The role of *Hand2* in branchial arch and head-shoulder patterning

Bettina Ryll

UCL

PhD

to Peter

Declaration

I, Bettina Ryll, confirm that the work presented in this thesis is my own. All data has been generated by myself unless indicated otherwise. Where information has been derived from other sources, I confirm that this has been indicated in the thesis.

_____

Bettina Ryll

Abstract

Comprehending gnathostome evolution requires insights into key cellular and molecular components of craniofacial and shoulder development.

For the work of this PhD, I made use of genetically modified mouse models to study aspects of mammalian head and shoulder morphogenesis by triple fluorescent RNA *in situ* hybridisation, immunohistochemistry and high resolution imaging.

First- I use a genetically defined sentinel cell population labelled by the *Hand*2-Cre transgene to establish the expansion of the distal-most branchial arch domain and correlate this by triple fluorescent RNA *in situ* hybridisation with the system controlling proximo-distal branchial arch patterning, the *Dlx* system. I find that the axis of the *Dlx* system does not correspond to the proximo-distal but an endodermal-ectodermal axis of the arch and rotates during development; the overall expansion of the arch is explicable by telescopic outgrowth along this new axis.

Second- I study the cellular and molecular characteristics of head/ shoulder skeleto-muscular connectivity and the contribution of limb lateral plate mesoderm to the shoulder girdle, which allows me to identify part of the *manubrium sterni* as the 'lost' mammalian procoracoid and to demonstrate that the interaction between lateral plate mesodermal subpopulations is non-random.

Third- I establish novel roles for *Hand*2 in lower incisor ameloblasts and in laminar dermal bone formation, suggesting a fundamental role for *Hand*2 in epithelial and mesenchymal cell layer arrangements. My detailed study of the murine frontal bone reveals that the establishment of an internal and an external layer initiates dermal bone formation; the latter shows intermediate molecular periosteal/ perichondrial characteristics and generates the intermediate layer by a *Hand*2-dependent invagination process.

For a comparative amphibian data set, I begin to establish genetic lineage labelling as technique in *Xenopus tropicalis*. I generate and test a *Xenopus Hand*2-Cre transgene and establish a stable generic *Xenopus tropicalis* Cre-reporter line by I-*Sce*I mediated transgenesis.

Table of Contents

Table of Figures

Chapter 1

Chapter 2

Chapter 3

Chapter 4

Chapter 5

Chapter 6

Chapter 7

Abbreviations

bHLH TF	basic Helix-Loop-Helix transcription factor
CMV	Cytomegalovirus
CMV'	Cytomegalovirus immediate early element
Cre	Cre recombinase
Cy3	Cyanine 3, excited maximally at 550nm, emits maximally at 570nm
Cy5	Cyanine 5, excited maximally at 649nm, emits maximally at 670nm
DABCO	1,4-diazobicyclo-[2.2.2]-octane
DAPI	4'-6-Diamidino-2-phenylindole = stain for double-stranded DNA
dH2O	double distilled water
DIG	Digoxigenin
DNA	Deoxyribonucleic acid
DNP	2,4-Dinitrophenol
dNTP	deoxyribonucleotide
EDTA	ethylenediaminetetraacetate
FITC	fluorescein isothiocyanate
GFP	Green Fluorescent Protein
H2O2	Hydrogenperoxide
***Hand*2 domain**	domain defined by the *Hand*2-Cre transgene
***hand*2 domain**	domain of *hand*2 RNA transcript expression
HCl	Hydrochloric acid
IHC	Immunohistochemistry
LB broth	Luria-Bertani broth
LoxP	locus of X-over P1
LPM	lateral plate mesoderm
M.	musculus/ muscle
Mm.	musculi/ muscles
mRFP	monomeric Red Fluorescent Protein
NaCl	Sodium chloride
NaOH	Sodium hydroxide
pBR	plasmid (designed and generated by) Bettina Ryll
PBS	Phosphate Buffered Saline
PCP	planar cell polarity
PCR	Polymerase Chain reaction
PFA	Paraformaldehyde
POD	Peroxidase
proc.	processus/ process
RFP	Red Fluorescent Protein
RISH	RNA *in situ* hybridisation
RNA	Ribonucleic acid
SCM	sternocleidomastoid muscle
SDS	sodium dodecyl sulfate

SOC	Super Optimal Broth with catabolite repression
SSC	saline sodium citrate buffer
TAE	400 mM Tris-acetate and 10 mM EDTA
TRIS	tris-hydroxymethyl-aminomethane
X-Gal	bromo-chloro-indolyl-galactopyranoside

Overview- genetically modified mice strains used in this thesis

Name	genetic modification	original publication	analysed crosses	described in this thesis in	obtained as/ from
***Hand*2-Cre**	transgene	Ruest et al. 2003[1]	*Hand*2-Cre$^{+/-}$; Rosa26LacZR$^{-/-}$ or *Hand*2-Cre$^{+/-}$; Rosa26EYFPR$^{-/-}$	Chapter 2, 3, 4	specimen and mice/ D. Clouthier- University of Colorado
***Wnt*1-Cre**	transgene	Danielian et al. 1998[2]	*Wnt*1-Cre$^{+/-}$; Rosa26LacZR$^{-/-}$	Chapter 3, 4	mice/ The Jackson Laboratory
***Hand*2 BA**	targeted deletion of regulatory region	Yanagisawa et al. 2003[3]	*Hand*2 BAenh$^{-/-}$	Chapter 4	specimen/ H. Yanagisawa- University of Texas/ Dallas
***Hand*2$^{fl/fl}$**	targeted insertion of LoxP sites into the coding region of *Hand*2	Hendershot et al. 2008[4]	*Hand*2$^{fl/fl}$; *Wnt*1-Cre$^{+/-}$; Rosa26LacZR$^{+/-}$	Chapter 4	specimen/ D.Clouthier- University of Colorado
Rosa26LacZR	targeted insertion, 'Rosa reporter'	Soriano 1999[5]	Rosa26LacZR$^{-/-}$	Chapter 2, 3, 4	mice/ The Jackson Laboratory
Rosa26EYFPR	targeted insertion, 'Rosa reporter'	Srinivas et al. 2001[6]	Rosa26EYFPR$^{-/-}$	Chapter 3	mice/ The Jackson Laboratory

1 General introduction

1.1 A genetic coordinate system patterning the branchial arches

Head, neck and shoulder are anatomical regions displaying a high degree of structural complexity. Understanding the genetic mechanistics underlying the development and the evolution of these regions therefore represents a formidable challenge. Particularly subjected to evolutionary transformation is the ventral and neural crest-derived side of the head comprising the face and the jaws which are derived from the first and to a lesser degree the second branchial arch (Figure 1.1 A, BA1 (red) and BA2 (blue) in an E10 mouse embryo, also see B). Branchial arches exist only as transient precursor structures during embryonic development; depending on the species, vertebrate embryos form between 4 and 7 arches that emerge in a cranio-caudal sequence as bilateral outpocketings on the ventral side of the embryo. Later, these outpocketings fuse in the midline around the later pharynx to create ring-shaped structures, the branchial (or pharyngeal) arches.

The future anatomy of the region is laid out in genetically encoded patterns within these branchial arches and three genetically defined axes are thought to create a 'genetic coordinate system' in which the branchial arches reside: the cranio-caudal (sometimes also called rostro-caudal), the proximo-distal and an ectodermal-endodermal axis (Figure 1.2). The patterning mechanism along the cranio-caudal axis is currently the best-understood and is the result of the overlapping expression domains of members of the *Hox* gene family. This provides each branchial arch with a distinct identity regarding its position along the cranio-caudal axis and is also referred to as the '*Hox*-code'[89,90,149] (Figure 1.2 A, axis 1).

Patterning along the proximo-distal axis within a given arch is less understood, although the family of *Dlx* genes has been shown to be expressed along this axis in a nested fashion that has been compared to the expression pattern of *Hox* genes. In mice, null mutations for *Dlx* genes- and especially double null mutations for paralogous *Dlx* genes- produced phenotypes in cranial anatomy that affected proximal and distal arch derivatives to varying degrees (most notably in the case of the *Dlx*5/6 knockout in which the lower jaw is replaced by an upper jaw[55,155]) so that in analogy to the cranio-

caudal *Hox* code[55,56] a proximo-distal '*Dlx* code' has been suggested for the patterning of the branchial arches (Figure 1.2 A, axis 2).

Cranio-caudal and proximo-distal branchial arch patterning are thereby not independent of each other but have been shown to be genetically linked. The loss of *Hox* gene expression in the second and more posterior branchial arches re-establishes in these arches gene expression patterns typical for the first branchial arch (under wild-type conditions, the first branchial does not express any *Hox* genes). The first arch state can therefore be considered a 'branchial arch default state' that can be overruled or modified by the expression of *Hox* genes[127,153].

The third and least-understood of the three axes extends between the inner endodermal lining and the outer ectodermal cover of the branchial arches (Figure 1.2 A axis 3 and B). Transplantation experiments in birds were able to demonstrate that the rotation of a patch of endoderm was sufficient to induce a concomitant rotation in the branchial arch-derived skeletal elements adjacent to the transplanted patch, clearly demonstrating the instructive properties of the endoderm[44]. The expression of FGF8 in the ectoderm on the other side has also been shown to be essential for the correct patterning of branchial arch elements[116,197], so that both endoderm and ectoderm are required to correctly pattern the intermediary branchial arches.

A detailed understanding of the working principle of this genetic coordinate system will bring us a step closer to understanding the developmental 'bauplan' of the vertebrate head skeleton. On a next level will the comparison between species help us to define the genetic differences at the origin of species-specific morphology and to elucidate evolutionary processes (such as the link between the evolution of a secondary jaw and the middle ear).

1.2 Establishing cellular origin by lineage labelling techniques

Vertebrate branchial arches are- with the exception of a mesodermal core later giving rise to muscle cells- filled with neural crest cells (Figure 1.1 B). The neural crest however only provides the embryonic material for the ventral and cranial part of the embryo including the head and neck (Figure 1.1 B, green), while the ventral caudal part

Figure 1.1- 1.2

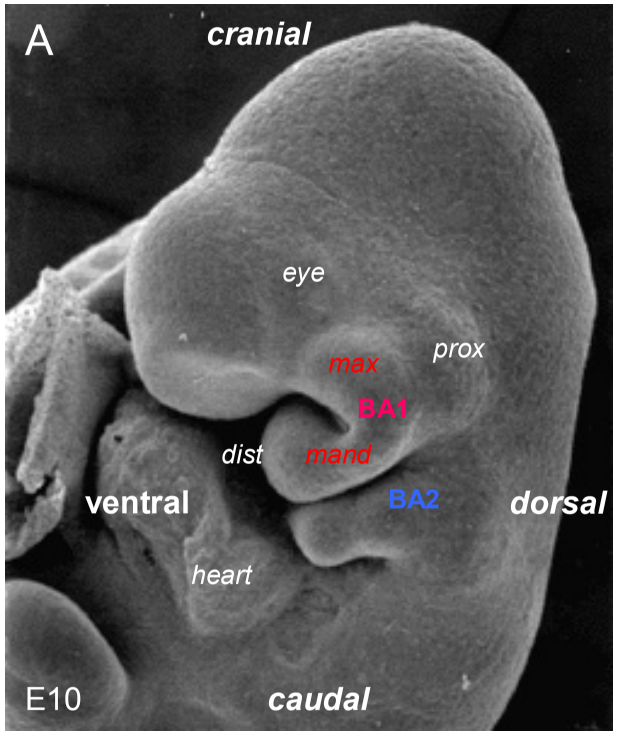
A
cranial
eye
prox
max
BA1
dist
mand
ventral
BA2
dorsal
heart
E10
caudal

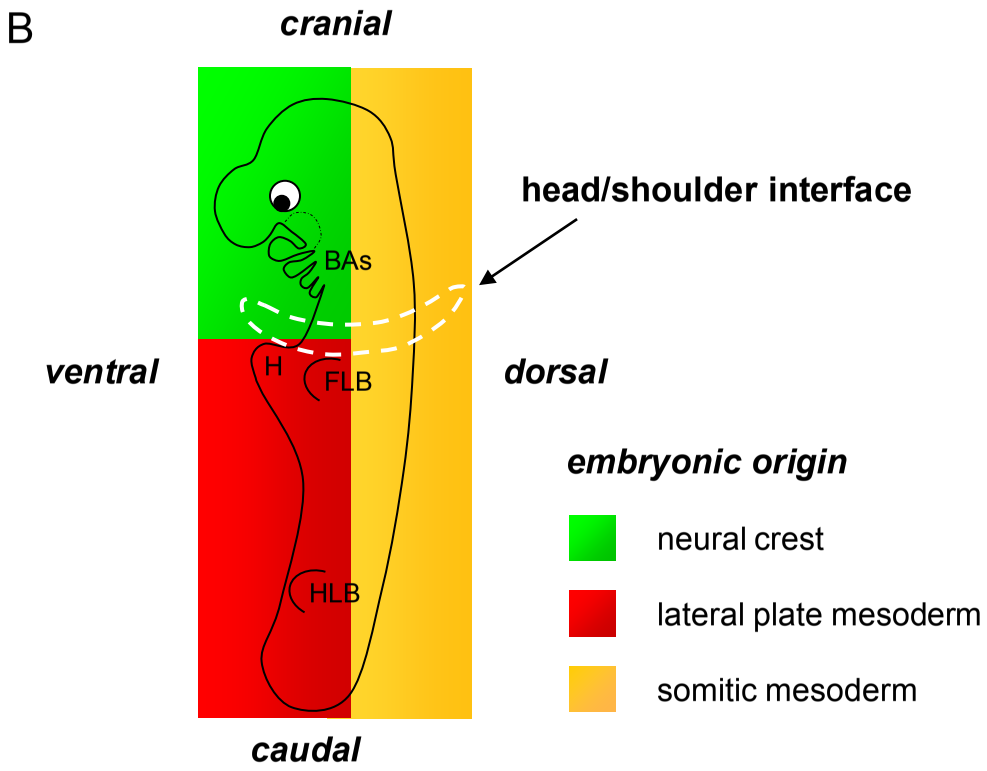
B
cranial
head/shoulder interface
BAs
ventral
H
FLB
dorsal
embryonic origin
neural crest
lateral plate mesoderm
somitic mesoderm
HLB
caudal

Figure 1.1 The vertebrate embryo

A Electron-microscopic image of an E10.0 mouse embryo in side-view with annotated axes (cranial to the top, caudal to the bottom, ventral to the left and dorsal to the right). At this time point in development, the first and the second branchial arch (BA1 and BA2) are already clearly established; the first branchial arch (BA1) can further be subdivided into a mandibular (mand) and a maxillary (max) process.

Source of the image: http://www.med.unc.edu/embryo_images/unit-hednk/hednk_htms/hednk012a.htm

B Cell populations of different embryonic origin contribute to the vertebrate embryo as depicted in this schematic side-view: While the dorsal part of the vertebrate embryo is mainly somitic mesoderm-derived (yellow), the cranial ventral side originates from the neural crest (green) and the caudal ventral side from the lateral plate mesoderm (red). The white underbroken line indicates the shoulder region which corresponds to an interface between all three cell populations.

BAs branchial arches 1-4 , ***BA1*** first branchial arch, ***BA2*** second branchial arch, ***dist*** distal, ***FLB*** forelimb bud, ***H*** heart, ***HLB*** hindlimb bud, ***mand*** mandibular, ***max*** maxillary, ***prox*** proximal

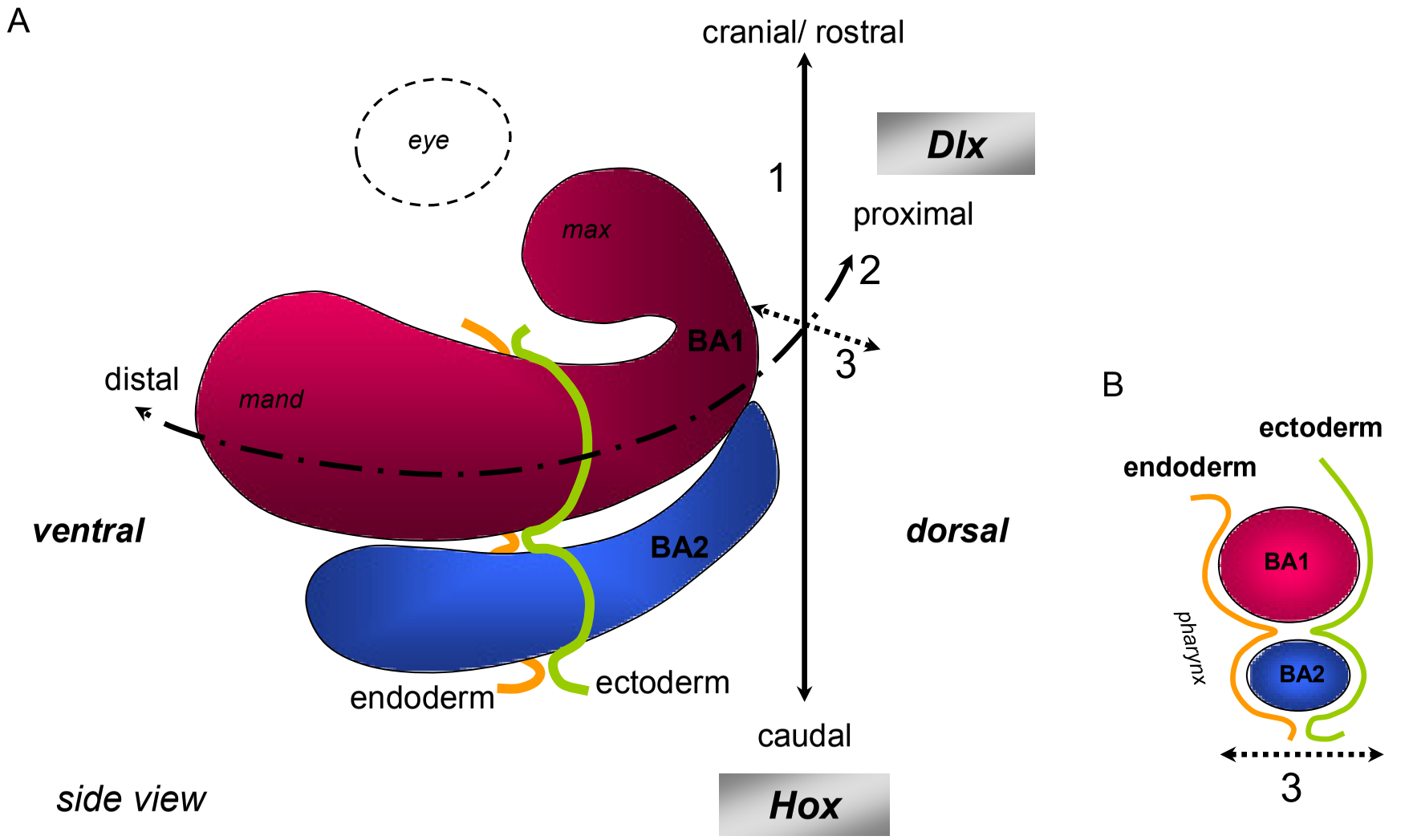
A
cranial/ rostral
eye
Dlx
1
proximal
max
2
BA1
3
distal
mand
ventral
dorsal
BA2
endoderm
ectoderm
caudal
side view
Hox
B
ectoderm
endoderm
BA1
pharynx
BA2
3

Figure 1.2 A genetic coordinate system patterning the branchial arches

A Schematic representation of the axes of a genetic coordinate system according to which the branchial arches are patterned. Represented are the first branchial arch (BA1, red) with the maxillary and mandibular process and the second branchial arch (BA2, blue) in side view; arches are orientated as in Figure 1.1 A with cranial to the top, caudal to the bottom, ventral to the left and dorsal to the right, the position of the eye is further indicated by the dashed circle.

Cranio-caudal identity between the branchial arches is defined by an overlapping pattern of *Hox* gene expression (axis **1**), it is noteworthy that the first branchial arch is devoid of Hox gene expression.

Branchial arches are thought be patterned in a similar way along their proximo-distal axis by the nested expression of *Dlx* genes (axis **2**). A further axis is defined between the inner, endoderm-facing side (yellow) and the outer, ectoderm-facing side (green) of the branchial arch though the genetic mechanism behind this patterning system is still less understood (axis **3** and in frontal view: **B**).

B Frontal view of the endodermal- ectodermal axis of the branchial arches (**3**, double arrow) at the position indicated in **A**. The contact between endoderm (yellow) and ectoderm (green) between the arches represents the location of the pharyngeal pouches (short arrow); the position of the pharynx at the inside of the branchial arches is indicated.

of the embryo is derived from the lateral plate mesoderm (red) and the dorsal part from the somitic mesoderm (yellow). By necessity, cell populations from different embryonic origin need to interact at their interfaces to give rise to a continuous and seamless organism and so far it is largely unknown by which mechanism(s) this is achieved. The plane where all three embryonic cell populations- neural crest, lateral plate mesoderm and somitic mesoderm- interact corresponds to the head/ shoulder interface of the embryo (indicated by a white dashed line in Figure 1.1 B). Also this region experiences major remodelling during evolution [122] and it is intriguing to think about how this could be achieved at such a complex embryonic interface.

In order to unravel the construction principle of an organism, it becomes crucial to understand the link between the origin and the final destination of cells. Tracing a cell and its progeny throughout development- so-called lineage labelling- can potentially reveal the patterning mechanisms these are subjected to, as e.g. lineage labelling experiments in the limb revealed that cells cannot cross a dorso-ventral lineage restriction plane[10]. Further, lineage labelling can give insight into the interactions at cell populations boundaries as e.g. in the case of the ontogenetically preserved connectivity of cells that form the connective tissue as well as the corresponding attachment sites of each muscle examined so far[102].

Different lineage labelling techniques have been used to follow cells and their progeny through development, all based on the principle that a detectable signal is passed on from the mother cell to all its daughters; this allows to establish a cell lineage tree. Early in the 20th century, staining of the neural ridge with vital dyes were used to observe early neural crest migration[85]; this technique was considerably improved by the discovery of lipophilic dyes such as DiI and DiO that specifically and strongly label cell membranes[11] and by the development of fluorescent conjugates of highmolecular dextrans that could serve as intracellular tracers. All direct labelling techniques unfortunately share the disadvantage that the marker or tracer is diluted with every cell division, limiting the use of this technique for long-term fate mapping. Grafting techniques in which labelled tissue is transplanted into an unlabelled host[157]or between two similar but not identical species (such as quail/ chick or between two xenopus species) require surgical skills and rely on the availability of anatomical landmarks but have been successfully used for long-term fate mapping in amphibian and bird embryos, e.g. work by Chibon[33-35], Noden[134-136], Le Douarin [summarized in 106], Koentges and Lumsden[102].

Genetic lineage labelling has the potential to overcome some of the limitations mentioned above and offers the additional advantage of being applicable to species with intrauterine development as long as transgenic techniques are available. The permanent labelling of a cell lineage is thereby achieved by the controlled expression of a recombinase (such as Cre or Flp) in a cell population of interest that subsequently leads to the irreversible activation of a generic reporter which produces a detectable signal (such as direct fluorescence). Today, the Cre/ Lox system is widely used for genetic lineage labelling in mouse (*Mus musculus*). The activation of the Cre-reporter occurs on DNA level and so creates an inheritable and permanent signal that is passed on from the mother to all daughter cells, thus defining a cell lineage tree. Generic Cre-reporter mouse strains such as the ROSA26LacZR[176] or ROSA26EGFPR[177] are nowadays commercially available from sources like e.g. The Jackson Laboratory/ US.
The specificity of the lineage labelling reaction is achieved by placing the Cre recombinase under the control of a suitable genetic element ideally only active in the cell population of interest. As soon as the Cre-reporter has been activated, recombinase activity becomes redundant, which makes the technique ideal for long-term lineage labelling.
Once the transgenic line is established, genetic lineage labelling is- in contrast to transplantation experiments- non-invasive, allowing to trace cells under physiological conditions. With the choice of a suitable genetic element for the controlled expression of the recombinase, genetic lineage labelling can further be used to trace genetically defined subpopulations of cells within otherwise anatomically homogenous structures. This not only reduces the dependency on anatomical landmarks but also offers the potential to considerably increase the resolution with which lineage labelling experiments can be conducted.
The genetic lineage labelling technique allowed me to address several aspects of head/ shoulder morphogenesis during the work for my PhD and the results of this study will be presented in the following chapters of this thesis. In particular, I made use of the *Hand*2-Cre mouse, an established transgenic mouse line in which the expression of Cre recombinase is under the control of 7.4kb upstream region of the transcription factor *Hand*2[158].

1.3 The transcription factor Hand*2*

*Hand*2 (formerly also called bHLHa26, E*hand*2, *Hed*, *Thing*2, d*Hand*) is a member of the basic-loop-helix (bHLH) transcription factor family, a group of transcription factors that control the specification, growth and differentiation of numerous cell types during embryogenesis[121]. The characteristic bHLH motif of this group of transcription factors mediates the dimerization between tissue-specific class B bHLH proteins with ubiquitous class A bHLH proteins (also called E-proteins). *Hand*2 is a bHLH transcription factor of the tissue-specific class B and was originally identified for its particular role in cardiogenesis[178].

Since then, *Hand*2 has been shown to also play an important role in the development of a variety of other tissues like the lateral plate mesoderm, the branchial arches, the limb buds, blood vessels and in the peripheral autonomous nervous system[46,63,79,80,129,175,212]. More recently, *Hand*2 has also been mentioned in the context of chondrogenesis [1], osteoblast differentiation [65] and epithelogenesis [208] which indicates that *Hand*2 also assumes a number of currently less-studied functions at later developmental stages.

The complete loss of *Hand*2 function is not compatible with life and *Hand*2 null mouse embryos do not survive past embryonic day 10.5. Cause of the embryonic lethality is heart failure due to right ventricular hypoplasia and defects in vascular development; in addition, *Hand*2 null mice display severely hypoplastic first and second branchial arches while posterior arches entirely fail to from[178,179,210].

*Hand*2 has been shown to exert its function as transcriptional activator via both DNA-binding dependent and independent mechanisms[109]: DNA-binding dependent *Hand*2 function requires the recognition of a specific DNA-motif, a so-called E-box (CANNTG). In order to in effect bind to the sequence, *Hand*2 imperatively needs to dimerize with other E-porteins[47]. Transcriptional activation occurs through an activation domain in the amino-terminal region of the *Hand*2 protein and can be controlled by masking or unmasking of this domain by intra- and intermolecular interactions[47]. Over-expression assays showed that *Hand*2 DNA-binding is not necessary for its role as transcriptional activator as even mutant *Hand*2 proteins with a defective DNA-binding domain were able to activate transcription[160,209]. A mouse mutant in which the *Hand*2 DNA-binding domain was abolished by homologous recombination confirmed this finding *in vivo* and was able to demonstrate that *Hand*2 regulates region- (and time) specifically gene expression in a DNA-binding dependent or independent manner:

While *Hand*2 function in the limb bud is fully dependent on the ability of the transcription factor to bind to DNA, the early development of the branchial arches and the heart were remarkably unaffected upon loss of the DNA-binding domain (both processes are severely affected in the *Hand*2 null mutant)[109,180].

Main regulatory elements controlling *Hand*2 expression have been identified in the vicinity of the *Hand*2 coding region[29,123,201]. In the wildtype, *Hand*2 expression is restricted to the distal part of all branchial arches[178] and -7.4kb of *Hand*2 upstream region were apparently able to replicate this *Hand*2 expression pattern (as well as expression in the heart but not in the lateral plate mesoderm nor the limb buds, Figure 1.3). Branchial arch expression was thereby governed by a genetic element located between -6.6 and -7.4kb upstream of the *Hand*2 transcriptional start site (the 'branchial arch enhancer', Figure 1.3 B); in combination with an artifical minimal promoter, this element replicated *Hand*2 branchial arch expression and was shown to be *endothelin*1-dependent and regulated by *Dlx*6[30]. Interestingly, the deletion of this 'branchial arch enhancer' only abolished the proximal but not the distal part of the *Hand*2 branchial arch expression, showing that this apparently homogenous *Hand*2 expression domain is composed of independently regulated subdomains[211]. A second element in the *Hand*2 upstream region located between -2.7 and -5.5kb was able to replicate *Hand*2 expression in the right heart and was therefore termed 'right cardiac enhancer'[123] (Figure 1.3 B). Neither a construct containing -7.4kb nor -11kb *Hand*2 upstream region were able to replicate endogenous *hand*2 expression in the lateral plate mesoderm[123]. When the previously assessed -7.4 kb of *Hand*2 upstream region were incorporated into the *Hand*2-Cre transgene and tested in mouse transgenesis (Figure 1.3 B, mouse line analysed for this thesis), the transgene showed the expected activity in the first and second branchial arch and in the heart (but not in the lateral plate mesoderm), in addition to an unexpected activity throughout the forelimb bud (Figure 1.3 B). *Hand*2 expression is normally confined to the posterior part of both forelimb and hindlimb bud and has been show to pre-pattern the limb prior to *sonic hedgehog* activity [30] (Figure 1.3 A). The posterior restriction of *Hand*2 is thereby achieved by anterior *gli*3-mediated repression[30,183]. A recent study identified two *gli*-response elements located at circa 10kb and 85 kb respectively downstream of the *Hand*2 coding region. The absence of these *gli*-response elements in the -7.4kb *Hand*2-Cre transgene would provide a possible explanation for the aberrant transgene behaviour[201]. The differences in expression between the *Hand*2-Cre transgene and the previously tested *Hand*2-LacZ

Figure 1.3

A

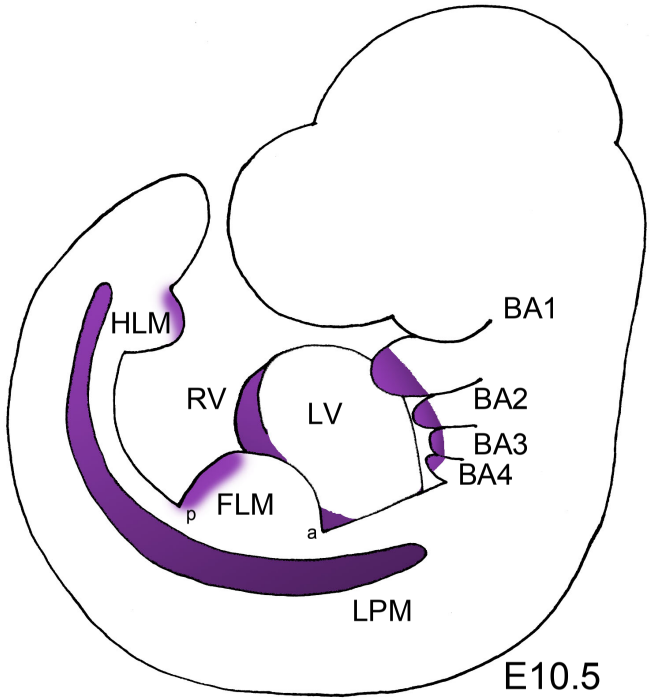

endogenous hand2 expression

B

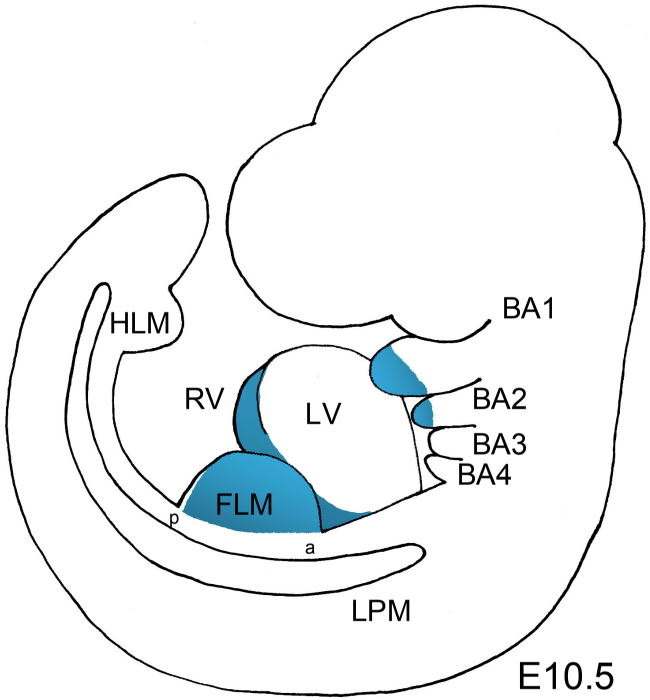

Hand2-Cre transgene

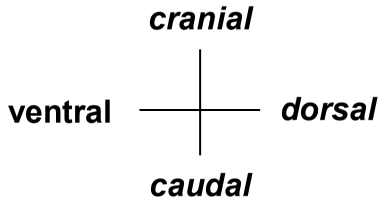

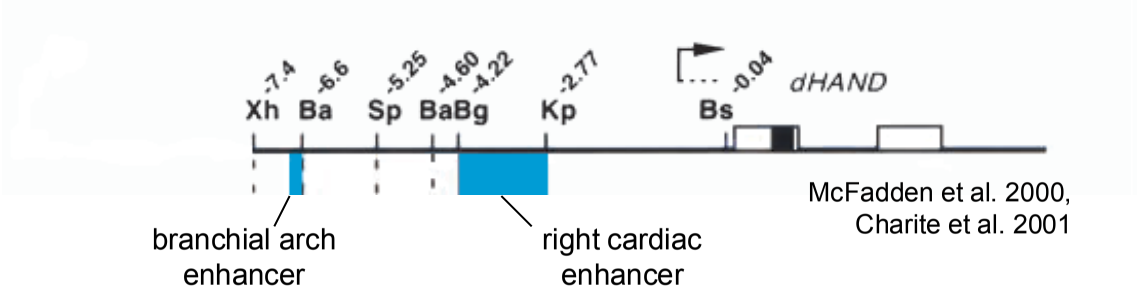

Figure 1.3 *Hand*2 endogenous expression and *Hand*2-Cre transgene expression in comparison

A The main endogenous *hand*2 expression domains in an E10.0 mouse embryo: *Hand*2 is expressed in the distal part of the branchial arches (BA1- BA4), the right ventricle (RV) of the heart, throughout the lateral plate mesoderm (LPM) and in the posterior parts of the forelimb (FLM) and hindlimb buds (HLM).

B The *Hand*2-Cre transgene (as characterised by McFadden et al. 2000, Charite et al. 2001 and Ruest et al. 2003) contains -7.4 kb genomic region upstream of the *Hand*2 transcriptional start site (bottom of the figure) and apparently replicates endogenous *hand*2 expression in the first and second (BA1 and BA2) but not in more posterior (BA3 and BA4) branchial arches. The genetic element responsible for this part of the expression pattern, the so-called *Hand*2 'branchial arch' enhancer has been located in the *Hand*2 upstream region between a *Bam*HI (-6.6 kb) and a *Xho*I (-7.4kb) site. Expression in the right ventricle of the heart is controlled by the right cardiac enhancer, located between -2.77 (*Kpn*I site) and -4.22 (*Bg* site) in the *Hand*2 upstream region. The *Hand*2-Cre transgene shows further expression throughout the forelimb bud (FLB), omitting only a slim rim at the posterior end of the forelimb bud; this part of the transgene expression does not replicate endogenous *hand*2 expression. The *Hand*2-Cre transgene shows no activity in the hindlimb bud (HLB) nor throughout the lateral plate mesoderm (LPM).

a anterior, ***BA*** branchial arch, ***FLM*** forelimb bud, ***HLB*** hindlimb bud, ***LPM*** lateral plate mesoderm, ***LV*** left ventricle, ***p*** posterior, ***RV*** right ventricle

enzymes in order of occurrence in the *Hand*2-Cre transgene: **Xh** *Xho*I, **Ba** *Bam*HI, **Sp** *Spe*I, **Bg** *Bgl*II, **Kp** *Kpn*I, **Bs** *Bss*HII

transgene (which both contain the same -7.4kb upstream *Hand*2 regulatory region) are most likely caused by position variegation effects in addition to the missing *gli*-response elements.

1.4 Introduction to the work of this PhD

During the work for this PhD, I made use of the above mentioned *Hand*2-Cre mouse, two different genetically modified mouse lines with partial inactivation of *Hand*2 function and the *Wnt*1-Cre mouse as a reference for neural crest origin (a separate overview of all genetically modified mouse lines used in this thesis is also part of the introductory chapter and directly proceeds this general introduction) to address specific points of head/ shoulder development that particularly intrigued me:

Chapter 2

However complicated the anterior part of the head is, its precursor structure, the first branchial arch, is a surprisingly simple half-round roll of cells. Morphological analysis does not reveal any signs of the later complexity that nevertheless must be already present and laid out in patterns of gene expression. I made use of a sentinel distal branchial arch population defined by the mouse *Hand*2-Cre transgene to study the outgrowth of the first branchial arch along the proximo-distal axis and correlated this domain by double/ triple fluorescent RNA *in situ* hybridisations to the system commonly recognised as responsible for proximo-distal branchial arch patterning, the *Dlx* system, which is content of Chapter 2.

Chapter3

In tetrapods, the head is connected to the shoulder girdle via a mobile muscular bridge, the neck. Different embryonic cell populations contribute to this complex region and I was interested in the mechanistics according to which these different embryonic cell populations interact in order to create a continuous functional system. The aberrant activity of the *Hand*2-Cre throughout the forelimb bud allowed me in this context to identify cells that originated within the limb bud within the lateral plate mesodermal domain. The anterior margin of the shoulder girdle corresponds to a major neural crest/

mesoderm interface and I studied the cellular and molecular characteristics of the attachments of the coracobranchial muscles onto this margin, as well as the contributions and interactions of different lateral plate mesoderm subpopulations to this region; these results will be presented in Chapter 3.

Chapter 4

Development can be described as a series of increasingly refined patterns for which the same genes are repeatedly deployed in different context[26]. Young embryos within the vertebrate group resemble each other surprisingly while species differences get markedly pronounced with ongoing development and result in very different adult morphology[202]. Which patterns make the difference between a mouse and a zebrafish? My interest in relatively late developmental patterns led me to discover a novel role for *Hand2* in the organisation of the incisor ameloblast layer and in dermal bone formation, which will be described in Chapter 4.

Chapter 5

The evolution of the middle ear within the tetrapod group has fascinated biologists and comparative anatomists for a very long time, e.g.[70]. It is now commonly accepted that a tympanic middle ear evolved several times independently within the tetrapod group which raises interesting questions about the homology of structures and the underlying genetic mechanistics[38,39]. Recent fossil evidence suggests that the middle ear of extant frogs still strongly resembles the ancestral condition of certain stemgroup tetrapods[154]. With the aim to understand how such a primitive middle ear could have arisen and to gain first insights into shared and divergent mechanisms of the evolution of the tympanic middle ear within the tetrapod group, we began to establish a genetic lineage labelling system based on the Cre/ Lox technique in a biological model system representing extant frogs, *Xenopus tropicalis*.
The establishment of a generic stable transgenic *X. tropicalis* Cre-reporter line, in addition to preliminary results for specific Cre-driving constructs will be presented in Chapter 5.

As each of the data sets addresses a different aspect of head/ shoulder morphogenesis, they will be treated as separate entities and introduced and discussed independently in

the relevant Chapter. A concluding general discussion follows in **Chapter 6** and a description of the material and the methods can be found in **Chapter 7**.

2 *Hand*2 in the context of proximo-distal branchial arch patterning and branchial arch outgrowth

2.1 Overview

The anterior head and the face are derivatives of the first two of a series of deceptively simple branchial arches. The complexity of the final structure is already encoded in the genetic patterns of these arches; understanding of the patterns will reveal how cranial morphology is defined, how the process of outgrowth from a simple branchial arch into a complex final structure is controlled and finally, by comparison with other species, which genetic differences stand behind the great diversity of vertebrate head morphology.

In this study, we make use of a sentinel branchial arch population defined by the murine *Hand*2-Cre transgene to evaluate the outgrowth of the first branchial arch by tracing cells originating from the distal branchial arch and their progeny through ontogeny. We further correlate the development of this distal branchial arch domain defined by the *Hand*2-Cre transgene by triple fluorescent RNA *in situ* hybridisation with endogenous *hand*2 expression and with the genetic system that is considered in control of intra-arch patterning along the proximo-distal axis, the *Dlx* system. We find that the distal domain of the first branchial arch experiences considerable extension during development, performing an inward and upward rotation. To our surprise, the axis of the *Dlx* system does not correlate with the proximo-distal axis of the branchial arch as generally suggested but rather with an axis that is established between the ectodermal and endodermal face of the arch. This alternative axis of the *dlx* system corresponds to the rotational axis of the *Hand*2 domain which is suggestible of an outgrowth of the first branchial arch under the control of *Dlx* genes.

2.2 Table of Contents

2.3 Introduction

2.3.1 The role of the neural crest in craniofacial development

The invention of neural crest cells is currently seen as one of the reasons for the emergence and the success of the vertebrate group as it allowed the evolution of advantageous complex craniofacial structures (the new head theory[66]). Neural crest cells detach from the dorsal-most aspect of the neural tube after an epithelial-to-mesenchymal transition and migrate into the periphery, filling the branchial arches. Cranial neural crest destined to form the anterior head leaves the neural tube at the level of the posterior midbrain and hindbrain and migrates in discrete streams that are defined by their level of origin and do not mix. The hindbrain shows a segmental organisation in regular bulges, so-called rhombomeres, and it is its rhombomeric origin that defines the destination of the emigrating cranial neural crest: Cells originating from rhombomere 1 and 2 thereby migrate into the first branchial arch, rhombomere 4 crest into the second arch and neural crest from rhombomere 6 and posterior populates the third and fourth branchial arch[112,113]. The segregated migratory pattern might result from the fact that neural crest cells emerging from rhombomere 3 and 5 predominantly die by apoptosis and do not contribute to skeletal craniofacial structures[73,74,113]. It is also the cranial neural crest component that accounts for the considerable variation in vertebrate craniofacial anatomy. For a long time, regional diversity in the head had been thought to be generally specified in pre-migratory neural crest cells. This assumption was based on results from early hetero- and isotopic grafting experiments of pre-migratory cranial neural crest in amphibian[83,203]and avian embryos[137] although only the mandibular but not other pre-migratory neural crest population appeared to be specified with respect to subsequent patterning. Consequently, the idea of pre-patterned cranial neural crest was challenged after a modification of the transplantation technique by Trainor et al. in which pre-migratory neural crest was now transplanted without the isthmus, a region of the neural tube with intrinsic signalling function: Neural crest cells transplanted without the isthmus no longer showed signs of the previously reported pre-specification but on the contrary, a high degree of plasticity as they developed according to surrounding patterning cues[194]. While these results promoted the idea of a high degree of plasticity in neural crest cells that receive their patterning information mainly from peripheral

signalling centres, even more recent inter-species transplantation experiments by Schneider and Helms provide new evidence for the previous concept of a pre-specified neural crest: transplantation of neural crest cells from the beak-forming regions between duck and quail always result in the formation of a beak according to the donor but not the host species. Donor neural crest cells thereby do not only form a donor-like beak but also instruct surrounding host ectoderm to develop into donor-like structures, demonstrating the inherent organizing capacity of the transplanted neural crest[162]. The disparity between the results from Trainer et al. and Schneider and Helm could be explained by differences in the way the transplantations were performed, as a larger transplant size might retain organizing capabilities in the neural crest due to community effects[193]. Current understanding is therefore that craniofacial patterning is achieved in a complex and yet not fully understood interplay between partially pre-specified neural crest cells that respond to signals coming from the surrounding tissue, e.g.[119] and that this response might differ from arch to arch.

2.3.2 Branchial arch patterning

The instructive surrounding required for correct craniofacial patterning is provided by the branchial arches into which neural crest cells immigrate. Branchial arches are metameric serial structures that arise during embryonic development in a rostro-caudal fashion on the ventral side of the cranio-facial region. Vertebrate embryos have between 4 to 7 branchial arches and while the two rostral-most arches (first and second branchial arch) are prominent in size, more posterior branchial arch material is occasionally only present in rudimentary form. Branchial arches are embryonic structures and transient in nature as they provide the 'building material'- and in all likelihood also the pattern- for the anterior head and neck region. While branchial arches appear as deceptively simple out-pocketings at the side of the vertebrate neck, the high complexity of the resulting head and neck region must have been encoded in earlier specific genetic patterns. Branchial arches are known to be patterned along several axes, whereby the patterning mechanism along the rostro-caudal axis by *Hox* genes is the best-understood. The unique identity of a given branchial arch is defined by its position on the rostro-caudal axis of the embryo and genetically specified by the overlapping expression of *Hox* genes which create a rostro-caudal '*Hox*-code' of branchial arch identity. Loss and gain

of function experiments in different species have for example demonstrated the role of *Hox*a2 as selector gene for second branchial arch identity[13,71,75,141,148,153]. So while the origin of inter-arch specificity is relatively well-understood, our understanding about intra-arch specificity, the definition of different identities within a given arch, is still somewhat less clear.

Based on their nested expression reminiscent of nested *Hox* gene expression, the transcription factor family of *Dlx* genes has been proposed to provide the proximo-distal equivalent to the rostro-caudal *Hox*-code, therefore named the '*Dlx*-code'[55,56]. In mice, there are six known *Dlx* genes (*Dlx*1, *Dlx*2, *Dlx*3, *Dlx*4 (previously: *Dlx*7), *Dlx*5 and *Dlx*6) that are expressed in a differential and nested pattern within the branchial arches[55]. Mammalian *Dlx* genes are arranged as tightly-linked paralogous pairs in a tail-to-tail fashion in the vicinity of *Hox* clusters (paralogues are *Dlx*1-2, *Dlx*3-4, *Dlx*5-6)[181, 146]. Paralogous *Dlx* gene pairs appear to share certain regulatory elements and to be expressed in similar branchial arch domains (for an extensive review on *Dlx* genes please see the publication by Depew et al. 2005[56] and references therein). The current view is that the distal-most part of the branchial arch is defined by the overlapping expression of all six *Dlx* genes, the intermediate part by *Dlx*1-2 and *Dlx*5-6 and the proximal part by *Dlx*1-2. Branchial arches are known to be at the origin of an ordered series of skeletal elements so that it was hypothesized that the nested expression of *Dlx* genes worked as a combinatorial code, specifying the identity, pattern and development of each skeletal element of the series. Loss-of-function mutants were able to confirm the postulated role of *Dlx* genes in the specification of intra-arch identity, as loss of gene function resulted in the loss or re-specification of discrete branchial arch elements, most spectacularly in the case of the $Dlx5^{-/-}$,$Dlx6^{-/-}$ double mutant where the lower jaw ('distal') was transformed into a second upper jaw ('proximal') proving that the combinatorial expression of *Dlx*5/6 is indeed specifying lower jaw identity[55].

2.3.3 The deep homology of patterning systems

Dlx genes are the mammalian homologues of the fly gene *distal-less*, that was originally identified in *Drosophila* mutants lacking the distal parts of their limbs. *Distal-less* is expressed in the central domain of a concentric genetic system in the *Drosophila* imaginal disc, controlling the telescopic outgrowth of the structure and specifying the

distal-most part of the appendage[108]. The nested expression pattern of *Dlx* genes, together with the ability to specify skeletal elements along a proximo-distal axis is common between mammalian branchial arches and invertebrate imaginal discs. The evolutionary co-option of existing genetic networks in a new context by non-homologous structures has been recently reviewed by Shubin et al. 2009[171]. An example cited by Shubin and co-authors is the co-option of the same *Drosophila* limb programme involving *distal-less* for horn development in the dung beetle *Onthophagus*. Although limbs and horns are not related, the same genetic network is deployed in the regulation of their outgrowth, a fact termed 'deep homology' by the same authors already in an earlier publication[170]. Against this background, it is tempting to speculate that mammals deploy a 'deeply homologous' mechanism based on distal-less/ *Dlx* genes to regulate the outgrowth of the embryonic branchial arch in a way that is reminiscent of the telescopic outgrowth of the *Drosophila* imaginal disc.

In order to study mammalian branchial arch outgrowth and patterning, we made use of a transgenic mouse line (*Hand*2-Cre mouse by Ruest et al.[158]) to analyse the behaviour of a subpopulation of cells within the branchial arch. The *Hand*2-Cre mouse allows us to specifically label cells from the distal-most part of the first two branchial arches and to follow their progeny through development. The relationship between the distal first branchial arch domain defined by the *Hand*2-Cre transgene and the *Dlx* system was established by double and triple fluorescent RNA *in situ* hybridisations on sections. The results of this study and a discussion of the topic are content of this chapter.

2.4 Results

2.4.1 A distal *hand*2 domain

The expression domain of *hand*2 was compared to the domains of other established proximo-distal markers by fluorescent double RNA *in situ* hybridisations on sections of wildtype branchial arches; the aim was to describe the position of *hand*2 in a coordinate system of proximo-distal markers and to identify potential patterns in the spatial arrangements of gene expression domains that could betray a common underlying genetic regulation. Stainings were repeated at least twice for each probe in independent rounds of stainings; sections were from unrelated embryos and the expression patterns were compared to published results. The embryonic stage chosen for analysis, E12.0, lies just prior to the formation of distinct upper and lower jaws; the underlying assumption is that any genetic pattern for future structures must have been laid down by this time-point. Branchial arches were sectioned along their entire proximo-distal axis, which due to the natural arch curvature corresponds to an angled transverse sectioning plane as depicted e.g. in Figure 2.1.

*Hand*2 is expressed in a clear domain in the distal part of the branchial arches and fills this region entirely (Figure 2.1 and 2.2). Nested within can be found the domain for *hand*1 (formerly called e*hand*, Figure 2.1 B). Adjacent to it, with overlap limited to a small triangular zone on the endodermal side of the branchial arch (arrow in Figure 2.1 A), lies the expression domain of *pitx*1. The expression domains of all three genes, *hand*1 and *hand*2 and *pitx*1, follow the same orientation and span the entire depth of the branchial arch from the endodermal to the ectodermal side (see also Figure 2.3). Other genes such as *msx*1 (Figure 2.1 C) and *gsc* (Figure 2.2 B) differ in that respect and follow an orientation perpendicular to the one of *hand*2. While not reaching as far distal as *hand*2, the *msx*1 expression domain resembles a cap on the ectodermal side of the arch. In comparison, the *gsc* expression domain is limited to a stripe in the medial third of the arch.

Another group of genes shows components of each orientation system, like *prx*1 and *barx*1 (Figure 2.1 A and Figure 2.2 A respectively), with a part of the expression domain following the *msx*1/ *gsc* axis and a part orientated along the *hand*2 axis. *Fox*c2 has a triangular zone of expression in the centre of the overlap of many expression

Figure 2.1- 2.2

2.1

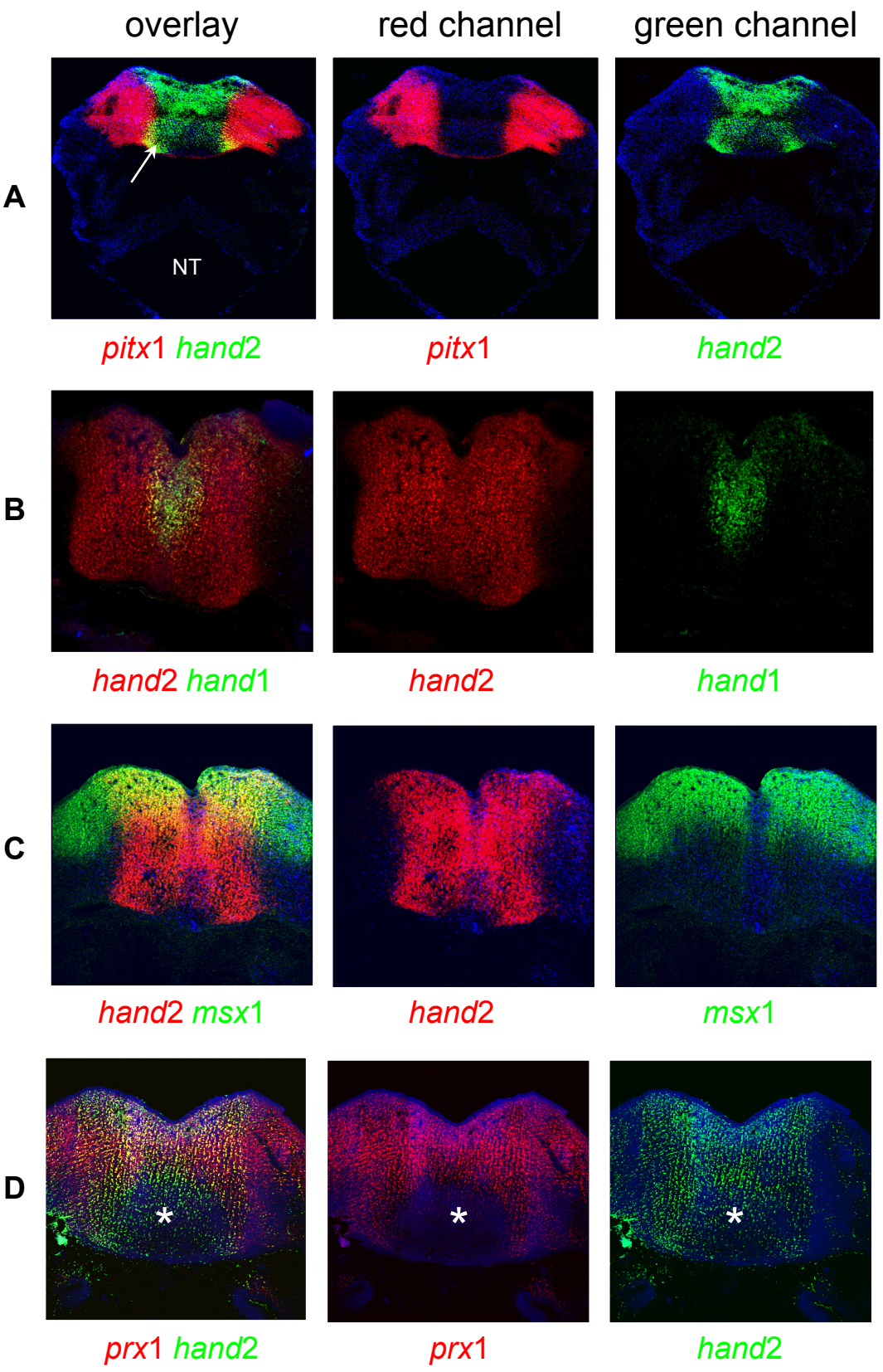
overlay
red channel
green channel
A
NT
pitx1 hand2
pitx1
hand2
B
hand2 hand1
hand2
hand1
C
hand2 msx1
hand2
msx1
D
*
*
*
prx1 hand2
prx1
hand2

E12.0

Figure 2.1 Gene expression in the distal part of the first branchial arch

Double fluorescent RNA *in situ* hybridisation for proximo-distal markers on sections of the first branchial arch of E12.0 wildtype mouse embryos. Sections were cut as indicated below as angled transverse sections to show the entire length of the branchial arch. RNA probes were either labelled with DIG and developed with Cy3 tyramide (red) or labelled with FITC and developed with FITC tyramide (green). Nuclear counterstain: DAPI (blue).

Images are shown as an overlay of all three channels (first column), red (second column) and green (third column) channel with or without DAPI. All images are orientated with ventral to the top and dorsal to the bottom. The position of the neural tube (NT) is marked in **A**.

A *Pitx*1 (red) and *hand*2 (green) show nearly mutually exclusive expression with the domain of *pitx*1 lying proximally to the *hand*2 domain. A small area of overlap exists at the endodermal side of the arch (arrow).

B The very distal expression domain of *hand*1 (formerly called *ehand*, green) is fully nested with the domain of *hand*2 (red).

C Expression of *msx*1 (green) is restricted to the ventral part of the branchial arch and expands further proximally than *hand*2 (red) expression.

D *Prx*1 (red) shows a strong ventral expression with an additional extension towards the dorsal side of the branchial arch; no expression is seen in the distal- most and central part of the arch which is *hand*2 positive (asterisk).

NT neural tube

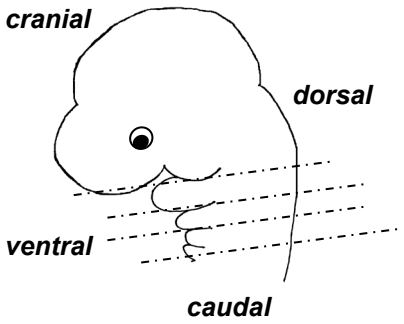

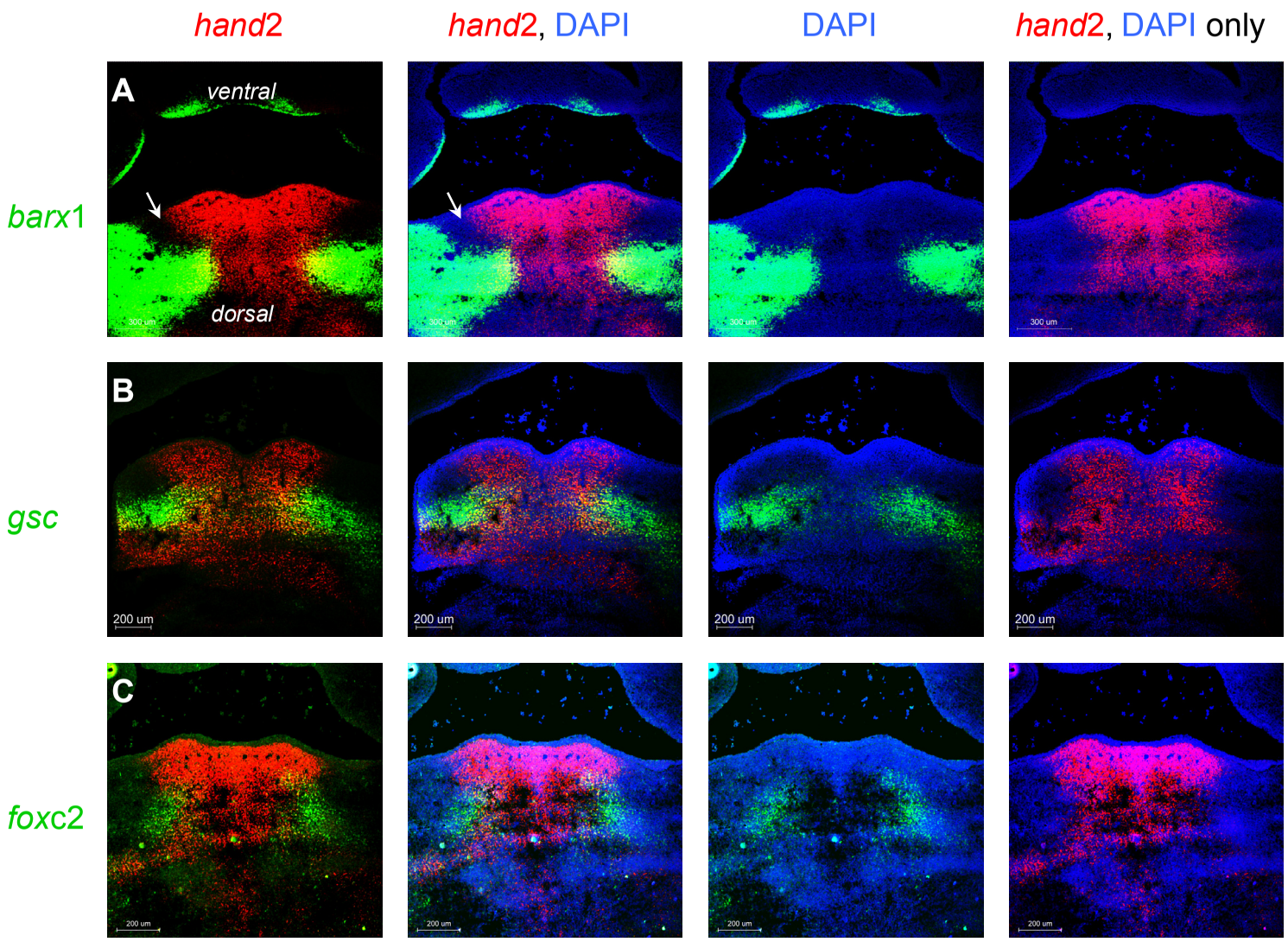
hand2
hand2, DAPI
DAPI
hand2, DAPI only
barx1
gsc
foxc2
A
B
C
ventral
dorsal
300 um
200 um

Figure 2.2 Gene expression in the distal part of the first branchial arch- 2

Double fluorescent RNA *in situ* hybridisation in the first branchial arch of E12.0 mouse embryos. Section were cut as angled transverse sections to be able to show the entire length of the branchial arch and as indicated below. Orientation of all sections is: ventral to the top, dorsal to the bottom.

RNA probes were labelled with DIG and developed with Cy3 tyramide (red) or labelled with DNP and developed with Cy5 tyramide (green). Counterstain: DAPI.

The first column shows the overlay of just the two probes, the second column the two probes with DAPI to demonstrate the anatomy. Third and forth column show the probes in separated images

A *Barx*1, *hand*2. *Barx*1 shows a distinctly shaped expression domain further proximal to the hand2 domain, with only very little overlap towards the dorsal end of the *hand*2 domain. Ventrally, there is a clear gap between both expression domains (arrows).

B *Gsc*, *hand*2. *Gsc* shows a stripe of expression in the middle third of the branchial arch, reaching into the *hand*2 expression domain.

C *Foxc*2, *hand*2. *Foxc*2 is expressed in a triangular area in the middle third of the branchial arch and touches the proximal hand2 expression boundary.

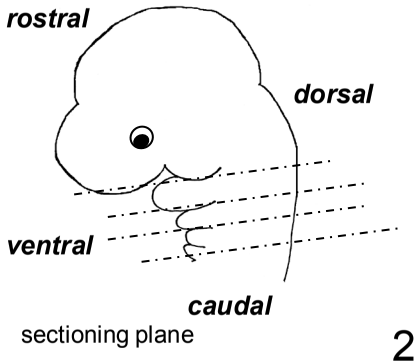

2.2

zones (Figure 2.2 C and Figure 2.3) but does not show orientation along any of the other axes. Figure 2.3 gives a schematic summary of all expression domains projected over each other (A) and individually. Though several gene expression domains seem to follow the same orientation, potentially suggesting a common genetic control, there is no overall unifying pattern recognisable that would betray the structure of an underlying genetic mechanism.

2.4.2 *Hand*2 gene and transgene within the *Dlx* system

To position endogenous *hand*2 expression and cre expression driven by the *Hand*2-Cre transgene within the *Dlx* system, triple fluorescent RNA *in situ* hybridisations on sections of *Hand*2-Cre$^{+/-}$; Rosa26LacZR$^{-/-}$ embryos were performed, with the aim of simultaneously answering the following questions:

1. How does *hand*2 expression relate to the *dlx* system?
2. In how far does the *Hand*2-Cre transgene replicate endogenous *hand*2 expression?
3. If divergent, how does the expression domain defined by the *Hand*2-Cre transgene relate to the *Dlx* system?

Because of *hand*2's distal expression, the supposedly distal-most *dlx* pair (*dlx*3, *dlx*4) and the intermediate *dlx* pair (*dlx*5, *dlx*6) were chosen for comparison. According to the textbook model about the nesting of *dlx* domains, we expected an overlap of the *hand*2 with the *dlx*3, *dlx*4 expression domain and a nesting of the *hand*2 domain within the *dlx*5, *dlx*6 domain. To our surprise, *hand*2 showed no overlap with the *dlx*3 domain (Figure 2.4 A, B) but with the *dlx*5 domain (Figure 2.4 C, D). This could be confirmed albeit less convincingly for the respective other candidate of the *dlx* pairs, *dlx*4 (paired with *dlx*3, Figure 2.6 A, B) and *dlx*6 (paired with *dlx*5, Figure 2.6 C, D).
As most studies are based on RNA *in situ* hybridisations in E10 embryos and to rule out specificity for a given time-point in development, RNA *in situ* hybridisations were repeated at two different time points (E10 and E11), with the consistent result that the 'intermediate' *dlx*5/6 domain reaches further distally than the 'distal' *dlx*3/4 domain

Figure 2.3- 2.6

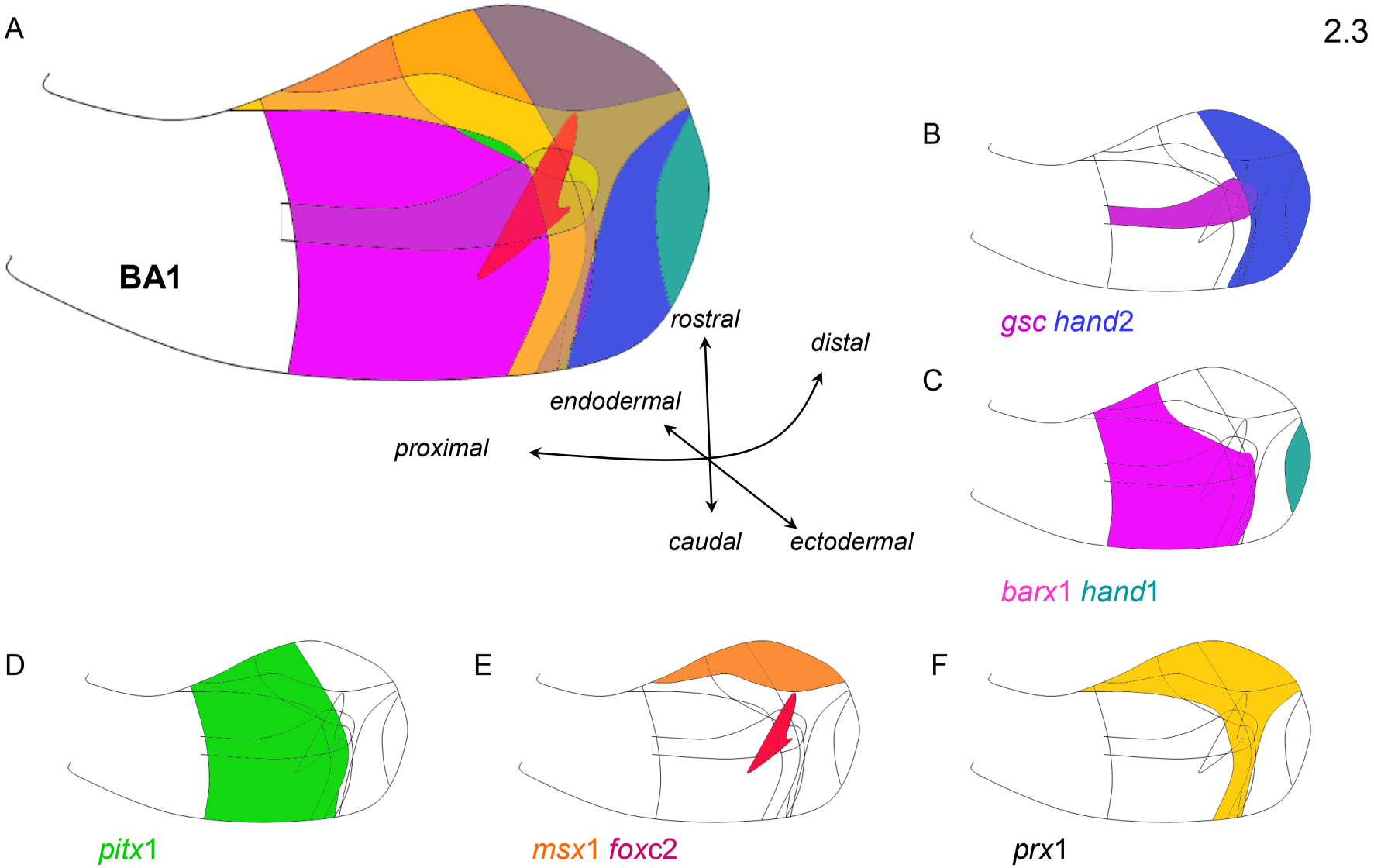
A
BA1
rostral
distal
endodermal
proximal
caudal
ectodermal
B
gsc hand2
C
barx1 hand1
D
pitx1
E
msx1 foxc2
F
prx1

Figure 2.3 Summary of gene expression patterns in the distal part of the first branchial arch

The gene expression domains of a number of proximo-distal markers in the first branchial arch are shown in a schematic side view in overlay (**A**) and also separately to give a clearer impression about the individual domains (**B**- **F**).

The expression domains do not appear to be orientated along a single underlying patterning system.

Some genes follow a proximo-distal expression along the entire breadth of the branchial arch (*hand*1 (**C**), *hand*2 (**B**), *pitx*1 (**D**) and to a certain degree, *barx*1 (**C**) and *prx*1 (**F**)), while others are orientated along an ectodermal-endodermal axis (*msx*1 (**E**), *gsc (***B***)*, partially *prx*1 (**F**)).

*Foxc*2 (**E**) has a central well-defined expression domain that appears to localise to the overlap of a number of other domains without following either a proximo-distal or ectodermal-endodermal orientation.

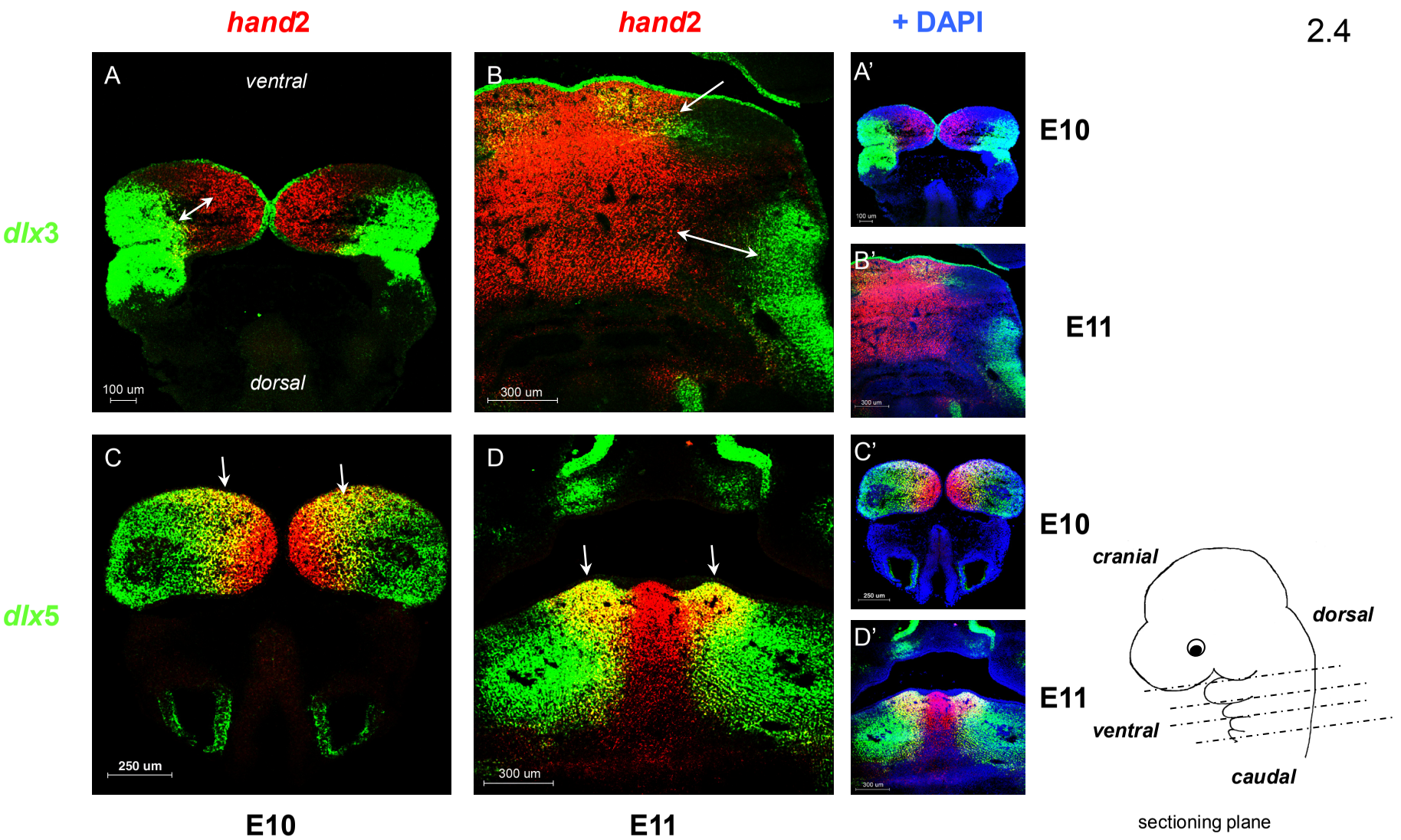
hand2
hand2
+ DAPI
dlx3
dlx5
A
ventral
dorsal
100 um
B
300 um
A'
B'
C
250 um
D
300 um
C'
D'
E10
E11
E10
E11
cranial
dorsal
ventral
caudal
sectioning plane

Figure 2.4 The *hand*2 domain in relation to the domains of *dlx*3 and *dlx*5

Triple fluorescent RNA *in situ* hybridisation for *hand*2 and (**A, B**) a 'distal' *dlx* gene, *dlx*3 or (**C, D**) an 'intermediate' *dlx* gene, *dlx*5 on sections of the first branchial arches of E10 (**A**, **C**) and E11 (**B**, **D**) *Hand*2-Cre +/-; Rosa26Lac -/- mouse embryos. *Hand*2 probes were DIG-labelled and developed with Cy3 tyramide (shown in red), *dlx*3/ 5 probes DNP-labelled and developed with Cy5 tyramide (shown in green), *cre* probes were FITC-labelled and developed with FITC tyramide (not shown). Nuclear counterstain: DAPI. Sections are orientated with ventral to the top and dorsal to the bottom.

A, B The major *dlx*3 and *hand*2 domain do not overlap (double arrows in the gap). At E11.0 (**B**) a small additional *dlx*3 expression domain becomes apparent distally (single arrow).

C, D The *dlx*5 and the *hand*2 domain clearly overlap in the ventral part of the branchial arch (region appearing yellow in **C**, **D**, arrows) and are adjacent or only marginally overlapping in the dorsal part.

A'- D' The nuclear counterstain with DAPI outlines the overall anatomy, sections identical to **A**- **D**.

2.5

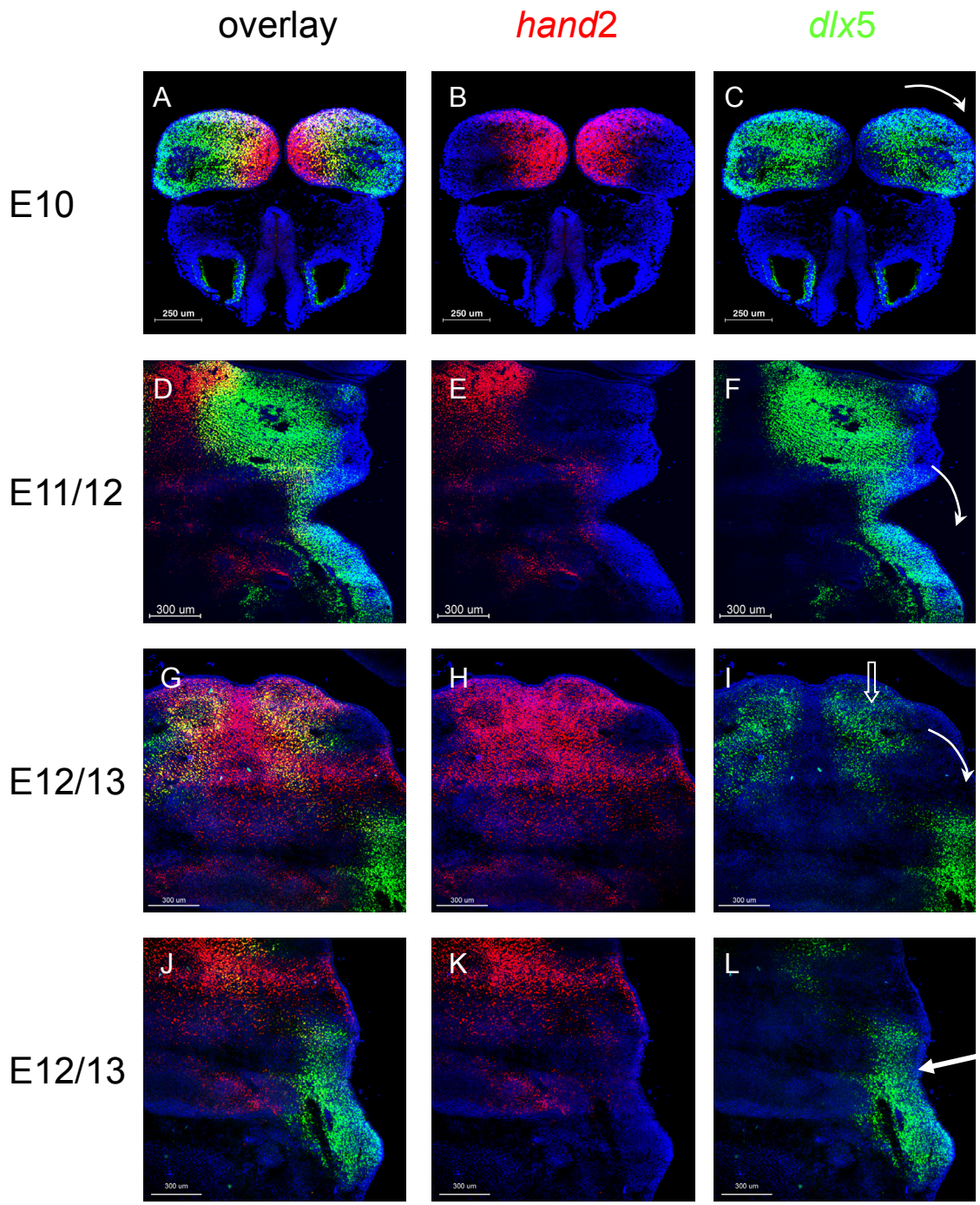
overlay
hand2
dlx5
E10
E11/12
E12/13
E12/13
A
B
C
D
E
F
G
H
I
J
K
L
250 um
300 um

Figure 2.5 Distal-to-proximal rotation of the *dlx*5 expression domain during development

Fluorescent triple RNA *in situ* hybridisations on sections of the first branchial arch of E10 (**A**- **C**), E11/12 (**D**- **F**) and E12/13 (**G**- **L**) embryos for *hand*2 (red) and *dlx*5 (green), nuclear counterstain is DAPI (blue).

Sections were cut in a tilted transverse orientation as indicated to display the arch along its entire proximo-distal length. Images are orientated with ventral to the top and dorsal to the bottom.

Images **G**- **L**: due to the size of the specimen, the distal domain (**G**- **I**) and the proximal domain (**J**- **L**) are shown separately.

The early *dlx*5 domain is distally located (**A, C**) and then moves proximally (E11/12, **D, F**, arrow).

Later in development (E12/13, **G**- **L**), distal *dlx*5 expression becomes weaker and appears associated with the forming incisor (**I**, empty arrow). The main expression domain has moved further proximally (**L**, full arrow).

Similar to the *dlx*5 domain, the *hand*2 domain is initially distally located (**B**) but then expands proximally (**E**, **H**, **K**).

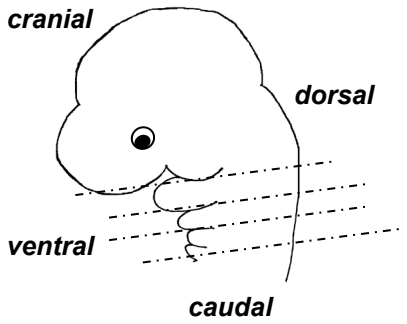

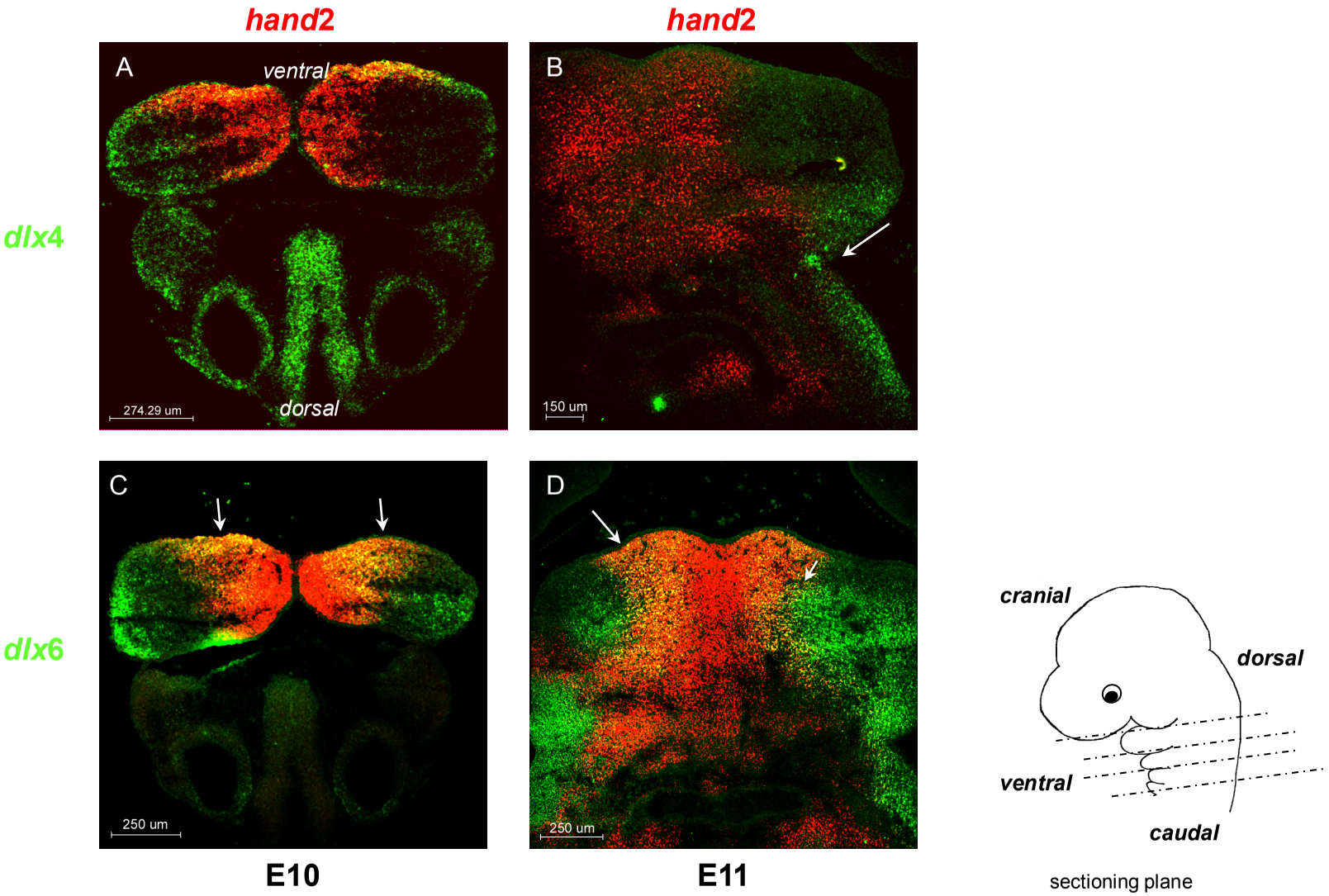
hand2
hand2
A
ventral
dorsal
274.29 um
B
150 um
dlx4
C
250 um
D
250 um
dlx6
E10
E11
cranial
dorsal
ventral
caudal
sectioning plane

Figure 2.6 The *hand*2 domain in relation to the domains of *dlx*4 and *dlx*6

Triple fluorescent RNA *in situ* hybridisation for *hand*2 and (**A, B**) the respective other 'distal' *dlx* gene, *dlx*4, or (**C, D**) other 'intermediate' *dlx* gene, *dlx*6, on sections of the first branchial arches of E10 (**A**, **C**) and E11 (**B**, **D**) *Hand*2-Cre +/-; Rosa26Lac -/- mouse embryos. *Hand*2 probes were DIG-labelled and developed with Cy3 tyramide (shown in red), *dlx*4/ 6 probes DNP-labelled and developed with Cy5 tyramide (shown in green), *cre* probes were FITC-labelled and developed with FITC tyramide (not shown). Nuclear counterstain: DAPI. Sections are orientated with ventral is to the top and dorsal to the bottom.

The expression patterns of *dlx*4 and *dlx*6 confirm that the 'intermediate' *dlx*5/6 expression domains reaches further distally than the domain of the 'distal' *dlx*3/4 group.

A, B *Dlx*4 expression seems restricted to an outer superficially located domain.

C, D *Hand*2 domain and *dlx*6 domain overlap, the overlap appears yellow (arrows).

(Figure 2.4 and 2.5). Interestingly, the *dlx* domains seem to rotate from distal to proximal over time, as illustrated for *dlx*5 in Figure 2.5.

When comparing *hand*2 gene and *cre* expression from the *Hand*2-Cre transgene, it becomes apparent that the domains widely overlap but that transgene expression reaches further proximally and cranially than gene expression (Figure 2.7 and Figure 2.8), most likely indicating the absence of *Hand*2 repressor elements in the 7.4kb upstream region incorporated into the *Hand*2-Cre transgene. In relation to *dlx*3 and *dlx*5 domains (Figure 2.9), the expression domain defined by the *Hand*2-Cre transgene reaches proximally up to the *dlx*3 domain (Figure 2.9 A, B). This is not the case for endogenous *hand*2 expression, where there is a clear gap between the *hand*2 and *dlx*3 domains (Figure 2.4 A, B). At E10, the transgene domain also shows a wider overlap with the *dlx*5 domain than endogenous *hand*2 (compare Figure 2.9 C to Figure 2.4 C). One day later in development, at E11.0, the transgene, similar to *dlx*5, is not expressed in the in midline of the first branchial arch (Figure 2.9D), an area, in which *hand*2 is normally expressed (Figure 2.4D). This reveals the existence of independent regulatory elements for *hand*2 expression in the branchial arch midline that are not present in the *Hand*2-Cre transgene.

Our results for *dlx* expression are inconsistent with the conventional model of nested *dlx* expression along the proximo-distal axis of the branchial arch as we find that the group of *dlx* genes commonly considered as 'intermediate', *dlx*5 and *dlx*6, is expressed further distally than the *dlx* genes of the 'distal' group, *dlx*3 and *dlx*4. A model summarizing our findings is shown in Figure 2.10. According to our alternative view, *dlx* domains still stack in a shell-like fashion but the axis of the 'stack' does no longer correspond to the proximo-distal axis of the branchial arch but is oriented almost perpendicular to it. *Hand*2 as a very distally expressed gene does not reach the outermost (but not distal-most) shells of *dlx*3 and *dlx*4 but overlaps with the *dlx*5, 6 domain. The *Hand*2-Cre transgene reaches further proximally and up to the *dlx*3 domain; both domain boundaries are indicated by dashed lines. Although the expression domains of *hand*2 and cre from the *Hand*2-Cre transgene are not congruent, the *Hand*2-Cre transgene nevertheless constitutes a valuable marker for origin from the distal part of the branchial arches as it marks the domain distal of the *dlx*3 domain.

Figure 2.7- 2.10

E10

2.7

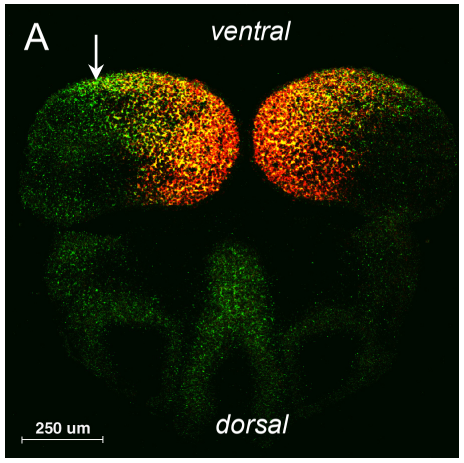

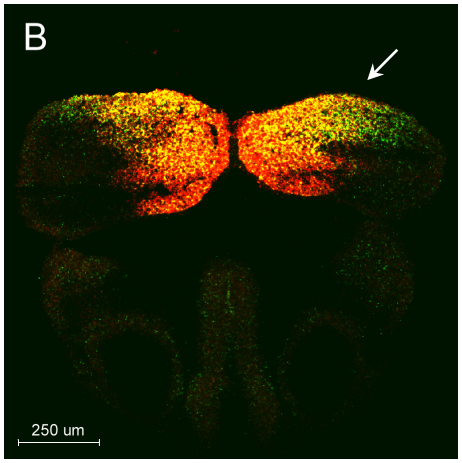

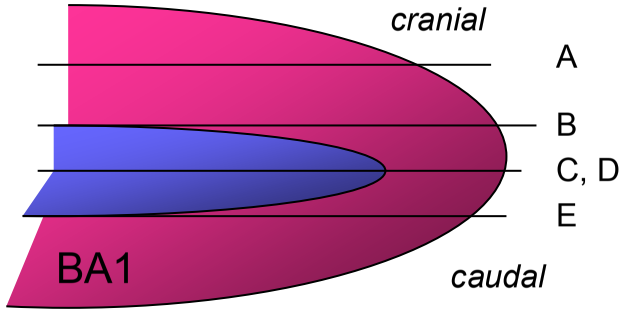

neural crest mesodermal core

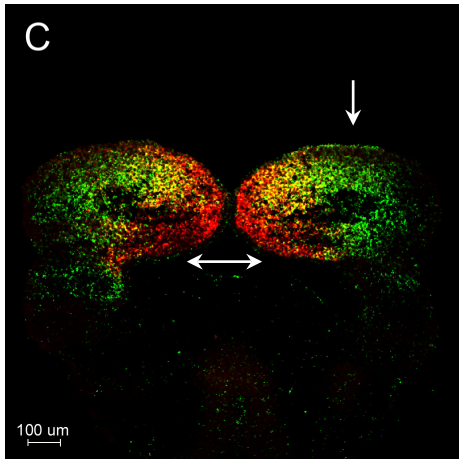

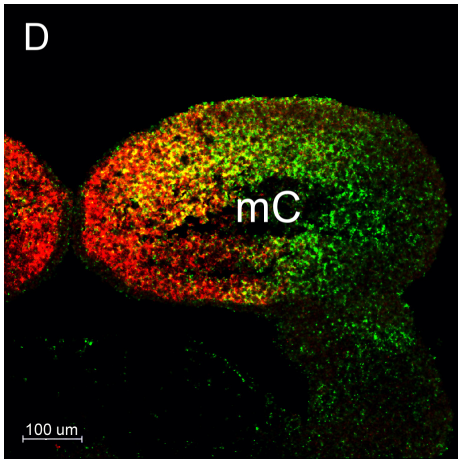

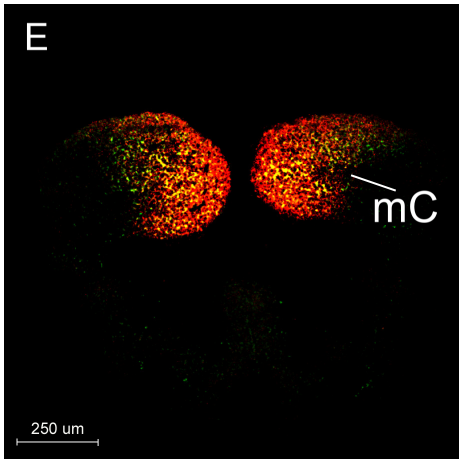

hand2 cre

Figure 2.7 Comparison of *hand*2 and *Hand*2-Cre transgene expression in the first branchial arch at E10

Triple fluorescent *in situ* hybridisation for *hand*2 and *cre* on sections of the first branchial arch of E10 Hand2-Cre+/-; Rosa26LacZ-/- embryos, shown are two channels only. *Hand*2 probes were DIG-labelled and developed with Cy3 tyramide (shown in red), *cre* probes were FITC-labelled and developed with FITC tyramide (shown in green). Sections are orientated with ventral to the top and dorsal to the bottom. The diagram indicates the position of the respective section within the first branchial arch. The mesodermal core (mC) of the branchial arch is labelled in blue.

A, **B** On top (cranial) of the first branchial arch, *Hand*2 and *cre* from the *Hand*2-Cre transgene are both expressed distally. Cre expression is localised more ventrally than endogenous *hand*2 expression and extends further proximally (arrows).

C, **D** In the middle of the branchial arch (**D** is a higher magnification of **C**), recognisable from the unlabelled mesodermal core (mC), transgene expression expands furthest proximally (arrow) but spares the distal-most part (double arrow).

E Transgene but not endogenous *hand*2 expression fades out on the caudal side of the mesodermal core (mC).

In summary, transgene expression is more ventrally localised and expands further proximally than endogenous *hand*2 expression.

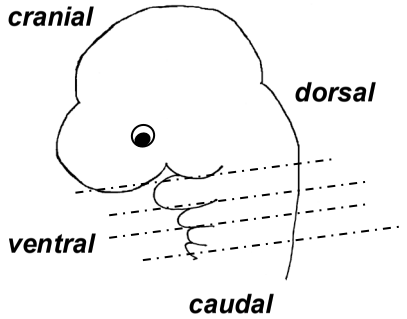

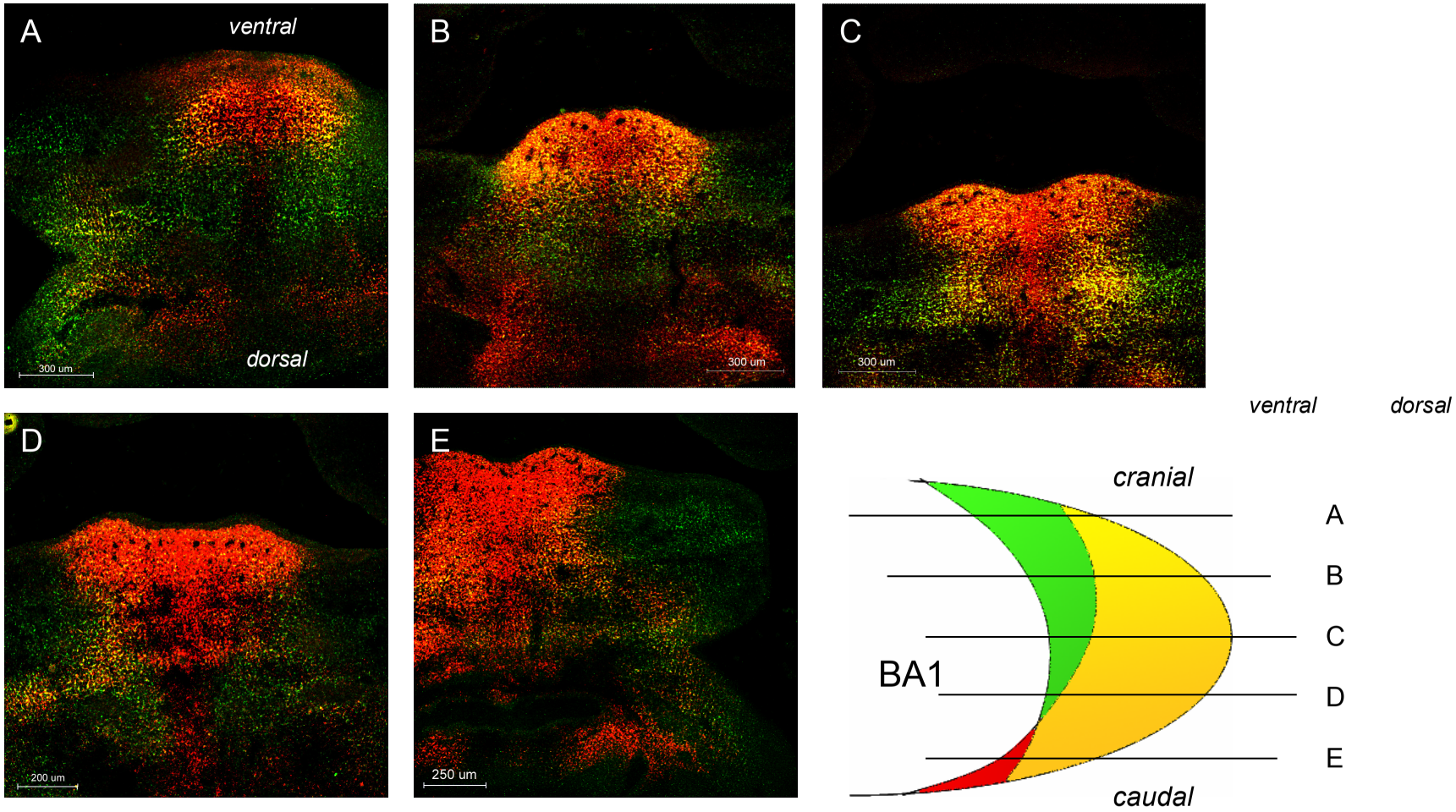
A
ventral
dorsal
300 um
B
300 um
C
300 um
D
200 um
E
250 um
ventral
dorsal
cranial
A
B
C
D
E
BA1
caudal
hand2 cre

Figure 2.8 Detailed comparison of *hand*2 and *Hand*2-Cre transgene expression in the first branchial arch at E11/ 12

Triple fluorescent *in situ* hybridisation for *hand*2 and *cre* on sections of the first branchial arch of E11/ 12 Hand2-Cre+/-; Rosa26LacZ-/- embryos, shown are two channels. *Hand*2 probes were DIG-labelled and developed with Cy3 tyramide (shown in red), *cre* probes were FITC-labelled and developed with FITC tyramide (shown in green). Sections are orientated with ventral to the top and dorsal to the bottom. The diagram indicates the position of the respective section within the first branchial arch and the relationship of the endogenous and transgene expression domain to each other.

*Hand*2 and *cre* from the *Hand*2-Cre transgene are both expressed in the distal part of the first branchial arch but the expression domains are not entirely congruent. On the upper (rostral) side of the arch (**A**), transgene expression reaches further dorsally than endogenous gene expression while the relationship is reversed towards the under (caudal) side of the arch, were *hand*2 expression but not transgene expression is found in the dorsal part of the arch (**E**). In three dimensions, this corresponds to an upwards tilt of the transgene expression in relation to the endogenous gene expression (see diagram).

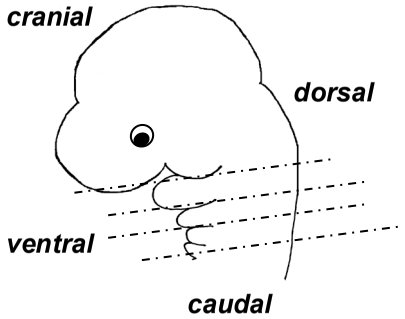

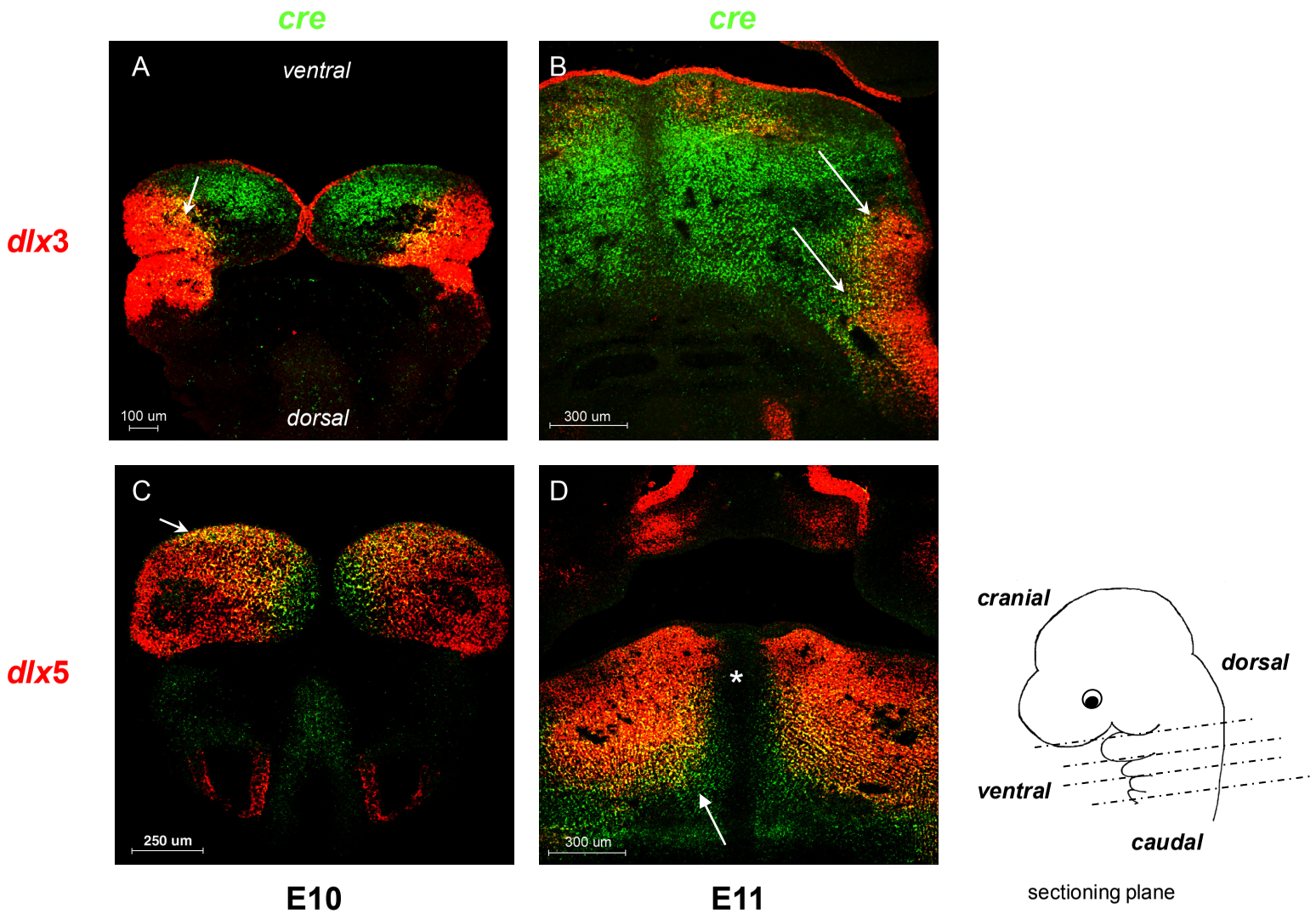
cre
cre
dlx3
dlx5
A
ventral
dorsal
100 um
B
300 um
C
250 um
D
300 um
E10
E11
cranial
dorsal
ventral
caudal
sectioning plane

Figure 2.9 Cre expression from the *Hand*2- Cre transgene in relation to the domains of *dlx*3 and *dlx*5

Triple fluorescent RNA *in situ* hybridisation on sections of the first branchial arches of E10 (A, C) and E11 (B, D) *Hand*2-Cre +/-; Rosa26Lac-/- mouse embryos. *Hand*2 probes were DIG-labelled and developed with Cy3 tyramide (not shown), *dlx*3/ 5 probes DNP-labelled and developed with Cy5 tyramide (shown in red), *cre* probes were FITC-labelled and developed with FITC tyramide (shown in green). Nuclear counterstain: DAPI. The sections are identical to the ones shown in Figure 2.4; however, this time, it is the *Hand*2-Cre transgene expression domain that is compared to the domains of *dlx*3 (**A, B**) and *dlx*5 (**C, D**).

A, B Cre expression from the *Hand*2-Cre transgene and *dlx*3 expression at two different time-points. **A** At E10, the *cre* expression from the *Hand*2-Cre transgene shows a clear overlap with the *dlx*3 domain **B** At E11, the *cre* expression domain reaches the lateral dlx3 expression domain (arrows).

C, D Cre expression from the *Hand*2-Cre transgene and *dlx*5 expression at two different time-points. **C** At E10, the *dlx*5 and the *cre* domain clearly overlap, ventrally more than dorsally (the overlapping region appears yellow). **D** At E11, both *cre* and *dlx*5 are not expressed in the medial part of the branchial arch, in contrast to endogenous *hand*2 domain (asterisk, and Figure 2.4 D). The overlap between *cre* and *dlx*5 is more pronounced dorsally than ventrally (arrow).

For comparison of endogenous *hand*2 expression in relation to the same *dlx*3 and *dlx*5 domains, see Figure 2.4.

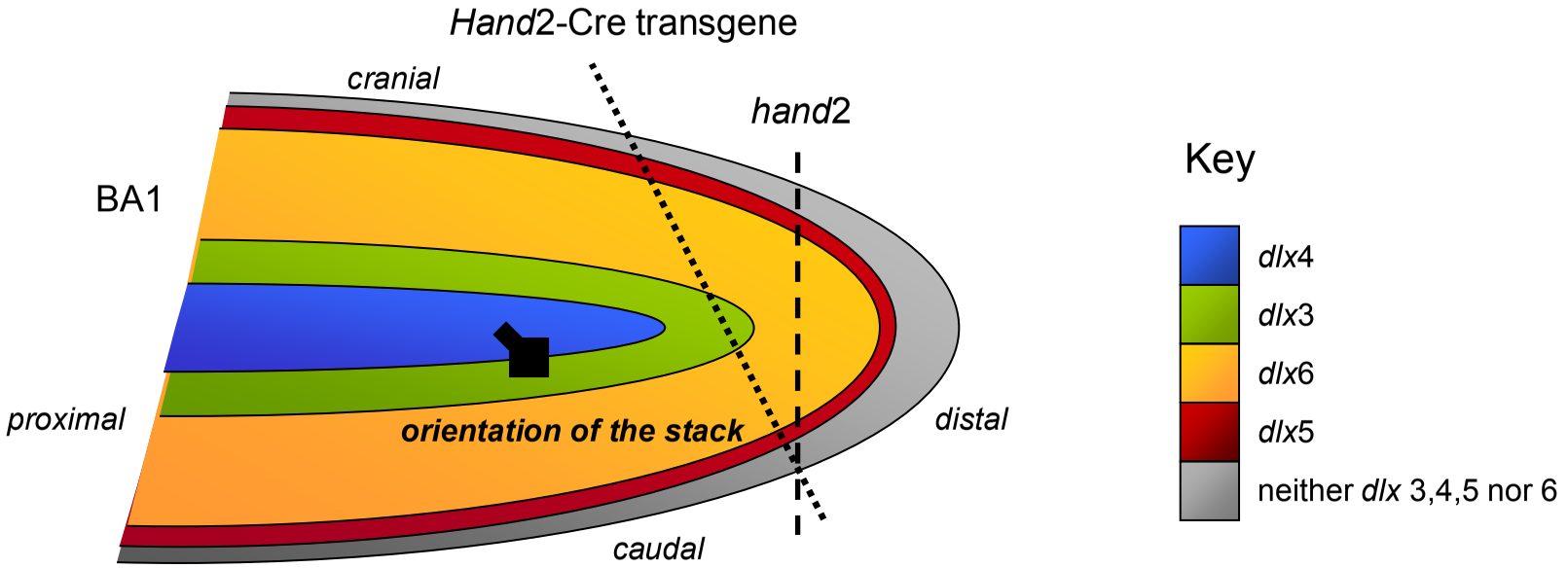

Figure 2.10 Summary of distal *dlx* expression domains in the first branchial arch in relation to endogenous *hand*2 and *Hand*2-Cre transgene expression

Dlx expression domains are arranged in shells with *dlx*4 forming the outer-most and *dlx*5 the inner-most shell among the four *dlx* genes analysed. The axis of the stack deviates from the general proximo-distal axis of the branchial arch, and expression of *dlx* genes of the 'intermediate group', *dlx*5/6, reaches further distally than the one of the 'distal group' *dlx*3/4.

Proximal domain boundaries of endogenous *hand*2 (overlap with *dlx*5 and *dlx*6 but not *dlx*3, dashed line) and *Hand*2-Cre transgene expression (overlap with *dlx*3, *dlx*5, *dlx*6, dotted line) are indicated in relation to the *Dlx* system.

2.10

2.4.3 Development of the *Hand*2 domain and branchial arch outgrowth

A previously published analysis of the *Hand*2-Cre$^{+/-}$; Rosa26LacZR$^{-/-}$ mouse did not make use of the domain defined by the transgene to address the question of branchial arch outgrowth[158]. We therefore performed a detailed analysis of the extent and the precise development of the domain established by the *Hand*2 transgene in skeletal and muscular structures of the head.

2.4.3.1 The extension of the *Hand*2 domain during development

Whole mount X-Gal stainings for ß-Galactosidase activity of *Hand*2-Cre$^{+/-}$; Rosa26LacZR$^{-/-}$ embryos of different developmental stages allow a first appreciation of the expansion of the *Hand*2 domain. At E9.0 and E10.0, the *Hand*2 domain is clearly defined (Figure 2.11) and limited to the distal aspect of the branchial arches, this aspect remains unchanged until stage E12.0 (date not shown). By E14.0, the extent of the *Hand*2 domain has suddenly expanded and resembles the final state (Figure 2.12, compare E14.0 and P0), encompassing the entire lower jaw and reaching up to the outer ear.

To address the apparent discrepancy between an early distinctly distal and an extended later expression domain, E13.0, E14.0 and E16.0 specimen were sectioned and ß-Galactosidase activity assessed by X-Gal staining (Figure 2.13). At E13.0, the *Hand*2 domain has assumed a pyramid shape, with the top of the pyramid at the midst of the outer ear (A) and an expanding base further caudally (B, C). The boundary between the labelled *Hand*2 domain and adjacent unlabelled tissue is distinct, horizontally orientated and corresponds to the boundary between upper and lower jaw (C). A day later, labelled structures of the lower jaw such as Meckel's cartilage and the ossifying dentary bone can be identified (D), while no labelling is detected in the upper jaw (D, E). On the outside of the forming lower jaw, separate labelled strands of connective tissue (D, arrows) indicates the beginning organisation of the outer masticatory musculature. At E16.0, the outline of the dentary bone already strongly resembles the final structure (Figure 2.13 F, G) and now reaches far dorsally and cranially, into the surrounding

Figure 2.11- 2.13

2.11

E9.0

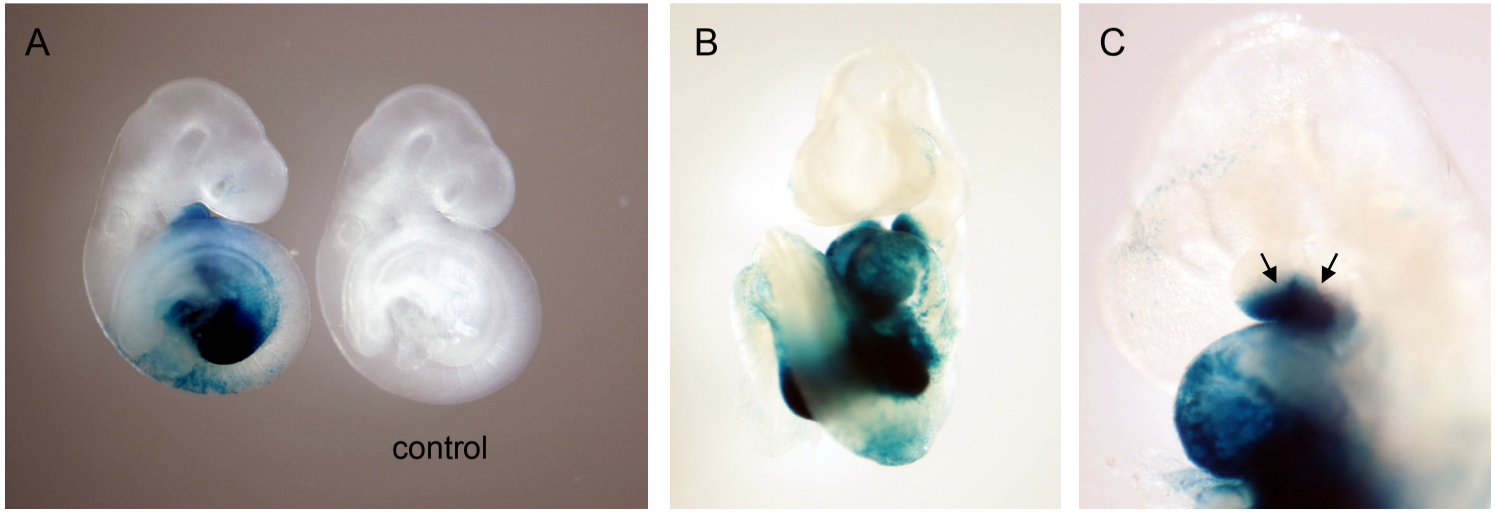
A
control
B
C

E10.0

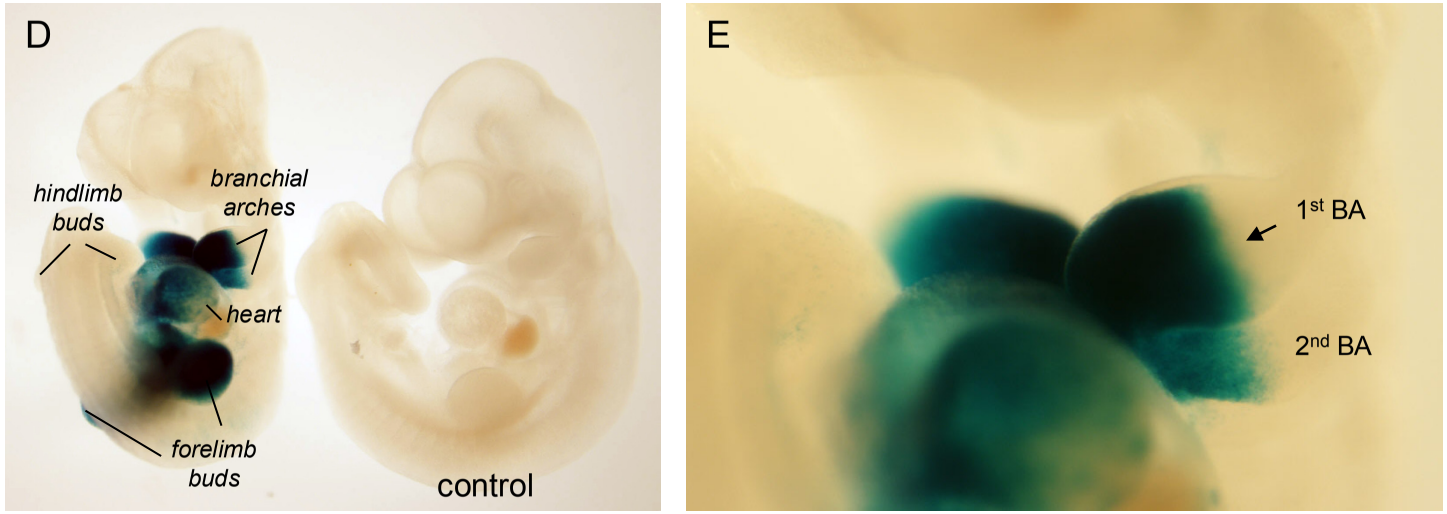
D
hindlimb buds
branchial arches
heart
forelimb buds
control
E
1st BA
2nd BA

Figure 2.11 The *Hand*2-Cre transgene labels a distal branchial arch domain

*Hand*2-Cre+/-; Rosa26LacZR-/- embryos after whole mount X-Gal staining for ß-Galactosidase activity. E9.0 (**A**- **C**) and E10.0 (**D**- **E**) embryos with transgenic and wild-type littermates (**A**, **D**).

At an early time point in development (E9.0 and E10.0), the Hand2-Cre transgene labels a well-defined distal branchial arch domain in the first and second branchial arch (**C**, **E**).

B and **C** show the frontal and lateral aspect of the domain labelled by the transgene at E9.0.

E14.0

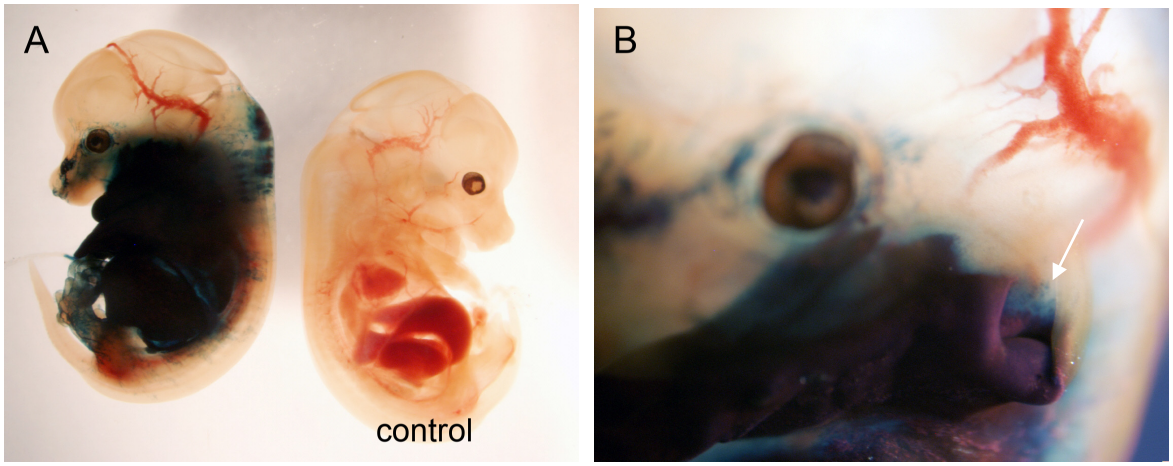

P0

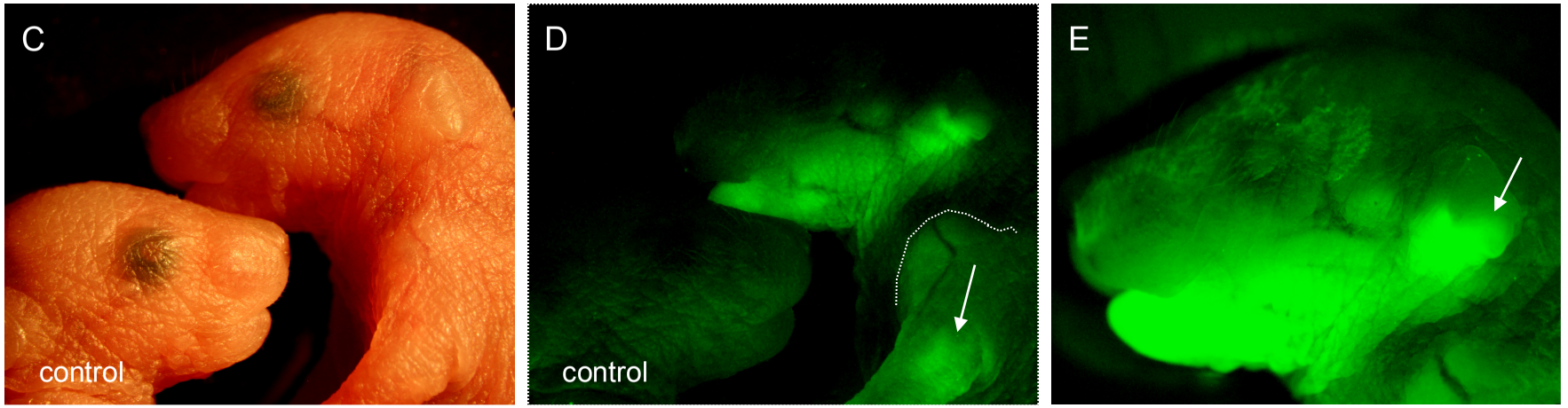

Figure 2.12 The *Hand*2-Cre transgene domain at later stages of development

A, B: E14.0 *Hand*2-Cre+/-; Rosa26LacZR-/- embryos and control littermates after whole mount X-Gal staining for ß-Galactosidase activity. The domain labelled by the transgene stretches back far dorsally and reaches till the outer ear (arrows in **B, E**).

C-E: P0 *Hand*2-Cre+/-; Rosa26EYFP-/- pups and control littermates. Transgenic pups show EYFP expression in the lower jaw and the upper limb (arrow and dotted line in **D**).

E13.0- transverse

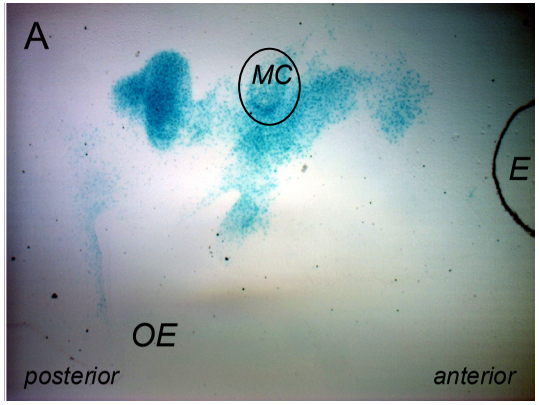

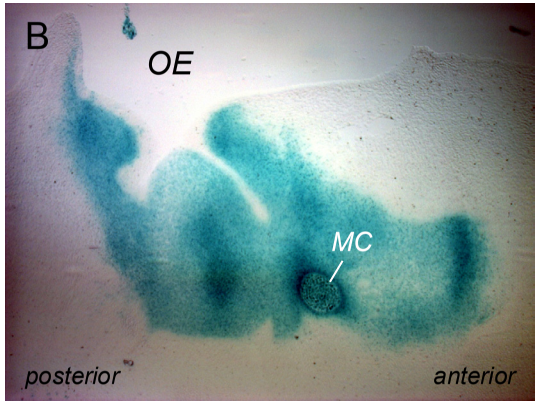

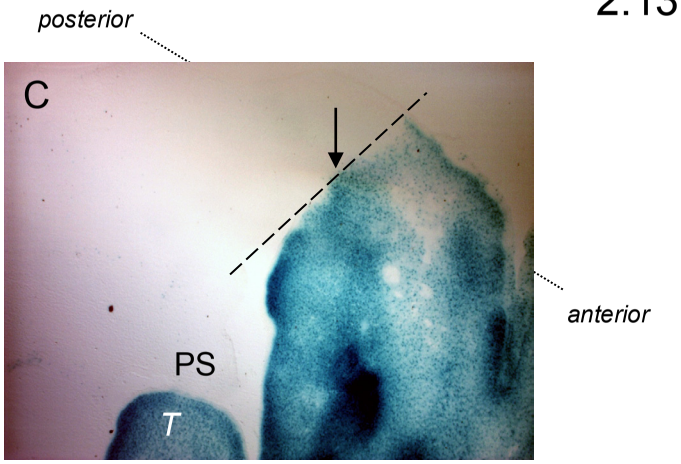

E14.0- frontal

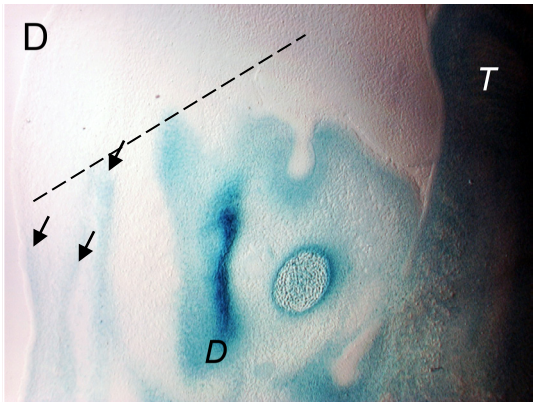

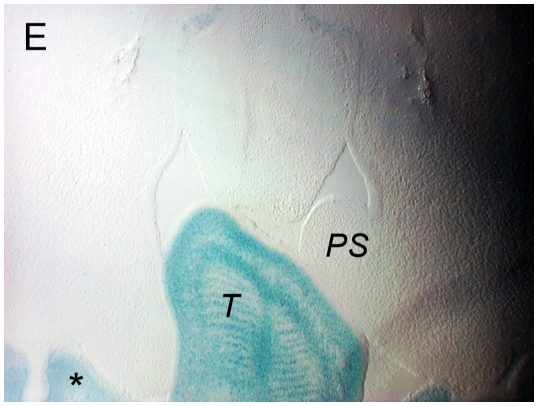

E16.0- frontal

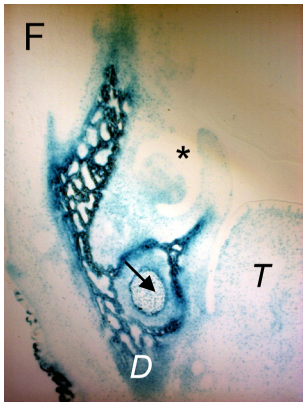

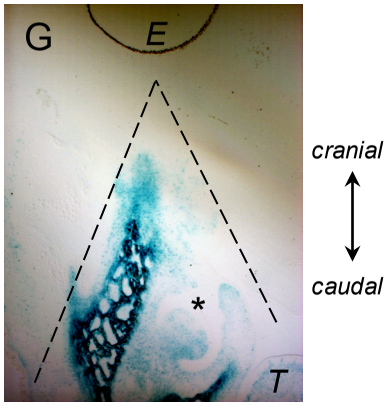

Figure 2.13 The *Hand*2 domain between E13.0- E16.0

X-Gal staining of sections of E13.0 (**A- C**), E14.0 (**D, E**) and E16.0 (**F, G**) *Hand*2-Cre+/-; Rosa26LacZR-/- embryos. The sectioning plane is transverse for E13.0 (**A- C**) and frontal for E14.0 and E16.0 (**D- G**) embryos. The orientation of the image is indicated.

A- **C** show a cranial to caudal series of the *Hand*2 domain at E13.0. **A** shows the cranial most extension of the domain, with faint labelling in the bay of the outer ear. **B** Further caudal, the Hand2 domain including Meckel's cartilage (MC) is sharply defined and passes through the auricular hillocks. **C** At the level of the oral cavity, the ventral *Hand*2 domain of the future lower jaw is clearly separated from the upper jaw (arrow). Strong labelling is also present in the tongue (T).

D- **E** At E14.0, the final architecture of the lower jaw becomes recognisable. **D** The ossification of the dentary bone on the lateral side of Meckel's cartilage is underway and streaks of labelled connective tissue (arrows) indicate a beginning of muscular organisation. **E** More medially, the labelled lower jaw (asterisk) and the labelled connective tissue of the tongue contrast sharply with the unlabelled upper jaw (PS, palatal shelf of the upper jaw).

F At E16.0, the dentary bone is outlined in its final shape and encases Meckel's cartilage (arrow). **G** The ectodermal invagination of a tooth bud (asterisk) shows no staining. The outline of the *Hand*2 domain is indicated by dashed lines.

Over time, the orientation of the *Hand*2 domain boundary at the upper/ lower jaw junction changes from horizontally (dashed lines in **C**, **D**) towards a pyramid- form (dashed line in **G**).

D dentary, ***E*** eye, ***MC*** Meckel's cartilage, ***OE*** outer ear, ***PS*** palatal shelf, ***T*** tongue

negative mesenchyme. The boundary of the domain stands no longer horizontally but is tilted towards the vertical, with an inner labelled domain reaching under the outer unlabelled domain.

2.4.3.2 The projection of the *Hand*2 domain onto the skeletal elements of the first and second branchial arch

Branchial arches form as metameric building blocks for the face and neck along the anterior- posterior axis of the embryo and each arch provides a set of elements (skeletal, muscular, nerve and blood vessel), among them transient embryonic cartilages that do not persist into adulthood. As the *Hand*2 domain appears pyramid- shaped on sections of E13 embryos (Figure 2.13), we went on to define the 'tip' of the pyramid for the first and second branchial arch as the most proximal extension of the *Hand*2 domain. Meckel's cartilage is the cartilaginous element associated with the first branchial arch and forms as a long rod (visible within the *Hand*2 domain in Figure 2.13). Later a dermal bone, the dentary, will form on the outside of the distal part of Meckel's cartilage and finally enclose it, meanwhile the upper part of the cartilaginous rod of Meckel's cartilage segregates from the rest to give rise to the malleus. Reichert's cartilage is the equivalent cartilaginous element of the second branchial arch and gives rise to the last element of the middle ear, the stapes, as well as the styloid and parts of the hyoid bone (in a proximal to distal order). Connections between the elements degenerate or can remain as ligamentous structures. We analysed the projection of the *Hand*2 domain boundary onto these transient embryonic cartilaginous elements at E13.0 and onto their respective derivatives at P0 to define the precise proximal extent of the *Hand*2 domain.

At E13.0, the *Hand*2 transgene domain is homogenously labelled (Figure 2.14 A- O) and its tip projects onto Meckel's cartilage (B), just above the segregation point between the future malleus and the remnant of Meckel's cartilage (M, N, O, arrows). Meckel's cartilage has been previously reported to contain a mix of cells labelled by the *Hand*2-Cre transgene and unlabeled cells[158]. We could confirm this only for the cartilage in newborns (P) as earlier stages show homogenous labelling.

Figure 2.14- 2.15

2.14

E13.0

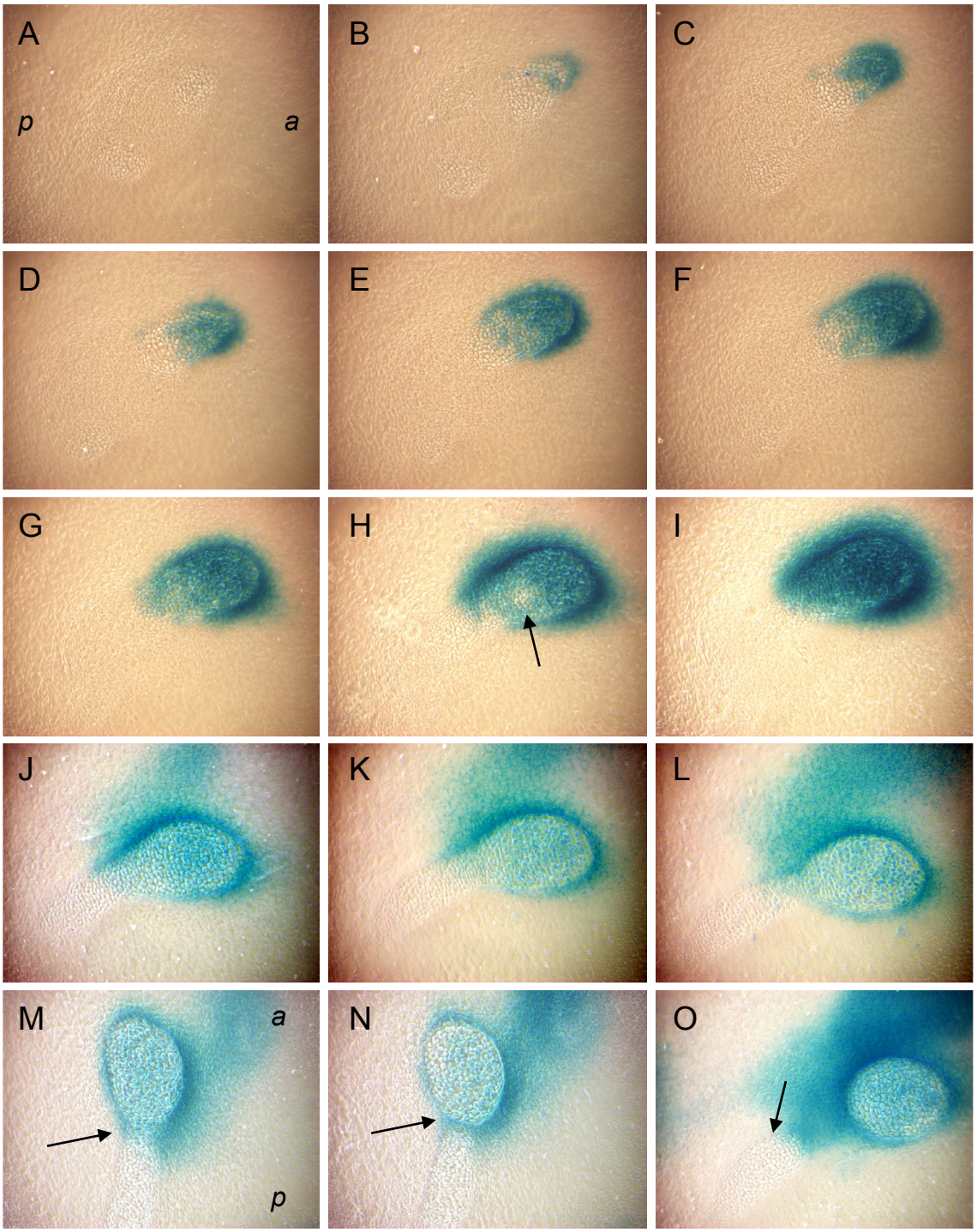
A
p
a
B
C
D
E
F
G
H
I
J
K
L
M
a
p
N
O

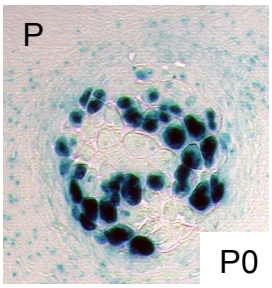
P
P0

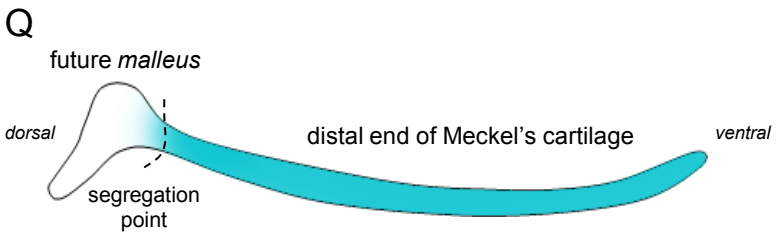
Q
future malleus
dorsal
distal end of Meckel's cartilage
ventral
segregation point

2.14

Figure 2.14 Projection of the *Hand*2 domain onto Meckel's cartilage

X-Gal staining on transverse (**A**- **O**, E13) and frontal (**P**, P0) sections of the head of *Hand*2-Cre+/-;Rosa26LacZR-/- embryos.10x magnification.

A- O Meckel's cartilage in a series from cranial to caudal.

P Meckel's cartilage in the distal part of the cartilage, located within the dentary bone of a newborn (P0), (detail image).

Orientation of slides: **A- O**: All but **M, N**: Anterior to the right, posterior to the left as indicated in **A**.

M,N: anterior to the top, posterior to the bottom as indicated in **M**.

P: frontal section with cranial to the top and caudal to the bottom.

Q: summary: projection of the *Hand*2 domain on to Meckel's cartilage

The upper and dorsal end of Meckel's cartilage does not originate from the *Hand*2 domain (**A**, **Q**).

The boundary between the labelled and unlabelled domain is relatively sharp (**B**- **O**, but also see arrow in **H**) and corresponds to the segregation point between the future malleus and the cartilaginous rod for the lower jaw (arrows in **M, N**). Only few labelled cells stay behind in the future malleus (arrow in **O**).

P While the labelling in Meckel's cartilage at E13.0 seems rather homogenous (**A- O**), Meckel's cartilage contains domains of labelled and unlabelled cells in a newborn mouse.

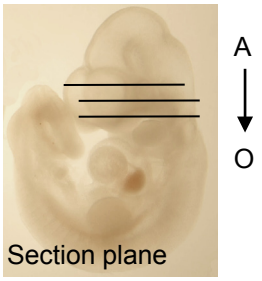

2.15

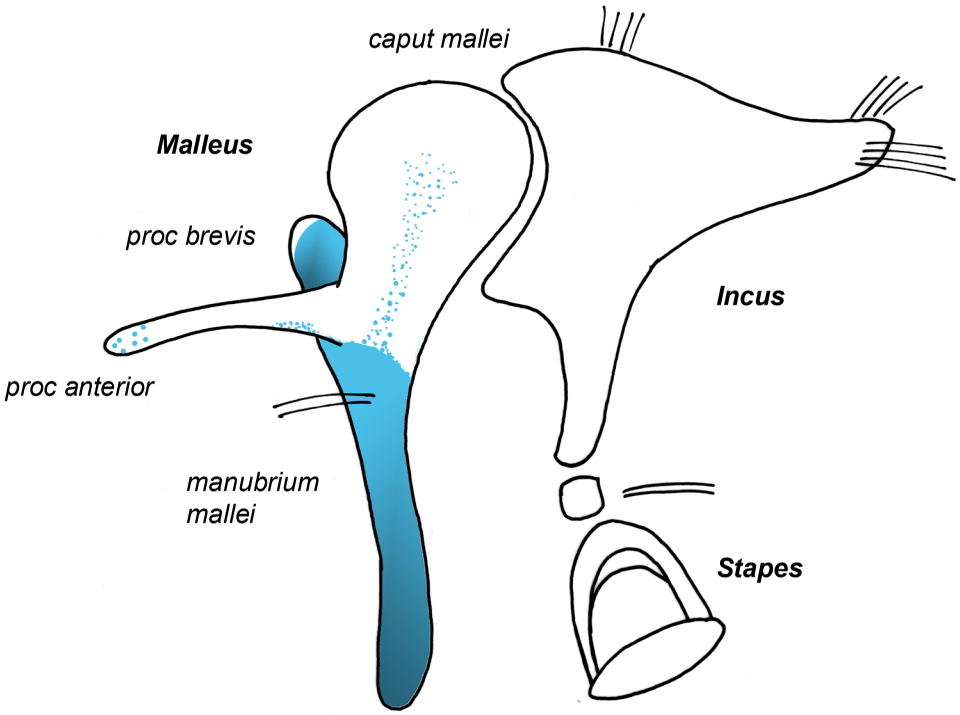

view onto the middle ear from medially and above

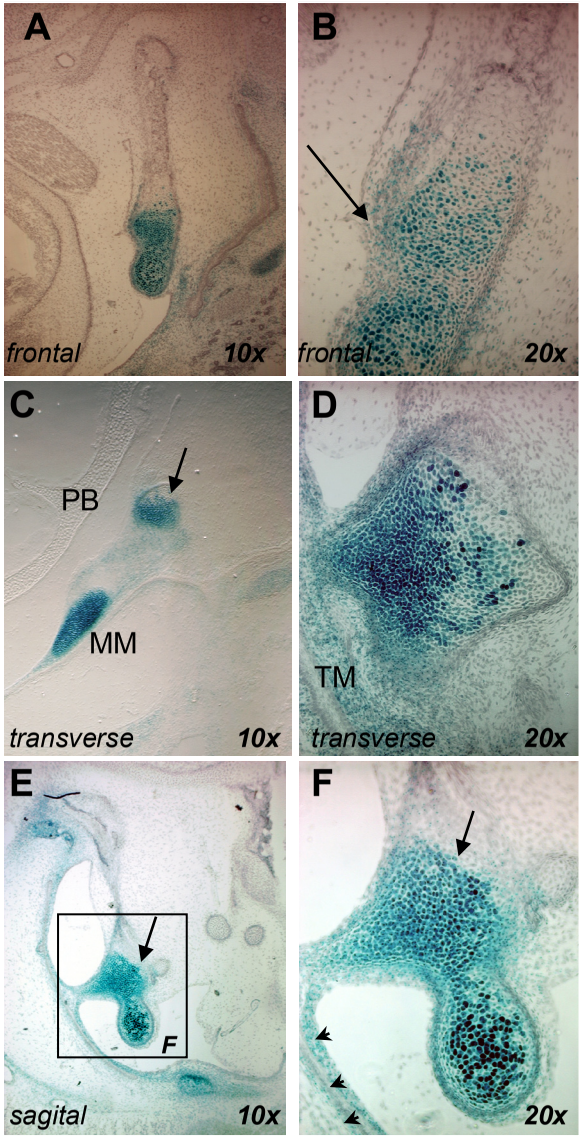

Figure 2.15 A sharp *Hand*2 domain boundary within the malleus

X-Gal staining of sections of the middle ear region of P0 *Hand*2-Cre+/-; Rosa26LacZR-/- mice. The orientation of the section plane is given.

A, B Frontal section through the malleus in different magnifications. The domain boundary appears relatively sharp. The connective tissue of the insertion of the M. tensor tympani contains labelled cells (B, arrow). Orientation of the image: cranial to the top, medial to the left.

C, D On transverse sections it becomes apparent that the labelling does not encompass the entire thickness of the malleus. The manubrium of the malleus is entirely labelled (**C**). The processus brevis is mainly labelled but contains a cap of unlabelled cells (**C**, arrow). A section through the body of the malleus shows that only the side facing the tympanic membrane is labelled (also see **E, F**). Orientation of the images: posterior to the top, medial to the left.

E, F Sagital sections confirm the sharp boundary in the body of the malleus (arrows), with the labelled domain facing the tympanic membrane. The three-layered tympanic membrane shows labelling in the outer and inner but not the middle layer (arrowheads). Orientation of the images: cranial to the top, anterior to the left.

PB processus brevis, ***TM*** tympanic membrane, ***MM*** manubrium mallei

To determine the overall projection of the *Hand*2 domain onto the fully formed middle ear space, we analysed middle ears at a later developmental stage (P0, Figure 2.15 and 16). The mammalian middle ear contains three ossicles (malleus, incus and stapes) linking the tympanic membrane held by the tympanic bone to the oval window, the entrance to the inner ear. The tympanic bone, tympanic membrane, malleus and incus are derivatives of the first branchial arch, while the stapes is a second arch derivative. The boundary of the *Hand*2 domain runs through the first element of the middle ear, the malleus, and is sharply defined. The frontier lies within the lower end of the body of the ossicle, with an entirely labelled manubrium mallei (Figure 2.16 E) and a mainly labelled proc brevis (the proc brevis shows a cap of unlabeled cells, Figure 2.15 C, arrow). The main part of the body of the malleus, as well as incus and stapes, are unlabelled (Figure 2.16 A, B, D). It is also worth noting the labelling on the anterior side of the malleus in the anchoring ligaments (Figure 2.16 D) and the positive connective tissue of the M. tensor tympani at its insertion site (Figure 2.15 A, B).
The manubrium of the malleus is embedded in the tympanic membrane which consists of three layers: The outer and inner layer of the membrane are labelled by the *Hand*2 transgene, while the middle, ectoderm-derived layer, is not (Figure 2.15 F, three arrowheads). The tympanic membrane is held by the ring-shaped tympanic bone; located cranially and laterally to the latter can be found a small dermal bone, the goniale. While the tympanic bone shows labelling throughout, only single labelled cells are incorporated into the goniale (Figure 2.16 C).
The second arch-derived ossicle of the middle ear, the stapes, is considered the proximal end of Reichert's cartilage. Stapes, styloid and the minor horn of the hyoid were easily identifiable in the *Hand*2-Cre mouse while their common embryonic precursor, Reichert's cartilage, could never be identified as a continuous cartilaginous structure similar to Meckel's cartilage.
As mentioned above, no signal was detectable in the stapes but a few labelled cells were found within the styloid process (Figure 2.17). The positive cells within the styloid process could not be localised with certainty to a specific continuous area (compare Figure 2.17 B and C). In the surrounding connective tissue, a labelled band, the stylo-hyoidal ligament, could be traced from the medial and posterior site of the process to the hyoid (Figure 2.17 B, C).
At E13.0, the hyoid itself was continuous with a broad *Hand*2 domain (Figure 2.18), representing the main dorsal domain boundary; only separate bands of connective tissue

Figure 2.16- 2.18

2.16

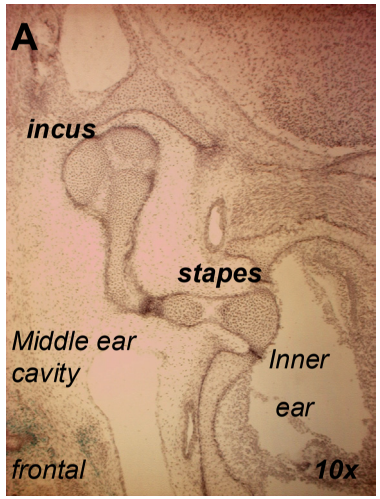

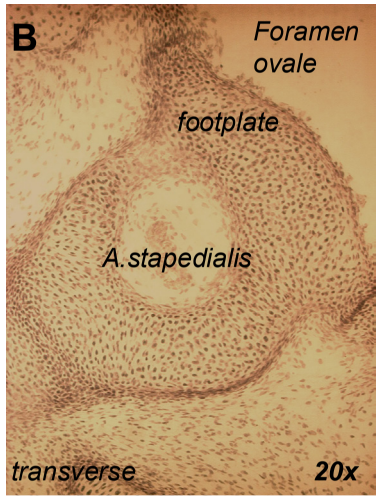

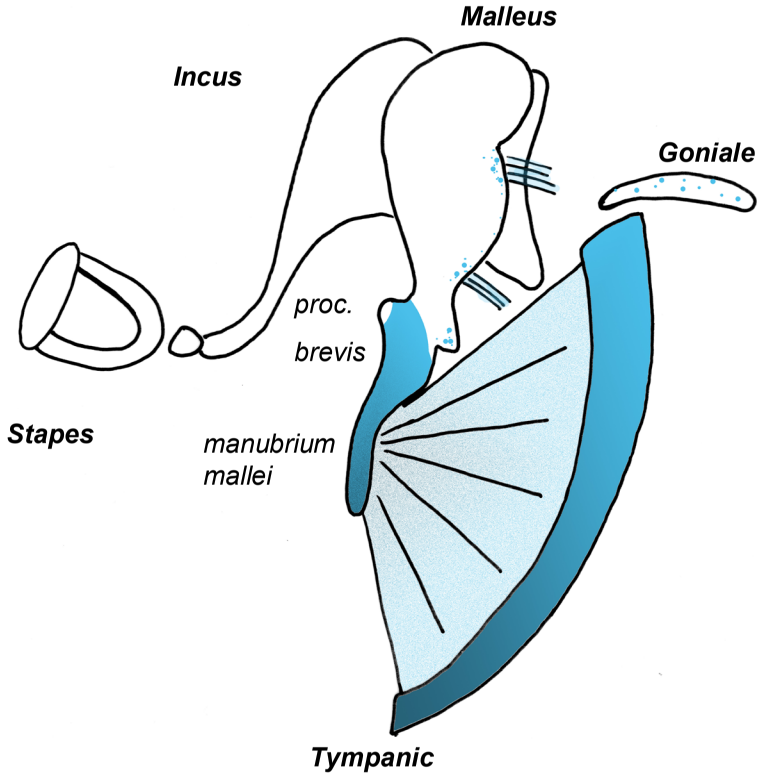

frontal view of a left middle ear

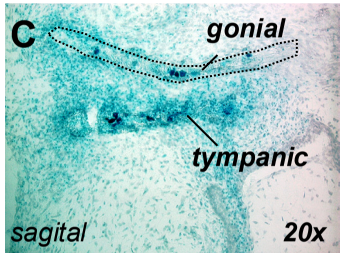

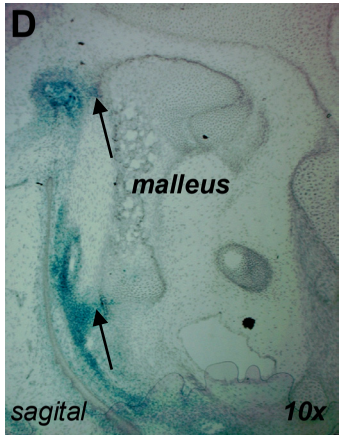

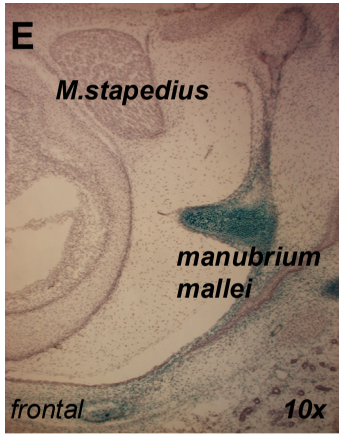

Figure 2.16 Overall projection of the *Hand*2 domain boundary onto the middle ear

X-Gal staining of sections of the middle ear region of P0 *Hand*2-Cre+/-; Rosa26LacZR-/- mice. The orientation of the section plane is given.

A, B Incus (**A**) and stapes (**A, B**) are not labelled by the *Hand*2-Cre transgene.

C, D The tympanic bone is fully labelled, while the overriding goniale (outlined) only contains single positive cells.

D On a sagital section, the anterior ligaments anchoring the malleus to the walls of the middle ear cavity are labelled by the *Hand*2-Cre transgene (arrows).

E The connective tissue of the M. stapedius is unlabelled. Also on this section: the labelled manubrium mallei.

Orientation of the images: **A** cranial top, medial right. **B** anterior bottom, medial right. **C**, **D** cranial top, anterior left. **E** cranial top, medial left.

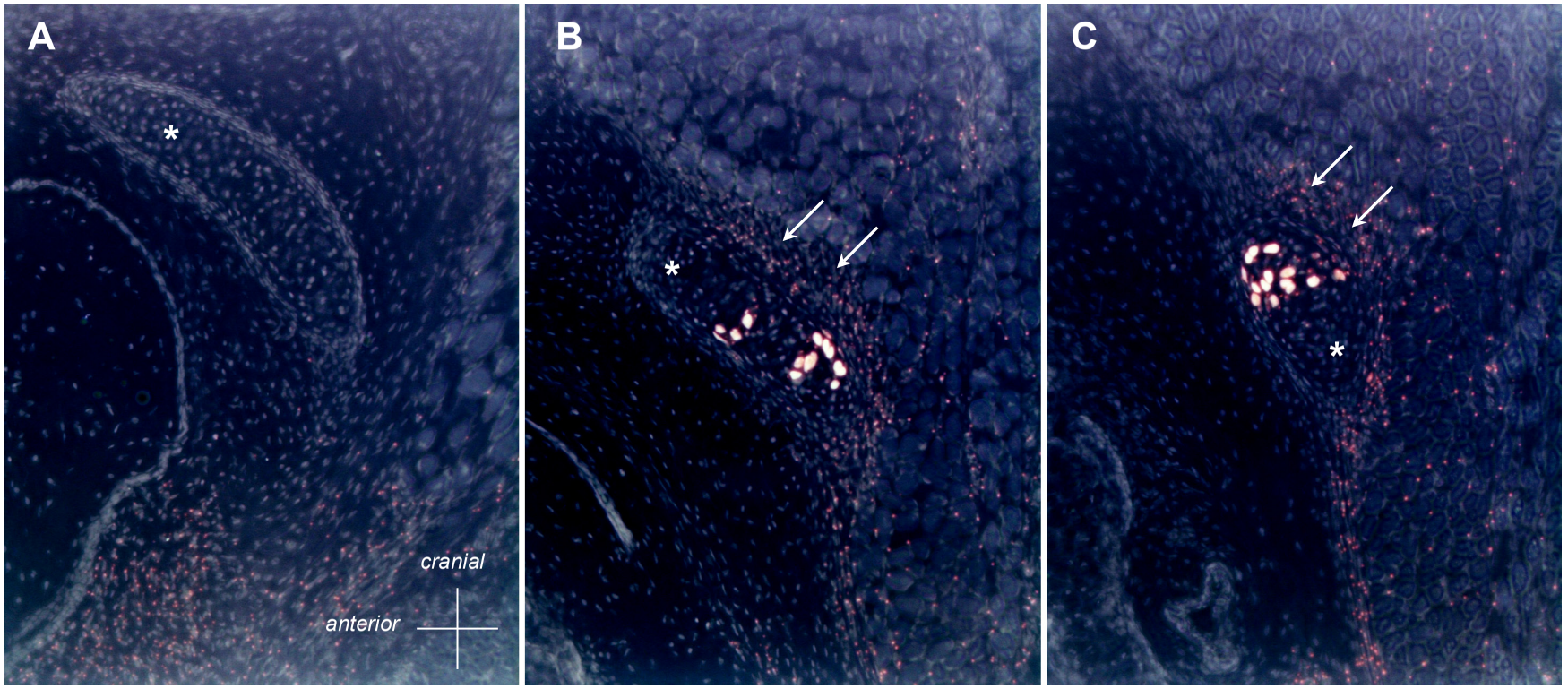

A to C: lateral to medial

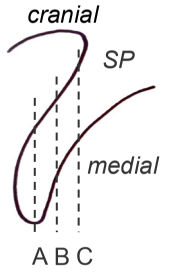

Figure 2.17 The *Hand*2-Cre domain reaches the styloid process

X-Gal staining of sagital sections of the cranial base of P0 *Hand*2-Cre+/-; Rosa26LacZR-/- mice. Cranial is to the top and anterior to the left of the image, magnification: 10x. Images are shown in inverted colours for enhanced contrast.

A-C: Series from lateral (A) to medial (C) sections as annotated in the frontal schematic representation of the styloid process (SP).

A On the most lateral level, no labelling can be found close nor within the styloid process (*).

B+ C Closer to the base, single strongly labelled cells can be found within the styloid process and on its posterior but not anterior face. Labelled cells within the process appear as groups which suggests clonal origin.

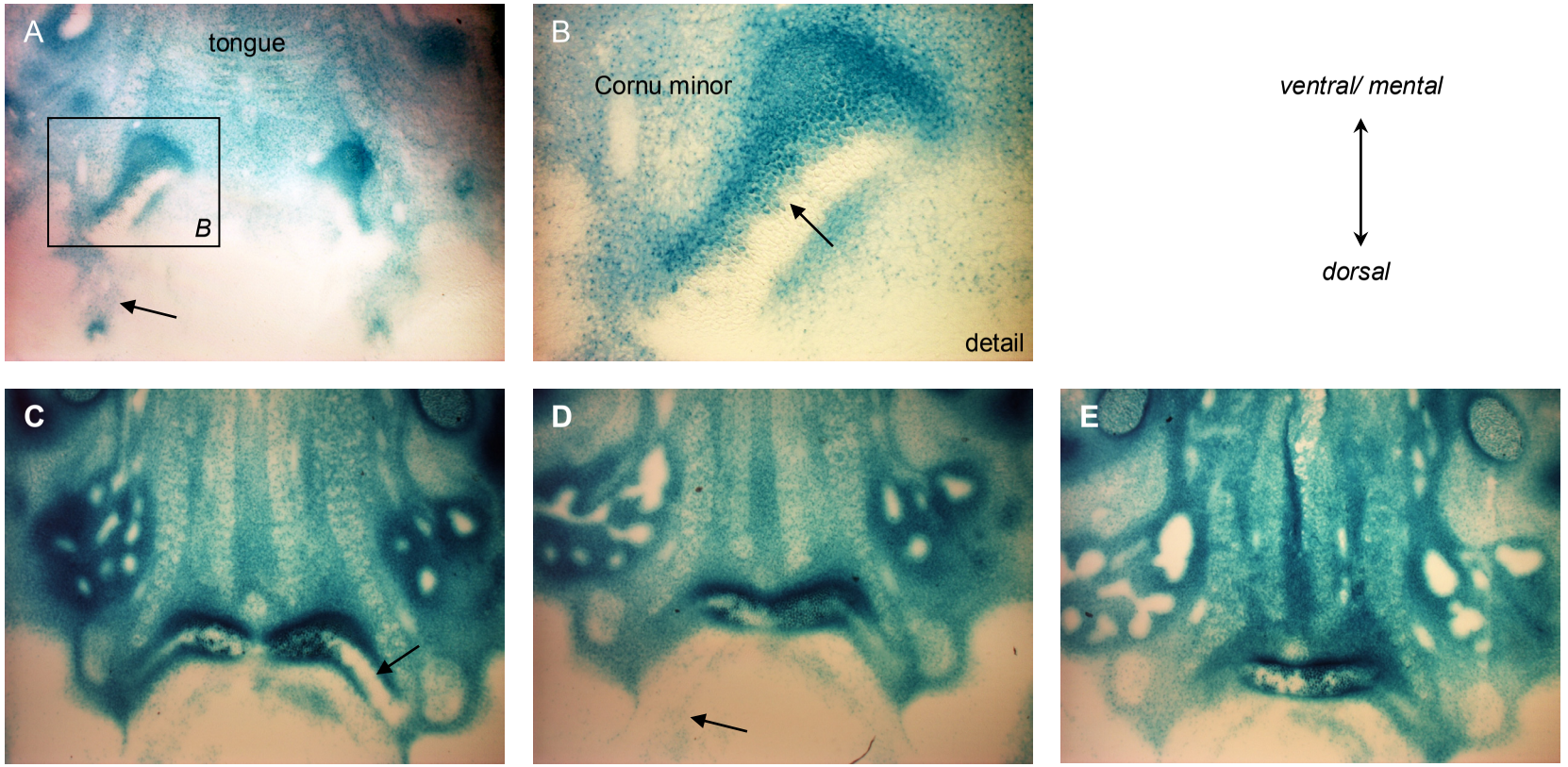
A
tongue
B
B
Cornu minor
detail
ventral/ mental
dorsal
C
D
E

Figure 2.18 Labelling in the hyoid of the *Hand*2-Cre mouse

X-Gal staining of transverse sections through the hyoid region of *Hand*2-Cre+/-;Rosa26LacZR-/- E14.0 embryos. Ventral (mental) is to the top, dorsal to the bottom of the image. Sections are shown from cranial to caudal from (**A**- **E**). **B** is a detail of **A** as indicated in the box.

A, **B** The boundary between labelled and unlabelled cells in the hyoid is distinct and for the upper part runs through the base of the cornu minor.

C On further caudal sections, only the outside of the cartilaginous hyoid appears labelled (arrow).

The boundary between the entire domain labelled by the *Hand*2-Cre transgene and the unlabelled domain mainly correponds to the dorsal side of theby the hyoid (**D,** also others). Dorsal to the hyoid, transgene labelling is limited to a few connective tissue tracks (arrows in **A**, **D**).

The tongue is always strongly labelled by the *Hand*2-Cre transgene (**A**- **E**).

point further dorsally (arrow in D). Labelling in the hyoid appears to be restricted to the outside of the element (C, arrow), with the exception of the entirely labelled cornu minor (A, B) that is separated by a distinct domain boundary (arrow). At birth (P0), the labelled domains of the hyoid lack the previous continuity (Figure 2.19). A few positive cells can be found in the ossified central part of the basihyoid (Figure 2.19 A, B). In the more lateral cartilaginous parts, labelling is restricted to the ventral (anterior) side of the hyoid (C- L), in addition to occasional small groups of labelled cells within the cartilage more dorsally (e.g. J). In the minor horn of the hyoid, transgene labelling becomes restricted to the outer layers of the cartilage (G, H, I, K), similar to the situation already observed at E13.0 (Figure 2.18). The major horn is unlabelled with the exception of a small group of cells at the ventral (anterior) tip (L). Figure 2.20 schematically summarizes the extent of the *Hand*2-Cre transgene labelling in the skeletal head and neck structures.

2.4.3.3 The extent of the *Hand*2 domain in the muscle connective tissue of head and neck

The labelling in the cranial muscle connective tissue *Hand*2-Cre mouse has been reported as spurious[158] but never been fully investigated. To appreciate the full extent of the *Hand*2 domain including the connective tissue of muscles of head and neck, we undertook a comprehensive study of the distribution of labelled muscle connective tissue in the *Hand*2-Cre mouse.

To evaluate the three-dimensional character of the domain, *Hand*2-$Cre^{+/-}$; Rosa26LacZ$R^{-/-}$ specimens were embedded in frontal, sagital and transverse orientation, sectioned and at least every 3rd slide subjected to X-Gal staining. The labelling within the muscle connective tissue of this mouse can only been seen clearly under higher magnification (40X and higher) but an image taken at this magnification lacks the anatomical overview necessary for later correct localisation. Thus, every section was photographed in low magnification and the extent of labelling annotated as seen in higher magnification. Figures 2.21 -2.23 show examples of sections in intermediate magnification with annotation of the extent of the labelled domain. Final representations

Figure 2.19- 2.23

2.19

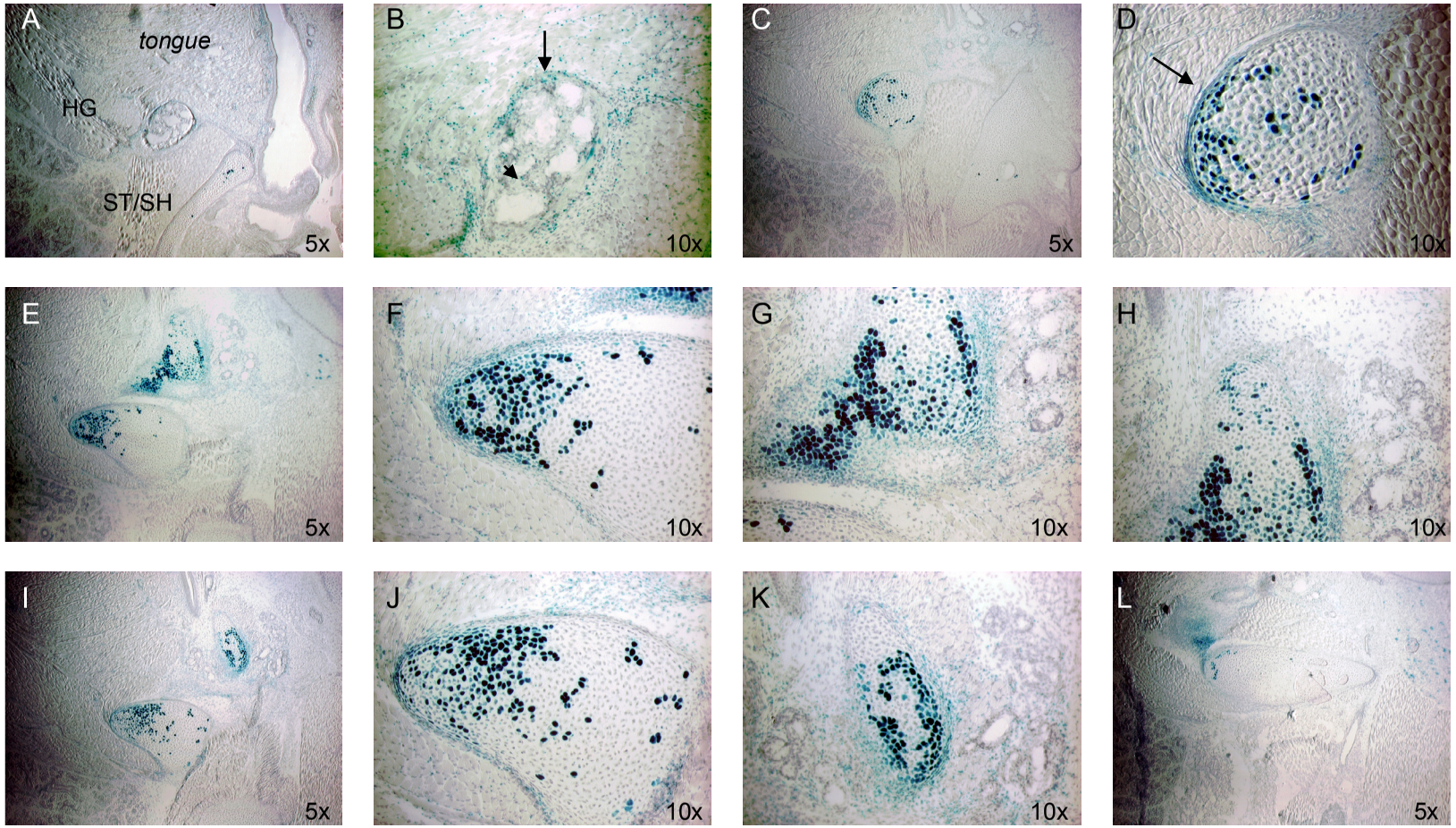
A
tongue
HG
ST/SH
5x
B
10x
C
5x
D
10x
E
5x
F
10x
G
10x
H
10x
I
5x
J
10x
K
10x
L
5x
cranial
anterior

P0

Figure 2.19 *Hand*2-Cre transgene labelling in the newborn hyoid bone

X-Gal staining of sagital sections through the hyoid region of P0 *Hand*2-Cre+/-; Rosa26LacZ-/- mice. Orientation of the images is cranial to the top and anterior to the left

A- L show positions along the hyoid bone from medial to lateral as indicated in the sketch below.

A, B Lower (**A**) and higher (**B**) magnification of the ossified basihyoid. Clear transgene labelling exists on the outside of the hyoid (long arrow) and single positive are found inside the bone (short arrow).

C, D In the cartilaginous part of the hyoid further laterally, labelling is mainly restricted to the ventral and caudal side of the hyoid, with groups of few labelled cells dispersed throughout.

E- H At the junction of cornu minor and major, labelling is strong in the ventral but not the dorsal part of the body of the hyoid (**E**, **F**). The base of the minor horn shows strong labelling, especially at the outside of the element (**G**, **H**).

I- K Staining in the body of the hyoid is once more restricted to the ventral aspect (**I**, **J**). The outer tip of the minor horn shows labelling on the outside but an unlabelled tip.

L The major horn of the hyoid is entirely unlabelled apart from a small ventral tip of positive cells.

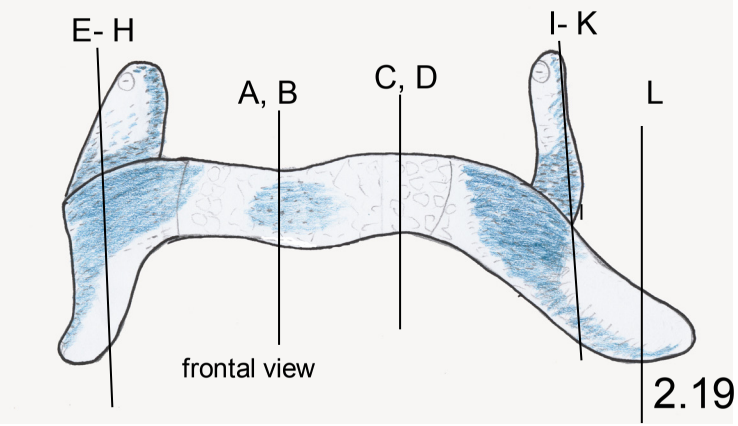

HG *M. hyoglossus*, ***ST***/***SH*** *M. sternothyroideus/ sternohyoideus*

A

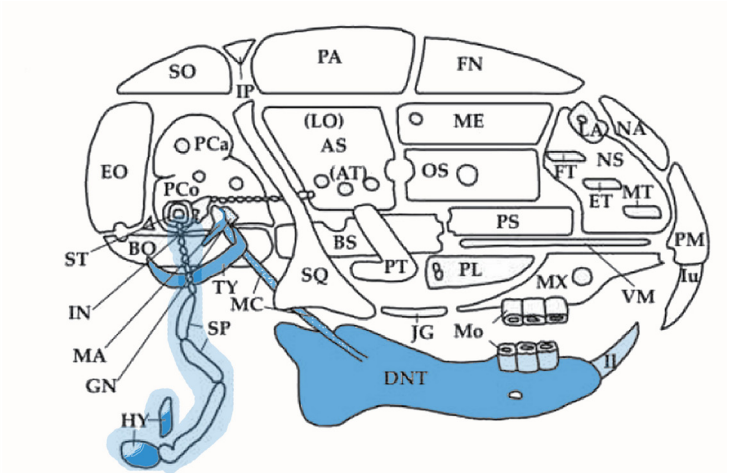

AS alisphenoid, **BO** basioccipital, **BS** basisphenoid, **DNT** dentary, **EO** exoccipital, **FN** frontonasal, **GN** goniale, **HY** hyoid, **Iu** upper incisor, **Il** lower incisor, **IN** incus, **JG** jugular, **LA** lacrimals, **MA** malleus, **MC** Meckel's cartilage, **Mo** molars, **Mx** maxilla, **NA** nasal, **NS** nasal septum, **PA** parietal, **PL** palatine, **PM** premaxilla, **PS** palatoshenoid, **PT** pterygoid, **SO** supraoccipital, **ST** styloid, **SQ** squamosum, **TY** tympanic, **VM** vomer

B

		proximal	distal
First arch	*splanchno cranium*	Ala temporalis	Malleus
		Incus	Meckel's cartilage
	dermato cranium	Palatine	Mandible
		Pterygoid	Tympanic
		Lamina obturans	Gonial
		Maxilla	
		Jugal	
		Squamosal	
Second arch	*splanchno cranium*	Stapes	Hyoid (lesser horn and upper body)
		Styloid	

Key

structure fully labelled by the *Hand*2-Cre transgene

structure partially labelled by the *Hand*2-Cre transgene

Figure 2.20 Summary of *Hand*2 domain-derived structures of the head

A Annotation of the *Hand*2-Cre transgene labelling in bone after X-Gal staining of P0 *Hand*2-Cre+/-; Rosa26LacZR-/- (template after Depew et al. 1999). Labelling in the structures of the first branchial arch is restricted to the dentary bone (DNT), the tympanic bone (TY), the gonium (GN), Meckel's cartilage (MC) and extends up to the boundary in the malleus (MA). The pulp of the lower incisors (II) and molars (Mo) is labelled while the enamel is not (indicated by light blue colouring). No labelling is detected in the upper jaw (maxilla, Mx, pre-maxilla, PM).

For the second branchial arch-derived structures, labelling is present in the hyoid (HY) and its surrounding connective tissue (labelled in light blue) and reaches up to the styloid process (ST).

B For the first branchial arch, all bones commonly considered distal (table based on Qiu et al. 1997) are either fully (dark blue) or partially (light blue) labelled by the *Hand*2-Cre transgene. Partially labelled elements are the most proximally located. For the second branchial arch, the situation is less clear as both hyoid (considered distal) and styloid (considered proximal) show partial labelling; this might reflect characteristics of the transgene.

References

Depew, M. J. *et al.* (1999), Qiu, M. *et al.* (1997).

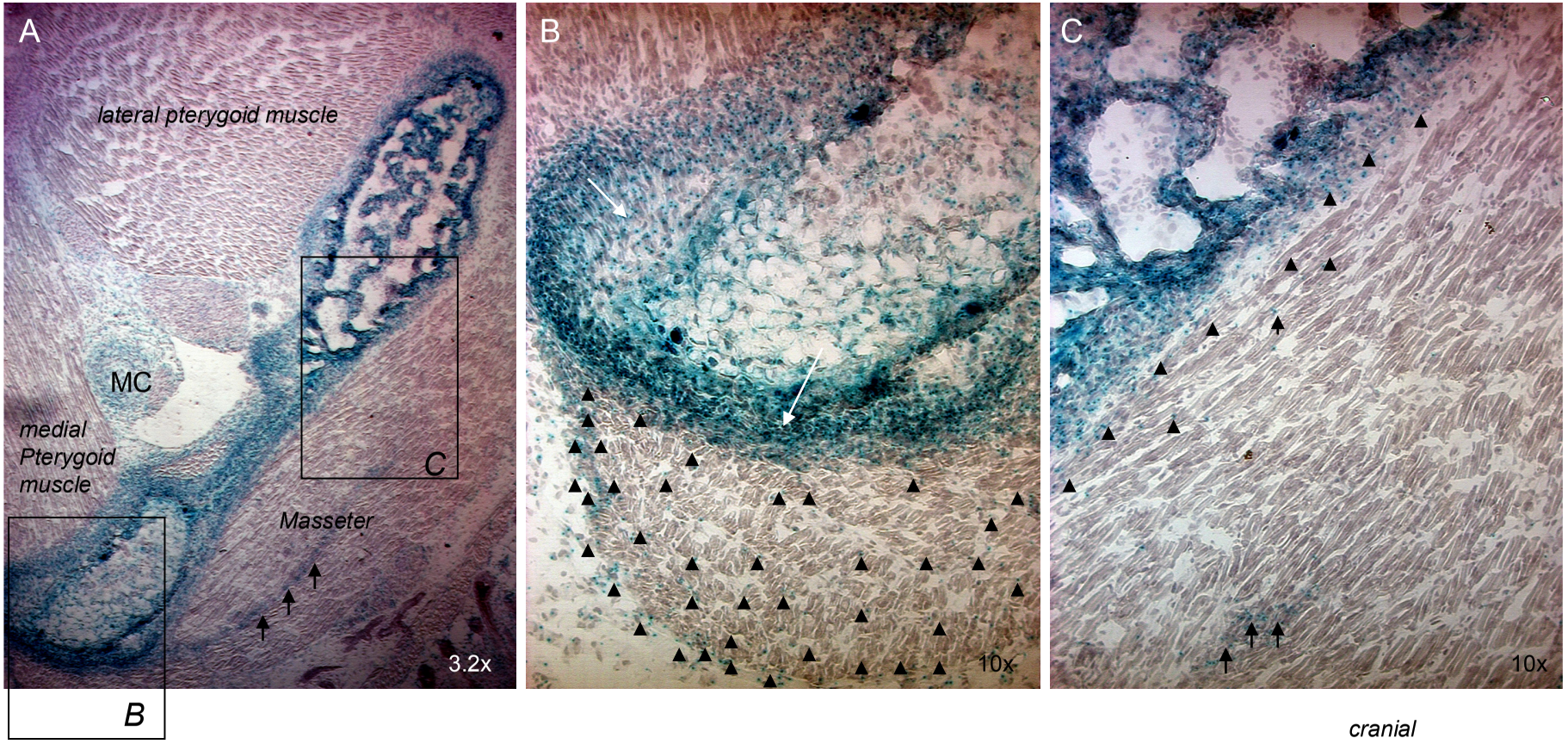
A
lateral pterygoid muscle
MC
medial
Pterygoid
muscle
C
Masseter
3.2x
B
B
10x
C
10x
cranial
medial
lateral
caudal

Figure 2.21 Labelled connective tissue in the masticatory muscles of *Hand*2- Cre+/-; Rosa26LacZR-/- mice

X-Gal staining of frontal sections of the head of P0 *Hand*2-Cre+/-; Rosa26LacZR-/- mice, Hematoxylin counterstain. Overview (**A**) and details of the masseter muscle (**B, C**). The extent of positively labelled connective tissue is indicated by black arrowheads.

A Frontal section through 3 out of the 4 masticatory muscles (masseter, the medial and lateral pterygoid muscle, missing is the temporal muscle) and their insertion points at the lower jaw.

B The lower jaw and in particular the muscular attachment regions (arrows) of the medial pterygoid muscle and the superficial part of the masseter are strongly labelled by the *Hand*2-Cre transgene. Out of the three parts of the masseter muscle, only the superficial part (here shown) has a major component of labelled connective tissue (arrowheads).

C Connective tissue along the dentary bone but not within the intermediate masseter part is labelled (arrowheads). Equally labelled the connective sheet separating the different masseter parts (arrows in **C**, also in **A**).

MC Meckel's cartilage

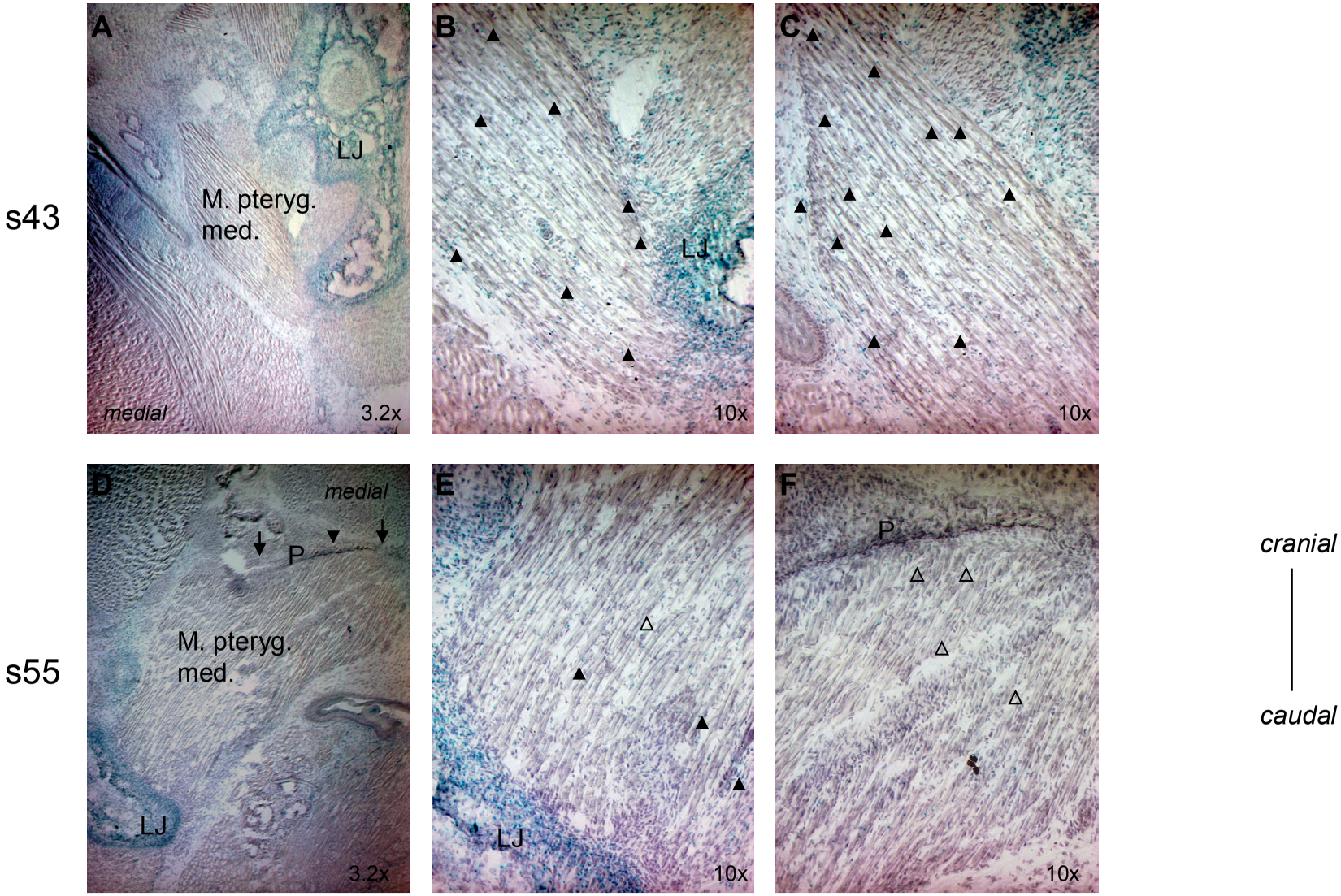
s43
s55
A
B
C
D
E
F
LJ
M. pteryg.
med.
medial
3.2x
10x
P
cranial
caudal

Figure 2.22 The *Hand*2-Cre transgene labels the anterior and distal part of the *M. pterygoideus medialis*

Frontal sections of the masticatory muscles of *Hand*2-Cre+/-; Rosa26LacZR-/- mice, PO. Images are orientated with cranial to the top, caudal to the bottom, the medial side of the section is indicated. This figure shows cross-sections of the medial pterygoid muscle (*M. pterygoideus medialis*), one on the ventral side (slide 43**, A- C**) and one more towards the dorsal side of the muscle (slide 55, **D**- **F**).

A Overview showing the lower jaw and the ventral side of the *M. pterygoideus medialis*.

B, C In higher magnification, the muscle connective tissue labelled by the *Hand*2-Cre transgene becomes visible. Connective tissue throughout the entire ventral front of the muscle is labelled (arrowheads).

B The distal part of the muscle with the insertion at the lower jaw.

C The proximal part of the muscle. As this is a cross-section through the muscle belly, it does not reach the origin at the pterygoid bone.

D Overview of a more dorsal section through the *M. pterygoideus medialis* including the muscle origin at the pterygoid bone (arrows in **D**).

E, F While most of the muscle connective tissue close to the insertion site at the lower jaw is still labelled (filled arrowheads in **E**), the area close to the origin shows no labelling (empty arrowheads).

A reconstruction of the entire *Hand*2 domain within the lateral pterygoid muscle can be found in Figure 2.24.

LJ lower jaw, ***P*** pterygoid

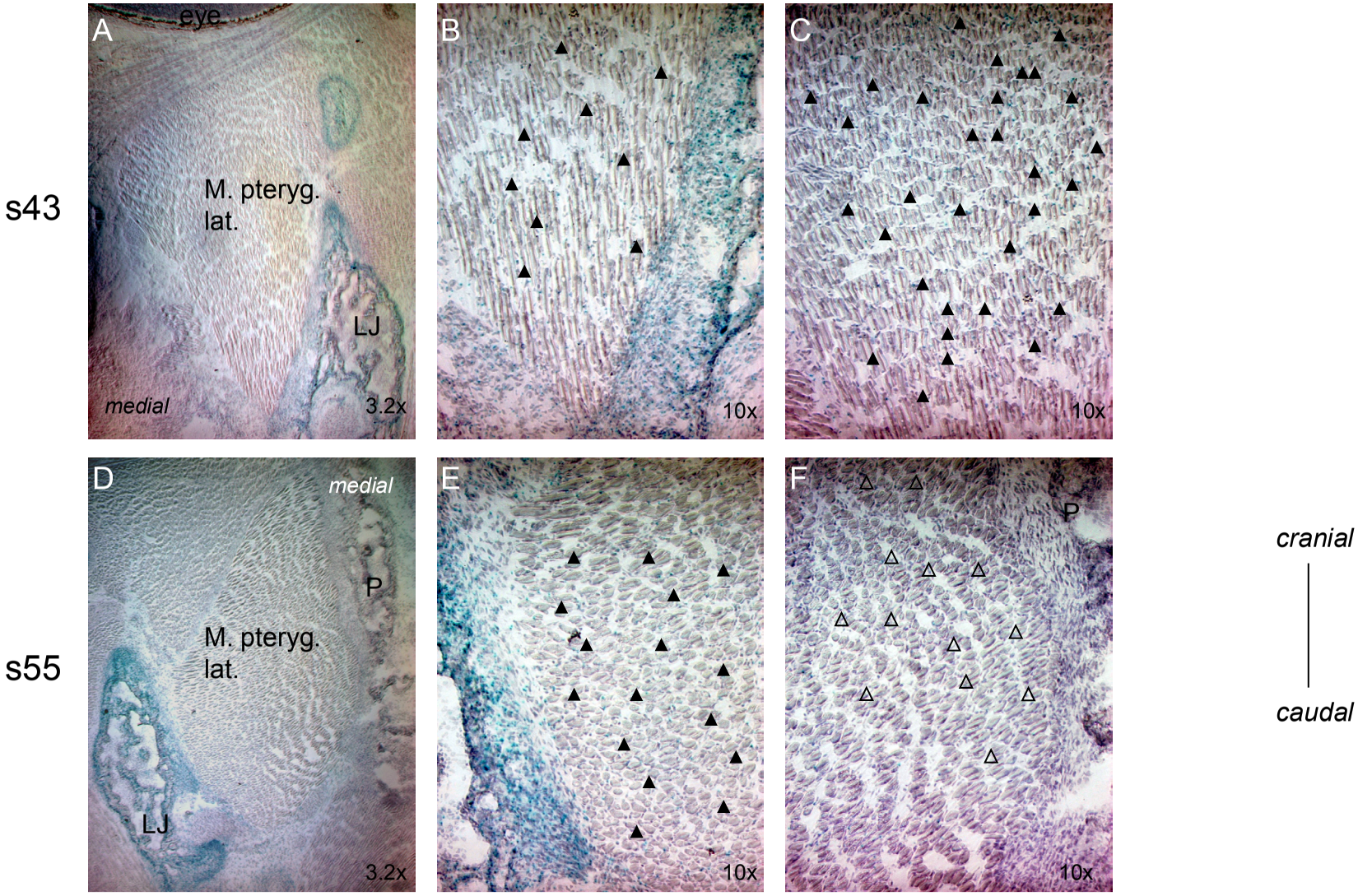
s43
s55
A
eye
M. pteryg.
lat.
LJ
medial
3.2x
B
10x
C
10x
D
medial
P
M. pteryg.
lat.
LJ
3.2x
E
10x
F
P
10x
cranial
caudal

Figure 2.23 The *Hand*2-Cre transgene labels the anterior and distal part of the *M. pterygoideus lateralis*

Frontal sections of the masticatory muscles of *Hand*2-Cre+/-; Rosa26LacZR-/- mice, PO. Images are orientated with cranial to the top, caudal to the bottom, the medial side of the section is indicated. This figure shows cross-sections of the other pterygoid muscle, the lateral pterygoid muscle (*M. pterygoideus lateralis*) at different dorso-ventral positions. **A**- **C** shows the ventral (slide 43), **D**- **F** a more dorsal aspect (slide 55) of the muscle.

A- C The ventral side of the lateral pterygoid muscle with insertion at the lower jaw (LJ).

Higher magnifications reveals the extent of labelling in the muscle connective tissue at the insertion site at the labelled lower jaw (**B**) and further medially towards the origin of the muscle (**C**).

D- F A more dorsal position within the lateral pterygoid muscle with its labelled insertion at the lower jaw (LJ) and unlabelled origin at the pterygoid (P). While the muscle connective tissue close to the insertion site is still positive (**E**), the labelling fades out towards the origin of the muscle at the pterygoid (**F**, indicated by empty arrowheads).

A reconstruction of the entire *Hand*2 domain within the *M. pterygoideus lateralis* can be found in Figure 2.24.

LJ Lower jaw, ***P*** pterygoid

of the domains as seen in Figure 2.24 and 2.25 are a reconstruction of all observations made along at least two axes. In accordance with *hand*2 gene and *Hand*2-Cre transgene expression being restricted to the neural crest-derived part of the branchial arches, no labelling was ever observed in mesoderm-derived muscle fibres.

2.4.3.3.1 Masticatory muscles

The masticatory muscles (*M. massentericus*, *M. temporalis*, *Mm. pterygoidei*) are a group of strong muscles originating from the first branchial arch and were of particular interest as they link the lower jaw labelled by the *Hand*2-Cre transgene with the unlabelled upper part of the skull. Common to all four muscles is that their connective tissue is labelled at the insertion site at the lower jaw and is unlabelled at the origin from the side and the base of the skull. The extent of labelling within the muscle connective tissue differs between different masticatory muscles: The labelling in the *M. temporalis* is restricted to its insertion area at the coronoid process of the lower jaw; the remaining muscle connective tissue shows no labelling. The murine masseter is split in at least three parts which differ in the proportion of labelled connective tissue (Figure 2.21). The superficial part of the masseter shows a zone of clear labelling at the caudal part of the muscle (Figure 2.21 B, Figure 2.24 for a summary). In the intermediate and inner parts, labelling is restricted to the attachment zone at the lower jaw (Figure 2.21 C). Both pterygoid muscles, located at the inside of the lower jaw, show an interesting pattern of labelling, with strong labelling at the anterior side of the muscle fading out towards the back of the muscle (Figure 2.22 and 2.23, compare the difference between the sections of different positions within the muscle). Laterally and distally, both muscles are labelled along their insertion at the lower jaw. Towards the origin of the muscles, the labelled domain becomes increasingly restricted to the anterior face of the muscle, creating a diagonal anterior *Hand*2-derived domain.

2.4.3.3.2 Mouth floor, suprahyal musculature and pharynx

The muscles of the mouth floor connect the first arch-derived lower jaw with the second arch-derived upper part of the hyoid, both labelled by the *Hand*2-Cre transgene (Figure 2.25). Muscles connecting labelled skeletal elements- in this case the dentary bone and

Figure 2.24- 2.25

A *M. massentericus*

superficial part

intermediate part

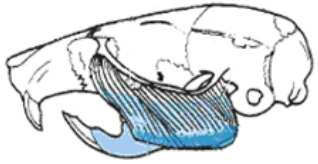

deep part

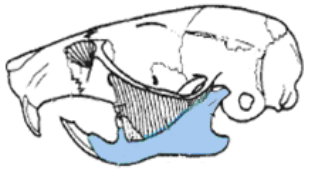

B *M. temporalis*

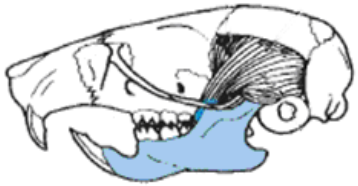

C *M. pterygoideus lateralis*

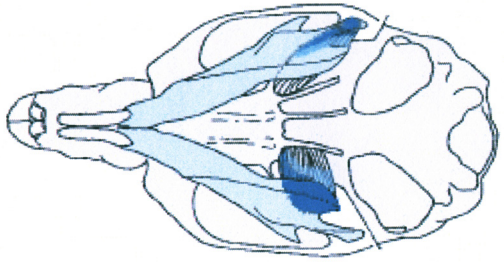

M. pterygoideus medialis

D

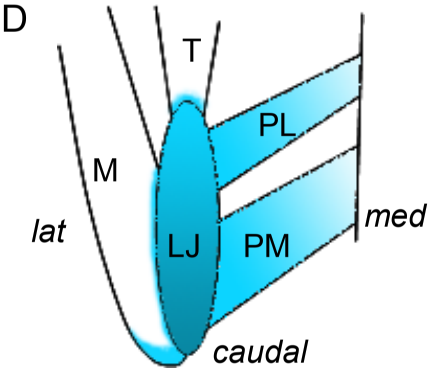

frontal view

Figure 2.24 Summary- labelling in the masticatory muscles of the *Hand*2-Cre+/-; Rosa26LacZR-/- mouse

Reconstruction of the *Hand*2 domain within the masticatory muscles based on the analysis of series of sections in at least two dimensions.

A The three parts of the murine *M. massentericus* (superficial, intermediate and deep part) are labeled to a varying degree by the *Hand*2-Cre transgene: the outer-most superficial part shows strong labelling at its caudal edge, the intermediate part shows a small zone of strong labelling in the caudal part of the muscle apart from connective tissue close to the insertion site (at the lower jaw) and the deepest part only shows labelling close to its insertion at the lower jaw.

B The *M. temporalis* behaves similarly to the deep part of the *M. massentericus* with only a very small zone of labelled connective tissue at the insertion of the muscle.

C The lateral and medial pterygoid muscles show transgene labelling ventrally, distally and caudally, creating a diagonal domain with strongest expression ventrally and fading out towards the dorsal and medial side.

D Schematic representation of the distribution of labelled muscle connective tissue within the masticatory musculature on a frontal view. The overall domain expands hardly to the lateral but mainly to the medial side.

M *M. massentericus,* ***T*** *M. temporalis,* ***PL*** *M. pterygoideus lateralis,* ***PM*** *M. pterygoideus lateralis*, ***LJ*** lower jaw.

A

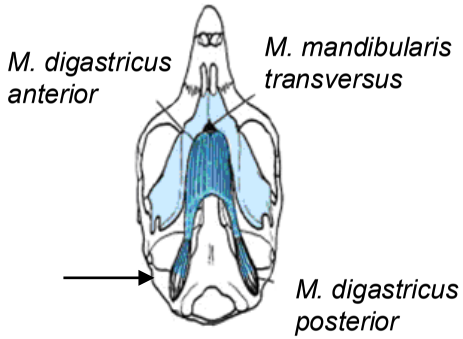

B

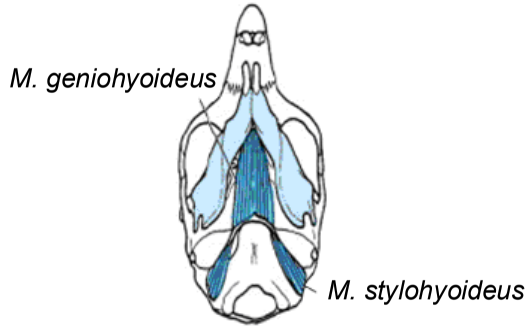

C

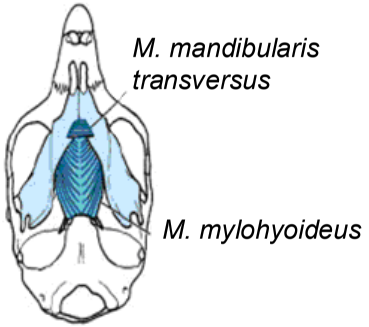

D

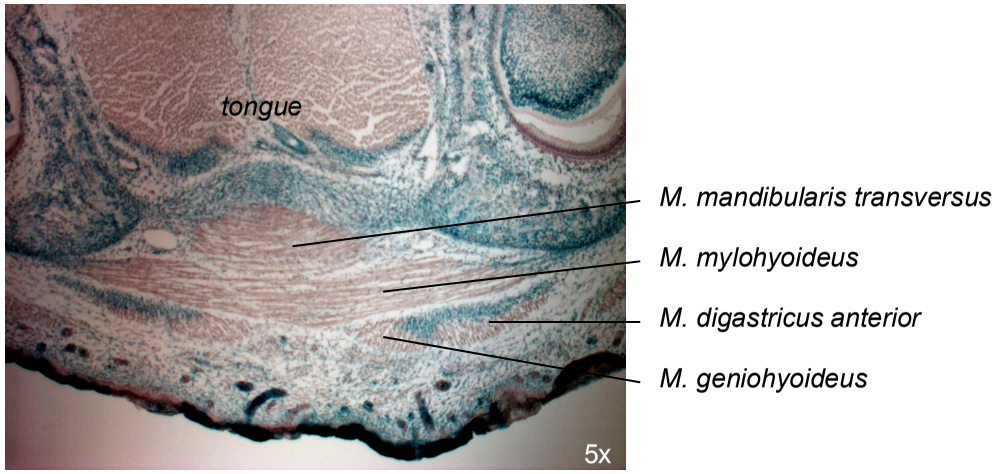

frontal section

Figure 2.25 Mouth floor and suprahyal musculature in the *Hand*2-Cre mouse

Schematic representation of the extent of labelling in the mouth floor and the suprahyal muscles of a *Hand*2-Cre+/-; Rosa26LacZR-/- newborn mouse.

A- **C** The different muscular layers of the region are shown in separate cartoons:

A Superficial layer of the suprahyal musculature with the anterior and posterior belly of the digastric muscle. The anterior belly (1st arch) of the M.digastricus is fully labelled and the posterior belly (2nd arch) is labelled up to two thirds of its length, with an unlabelled attachment at the skull base (arrow pointing to the boundary).

B Intermediate layer of the suprahyal musculature with the geniohyoid and stylohyoid muscle both of which contain entirely labelled connective tissue.

C Deep layer of the suprahyal musculature forming the floor of the mouth cavity. The muscle connective tissue of the M.mylohyoideus and M.mandibularis transversus that connect both arms of the lower jaw is also entirely labelled.

D Frontal section of a *Hand*2-Cre+/-; Rosa26LacZR-/- newborn, X-Gal staining with hematoxylin counterstain, showing the anatomy of the mouth floor with labelling in the connective tissue throughout the region.

the hyoid- such as the *M. mandibularis transversus*, the *M. mylohyoideus* and the *M. geniohyoideus* show fully labelled connective tissue. Similarly, the anterior belly of the digastric muscle which is connected to the hyoid via an intermediate tendon, shows labelled connective tissue throughout. From the entire group, only the posterior digastric belly shows partial labelling: the connective tissue is labelled for two thirds of the length of the muscle towards its hyal attachment, while its insertion at the skull base is unlabelled. In the newborn, the labelling in the connective tissue dorsal of the hyoid reaches behind the pharynx (Figure 2.26), showing also a major dorsal and medial extension of the *Hand*2 domain of the second branchial arch.

2.4.3.3.3 The *Hand*2 domain defines the corner of the mouth

In the *Hand*2-Cre mouse, the second arch-derived muscles of lips and mouth connect- similarly to the afore mentioned masticatory muscles- the labelled domain of the lower jaw with the unlabelled domain of the upper jaw, thereby forming the mouth cavity. At E16.0, the overall *Hand*2 domain boundary in the structures of the face runs half-way between upper and lower jaw (Figure 2.27 A, B); the same situation can still be observed at P0 (Figure 2.27 C, D), indicating stability of the boundary. With regards to the muscles forming the lips and the mouth, the *Hand*2 domain encompasses the lower half of the *M.orbicularis oris*, just ending below the crossing point of fibres of the lower and upper part (Figure 2.28 C, D, see also the schematic representation). This split into a positive lower and a negative upper half can equally be seen in the buccinator muscle, the muscle that forms the walls of the mouth cavity (Figure 2.29, IHC for ß-Galactosidase, noteworthy is also immunoreactivity in the oral ectoderm which will be addressed in Chapter 4 of this thesis). The *Hand*2 domain therefore divides the second-arch derived muscles of lips and mouth into an upper and a lower part, and so demarcates the corner of the mouth.

Figure 2.26- 2.29

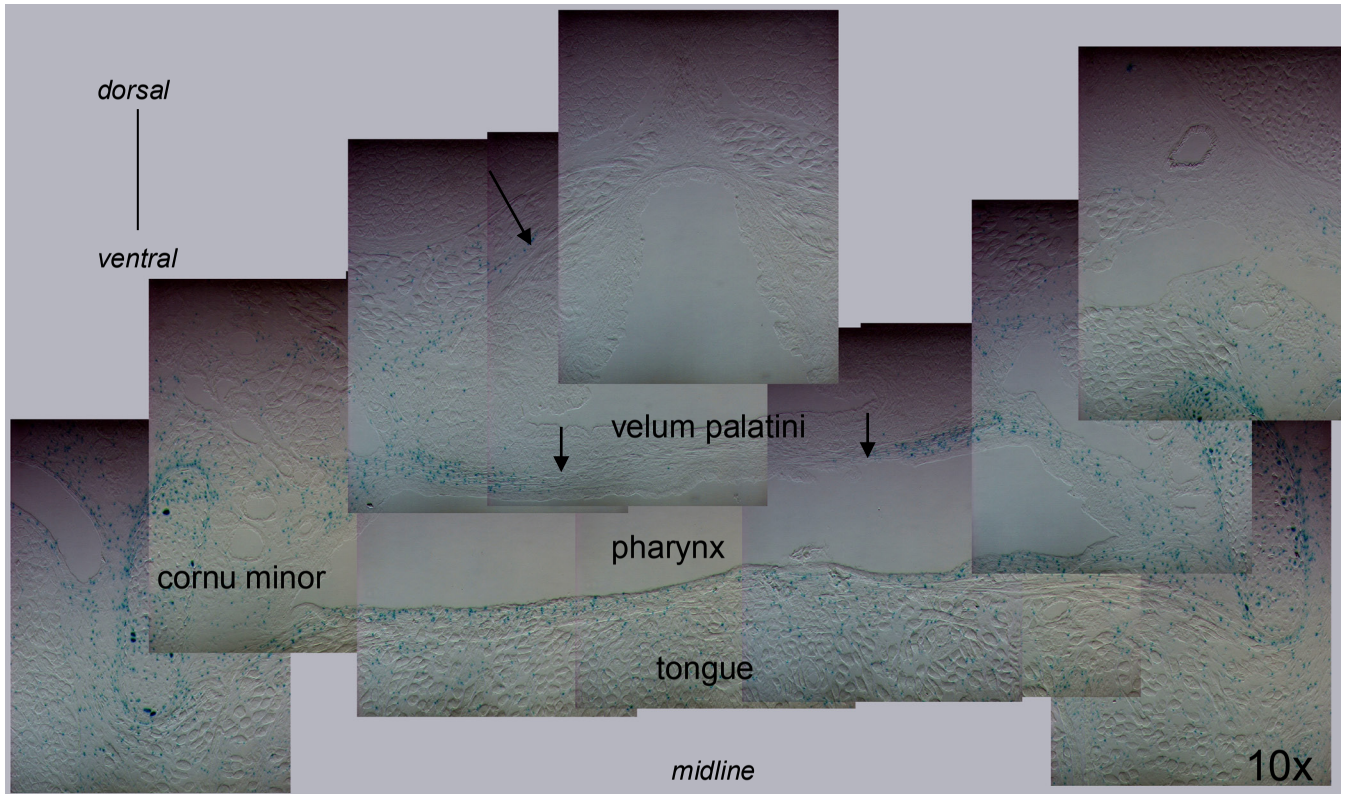

Figure 2.26 The *Hand*2 domain in the pharyngeal region

X-Gal staining of a transverse section through the base of the tongue of a newborn *Hand*2-Cre+/-; Rosa26LacZR-/- mouse. Separately acquired images in overlay to show the full extent of the domain.

The labelled cells of the *Hand*2 domain reach far medially and dorsally, with a contribution to the velum palatini (short arrows) and towards the oropharynx (long arrow).

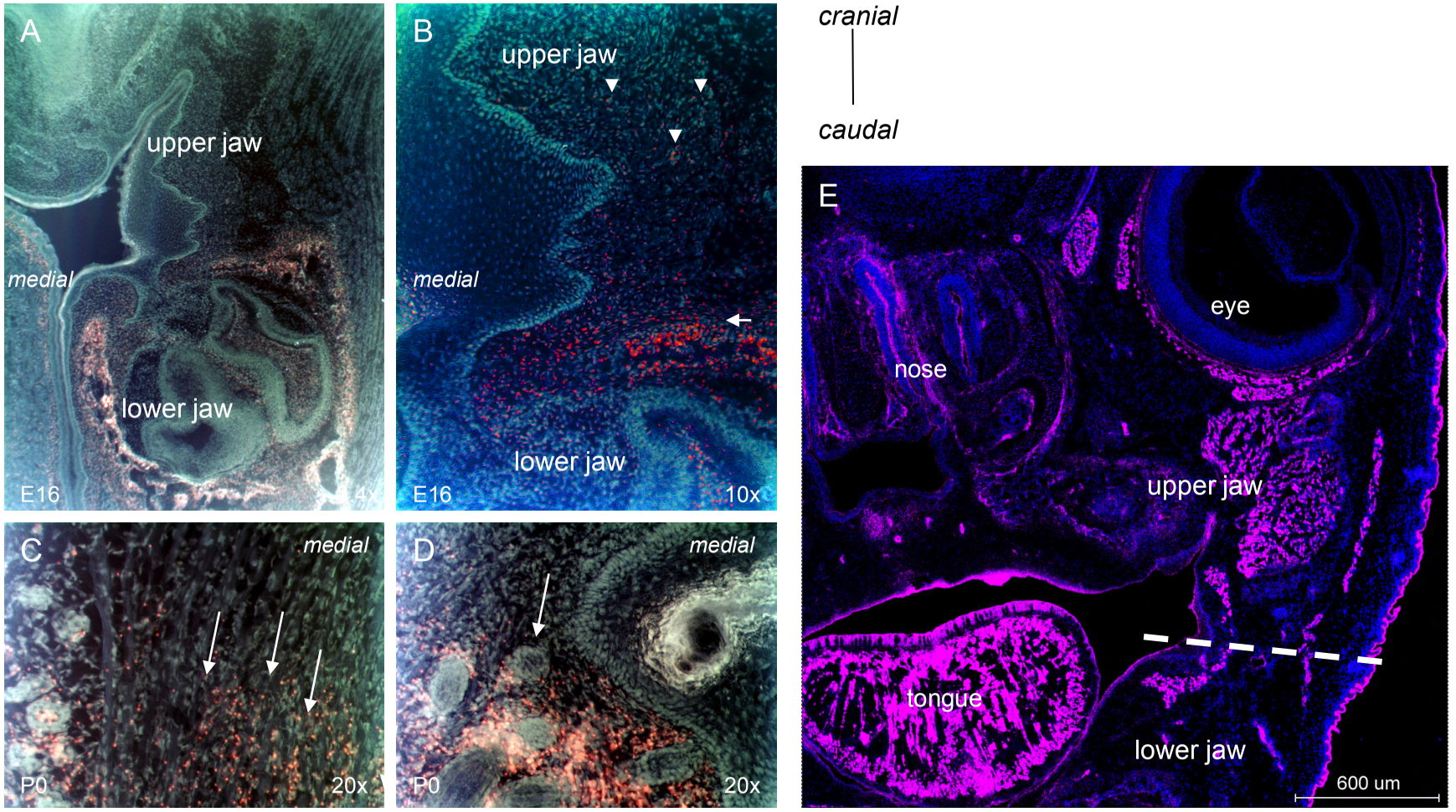
A
upper jaw
medial
lower jaw
E16
4x
B
upper jaw
medial
lower jaw
E16
10x
C
medial
P0
20x
D
medial
P0
20x
cranial
caudal
E
eye
nose
upper jaw
tongue
lower jaw
600 um

Figure 2.27 The *Hand*2 domain boundary coincides with the boundary between upper and lower jaw

X-Gal staining on frontal sections of E16.0 (**A, B**) and PO (**C, D**) *Hand*2-Cre+/-; Rosa26LacZR-/- mice. Images are shown in inverted colours for better contrast. Orientation of the images: cranial to the top, caudal to the bottom and medial to the left (**A**, **B**) or to the right (**C**, **D**) as indicated.

A Lower magnification to show a *Hand*2 domain derived lower jaw and an unlabelled upper jaw.

B Higher magnification with increased saturation of the red channel allows a better appreciation of the boundary (arrow). Single positive cells can be found above (arrowheads).

C, D The sharp boundary is maintained at P0 and crossed right through the buccinator muscle (C, arrows) and continues through adjacent connective tissue until just below the oral ectoderm (D, arrow, ectoderm to the right).

E Positioning of the boundary in relation to the overall anatomy (unrelated image, chosen for the anatomical overview; stained with Rhodamine-Phalloidin (magenta), DAPI; this is the same image as in Figure 2.29 A).

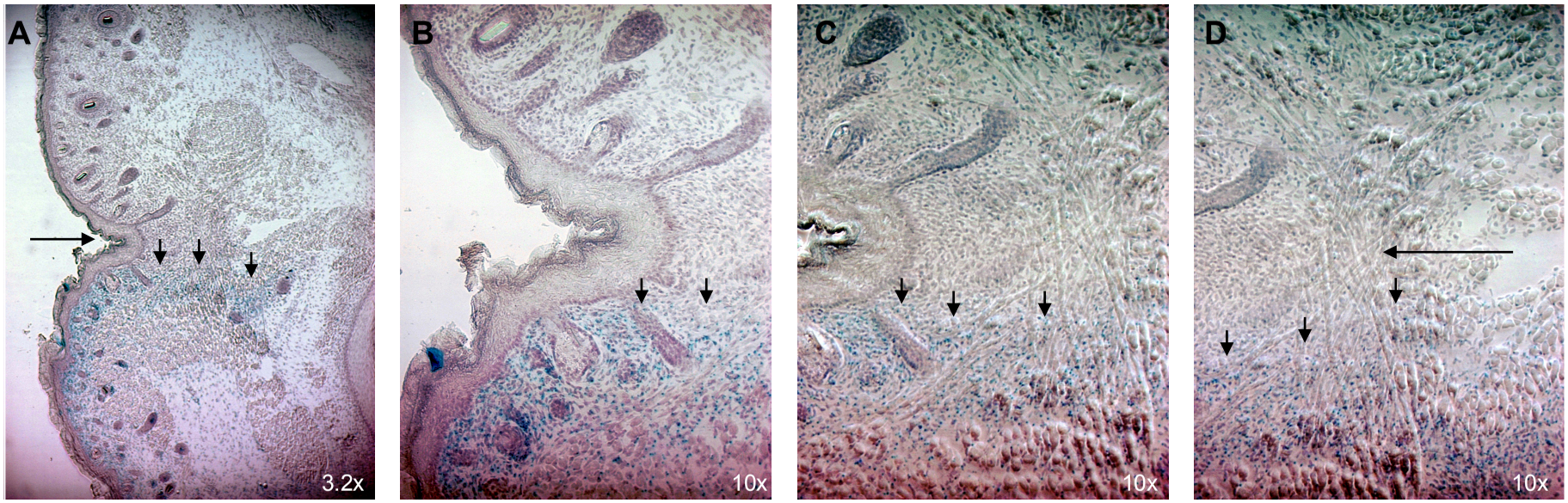
A
3.2x
B
10x
C
10x
D
10x

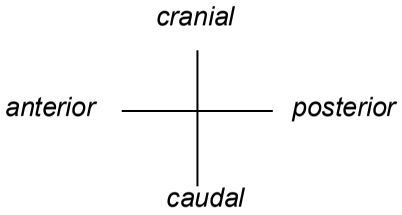
cranial
anterior
posterior
caudal

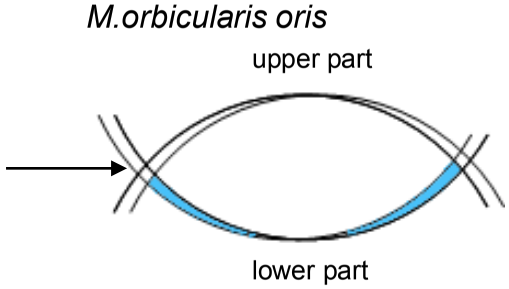
M.orbicularis oris
upper part
lower part

Figure 2.28 Projection of the *Hand*2 domain onto the *M. orbicularis oris*

X-Gal staining of sagital sections through the mouth corner of P0 *Hand*2-Cre+/-; Rosa26LacZR-/- mice. Images are orientated with cranial to the top and anterior to the left.

A Lower magnification shows the boundary between upper and lower jaw (long arrow) at the indentation of the mouth corner. Labelled connective tissue is visible just below this boundary (short arrows).

Higher magnification shows the extent of the *Hand*2 domain from anterior to posterior (**B**- **D**, short arrows), which runs just below the indentation of the outer ectoderm (**B**) and the cross of the muscle fibres of the *M.orbicularis oris* (**C**, arrow in **D** and cartoon).

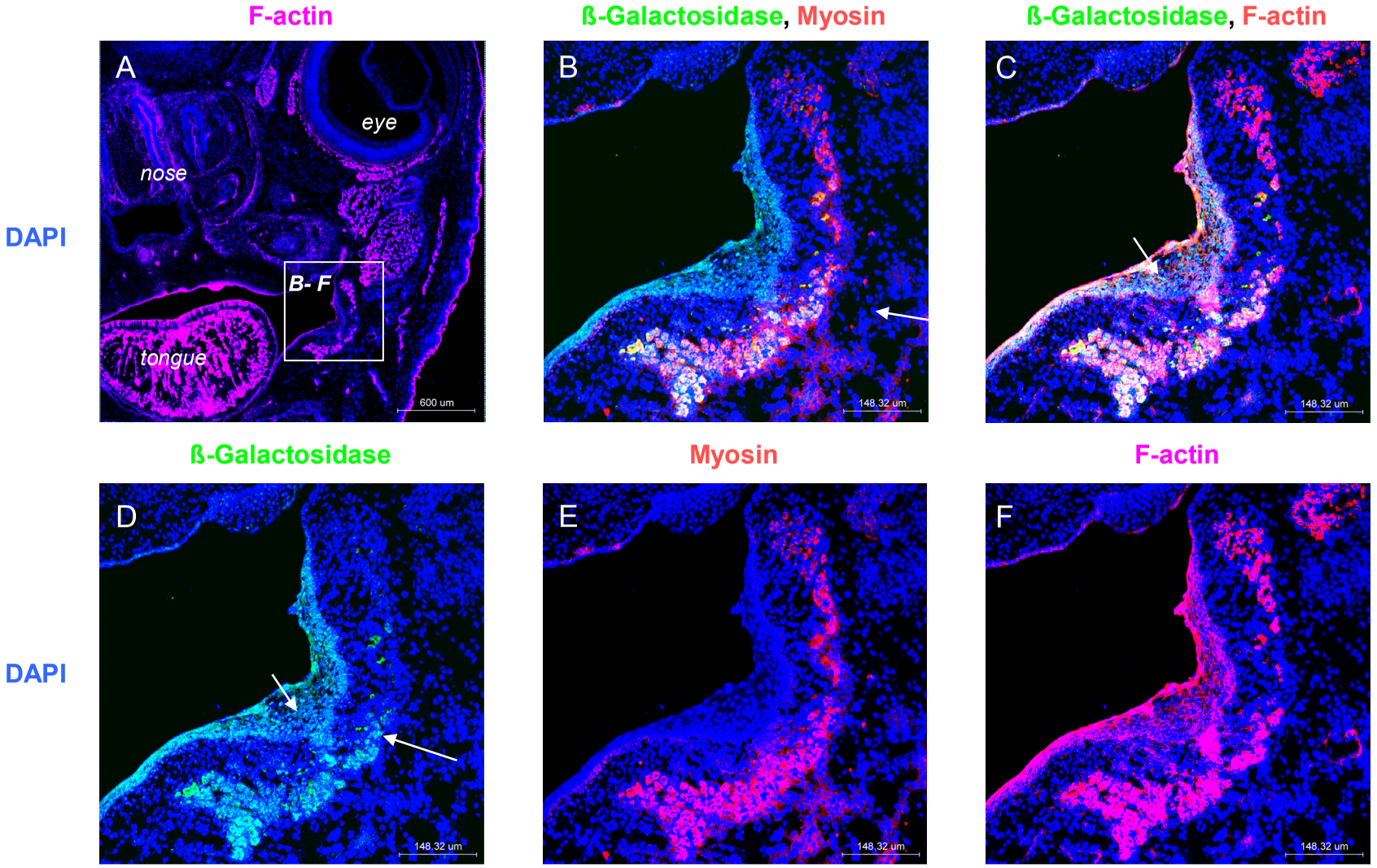
F-actin
ß-Galactosidase, Myosin
ß-Galactosidase, F-actin
DAPI
A
eye
nose
B- F
tongue
600 um
B
148.32 um
C
148.32 um
ß-Galactosidase
Myosin
F-actin
DAPI
D
148.32 um
E
148.32 um
F
148.32 um

Figure 2.29 The *Hand*2 domain defines the lower half of the cheek muscle (*M. buccinator)*

Frontal section through the anterior head of an E16.0 *Hand*2-Cre+/-; Rosa26LacZR-/- embryo. IHC for ß-Galactosidase (green) and Myosin (red in **B**). Counterstain with DAPI (blue) and Alexa633- Phalloidin (magenta in **A** and for better contrast red in **C**). Cranial is to the top of the image, caudal to the bottom.

A Overview of the anatomy of the region in lower magnification The buccinator muscle forms the muscular layer of the cheek and connects the upper and the lower jaw. The box indicates the position of **B- F**.

B- F The *M. buccinator* in higher magnification.

Anti- Myosin staining shows the course of the muscle fibres. The expression of ß-Galactosidase is restricted to the caudal half of the muscle, the boundary is indicated by the arrow (**B**). In the separation of the channels (**D, E**), this becomes even more obvious.

In addition to the muscle, Phalloidin also outlines the oral ectoderm (**C, F** and arrow in **C**). Cells staining positive for ß-Galactosidase clearly localise to this ectodermal layer (arrows in **C, D**)and *Hand*2 ectodermal expression will be discussed in Chapter 4.

2.4.3.4 X-Gal staining specifically detects cells originating from the distal branchial arch

To exclude late gene and/ or transgene expression in the *Hand*2-Cre mouse as explanation for the extent of the *Hand*2 domain in the middle ear and the lower jaw, fluorescent double RNA *in situ* hybridisations for *hand*2 and cre expression from the *Hand*2-Cre transgene were also performed at later stages of development (Figure 2.30). No *hand*2 nor cre RNA transcripts expression could be detected in the ossicles of the middle ear at E14.0 (Figure 2.30 A). As this excludes independent late *hand*2 (or transgene) expression in this region, the labelling in the malleus we were able to detect by X-Gal staining genuinely indicates distal branchial arch origin.
However, *hand*2 as well as cre are expressed in the dermal bone of the lower jaw, with a few remaining positive cells in Meckel's cartilage (Figure 2.30 B and C, E16). Interestingly, *hand*2 gene and *Hand*2-Cre transgene expression are also detected in other dermal bones, such as the frontal bone and in the dermal cover of the clavicle though no ß-Galactosidase activity can be detected in these with X-Gal stainings (Figures 4.13- 4.15). *Hand*2 also seems expressed in the molar tooth bud of the lower jaw (Figure 2.30 B). As expected from the strong staining for ß-Galactosidase in the tongue (Figure 2.18), *hand*2 and cre show strong albeit not entirely congruent expression here (Figure 2.30 D, E11). At the same stage, *hand*2 and cre expression were found in the auricular hillocks of the forming outer ear, both in the mesenchyme and the ectoderm (E). Strong *hand*2 expression was also observed in hair follicles as late as E16 (F).
H*and*2 and *cre* RNA expression was thereby more widespread than could be expected from the analysis of the *Hand*2-Cre$^{+/-}$; Rosa26LacZR$^{-/-}$ mouse by X-Gal staining. This inconsistency could be resolved as a sensitivity issue by highly sensitive immunohistochemistry with an additional tyramide-amplification step for ß-Galactosidase. Cre-mediated activation of the Rosa26LacZR reporter and the subsequent expression of ß-Galactosidase is an all-or-nothing event occurring in any given cell. Although the activation of both reporter alleles in a homozygous reporter mouse might not occur simultaneously if Cre concentrations are low, the cell will start producing and accumulating ß-Galactosidase once the excision of the stop cassette from the reporter allele has taken place. A cell in which the activation of the reporter has only taken place at a late stage in development will therefore have low levels of ß-

Figure 2.30

Hand2-Cre+/-; Rosa26LacZR

2.30

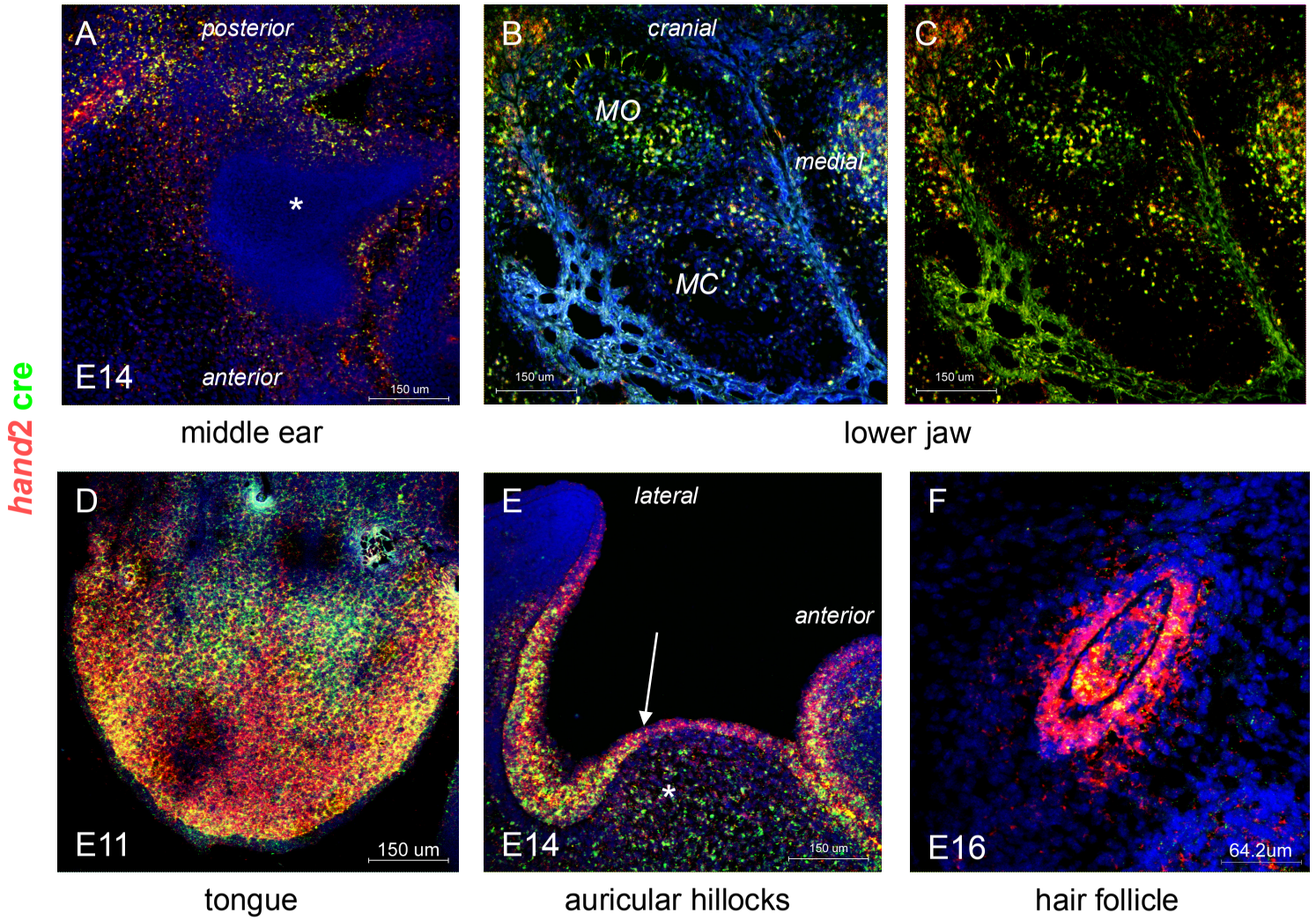

Figure 2.30 Late *hand*2 and *Hand*2-Cre transgene expression domains

Double RNA *in situ* hybridisation for *hand*2 (red) and cre (green) on sections of different regions of *Hand*2-Cre+/-; Rosa26LacZR-/- embryos. **A**- **C** transverse sections at two different time-points of development: E11 (**A**) and E14 (**B**- **C**). **D**- **F** frontal sections, E16.

A The middle ear region at E14.0. No *hand*2 gene nor *Hand*2-Cre transgene expression is seen in the forming middle ear ossicles (asterisk); however, expression of both is seen in the surrounding connective tissue.

B, **C** (same image, with and without DAPI, E16). *Hand*2 and the *Hand*2-Cre transgene are expressed in the dermal bone of the lower jaw. Meckel's cartilage (MC) shows single positive cells but is mainly unlabelled. Further expression is seen in the forming lower jaw molar (MO).

D The tongue is an area of strong *Hand*2 expression (red). Also the *Hand*2-Cre transgene shows expression although the two domains do not entirely overlap (green).

E *Hand*2 and *Hand*2-Cre transgene expression in the auricular hillocks of the forming outer ear. Expression is found in the mesenchymal tissue (asterisk) but also in the overlaying ectoderm (long arrow).

F *Hand*2 and to a lesser degree *Hand*2-Cre transgene expression is also found in hair follicles (here in a hair follicle of the craniofacial region at E16.0).

Galactosidase that are below the sensitivity threshold for conventional X-Gal staining. The differences in sensitivity between X-Gal staining and tyramide-amplified IHC allow in the case of the *Hand*2-Cre$^{+/-}$; Rosa26LacZR$^{-/-}$ mouse to distinguish between early (X-Gal positive, IHC positive) and late (X-Gal negative but IHC positive) developmental roles of *Hand*2: Analysis based on conventional X-Gal staining allows to trace cells originating from an early distal branchial arch domain and to analyse the extent of the *Hand*2 domain. Later widespread and unrelated expression domains of *Hand*2 do not interfere with this analysis, as they require more sensitive detection methods; the late expression of *Hand*2 in forming dermal bone and in teeth will be investigated separately and are content of Chapter 4.

2.4.4 Summary of the results

- *Hand*2 is an appropriate marker for distal branchial arches and overlaps with the *dlx*5/6 domain but not the *dlx*3/4 domain.
- The *Hand*2-Cre transgene does not fully replicate endogenous *hand*2 expression but provides a suitable marker for distal branchial arch identity.
- The domain labelled by the *Hand*2-Cre transgene expands greatly during development, from an early very distal domain to the demarcation of the mouth corner ventrally and to a far dorsally (middle ear, styloid) and medially (pterygoid muscles, connective tissue behind the pharynx) reaching domain. During its expansion, the *Hand*2 domain performs an inward and upward rotation.
- The axis of the stacked *dlx* domains does not correspond to the proximo-distal axis proper of the branchial arch but to an axis between the ectoderm and endoderm of the branchial arch. During development, *Dlx* expression domains rotate slightly from distal to proximal.

2.5 Discussion

The analysis of craniofacial bones labelled by the *Hand*2-Cre transgene (as summarized in Figure 2.20[54]) shows that all first arch elements associated with the lower jaw are either fully or at least partially derived from the distal-most part of the arch as defined by the *Hand*2-Cre transgene as late wide-spread transgene activation was excluded as reason for the extended labelling (Figure 2.30). Labelling in the first arch of the *Hand*2-Cre mouse extends into the malleus but not the incus and was never observed in the upper jaw of the mouse (e.g. Figure 4.5). The mammalian malleo-incudal joint is commonly considered to be the tetrapod homolog to the teleost primary jaw-joint (with the malleus being homologous to the articular (lower jaw) and the incus to the quadrate (upper jaw))[70,152] so that nearly the entire ancient lower jaw is labelled by the *Hand*2-Cre transgene. With the evolution of a secondary jaw joint in mammals- located between dentary and squamosum external to the original jaw articulation- the mammalian jaw joint no longer represents the ancient boundary between upper and lower jaw, this boundary now shifts into the middle ear. The results from the analysis of the *Hand*2-Cre mouse suggest that the *Hand*2-Cre transgene can be considered a useful proxy for the ancient lower jaw and demonstrates that nearly the entire lower jaw originates from the domain of the first branchial arch distal to the *dlx*3 expression domain (Figure 2.9).

This is consistent with a recent observation made by Cerny et al.[27]: the authors traced cells originating from the distal, so-called 'mandibular', mesenchymal condensation and from the proximal, so-called 'maxillary' mesenchymal condensation of the axolotl first branchial arch by DiI injection. Cells originating from the distal 'mandibular' condensation of the first branchial arch were found both in mandibula and maxilla, while cells coming from the proximal 'maxillary' condensation only became part of the trabeculae. This indicates that the lower as well as the upper jaw originate from the same distal 'mandibular' mesenchymal condensation of the first arch that was so far considered to only give raise to the lower jaw; following their results, the authors suggest to rename this condensation as 'maxillo-mandibular'.

The domain genetically marked by the *Hand*2-Cre transgene in all likelihood therefore corresponds to the distal part of this 'maxillo-mandibular' mesenchymal condensation studied by Cerny et al.[28]. This notion is further supported by lineage labelling results

with a murine *Pitx*1-Cre transgene. *Pitx*1 is expressed in a proximal domain directly adjacent to the *hand*2 domain (Figure 2.1 A, *pitx*1 in red) and the *Pitx*1-Cre transgene allows to genetically label cells originating from this proximal domain; in the newborn *Pitx*1-Cre mouse, the upper jaw is clearly labelled[208]. Taken together, this suggests that the distal 'maxillo-mandibular' *sensu* Cerny et al. mesenchymal condensation of the first branchial arch is genetically subdivided into a proximal *pitx*1 positive part giving rise to the upper jaw and a distal *hand*2 (transgene) positive part giving rise to the lower jaw.

In mammals, a highly characteristic set of muscles in control of the expression of the face is intercalated between the head skeleton and the skin. This facial or mimic musculature originates from the second branchial arch and migrates over first arch territory to its final position. Part of this muscle group are the muscles forming the mouth cavity by linking the upper and lower jaw, the *M. buccinator* and *M. orbicularis oris*. Both muscles respect the architecture established by first arch structures: The boundary between labelled and unlabelled cells in the *Hand*2-Cre mouse corresponds to the corner of the lips and runs half-way through the cheek (Figure 2.27- 2.29), clearly defining a (labelled) lower and an (unlabelled) upper half of the mouth, corresponding to the labelled lower and unlabelled upper jaw.

The considerable expansion of the *Hand*2 domain during development allows us to address the question of how the first branchial arch grows. By analogy to the outgrowth of the limb (for detailed reviews on limb patterning see e.g.[41,58,185-192]), a progress zone type model is possible where differentiating cells drop out of a proliferative zone at the tip of the growing domain (Figure 2.31 A, left). If this model was applicable to the first branchial arch, all first arch-derived structures, including both the upper and lower jaw (Figure 2.31 A) would be distal domain-derived. The analysis of the *Hand*2-Cre$^{+/-}$; Rosa26LacZR$^{-/-}$ mice shows no labelling in the upper jaw which allows us to discard a progress zone-type model for the outgrowth of the fist branchial arch.

The compartment model assumes that genetically distinct compartments lead to anatomically distinct structures (Figure 2.31 B, boundaries in the upper jaw were not investigated in this study and are therefore depicted as fuzzy) and is compatible with the existence of a boundary between distally and proximally derived cells in the lower jaw as seen in the *Hand*2-Cre mouse.

So while the distal *Hand*2 domain appears to behave like a compartment, its development can not be understood as a simple expansion of a distal branchial arch

Figure 2.31

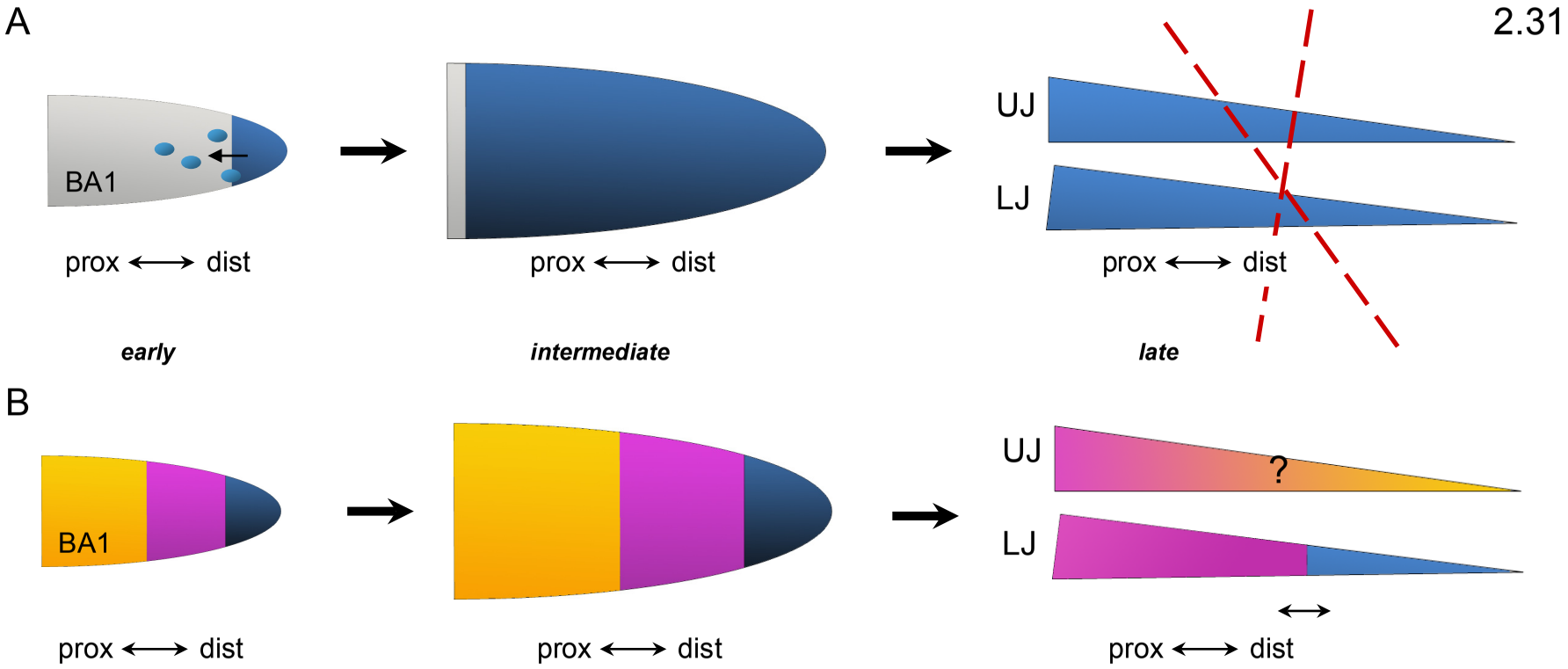

Figure 2.31 Different models of branchial arch outgrowth

Early, intermediate and late stages of first branchial arch (BA1) development according to

A the progress zone model and **B** the compartment model. Please see associated text for a detailed discussion.

UJ upper jaw, ***LJ*** lower jaw

compartment. With ongoing maturation of the facial precursor structures, the *Hand*2 domain performs an inward and upward rotation (summarized in Figure 2.32). During this process, the early vertical domain boundary rotates and shifts proximally (Figure 2.32 B- D). The final *Hand*2 domain extends cranially and towards the midline with labelling in the medially located *Mm. pterygoidei* but very little labelling in the lateral *M. massentericus* (Figure 2.32 E). Interestingly, we also observe a shift of some *dlx* domains in the same direction (shown for *dlx*5 in Figure 2.5, see also Robledo et al.[155] (Figure 2.C and D)). *Dlx* genes with their nested expression pattern have been shown to be responsible for proximo-distal branchial patterning[56,151], creating a proximo-distal '*Dlx* code' for intra-arch identity similar to the rostro-caudal '*Hox* code' for inter-arch specificity; this makes them likely candidates for the regulation of branchial arch outgrowth. The results from RNA *in situ* hybridisations on sections of the first branchial arch presented in this study demonstrate that the orientation of the *dlx* stack does not coincide with the proximo-distal axis of the branchial arch as previously suggested based on results from whole mount RNA *in situ* hyridisations[56] but rather seems orientated between the endoderm and the ectoderm (Figure 2.33). An endodermal-ectodermal axis would also be supported by the fact that both are sources for different signalling molecules (FGF8 signalling versus Endothelin signalling) and *dlx* pairs have been shown to be regulated by either pathway: *Dlx*1/2 expression can be activated by FGF8 expression[147,169] and *dlx*5/6 expression has been shown to depend on Endothelin signalling[29,159].

Telescopic outgrowth has been described as growth pattern for nested domains, foremost for the *Drosophila* leg disc, where the central-most domain telescopes out to become the distal-most part of the leg[108]. A model of telescopic growth along the proximo-distal axis of the branchial arch would not be able explain how distally derived cells would arrive at a dorsal and medial position (Figure 2.34 A). However, telescopic growth of the *Dlx* system along an ectodermal-endodermal axis, in combination with the afore mentioned rotation, provides a plausible model for the dorsal, cranial and medial extension of the distal branchial arch domain during development (B).

Future work will be required into the role of *Dlx* genes as control genes for branchial arch outgrowth, for example by studying how the loss of function of single members of the gene family effects the overall growth process. The data presented in this chapter thereby clearly demonstrates the three-dimensional nature of gene and transgene expression domains (e.g. in Figure 2.7 and 2.8). While the analysis on sections provides

Figure 2.32- 2.34

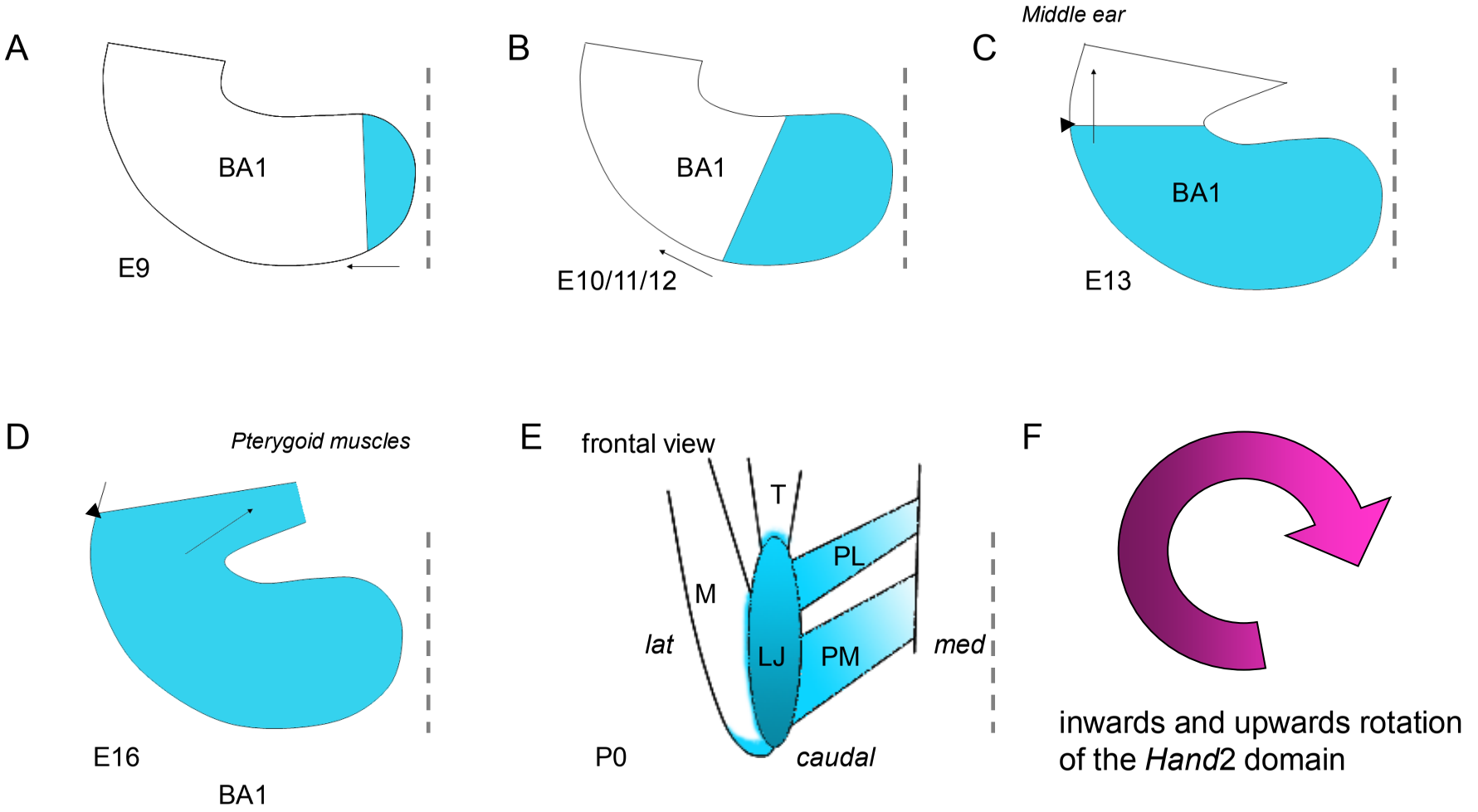
A
BA1
E9
B
BA1
E10/11/12
C
Middle ear
BA1
E13
D
Pterygoid muscles
E16
BA1
E
frontal view
T
PL
M
lat
LJ
PM
med
P0
caudal
F
inwards and upwards rotation
of the Hand2 domain

Figure 2.32 Inwards and upwards rotation of the *Hand*2 domain in development

Schematic idealised development of the *Hand*2 domain in the first branchial arch based on the analysis of the *Hand*2-Cre+/-; Rosa26LacZR-/- mouse. **A**- **D** represent transverse sections of the right first branchial arch, the midline of the embryo is indicated by a dashed line. **E** summarizes the labelling in the masticatory musculature of the newborn (also see Figure 2.24).

A Early in branchial arch development (around E9), the *Hand*2 domain boundary stands vertically and only a very small distal branchial arch population is labelled by the *Hand*2-Cre transgene.

B The *Hand*2 domain expands and the ventral axis begins to shift laterally (E10).

C The *Hand*2 domain has by now expanded very far laterally, reached the middle ear and demarcates the boundary between upper and lower jaw (E13.0).

D, E Between E16.0 and P0 the domain expands further, now more towards the midline of the embryo (**D**). The final extent of the *Hand*2 domain in the newborn (**E**).

F The summary of all directional movements of the *Hand*2 domain results in an overall inwards and upwards domain extension (for the right branchial arch: clock- wise).

M *M. massentericus,* ***T*** *M. temporalis,* ***PL*** *M. pterygoideus lateralis,* ***PM*** *M. pterygoideus lateralis*, ***LJ*** lower jaw.

A

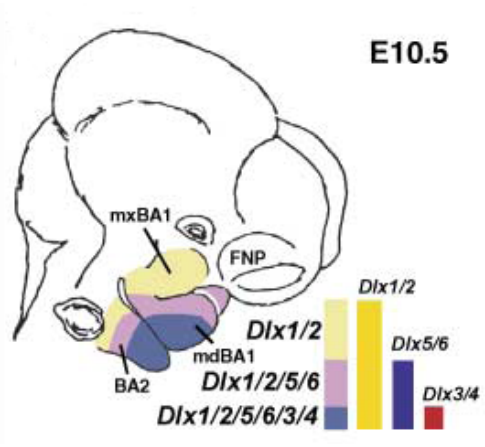

from Depew et al. 2005, Figure 3

B

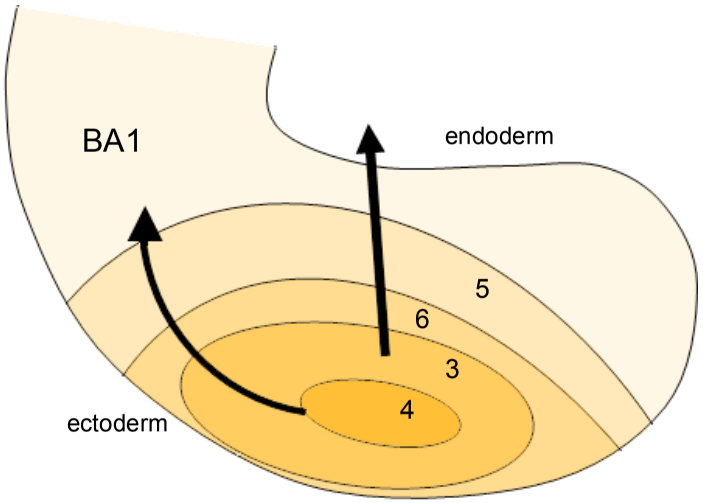

Figure 2.33 An alternative view on the *Dlx* system

A Standard view of the *Dlx* system (from Depew et al. 2005) with stacking of the *dlx* domains along the proximo- distal axis of the branchial arch.

B An alternative model for the *Dlx* system: Schematic representation of the arrangement of *dlx* 3- 6 domains in the first branchial arch. The axis of the stack does not correspond to the proximo- distal axis of the arch but rather to an axis between the ectodermal and endodermal face of the rach. The *dlx* 5/6 domain reaches further distally then the *dlx* 3/4 domain.Telescopic growth along the axis of the stack (straight arrow) and a rotation of the axis from distal to proximal (bent arrow) provides a model that is able to explain the presence of cells originating from the distal part of the first branchial arch in proximal and medial regions of the face.

Reference

Depew, M. J., Simpson, C. A., Morasso, M. & Rubenstein, J. L. Reassessing the Dlx code: the genetic regulation of branchial arch skeletal pattern and development. *J. Anat.* **207**, 501-561 (2005)

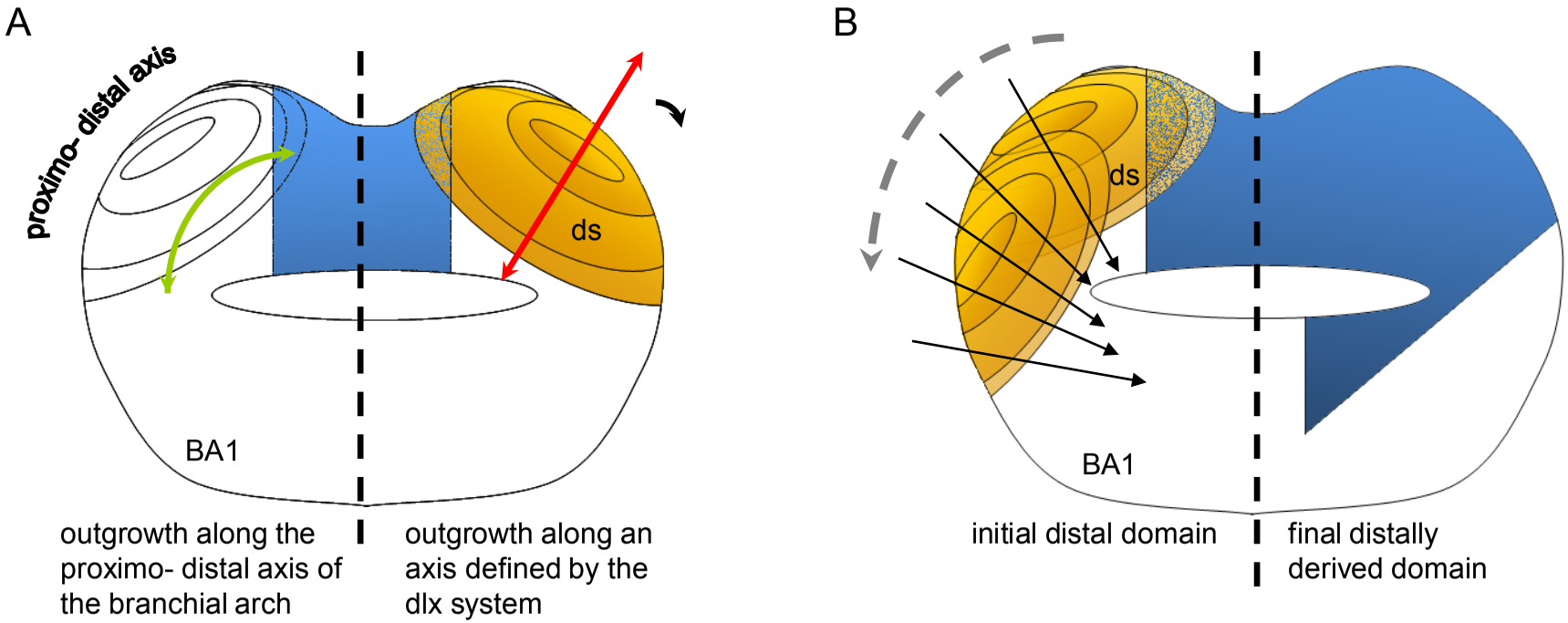

Figure 2.34 Final summary

A Comparison between an outgrowth of the arch along the proximo-distal axis with no correlation to the *Dlx* system (left, green arrow) and telescopic growth along the axis of the dlx system (right, red arrow).

B Outgrowth of the initially distal branchial arch domain (left) along the axis of a rotating *Dlx* system can explain the extent of the final distally derived domain (right).

For a detailed discussion, please see associated text.

ds *Dlx* system simplified as system of concentric yellow circles

us with a good resolution on cellular level, the overall character and three-dimensional extension of a domain is hard to appreciate. Confocal imaging of whole mount stainings, followed by reconstruction in 3D, could potentially reveal the spatial dimensions of smaller domains while still maintaining cellular resolution.

A recent imaging technique that makes use of a different optical principle, the so-called optical projection tomography (short OPT), was actually developed with the larger mouse embryo in mind and would have presented an interesting additional technique to appreciate for example the development of the *hand*2 or the *dlx* domains within the embryo[166-168]. While forfeiting cellular resolution, OPT is able to reveal an astonishing amount of anatomical detail as the technique makes use of both non-fluorescent and fluorescent signals. The scanning of the auto-fluorescence of the embryo can thereby provide anatomical detail against which expression domains, such as the *Hand*2-Cre transgene expression domain would have been interesting to judge, as e.g. in the case of the development of the shoulder blade.

The combination of double/ triple fluorescent RNA *in situ* hybridisations on sections with confocal imaging and of whole mounts with optical projection tomography will provide us in the future with both detailed cellular information as well as the exact spatial dimensions of gene expression domains and allow us to study genetic patterning systems in unsurpassed resolution and accuracy.

3 *Hand*2 and the head-shoulder divide

3.1 Overview

Head, neck and shoulder are regions of major evolutionary and developmental interest. Our understanding of the complex processes that led to the transformation of an immobile ancestral bony headshield to the mobile neck and shoulder region as we know it from modern tetrapods will depend on the exact knowledge of the contributions of cells from different embryonic origin, their respective boundaries and their interaction at these boundaries. With help of a transgenic mouse line, the *Hand*2-Cre mouse, we here determine the contribution of the limb lateral plate mesoderm to the shoulder girdle; this allows us (1)- to identify a part of the *manubrium sterni* as proximal element of the limb skeleton and therefore as a likely candidate for the 'lost' mammalian procoracoid and (2)- to study the behaviour between different lateral plate mesoderm subpopulations during the development of the mammalian shoulder blade.

The anterior margin of the shoulder girdle coincides with a major neural crest/ mesoderm interface which corresponds to the attachments sites of the neural crest-derived coracobranchial muscles on to the mesodermal shoulder girdle[122]. Genetic lineage labelling of neural crest (*Wnt*1-Cre mouse), in combination with immunohistochemistry for perichondrial and fibrillar molecular markers and imaging in high resolution provides us with a detailed image about the embryonic, morphological and molecular characteristics of these attachment sites and gives first insights into the cellular interactions in the process of their establishment at the neural crest/ mesoderm interface.

3.2 Table of Contents

3.3 Introduction

3.3.1 The evolution of the shoulder girdle

The development of limbs in a fish-like ancestor around 390 Million years ago gave rise (and the name) to a new group, the tetrapods. The transition from an aquatic to a terrestrial lifestyle coincided with major changes to the overall anatomy of the animal, including the evolution of limbs, and heavily affected the head and shoulder region. The ancestral shoulder girdle is hardly more than the posterior end of a box-shaped skull and is dominated by large dermal bones with directly attaching fins (Figure 3.1 A). The evolution of the upper limb coincides with the separation of the shoulder girdle from the head and the formation of a mobile neck (B). With this decoupling of the dermal shoulder girdle from the skull, the dominant outer dermal skeletal elements gradually shrink and the underlying endochondral scapulocoracoid gains in importance (a detailed description about the fish-to-tetrapod transition can e.g. be found in the book 'Gaining Ground' by J.Clack [37]).

The evolution of the endochondral element of the shoulder girdle, the scapulocoracoid, is central to this chapter and will be briefly summarised here and in Figure 3.2 (for a review on the evolution of the procoracoid, please see also Vickaryous et al.[200]): In basal tetrapod-like fish such as *Eusthenopteron*, the shoulder girdle is still dominated by dermal bones, with an insignificant scapulocoracoid on the inside of a sizable dermal cleithrum (A). With the evolution of digit-bearing limbs like in *Acanthostega* (B), the proportion of dermal to endochondral elements in the shoulder girdle begins to shift: the dermal elements shrink, while the scapulocoracoid enlarges and begins to dominate the shoulder region. The situation in an amniote sister group (*Seymouria*, (C)) illustrates a plausible next step in the evolution of the scapulocoracoid, in which it splits into a dorsal scapula and a ventral coracoid. In amniotes, a group containing mammals (D) and reptiles including birds (E), the coracoid is then further subdivided into a procoracoid and a metacoracoid. While both elements of the former coracoid are still present in some mammals like synapsida (D), they regress during the evolution of the placental group. In therians, to which rodents belong (F shows a murine scapula), the metacoracoid is thought not to represent more than the coracoid process of the scapula.

Figure 3.1- 3.2

A

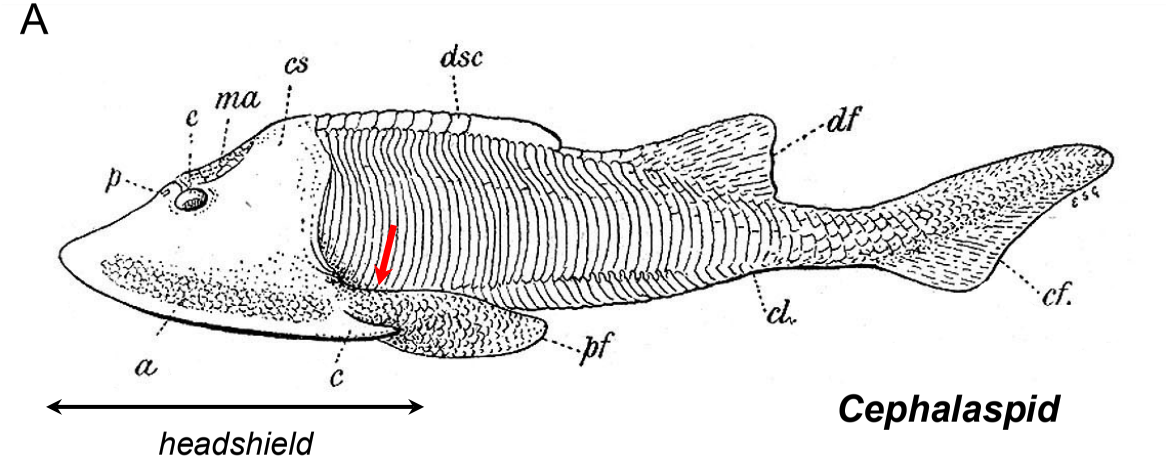

The ancestral condition of the head/ shoulder region (here in *Cephalaspid,* a jawless fish, about 400 Million years old) consists in a ”headshield”: Head and the shoulder region form a continous structure to which the limb directly articulates (arrow).

Image courtesy of P. Ahlberg

B

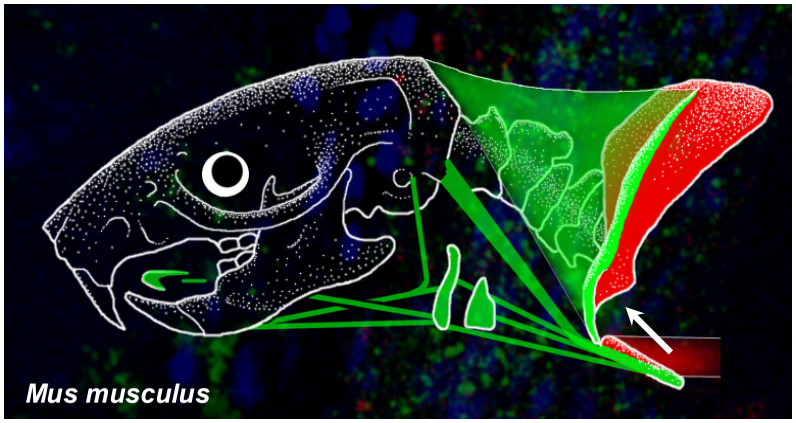

Modern tetrapods (here a mouse) show a clear separation of head and shoulder region. The original skeletal continuity has been replaced by strong muscular connections. The forelimb articulates with the shoulder blade (arrow).

Image Matsuoka, T. *et al.* (2005) *(title cover)*

neural crest-derived mesoderm-derived

Figure 3.1 The evolution of the shoulder girdle

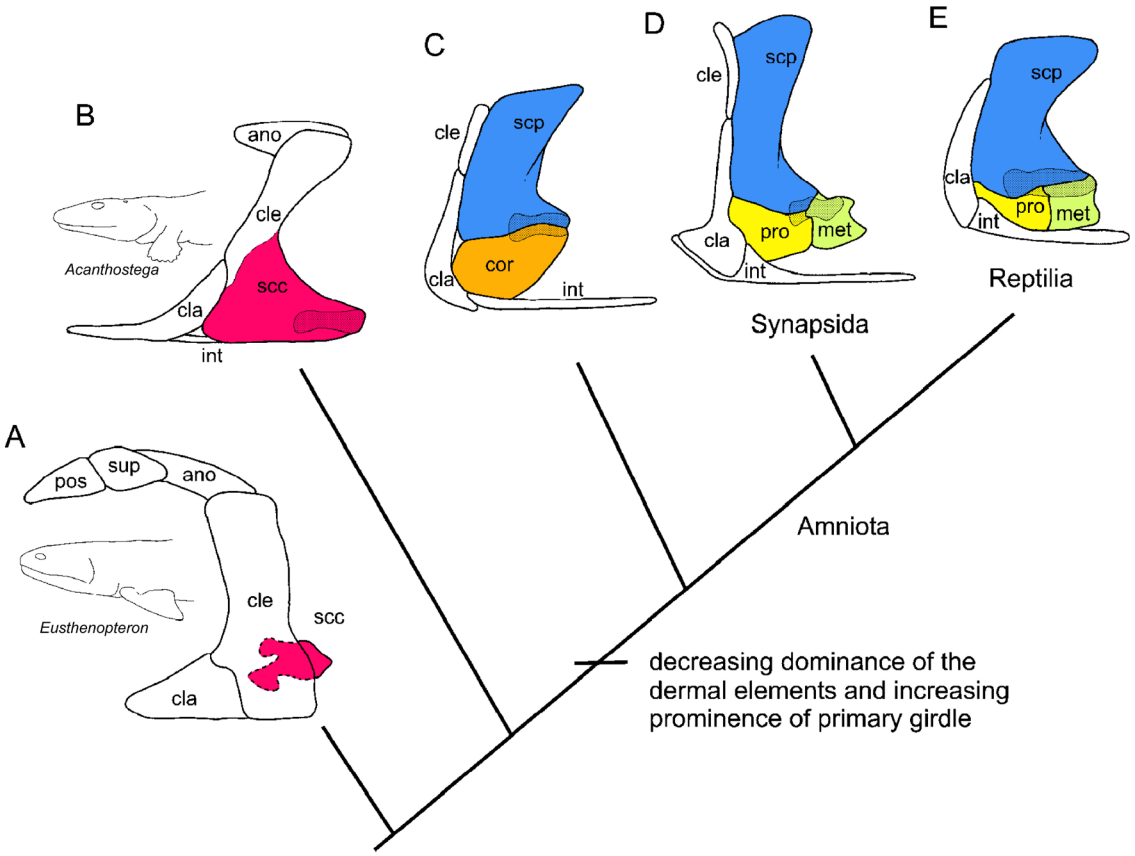
A
pos
sup
ano
cle
scc
cla
Eusthenopteron
B
ano
cle
scc
cla
int
Acanthostega
C
cle
scp
cor
cla
int
D
cle
scp
pro
met
cla
int
E
scp
cla
pro
met
int
Reptilia
Synapsida
Amniota
decreasing dominance of the
dermal elements and increasing
prominence of primary girdle

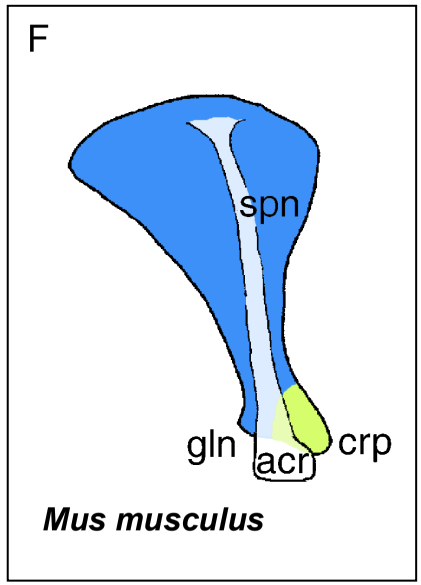
F
spn
gln
acr
crp
Mus musculus

Figure 3.2 The evolution of the scapulocoracoid

In very basal tetrapods before the evolution of digit-bearing limbs (**A**) the shoulder girdle is dominated by dermal elements, with a small scapulocoracoid on the inside. With evolution of the tetrapod lineage with digit-bearing limbs and the re-modelling of the shoulder girdle, the dermal contributions to the shoulder girdle decreases while the scapulocoracoid simultaneously increases in size (**B**). In a sistergroup to amniotes (**C**), the scapulocoracoid then splits into the scapula and a coracoid. In the amniote lineage (**D** and **E**), the coracoid occurs further subdivision into a procoracoid and a metacoracoid. In mammals (**F**), the scapula has become the dominant element remaining from the former scapulocoracoid; the metacoracoid remains as coracoid process and the procoracoid is thought to be lost or incorporated into the manubrium sterni (marsupials). Figure annotated after Vickaryous et al. 2006

ano anocleithrum, ***acr*** acromion, ***cla*** clavicle, ***cle*** cleithrum, ***cor*** coracoid, ***crp*** coracoid process, ***gln*** glenoid, ***int*** interclavicular, ***met*** metacoracoid, ***pos*** post-temporal, ***pro*** procoracoid, ***scc*** scapulocoracoid, ***scp*** scapula, ***spn*** spine, ***sup*** supracleithrum

Reference

Vickaryous, M. K. & Hall, B. K. (2006)

The mammalian procoracoid is commonly considered as lost (e.g.[125,165]), although it has already been suggested that in marsupials, the procoracoid material becomes incorporated into the *manubrium sterni*[101,114].
In summary, the primarily minor endochondral scapulocoracoid assumes an important function during the evolution of the tetrapod shoulder girdle and eventually subdivides into several elements. In placentals, the scapula is retained as the predominant element; the derivatives of the coracoid complex continue to exist in form of the coracoid process (the former metacoracoid) or are considered lost (the former procoracoid).

3.3.2 The shoulder girdle receives contributions from different embryological cell populations

The mammalian shoulder region consists of the upper limb, the scapula, the clavicle, the sternum and the ribs (Figure 3.3 A and B). The high degree of mobility that is characteristic for the modern tetrapod forelimb is achieved by a system relying on muscular suspension: The upper limb does not articulate directly with the trunk, but with the scapula, a triangular bone held in place by a system of muscles attaching it dorsally to the spine and rib cage and laterally to the limb. The scapula's only bony connection to the thorax is via its articulation with the lateral end of the clavicle. On the medial side, the clavicle articulates with the sternum; sternum, ribs and dorsally the vertebral column define the thorax. Sternum and vertebral column are predominantly derived from the lateral plate and the somitic mesoderm respectively[31]. The opinions about the embryonic origin of the ribs differ, they are either considered to be of somitic[88] or of mixed lateral plate/ somitic origin[24,140]. The forelimb forms as an outbudding from the lateral plate mesodermal domain; and the scapula, the linking element between forelimb and trunk, contains a major lateral plate mesoderm contribution[60]. The somitic mesoderm appears to participate to a varying degree in the formation of the scapular blade, depending on the analysed species[31,60,87,199]. The clavicle is often assumed to be lateral plate mesoderm derived[32] but a neural crest contribution has been demonstrated for the attachment sites of the coracobranchial system[122].

Figure 3.3

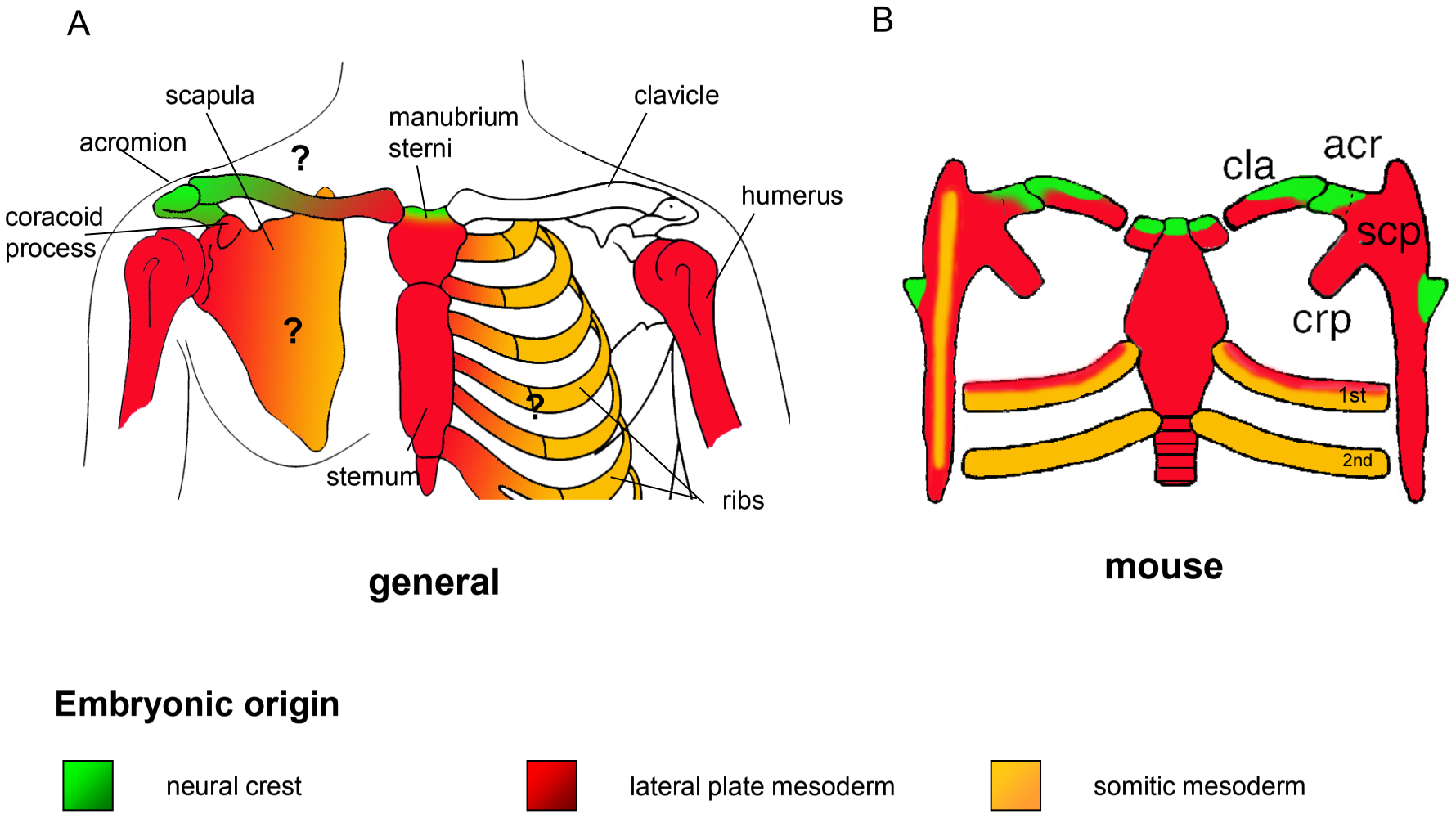
A
scapula
acromion
?
manubrium
sterni
clavicle
humerus
coracoid
process
?
?
sternum
ribs
general
B
cla
acr
scp
crp
1st
2nd
mouse
Embryonic origin
neural crest
lateral plate mesoderm
somitic mesoderm

Figure 3.3 The embryonic origin of the tetrapod shoulder girdle

The contribution of the different embryonic cell populations to the shoulder girdle in schematic overview (neural crest- green, lateral plate mesoderm- red, somitic mesoderm- yellow).

A Summary of current knowledge about the origin of the shoulder girdle based on work in different species and projected on to human anatomy (the original version of the figure can be found under *http://en.wikipedia.org/wiki/File:Pectoral_girdles-en.svg).* Areas of unclear contribution are indicated with a question mark. The neural crest contribution to the shoulder girdle (green) is restricted to the acromion, a part of the clavicle and the attachment sites of the sternocleidomastoid muscle to the sternum. Limbs, the shoulder blade, the major part of the sternum and most likely part of the ribs are lateral plate mesoderm derived. The spine (not shown), the ribs and part of the scapula are of somitic mesodermal origin. Please see the associated text for a more detailed description and references.

B Summary of the data solely obtained in mouse. The contribution of lateral plate mesoderm is based on the analysis of the *Prx*1-Cre mouse (Durland et al. 2003), the neural crest contribution of the neural crest based on the *Wnt*1-Cre mouse (Matsuoka et al. 2005) and the somitic mesodermal contribution on the *Pax*3-Cre mouse (Valasek et al. 2010).

The overall contribution of the lateral plate mesoderm (LPM) to the murine shoulder girdle has been mapped by genetic lineage labelling with help of the *Prx*1-Cre transgene[60]. As lateral plate mesoderm- in contrast to its somitic counterpart- lacks overt segmental behaviour[24,139], the contribution and the behaviour of subpopulations within the domain of the lateral plate mesoderm are however not well understood.
Forelimb and hindlimb buds originate from the lateral plate mesoderm at distinct, genetically controlled rostro-caudal positions along the body axis[25]; prior to limb bud initiation, *hand*2 is expressed throughout the entire lateral plate mesoderm[30] (Figure 3.4 A left). An outbudding from the lateral plate mesoderm for the later forelimb can be seen under the electron microscope as early as E9.0[4]. At this time, *hand*2 expression can only be observed in the caudal flank but no longer in the forelimb field (somite 7-12) of the lateral plate mesoderm[30]. Half a day later, at E9.5, *hand*2 expression then comes up within the posterior forelimb and continues in the flank[30]. The *Hand*2-Cre transgene deviates from endogenous *Hand*2 expression in that it shows no activity throughout the lateral plate mesoderm and in the hindlimb (Figure 3.4 A right). In contrast to the posterior restricted endogenous *Hand*2 expression in the forelimb (Figure 3.4 A left), the *Hand*2-Cre transgene labels the entire forelimb bud at E9.0 with the exception of a small posterior rim[158] (Figure 3.4 A right, also C). This particularity of the *Hand*2-Cre transgene that does not reflect endogenous *Hand*2 function, provides a useful tool as it allows to distinguish between the lateral plate mesoderm cell population forming forelimb bud (now called 'limb lateral plate mesoderm', Figure 3.4 A) and the reminder of the lateral plate mesoderm of the trunk (now referred to as 'trunk lateral plate mesoderm' Figure 3.4 A). At the anatomical interface of the shoulder region, the *Hand*2-Cre transgene can therefore be used to locate elements originating from the forelimb bud within the structures known to be lateral plate mesoderm-derived[60]. It further allows to study the interaction between lateral plate mesodermal populations from different origin (forelimb versus trunk), despite their lack of overt segmented behaviour.
A precise map of the cellular contributions to the mammalian shoulder girdle and the principles according to which different cell populations interact will eventually provide us with a detailed understanding of the development and the evolution of this interface.

Figure 3.4

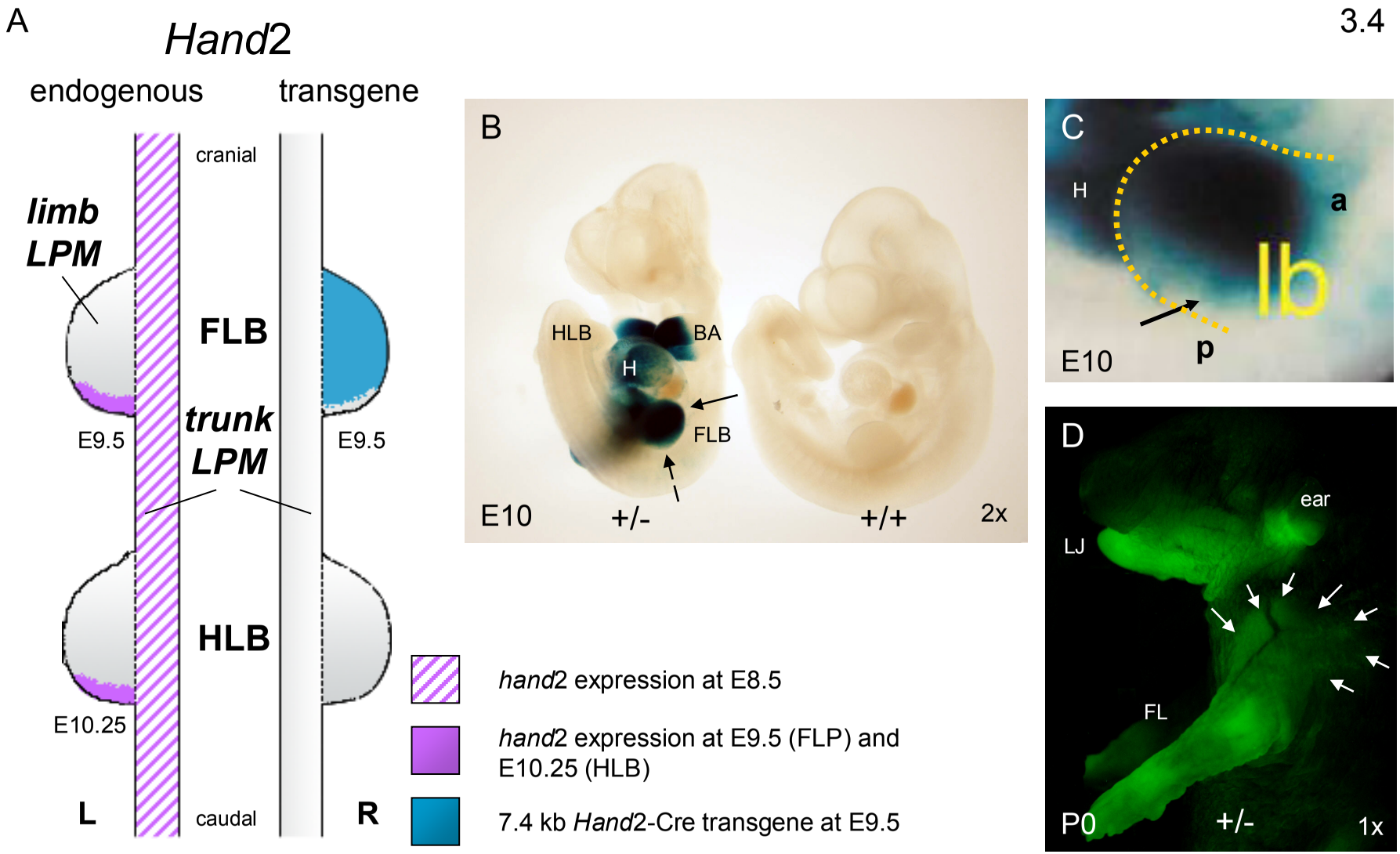
A
Hand2
endogenous
transgene
cranial
limb LPM
FLB
trunk LPM
E9.5
E9.5
HLB
E10.25
L
caudal
R
B
HLB
BA
H
FLB
E10
+/-
+/+
2x
C
H
a
lb
p
E10
D
ear
LJ
FL
P0
+/-
1x
hand2 expression at E8.5
hand2 expression at E9.5 (FLP) and E10.25 (HLB)
7.4 kb Hand2-Cre transgene at E9.5

Figure 3.4 The *Hand*2-Cre transgene labels the lateral plate mesoderm of the forelimb bud

A Comparison between endogenous *hand*2 RNA expression on the left (L, magenta) and the expression driven by the transgene containing 7.4kb upstream region of *Hand*2 (Ruest et al. 2003) on the right (R, blue). Endogenous hand2 expression can be found throughout the lateral plate mesoderm as early as E8.5; expression in the posterior domain of the forelimb and hindlimb buds comes up at E9.5 and E10.5 respectively (Charite et al. 2000). The Hand2-Cre transgene in contrast does not replicate endogenous expression in the lateral plate mesoderm at all and deviates from endogenous *hand*2 expression in the limb bud in that it is expressed throughout the entire lateral plate mesoderm-derived mesenchyme of the forelimb bud (with the exception of a small dorsal rim) but not the hindlimb bud (Ruest et al. 2003). As no expression was ever observed in myocytes, the *Hand*2-Cre transgene provides a useful marker for the lateral plate mesoderm-derived limb mesenchyme ('limb lateral plate mesoderm').

B Whole mount X-Gal staining of E10.0 embryos from a *Hand*2-Cre/ Rosa26Lac cross. Transgenic embryos (+/-) show the different expression domains of the *Hand*2-Cre transgene: In the first and second branchial arch (BA), in the heart (H) and in the forelimb but not the hindlimb bud (FLB, HLB). Expression in the anterior limb bud (black arrow) is excluded from a rim at the posterior side of the bud (dashed arrow). For comparison, a non-transgenic littermate (+/+). 2x magnification.

C Forelimb bud in higher magnification from the original publication (Ruest et al. 2003) demonstrating *Hand*2-Cre transgene expression throughout the forelimb bud (dotted yellow line, lb) with the exception of a small posterior domain. Also labelled is the heart (h).

D A newborn *Hand*2-Cre+/-;Rosa26EYFP-/- viewed under UV illumination under a dissecting microscope. Derivatives of the distal branchial arches (lower jaw, LJ), the forelimb bud (FL) and parts of the shoulder girdle are labelled. The proximal boundary of the limb lateral plate mesoderm is indicated by arrows.

a anterior, **FLB** forelimb bud, **h** heart, **HLB** hind limb bud, **lb** limb bud, **LJ** lower jaw, **LPM** lateral plate mesoderm, **p** posterior

3.3.3 Cell population boundaries, muscle attachment sites and the rule of connectivity

The boundaries between the different cell populations that contribute to head, neck and shoulder are without anatomical correlate. However, this does not reflect the absence of organisation, as genetically defined cell populations of the same origin stay connected throughout ontogeny[102]. Muscles play a particular role in this system, as the connective tissue of a muscle and its attachment originate from the same embryonic cell population. This applies to neural crest subpopulations[17] as well as cell populations at the neural crest/ mesoderm interface[122] and suggests that a 'rule of connectivity' is an integral part of the underlying bauplan of the organism. The muscle scaffold of head and neck shows a higher degree of evolutionary conservation than the associated skeletal elements[122] so that the interaction of cell populations at muscle attachment sites in this area is also of evolutionary relevance. The establishment of an attachment as the functional connection between muscle and skeleton requires the coordinated behaviour of muscle, tendon and bone progenitor cells but so far the process itself and the role of different cell populations in it are not well understood. Our current understanding is predominantly based on studies on limb muscles which initially develop as independent muscle and tendon progenitor cell populations before they interact at a later time-point in development[6]. Muscle positioning necessary for the attachment to the correct skeletal element is then achieved with help of another mesenchymal cell population under control of the canonical *Wnt* pathway[96,97]. However, this process seems more permissive than instructive, so that it is still unclear how the final attachment is established and in how far the observations made in limb muscles can be applied to other muscle groups.

Here, genetic lineage labelling of neural crest in combination with immuno-histochemistry and high resolution imaging is used to study the cellular, embryological and molecular characteristics of muscle attachment sites at the cryptic neural crest/ mesoderm interface at the anterior margin of the shoulder girdle.

3.4 Results

3.4.1 The participation of proximal limb elements in the formation of the shoulder girdle

As described in detail in Chapter 2, the *Hand*2-Cre transgene replicates *Hand*2 branchial arch expression and can be used to trace distal branchial arch neural crest populations. In addition and deviating from endogenous *Hand*2 expression, the 7.4kb *Hand*2-Cre transgene consistently labels the lateral plate mesoderm of the anterior limb bud at an early developmental stage[158]. This property of the transgene allows us to distinguish lateral plate mesoderm populations associated with the limb from trunk lateral plate mesoderm and to establish in this way the contribution of proximal limb elements to the mesodermal shoulder girdle (Figure 3.4 A, arrows in B indicate the proximal extension of the limb lateral plate mesoderm contribution as visible through the skin).

X-Gal staining of sections of the shoulder girdle of newborn *Hand*2-Cre$^{+/-}$; Rosa26LacZR$^{-/-}$ mice reveals a contribution of labelled cells to the upper part of the *manubrium sterni* (Figure 3.5). Despite the fact that groups of unlabelled cells are present within this labelled domain (white arrows in A and B), the domain boundary between the labelled and the unlabelled part of the manubrium is clear (black arrows in C, D). A distinct boundary also exists between the labelled part of the *manubrium sterni* and the articulating first rib (Figure 3.6 A, B). Cells labelled by the *Hand*2-Cre transgene do not seem to contribute to the ribs (shown here for the first and second rib); the labelling in the surrounding connective tissue is restricted to the area cranial and caudal to the first rib, reaching from below the clavicle (Figure 3.7) to the first rib (Figure 3.6 B) and the cranial half of the first intercostal muscle (Figure 3.6 C, E). Only very few positive cells are detected cranial to the second rib and even fewer below (Figure 3.6 F and data not shown). With the exception of a negligible number of cells, no labelling of the *Hand*2-Cre transgene can be found in the clavicle itself, independent of the medio-lateral position. However, the surrounding connective tissue close to the lower and slightly anterior edge of the clavicle is consistently labelled (Figure 3.7). This domain anterior to the clavicle is already established at E13 (Figure 3.8 A) and is

Figure 3.5- 3.8

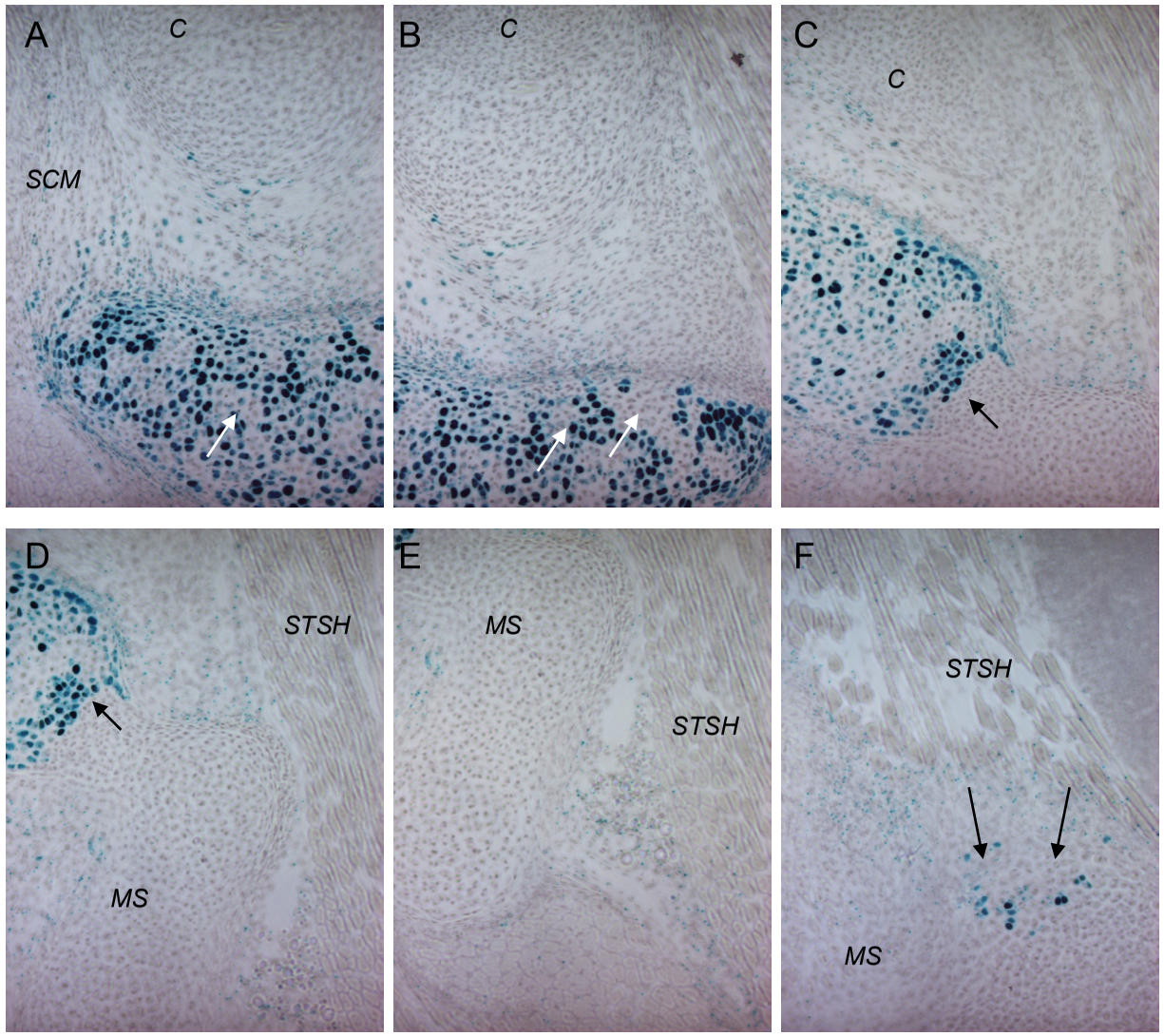
A
C
SCM
B
C
C
C
D
STSH
MS
E
MS
STSH
F
STSH
MS

P0

3.5

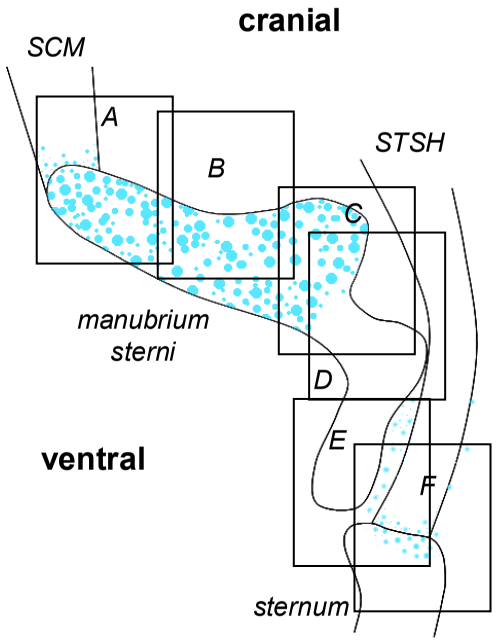
cranial
SCM
A
B
STSH
C
manubrium
sterni
D
ventral
E
F
sternum

10x

Figure 3.5 The *Hand*2-Cre transgene labels the upper part of the manubrium sterni

X-Gal staining of sagital sections of the sternal region of newborn *Hand*2-Cre+/-; Rosa26LacZR-/- mice (P0). Images are orientated with anterior to the left and cranial to the top as indicated on the cartoon to the right. Magnification: 10x.

Labelling by the *Hand*2-Cre transgene is restricted to the upper part of the manubrium sterni (**A**, **B**, **C**, **D**), with a clearly recognisable domain boundary (black arrow in **C**, **D**).

Despite a well-defined domain boundary, the domain of the *Hand*2-Cre transgene contains groups of unlabelled cells (white arrows in **A**, **B**).

A number of labelled cells can also be found in the otherwise unlabelled part of the manubrium, close to the insertion site of the sternothyroid/ sternohyoid (STSH) muscle (arrows in **F**).

C clavicle, ***MS*** manubrium sterni, ***SCM*** sternocleidomastoid muscle, ***STSH*** sternothyroid/ sternohyoid muscle

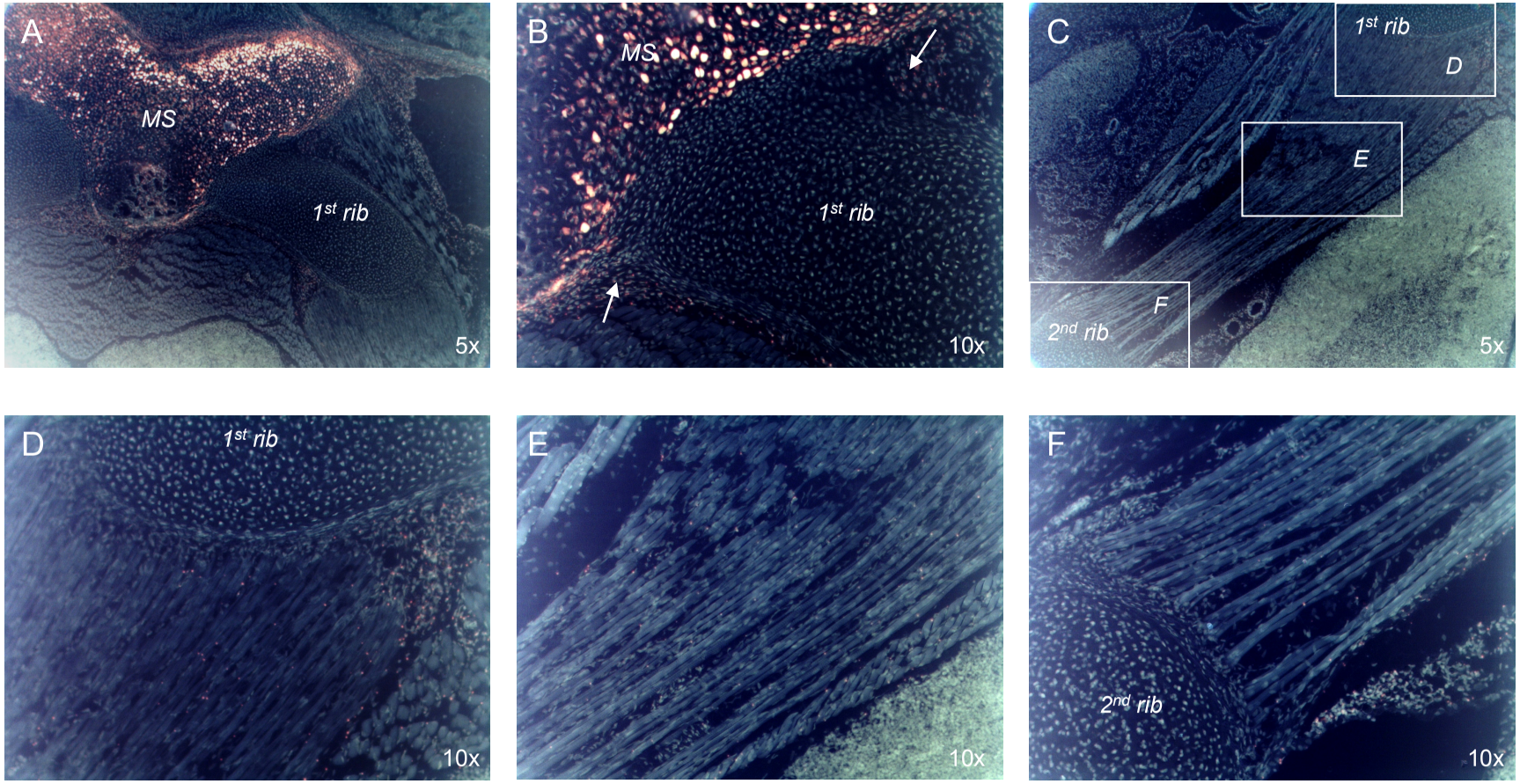
A
MS
1st rib
5x
B
MS
1st rib
10x
C
1st rib
D
E
F
2nd rib
5x
D
1st rib
10x
E
10x
F
2nd rib
10x

P0

Figure 3.6 The *Hand*2-Cre transgene labels the upper part of the manubrium sterni but not the first rib

X-Gal staining of frontal sections of the sternal region of newborn *Hand*2-Cre+/-; Rosa26LacZR-/- mice (P0). Light microscopic images are shown in inverted colours for better contrast (X-Gal staining appears reddish against a dark backdrop) and are orientated with cranial to the top. (**A**- **B**) first costo-sternal articulation and (**C- F**) first intercostal muscle.

A, **B** While the *Hand*2-Cre transgene labels the upper manubrium sterni (MS, **A**), no contribution of labelled cells is found in the first rib (**B**). However, positive cells are present in the connective tissue surrounding the first rib (arrows in **B**).

C- **F** In the first intercostal muscle, labelling by the *Hand*2-Cre transgene is restricted to the cranial side of that muscle facing the first rib (**C**, **D**) and fades out towards the middle (**E**). Only very few cells are found next to the muscle insertion at the second rib (**C**, **F**).

MS manubrium sterni

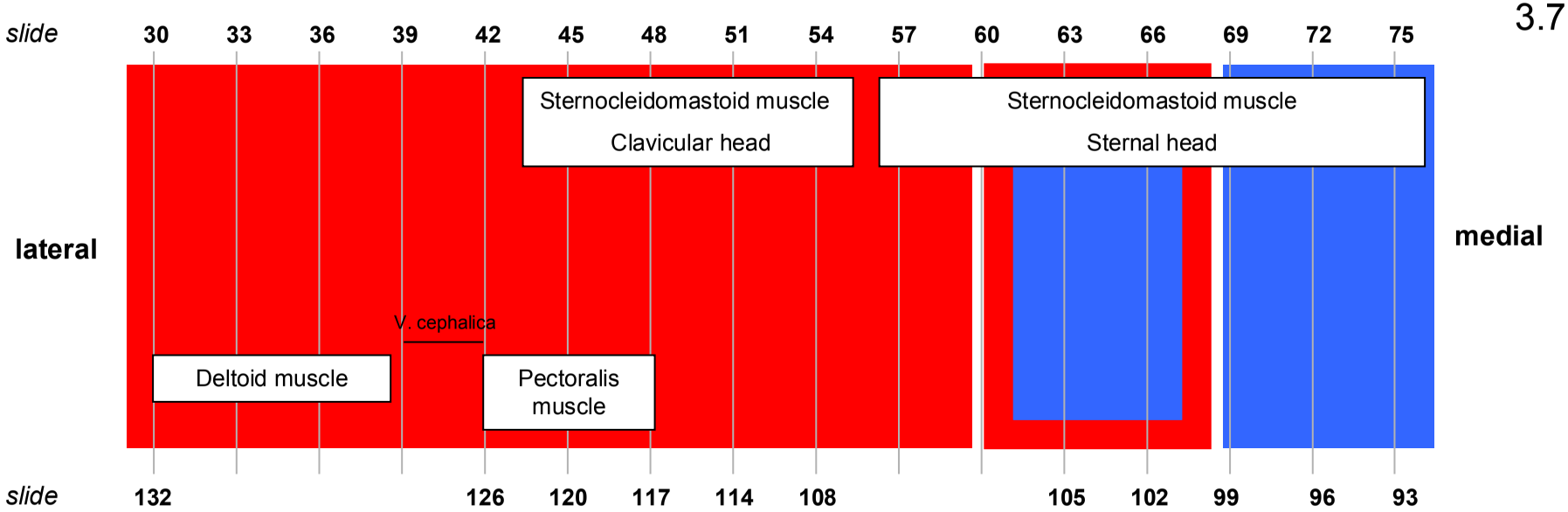

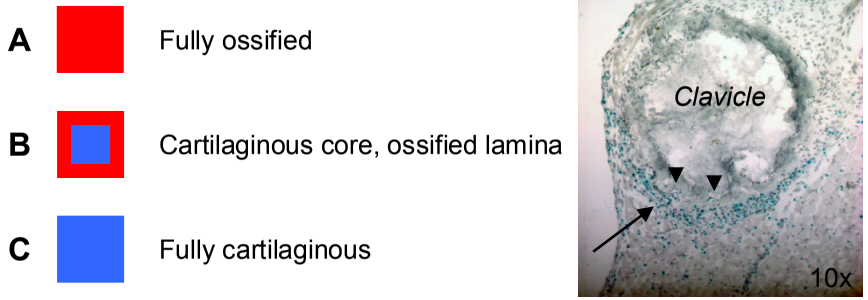

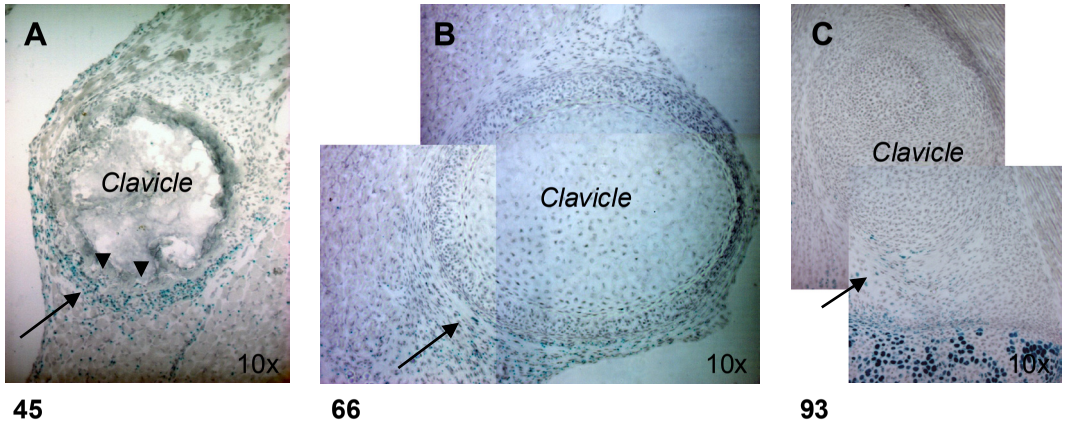

***Hand*2-Cre+/-, Rosa26LacZR-/-, P0**

Figure 3.7 The clavicle receives no contribution from cells labelled by the *Hand*2-Cre transgene

X-Gal staining of sagital sections of the clavicle of a newborn *Hand*2-Cre+/-; Rosa26LacZR-/- mouse (P0). The representation of the ossification status and the contribution of the *Hand*2-Cre transgene are based on a series of parallel sections through the left and right clavicles of a single specimen; the number of the slides are indicated. Examples for each of the three different ossification stages are shown: **A**, **B**, **C** correspond to section 45, 66, 93 respectively, 10x magnification.

A At the time of birth, more than the lateral half of the clavicle was fully ossified.

B Towards the centre of the clavicle, dermal ossification was seen around a cartilaginous core.

C The most proximal/ ventral part of the clavicle was still purely cartilaginous at this time-point of development.

Cells labelled by the *Hand*2-Cre transgene were hardly ever detected within the clavicle (e.g. arrowheads in **A**). However, the surrounding connective tissue showed labelling at the lower and lower anterior edge of the clavicle (arrows in **A**- **C**).

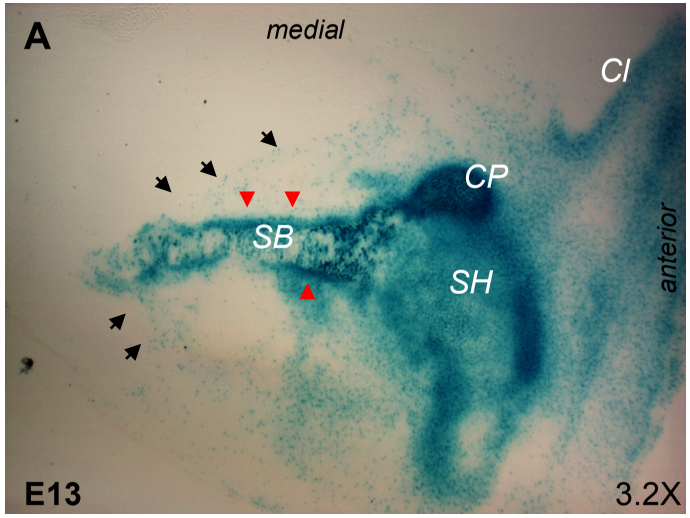

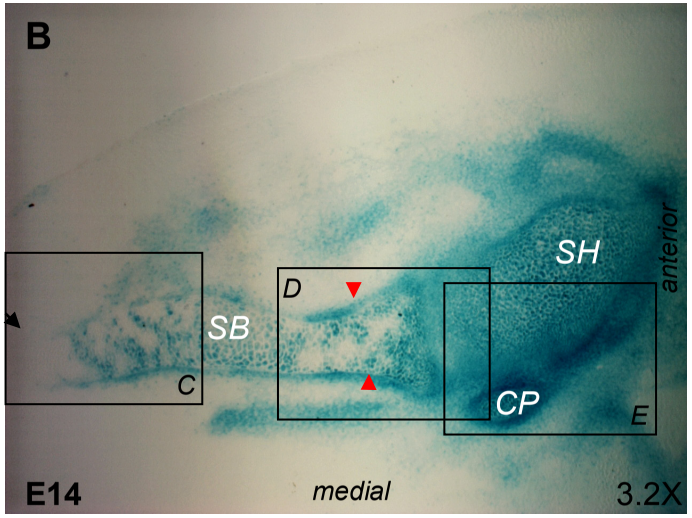

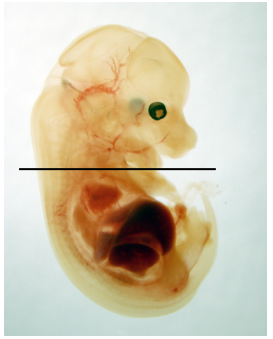

sectioning plane-
transverse

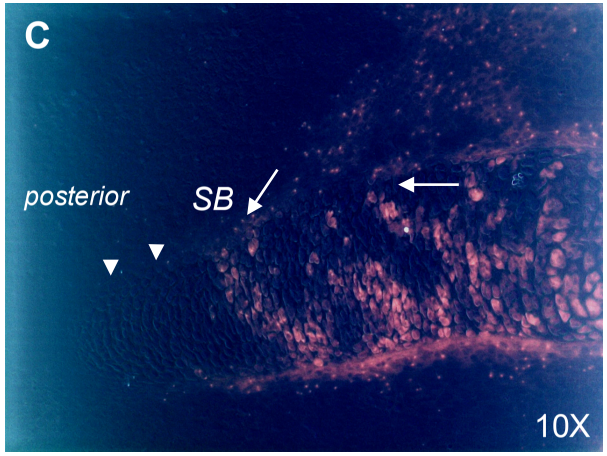

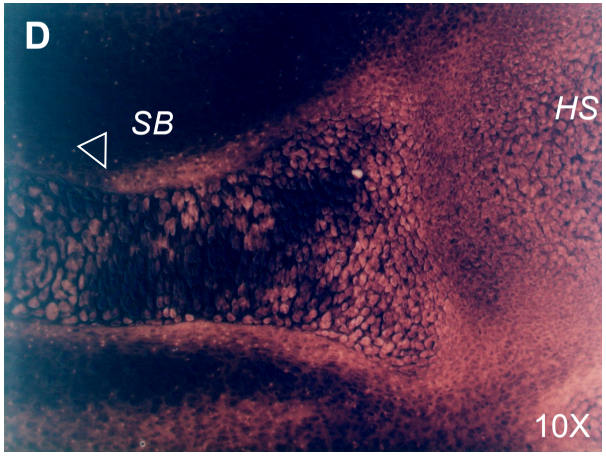

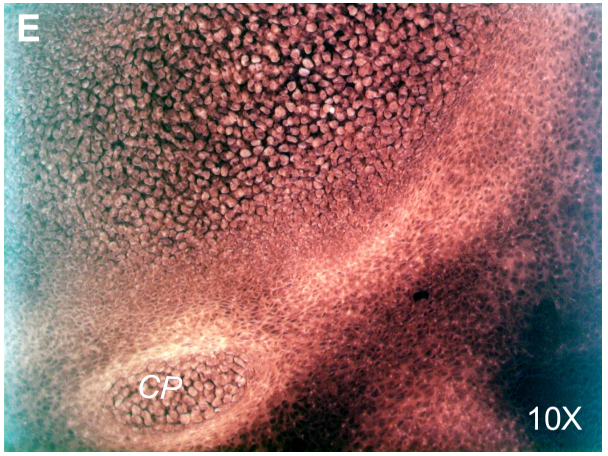

Figure 3.8 The development of the shoulder blade in the *Hand*2-Cre mouse

X-Gal staining on transverse sections of E13 (**A**) and E14 (**B**- **E**) *Hand*2-Cre+/-; Rosa26LacZR-/- embryos. Images **C**- **E** are shown in inverted colours for better contrast (X-Gal staining appears reddish against a dark backdrop).

A At E13, the shape of the future scapula is recognisable as mesenchymal condensation within an area labelled by the *Hand*2-Cre transgene. The coracoid process (CP) and the head of the scapula (SH) are entirely labelled while the scapular blade develops in a triangle of positive connective tissue (designated by black arrowheads) but is not labelled throughout. Cells labelled by the *Hand*2-Cre transgene locate rather to the outside of the blade than to the inside (red arrowheads in **A**, also **B**).

B- **E** At E14, the coracoid process and the scapular head are entirely composed of labelled cells (**B**, **E**) while the middle part of the blade is only strongly labelled on the outside (**B**, **D**). Towards the posterior end of the blade, labelled cell populations alternate with unlabelled ones, creating a stripe pattern (**B**, **C**). Labelling does not end at the outside of the blade but continues into the surrounding mesenchyme (arrows in **C**).

Cl clavicle*,* ***CP*** coracoid process*,* ***SB*** *scapular* blade*,* ***SH*** scapular head

continuous with the area in which the shoulder blade forms. At this time-point, the head of the scapula, the coracoid and the scapular blade are clearly identifiable and appear to develop in a triangle of positive connective tissue (black arrows in Figure 3.8 A). While the scapular head and the coracoid are fully labelled (A, B, E), the situation is different for the blade: early *Hand*2-Cre transgene labelling is strong on the outer cranial part of the blade (red arrowheads in A and B, also D) while the inside of the blade is unlabelled. At E14, the external labelling continues on the medial side and close to the head on the lateral side (empty triangle in D). Towards its dorsal end, the scapular blade shows a stripy pattern of labelled and unlabelled domains (C) that interestingly continue into the connective tissue on the lateral side of the blade (arrows in C). The dorsal-most edge of the blade is entirely unlabelled (arrowheads in C). At birth, the situation has changed and the previously entirely labelled coracoid now shows a considerable proportion of unlabelled cells (Figure 3.9 B). The acromion only sporadically contains labelled cells (same Figure, A). In the now ossified blade of the scapula, positive cells predominantly localise to the outer side of the element (arrows in C1 and C2). Additionally, scattered cells can be found within the blade and also within adjacent muscles (arrowheads in C1 and C2). In the caudal and still cartilaginous part of the scapular blade, we find a stripe pattern of labelled and unlabelled cells but labelling is absent form the dorsal-most edge (D, arrow in D1). Labelling in the blade is strongest ventrally and cranially, especially in the coracoid and the scapular head, considerably less pronounced in the caudal part of the blade and virtually absent from the dorsal edge (summarised in Figure 3.10).

3.4.2 The muscle connective tissue in the shoulder girdle reflects the mixed labelling pattern of the skeletal elements

The functionality of the mammalian shoulder region relies heavily on muscles and labelling of the *Hand*2-Cre transgene was not restricted to the skeletal elements of the region but extended into the surrounding mesenchyme, outlining the course of muscles (e.g. Figure 3.8). The muscles of the shoulder region where therefore analysed on sections (in all three orientations: frontal, transverse and sagital) of newborn *Hand*2-

Figure 3.9- 3.10

3.9 overview details

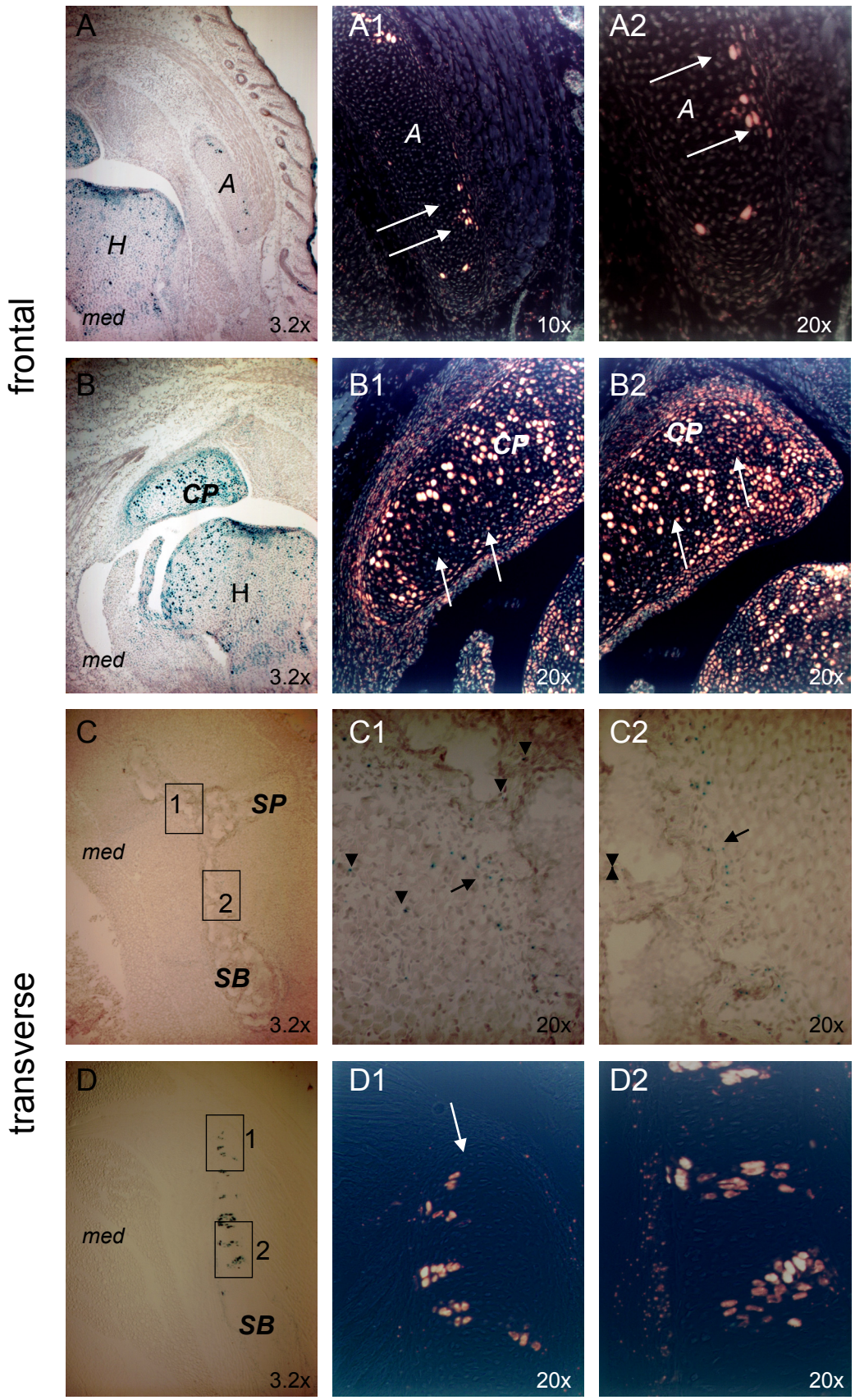

Figure 3.9 The shoulder blade in the newborn *Hand*2-Cre mouse

X-Gal staining of frontal (**A**, **B**) and transverse (**C**, **D**) sections of the shoulder region of newborn *Hand*2-Cre+/-; Rosa26LacZR-/- mice (P0). Areas are shown in overview (left column) and in detail (middle and right column).

At birth, the staining pattern within the scapula has changed in comparison with earlier stages of development (also see Figure 3.7).

A Only single cells labelled by the *Hand*2-Cre transgene can be found within the acromion (arrows in A1 and A2).

B The coracoid is still predominantly composed of labelled cells but now also shows groups of unlabelled cells (arrows in B1 and B2). The humerus (H) equally contains a mixture of labelled and unlabelled cells.

C At the height of the scapular spine, labelled cells are scattered throughtout the scapular blade but mainly localise to the outside of the element (C1 and C2, arrows).

D In the caudal and cartilaginous part of the blade, stripes of labelled and unlabelled cells are seen, similar to the ones observed at earlier stages (Figure 3.7).

A acromion***, H*** humerus, ***SB*** scapular blade, ***SP*** scapular spine

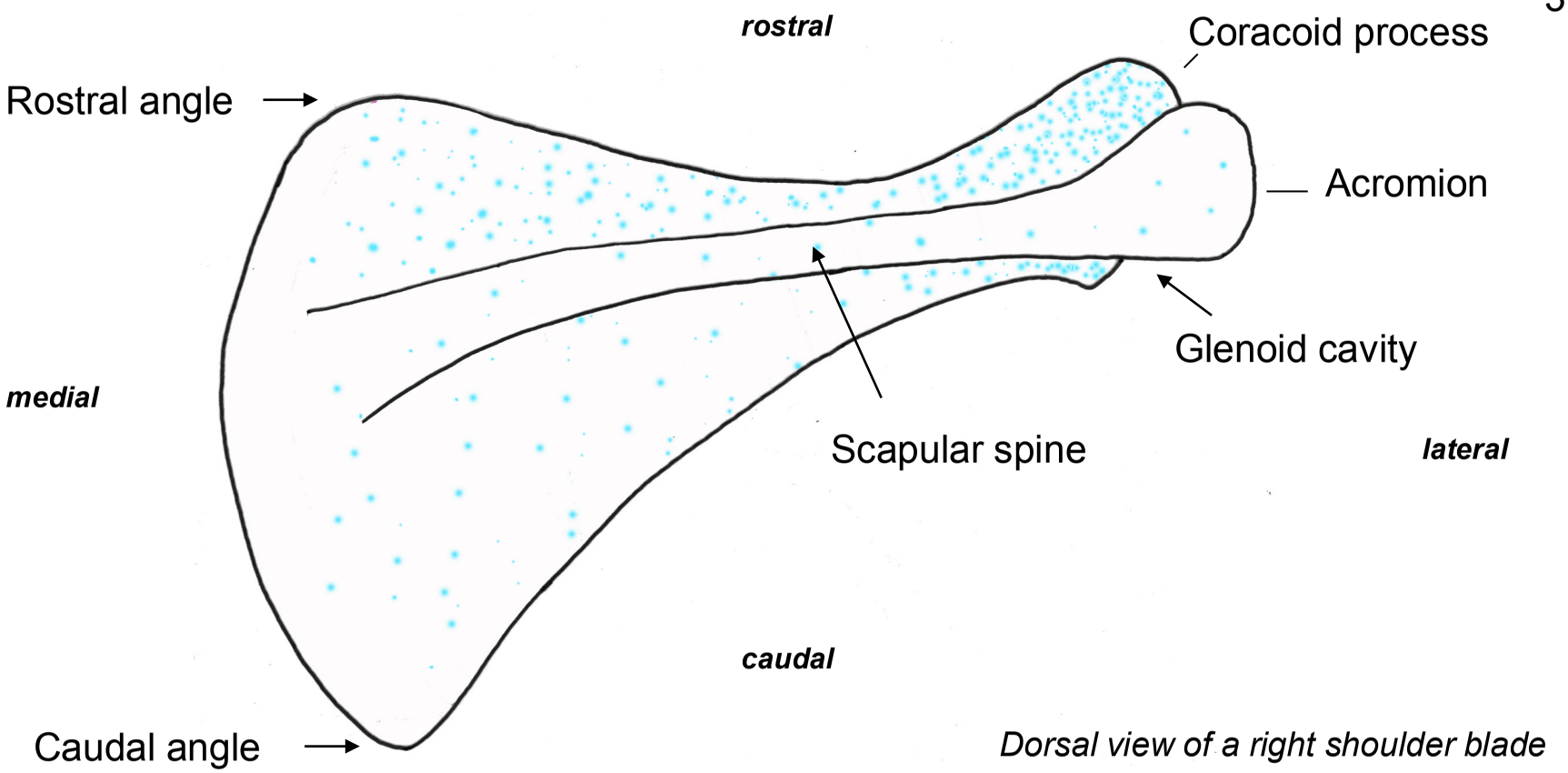

Figure 3.10 Schematic representation of shoulder blade labelling in the *Hand*2-Cre+/-; Rosa26LacZR-/- mouse
No labelling is found on the medial side of the shoulder blade but labeled cells are dispersed throughout the rest of the shoulder blade. A higher proportion of positive cells is found in the coracoid process; the acromion is hardly labelled.

$Cre^{+/-}$; Rosa26LacZR$^{-/-}$ mice with respect to the contribution of connective tissue labelled by the *Hand*2-Cre transgene; the results are schematically summarized in Figure 3.11. As a rule, the contribution of labelled connective tissue to the muscles of the shoulder region was generally only minor, 'fuzzy' and not clearly restricted to a certain part of the muscle (see Figure 3.9 C1 for the example of the subscapularis muscle). All muscles attaching at the scapular blade- with the exception of the three muscles inserting along the dorsal edge (M. serratus (15) on the internal (costal) side, M. levator scapulae (1) and Mm. rhomboidei (2) on the outer side, red in Figure 3.10)- received some contribution of labelled cells. In the case of the M. omohyoideus (9) and M. trapezius (7), this was limited to some cells at the insertion point of the muscle (green). Muscles attaching to the caudal edge of the clavicle contained labelled connective tissue (M. subclavius (10) and M. pectoralis (11)), consistent with the previously described presence of labelled connective tissue on the caudal side of the clavicle (Figure 3.8). The sternocleidomastoid muscle inserts with a single head at the mastoid process at the base of the skull but originates from two separate heads, a lateral head from the clavicle and a medial head from the sternum. While the lateral clavicular origin shows no labelling by the *Hand*2-Cre transgene (12), the medial sternal insertion is peculiar in so far in that the boundary of the labelled domain coincides sharply with the muscle attachment (Figure 3.12 A- B, arrows in B). With the exception of the lateral side of the attachment (arrowheads in B, also Figure 3.5 A), hardly any labelled cells are found within the connective tissue of the sternocleidomastoid muscle and the boundary at the sternal attachment site appears very sharp. This stands in contrast with previous findings (e.g. in the masticatory muscles, Figure 2.21) where *Hand*2-Cre transgene labelling always spans the attachment site according to the rule of muscle connectivity that states that muscle connective tissue and its insertion site share the same embryonic origin[102,122].

The interesting observation made at the sternal head of the sternocleidomastoid muscle was the starting point of an investigation into the morphology and embryological origin of the attachment sites of the sternocleidomastoid muscle; the results will be content of the next sections of this chapter.

The complete analysis of the distribution of labelled connective tissue in the muscles of the *Hand*2-Cre mouse can be found in the Appendix.

Figure 3.11- 3.12

1 *M. levator scapulae*

2 *Mm. rhomboidei*

3 *M. supraspinatus*

4 *M. infraspinatus*

5 + 6 *Mm. teres minor et major*

7a *M. trapezius; spinal insertion*

7b *M. trapezius; clavicular insertion*

8 *M. deltoideus*

9 *M. omohyoideus*

10 *M. subclavius*

11 *M. pectoralis*

12 *M. sternocleidomastoideus, clavicular insertion*

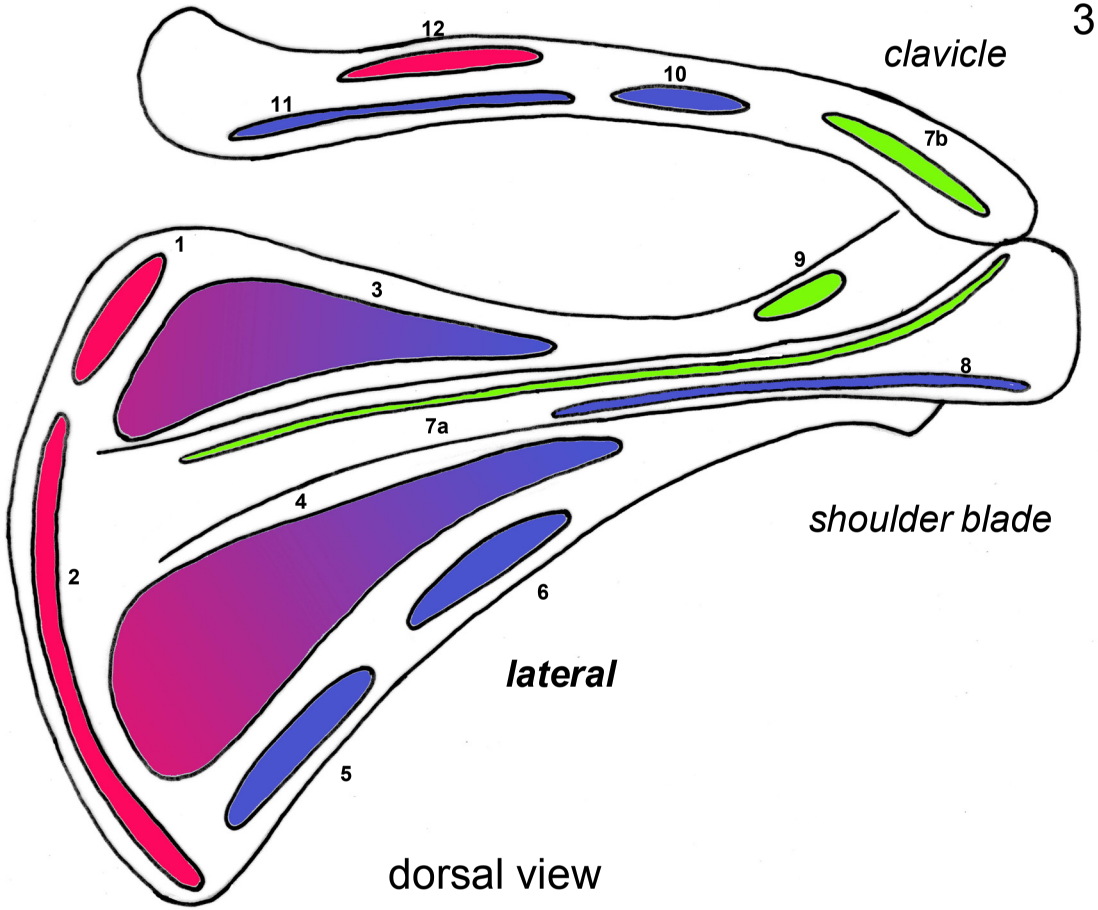

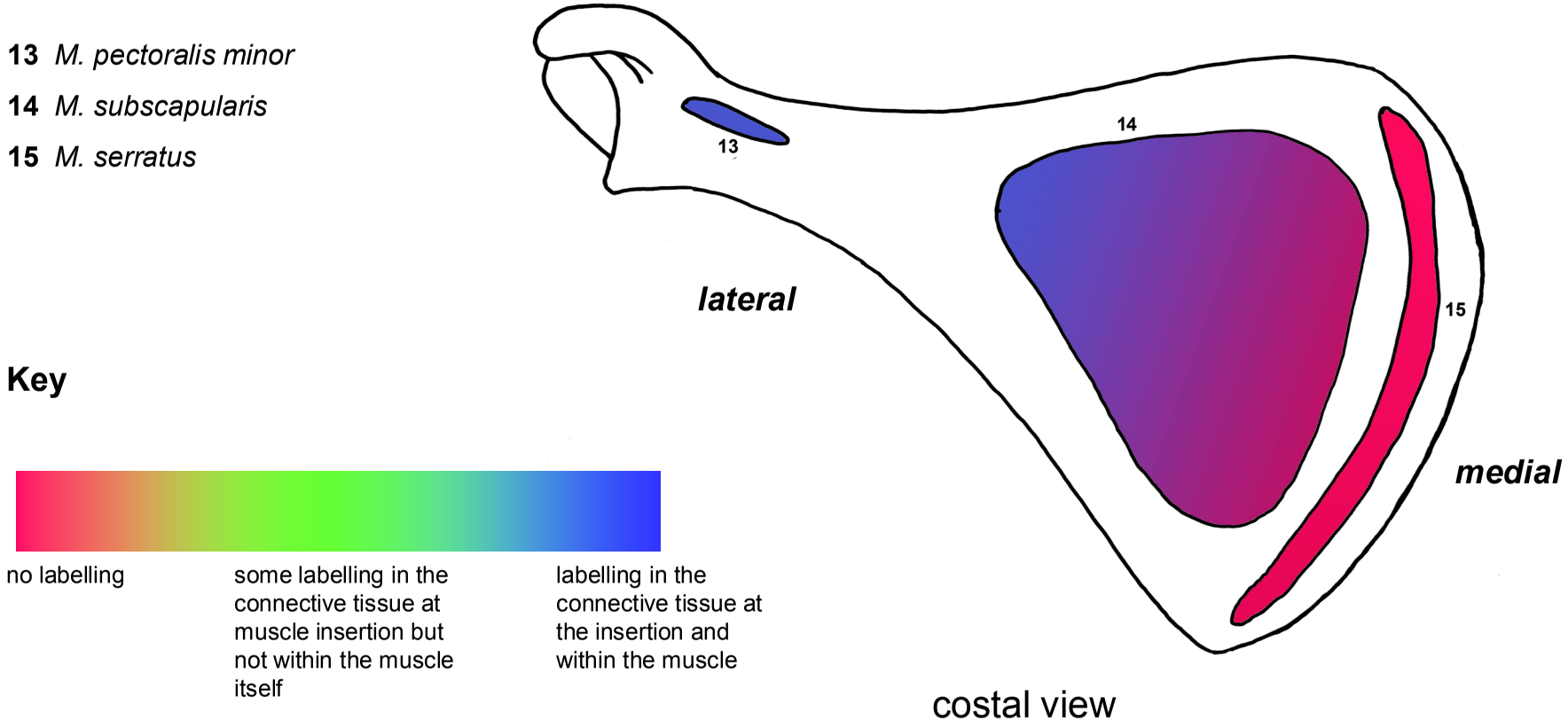

Figure 3.11 Summary of labelling in muscle attachment sites in the shoulder girdle of the *Hand*2-Cre+/-; Rosa26LacZR-/- mouse

3.11

Hand2-Cre

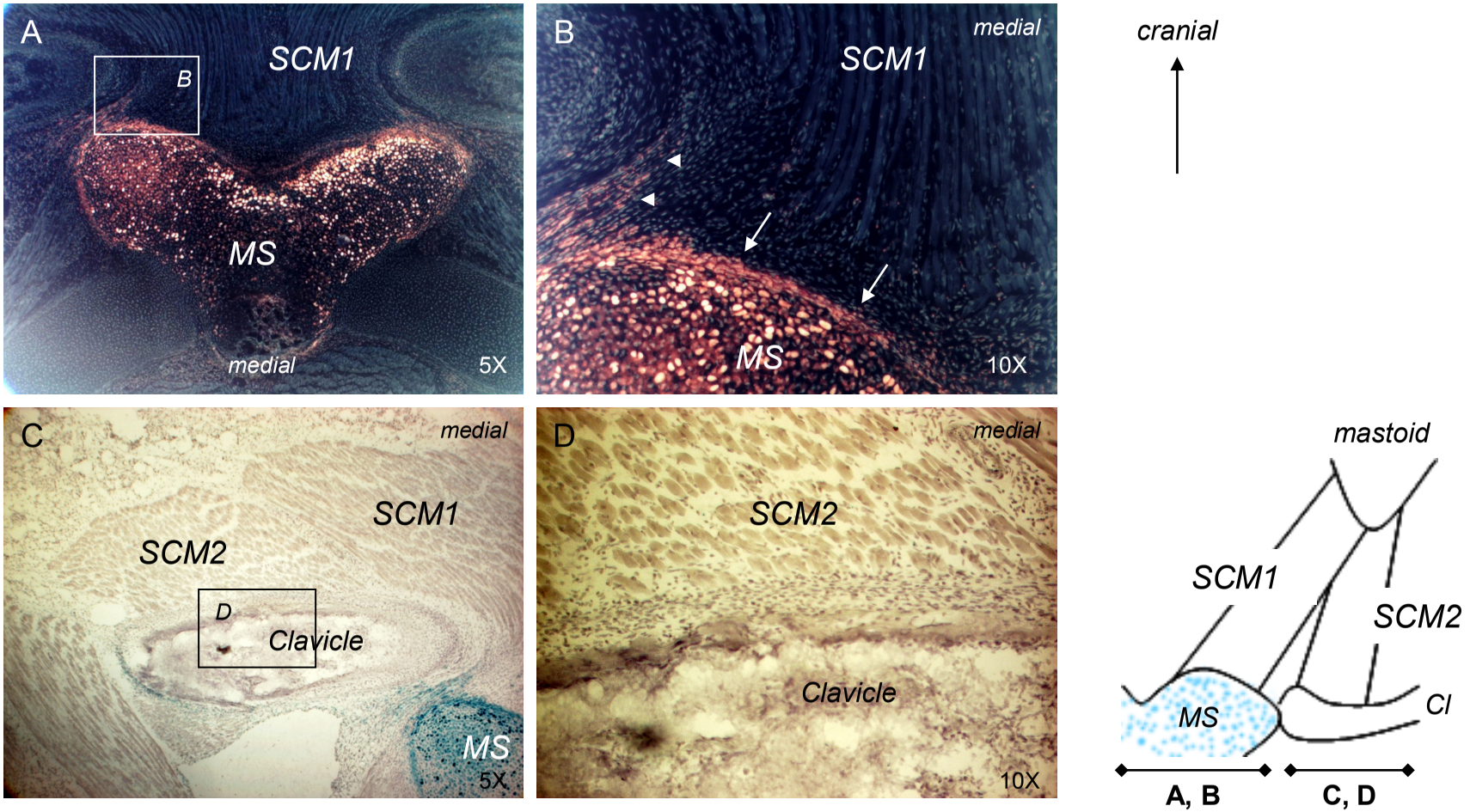
A
SCM1
B
MS
medial
5X
B
medial
SCM1
MS
10X
C
medial
SCM1
SCM2
D
Clavicle
MS
5X
D
medial
SCM2
Clavicle
10X
cranial
mastoid
SCM1
SCM2
MS
Cl
A, B
C, D

Figure 3.12 The attachment of the sternocleidomastoid muscle to the shoulder girdle

X-Gal staining on frontal (A, B, E, F) sections of newborn *Hand*2-Cre+/-; Rosa26LacZR-/- mice. **A**, **B** Images are shown in inverted colours for better contrast (X-Gal staining appears reddish against a dark backdrop).

The sternal (**A- B**) but not the clavicular attachment site (**C- D**) of the sternocleidomastoid muscle on to the shoulder girdle is labelled by the *Hand*2-Cre transgene.

The muscle connective tissue of the SCM is unlabelled with the exception of cells at the lateral edge of the sternal attachment (arrowheads in **B**). The boundary between labelled and unlabelled tissue apparently coincides with the boundary between muscle and *manubrium sterni* (**B**).

Cl *clavicle,* ***MS*** *manubrium sterni,* ***SCM1*** sternocleidomastoid muscle, sternal head, ***SCM2*** sternocleidomastoid muscle, clavicular head

3.4.3 The sternal attachment of the sternocleidomastoid muscle- an exception to the 'connectivity rule'?

3.4.3.1 Background

Although the boundaries between the different cell populations that contribute to the head and the neck find no reflection in anatomical boundaries, cells belonging to the same genetically defined population will stay connected throughout ontogeny[102]. Following this rule of connectivity, the attachment site of a cranial muscle is thereby composed of cells of the same embryonic origin as the muscle connective tissue (but not the muscle itself) and so far, there is no known exception to that rule[102,122]. During the analysis of the *Hand*2-Cre mouse, the sternal origin of the sternocleidomastoid muscle attracted our attention, as a muscle with entirely unlabelled connective tissue (the sternocleidomastoid muscle) appeared to attach to a labelled domain (the upper part of the sternum, the *manubrium sterni*); this suggests the interface of two genetically distinct cell populations (Figure 3.12).

The sternocleidomastoid muscle (SCM) originates with one head from the clavicle and one head from the *manubrium sterni* and inserts at the mastoid process. As a coracobranchial muscle, the connective tissue of the SCM is of neural crest origin. Although the muscle originates and inserts in mesodermal territory, the attachment sites are neural crest-derived[122]. In the *Hand*2-Cre mouse, no transgene labelling is detected in the SCM clavicular head nor the clavicle (Figure 3.12). In contrast, the equally unlabelled SCM sternal head originates from a labelled *manubrium sterni*. With the exception of labelling at the lateral side of the attachment (arrowheads in B), the domain boundary defined by the *Hand*2-Cre transgene apparently corresponds to the skeletal side of the muscle attachment.

The correspondence of the boundary between two genetically distinct cell populations to a muscle attachment site contradicts the 'connectivity rule' as well as the previously reported neural crest contribution to the sternum[102,122] (Figure 3.13A). An hypothesis in accordance with the 'connectivity rule' was therefore that the neural crest/ mesoderm

Figure 3.13

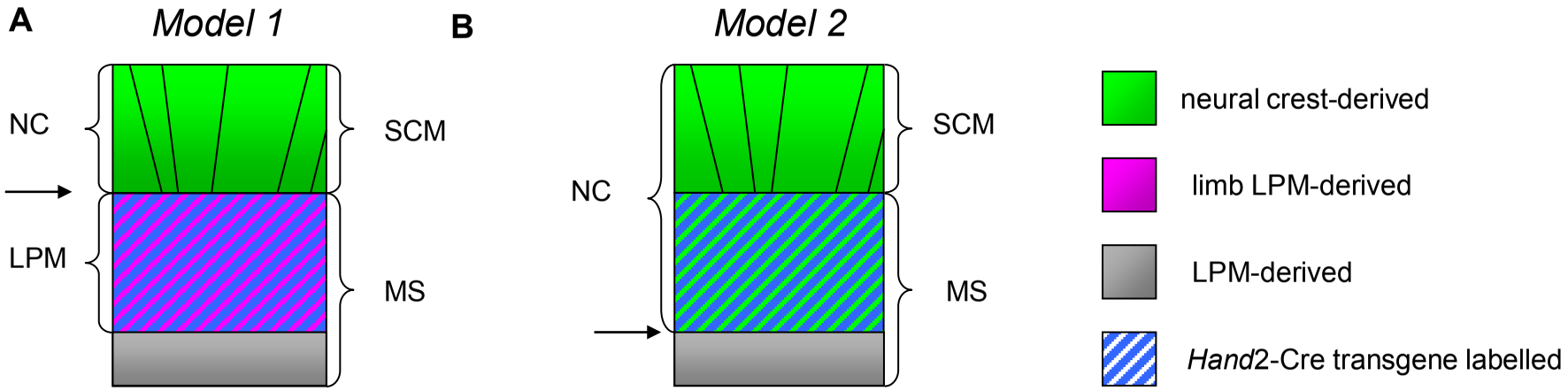

Figure 3.13 Working hypotheses

(A) Model 1: The boundary between domains originating from either the neural crest (green) or limb lateral plate mesoderm (magenta) as labelled by the *Hand*2-Cre transgene (blue stripes) corresponds to the anatomical boundary between the sternocleidomastoid muscle and the *manubrium sterni*, contradicting the 'connectivity rule'.

(B) Model 2: The boundary between the domains derived from neural crest and lateral plate mesoderm lies within the manubrium sterni. This model assumes the activity of the *Hand*2-Cre transgene in caudal distal neural crest and could indicate a potential role for *Hand*2 in the formation of the SCM attachment.

LPM lateral plate mesoderm ***MS*** *manubrium sterni*, ***NC*** neural crest, ***SCM*** sternocleidomastoid muscle

boundary lies within the *manubrium sterni* (Figure 3.13 B). In this scenario, the domain labelled by the *Hand*2-Cre transgene would correspond to a caudal distal brachial arch population (the function of the *Hand*2-Cre transgene in posterior neural crest was never thoroughly investigated, personal communication of D. Clouthier). *Hand*2 belongs to the family of bHLH transcription factors; considering the fact that another member of the group, *Scleraxis*, has been shown to crucially control tendon development[130,164], it would be conceivable that *Hand*2 plays a specific role in the formation of the sternal attachment of the sternocleidomastoid muscle.
The sternal origin of the sternocleidomastoid muscle was therefore analysed in detail regarding the cellular and embryological characteristics of the attachment site, in particular the relationship between attachment fibres and the periost. The potential role of *Hand*2 in posterior neural crest for the establishment of the sternal attachment of the sternocleidomastoid muscle was further investigated in a mouse with a neural-crest specific ablation of *Hand*2 function.

3.4.3.2 The sternal attachment of the sternocleidomastoid muscle is limited to a single layer of cells

The outer-most layers of cartilaginous and osseous elements are fibrous and called the perichondrium and periost respectively. A connection between a muscle and a skeletal element therefore by necessity also involves the perichondrium/ periost as intermediate and attachment layer. To gain a better understanding of the nature of the sternocleidomastoid muscle attachment to the sternum, we investigated the spatial relationship between muscle attachment fibres and the sternal perichondrium by immunohistochemistry for perichondrial and fibrillar markers and high resolution imaging.
A recent microarray study supported by RNA *in situ* hybridisation of candidate genes was able to identify specific genetic markers for the perichondrium and the periost of avian long bones[14]. Decorin, cellular retinoic acid binding protein 1 (CRABP1) and Undulin were identified as specific markers for the inner (Decorin) and outer (CRABPI) perichondrium or as a general perichondrial/ periosteal marker (Undulin). The validity

of these markers for the murine head/ shoulder region was tested by immunohistochemistry on sections of the cranial region (Figure 3.14, details about the antibodies used can be found under 'Materials and Methods', section 7.6.4.2). Decorin labels perichondria in the head region (brain capsule, styloid process, hyoid, Figure 3.14 A and B). Strong immunoreactivity is detectable in the perichondrial lining but can also be seen in single cells within the cartilage, usually in parallel to the perichondrium. The styloid process appears fully composed of Decorin positive cells which is most likely a consequence of the small diameter of the element as the larger hyoid (B) only shows immunoreactivity in the outer cell layer. The perichondria of the brain case, the styloid process and Meckel's cartilage shows strong immunoreactivity for CRABP1 (C, D). CRABP1 is also expressed in the forming bone of the lower jaw (arrow, D). In areas with ongoing endochondral ossification, Undulin (also: Collagen XIV) is present in a continuity between periost and perichondrium (E, rib). As a Collagen, Undulin is not restricted to skeletal structures but also forms an important component of e.g. the dermis (F).

Decorin, CRABP1 and Undulin therefore represent generally valid perichondrial marker but have also been described as expressed in tendons[130,215], similar to another perichondrial marker, Ephrin Receptor A4 (EphA4)[130] and were used for further analysis. The fibres of the attachment of the sternocleidomastoid muscle were visualised with antibodies against Collagen I (main component of tendinous collagenous matrix and general marker for tendons[14]), Collagen III (expressed in epi- and endotenon, regulates fibrillogenesis of Collagen I fibers[18,105]) and Periostin (originally identified as periostal marker[84] but also expressed in attachment fibres). Independent of the fibrillar marker used, the attachment of the sternocleidomastoid muscle on to the sternum is surprisingly superficial. Attachment fibres never reach into the cartilage; Collagen III fibres end blind on the outside of the attachment (Collagen III, C) while Periostin and Collagen I fibres connect to an interwoven perichondrium (Periostin, A and Collagen I, D). Decorin as 'perichondrial' marker is also expressed by the attaching tendon cells and a row of cartilage cells below the attachment, thereby labelling cells on both sides of the perichondrium and defining a molecular 'attachment zone'(Figure 3.15 A, B arrows). Nested within this Decorin attachment zone, Ephrin Receptor A4 (EphA4) is expressed in the attachment fibres and the outer cell layer of the perichondrium. Even further restricted, CRABP1 only labels attachment fibres and a very superficial layer of the perichondrium (D, E). The relationship between the different marker domains and

Figure 3.14- 3.16

3.14

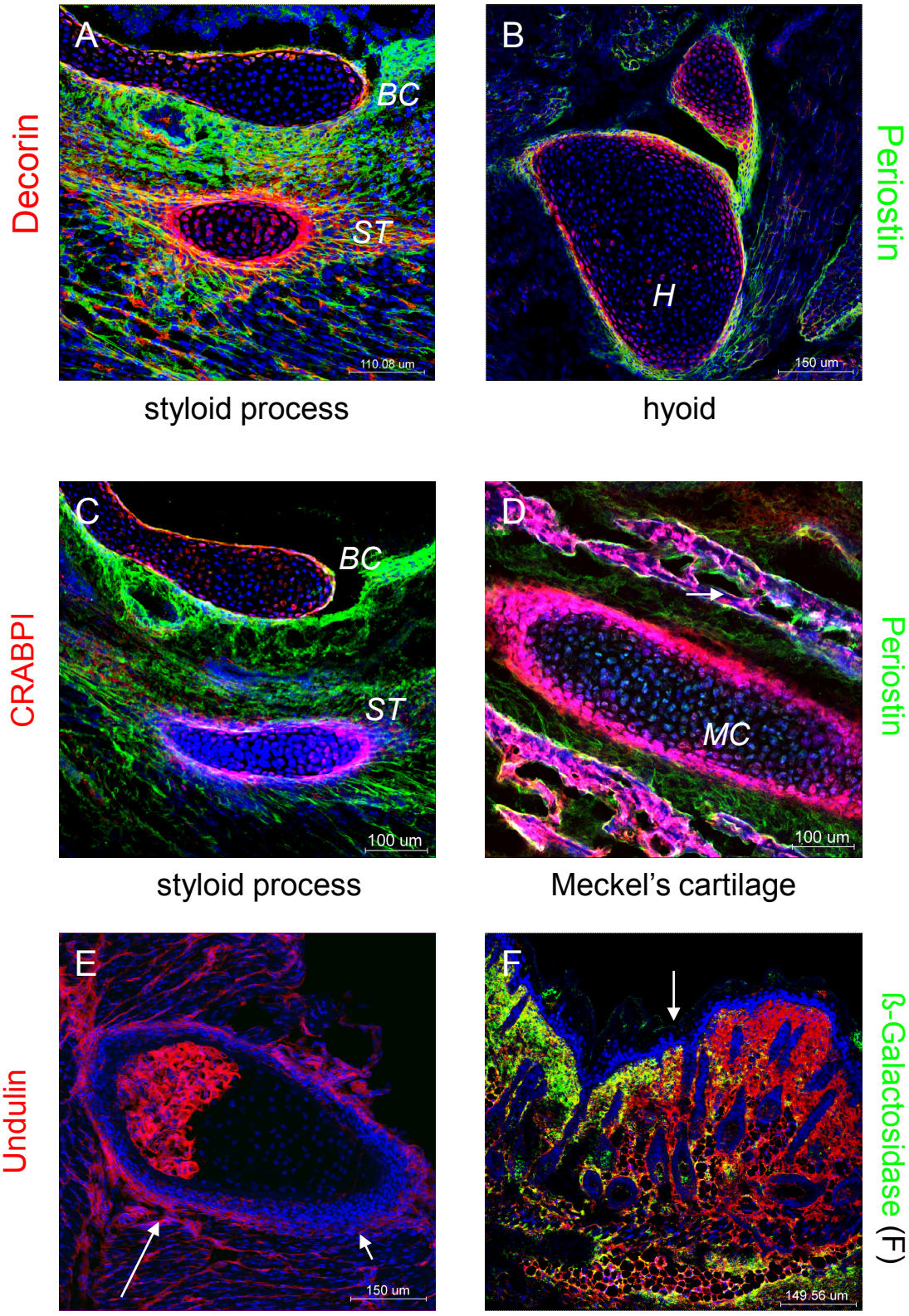
A
BC
ST
110.08 um
B
H
150 um
Decorin
Periostin
styloid process
hyoid
C
BC
ST
100 um
D
MC
100 um
CRABPI
Periostin
styloid process
Meckel's cartilage
E
150 um
F
149.56 um
Undulin
ß-Galactosidase (F)
rib
dermis

Figure 3.14 The general validity of perichondrial markers

IHC* for different perichondrial markers (Decorin red in **A**, **B**, CRABPI red in **C**, **D**, Undulin red **E**, **F**) and ß-Galactosidase (**F**, green) on sagital sections of E18 *Wnt*1-Cre+/-; Rosa26LacZR embryos (**A**, **C** styloid process, **B** hyoid, **D** Meckel's cartilage, **E** rib, **F** dermis).

A Decorin labels the perichondrium of cartilaginous structures irrespective of their embryological origin, here the mesodermal brain capsule (BC) and the neural crest-derived styloid (ST). In addition, single Decorin positive cells are found within the cartilage in parallel to the overlying perichondrium.

B Nearly complete labelling of the styloid process in (**A**) is most likely a consequence of the small diameter of the element as the larger hyoid only shows periochondrial labelling below a Periostin envelope.

C CRABPI labels- similarly to Decorin- the perichondrium of both the brain capsule an the styloid process.

D The perichondrium of Meckel's cartilage (MC) shows particulary strong labelling for CRABPI. It is noteworthy that CRABPI is also expressed in bone (arrow in the lower jaw).

E A section through a rib undergoing endochondral ossification demonstrates the continuity of Undulin expression in the perichondrium (short arrow) and the periost (long arrow).

F Undulin is not specific to the periosteal/ perichondrial layer but also strongly expressed in the dermis, here the transition of neural crest (*Wnt*1-Cre, ß-Galactosidase is green, yellow in overlay with red from Decorin expression) to mesoderm-derived dermis in the neck.

BC brain capsule, ***H*** hyoid, ***MC*** Meckel's cartilage, ***SP*** styloid process

* IHC was performed according to standardized conditions; a detailed description of conditions and antibodies (primary and secondary) can be found in the relevant section under 'Materials and Methods' (Chapter 7.5.4).

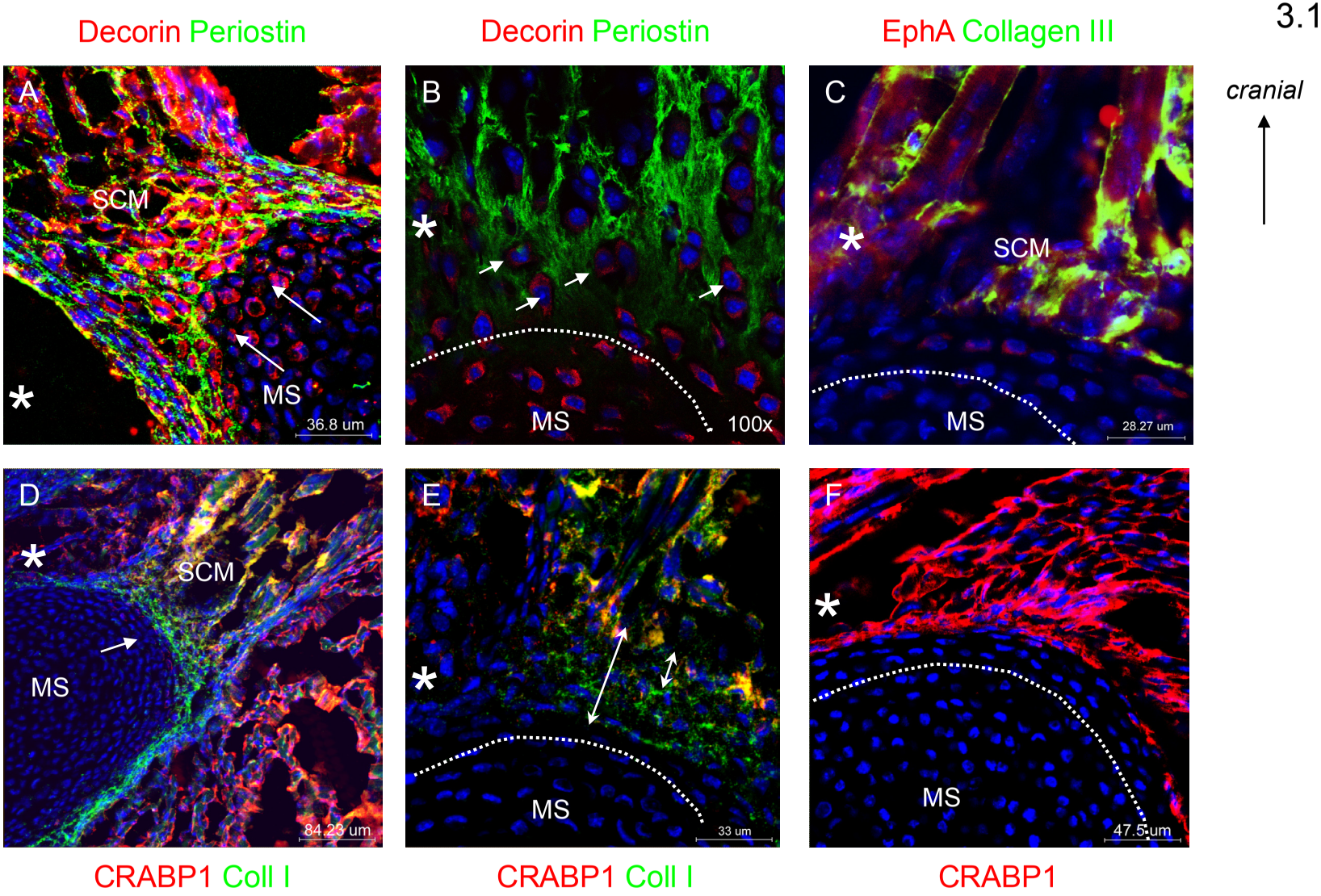
Decorin Periostin
Decorin Periostin
EphA Collagen III
cranial
A
SCM
MS
36.8 um
B
MS
100x
C
SCM
MS
28.27 um
D
SCM
MS
84.23 um
E
MS
33 um
F
MS
47.5 um
CRABP1 Coll I
CRABP1 Coll I
CRABP1

Figure 3.15 The sternocleidomastoid muscle only inserts at the outer-most cell layer of the sternal perichondrium

IHC* on sagital sections of the sternal region for Decorin and Periostin (**A**), Ephrin Receptor A and Collagen III (**B**) and CRABPI and Collagen I (**C**), nuclear counterstain: DAPI (blue). Confocal images show the insertion point of the sternocleidomastoid muscle (SCM) onto the *manubrium sterni* (MS) and are orientated with cranial to the top, the ventral side of the specimen is marked with an asterisk. The dotted lines in **B**, **C**, **E**, **F** indicate the transition between cells with elongated nuclei most likely belonging to the periost to cells with round nuclei belonging to the cartilaginous matrix of the *manubrium sterni*.

Sternocleidomastoid muscle attachment fibres (labelled with Periostin, **A**, Collagen III, **C**, Collagen I, **D**- **E**) only attach to the very outside of the sternal perichondrium, either ending blind (Collagen III, **B**) or linked with the woven perichondrium (Periostin, **A**, and Collagen I, **C**). Decorin (**A**, **B**), Ephrin A (**C**), Collagen I (**D**- **F**) and CRABPI (**D**- **F**) label attachment fibres as well as a varying proportion of the perichondrial layer.

A, **B** Decorin can be found below the fibre attachment (arrows in **A**) but also in the tendon cells making up the attachment (**B**, a single optical section in high resolution, arrows) and below the perichondrial layer within the cartilaginous matrix.

C Ephrin Receptor A is diffusely expressed in the attachment fibres and in single superficial cells of the perichondrium, but does not extend into the cartilaginous matrix.

D- **F** Collagen I labels the perichondrium (**D**, long double arrow in **E**) as well as attachment fibres. CRABP1 labels attachment fibres but only the most superficial layer of the periost (short double arrow in **E** and **F**).

MS *manubrium sterni*, ***SCM*** sternocleidomastoid muscle

* IHC was performed according to standardized conditions; a detailed description of conditions and antibodies (primary and secondary) can be found in the relevant section under ‘Materials and Methods’ (Chapter 7.5.4).

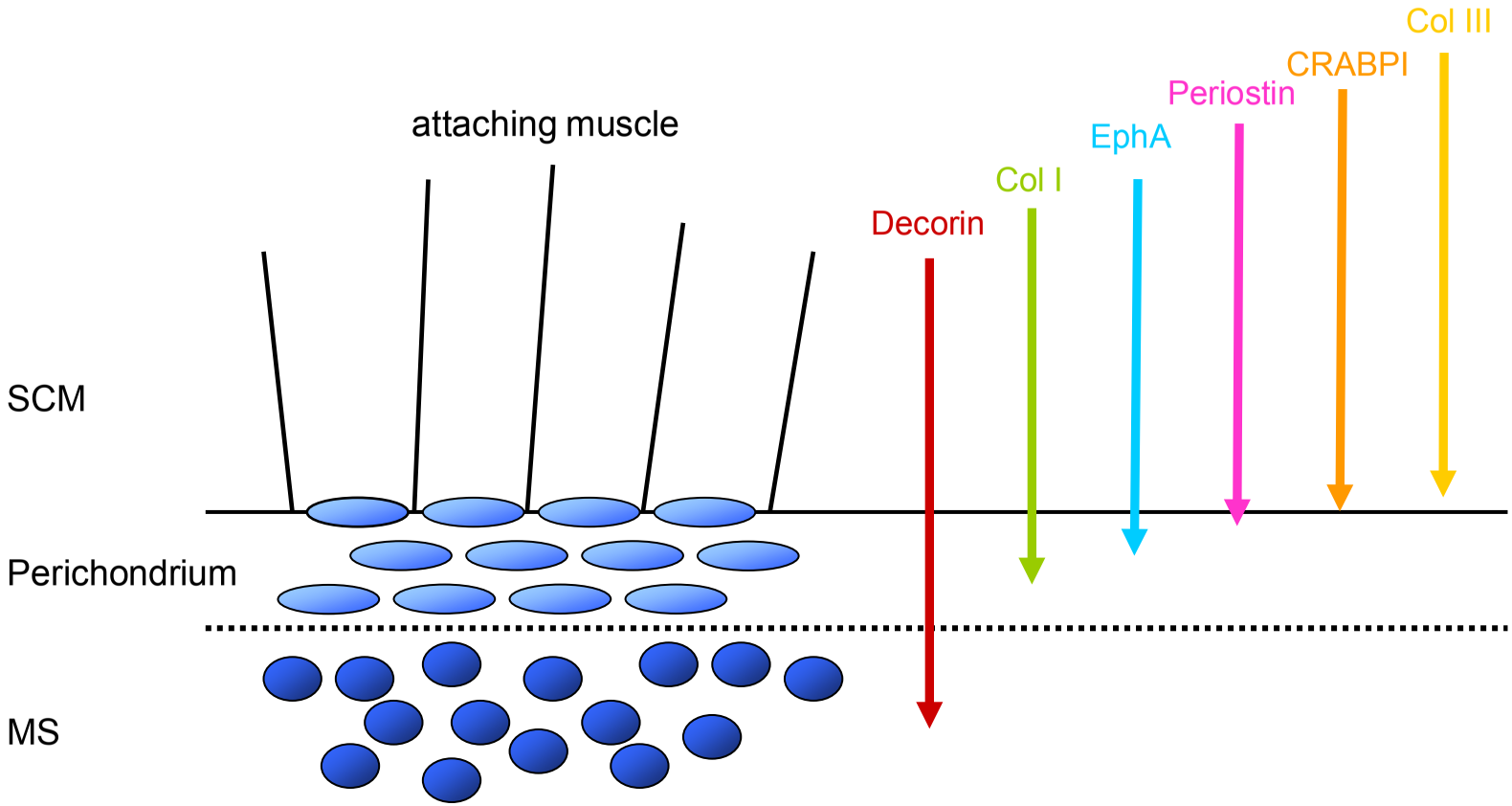
attaching muscle
Col III
CRABPI
Periostin
EphA
Col I
Decorin
SCM
Perichondrium
MS

Figure 3.16 Schematic summary of differential marker expression for the sternal sternocleidomastoid attachment

All analysed markers (Decorin, Collagen I, Ephrin A4, Periostin, CRABPI, Collagen III) are expressed in the muscle connective tissue but show a differential display with regards to the expression in the perichondrial layer of the attachment site as indicated by the tip of the arrow on the right site of the figure. For clarity, arrows are displayed next to the schematic muscle attachment.

In addition to the expression in attachment fibres, markers localise as follows:

Decorin expression spans the entire region; it is expressed in attachment fibres, the perichondrium and an outer layer within the cartilaginous matrix of the *manubrium sterni.*

Collagen I is expressed in the outer two thirds of the perichondrial layer.

Ephrin A4 is expressed in a few cells in the outer third of the perichondrial layer.

Periostin is expressed in the attachment layer.

CRABPI is expressed in the superficial attachment layer.

Collagen III is expressed in the attaching fibres but not the attachment layer.

SCM sternocleidomastoid muscle, ***MS*** *manubrium sterni*

attachment fibres to the sternal perichondrium is schematically summarised in Figure 3.16.

3.4.3.3 The sternal attachment of the sternocleidomastoid muscle is neural-crest derived

To determine the neural crest contribution to the superficial sternal attachment of the sternocleidomastoid muscle, corresponding sections of the sternal region of *Wnt*1-Cre$^{+/-}$; Rosa26LacZR$^{-/-}$ mice in which neural crest is permanently labelled by the expression of ß-Galactosidase[50] were analysed. Conventional X-Gal staining shows a superficial neural crest contribution that is limited to the area of the sternocleidomastoid muscle but does not include the sternum nor the perichondrium (Figure 3.17 A). Highly sensitive immunohistochemistry for ß-Galactosidase, Decorin, the marker with the widest expression in the attachment zone, and Periostin as marker for attachment fibres demonstrates that a neural crest contribution is limited to the attachment fibres contacting the outer-most layer of the perichondrium (C, D) but does not span the entire depth of the perichondrium (E). The sternal attachment of the sternocleidomastoid muscle is therefore in its very superficial nature fully neural crest-derived.

3.4.3.4 The *Hand*2-Cre transgene does not label posterior distal neural crest

Hyoid and thyroid cartilage are neural crest-derived structures of the anterior midline and originate from the second and third and third and fourth branchial arch respectively (the *Wnt*1-Cre transgene is here used to demonstrate neural crest origin, Figure 3.18 A). Structures of the anterior midline originate from the distal part of the branchial arches and labelling of the *Hand*2-Cre transgene can be found in the midline of first and second branchial arch territory but with the exception of isolated single cells not in the thyroid cartilage (B). This shows that the *Hand*2-Cre transgene replicates endogenous *Hand*2 expression in the neural crest of the first and second branchial arch as previously

Figure 3.17- 3.18

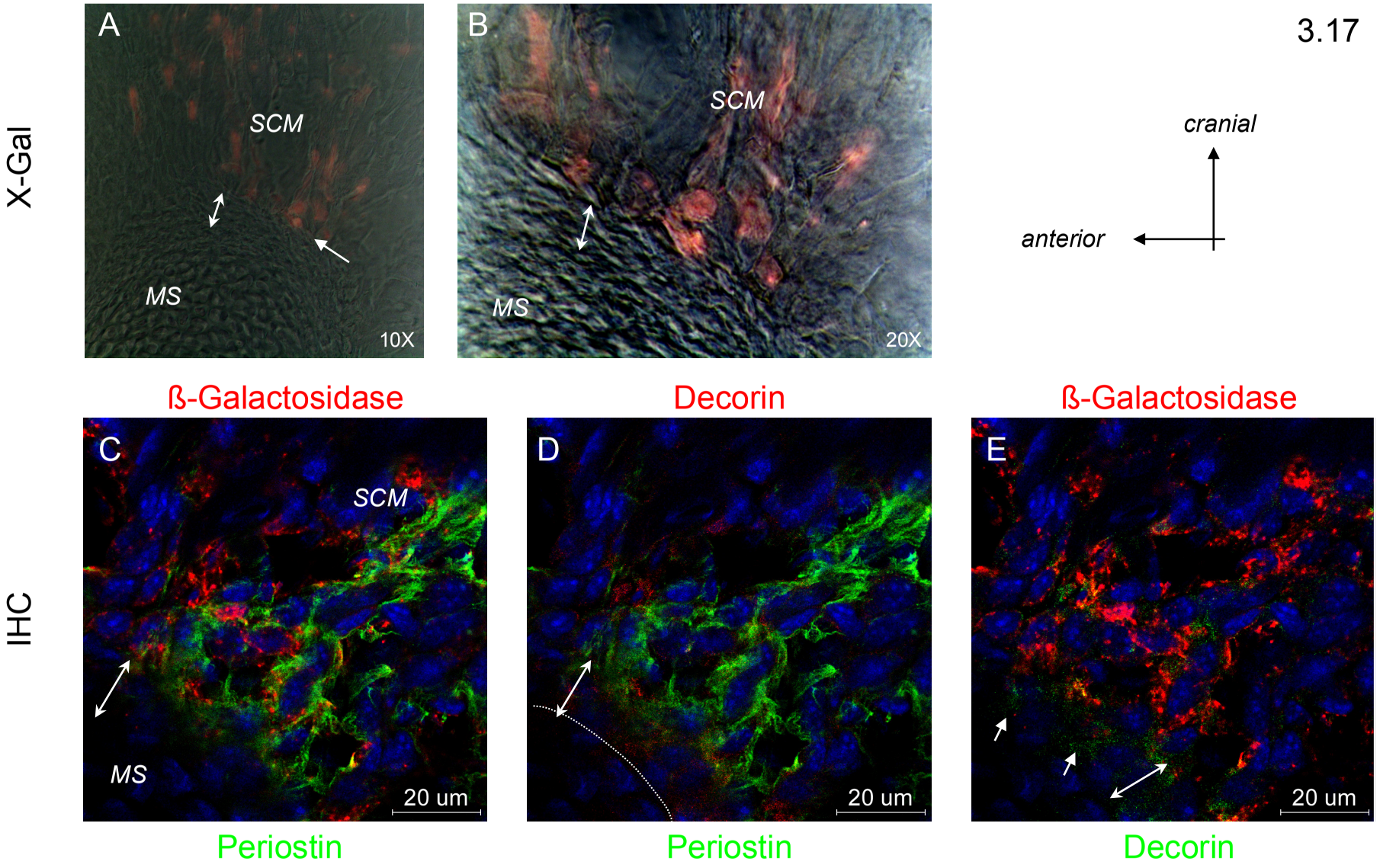
X-Gal
A
SCM
MS
10X
B
SCM
MS
20X
cranial
anterior
ß-Galactosidase
Decorin
ß-Galactosidase
IHC
C
SCM
MS
20 um
D
20 um
E
20 um
Periostin
Periostin
Decorin

Figure 3.17 The sternal attachment of the sternocleidomastoid muscle is neural crest-derived

Sagital sections of the sternal region of E18.0 *Wnt*1-Cre+/-; Rosa26LacZR-/- mice. The images shows the sternal attachment point of the sternocleidomastoid muscle (SCM) in detail.

A- B X-Gal staining for Beta-Galactosidase activity. For better contrast, the inverted image of the light-microscopic image is shown (X-Gal staining is now appearing red). **C**- **E** IHC* for Periostin (green), Decorin (red in **D**, green in **E**) and ß-Galactosidase (red), a single optical section of a confocal z-stack in is shown. At any one time, two out of the three markers are shown in overlay in the combination with DAPI (blue) as counterstain. The double arrow indicates the width of the perichondrium.

A, **B** X-Gal staining indicates that the neural crest contribution to the SCM sternal attachment is limited to the muscle connective tissue but excluded from the perichondrium (double arrow) and the *manubrium sterni* (MS) itself.

C Highly sensitive IHC for ß-Galactosidase confirms that the neural crest contribution (as indicated by expression of Beta-Galactosidase in the *Wnt*1-Cre+/-; Rosa26LacZR-/- mouse) is limited to the connective tissue of the attaching fibres.

D Fibres do not penetrate the Decorin-labelled perichondrium (dotted line in **D**).

E ß-Galactosidase expression is equally limited to the outer part of the Decorin expression domain and does not cross the perichondrial layer (arrows indicated the inner boundary of Decorin expression/ perichondrium).

SCM sternocleidomastoid muscle, ***MS*** *manubrium sterni*

* IHC was performed according to standardized conditions; a detailed description of conditions and antibodies (primary and secondary) can be found in the relevant section under ‘Materials and Methods’ (Chapter 7.5.4).

3.17

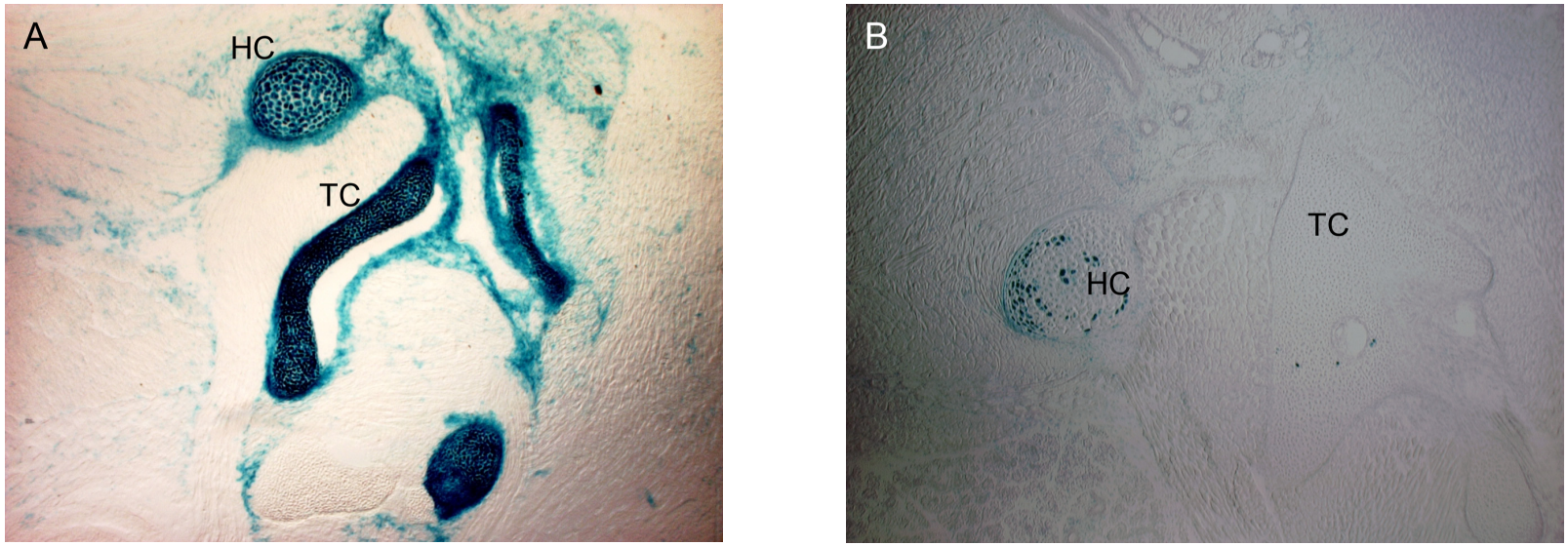

Figure 3.18 The *Hand*2-Cre transgene does not label posterior distal arch neural crest

X-Gal staining of sagital sections of the hyoid/ thyroid region of Rosa26LacZR-/- mice interbred with a *Wnt*1-Cre mouse (labelling all neural crest) (**A**) and a *Hand*2-Cre mouse (**B**). Magnification: 5x

Hyoid and thyroid cartilage are neural crest- derived structures (**A**) but labelling of the *Hand*2-Cre transgene is limited to groups of cells in the anterior hyoid and single cells with the thyroid cartilage (**B**). The hyoid/ thyroid area is derived from branchial arch 3 and 4 and its anatomical position in the midline suggests origin from distal neural crest. Absence of labelling with the exception of isolated cells in the thyroid cartilage (**B**) therefore indicates that the activity of the *Hand*2-Cre transgene does not extend beyond the first and second branchial arch.

HC hyoid cartilage, ***TC*** thyroid cartilage

reported[158] but is most likely not active in more posterior branchial arches (also see Figure 3.4).

3.4.3.5 Loss of *Hand*2 function does not affect the integrity of the *manubrium sterni* nor the sternocleidomastoid attachment site

To finally rule out a role of *Hand*2 in posterior distal neural crest for the correct formation of the sternal attachment of the sternocleidomastoid muscle, we made use of a genetically modified mouse with a neural crest-specific ablation of *Hand*2 (*Hand*2$^{fl/fl}$;*Wnt*1-Cre$^{+/-}$;Rosa26LacZR$^{-/-}$[80,122], Figure 3.19). The ablation of *Hand*2 function specifically in neural crest cells is thereby achieved by crossing a mouse line with a partially floxed coding region of *Hand*2 with the *Wnt*1-Cre line that confers neural crest specificity[50,80]. By additional crossing into the Rosa26LacZR reporter line[176], the activity of Cre recombinase not only causes the inactivation of *Hand*2, but can also be visualised by staining for ß-Galactosidase. The *manubrium sterni* of *Hand*2$^{fl/fl}$;*Wnt*1-Cre$^{+/-}$;Rosa26LacZR$^{-/-}$ mice shows no anatomical anomalies (A) and the attachment site of the sternocleidomastoid muscle is intact (B) despite the lack of *Hand*2 function in the cells at the attachment site (C, red). Immunohistochemistry for ß-Galactosidase also confirms again the superficial nature of the neural crest contribution to the sternal attachment of the sternocleidomastoid muscle.

3.4.3.6 Summary

The sternocleidomastoid muscle attaches to a single layer of cells on the outside of the sternal perichondrium and the contribution of the neural crest is limited to the attachment fibres and the thin attachment layer. The cell population labelled by the *Hand*2-Cre transgene in the upper part of the *manubrium sterni* therefore does not represent a posterior and distal branchial arch population but a contribution from the second domain labelled by the *Hand*2-Cre transgene, the limb lateral plate mesoderm. Neural crest-specific ablation of *Hand*2 confirms that *Hand*2 is not involved in the establishment of the sternal attachment of the sternocleidomastoid muscle .

Figure 3.19

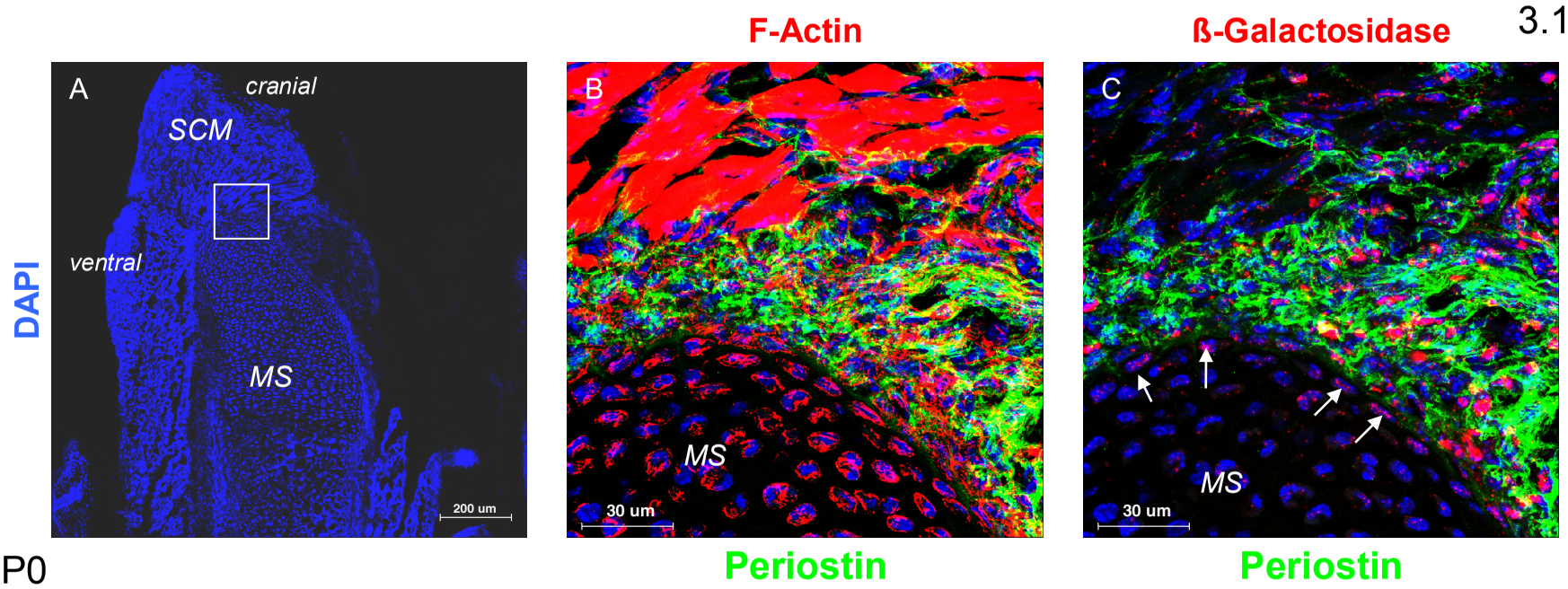

D *Hand*2fl/fl; *Wnt*1-Cre+/-; Rosa26LacZR+/-

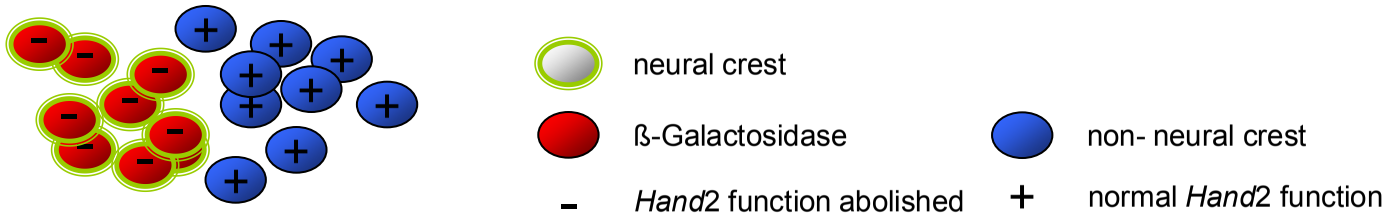

Figure 3.19 The sternal insertion of the sternocleidomastoid muscle is not affected by the loss of *Hand*2 function

IHC* for Periostin (green in **B** and **C**) and ß-Galactosidase (red in **C**) on sagital sections of the insertion of the sternocleidomastoid muscle (SCM) at the manubrium sterni (MS) of *Hand*2fl/fl, *Wnt*1-Cre+/-, Rosa26LacZR-/- newborn mice (P0). F-Actin fibres are stained with Rhodamine-Phalloidin (**B**), nuclear counterstain is DAPI (blue).

A shows an overview of the anatomy of the sternal attachment site of the sternocleidomastoid muscle; images **B** and **C** are higher magnifications of the region boxed in **A**.

B Neural crest-specific loss of *Hand*2 function does not affect the structure of the manubrium sterni (MS) nor the sternocleidomastoid muscle insertion.

C Control staining for ß-Galactosidase shows that Cre-mediated recombination (leading to the inactivation of *Hand*2) has indeed taken place in the neural crest cells forming the attachment site. The neural crest contribution to the attachment site is limited to the attachment fibres and a thin outer layer of cells (arrows).

D Principle of the *Hand*2fl/fl, *Wnt*1-Cre+/-, Rosa26LacZR-/- cross: neural crest cells (green outer rim) are ß-Galactosidase (red cell body) positive and lack *Hand*2 function (minus). Hand2 is fully functional (plus) in non-neural crest (blue cell body).

MS manubrium sterni, ***SCM*** sternocleidomastoid muscle

* IHC was performed according to standardized conditions; a detailed description of conditions and antibodies (primary and secondary) can be found in the relevant section under ‘Materials and Methods’ (Chapter 7.5.4).

3.5.2 A comparative approach- tracing the lost mammalian procoracoid

X-Gal staining allows to identify two independent expression domains in the *Hand*2-Cre mouse: neural crest originating from the distal part of the cranial two branchial arches and lateral plate mesoderm associated with the limb. The fact that the neural crest contribution to the *manubrium sterni* is restricted to the superficial attachment of the sternocleidomastoid muscle comprising a single layer of cells, also supported by the fact that the neural crest-specific loss of *Hand*2 function does not affect the *manubrium sterni* nor the attachment site of the sternocleidomastoid muscle identifies the labelled cell population within the *manubrium sterni* of the *Hand*2-Cre mouse as belonging to the limb lateral plate mesoderm domain of the *Hand*2-Cre transgene.
The central position of the sternum in the body midline suggests that the cell population labelled by the *Hand*2-Cre transgene in the *manubrium sterni* must have been established as a very proximally (close to the body centre) located limb lateral plate mesoderm. The scapulocoracoid complex (also see the Introduction to this chapter) represents the link between limb and the trunk skeleton. The contribution of the limb lateral plate mesoderm to the scapula was determined in this study with the help of the *Hand*2-Cre transgene (section 3.4.1), the results show that parts of the scapula can be considered proximal limb elements. The scapula is the only element of the scapulocoracoid complex that is retained as a distinct element in mammals, with which the former metacoracoid fuses to give rise to the coracoid process (also labelled by the *Hand*2-Cre transgene, Figure 3.8). The other element of the coracoid, the procoracoid, is thought to be lost in mammals[125,165] but has also been suggested to be incorporated in the *manubrium sterni* of a therian sister group, the marsupials[101,200]. The presence of a limb lateral plate mesodermal cell population in the murine upper *manubrium sterni* now suggests that this scenario might actually not only apply to monotremes but also to placental mammals like the mouse; the labelled cell population in the *manubrium sterni* of the *Hand*2-Cre mouse would then represent the 'lost' procoracoid of placentals.

To test whether the *Hand*2-Cre transgene can indeed be used to 'trace' the scapulocoracoid through evolution, the transgene was tested by Tol2 transgenesis in zebrafish, a species retaining a full scapulocoracoid (Figure 3.20).

Figure 3.20

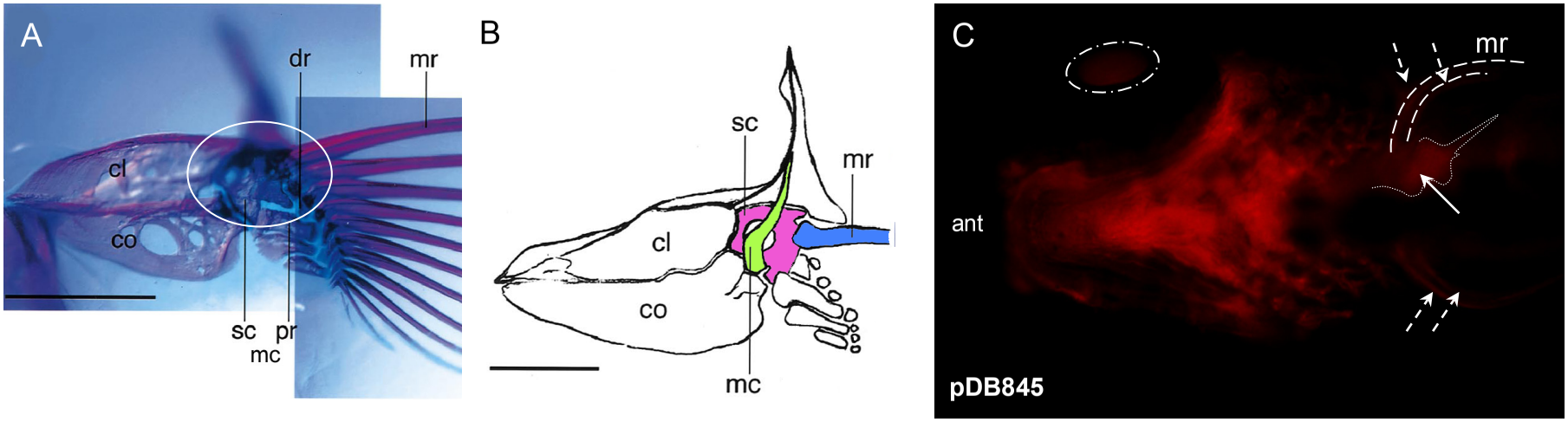
A
dr
mr
cl
co
sc
pr
mc
B
sc
mr
cl
co
mc
C
mr
ant
pDB845

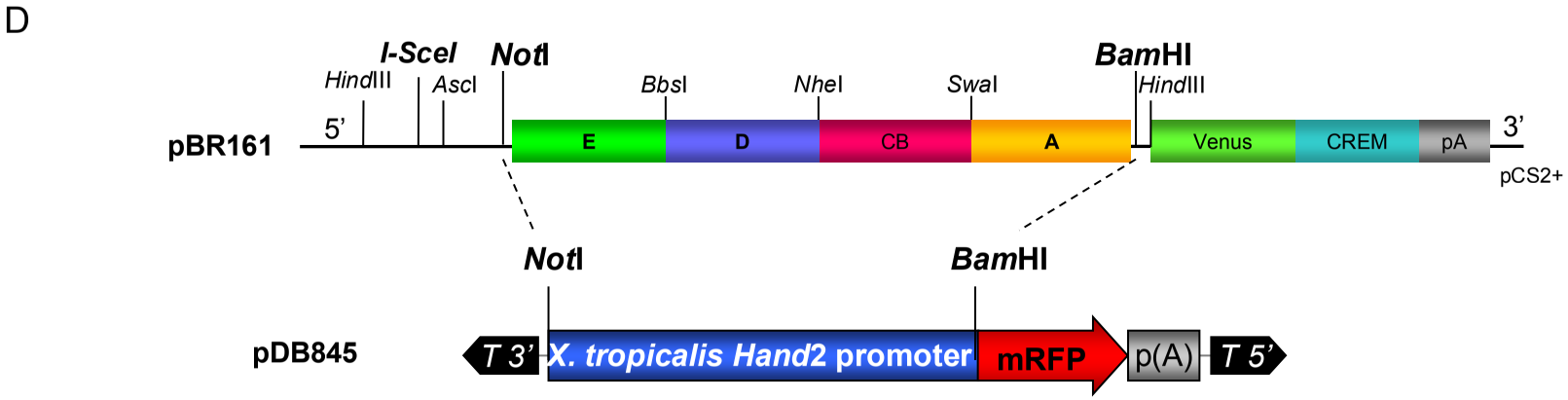
D
I-SceI
NotI
BamHI
HindIII
AscI
BbsI
NheI
SwaI
HindIII
pBR161
5'
E
D
CB
A
Venus
CREM
pA
3'
pCS2+
NotI
BamHI
pDB845
T 3'
X. tropicalis Hand2 promoter
mRFP
p(A)
T 5'

Figure 3.20 A *Xenopus Hand*2 transgene labels skeletal elements in the *zebrafish* shoulder girdle most likely corresponding to the scapula and the mesocoracoid

A, **B** Anatomy of the *zebrafish* shoulder girdle annotated after Grandel et al.1998. (**A**) Alzian-Blue/ Alizarin-Red stained shoulder region of a subadult, the circle indicates the position of the scapula and the proximal metacoracoid. (**B**) Shoulder region in a schematic view; scapula (sc), metacoracoid (mc) and the marginal ray (mr) are highlighted. The scale bar corresponds to 1mm in a 17mm subadult specimen. **cl** cleithrum **co** coracoid **dr** distal radius **mr** marginal ray **mc** mesocoracoid **pr** proximal radials **sc** scapula

C Ventral view of a 5 day-old transgenic zebrafish created with the Tol2 method with plasmid pDB845, a plasmid containing a red fluorescent protein (mRFP) under the control of the the *X.tropicalis Hand*2 promoter (construct in detail under **D**). The rapid development of zebrafish embryos and the high stability of mRFP allows the tracing of cells for some time after they stopped synthesising mRFP (personal communication D. Balciunas). Transgenesis with pDB845 in zebrafish conferred expression to the lower jaw and the distal branchial arch region, compatible with the extent of the *Hand*2 domain in mouse (see Chapter 2). Two fin rays can be visualised (dashed arrows and lines). On the left (here: upper) side of the specimen, labelling can be recognised in the skeletal element (dotted line) at the base of the marginal ray. The positioning and the outline of the labelling correspond to the position of the scapula and mesocoracoid. Labelling is only detectable on one side, as the specimen is slightly tilted (which is also recognisable by the fact that the lens of the upper but not the lower eye is visible, marked by the ellipse). The same staining pattern was observed in 5 independent specimens and stable transgenic lines for a detailed analysis are currently being established.

D Plasmid pDB845 for Tol2 transgenesis in zebrafish contains the *Xenopus tropicalis Hand*2 upstream region from plasmid pBR161 as a *Not*I- *Bam*HI fragment 5' of a red fluorescent protein (mRFP). The generation of construct pBR161 will be described in detail in Chapter 3 and was performed by the author. The sub-cloning of the *Hand*2 upstream region from pBR161 into miniTol2 (plasmid pDB845) and zebrafish transgenesis were performed by D. Balciunas.

Reference

Grandel, H. & Schulte-Merker, S. (1998)

The activity of the 7.4kb *Hand*2-Cre transgene in the limb bud, although replicable in independent transgenic mouse lines[158], does not reflect endogenous *Hand*2 expression. *Hand*2 is normally expressed at the posterior margin of the limb bud and is actively excluded from the anterior margin[183]. The fact that the *Hand*2-Cre transgene is able to drive expression at the anterior margin is therefore most likely due to missing repressor elements in the transgene. *Hand*2 expression in the limb/ fin has been shown to be conserved between mouse, *Xenopus* and zebrafish[9,30,178] and anterior-posterior patterning in the both the *mouse* limb and zebrafish fin buds is achieved by an interplay between *Sonic hedgehog* and *Hand*2[52]. The fact that *Hand*2 expression as well as anterior-posterior limb patterning appeared conserved within the gnathostome group, we were cautiously optimistic that the *Hand*2-Cre transgene would behave similarly in mouse and zebrafish. The fact that limbs and fins are homologous and well-defined structures further allows us to unambiguously assess correct transgene behaviour (in this case: the same deviation from endogenous *Hand*2 expression).

As the mouse *Hand*2-Cre transgene has been reported not to be functional in zebrafish (personal communication D.Clouthier), a transgene containing the equivalent *Hand*2 upstream region of *Xenopus tropicalis* was tested instead (construct design and cloning are described in detail in Chapter 5).

First results in the founder generation show that the *X. tropicalis Hand*2 transgene indeed labels skeletal elements at the base of the anterior fin rays which correspond positionally to the scapula and the mesocoracoid (Figure 3.20 A[76]). Transgenic fish are currently being raised to establish stable transgenic lines for an assessment of transgene behaviour and a detailed skeletal analysis that would confirm that the *Hand*2-Cre transgene can be used to trace the ancient scapulocoracoid complex.

3.5.3 The attachment sites of the sternocleidomastoid muscle

To evaluate whether the sternal attachment was specific or typical for the sternocleidomastoid muscle, the morphology of the second origin of the muscle at the clavicle, its insertion point at the mastoid process and the origin of the trapezius muscle, the muscle from which the sternocleidomastoid muscle is thought to be derived[19], were analysed.

3.5.3.1 The clavicular origin of the sternocleidomastoid muscle

The sternocleidomastoid muscle originates with one head from the sternum and a second head from the medial part of the clavicle. Similar to the sternal origin, attachment fibres at the clavicular origin do not penetrate into the clavicular bone but link up superficially with a mesh of periosteal fibres (Figure 3.21 A). Labelling by the *Wnt*1-Cre transgene indicates the neural crest origin of the sternocleidomastoid muscle connective tissue and attachment. Interestingly, the periosteal cells directly beneath the attachment site show no immunoreactivity for ß-Galactosidase (arrow in A). At the medio-lateral position of the clavicular attachment, most cells of the clavicle are neural crest-derived, like the cartilaginous core (B, D) and the dermal outside (B- D). However, unlabelled cells related to blood vessels can be found within the outer dermal shell (asterisks in B, C). The clavicle is a composite bone of neural crest and mesodermal origin, demonstrated here on a section from a more lateral position, where the neural crest contribution becomes limited to attaching fibres belonging to the omohyoideus system (E).
The morphology of the attachments of the sternocleidomastoid muscle at its origin from the shoulder girdle therefore resemble each other strongly (Figure 3.22). Both at the sternum (A- C) and the clavicle (D- F), the neural crest-derived attachment is extremely superficial and no further neural crest contribution is found in the sternum. In contrast, neural crest cells are present in the clavicle; the cells directly below the attachment, however, are not neural crest-derived (F, asterisk, also see Figure 3.21 A). Higher magnification reveals that the actual clavicular attachment is formed between cells

Figure 3.21- 3.22

*Wnt*1-Cre+/-; Rosa26LacZR-/-

3.21

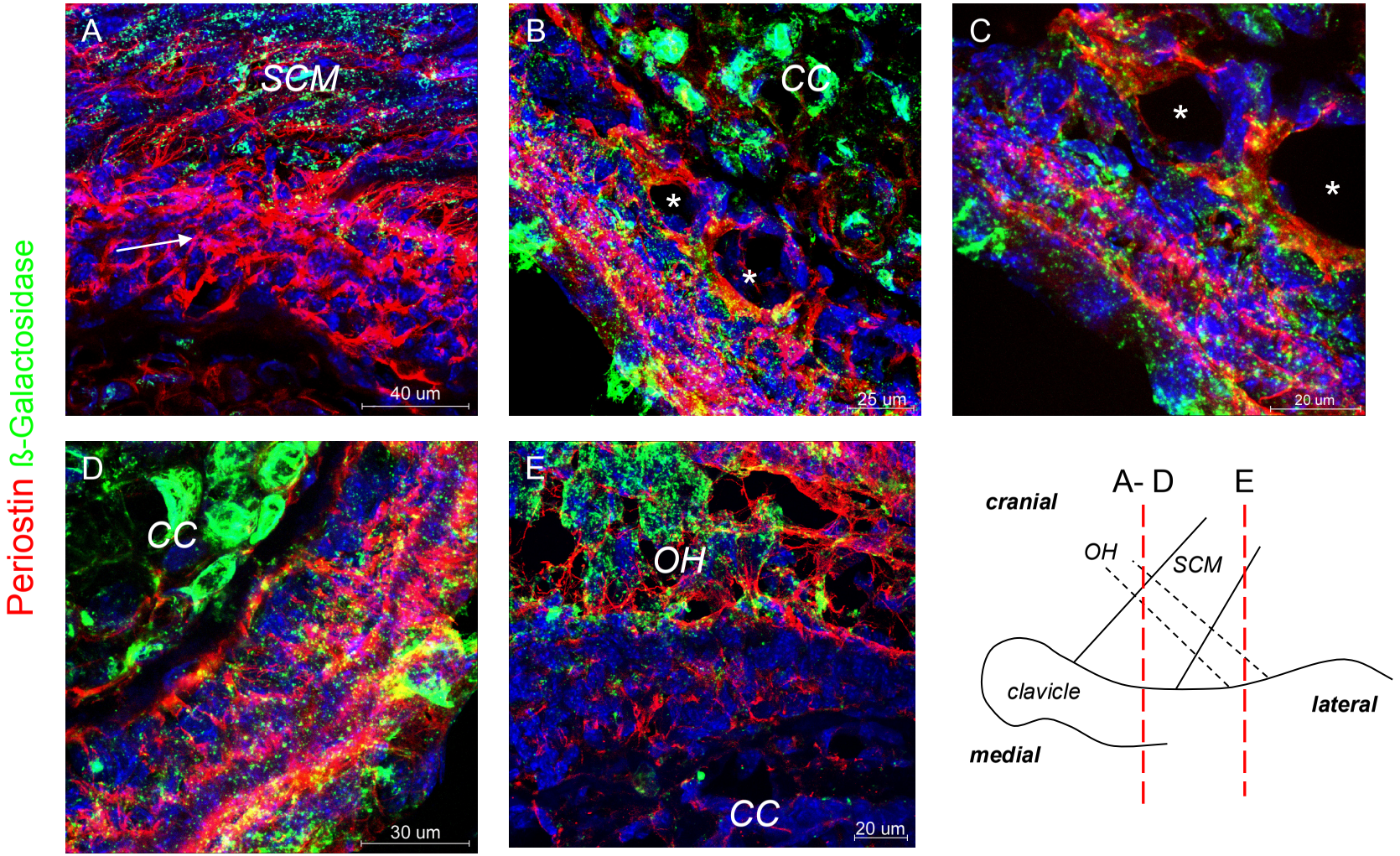

Figure 3.21 The clavicular attachment of the sternocleidomastoid muscle

IHC* for Periostin (red), ß-Galactosidase (green); nuclear counterstain is DAPI (blue). Sagital sections of the clavicle of E18 *Wnt*1-Cre+/-; Rosa26LacZR-/- mice. **A**- **D** represent different areas along the circumference of the clavicle at the same medio- lateral position while the section shown in **E** lies more laterally.

A At the insertion of the SCM muscle on to the clavicle, the contribution of the neural crest is limited to the muscle connective tissue and the superficial attachment while the underlying mesenchyme appears unlabelled (arrow).

B The anterior aspect and the cartilaginous core of the clavicle appear nearly entirely neural crest-derived; however, cells associated with bloodvessels (asterisks) show less labelling (also see C).

C Area containing bloodvessels in higher magnification (marked with asterisks in B and C).

D The posterior aspect of the clavicle shows neural crest labelling throughout.

E In contrast, a more lateral position of the clavicle. Neural crest labelling is mainly restricted to the connective tissue associated with the omohyoid (OH) muscle; only few neural crest cells are found within the clavicle.

CC cartilaginous core of the clavicle*,* ***OH*** omohyoid muscle, ***SCM*** sternocleidomastoid muscle

* IHC was performed according to standardized conditions; a detailed description of conditions and antibodies (primary and secondary) can be found in the relevant section under ‘Materials and Methods’ (Chapter 7.5.4).

3.22

cranial
Wnt1-Cre+/-; Rosa26LacZR+/-
Periostin Undulin
Periostin BG
BG Undulin
BG CRABPI
Periostin CRABPI
Periostin BG
A
B
C
D
E
F
SCM
SCM
20 um
20 um
20 um
30 um
30 um
30 um
*
sternum
clavicle

Figure 3.22 The attachment sites of the sternocleidomastoid muscle on to the shoulder girdle

IHC* for Periostin (green, **A**, **B**, **D**, **E**), Undulin (red, **A**, **C**), CRABP1 (red, **D**, **F**) and ß-Galactosidase (red in **B**, **E**; green in **C**, **F**) on sagital sections of the sternum (**A**- **C**) and the clavicle (**D**- **F**) of a *Wnt*1-Cre+/-; Rosa26LacZR-/- mouse (E18). High resolution images of the sternal and the clavicular attachment sites of the sternocleidomastoid muscle (SCM) were acquired by confocal microscopy; at any one time, two of the three markers are shown in overlay in addition to the counterstain (DAPI, blue).

At both insertion sites, the nature of the SCM muscle attachment is very superficial; attachment fibres end at the outer-most layer of the perichondrium/ periost to which they connect. Fibre strands coming from a tendon cell can be seen in continuity with the fibres from perichondrial/ periosteal cells (**A**, **D** arrows), forming an 'attachment system'. Both at the sternum and the clavicle, this 'attachment system' is neural crest- derived (**B**, **E**). At the sternum, immunoreactivity for ß-Galactosidase indicating neural crest origin does not extend below the outer layer of the perichondrium (**B**, **C**). At the clavicle, the mesenchyme below the attachment consists of several layers of cells; the outer and inner layer are organised sheet-like with elongated cell nuclei, are CRABP1 positive and sandwich a CRABP1 negative cell population of different morphology (**F**, asterisk). While the outer layer of CRABP1 positive cells is neural crest-derived (**F**, arrow), the intermediate cell population and lower CRABP1 layer only contain a few ß-Galactosidase positive cells.

Neither Undulin (**A**, **C**) nor CRABP1 (**D**, **F**) are specific to the perichondrium/ periost; low levels of Undulin are also found in the SCM attachment fibres (**A**, **C** arrowheads). Cells forming the 'attachment system' are both CRABP1 positive (**D**, **F**).

BG ß-Galactosidase, ***SCM*** sternocleidomastoid muscle

* IHC was performed according to standardized conditions; a detailed description of conditions and antibodies (primary and secondary) can be found in the relevant section under 'Materials and Methods' (Chapter 7.5.4).

sitting on the outside of muscle fibres and cells that are part of the outer perichondrial layer; both cells of this anchoring complex are neural crest-derived and express CRABP1 (D- F).

3.5.3.2 The insertion site of the sternocleidomastoid muscle at the mastoid process

The sternocleidomastoid muscle- despite its neural crest-derived connective tissue- does not only originate from mesoderm-derived skeleton (clavicle, sternum) but also inserts at the mesodermal skull base at the mastoid process. The situation of a neural crest-derived muscle attaching to a mesodermal base was therefore common to both the origin and the insertion of the muscle and we were interested to see whether this found a reflection in the morphology of the attachments. The insertion of the sternocleidomastoid muscle at the mastoid process indeed resembles the attachment at the sternum with a 'veneer' of neural crest on a mesodermal base (Figure 3.23). The attachment fibres only reach the outer perichondrial layer of the mastoid process and attach to an outer Decorin positive cell layer in which cells are encased by Periostin fibres (A, the perichondrium is labelled with Decorin, the arrow points to the layer of encased cells). Although fibrous structures can be seen within the cartilage, these do not appear to stand in relation with the attachment site. The neural crest contribution is once more restricted strictly to the attachment site and does not appear to extend into the cartilage (B, arrows) with the exception of isolated neural crest cells located deep in the mastoid process (B, arrowheads).

3.5.3.3 The attachment of the *M. trapezius* at the spinous process

The sternocleidomastoid muscle is considered to be an anterior division of the dorsal trapezius muscle[19], that originates from the spinous processes of the mesodermal vertebral column. Neural crest origin has been described for its connective tissue as well as its attachment[122]. The attachment fibres of the trapezius muscle on to the spinous

Figure 3.23

*Wnt*1-Cre +/-; Rosa26LacZR-/-

3.23

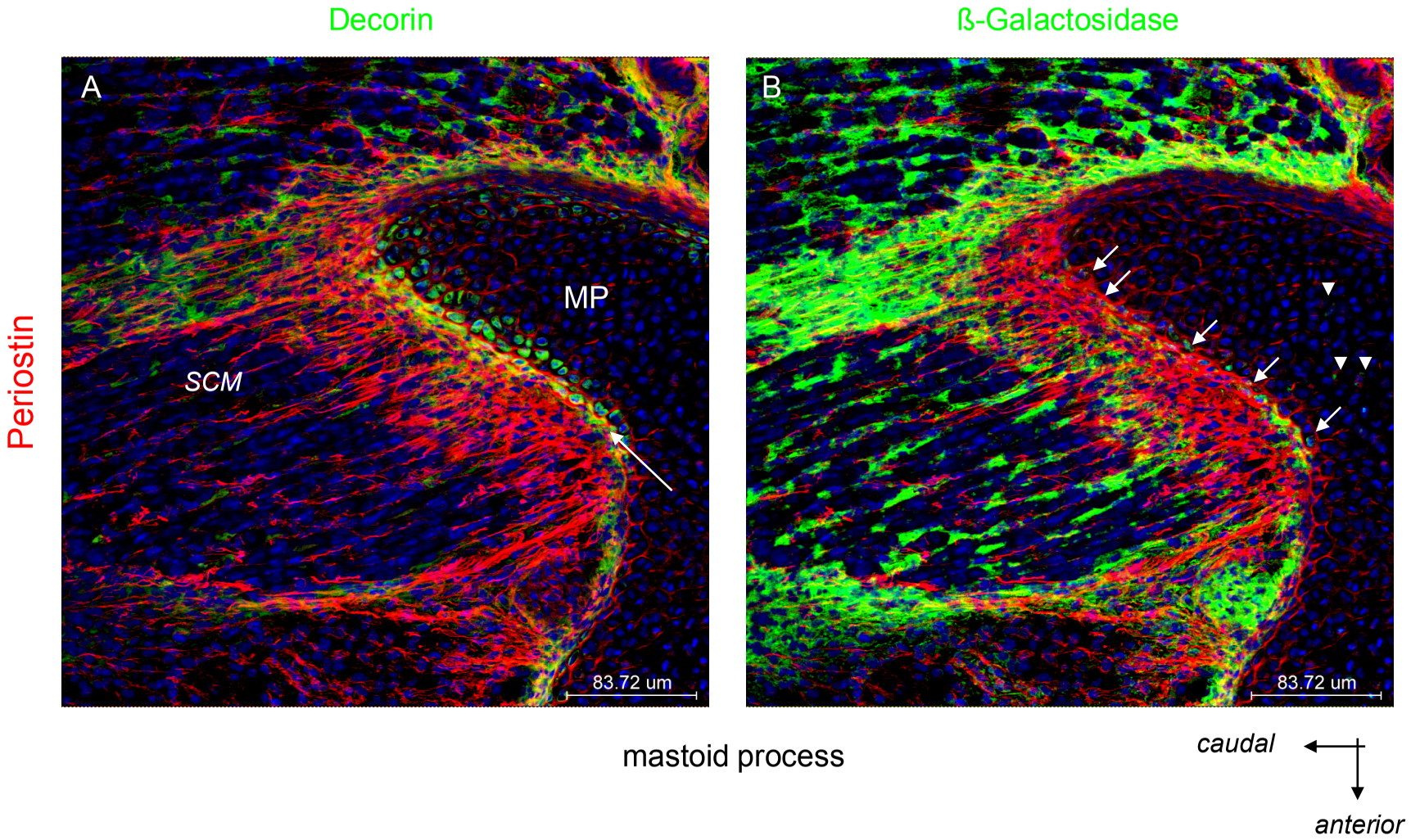

Figure 3.23 The sternocleidomastoid muscle at its origin from the mastoid process

Sagital sections of the origin of the sternocleidomastoid muscle from the mastoid process of E18.0 *Wnt*1-Cre+/-; Rosa26LacZR-/- mice. IHC* for Periostin (red), Decorin (green in **A**) and ß-Galactosidase (green in **B**). Images show the actual attachment area and orientated with anterior to the bottom and dorsal to the left.

A At the origin of the sternocleidomastoid muscle at the mastoid process, attachment fibres insert on the outside of the periost, onto a layer of Decorin positive cells encased by Periostin fibres (arrow). Decorin positive cells are also found further inside the cartilage, paralleling the perichondrium.

B Within the attachment, the contribution of the neural crest is limited to the side of the attaching muscle (arrows) and does not further extend into the cartilage. Structurally unrelated single neural crest cells are found within the mastoid process (arrowheads).

MP mastoid process

* IHC was performed according to standardized conditions; a detailed description of conditions and antibodies (primary and secondary) can be found in the relevant section under ‘Materials and Methods’ (Chapter 7.5.4).

process end similarly superficially like previously found for the attachment sites of the sternocleidomastoid muscle (Figure 3.24). The muscle connective tissue of the trapezius muscle shows strong immunoreactivity for ß-Galactosidase, confirming its origin from the neural crest (*Wnt*1-Cre mouse, A, B, D). As previously reported[122], neural crest cells can also be detected within the spinous process itself (A, arrow in D). The neural crest cells forming the attachment site show strong immunoreactivity for Decorin, demonstrating that the attachment of the trapezius muscle on to the spinous process is indeed accomplished by the neural crest (C, E, F). Interestingly, cells within the spinous process directly below the neural crest-derived attachment site show no immunoreactivity for ß-Galactosidase (arrow in D), despite the fact that further ß-Galactosidase immunoreactive neural crest cells are present deeper within the bone. This resembles the situation already observed for the clavicular origin of the sternocleidomastoid muscle, suggesting a general characteristic.

3.5.3.4 Summary

The sternal attachment of the sternocleidomastoid muscle can be considered typical for the attachment sites of the muscle, which are all extremely superficial in nature and limited to the outer-most cell layer of the perichondrium/ periost. All attachments are effected by neural crest cells, following the 'rule of connectivity' and consistent with the neural crest origin of the muscle connective tissue. The boundary between neural crest and mesoderm runs within the perichondrial layer as the mesenchymal cell population directly beneath the attachment is always of non-neural crest origin. At sites, where the sternocleidomastoid muscle attaches to a cartilaginous element (here: sternum, mastoid), the neural crest contribution is limited to the attachment site with only very isolated neural crest cells within the cartilage. However, at attachment sites on to bone (here: clavicle, also spinous process), the neural crest provides an important contribution to the bony element, although the cell population beneath the attachment remains mesodermal in origin.

Figure 3.24

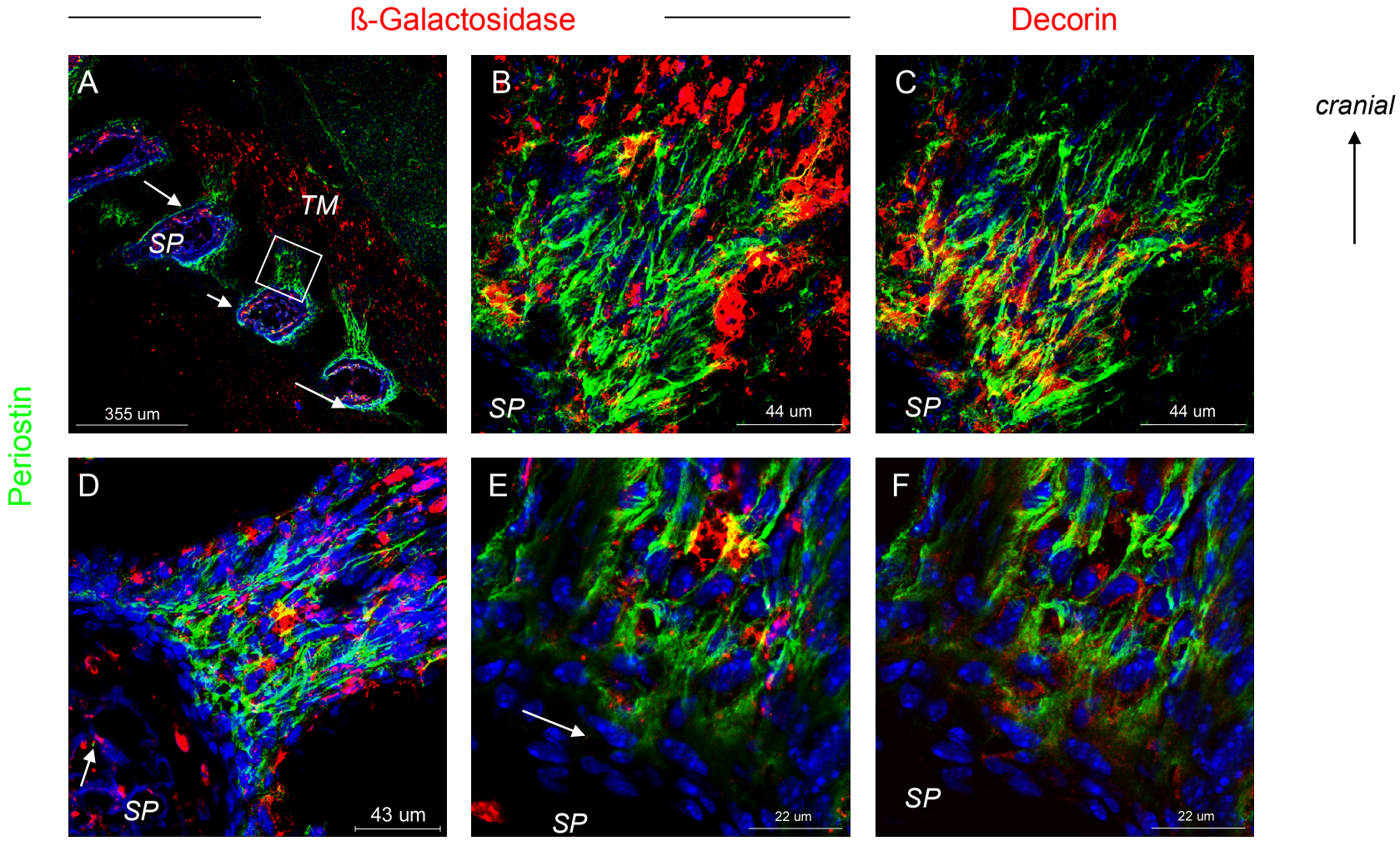
ß-Galactosidase
Decorin
cranial
Periostin
A
TM
SP
355 um
B
SP
44 um
C
SP
44 um
D
SP
43 um
E
SP
22 um
F
SP
22 um

Figure 3.24 The attachment of the trapezius muscle on to the spinosus process is superficial and neural crest-derived

IHC* for Periostin (green), ß-Galactosidase (red in **A**, **B**, **D**, **E**) and Decorin (red in **C**, **F**) on sagital sections of the vertebral column of P4 *Wnt*1-Cre+/-;Rosa26LacZR-/- mice. Confocal images of the direct attachment of the trapezius muscle (TM) on to the spinosus process (SP) of the vertebral column.

A Overview of the attachment of the trapezius muscle on to the spinosus processes (SP) of the vertebrae. The presence of neural crest cells within the trapezius muscle (TM) and in the spinosus processes is easily detectable (arrows, also see **D**).

B, **C** The connective tissue of the attachment is neural crest-derived (**B**) and the attachment itself characterised by the expression of Decorin (**C**).

D Attachment fibres of the trapezius muscle end superficially on the outside of the spinosus process and do not penetrate into the bone. Neural crest cells are found within the connective tissue of the muscle as well as in the bone (arrow).

E, **F** Higher magnification shows that Decorin specifically marks cells between the periostin fibres of the attachment (**F**) and that these are neural crest-derived (**E**). However, the mesenchymal tissue directly underneath the attachment does not appear to be neural crest-derived (arrow in **E**).

TM trapezius muscle***, SP*** spinosus process

* IHC was performed according to standardized conditions; a detailed description of conditions and antibodies (primary and secondary) can be found in the relevant section under ‘Materials and Methods’ (Chapter 7.5.4).

3.5.4 Summary of the results

- The analysis of the *Hand*2-Cre mouse confirms the origin of the mammalian scapular blade from the lateral plate mesoderm and more precisely defines the contribution from lateral plate mesoderm associated with the limb to it. The behaviour of limb lateral plate mesoderm in relation to trunk lateral plate mesoderm in the shoulder blade shows signs of initial organisation that is then lost in later development.
- The contribution of limb lateral plate mesoderm to the *manubrium sterni* presents evidence that the mammalian sternum receives a contribution from the former scapulocoracoid, most likely the procoracoid. Preliminary data in zebrafish for a comparative genetic lineage labelling study support this notion.
- The attachment sites of the sternocleidomastoid muscle are limited to the outer perichondrial cell layer and fulfil the minimal conditions of the 'connectivity rule' as they are- as the connective muscle tissue- neural crest-derived. The morphological and molecular analysis of the sternal attachment of the sternocleidomastoid muscle shows a clearly layered organisation of the periost.

3.5 Discussion

3.5.1 The contribution of the limb lateral plate mesoderm to the shoulder girdle

The results from this study demonstrate the contribution of the lateral plate mesoderm associated with the limb to the shoulder girdle and confirm the origin of the mammalian scapula from the lateral plate mesoderm as reported by Durland et al.[60] The authors also noted an unlabelled- and therefore not lateral plate mesoderm-derived dorsal-most edge of the scapular blade, together with the absence of labelling in muscles inserting in this region (*M. rhomboideus*, *M. serratus* and *M. levator scapulae*), similar to the results of this study. This is suggestive of a very limited dorsal somitic contribution to the mammalian shoulder blade and contrasts with the situation in birds where the scapular blade has been shown to be entirely of somitic origin[31,87]. Experiments in the salamander *Ambystoma maculatum* demonstrate indirectly that the amphibian shoulder blade is derived from the lateral plate mesoderm like its mammalian counterpart[23], indicating that the avian condition can not be considered representative for tetrapods. The fact that the avian shoulder girdle is highly modified in the adaptation to flight might serve as a tentative explanation for this finding. The results obtained for the avian scapula also highlight a difference in the patterning of the somitic mesoderm and the lateral plate mesoderm: Huang et al.[87] showed that the somitic contribution to the scapular blade is clearly segmented, resulting in distinct stripes of cells originating from a defined axial level that do not mix with neighbouring cells. Early in the development of the murine scapular blade, limb lateral plate mesodermal cells labelled by the *Hand*2-Cre transgene form a homogenous cell population (Figure 3.5), in particular in the area of the scapular head and the coracoid. At later stages, the shoulder blade is then composed of a mix of labelled and unlabelled cells (Figure 3.9) which indicates that lateral plate mesodermal cells are not prevented from intermingling to the degree that somitic mesodermal cells apparently are. However, early domains of lateral plate mesodermal cells are well-defined and appear to play an organising role, so at E14, where the *Hand*2-Cre transgene domain apparently defines not only the shape of the scapula but also the layout of the surrounding muscles (Figure 3.8 B). The interaction

between labelled and unlabelled cell populations is non-random as can be seen from the organised, finger-like intercalations in the scapular blade (Figure 3.8 C). The intermixing of cell populations within the lateral plate mesoderm domain is not restricted to the scapula, as also the humerus is composed of mingled labelled and unlabelled cell groups, despite the fact that only the posterior-most edge of the limb bud is not labelled by the *Hand*2-Cre transgene[158] (Figure 3.8). Based on the observations in the mammalian scapula and in the upper limb, lateral plate mesoderm patterning appears to follow a three-step model:

At a first early stage, the initial shape of an element is defined; cell populations from different origins do not or hardly mix. A second stage is characterised by defined interactions between different cell populations within the now determined shape (as seen from the intercalation in the scapular blade). In the third and final stage, cell populations intermingle in a fully formed element. Whether the latter reflects the difference in patterning between lateral plate and somitic mesoderm[126,139] or could represent a more general phenomenon also valid for other cell populations remains to be seen and will require further studies into the stability of cell population boundaries throughout development.

We found no contribution of limb lateral plate mesodermal cells labelled by the *Hand*2-Cre transgene to any of the ribs. This is compatible with the results by Durland et al.[60] who observed that only the first rib received a lateral plate mesodermal contribution; based on our results, this contribution can now be identified as trunk lateral plate mesodermal. The *Hand*2-Cre transgene does not allow to distinguish trunk lateral plate mesoderm from somitic mesoderm but in combination with the results of Durland et al., murine ribs appear to be predominantly of somitic origin (with the afore mentioned minor contribution of trunk lateral plate mesoderm to the first rib). This contrasts with the view, mainly based on results in birds, that ventral ribs are like the sternum of lateral plate mesodermal origin[24,140,145]. (The murine Hoxb2 and Hoxb4 gene knockout mice cited as proof of lateral plate mesoderm origin of the sternal ribs show a major medial fusion defect of the sternal bands while ribs are still normally attached to the lateral aspect of these sternal bands[24,118]. This identifies the defect of the ventral body wall as fusion defect rather than caused by specifically affected lateral plate mesoderm). The differences in the embryonic origin of avian and mammalian ribs, together with the already noted differences in the shoulder blades, signify that functionally homologous

shoulder girdle structures between birds and mammals cannot be considered cellular homologues as they are derived from different embryological material.

3.5.2 The mammalian procoracoid

The analysis of the shoulder girdle of *Hand*2-Cre mice revealed that the upper part of the sternum (*manubrium sterni*) receives a contribution of cells marked by the *Hand*2-Cre transgene. Comparative analysis of the *Wnt*1-Cre mouse could rule out neural crest origin for these cells that must therefore be considered associated with the second domain labelled by the *Hand*2-Cre transgene, the lateral plate mesoderm of the forelimb. The incorporation of proximal limb elements into the *manubrium sterni* has already been suggested for marsupials as the cellular condensation of the procoracoid appear to merge into the upper sternum[101,200]. Although the *Hand*2-Cre transgene does not allow the identification of subparts of the scapulocoracoid complex, the comparison with the situation in marsupials suggests that the labelled cell population in the upper mouse *manubrium sterni* corresponds to the 'lost' procoracoid of placental mammals. A potential developmental scenario based on the results of this study and previous knowledge is depicted in Figure 3.25: The embryonic domain of limb lateral plate mesoderm that encompasses the scapula, and both elements of the coracoid (the metacoracoid and the procoracoid) reaches far proximally and ventrally (A). During the development of placental mammalians, neither of the coracoid elements is retained as separate entities as the metacoracoid becomes the coracoid process of the scapula and the procoracoid fuses with the *manubrium sterni* (B). This applies to the entire group of placentals. The procoracoid (also see introduction) is therefore not simply 'lost' in the evolution of the mammalian group but fuses with the sternal bands to give rise to the *manubrium sterni*.

The labelling observed in the muscle connective tissue surrounding the first and second rib most likely represents the remnants of the original limb lateral plate mesodermal domain into which somitic ribs then later invade. The schematic representation in (B) is imprecise in so far in as the scapular blade reaches beyond the second rib; absence of labelling in the caudal aspect of the scapular blade can be due

Figure 3.25

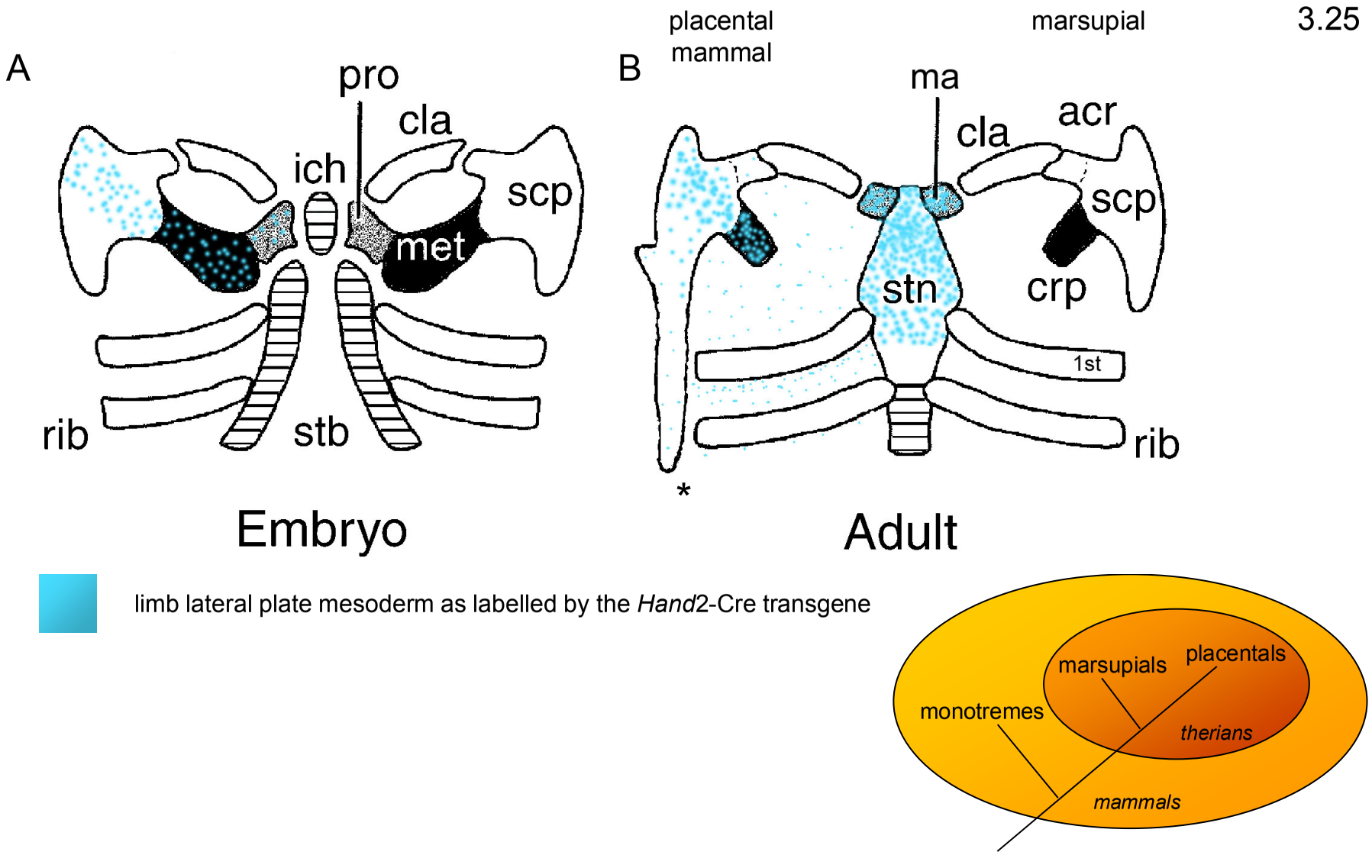
A
pro
cla
ich
scp
met
rib
stb
Embryo
placental
mammal
marsupial
B
ma
cla
acr
scp
stn
crp
1st
rib
*
Adult
limb lateral plate mesoderm as labelled by the *Hand*2-Cre transgene
marsupials
placentals
monotremes
therians
mammals

Figure 3.25 Scenario for the contribution of the limb lateral plate mesoderm to the shoulder girdle

A In embryonic development, the limb lateral plate mesoderm domain as visualised by the *Hand*2-Cre transgene reaches far proximally and ventrally, with the scapulocoracoid (scapula, coracoid= metacoracoid + procoracoid) complex as proximal-most element of the limb skeleton.

B Therians only retain the scapula as fully formed element; neither of the coracoid elements continues to exist as separate entities: the metacoracoid condensation becomes the coracoid process of the scapula and the procoracoid fuses with the manubrium sterni. This corresponds to the situation previously reported for marsupials (Klima 1987, Vickaryous et al. 2006). The labelling observed in the muscle connective tissue surrounding the first and second rib correspond to the remnants of the original limb lateral plate mesodermal domain into which somitic ribs then later invade. The unlabeled caudal aspect of the scapular blade can be due to the fact that the *Hand*2-Cre transgene does not label the posterior margin of the forelimb bud (Figure 3.4 and Ruest et al.) or due to a contribution of non-limb lateral plate mesoderm. A somitic contribution can be excluded as Durland et al. showed that this is limited to the dorsal-most edge of the blade. Placentals and marsupials belong to the therians, a sistergroup to monotremes; therians and monotremes form the mammalian group.

(Asterisk) The schematic representation of the scapular blade on the left (B) is imprecise in so far as it reaches beyond the second rib. Figure modified after Vickaryous et al. 2006.

acr acromion, ***cla*** clavicle, ***crp*** coracoid process, ***ich*** inter-clavicle, ***ma*** manubrium, ***met*** metacoracoid ***pro*** procoracoid, ***scp*** scapula, ***stb*** sternal bands, ***stn*** sternum

References

Durland, J. L., Sferlazzo, M., Logan, M. & Burke (2008); Klima, M. (1987); Ruest, L. B. *et al.* (2003); Vickaryous, M. K. & Hall, B. K. (2006)

to either the fact that the *Hand*2-Cre transgene does not label the posterior margin of the forelimb bud (Figure 3.4 and Ruest et al.[158]) or due to a contribution of trunk lateral plate mesoderm. A somitic contribution can be excluded, as Durland et al.[60] showed that the entire murine scapular blade is lateral plate mesoderm-derived with a somitic contribution limited to the dorsal-most edge of the blade.
The identification of the upper part of the murine *manubrium sterni* as element of the ancient scapulocoracoid complex shows once more that skeletal elements are not simply 'lost' in evolution but rather cease to exist as distinct entities after fusion with adjacent skeletal elements[122]. Future understanding of the developmental and evolutionary processes governing the formation of the shoulder girdle will therefore essentially rely on our ability to disentangle the different cellular contributions that the latter receives.

3.5.3 A 'minimal' connectivity rule and general aspects of attachment formation

The detailed analysis of the attachment sites of the sternocleidomastoid muscle proves once more the general validity of the 'connectivity rule' according to which the attachment and the connective tissue of a muscle originate from the same embryonic cell population[102]. The attachment sites of the sternocleidomastoid muscle thereby fulfil the minimal condition of the 'connectivity rule': a neural crest-derived muscle attaches to a single layer of neural crest cells on a mesodermal base. This disproves both of our working hypotheses for the sternal attachment of the sternocleidomastoid muscle (Figure 3.26): the attachment of the neural crest-derived muscle is effected by neural crest cells, according to the connectivity rule and falsifying working hypothesis 1. Despite the fact that the attachment follows the connectivity rule, it only fulfils the minimal requirement- a single layer of cells- as there is no major neural crest contribution to the *manubrium sterni*, this falsifies working hypothesis 2. This superficial nature of the attachment site with a neural crest 'veneer' on a mesodermal background is not restricted to the sternal origin but equally applies to the clavicular origin and the insertion of the muscle at the mastoid process. Also the trapezius muscle, as whose anterior division the sternocleidomastoid muscle is considered,

Figure 3.26

Conclusion: a ‘minimal connectivity rule’

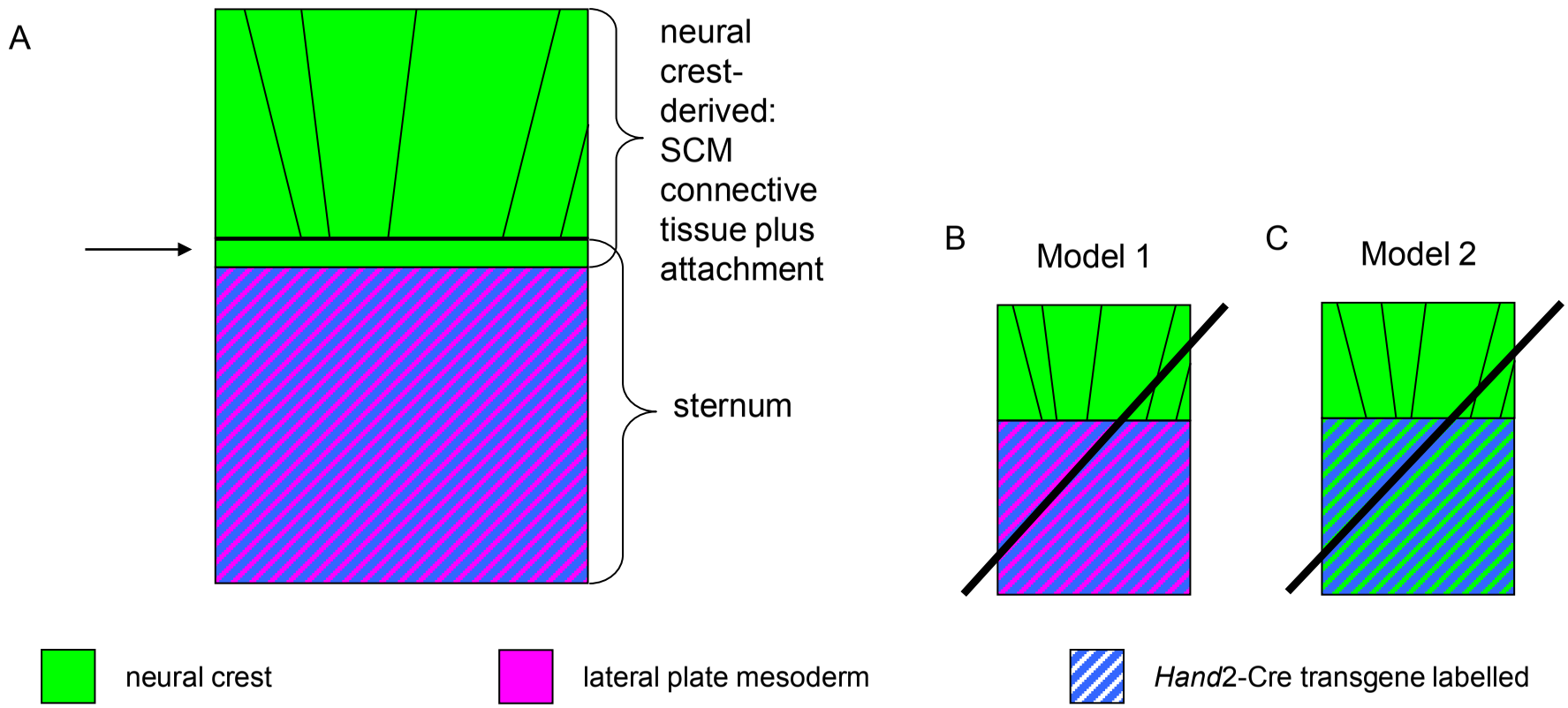

Figure 3.26 Summary: a ‘minimal connectivity rule’

A The muscle connective tissue of the sternocleidomastoid muscle (SCM) including its superficial attachment comprising a single layer of cells are neural crest-derived, while the sternum is of lateral plate mesodermal origin. This fulfils the minimal condition for the ‘connectivity rule’ (here called ‘minimal connectivity rule), according to which muscle connective tissue and attachment site are of shared embryonic origin.

B, **C** Neither of the original models was correct as the boundary between neural crest and lateral plate mesoderm in the sternum lies very superficially but nevertheless below the neural crest-derived attachment of the sternocleidomastoid muscle (**B**). The labelling in the manubrium sterni by the *Hand*2-Cre transgene reflected a contribution of the limb-associated lateral plate mesoderm to the manubrium and not a new *Hand*2-positive neural crest domain (**C**).

shows similar attachment sites at the spinous processes. This 'veneer' of neural crest on a mesodermal base at the attachment sites of the sternocleidomastoid muscle is comprehensible in the light of the evolution of the muscle. As anterior division of the dorsally located neural crest-derived trapezius muscle, the sternocleidomastoid muscle, migrates in evolution anteriorly and ventrally over mesodermal territory, taking its neural crest attachment with it; this results in a neural crest veneer on a mesodermal base at its attachment sites. The mammalian trapezius muscle itself has experienced considerable dorsal and caudal expansion during evolution, which is still reflected in its neural crest-derived attachment sites at the spinous processes of the otherwise mesodermal vertebral column.

Although all these attachments apparently occur at a neural crest/ mesodermal interface, a considerable neural crest contribution is found within the clavicle and in the spinous processes, both of which are undergoing ossification at the time-point of analysis. A contribution of neural crest has also been reported for the mastoid process and the upper part of the sternum[122] which this study does not appear to confirm. However, as both of these structures are still cartilaginous at the time-point of analysis, this in all likelihood represents different stages of attachment formation and maturation. A possible scenario could therefore be that attachments at the anterior margin of the shoulder girdle are initially established at the neural crest/ mesoderm interface and that a neural crest contribution to the underlying skeletal element occurs secondarily.

The molecular perichondrial/ periosteal markers used in this study also label the fibres effecting the muscle attachment; this underligns the unity and continuity of muscle, attachment and perichondrium/ periost on a molecular level. The cellular retinoic acid binding protein 1 (CRABP1) was identified as specifically expressed at muscle attachment sites[14]. Immunohistochemistry combined with confocal imaging in high resolution could demonstrate that the actual muscle attachment is established between two cells that are immunoreactive for CRABP1 (Figure 3.22). Retinoic acid is necessary for the establishment of myotendinous junctions[156], but the presence of cellular retinoic acid binding protein 1 (CRABP1) in attachment cells could indicate that retinoic acid also controls the establishment of the tendon-bone junction.

Future work will be required to better understand the temporal aspects of attachment formation, in particular the roles of the different cell populations involved and the molecular processes by which these are controlled.

4 *Hand*2 controls aspects of epithelial and mesenchymal cell layer formation

4.1 Overview

The transcription factor *Hand*2 is involved in a range of early developmental processes, such as cardiogenesis, the patterning of limbs and the branchial arches and the development of the autonomous nervous system[1,46,63,63,79,80,123,124,129,158,178,180,212]. Highly sensitive fluorescent RNA *in situ* hybridisation in late stages of intrauterine mouse development identifies here additional and previously unknown expression domains of *Hand*2 in the dental epithelium and at sites of forming dermal bone. This is suggestive of additional functions of *Hand*2 in later developmental processes. The two *Hand*2 expression domains in the dental epithelium and in dermal bone appeared unrelated at first sight; however, *Hand*2 function in both systems was governed by the same 750bps regulatory module which suggests a mechanistic link between the two processes. The specific alterations in the anatomical architecture we observe after the loss of *Hand*2 function in both the dental epithelium and dermal bone reveal a perturbed organisation of cellular layers. Two recent publications have suggested a role for *Hand*2 in the establishment of epithelial polarity which allows cells to arrange and move in layers or sheets[195,208]. Against this background, *Hand*2 appears fundamentally involved in the control of epithelial and mesenchymal cell layer formation across a diversity of organ systems.

4.2 Table of Contents

4.3 Introduction

Cellular organisation in layers requires planar cell polarity

The organisation and coordinated behaviour of cells in layers or sheets is crucial to many morphogenetic processes. Epithelia are the most obvious example of layered cellular organisation which occurs along two axes: The first axis describes the polarity between the basal membrane and the apical surface of the epithelium- called apico-basal polarity- and is almost always prerequisite for the correct functioning of the system, e.g. in the renal or the intestinal epithelium. Perpendicular and genetically linked[57,182] to the first axis lies the second axis- called planar cell polarity (short: PCP, previously also called tissue polarity)- which describes the organisation of cells along the plane of the epithelium. PCP has long been recognised and extensively studied in *Drosophila*, where most adult cuticular structures and the omatides of the eye show evidence of PC polarity[173,207]. However, PCP is neither restricted to invertebrates nor epithelia, as vertebrate mesenchymal processes such as gastrulation and neurulation have been shown to be similarly controlled (review on vertebrate PCP[173]). In mesenchymal processes like the convergent extension during gastrulation, planar cell polarity ensures the coordinated and directed behaviour of cells within a cellular sheet that is required for cell migration and cell intercalation.

The genetic pathway traditionally associated with planar cell polarity is the evolutionary conserved non-canonical *Wnt*/PCP pathway (reviewed in e.g. [48,62,72,98,99,173]). The central components of the *Wnt*/PCP pathway are thought to be common to all structures with planar cell polarity and that specificity results from the interaction with tissue-specific factors[172]. In the example of epithelia, canonical *Wnt* signalling, the *Notch* and the *TGF*ß/*BMP* pathway converge to control single aspects of epithelial behaviour and are transduced to the non-canonical *Wnt* pathway for planar cell polarity and controlled cell movement and to the canonical *Wnt* pathway for tissue differentiation[100]. However, recent evidence suggests that other pathways besides the *Wnt*/ PCP pathway are directly controlling aspects of planar cell polarity, such as the member *Nodal* of the *TGF*ß family in *Xenopus* gastrulation[115].

To our knowledge, there are no known reports of interactions between the transcription factor *Hand*2 and the *Wnt*/PCP pathway. However, Trinh et al. report that loss of *Hand*2 function in the zebrafish myocardial epithelium leads to a disruption of the myocardial cell sheet and a randomised expression of apico-basal cell markers[195], which provides first evidence for a role of *Hand*2 in the organisation of cellular sheets. In a different publication, Xiong et al observe a disruption of the architecture of the oral epithelium after the inactivation of *Hand*2[208], further supporting an involvement of *Hand*2 in the formation of cell layers.

Data showing that *Hand*2 plays a role in the establishment of cell layers in two further and unrelated tissues, the dental epithelium and in dermal bone, which suggests a truly general phenomenon, will be presented and discussed in this chapter.

4.4 Part 1- A role for Hand2 in the formation of the dental epithelium

4.4.1 Background

The dental epithelium

Teeth are structures of mixed embryological origin and develop in an interaction between the oral ectoderm and the underlying mesenchyme (see Figure 4.1). Tooth formation begins as a circumscribed thickening of the oral epithelium (A, B) that then continues to proliferate, starts to invaginate into the underlying mesenchyme and induces a condensation of the surrounding mesenchymal tissue (C, arrow). The morphology of the invaginating epithelium changes from bud-shaped to bell-shaped (C, D) and the ectodermal 'bell' starts to enclose the underlying condensed mesenchyme, which will later form the papilla of the tooth (E). The change from bud to bell- shape coincides with a differentiation of the epithelium into an outer and inner dental epithelium (D, E). With ongoing development, the upper connection to the dental epithelium disappears, leaving behind the tooth germ enclosed by mesenchyme and without a connection to the oral epithelium from which it originated. In succession, the inner dental epithelium develops into enamel-producing ameloblasts, a process that is dependent on the interaction with the underlying mesenchyme. Amelogenesis involves three major stages: pre-secretory, secretory and maturation stages, during which the cells change their polarity and take on a characteristic highly polarised morphology[132]. Ameloblast polarisation has been shown to be linked to secretory activity[42] and the rodent incisor provides a good example for this. As a particularity, the rodent incisor is covered with enamel only on the labial but not the lingual side of the tooth which creates a sharp cutting edge at the tip[69]. Enamel production thereby correlates with ameloblast differentiation on the labial side of the tooth and is absent in the area of undifferentiated ameloblasts on the lingual side[42]. On the level of gene regulation, Follistatin has been shown to be at the source of this asymmetry as it specifically inhibits ameloblast differentiation on the lingual side of the incisor[205]. To our knowledge, *Hand*2 expression in the dental epithelium has not been previously reported. Dental *Hand*2 expression is currently considered to be specific to the mesenchyme of

Figure 4.1

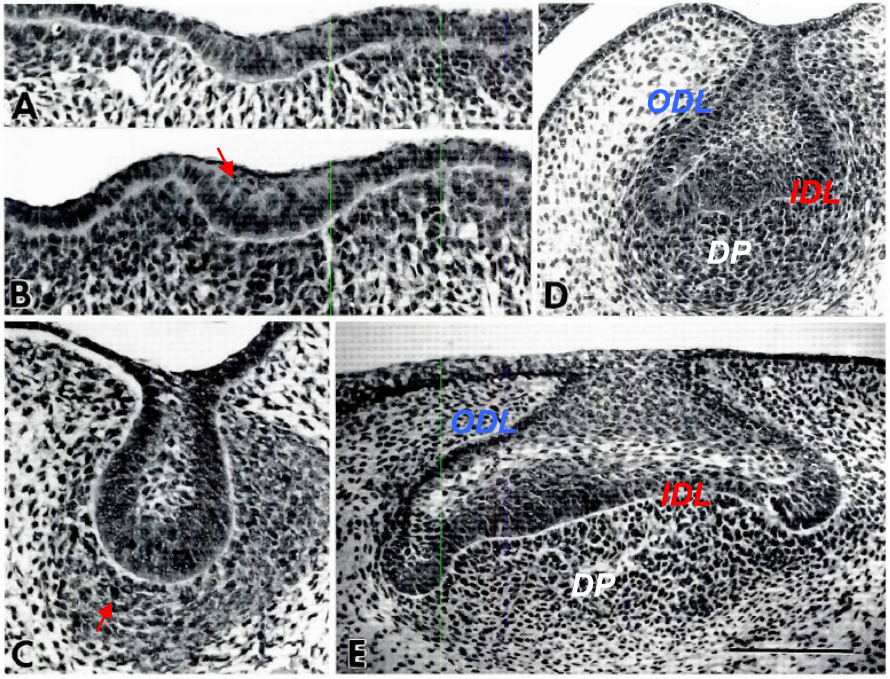

annotated after Zeichner-David et al. 1995 (Figure 2)

Figure 4.1 Early stages of murine tooth morphogenesis

A E9/10 The odontogenic placode is recognisable as a slight thickening of the oral epithelium.

B E10/E11 Local proliferation in the epithelium leads to formation of the dental lamina (arrow).

C E12 The dental lamina further proliferates and invaginates into the underlying mesenchyme, inducing a reaction in the surrounding mesenchymal tissue (arrow) and forming a tooth bud.

D E14 Early cap stage. Outer (ODL, blue) and inner (IDL, red) dental epithelium have formed.

E E15 Cap stage. Outer and inner dental epithelium show now distinct morphologies.

DP dental papilla, ***IDL*** inner dental epithelium, ***ODL*** outer dental epithelium

Scale bar 100 µm

the lower incisor; the authors had also antagonised *Hand*2 function in explanted incisors with antisense oligodeoxinucleotides and had observed an effect on both odontoblasts and ameloblasts, but had interpreted the effect on ameloblasts as indirect[2].

4.4.2 Results

4.4.2.1 *Hand*2 expression in the dental epithelium

Sensitive fluorescent RNA *in situ* hybridisations of the lower jaw of E14.0 and E16.0 *Hand*2-Cre mouse embryos (Figure 4.2 and 4.3) reveal that *Hand*2 expression is in contrast to previous reports not specific to the mesenchyme of the lower incisor[2]. According to our results, *Hand*2 is generally expressed in the dental epithelium of developing tooth buds of both lower and upper jaw. At E14.0, *Hand*2 expression can be seen within the mesenchyme of the tooth buds but is mainly found lining the invaginating layer from the oral ectoderm (Figure 4.2, arrows). The expression thereby appears slightly stronger on the lingual than on the labial side of the forming bud. Two days later, at E16.0, *Hand*2 is clearly expressed throughout the entire dental epithelium and in particular in the inner dental epithelium (Figure 4.3 shows *Hand*2 expression in molar tooth buds).

4.4.2.2 *Hand*2 expression defines a morphologically distinct ameloblast subpopulation in the lower incisor

*Hand*2 expression in the lower incisor shows a particularity in so far in that gene expression in the inner dental epithelium is restricted to the labial part and excluded from the lingual part of the tooth (Figure 4.4). The difference in *Hand*2 expression reflects a morphological change in the ectodermal layer: the part devoid of *Hand*2 expression appears as a monolayer of cubic cells, whilst the *Hand*2 positive part corresponds to a stratified epithelium. Interestingly, double fluorescent RNA *in situ* hybridisation (RISH) for *Hand*2 and *cre* reveal that the regulatory elements for endogenous *Hand*2 expression in the dental epithelium are contained within the 7.4kb

Figure 4.2- 4.4

*Hand*2-Cre+/-; Rosa26LacZR-/-

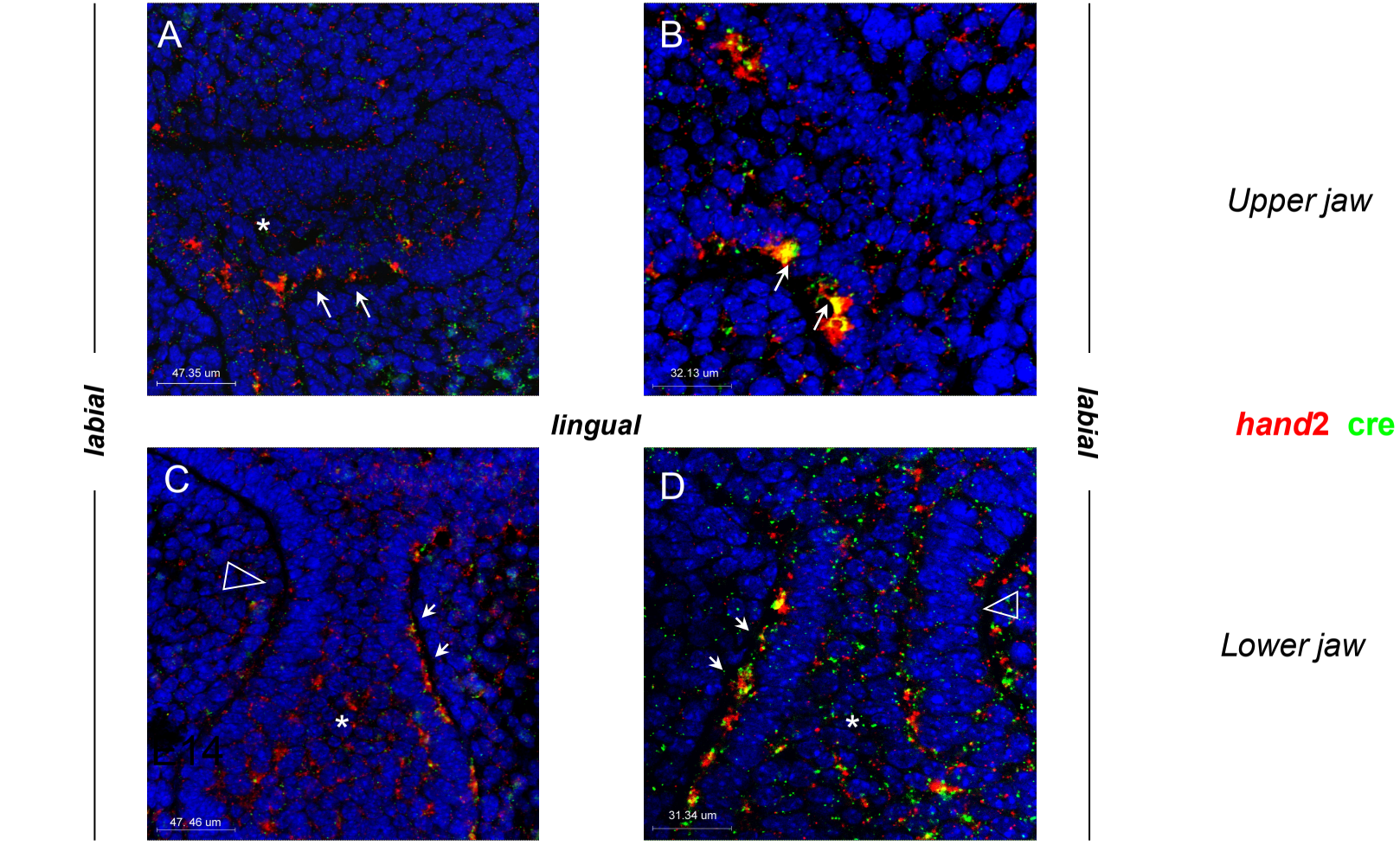

Figure 4.2 *Hand*2 is differentially expressed on the lingual side of upper and lower tooth buds

Fluorescent double RNA *in situ* hybridisation for endogenous *hand*2 expression (red) and cre expression (green) from the *Hand*2-Cre transgene, counterstain is DAPI (blue). Transverse sections of E14 *Hand*2-Cre+/-; Rosa26LacZR-/- embryos of upper (**A**, **B**) and lower (**C**, **D**) jaw tooth buds, the labial and lingual orientation of the bud is indicated.

A, B Upper tooth buds of the left and right side. *Hand*2 expression (red) is particularly strong in an area on the lingual side of the tooth bud (arrows), replicated by weaker cre expression of the *Hand*2-Cre transgene (green).

C, D: Left and right lower tooth buds. Also in tooth buds of the lower jaw, *hand*2 expression is stronger on the lingual (arrows) than on the labial side of the bud (empty triangle). *Hand*2 gene and cre expression from the *Hand*2-Cre transgene are here also seen within the bud (asterisk).

*Hand*2-Cre+/-; Rosa26LacZR-/-

4.3

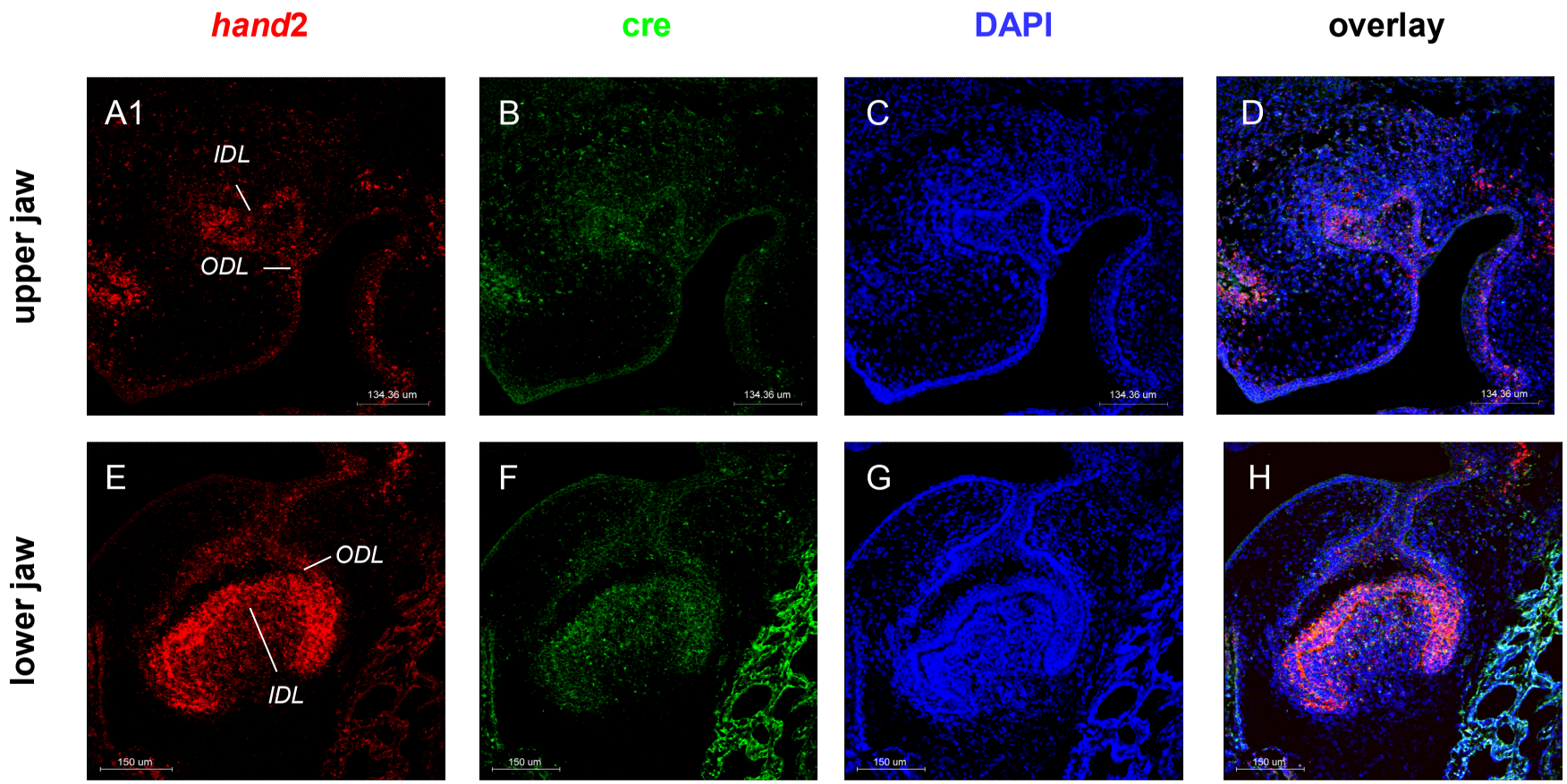

E16

Fig 4.3 *Hand*2 expression and Cre expression from the *Hand*2-Cre transgene in E16 tooth germs at cap stage

Fluorescent RNA double *in situ* hybridisation for *hand*2 (red) and cre (green) from the *Hand*2-Cre transgene, counterstained with DAPI (blue), on frontal sections of upper jaw(**A- D**) and lower jaw (**E- H**) tooth germs at early (**A- D**) and later (**E- H**) cap stage (E16 *Hand*2-Cre +/-; Rosa26Lac -/- embryos). For better visibility, channels are first shown separately (**A- C**, **E- G**) and then in overlay (**D**, **H**).

*Hand*2 is expressed in the inner and outer dental epithelium (IDL, ODL) at cap stage (**A**, **E**). Expression in the IDL increases during cap stage development (**A, E**) with persistent weaker expression in the ODL (**D**).

The *Hand*2-Cre transgene replicates endongenous *Hand*2 expression (**B, F**), albeit with a certain delay in the expression.

IDL inner dental epithelium

ODL outer dental epithelium

*Hand*2-Cre+/-; Rosa26LacZR-/-

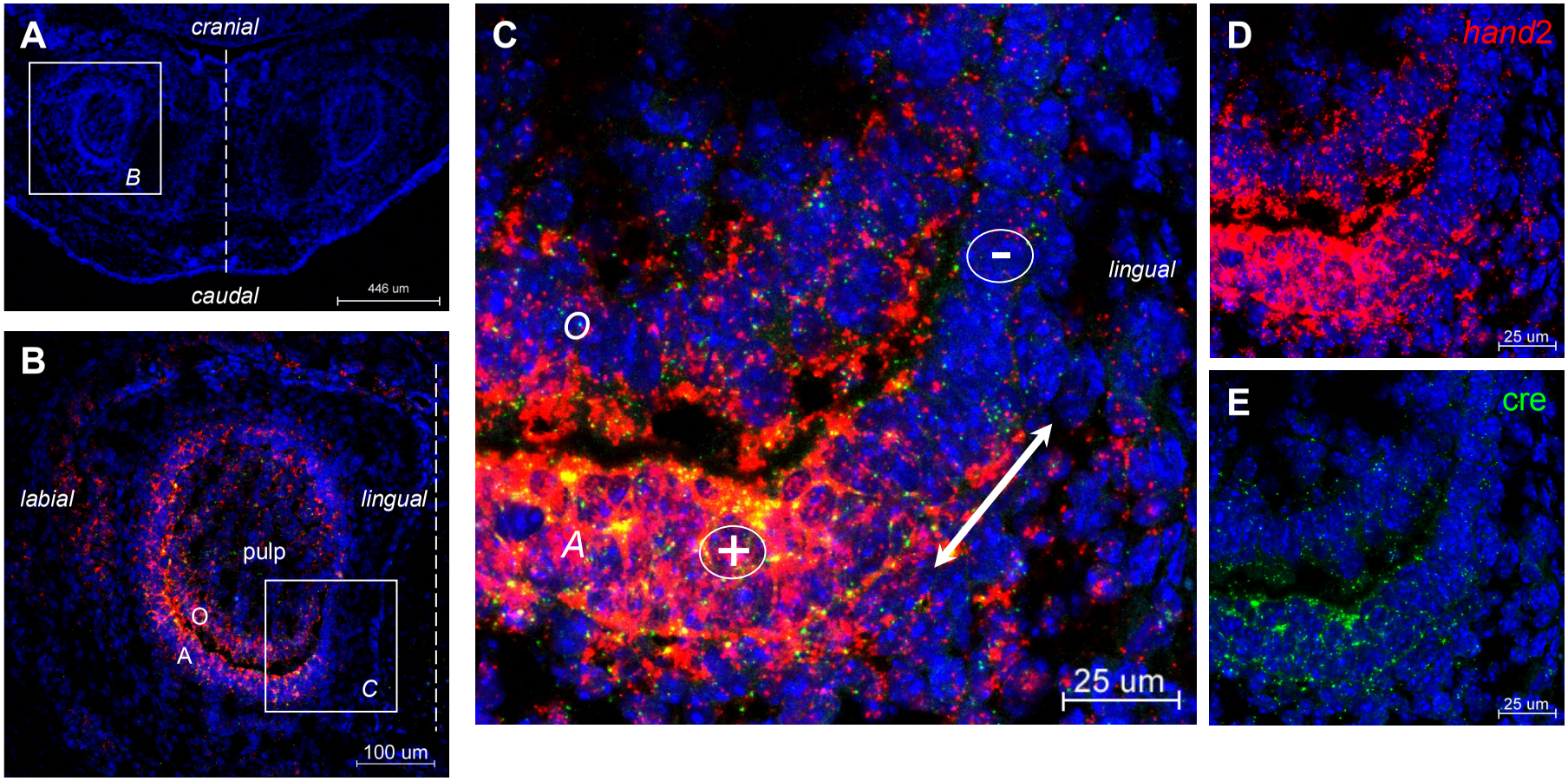

E16

Fig 4.4 *Hand*2 and *Hand*2-Cre transgene label the dental epithelium on the labial but not the lingual side of the lower incisor

Fluorescent double RNA *in situ* hybridisation for *hand*2 (red) and cre (green) on frontal sections of the lower incisor region of E16.0 Hand2- CRE+/-; Rosa26LacZR-/- embryos, counterstained with DAPI (blue). **B- E** are higher magnifications of the incisor boxed in A.

A Overview of the lower jaw with incisors (DAPI channel only). The midline of the specimen is indicated by a dashed line.

B The boxed incisor of A shown in slightly higher magnification. *Hand*2 expression can be found on the labial but not the lingual side of the lower incisor.

C Higher magnification of the area indicated in **B** shows the boundary of the *hand*2 expression domain with no expression on the lingual side (-). Hand2 expression coincides with a change of morphology in the dental epithelium: while the *hand*2 negative part (-) of the dental epithelium displays cell arrangement in a monolayer, the *hand*2 positive part (+) is multilayered (arrow indicates the transition). For better appreciation of the signal, the red and green channel are shown separately in **D** and **E** respectively, showing endogenous *hand*2 (**D**) and cre (**E**) expression from the *Hand*2-Cre transgene. Albeit weaker, the transgene replicates endogenous *hand*2 expression.

A ameloblasts

O odontoblasts

of *Hand*2 upstream region as the *Hand*2-Cre transgene replicates endogenous *Hand*2 expression (Figures 4.2- 4.4). This apparently contradicts the results obtained by conventional X-Gal staining on sections of *Hand*2-Cre$^{+/-}$;Rosa26LacZR$^{-/-}$ newborn mice (Figure 4.5 and 4.6). With conventional X-Gal staining, no signal is detectable in the upper jaw, including upper teeth (Figure 4.5 A- C and Figure 4.6 A- B). Labelling in the lower half of the face is restricted to neural crest-derived parts such as the dentary and surrounding connective tissue. Signal in teeth of the lower jaw is restricted to the neural crest-derived odontoblasts (O) but excluded from the ectodermal ameloblast layer (A) and the stratum intermedium (SI), (Figure 4.5 E (asterisk), F and Figure 4.6 D). The discrepancy between the results obtained by RISH and X-Gal could be resolved as a sensitivity issue because immunohistochemistry (IHC) against ß-Galactosidase was able to validate the RISH results (Figure 4.6 and 4.7).

Immunohistochemistry for ß-Galactosidase in *Hand*2-Cre$^{+/-}$; Rosa26LacZR$^{-/-}$ mice on sections of lower incisors uncovers molecular differences at the base of the morphological differences between incisor ameloblast subpopulations (Figure 4.7). Ameloblasts immunoreactive for ß-Galactosidase , indicating past or present expression of *Hand*2, form a highly structured monolayer with a strictly parallel alignment of cells (D, E). The clear polarisation of the layer is recognisable by basally located elongated nuclei (E, with exception of the transitional zone shown in D) and mirrored in a stratum intermedium with regular architecture consisting of a layer of cubic cells encased by Periostin 'boxes' (arrows in D, E). In contrast, the ß-Galactosidase-negative ameloblast subpopulation forms a multi-layered epithelium with rounded nuclei and no sign of orientation (C). The lack of organisation also extends to the underlying stratum intermedium that instead of the 'Periostin boxes' of the organised region shows long Periostin fibres (arrows in C). The boundary between unorganised/ unlabeled and organised/ labeled ameloblasts and stratum intermedium is distinct (arrow in D), with a small intermediate zone of approximately 10 cells with weaker labelling for ß-Galactosidase and elongated but not (yet?) basally located nuclei. The underlying stratum intermedium equally shows an intermediate state with stronger Periostin immunoreactivity than in the unorganised part but still lacks the characteristic 'Periostin boxes'.

Signs of present or past *Hand*2 expression in the dental epithelium are not specific for the ameloblast layer of lower incisors but also seen in the ameloblasts of upper molars. However, a similar transition between labelled and unlabelled ameloblast as found in

Figure 4.5- 4.7

4.5

Upper jaw

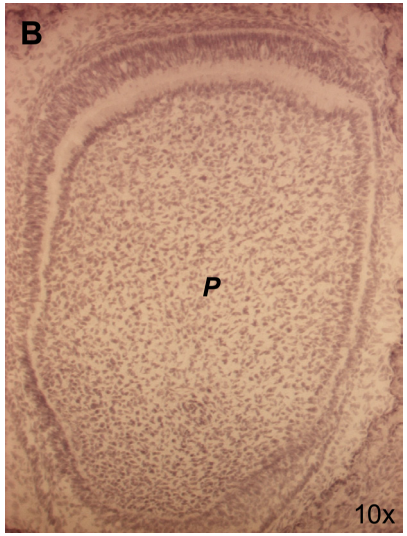

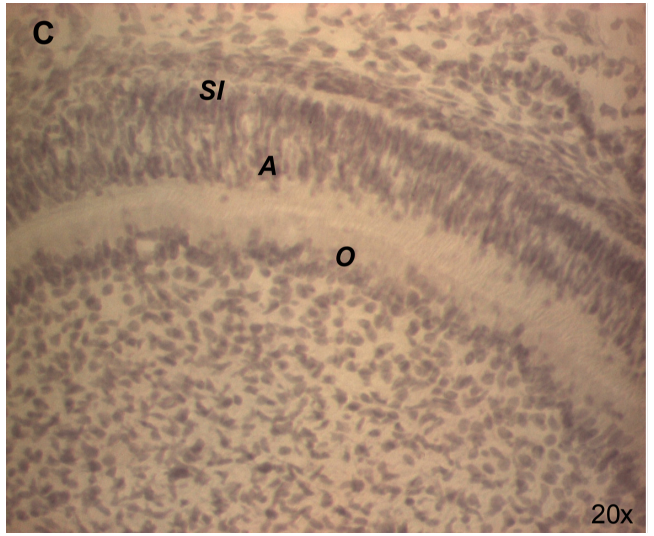

Lower jaw

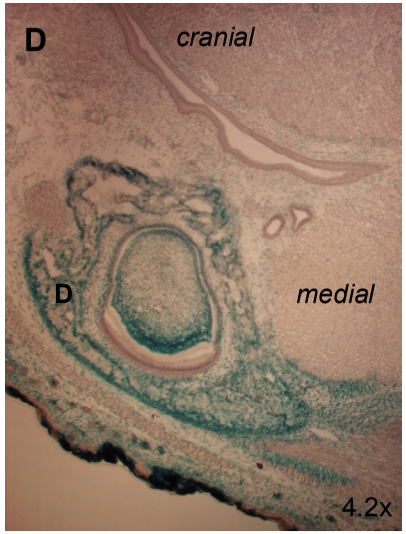

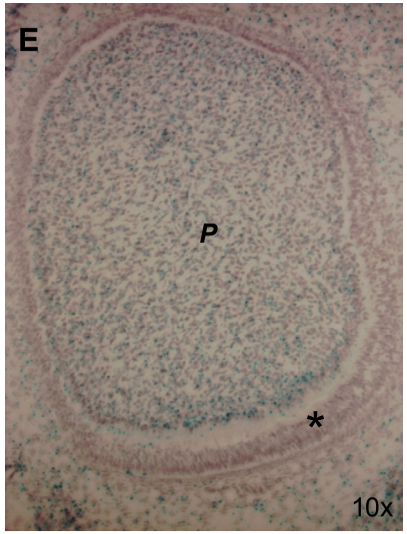

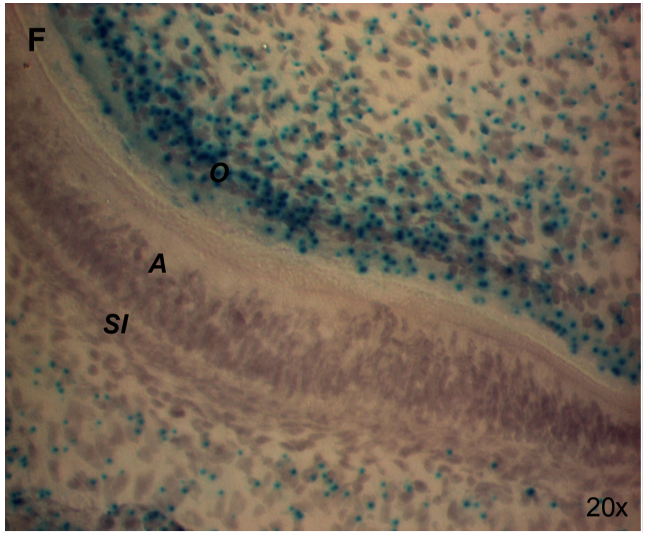

Figure 4.5 Comparison of *Hand*2-Cre transgene labelling in upper and lower incisors

ß-Galactosidaseand Hematoxylin Staining of frontal sections of the anterior jaw region of *Hand*2-Cre +/-, Rosa26LacZR -/- newborn mice. Increasing magnification of upper (**A- C**) and lower (**D- F**) incisors.

The upper incisor (**A- C**) is entirely unlabeled by the *Hand*2-Cre transgene, while the lower jaw shows labelling in the dentary bone (***D***, **D**) as well as the pulp (***P***, **E**) and the odontoblasts (***O*****, F**) of the lower incisor. No staining for ß-Galactosidasecan be found in the ectodermally derived ameloblasts and stratum intermedium in neither upper (**C**) nor lower (**F**) incisor.

A ameloblasts, ***D*** dentary bone, ***O*** odontoblasts, ***P*** pulp, ***SI*** stratum intermedium.

Upper jaw

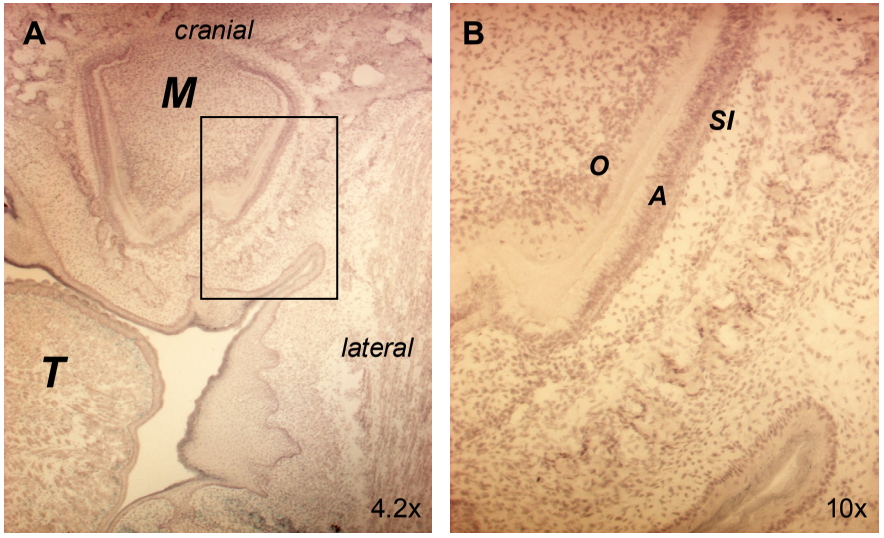

Lower jaw

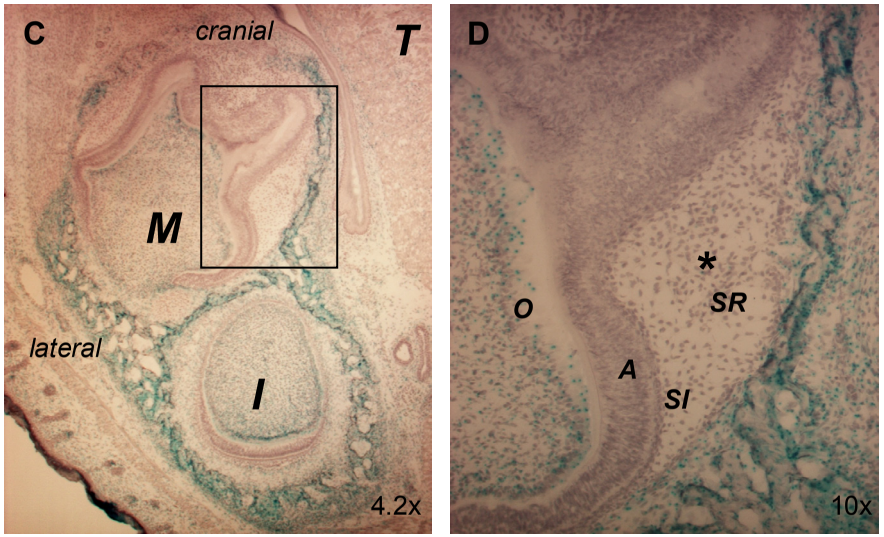

Figure 4.6 *Hand*2-Cre transgene labelling in molars of the upper and lower jaw

Frontal section of the oral region of a *Hand*2-Cre+/-; Rosa26LacZR -/- newborn mouse with upper and lower molars. X-Gal staining with Hematoxylin counterstain. Upper (**A, B**) and lower (**C, D**) molars are shown in overview (**A, C**) and detail (**B, D**), magnification as indicated.

A, B No signal from the *Hand*2-Cre transgene can be detected with X-Gal staining in the molars of the upper jaw nor in the upper jaw bone itself.

C, D The odontoblasts (*O*) of lower molars stain positively for Beta- Galactosidase, while the ameloblast layer (*A*) and the stratum intermedium (*SI*) appear entirely unlabeled. Equally unlabelled is the stratum reticulare (*SR*, asterisk in **D**).

A ameloblasts, ***I*** incisor, ***M*** molar, ***O*** odontoblasts, ***SI*** stratum intermedium, ***SR*** stratum reticulare, ***T*** tongue.

4.7

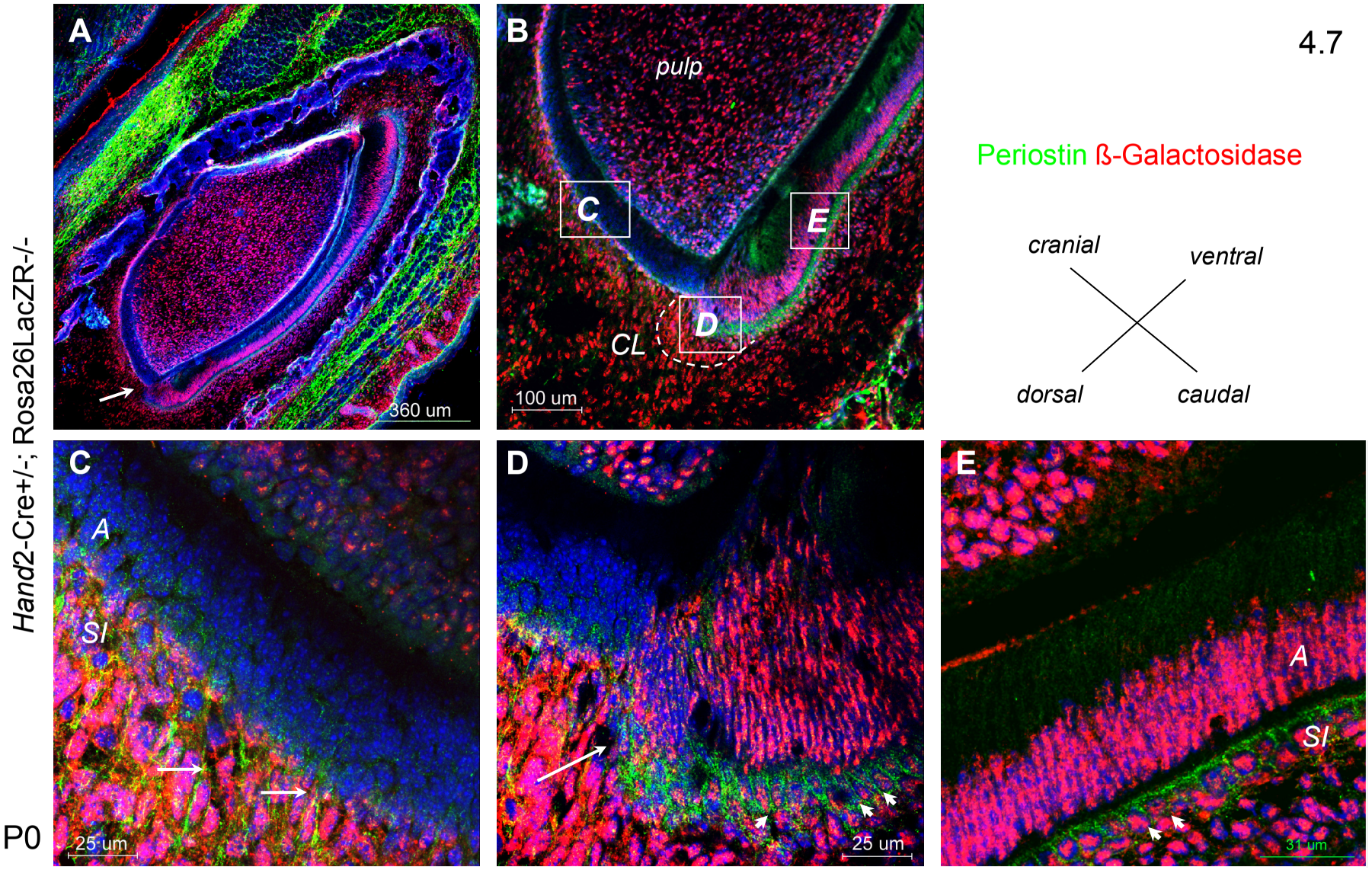
Hand2-Cre+/-; Rosa26LacZR-/-
P0
A
B
pulp
C
E
D
CL
360 um
100 um
Periostin ß-Galactosidase
cranial
ventral
dorsal
caudal
C
A
Sl
25 um
D
25 um
E
A
Sl
31 um

Figure 4.7 The *Hand*2-Cre transgene defines a subpopulation of incisor ameloblasts

Sagital sections of the head of *Hand*2-Cre+/-; Rosa26Lac-/- newborns. IHC* for Periostin (488, green), ß-Galactosidase(POD-conjugated, Cy3- tyramide amplified, red), nuclear counterstain: DAPI (blue).

A Overview of the lower incisor. The arrow indicates the transition between labeled and unlabeled ameloblasts in the lower incisor.

B Higher magnification of the transition area with the boundary between labeled and unlabeled ameloblasts (as indicated by the arrow in **A**) and the positioning of the details shown in **C**- **E**. The cervical loop and the polarised ameloblast layer are labelled by the *Hand*2-Cre transgene.

C Ameloblasts (A) unlabeled by the Hand2-Cre transgene show round nuclei and no morphological signs of cell polarisation. The underlying stratum intermedium (SI) shows losses Periostin fibers but not strict organisation.

D In the area of the cervical loop (as indicated by the dashed line in **B**), ameloblast morphology can be corelated with abent or present transgene expression: round ameloblasts from the mulitlayered part on the left are not labelled by the Hand2- Cre transgene; elongated monolayered ameloblasts on the right express the transgene. Between the two ameloblast populations with distinctly different morphology, a cell population with intermediate characteristics is found (long arrow). The stratum intermedium below the elongated monolayered ameloblasts shows a characteristic organisation with cells ‘sitting in Periostin boxes’ (short arrows)

E Ameloblasts labeled by the *Hand*2-Cre transgene are characterised by elongated nuclei and clear cell polarisation. The stratum intermedium shows a clear boxed organisation (short arrows).

A ameloblasts ***CL*** cervical loop ***SI*** stratum intermedium

* IHC was performed according to standardized conditions; a detailed description of conditions and antibodies (primary and secondary) can be found in the relevant section under ‘Materials and Methods’ (Chapter 7.5.4).

4.7

the lower incisor is not observed (Figure 4.8 and 4.7 for the lower incisor). Surprisingly, also the odontoblasts of the upper molars show immunoreactivity for ß-Galactosidase. As a control for the specificity of the anti-ß-Galactosidase antibody, the neural crest contribution to the lower incisor of E18.0 *Wnt*1-Cre$^{+/-}$; Rosa26LacZR$^{-/-}$ mice was therefore comparatively evaluated by conventional X-Gal staining and immunohistochemistry for ß-Galactosidase under conditions identical to the ones used for the analysis of the *Hand*2-Cre+/-; Rosa26LacZR$^{-/-}$ mice (Figure 4.9). *Wnt*1-Cre mice have been described previously[50]; the *Wnt*1-Cre transgene serves as a lineage marker for the neural crest. ß-Galactosidase is neither detected by X-Gal staining nor by immuno-histochemistry in the ameloblast layer and in the stratum intermedium of the lower incisor, both of which can be easily identified due to their characteristic architecture: ameloblasts are elongated, highly polarised cells with basally localised nuclei and basally localised endoplasmic reticulum. The stratum intermedium (SI) consists of small round cells in a network of F-actin fibres. This confirms that ameloblasts and stratum intermedium are indeed not neural crest-derived and that the antibody for ß-Galactosidase does not unspecifically recognize these structures.
The immunohistochemical signal detected in the teeth of *Hand*2-Cre mice must therefore be considered to reflect real *Hand*2 function.

4.4.2.3 Loss of *Hand*2 function leads to polarity defects in the ameloblast layer of the lower incisor

The correlation between past and present *Hand*2 expression and the polarised ameloblast morphology in the lower incisor led us to test the role of *Hand*2 in the process of ameloblast polarisation by loss-of-function experiments.
The total inactivation of *Hand*2 function in mice does not produce viable off-spring as embryos do not survive past embryonic stage 10[180]. To circumvent the problem of embryonic lethality, genetically modified mouse lines have been created that allow partial inactivation of *Hand*2 ([79,211], also see the overview in the Introduction of the genetically modified mouse lines used for this thesis). In one of the lines, the *Hand*2 branchial arch enhancer knockout (*Hand*2 BAenh$^{-/-}$), Yanagisawa et al. deleted a *Xho*I-

Figure 4.8- 4.9

*Hand*2-Cre+/-; Rosa26LacZR-/-

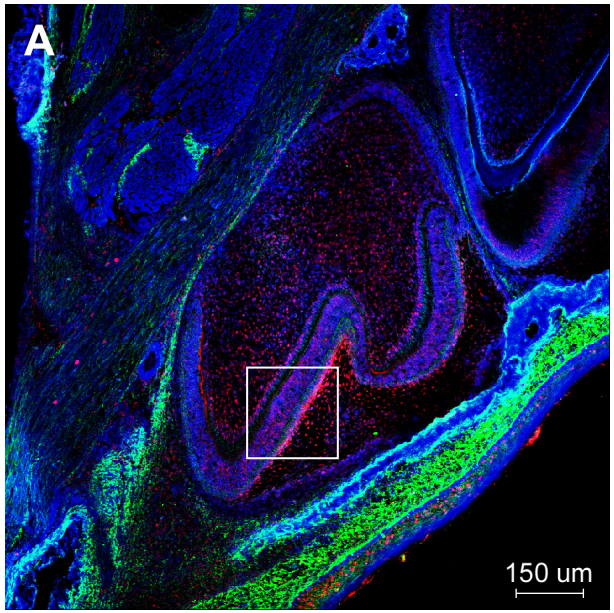

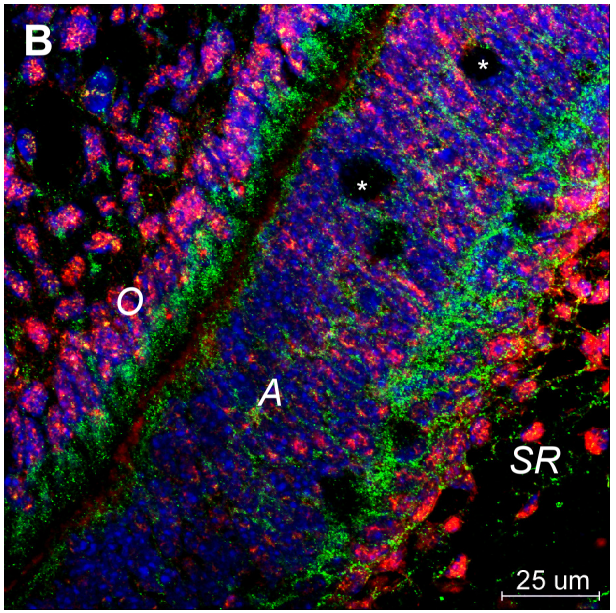

Periostin ß-Galactosidase

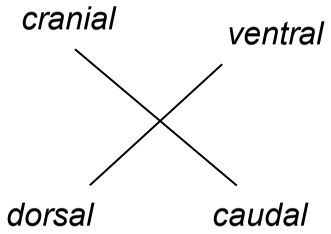

P0

Figure 4.8 The *Hand*2-Cre transgene also weakly labels ameloblasts of the upper molar

Sagital sections of the head of *Hand*2-Cre+/-; Rosa26LacZR-/- newborns. IHC for Periostin (488, green), ß-Galactosidase (POD- conjugated, Cy3- tyramide amplified, red) and DAPI (blue). Images show a molar in the upper jaw in an overview (**A**) and its ameloblast layer in higher magnification (**B**).

A Overview of the upper molar with box indicating the location of (**B**). Impossible to judge from this magnification but all ameloblasts of the upper molars stain weakly positive for ß-Galactosidase as shown in (**B**).

B The higher magnification reveals that also ameloblasts (*A*) of the upper jaw molars show albeit weak labelling by the *Hand*2-Cre transgene. Strong labelling is further observed in odontoblasts (*O*) and in the stratum reticulare (SR). The black circular structures (asterisks) are artefacts.

A ameloblasts, ***O*** odontoblasts

* IHC was performed according to standardized conditions; a detailed description of conditions and antibodies (primary and secondary) can be found in the relevant section under ‘Materials and Methods’ (Chapter 7.5.4).

*Wnt*1-Cre+/-; Rosa26LacZR-/-

4.9

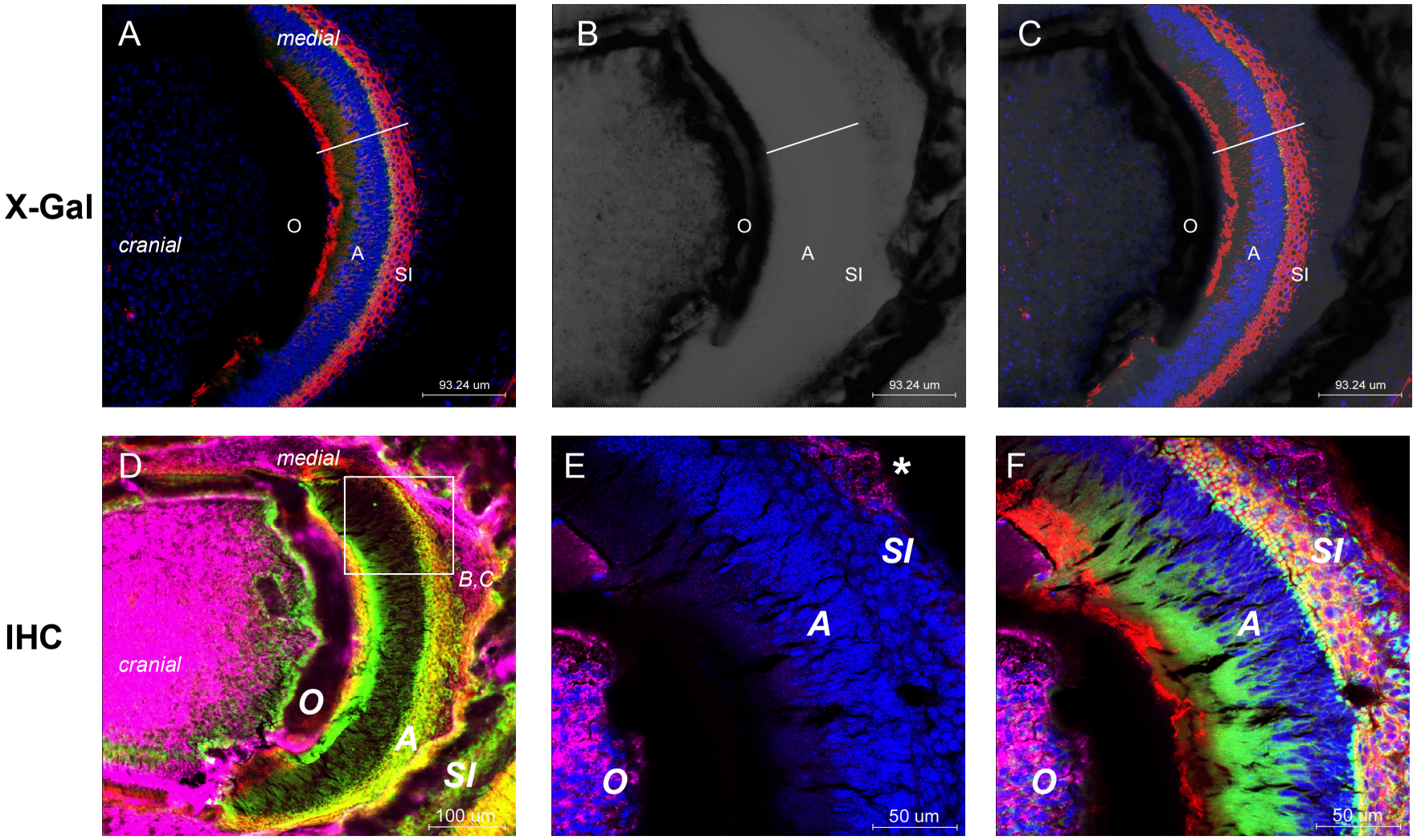

Fig 4.9 Ameloblasts and stratum intermedium are not neural crest- derived

Frontal section through the lower incisor of a E18.0 *Wnt*1-Cre+/-; Rosa26LacZR -/- mouse. Detection of ß-Galactosidase activity by X-Gal Staining (**A**- **C**, X-Gal staining and staining for endoplasmic reticulum (ER stain, green), F-Actin fibres (Rhodamine- Phalloidin, red) and nuclei (DAPI, blue)) or Immunohistochemistry* (**D**- **F**, IHC for ß-Galactosidase (magenta) in addition to the same staining for ER, F-Actin and DAPI as in **A**- **C**. Images were acquired by confocal microscopy (X-Gal staining was imaged as transmission image) and show the characteristic ameloblast layer on the caudal side of the incisor.

A Ameloblasts and Stratum intermedium stained for F-actin fibres (Rhodamine- Phalloidin, red) and endoplasmic reticulum (ER- stain, green), counterstain DAPI revealing the characteristic organisation of the layer. **B** Transmission image showing ß-Galactosidase staining of neural crest cells labeled by the *Wnt*1-Cre transgene. Clear absence of staining in the intermediate space (white line). **C** The overlay of **A** and **B** shows that the ameloblasts and stratum intermedium layer corresponds to the space devoid of *Wnt*1-Cre transgene labelling, indicating that these cells are not neural crest-derived.

IHC for ß-Galactosidase replicates the X-Gal staining, confirming the non- neural crest origin of the ameloblast layer and the stratum intermedium as well as the specificity of the anti-ß-Galactosidase antibody.

D Overview of the lower incisor. The white square indicates the position of the higher magnification shown in **B** and **C**.
E Overlay of staining for ß-Galactosidase (magenta) and DAPI (blue). Ameloblasts and stratum intermedium are recognisable due to their specific structure and show no immunoreactivity for ß-Galactosidase, in contrast to odontoblasts and adjacent lower jaw (*). **F** The overlay of all four channels with ß-Galactosidase (magenta), F-actin (red), ER (green) and DAPI (blue), unambiguously identifies the ameloblast layer and the stratum intermedium as the layer with no immunoreactivity for ß-Galactosidase

A ameloblasts, ***O*** odontoblasts, ***SI*** stratum intermedium

* IHC was performed according to standardized conditions; a detailed description of conditions and antibodies (primary and secondary) can be found in the relevant section under ‘Materials and Methods’ (Chapter 7.5.4).

*Bam*HI 754bps fragment in the upstream region of the gene by homologous recombination in order to study the role of *Hand*2 in branchial arch patterning[211]. The *Xho*I-*Bam*HI fragment had been previously identified as the *'Hand*2 branchial arch enhancer' as it contains necessary regulatory elements for *Hand*2 branchial arch expression[29]. As the focus of the original study was on branchial arch patterning, little intention has been paid to potential other functions of this so-called 'Branchial arch enhancer'. The results presented in this study now suggest that the deleted *Xho*I-*Bam*HI fragment in the *Hand*2 BAenh$^{-/-}$ also controls other aspects of *Hand*2 function, as in the dental epithelium and in dermal bone.

To assess a potential function of *Hand*2 in the dental epithelium, lower incisors of wildtype embryos were compared with lower incisors of *Hand*2 BAenh$^{-/-}$ mutants (Figures 4.10 and 4.11). First, potential markers for cellular morphology and polarisation were tested in the lower incisors of wildtype embryos. (Figure 4.10, F-Actin (Rhodamine-Phalloidin, Chemicon, ZO1 (anti-ZO1, Hybridoma), Vinculin (anti-Vinculin, Chemicon), Collagen I (anti-Collagen I, abcam), CRABPI (anti-CRABPI, abcam), Fibronectin (anti-Fibronectin, abcam), endoplasmic reticulum (ER stain, Chemicon)). The combination of a staining for F-actin filaments to reveal the outline of the cell and for the endoplasmatic reticulum to indicate functional polarisation was judged the most informative (Rhodamine-Phalloidin, ER staining, both Chemicon, Figure 4.10, A) and used for further analysis.
Figure 4.11 shows the comparison between wildtype and mutant (*Hand*2 BAenh$^{-/-}$) incisors of the upper and lower jaw. In order to distinguish between defects in neural crest and non-neural crest-derived structures, the panel on the left of the figure shows wildtype morphology but in a transgenic background that allows to identify neural crest (*Wnt*1-Cre$^{+/-}$; Rosa26LacZR$^{-/-}$ mice[49]). The incisors of the upper jaw of *Hand*2 BAenh$^{-/-}$ mice are misshapen, with a reduction of the neural crest-derived pulp stroma that further assumes a 'meshy' structure (compare Figure 4.11 A to B, asterisks). This is consistent with the results from *Hand*2-Cre mice that indicated *Hand*2 activity in the odontoblasts of the upper jaw (Figure 4.8 B). The ectoderm-derived part of the tooth, however, appears unaffected; the stratum intermedium (SI) is tightly linked and the ameloblasts are organised in a clearly polarised monolayer with a continuous apical membrane and a basal localisation of nuclei and endoplasmic reticulum ((C, D) arrows). The lower *Hand*2 BAenh$^{-/-}$ incisor displays the same reduced and mesh-like structure in the pulp

Figure 4.10- 4.11

4.10

A

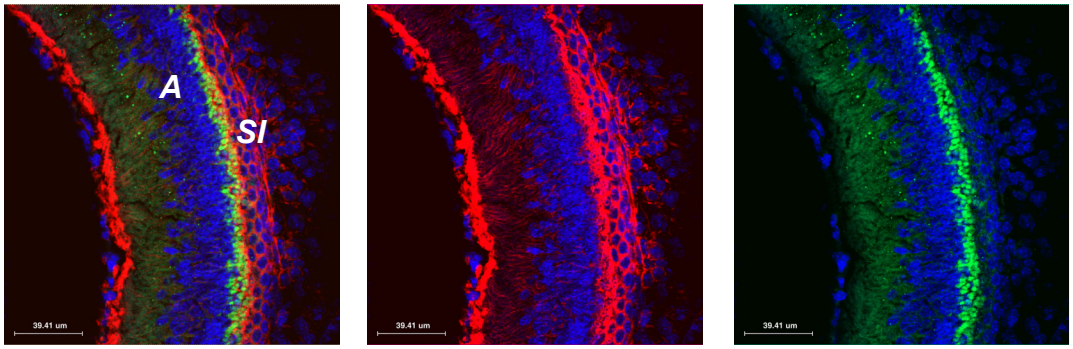

F-actin ER DAPI

B

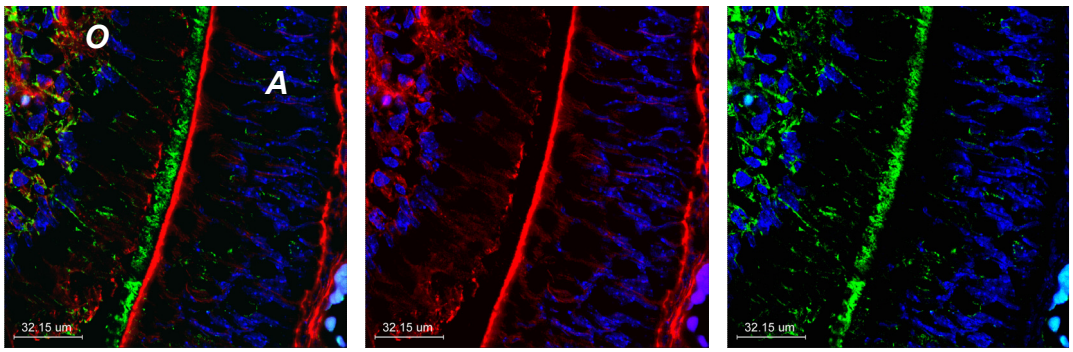

F-actin Vinculin DAPI

C

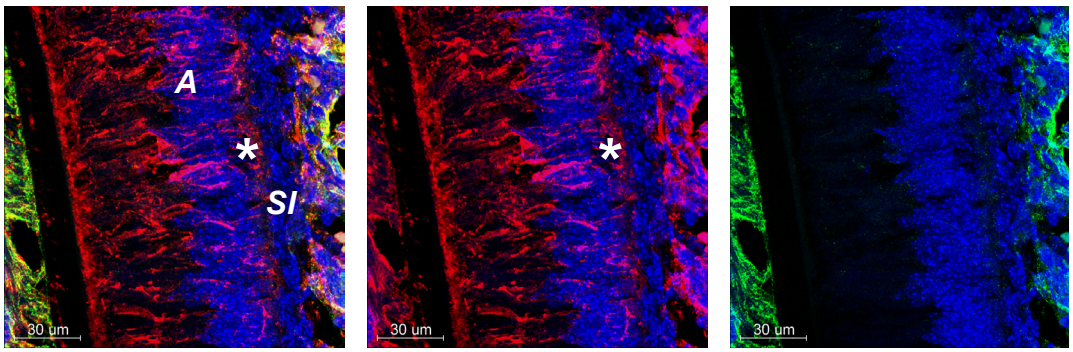

ZOI Fibronectin DAPI

D

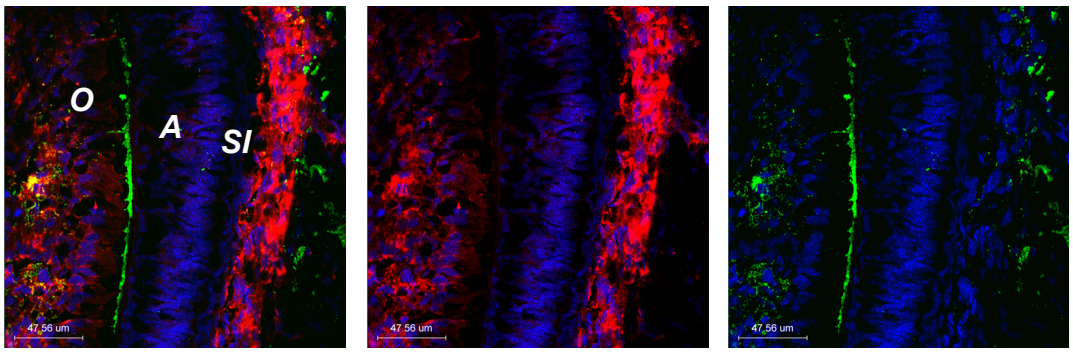

CRABPI Col I DAPI

4.10

Figure 4.10 Identification of polarisation markers for ameloblasts

IHC* and staining for sub-cellular markers on frontal sections of wildtype newborn incisors in search for suitable polarisation markers. Images are all arranged that anatomical structures from left to right are: odontoblasts- ameloblasts- stratum intermedium. The first panel shows both markers in overlay (plus DAPI), the second and third panel the red respective green channel (plus DAPI) separately. Details of the antibodies can be found in the relevant Material and Methods section.

A F-actin (Rhodamine- Phalloidin, red), endoplasmic reticulum (ER stain, green), DAPI (blue). The ER staining reveals clear basal localisation of the endoplasmic reticulum in ameloblasts (*A*). Rhodamine- Phalloidin shows the organisation of ameloblasts (*A*) and stratum intermedium (*SI*).

B F-actin (Rhodamine- Phalloidin, red, as in **A**), Vinculin (anti- Vinculin, green), DAPI (blue). Vinculin outlines the organisation of odontoblasts (*O*) but not of ameloblasts (*A*).

C Zonula occludens protein I (anti- ZOI, red), Fibronection (anti- Fibronectin, green), DAPI (blue). ZOI as basal marker shows basal localisation in ameloblasts (*). Fibronectin is not expressed in ameloblasts (*A*) nor stratum intermedium (*SI*).

D CRABPI (anti- CRABPI, red), Collagen I (anti- Collagen I, green), DAPI. CRABPI and Collagen I label surrounding structures, but are not present in ameloblasts (*A*) nor stratum intermedium (*SI*).

* IHC was performed according to standardized conditions; a detailed description of conditions and antibodies (primary and secondary) can be found in the relevant section under ‘Materials and Methods’ (Chapter 7.5.4).

4.11

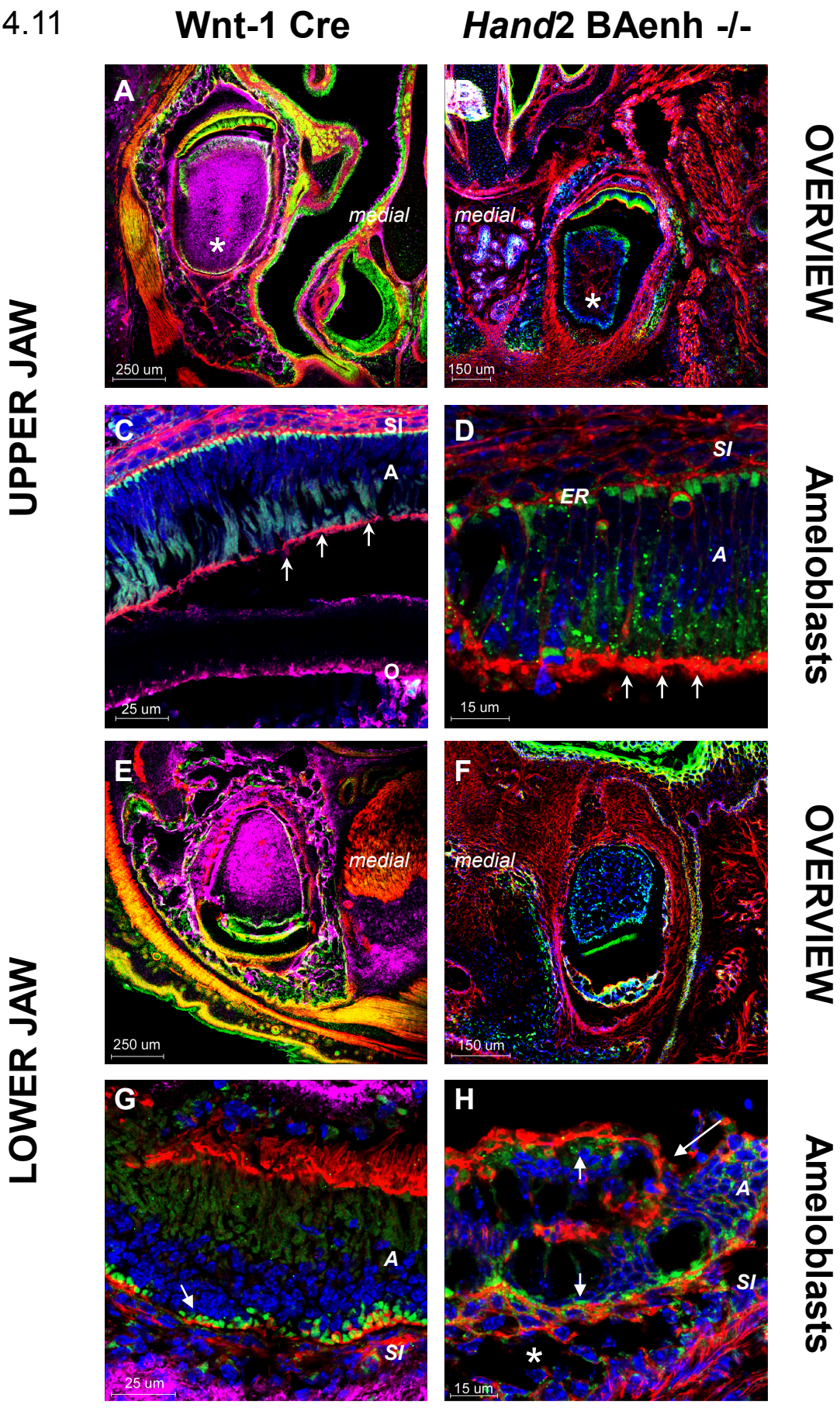
Wnt-1 Cre
Hand2 BAenh -/-
UPPER JAW
LOWER JAW
OVERVIEW
Ameloblasts
OVERVIEW
Ameloblasts
A
B
C
D
E
F
G
H
medial
SI
A
O
ER
250 um
150 um
25 um
15 um

Figure 4.11 Comparison of incisor morphology between phenotypically wildtype Wnt1-Cre+/-;Rosa26LacR-/- and *Hand*2 branchial arch enhancer knockout mice

Staining for endoplasmic reticulum (ER staining, green) and F-actin (Rhodamine- Phalloidin, red) on frontal sections of the face of phenotypically wild-type *Wnt*1-Cre+/-; Rosa26LacZR-/- mice (*Wnt*1-Cre, P4, left panel) and mutant *Hand*2 branchial arch enhancer knockout mice (*Hand*2 BAenh-/-), P0, right panel).

To indicate neural crest contribution to affected areas, additional immunohistochemistry for ß-Galactosidase was performed on the sections of the *Wnt*1-Cre+/-;Rosa26LacLZ-/- mouse (magenta, left panel).

The vertical axis of the images corresponds to the cranio-caudal axis of the specimen, the medial side is annotated.

A- D Upper incisors.

A, B Upper incisors appear only lightly affected in the *Hand*2 BAenh-/- knockout with a reduction of the pulp stroma (asterisk).

C, D Ameloblasts of the upper incisors of *Hand*2 BAenh-/-knockout resemble the wildtype condition with an elongated cell shape and parallel cell alignment. Cell nuclei and the endoplasmic recticulum are basally localised and the apical membrane forms a continuous structure (arrows).

E- H Lower incisors.

E, F Incisors of the lower jaw of *Hand*2 BAenh-/- mice show a rarefication of the pulp stroma similar to the one observed in the upper incisor (compare **F** to **B**).

G, H In addition, the architecture of the ameloblast layer and the stratum intermedium is perturbed (also visible in **F**). In the *Hand*2 BAenh-/- mouse, ameloblast nuclei in the lower incisor loose their basal location, the same applies to the endoplasmic reticulum (short arrows in **H**). The apical membrane of the ameloblast layer becomes discontinuous and folds back and inwards (long arrow in **H**). Also the stratum intermedium is affected and displays rarified stroma with large cell-free spaces (asterisk in **H**).

A ameloblasts, ***ER*** endoplasmic reticulum, ***SI*** stratum intermedium.

* IHC was performed according to standardized conditions; a detailed description of conditions and antibodies (primary and secondary) can be found in the relevant section under ‘Materials and Methods’ (Chapter 7.5.4).

already observed in the upper incisor (compare Figure 4.11 B and F). In addition, the stratum intermedium (SI) disintegrates, leaving behind large holes in the structure (asterisk in H). The associated ameloblast layer shows signs of perturbed polarisation: normally basally located within the ameloblast epithelium, nuclei and endoplasmatic reticulum (short arrows in G and H) are now also found on the apical side of the epithelium. The apical membrane is now discontinuous and folding backwards (long arrow in H). So while the partial inactivation of *Hand*2 function in the *Hand*2 BAenh$^{-/-}$ mouse affects the neural crest-derived pulp of the lower and upper incisors, the loss of polarisation is restricted to the epithelial derivatives (ameloblasts and stratum intermedium) of the lower incisor.

4.4.2.4 Summary of findings

- *Hand*2 expression in teeth is not limited to the mesenchyme of the lower incisor. Previously unknown *Hand*2 expression domains exist in the dental epithelium of the tooth buds of both upper and lower jaw.

- *Hand*2 expression correlates with a highly polarised ameloblast subpopulation in the lower incisor. Loss of function experiments support the functional significance of this finding and establish a role for *Hand*2 in dental epithelial polarity.

- Regulatory elements controlling *Hand*2 expression in the dental epithelium are- at least partially- contained in the 7.4kb *Hand*2 upstream region present in the *Hand*2-Cre transgene used by Ruest et al. 2003[158] and involve the so-called *Hand*2 branchial arch enhancer.

4.4.3 Discussion

The fact that *Hand*2 is generally expressed in the dental epithelium suggests a new role for *Hand*2 in tooth formation beyond the known involvement in incisor formation[2]. Recently, correct function of *Hand*2 in the oral epithelium but not in the underlying mesenchyme has been shown to be necessary for correct palate fusion[208], substantiating a general role of *Hand*2 in epithelial structures. Although *Hand*2 is expressed throughout the dental epithelium, the finding in the lower incisor- the expression of *Hand*2 correlates with a distinct cellular morphology- allows us to identify a function of the transcription factor in the context of ameloblast layer formation.

Analysis of incisors of *Hand*2-Cre+/-; Rosa26LacZR-/- mice reveal that only strictly organised and polarised ameloblasts express or have expressed *Hand*2 during their development. Rodent incisors are particular in so far as only the labial but not the lingual side of the tooth is covered with enamel. Enamel is exclusively produced by differentiated, elongated and clearly polarised ameloblasts on the labial side of the tooth but not by the unstructured ameloblasts on the lingual side[42]. The *Hand*2 positive ameloblast subpopulation in *Hand*2-Cre mice unequivocally corresponds to the highly organised cell population on the labial (and therefore enamel producing) side of the incisor (Figure 4.7). The perturbed tissue architecture in the partial *Hand*2 knockout (*Hand*2 BAenh$^{-/-}$; Figure 4.11) further supports the notion that correct architecture in the labial ameloblast layer is achieved by a process dependent on *Hand*2. This process is cell-autonomous as it is not replicated in mice with neural-crest specific ablation of *Hand*2 (personal communication from D.Clouthier). So far it is not fully understood how the asymmetry between ameloblast populations in the lower incisor is achieved; it is known, however, that only the labial but not the lingual dental epithelium is able to differentiate into ameloblasts in response to inducing signals from the mesenchyme and that modulation of TGFß/BMP signalling is crucial [6,7,204,205]. Whether *Hand*2 plays a specific role in the process of lingual ameloblast differentiation or whether *Hand*2 expression in this specific ameloblast population rather reflects its highly polarised nature will require future work.

The genetic regulation of *Hand*2 expression in epithelia is so far unknown. The *Hand*2-Cre transgene[158] replicates endogenous *Hand*2 epithelial expression, so necessary regulatory elements must be at least partially contained in the 7.4 kb *Hand*2 upstream

region present in the transgene. As the deletion of a small regulatory element- the so-called branchial arch enhancer, originally identified as regulating *Hand*2 expression in the distal part of branchial arches- is sufficient to disrupt the architecture of the ameloblast layer in the lower incisor, necessary regulatory elements for *Hand*2 epithelial expression can further be localised to this specific genetic region.
Although this work mainly focused on the role of *Hand*2 in the ameloblast layer of the lower incisor, the results obtained from *Hand*2-Cre mice and *Hand*2 BAenh$^{-/-}$ mice suggest that this does not fully cover the function of *Hand*2 in teeth; the factor also seems potentially involved in the formation of the pulp of teeth in both the lower and upper jaw (both were affected in the *Hand*2 BAenh$^{-/-}$ mouse) and of ameloblasts layers of different teeth.

4.5 Part2- Hand2 plays a role in the laminar formation of dermal bone

4.5.1 Background

Dermal bone

Bone is a characteristic feature of vertebrates and can develop according to two different mechanistics. Most bone of the trunk skeleton develops by replacement of a cartilage precursor in a process known as enchondral (or indirect) ossification. The bones of the skull in contrast develop directly in the mesenchymal tissue of the dermis; the process is therefore called dermal (or direct) ossification. A special form of dermal ossification is the perichondrial ossification that occurs on the outside of cartilage precursor elements.

Dermal ossification is thought to begin with increased vascularisation within the dermis, followed by proliferation and condensation of mesenchymal cells; these cells then later differentiate into osteoid-producing osteoblasts[77]. Once osteoblasts become encased in their own matrix, they differentiate into mature osteocytes (Figure 4.12). Initial dermal bone formation is thought to conclude with the addition of an inner and outer compacta and the establishment of a periost (see textbooks for histology e.g.[67,94]) .

So far, the only known role for *Hand*2 in osteogenesis is its control of bone differentiation by the inhibition of the osteogenic master regulator gene, *Runx*2[65].

Figure 4.12

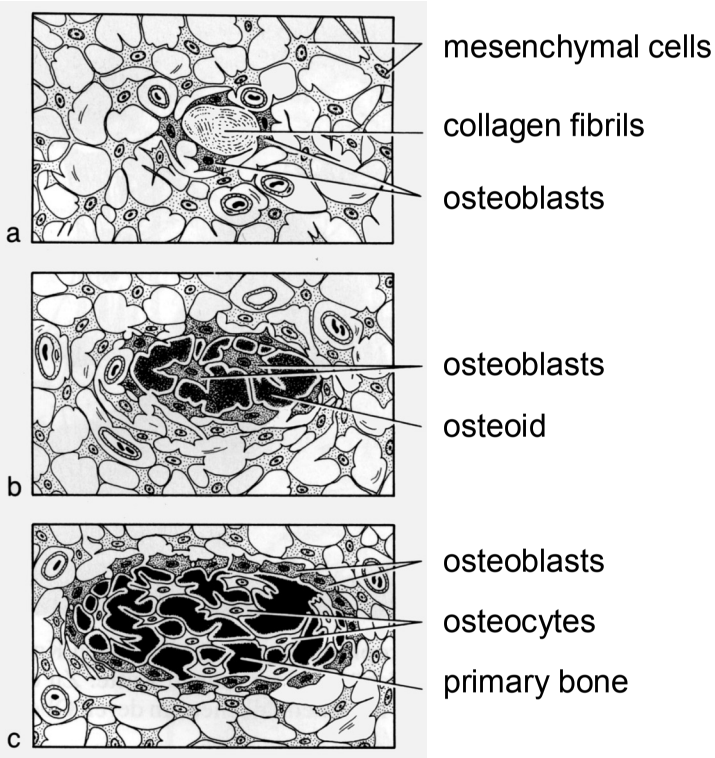

Figure 4.12 The current model of the initiation of dermal bone formation

Dermal bone formation is described as beginning spontaneously in mesenchymal tissue.

a) Loose mesenchymal tissue condensates and

b) begins to deposit osteoid between the cells that become osteoblasts.

c) Once encased, osteoblasts differentiate into osteocytes. The network of deposited matrix and osteocytes forms the primary bone.

after Junqueira, *Histologie,* Springer 1991 and Fawcett, *A textbook of histology,* 11th Ed., Saunders

4.5.2 Results

4.5.2.1 A novel expression domain of *Hand*2 at sites of forming dermal bone

A previously unreported expression domain of *Hand*2 at sites of forming dermal bone was detected by RNA *in situ* hybridisation on sections, supporting a role for *Hand*2 in osteogenesis[65] (Figure 4.13). In the developing murine frontal bone as an example of a dermally ossifying bone, *Hand*2 expression is found in sheets of condensing mesenchyme at E16 (Figure 4.13 F- H). *Hand*2 expressing cells align in two distinct cell layers facing each other, with an intermediate cell-free space, an arrangement described for pre-osteoblasts (asterisk F, H)[64]. Endogenous *hand*2 expression in these cell layers is mirrored by *cre* expression from the *Hand*2-Cre transgene; this allows to locate necessary regulatory elements for *Hand*2 bone expression within the 7.4kb of *Hand*2 upstream region that are present in the transgene (compare Figure 4.13 G and H).

The importance of *Hand*2 in dermal bone formation is supported by lineage labelling results from *Hand*2-Cre mice; Immunohistochemistry for ß-Galactosidase reveals that quasi all cells of the nasal bone either expressed *Hand*2 at some stage of their development or are descendents of *Hand*2 positive cells (Figure 4.14). The fact that 1. neither frontal nor nasal bone of the *Hand*2-Cre mouse stain positive with the conventional X-Gal method (Figure 2.20) and 2. *cre* message from the transgene is detected by RNA *in situ* hybridisation in these areas indicating an active transcription event allow to conclude that this is a new and independent function of *Hand*2 in the formation of dermal bone, which is unrelated to the *Hand*2 branchial arch expression domain.

Consistent with a role in dermal bone formation, *hand*2 message is also expressed in the dermally ossifying outer part of the clavicle at E14.0 (Figure 4.15). Additional but weaker *hand*2 expression exists within the cartilaginous core, most likely reflecting the only very recently reported function of *Hand*2 in chondrogenesis[1]. *Hand*2 expression in the clavicular dermal cover appears to be- like in the frontal bone- controlled by regulatory elements contained within 7.4kb *Hand*2 upstream region as *cre* message from the *Hand*2-Cre transgene seems to copy endogenous *hand*2 expression, albeit with a delay in expression (Figure 4.15 E).

Figure 4.13- 4.15

4.13

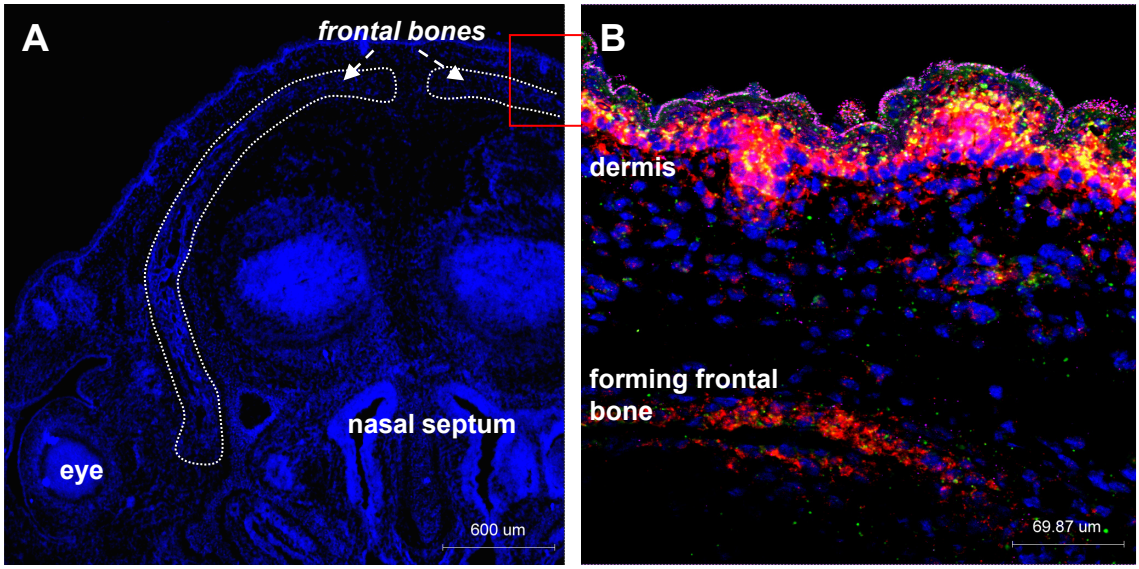

DAPI

hand2 cre *brn1* DAPI

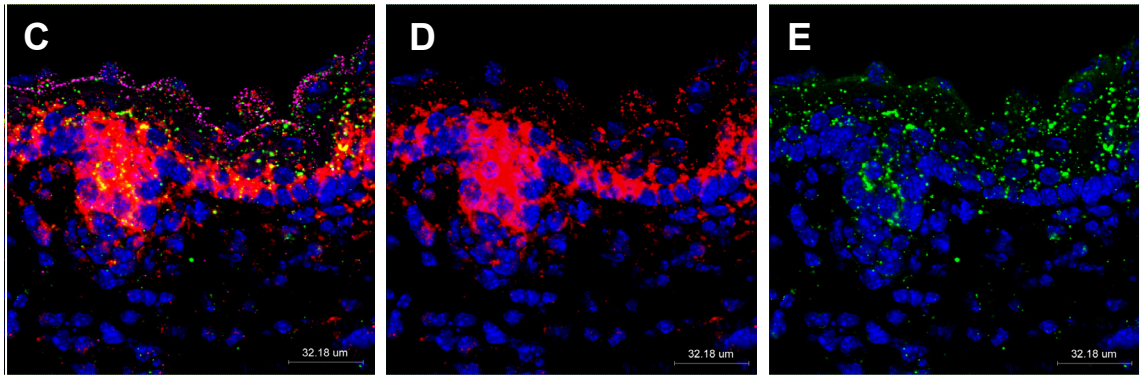

hand2 cre *brn1* DAPI

hand2 DAPI

cre DAPI

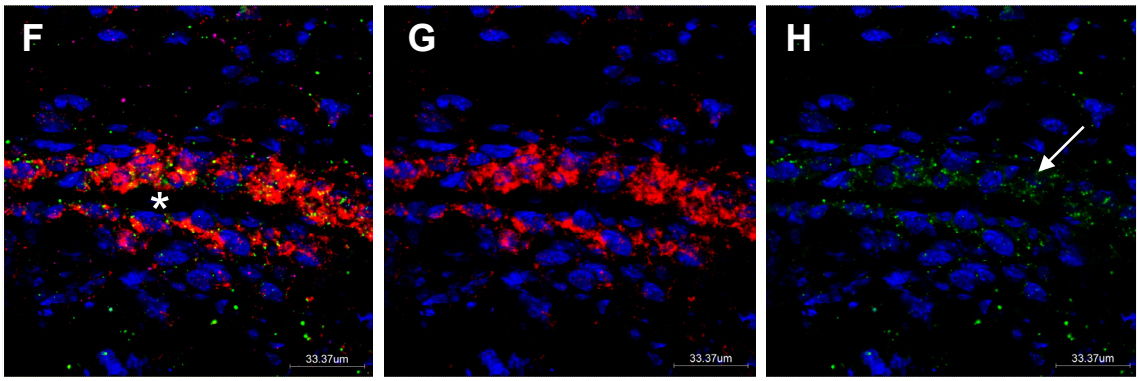

hand2 cre *brn1* DAPI

hand2 DAPI

cre DAPI

E16.0

4.13

Figure 4.13 *Hand*2 expression domains in the skin and in dermal bone at E16.0

Triple fluorescent RNA in situ Hybridisations on frontal sections of the anterior head of E16 *Hand*2-Cre+/-; Rosa26Lac-/- embryos for *hand*2 (red), cre from the *Hand*2-Cre transgene (green) and *brn*1 as control (magenta). Counterstain is DAPI (blue). The vertical axis of the images corresponds to the cranio-caudal orientation of the specimen.

A Anatomical overview shown for the DAPI counterstain. The outline of the frontal bones is stippled and the position of **B- H** indicated by the red square.

B *Hand*2 is expressed strongly in the upper part of the skin, as well as in the forming frontal bone.

C- E: *Hand*2 expression in the skin in higher magnification. Overlay (**C**), and separated *hand*2 (**D**) and cre (**E**) expression.

*Hand*2 is expressed in and above the germinative layer of the dermis (**C, D**) while cre is mainly located above (**E**). Expression of *brn*1 can be detected specifically in the epiderm but not in all other *hand*2 and cre positive areas.

F- H: *Hand*2 is expressed in forming dermal bone, here the frontal bone. Overlay (**F**) and separated *hand*2 (**G**) and cre expression (**H**). The asterisk indicates the cell-free space between the two cell layers.

*Hand*2 and cre expression from the *Hand*2 BAenh-/- transgene but not *brn*1 can be detected in the forming frontal bone. Though there is no structural organisation comparable to the skin with cells aligned on a basal membrane, two cell rows made up of *hand*2 and cre positive cells can be distinguished.

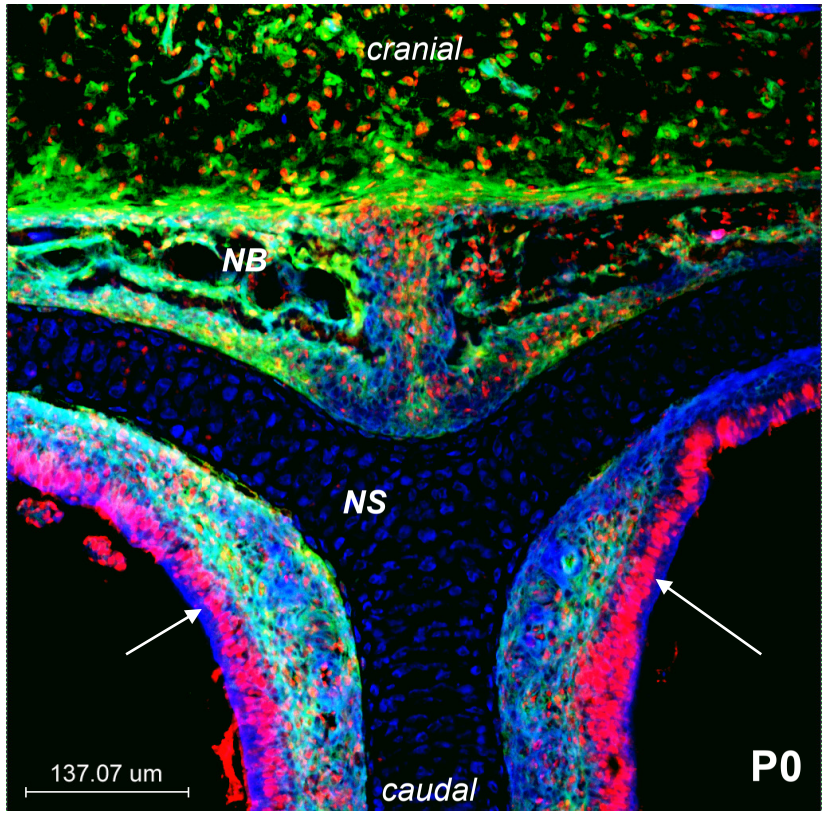

ß-Galactosidase Vinculin F-actin

Figure 4.14 Dermal bone forms through a process involving *Hand*2

IHC* of a frontal section of the anterior head of a *Hand*2-Cre+/-; Rosa26LacZR-/- newborn mouse. ß-Galactosidase (red) reveals past and present *Hand*2 activity; Vinculin (green) and F-actin (Rhodamine- Phalloidin, blue) indicate the outline of the tissue.

The nasal bone (NB) is nearly entirely made up of cells immunoreactive for ß-Galactosidase . Immunoreactive cells can also found in the skin above. In both areas, conventional X-Gal staining reveals no ß-Galactosidase activity.

ß-Galactosidase can also be detected by IHC in the nasal epithelium, particularly in the outer layers (arrows).

NB nasal bone ***NS*** nasal septum

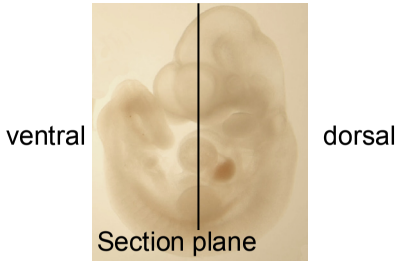

* IHC was performed according to standardized conditions; a detailed description of conditions and antibodies (primary and secondary) can be found in the relevant section under 'Materials and Methods' (Chapter 7.5.4).

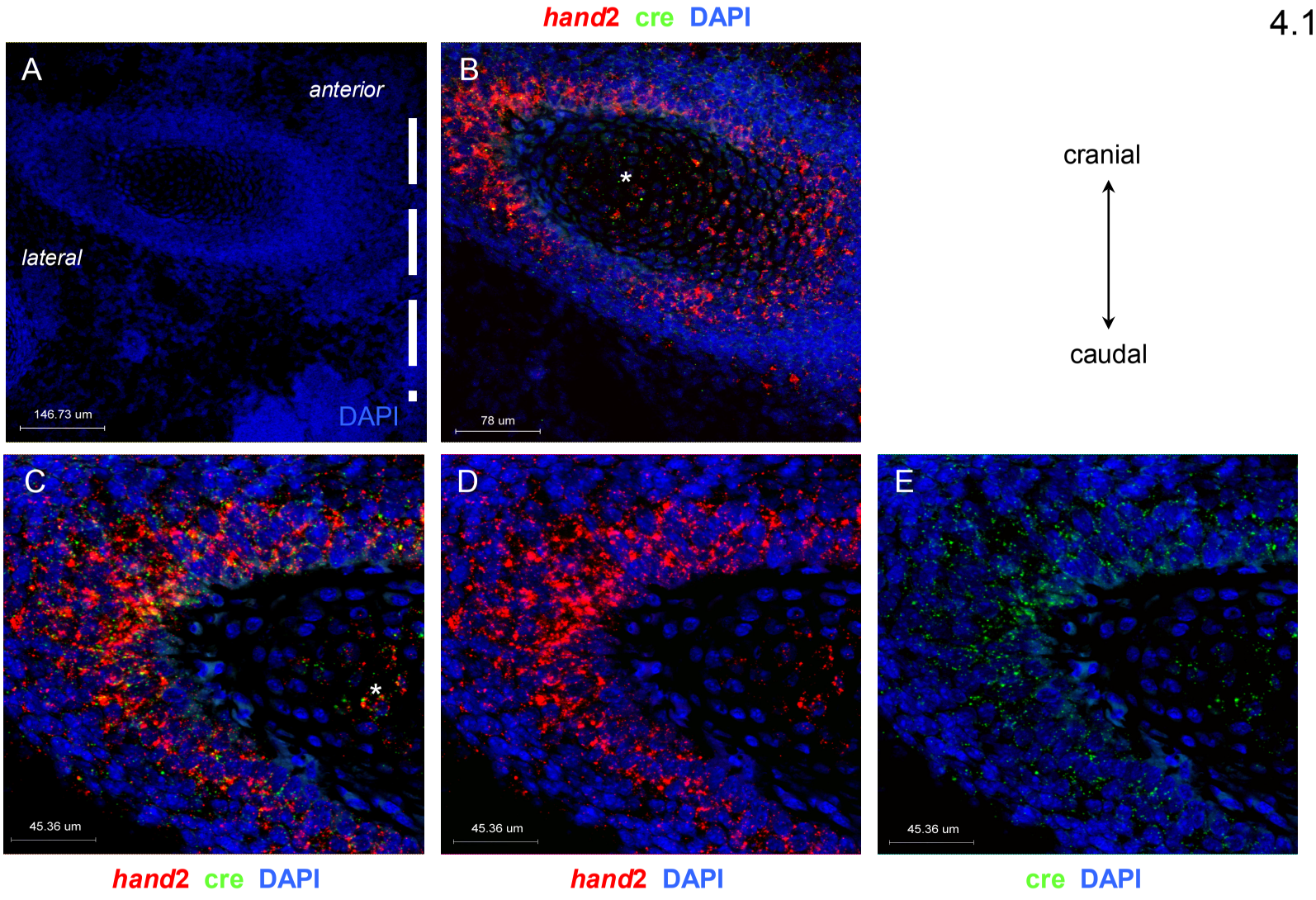
hand2 cre DAPI
A
anterior
lateral
DAPI
146.73 um
B
78 um
cranial
caudal
C
45.36 um
D
45.36 um
E
45.36 um
hand2 cre DAPI
hand2 DAPI
cre DAPI

E14.0

Figure 4.15 *Hand*2 is expressed in the forming outer layer of the clavicle

Fluorescent double *in situ* hybridisation for *hand*2 (red) and cre expression from the *Hand*2-Cre transgene (green) on transverse sections of the shoulder region of E14 *Hand*2+/-; Rosa26LacZR-/- mice. Nuclear counterstain: DAPI (blue).

A Anatomical overview of the clavicular region in low magnification, shown is only the nuclear counterstain. The midline of the specimen is indicated by the bold dashed line on the right.

B Higher magnification shows *hand*2 expression in the cells of the outer clavicular cover; additional weaker expression can be observed in the cartilaginous core of the clavicle (asterisk).

C Highest magnification shows that endogenous *hand*2 (red) expression in the outer clavicular layer is replicated by cre expression from the *Hand*2-Cre transgene (green). Cartilaginous expression is indicated by an asterisk.

D, E Separated red and green channel of (**C**) allow to appreciate the extent of *hand*2 and cre expression.

4.5.2.2 Loss of function confirms a role of *Hand*2 in bone formation

To study the role of *Hand*2 in the formation of the dermal cover of the clavicle, we made use of a further existing knockout/ transgenic mouse cross (*Hand*2$^{fl/fl}$;*Wnt*1-Cre), in which the entire function of *Hand*2 is specifically ablated in neural crest cells[79]. Further crossing into the Rosa26LacZ reporter line[176] allows us to identify *Hand*2$^{-/-}$ cells due to their expression of ß-Galactosidase (for an overview of all genetically modified mice used in this thesis, please see the relevant section in the Introduction).The mammalian clavicle develops via a mixed ossification modus, with direct dermal ossification in the lateral part and endochondral ossification under a dermal cover in the medial part[86]. The insertion point of the sternocleidomastoid muscle on to the clavicle has been shown to be neural crest-derived[122] and was therefore chosen as anatomical landmark. Figures 4.16- 4.18 show the comparison between the clavicles of wildtype mice and mice with neural crest-specific ablation of *Hand*2 (*Hand*2$^{fl/fl}$;*Wnt*1-Cre$^{+/-}$;Rosa26LacZR$^{+/-}$) with the attachment of the sternocleidomastoid muscle as anatomical reference point. Wildtype clavicles show a layered structure of the dermal cover suggesting that the formation of the bone occurs in successive layers. The concentric arrangement of cell sheets is made visible by the parallel arrangement of radial Periostin and F-Actin fibres (Figure 4.16 A, B and Figure 4.18). Especially F-Actin fibres do not seem to span more than a single layer of cells (Figure 4.18 F). In contrast, the dermal cover of knockout mouse clavicles lacks this apparent organisation; while the outer shell of the clavicle still forms, it lacks the inner layered structure (Figure 4.18). Periostin fibres no longer run strictly radially but are sparse and appear 'loose'(compare Figure 4.18 B to Figure 4.18 C). Instead of consecutive cell layers defined by Periostin fibres, cells are no longer aligned in cellular sheets but 'sandwiched' between an inner and an outer Periostin ring (Figure 4.18 B and C). Although F-Actin fibres maintain their radial orientation, they also reflect the overall loss of organisation and now span more than a single layer of cells (compare Figure 4.18 D- F to Figure 4.18 D- F). Immunohistochemistry for ß-Galactosidase confirms that the disorganised layer is indeed filled by cells lacking *Hand*2 function and that by conclusion *Hand*2 is necessary for the establishment of the layered structure in the dermal part of the clavicle (Figure 4.18 C).

Figure 4.16- 4.18

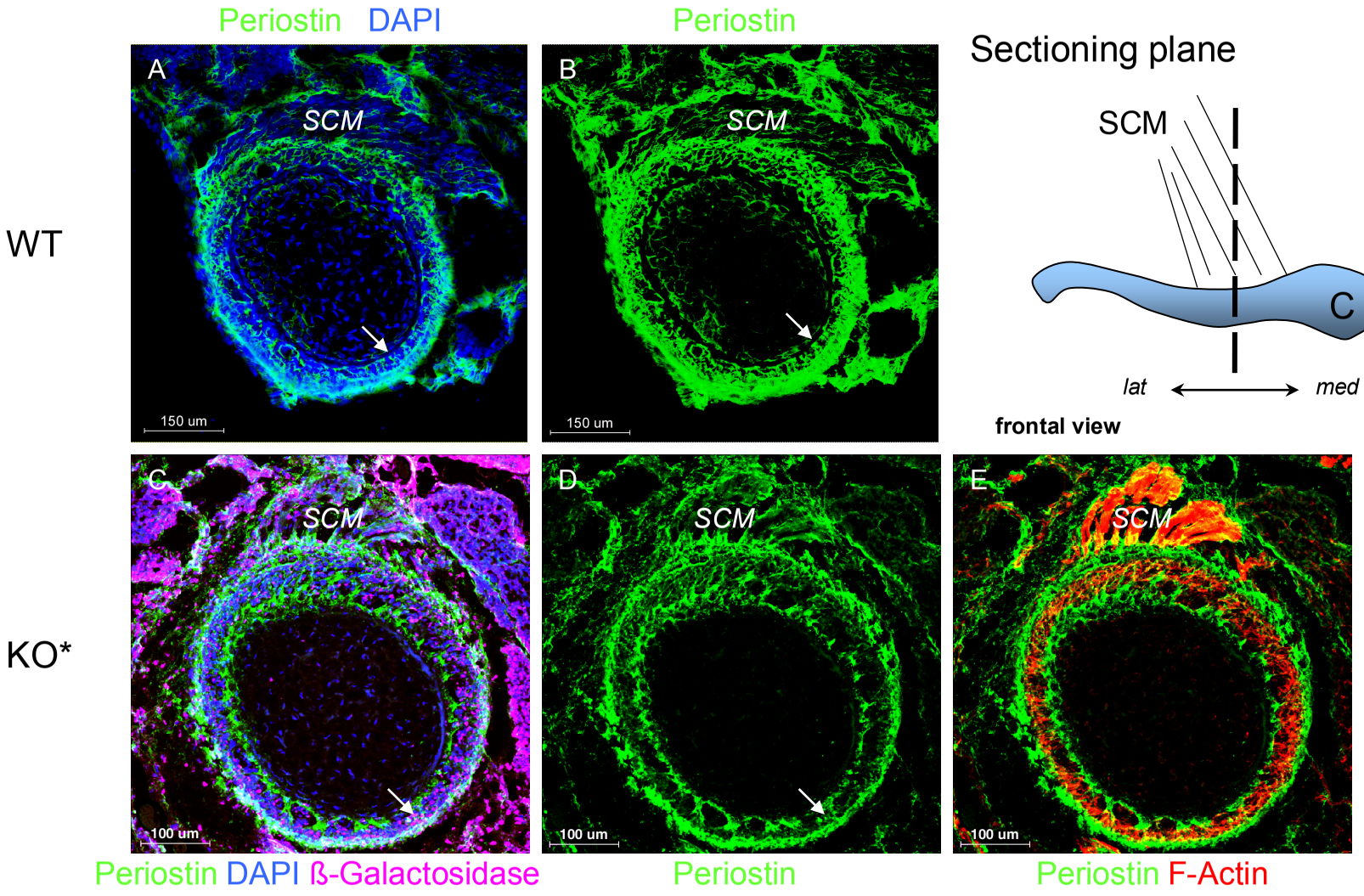

* Hand2fl/fl-/-; *Wnt*1-Cre+/-;Rosa26LacZ+/-

Figure 4.16 Neural crest specific loss of *Hand*2 disrupts the architecture of the clavicular dermal bone cover

IHC* against Periostin (A- E, green), ß-Galactosidase (C, magenta) and staining for F-Actin (E, red) and DAPI (A, C. blue) on sagital sections of the clavicle of wildtype E18 (**A**, **B**) and *Hand*2fl/fl-/-; *Wnt*1-Cre+/-;Rosa26LacZ+/- P0 (**C- E**) mice. Crossing of the knockout (Hand2fl/fl-/-; *Wnt*1-Cre) into a Rosa26LacZ background serves as control for affected cell populations. The insertion of the clavicular portion of the sternocleidomastoid muscle (SCM) was chosen as anatomical landmark for comparability of the regions and the sectioning plane is indicated in the comic. Images are orientated with cranial to the top and anterior to the left.

A, **B** The dermal cover of wildtype clavicles shows a layered architecture (arrow in **A**) as visible here in the staining for Periostin fibres.

C Loss of *Hand*2 function affects the entire outer cover of the clavicle as indicated by immunoreactivity for ß-Galactosidase (magenta).

D The periostin system in the of *Hand*2-deficient dermal cover appears rarified compared to the wildtype situation (compare to **B**).

E Periostin and F-Actin fibres in overlay clearly indicate the insertion of the sternocleidomastoid muscle. The system of F-Actin fibres is contained within the ring of loose Periostin fibres.

* IHC was performed according to standardized conditions; a detailed description of conditions and antibodies (primary and secondary) can be found in the relevant section under ‘Materials and Methods’ (Chapter 7.5.4).

SCM sternocleidomastoid muscle

WT

4.17

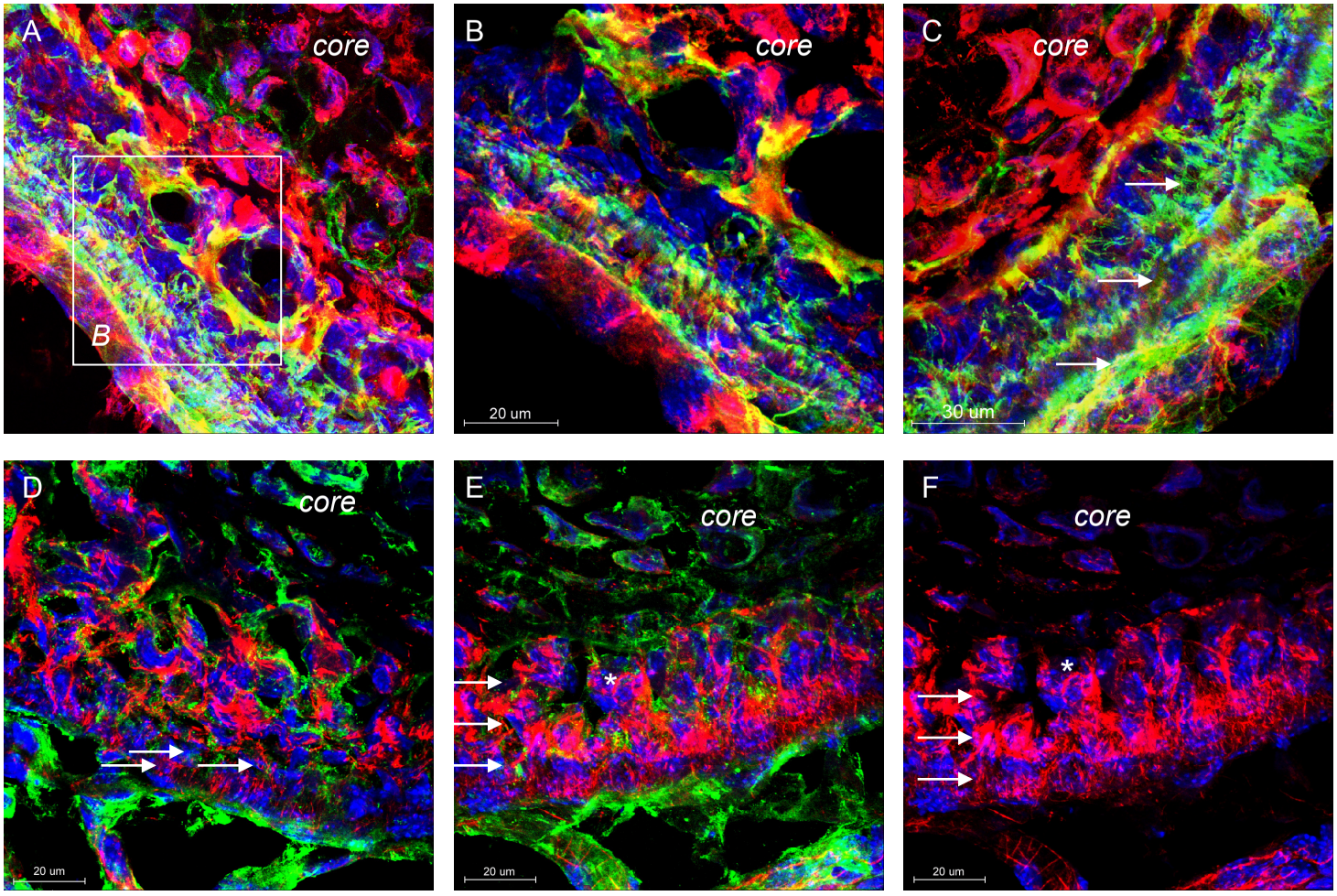
Undulin
Periostin
DAPI
A
core
B
B
core
20 um
C
core
30 um
F-Actin
Undulin
DAPI
D
core
20 um
E
core
*
20 um
F
core
*
20 um

Figure 4.17 Organisation of the outer clavicle in the wildtype

IHC* on sagital sections of the clavicle of wildtype E18.0 mice at the medio-lateral position of the sternocleidomastoid muscle insertion. (**A- C**) Undulin (red), Periostin (green), DAPI (blue). (**D- F**) Undulin (green), Rhodamine- Phalloidin (red) and DAPI. The position of the core of the clavicle is indicated.

A, B The layered organisation on the outside of the clavicle becomes apparent in this staining for Periostin fibres, visible are also two bloodvessels. **B** shows a detail of **A** in higher magnification and a thinner z-stack.

C At a different position along the outer circumference of the clavicle lacking bloodvessels the layered architecture of the dermal cover made up by different Periostin fibre systems is clearly visible (arrows).

D The organisation of F-Actin fibres (red) replicates the layered architecture of the Periostin fibres (arrows).

E, F In the dermal clavicular cover, parallel F-Actin fibres are arranged in continuous layers of varying density (arrows). With exception of the inner most layer (asterisk), fibres only span the height of a layer of one cell.

* IHC was performed according to standardized conditions; a detailed description of conditions and antibodies (primary and secondary) can be found in the relevant section under ‘Materials and Methods’ (Chapter 7.5.4).

*Hand*2fl/fl-/-;
*Wnt*1-Cre+/-,
Rosa26LacZ+/-

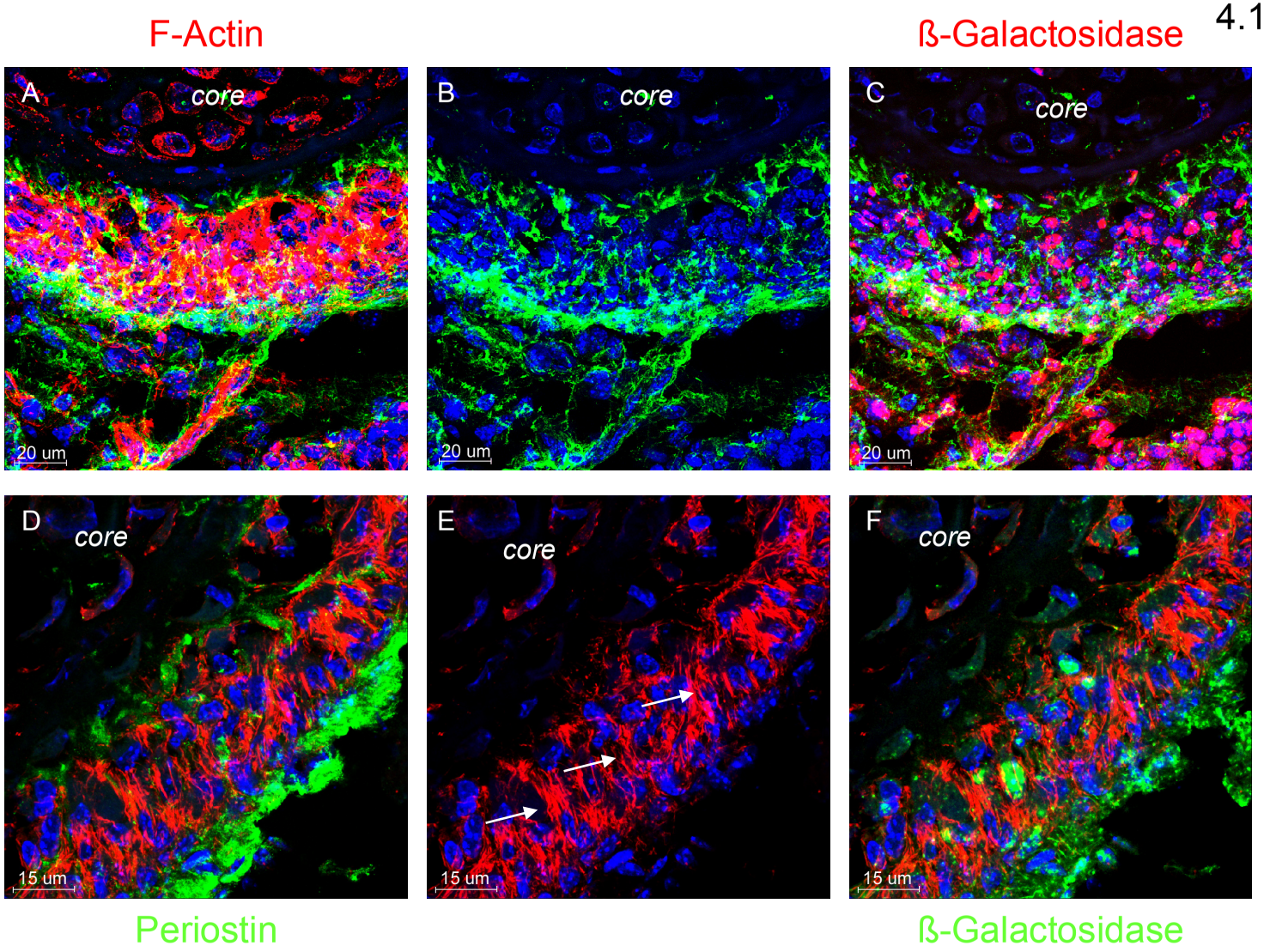

Figure 4.18 Loss of *Hand*2 function causes a disruption of the layer formation in the dermal outer clavicle

IHC* on sagital sections of the middle part of the clavicle of *Hand*2fl/fl-/-; *Wnt*1-Cre+/-;Rosa26LacZ +/- P0 mice at the insertion of the sternocleidomastoid muscle. Periostin (**A- D,** green), ß-Galactosidase (**C**, red and **F**, green) and staining for F-Actin (**A**, **D- F**, red). Nuclear counterstain: DAPI (blue). The position of the core of the clavicle is indicated.

The outer part of the clavicle which corresponds to the dermal cover is affected by *Hand*2 ablation as revealed by immunoreactivity for ß-Galactosidase (**C**). Loss of *Hand*2 function causes a loss of the wildtype architecture with circumferential layers of radial Periostin fibres; Periostin fibres in the part of the clavicle lacking *Hand*2 function appear rarified and only show loose organisation (**A**, **B**).

The ring formed by the remaining Periostin fibres of the outer clavicle is filled with F-Actin fibres (**A**, **D**). F-Actin fibres keep their radial orientation but now span more than a single layer of cells (arrows in **E**). Immunoreactivity for ß-Galactosidase reveals that the part with abnormal structure is made up of cells lacking *Hand*2 function (**F**).

* IHC was performed according to standardized conditions; a detailed description of conditions and antibodies (primary and secondary) can be found in the relevant section under ‘Materials and Methods’ (Chapter 7.5.4).

4.5.2.3 *Hand*2 expression in bone is at least partially controlled by the so-called *Hand*2 'branchial arch' enhancer

The *Hand*2 BAenh$^{-/-}$ mouse line was designed with the aim to specifically abolish *Hand*2 expression in the branchial arches[211]. *Hand*2 BAenh$^{-/-}$ mice had unexpected ossification defects in cranial dermal bones (personal communication H.Yanagisawa), which let us to suspect that *Hand*2 expression in dermal bone must be at least partially controlled by the so-called 'Branchial arch' enhancer. The analysis of the anterior skull roof of *Hand*2 BAenh$^{-/-}$ mice indeed shows structural alterations of the frontal bone (Figure 4.19). The outline of the frontal bone with the internal (IL) and external (EL) layer appears normal but the structure of the intermediate part of the bone is disrupted (compare A, B to C). Cells from the external layer still invaginate into the underlying space (B, arrows) but do not form the cellular sheets seen in the wildtype (C). In contrast, processes on the brain-facing side of the bone seem less affected as the c-shaped or round formations found in the wildtype frontal bone are still recognisable in the *Hand*2 BAenh$^{-/-}$ mouse (long arrow in A). These results confirm our hypothesis that *Hand*2 expression in dermal bone is at least partially controlled by the genetic region previously identified as the *Hand*2 'Branchial arch' enhancer[29].

4.5.2.4 Dermal bone development- the example of the frontal bone

Dermal bone formation occurs in a laminar fashion

The distinct alteration of the layered architecture of dermal bone in mice with neural crest-specific ablation of *Hand*2 or a deletion of a specific regulatory region for *Hand*2 let us to investigate dermal bone development in more general terms. The E18 mouse frontal bone is an ideal study subject for dermal bone development as it shows different stages of bone maturation along its height (Figure 4.20). At the coronal suture, where the frontal bones contact the parietal bones, lies the most immature part of the bone. Towards the nasal end of the bone, the inner bone structure increases in complexity and shows the cancellous architecture typical for mature bone. The frontal bone consists of three distinct layers: an external, intermediate and internal layer, for simplicity

Figure 4.19- 4.20

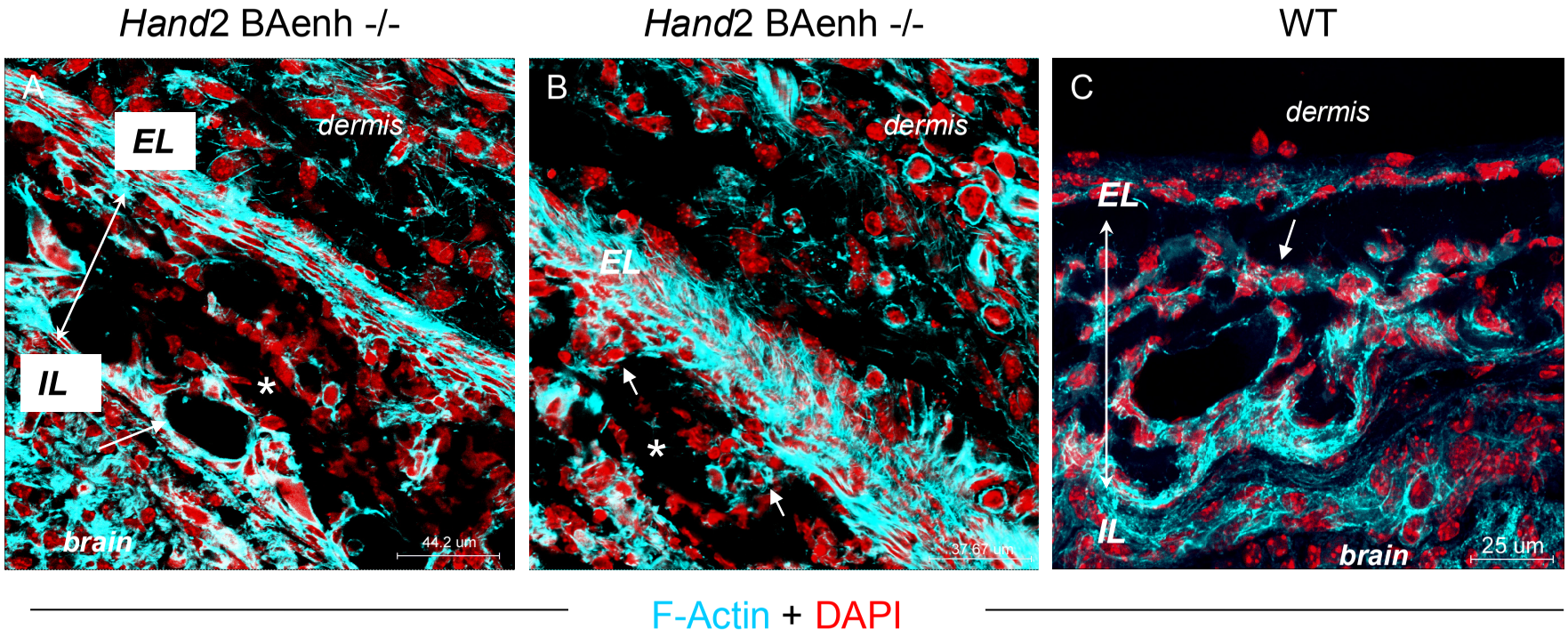
*Hand*2 BAenh -/-
*Hand*2 BAenh -/-
WT
A
EL
dermis
IL
*
brain
44.2 um
B
dermis
EL
*
37.67 um
C
dermis
EL
IL
brain
25 um
F-Actin + DAPI

Figure 4.19 Perturbed layer formation in the frontal bone of the *Hand*2 Branchial arch enhancer knockout mouse

DAPI (red) and Rhodamine-Phalloidin (turquoise) staining of frontal sections of the frontal bone of *Hand*2 BA enh-/- (**A**, **B**) and wildtype (**C**) mice. Images are orientated with the dermis to the top and the brain to the bottom.

In *Hand*2 BA enh-/- knockout mice, the external layer (EL) of the frontal bone appears multi-layered and disorganised (both **A** and **B**). Pillars of cells 'drop' from the external layer into the underlying space (**B**, arrows) but do not expand. Cells in the intermediate space between the external and internal layer clearly lack organisation (**A**, **B**, asterisk) and do not show the arrangement of continuous parallel cellular layers seen in the wildtype (**C**, arrow). However, the bottom part of the intermediate space adjacent to the internal layer appears less affected as it shows a rather normal organisation with a curved cell layer forming c-shapes (arrow in **A**).

EL external layer, ***IL*** internal layer

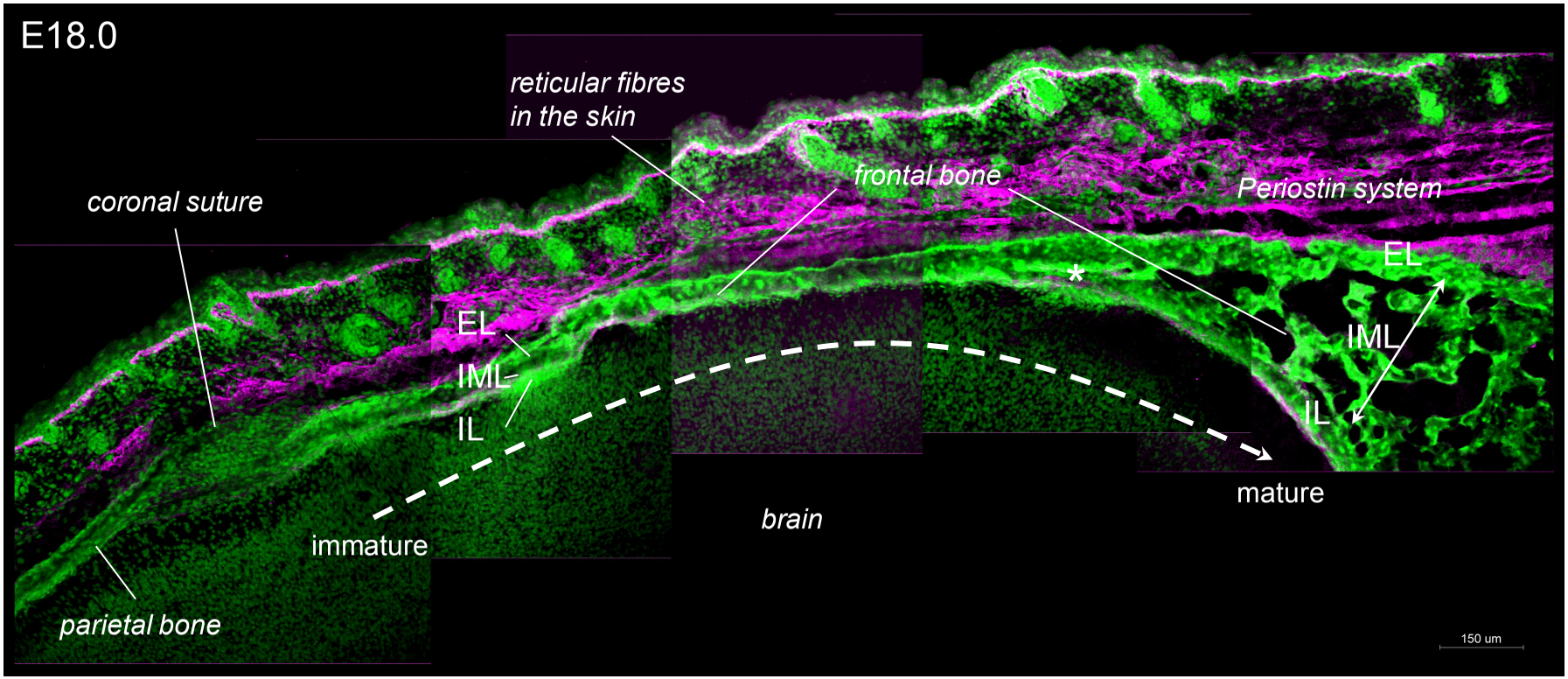

Periostin DAPI

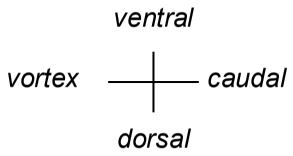

Figure 4.20 Overview of the frontal bone

Sagital section through the frontal bone of a E18.0 *Wnt*1-Cre+/-; Rosa26LacZ-/- mouse. The overlay of independently acquired images along the entire height of the bone demonstrates the overall anatomy. Scale bar 150 µm.

IHC* for Periostin (magenta), counterstained with DAPI (green).

The frontal bone shows different stages of bone maturation along its height: from immature close to the coronal suture (left) to ossified and re-structured towards the nose (right). Three layers are morphologically identifiable: the external layer (EL), the intermediate layer (IML) and the internal layer (IL). The external and internal layer are each contiguous layers; the expansion of the bone thickness towards the nasal end occurs on the expense of the intermediate layer (IML, double arrow).

A system of vertical Periostin fibres organised in layers or sheets runs parallel to the outside of the frontal bone.

Squares of fainter staining are due to photo-bleaching caused by previous scans.

EL external layer, ***IL*** internal layer, ***IML*** intermediate layer

* IHC was performed according to standardized conditions; a detailed description of conditions and antibodies (primary and secondary) can be found in the relevant section under ‘Materials and Methods’ (Chapter 7.5.4).

4.20

abbreviated as EL, IML, IL respectively (Figure 4.20). The external and internal layer are each continuous laminar structures; the thickness of the frontal bone towards the nasal end occurs due to the increase the intermediate layer. In a parallel cross-section, the frontal bone appears pre-constructed in parallel cellular sheets (dashed lines indicate two of the at least four sheets, Figure 4.21 A), before layers fold and contact each other to produce the final honeycomb structure. In the immature part of the bone close to the coronal suture, only the external and internal layers are clearly established, whilst the space between the two is filled with loose and sparse mesenchyme (A). In the case of the frontal bone, the loose mesenchyme is of mesodermal origin, sandwiched between a neural crest-derived external and internal layer (Figure 4.21 A, also Figure 4.22 A). At certain intervals, cells belonging to the external layer can be seen kinking and invaginating into the underlying space (Figure 4.21 C). These 'kinks' coming from the external layer are then actively connected with the next available deeper layer (H, connection to the closest intermediate layer: long arrow; connection to the internal layer: short arrow). The connection between 'kink' and underlying layer is established by a cell population of particular morphology that will be described later in more detail. Once part of the intermediate layer systems, cells from 'kinks' do not develop uniformly but are submitted to re-structuration (E-G), proliferate into ball-shapes (E) and finally form ring structures (F, G). It is noticeable that at all times the continuity and morphology of the external (EL) and internal (IL) layers is preserved. The absolute increase of the thickness of the frontal bone is due to an elaboration of the mesodermal and neural crest material belonging to the intermediate layer (H). After immigration from the external layer into the underlying space, cells organise in cellular sheets or layers which leads to a gradual filling of the intermediate space with an ontogenetic series of cell sheets. Cell sheets close to internal layer will be the ontogenetically oldest and those close to external layer the youngest in that series. During further development, cell layers assume a wavy morphology and begin to contact each other (H, arrows), providing the framework for the later cancellous structure of the intermediate layer.

Based on labelling with the *Wnt*1-Cre transgene, the murine frontal bone is traditionally thought to be solely derived from neural crest[93]. In contrast to that claim, we find that not only the original mesenchymal condensation for the frontal bone, sandwiched between the external and internal layer (Figure 4.22 A and D, asterisk), is not of neural

Figure 4.21- 4.22

Wnt1-Cre+/-;Rosa26Lac -/-

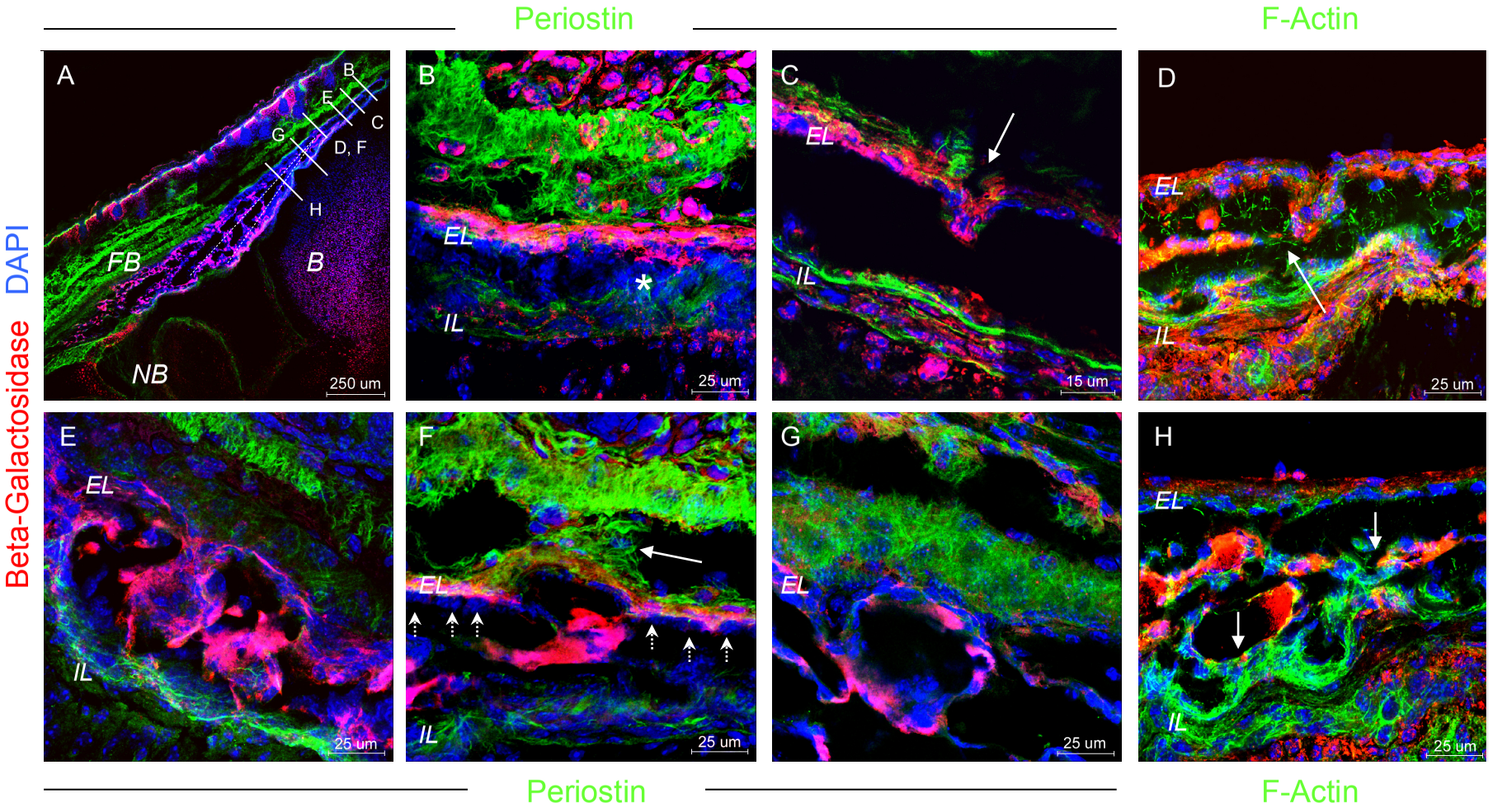

Figure 4.21 Laminar development of the frontal bone

IHC* for Beta-Galactosidase (red), Periostin (**A- C**, **E- G**, green) or F- Actin (**D**, **H**, green), counterstained with DAPI (blue) on sagital section of the frontal bone of a E18.0 *Wnt*1-Cre+/-; Rosa26LacZR-/- mouse. The position from where **B**- **H** are derived is indicated.

A Overview of the frontal bone in low magnification (FB, orientation: anterior to the left, cranial to the top). Different parallel cell layers are recognisable within the frontal bone, two of them are outlined by dashed lines.

B In the immature part of the bone close to the coronal suture, only the external (EL) and internal (IL) layer of the forming bone are established. The intermediated space (asterisk) is filled with loose mesenchyme lacking overt organisation. The outer layer EL shows strong immunoreactivity for ß-Galactosidase, while the space below lacks signal.

C At certain intervals, the external layer (EL) kinks and invaginates into the underlying space (arrow) which in this very thin optical stack appears empty but corresponds to the same region marked with asterisk in **B**. The external (skin-facing) side of the external layer is covered by a layer of Periostin fibres. The different intensities of the staining between the left and right side of the image are due to photobleaching of the right side caused by a previous scan of the area.

D 'Kinks' from the external layer (EL) into the underlying space are then actively connected with intermediate cell layers within the bone (long arrow) by a particular cell population analysed in detail in Figure 4.23.

E 'Kinks' from EL into the intermediate space can also develop into whirls of cells, note the continuity of the external layer in this process.

F, **G** Layers eventually interconnect and can often been seen forming circular structures (**G**), obscuring the original outlay in layers.

H Also cell layers in the intermediate space interconnect (arrows), forming a wavy and eventually circular pattern.

EL external layer, ***IL*** internal layer, ***FB*** frontal bone, ***NB*** nasal bone

* IHC was performed according to standardized conditions; a detailed description of conditions and antibodies (primary and secondary) can be found in the relevant section under 'Materials and Methods' (Chapter 7.5.4).

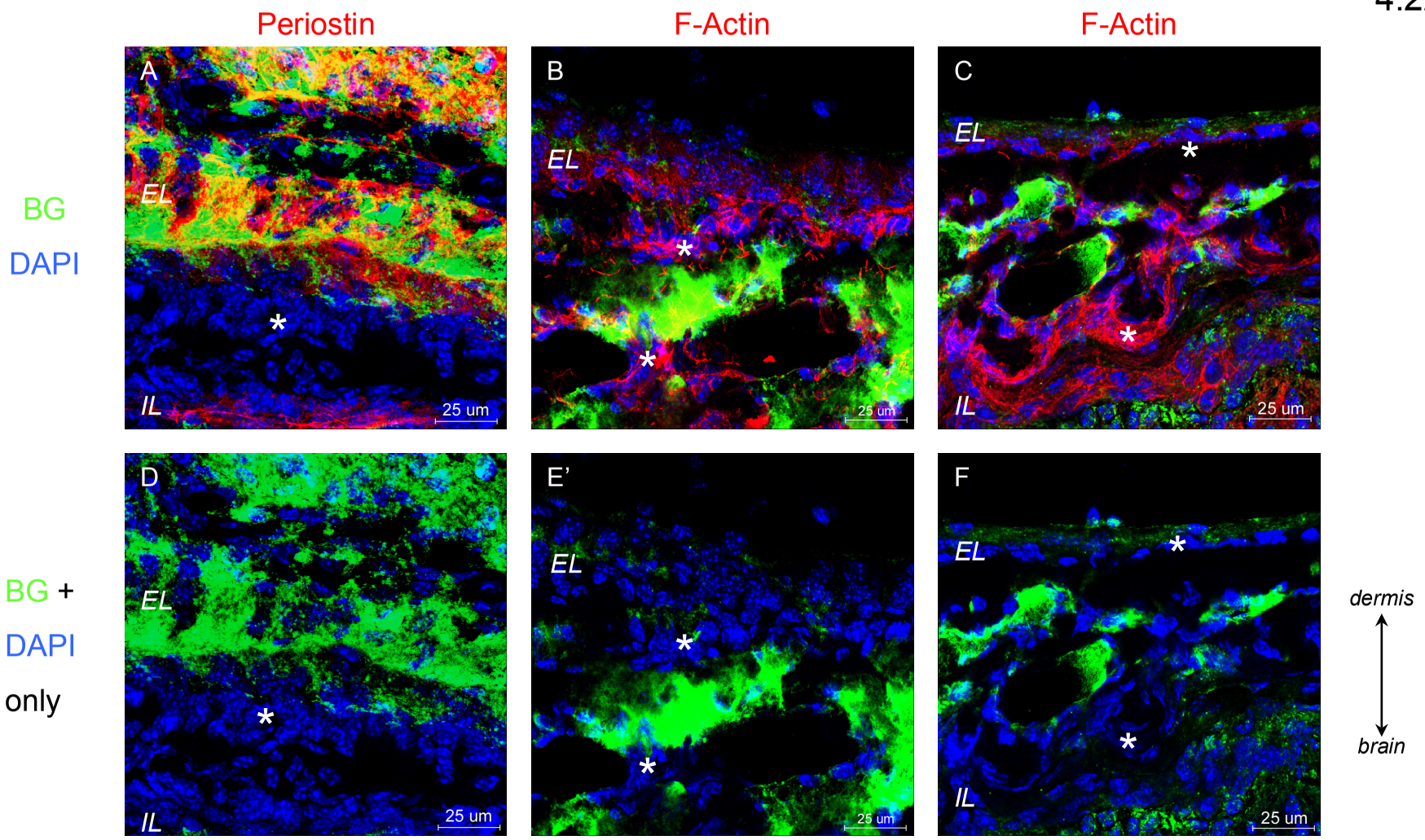
Periostin
F-Actin
F-Actin
BG
DAPI
BG +
DAPI
only
A
B
C
D
E'
F
EL
IL
25 um
dermis
brain

Figure 4.22 The murine frontal bone is of mixed embryonic origin

IHC* on sagital section of the frontal bone of a E18.0 Wnt1-Cre+/-; Rosa26LacZ -/- mouse in which the presence of Beta-Galactosidase indicates neural crest origin. Beta-Galactosidase (green) and either Periostin (**A**) or staining for F- Actin (Rhodamine-Phalloidin, **B** and **C**), counterstained with DAPI (blue) to show bone morphology. Images **D**, **E** and **F** in the lower row are identical to sections **A**, **B** and **C**; to appreciate the extent of neural crest contribution, only the green channel (Beta-Galactosidase) and the blue channel (DAPI) are shown. Images are orientated with the dermis to the top and the brain to the bottom.

A In the frontal bone at an immature state close to the coronal suture, the mesenchyme (asterisk) between the external layer EL and the internal layer IL (both positive for Periostin) is not labelled by the *Wnt*1-Cre transgene, indicating that it does not originate from the neural crest but must be derived from cranial mesoderm.

B, C In a part of the frontal bone in which dermal bone formation is more advanced, neural crest and mesodermal layers (asterisks) and areas alternate.

BG Beta-Galactosidase, ***EL*** external layer, ***IL*** internal layer

* IHC was performed according to standardized conditions; a detailed description of conditions and antibodies (primary and secondary) can be found in the relevant section under ‘Materials and Methods’ (Chapter 7.5.4).

crest but most likely mesodermal origin (mesodermal origin is concluded from the absence of ß- Galactosidase staining in the *Wnt*1-Cre mouse) but these unlabelled cell layers and groups are found throughout the frontal bone (B, C, asterisks). Sheets of neural crest cells appear to have invaded a mesodermal territory, resulting in layered structure of mixed embryonic origin (B, C).

A particular 'chestnut' cell population in immature frontal bone

In the immature part of the frontal bone close to the coronal suture, I was able to image a cell population of distinct morphology (Figure 4.23). Cells are perfectly round and large (15 µm, Figure 4.23 D, E), with an asymmetrically localised large nucleus and F-Actin spikes, giving them the appearance of 'chestnuts' (as which they will be referred to from now). They also show immunoreactivity for Undulin, a general periosteal marker[14]. Chestnut cells can bee seen apparently moving between the internal and the external layer (B, arrows show cells that fuse with or emerge from one of the layers) and merge with or emerge from nuclei of the external bone layer (F, arrows), suggesting a cellular movement between the two outer layers. The transformation of osteoblasts into osteocytes has been described as a process of cells moving from the organised layer of osteoblasts into the underlying space as pre-osteocytes while simultaneously reducing their cytoplasm[64]. Judged by their behaviour of a potential emergence from the upper layer of forming bone, 'chestnut cells' could theoretically represent pre-osteocytes although they do not seem to reduce but rather increase in size in comparison to the osteoblasts of the upper layer.

Some but not all chestnut cells are of neural crest origin (red in C), indicating that embryonic origin is not defining for this cell population. Though most abundant and easiest discovered under the immature part of the forming frontal bone (Figure 4.23 A-F), chestnut cells are also found in the upper but not the lower systems of the more mature frontal bone (G, H, arrows). Cells of similar morphology seem to fulfil a structural role in the development of the frontal bone as they are seen linking separate bone layers (empty arrowheads, Figure 4.23 G, H).

Figure 4.23

*Wnt*1-Cre+/-, Rosa26LacZR-/-

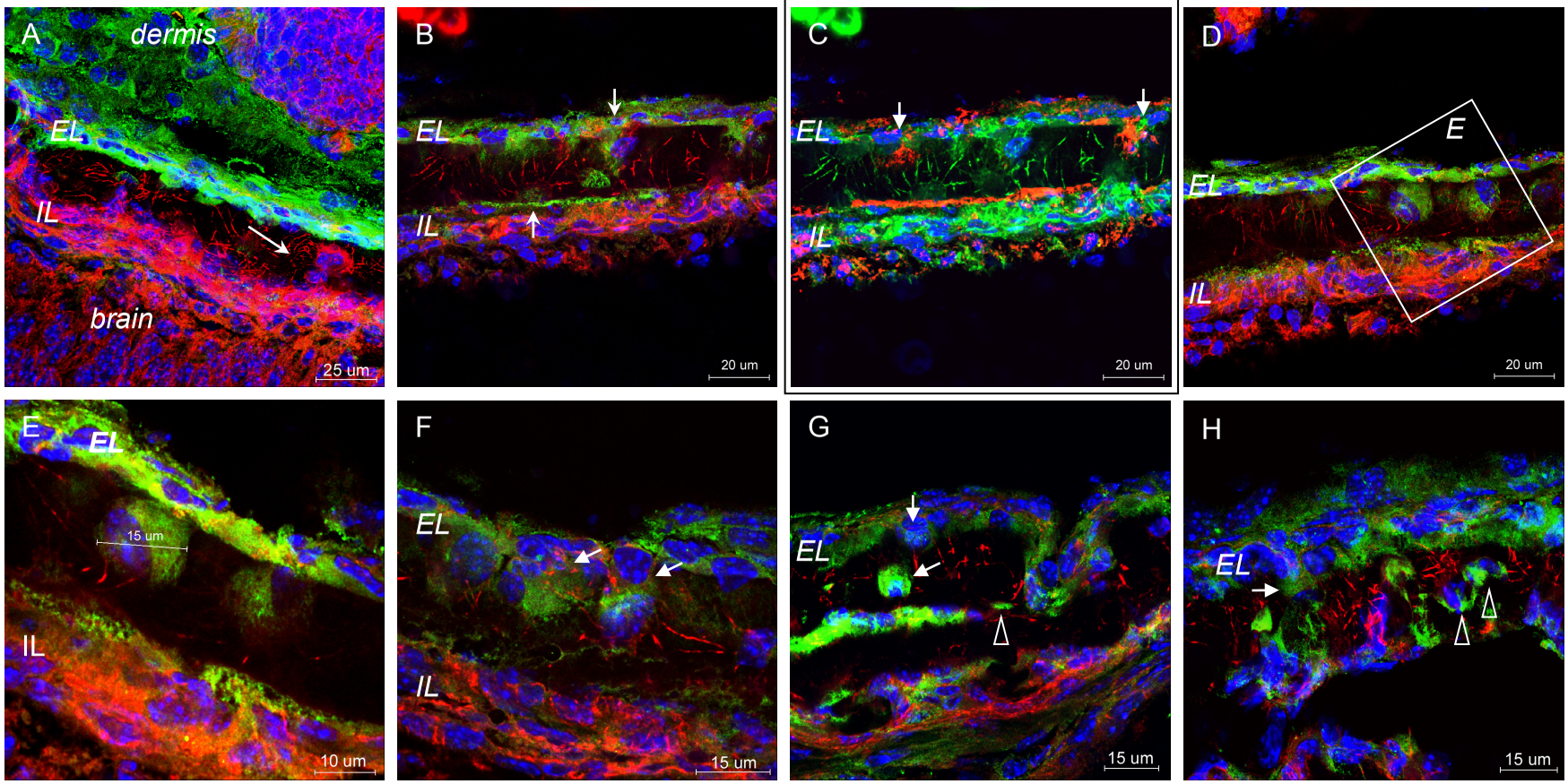

F-Actin Undulin

Figure 4.23 'Chestnut cells' in the frontal bone

IHC* on sagital sections of the frontal bone of a E18.0 Wnt1-Cre+/-; Rosa26LacZ-/- mouse. Images are orientated with the dermis to the top and the brain to the bottom. All but **C**: IHC for Undulin (green), F- Actin (red), DAPI (blue). **C**: IHC for Beta-Galactosidase (red), F- Actin (green), DAPI (blue).

A Projection of a thick z-stack to show the location of the chestnut in the intermediate layer of the forming frontal bone.

B A stack of fewer z- sections reveals the morphology of chestnut cells and shows that they emerge from or fuse with both the external and internal layer of the bone.

C Same section as in **B** but showing immunoreactivity against Beta-Galactosidase to indicate neural crest origin (red) and against F-Actin (green) to show the cell outline. Despite indistinguishable morphology, chestnuts can be of either neural crest or mesodermal origin (red cells are neural crest-derived, marked by arrows).

D, E Chestnut cells are round and large (15 µm), with an asymmetrically localised large nucleus and stain Undulin positive.

F Chestnut cells most likely fusing with the external layer (EL) of the frontal bone (arrows).

G, H Chestnut cells are mainly found in the intermediate layer of immature bone but are also present in the outer-most (skin-facing) part of the intermediate layer in more advanced bone (arrows). Cells of similar but not identical morphology can be seen to apparently fulfil structural tasks as in linking bone layers (empty arrows).

EL external layer, ***IL*** internal layer

* IHC was performed according to standardized conditions; a detailed description of conditions and antibodies (primary and secondary) can be found in the relevant section under 'Materials and Methods' (Chapter 7.5.4).

The external layer of the forming bone expresses molecular markers of both periost and perichondrium and is connected to dermal Periostin fibre systems

The study of frontal bone development suggests that the external layer plays a fundamental role in the formation of the bone as it is the layer providing the material for further internal layers. Before the establishment of a true bony structure, the external layer architecturally resembles a simple periost, with an outer layer of flattened cells and an inner layer of cubic cells[77] (Figure 4.24). The periost is known to play a fundamental role in bone, development, growth and regeneration; it has been proposed to be the tissue origin of bone and to recruit osteoprogenitor cells[43,84]. A specific set of markers characterises the periost of long bones and distinguishes it from perichondrium and the underlying bone[14]. The external periost-like layer is molecularly distinct from the intermediate and internal layer and expresses a mixture of both perichondrial and periosteal markers, namely Undulin (as expressed in both the periost and the perichondrium), Decorin (as marker for the perichondrium and also for early osteoblasts) and CRABPI (expressed in the perichondrium) (Figure 4.24). The external layer not only invaginates into the intermediate space but in regular intervals also makes contact with the Periostin fibre systems of the dermis (Figure 4.25 A and B, empty triangles). As the name suggests, Periostin was first isolated from the periost, although Periostin fibres are also found in other locations. Distinct parallel sheets of well-organised vertical Periostin fibres are present in the dermis (Figure 4.25 C, also Figure 4.19, 20 A). Interestingly, Periostin sheets show an internal organisation with flattened cells on the upper (skin-facing) side (Figure 4.25, B, C, arrows) and round cells (B, C, arrowheads) within the system. The overall orientation of the dermal Periostin sheets parallels the front of the forming frontal bone; layers occasionally split (C, dotted arrow), interconnect with other fibre systems (C, dashed arrow) and with the surface of the external layer (A, B). The interconnections close to the bone surface appear to ‘tie’ Decorin (A) and Undulin (B) positive cells to the surface of the forming bone, potentially recruiting cells to this layer.

Figure 4.24- 4.25

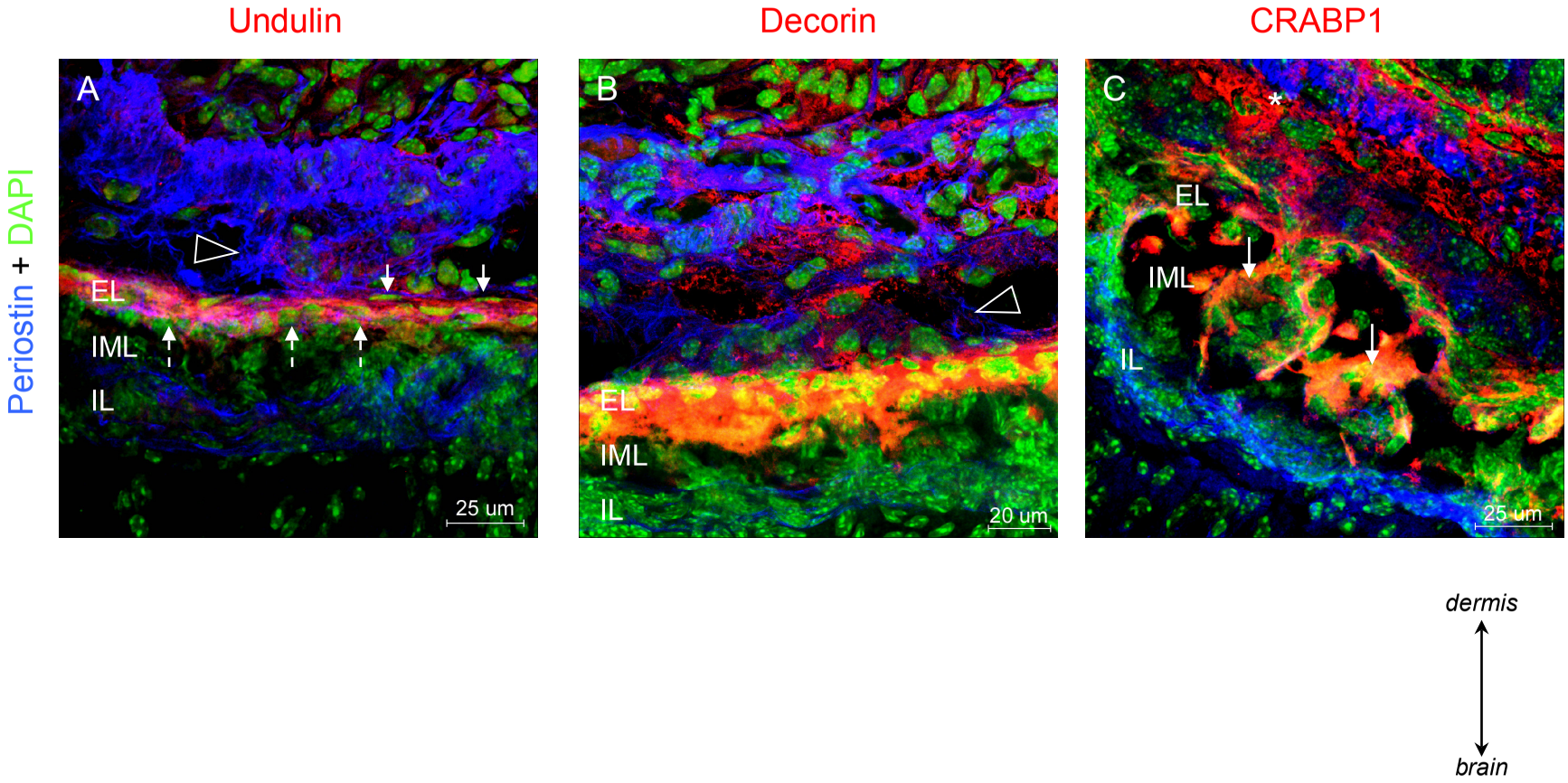
Undulin
Decorin
CRABP1
Periostin + DAPI
A
B
C
EL
IML
IL
25 um
20 um
25 um
*
dermis
brain

Figure 4.24 The external layer of dermal bone is molecularly distinct from the intermediate and internal layers

IHC* on sections of relatively immature frontal bone close to the coronal suture for Periostin (blue) and different periosteal/ perichondrial markers (red), nuclei are counterstained with DAPI (green). Markers: Undulin (**A**), Decorin (**B**) and CRABP1 (**C**).

A The external layer (EL) but not the intermediated layer (IML) nor the internal layer (IL) closest to the brain are Undulin positive. The external layer also shows a particular organisation with flattened cells on the top (full arrows) and cubic cells on the bottom of the layer (dashed arrows).

B Decorin is present in the external but not the other two layers. Decorin is also found in the dermis above to the forming bone in vicinity to Periostin fibre systems.

C CRABP1 is present in the external layer and on the surface of the invaginations from the external layer (EL) into the underlying space of the intermediate layer (arrows). Similar to Decorin, CRABP1 is also observed in the dermis.

* IHC was performed according to standardized conditions; a detailed description of conditions and antibodies (primary and secondary) can be found in the relevant section under ‘Materials and Methods’ (Chapter 7.5.4).

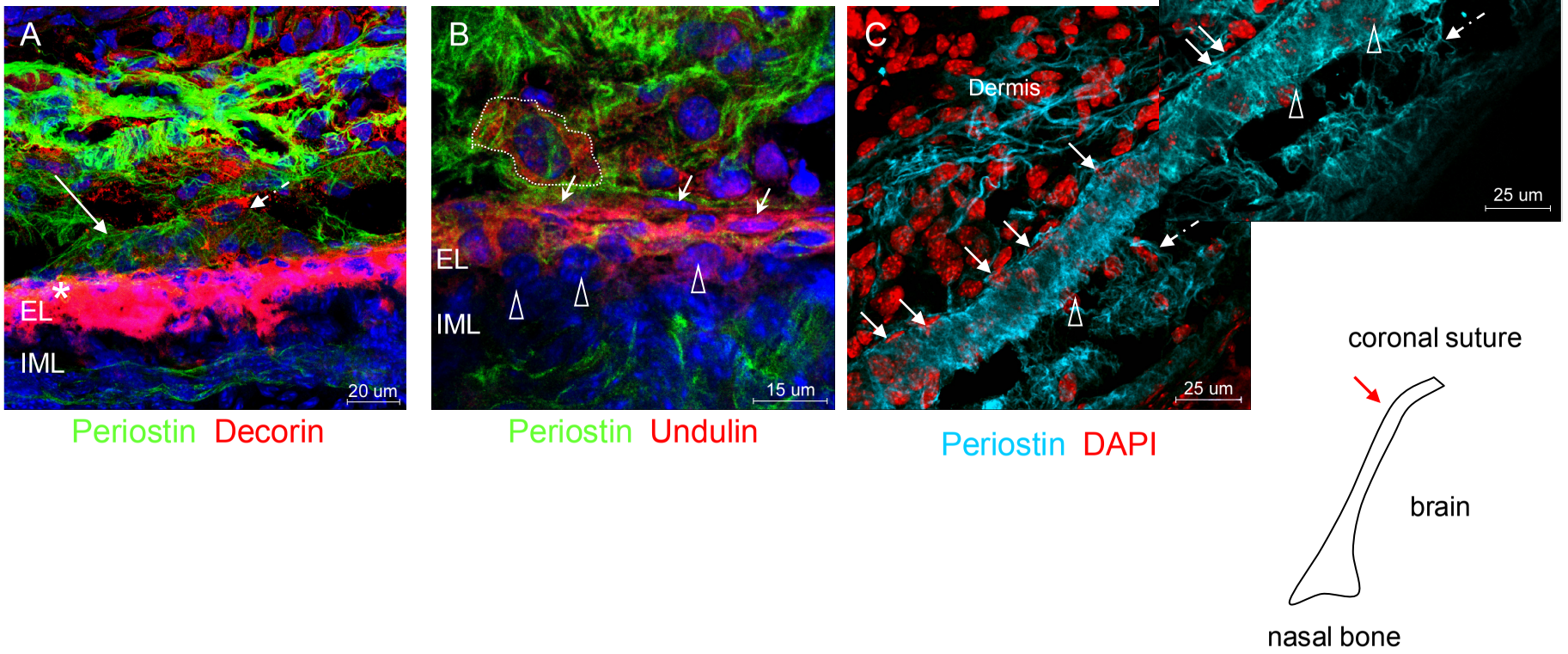
A
EL
IML
20 um
Periostin Decorin
B
EL
IML
15 um
Periostin Undulin
C
Dermis
25 um
Periostin DAPI
25 um
coronal suture
brain
nasal bone

Figure 4.25 Systems of Periostin fibres in the dermis

IHC* on sagital sections of the frontal bone of E18 mice for Periostin (**A**- **E**), Decorin (**A**, **D**, red), Undulin (**B**, red), counterstained with DAPI.

A The external layer (EL) with strong immunoreactivity for Decorin stands in contact with Periostin fibre systems in the dermis (solid arrow) giving the impression that cells- some of which are Decorin positive (dashed arrow)- get actively recruited to the surface of the forming frontal bone.

B Large Undulin positive cells (dotted outline) are tied by Periostin fibres to the external layer (EL) of the forming frontal bone. The organisation of the external layer (EL) with flattened cells on the outside (arrows) and large, round cells on the inner side of the layer (arrowheads) is clearly visible.

C The dermis is interwoven with large sheets of parallel running Periostin fibres. Occasionally, sheets are seen to split (dashed arrow on the right side of the image). The organisation of these Periostin sheets in the dermis resembles the one of the external layer of the forming dermal bone with flat cells on the top (dermis-facing side, arrows) and large rounded cells on the bottom (brain-facing side, arrowheads) of the system.

EL external layer, ***IL*** internal layer

* IHC was performed according to standardized conditions; a detailed description of conditions and antibodies (primary and secondary) can be found in the relevant section under ‘Materials and Methods’ (Chapter 7.5.4).

4.5.2.5 Summary of findings

- *Hand*2 is expressed at sites of forming dermal bone
- Loss of *Hand*2 function results in the loss of the layered architecture in the dermal cover of the clavicle as well as in the frontal bone.
- *Hand*2 expression in bone is at least partially controlled by the so-called *Hand*2 branchial arch enhancer and this enhancer controls a specific aspect of bone formation.
- The mouse frontal bone develops in an interaction between neural crest and mesoderm and from three distinct layers or sheets of cells: an external layer, several intermediate and an internal layer. The internal (IL) and external (EL) layer of the bone are established first, cells then invaginate from the external layer into the intermediated space, arrange themselves horizontally in new intermediate layers and finally re-organise to create the cancellous intermediate layer space (IML).
- The external layer of the forming frontal bone structurally resembles a primitive periost and expresses a mixture of periosteal and perichondrial markers[14].

4.5.3 Discussion

The novel expression domain of *Hand*2 RNA transcripts in forming dermal bone and the defects in bone architecture caused by the loss of *Hand*2 function reported in this thesis support a general role of the transcription factor in dermal bone formation. So far, the disturbed bone architecture in the lower jaw of *Hand*2 BAenh$^{-/-}$ mice who lack the regulatory element for *Hand*2 branchial arch expression has been interpreted as the consequence of the loss of *Hand*2 function in the distal first branchial arch[65]. However, I find that *Hand*2 expression is not restricted to bones derived from the *Hand*2 distal branchial arch domain such as the lower jaw, but is also present in e.g. the frontal bone and the clavicle (for an overview of bones of distal branchial arch origin, please see Figure 2.20).

Loss of *Hand*2 function results in a perturbed layered architecture of the bone and was the starting point for me to investigate dermal bone formation in detail. In mammals, purely dermally ossifying elements are restricted to the skull; the frontal bone was chosen in this study as it shows different maturation stages along its height. The observations I made about the formation of the frontal bone are not consistent with the current textbook model of dermal bone growth which assumes that dermal bone formation starts spontaneously in the mesenchyme and that an inner and outer corticalis layer are established afterwards (see Figure 4.12) but rather suggest a model of dermal bone formation according to which dermal bone begins to form as a 2-layered structure with an external and an internal layer, followed by the invagination of cells from the external layer into the underlying space. Eventual horizontal extension and elaboration of these invaginations will finally give rise to a cancellous intermediate layer and result in an overall 3-layered bone structure; the intermediate layer is therefore ontogenetically not the oldest but the youngest of the three layers (Figure 4.26).

In the formation of the frontal bone, the external layer is of particular importance as it is the generative layer for the ontogenetically younger intermediate layer. This particular role is reflected in a distinct molecular signature that sets apart the external layer from the intermediate and also the internal layer. Although the frontal bone is only laid out in cellular layers at the time of the analysis, I observe that the external layer expresses periosteal markers, suggesting that a periost-like external layer is established before and independently of underlying bone and not as commonly thought as last step in the

Figure 4.26

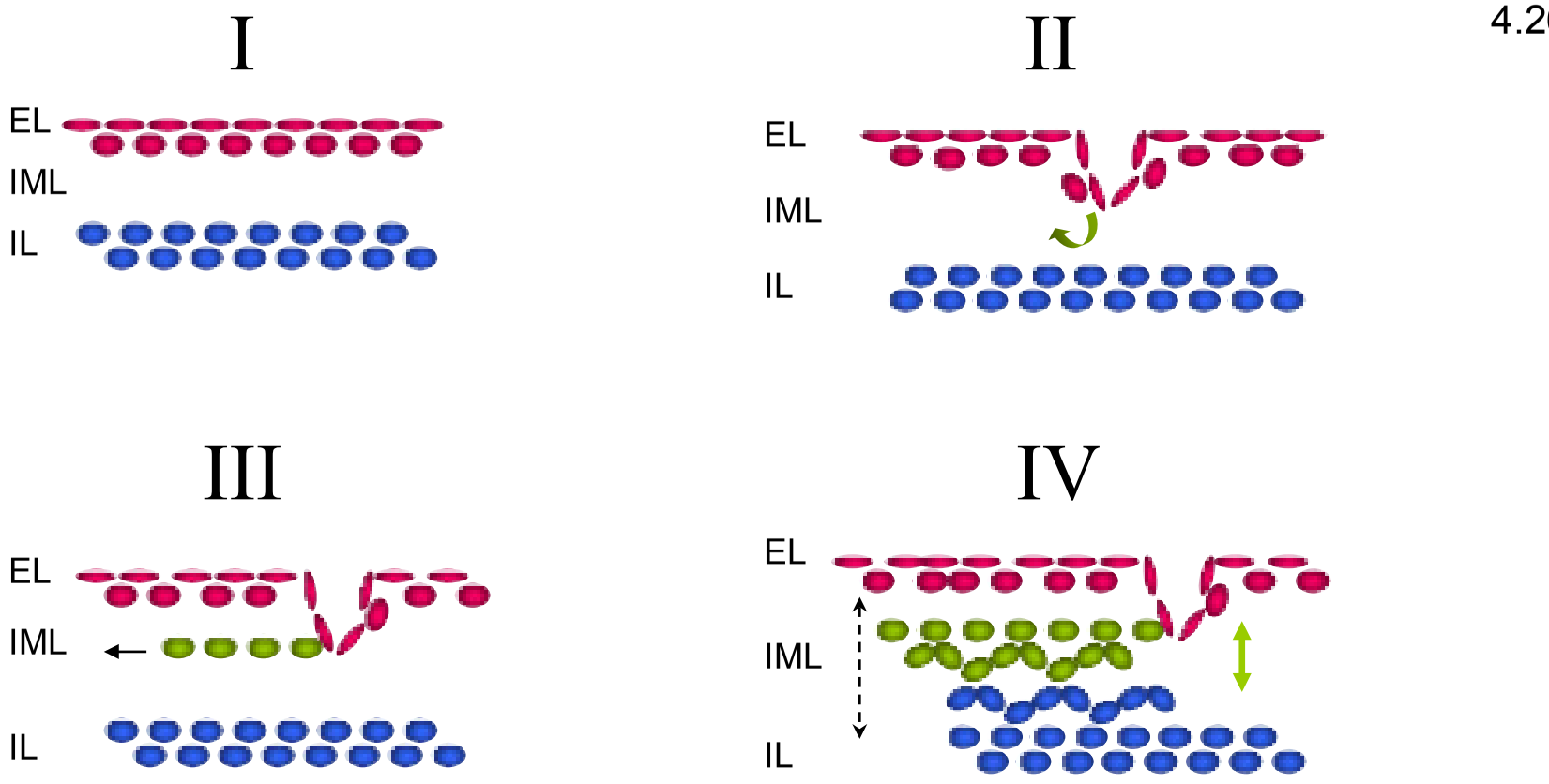

EL external layer facing the dermis

IML intermediate layer

IL internal layer facing the brain

Figure 4.26 A novel model for dermal bone growth

Based on the results of this study, the following model for the initiation of mammalian dermal bone formation is proposed:

Phase I: The mesenchyme in the dermis condenses into two discrete layers. The external Layer EL assumes the architecture of a simple periost with flattened cells on the outside and cubic cells on the inside.

Phase II: the external Layer EL begins to fold and invaginates vertically into the underlying space.

Phase III: Cells originating from the external Layer experience horizontal elaboration in the intermediate space and form distinct cell sheets.

Phase IV: Re-configuration of several cell sheets results later in the fully formed cancellous intermediate Layer (double arrow). Note that also cells from the external Layer participate in the formation of the bottom part of the intermediate Layer IML. It is this green part of the intermediate Layer (green double arrow) that is specifically affected by in the *Hand*2 BA enh-/- mutant.

formation of dermal bone[67,94]. Interestingly, the external layer not only expresses markers identified as characteristic for the periost but also for the perichondrium of long bones[14], suggesting an intermediate identity between periost and perichondrium. This is notable as dermal osteoprogenitors have recently been shown to genetically differ from enchondral osteoprogenitors in that they express both markers for osteogenesis as well as chondrogenesis [3]. The intermediate periost/ perichondrium identity of the external layer of the dermal frontal bone would thereby correlate with an intermediate molecular cartilage/ bone identity of its dermal osteoprogenitors.

I find that the intermediate layer forms from invaginations from the external layer into the underlying space, followed by a horizontal extension of these cells in layers and subsequent re-structuration, most likely occurring around forming bloodvessels, that obscure the original laminar nature. Interestingly, I also observe that it is this process of horizontal extension and cellular layer formation within the upper part of this intermediate layer IML that is particularly affected by the loss of *Hand*2 function (Figure 4.19). Cells from the external layer still invaginate but are no longer able to expand in horizontal layers, leaving behind pillars of cells and an empty space where the upper cancellous intermediate layer should have been (Figure 4.19). This suggests differences in the generative mechanisms of the upper and the lower part of the intermediate layer of the frontal bone, further supported by the results of the lineage experiments in the *Wnt*1-Cre mouse that show that only the upper part of the intermediate layer is neural crest-derived (Figure 4.22 C, F). In contrast, the lower part of the intermediate layer is- like the internal layer IL- not labelled by the *Wnt*1-Cre transgene, suggesting mesodermal origin of this part of the bone (Figure 4.22 C, F). The intermediate layer IML appears therefore to be the result from invaginations from the external layer EL into the underlying space followed by a *Hand*2-dependent horizontal elaboration of these cell sheets and in a further contribution from the internal layer as suggested by the shared non neural-crest origin of the internal layer and the lower part of the intermediate layer. The exact nature of the process of how the internal layer contributes to the intermediate layer IML was not investigated in this study. However, the mechanism by which the morphologically similar wavy cell layers of the lower part of the intermediate layer IML are generated is not controlled by the same mechanism dependent on the *Hand*2 branchial arch enhancer by which the cell layers in the upper part are established, as the specific deletion of the *Hand*2 branchial arch enhancer only

affects the upper but not the lower part of the intermediate layer (Figure 4.22 C, F, Figure 4.19).

So *Hand*2 function in dermal bone is- at least partially- controlled by the a short regulatory element that has been previously identified as the *Hand*2 'branchial arch' enhancer[29] as the deletion of this element is sufficient to disrupt a specific part of the layered bone architecture of the frontal bone. The fact that *Hand*2 is generally expressed in the early stages of dermal bone formation (Figure 4.13, 4.15), that the entire dermal nasal bone appears to be constituted of cells that have expressed *Hand*2 at some stage of their development or are descendants from a *Hand*2 expressing cell (Figure 4.14) and that neural crest-specific loss of *Hand*2 function disrupts the entire layer formation in the neural crest-derived part of the clavicular cover (Figure 4.16, 4.18) suggest however that additional regulatory elements are necessary to replicate endogenous *Hand*2 expression in dermal bone.

*Hand*2 has been reported to antagonize *Runx*2 function in osteogenesis[65]; the specific anatomical alterations after loss of *Hand*2 function at a time point prior to ossification reported in this thesis suggest however that this is not caused by a general ossification defect but rather a very specific function of *Hand*2 in the formation of the bone linked to the organisation of cellular layers.

The murine frontal bone apparently develops in an interplay between neural crest and mesoderm; neural crest from the external layer invaginates into a presumably mesodermal cell population, resulting in an arrangement of layers of different embryonic origin. As neural crest origin in this study is defined by expression of the *Wnt*1-Cre transgene, potential gaps in the expression of the transgene are a possible explanation. However, the situation observed in the murine bone mirrors the situation in chick, where a mixed neural crest/ mesodermal origin of the frontal bone has been demonstrated[61,107]. The location of mesodermal osteoblastic cells in the chick frontal bone has been experimentally demonstrated by fate-mapping of mesodermal cells (Figure 4.B3[61]) and exactly corresponds to the findings here in the mouse frontal bone (Figure 4.22 C, asterisk). The commonly held notion of a purely neural crest-derived mammalian frontal bone[93] might therefore have to be reconsidered.

4.6 Conclusion and perspective

A role for *Hand*2 in the arrangement of cells in layers and epithelial integrity has previously been described for the zebrafish myocardial epithelium[195] and the murine oral epithelium[208]. I show with the data presented in this chapter that dermal bone formation occurs through laminar stages dependent on *Hand*2 function and that *Hand*2 is equally necessary for the correct organisation and polarisation of the ameloblast layer in the murine lower incisor. The fact that the deletion of the short regulatory region of 745 bps (*Xho*I- *Bam*HI fragment[211]) of the so-called 'branchial arch enhancer' in the *Hand*2 BAenh$^{-/-}$ mouse is sufficient to disrupt both layer formation in dermal bone and the organisation of the incisor's ameloblast layer is highly suggestive of a shared genetic mechanism linking both systems, most likely in the organisation of cellular layers in both epithelia and mesenchyme. Future work will be required to identify the specific mechanistic role of *Hand*2 in the establishment of these cellular layers, in how far this mechanism is generalisable and to establish links between the transcription factor and known effectors of planar cell polarity, in particular the *Wnt*/PCP pathway. The interesting observation, that the expression of *Hand*2 in cellular layers is controlled by the short stretch of non-coding DNA that also controls expression in distal branchial arches will also require further investigation into the potentially complex mechanistics of this regulatory element.

5 Genetic lineage labelling in *Xenopus tropicalis*

5.1 Overview

Our understanding of the evolution of vertebrate head, neck and shoulder evolution will crucially depend on how well we are able to explain and compare the developmental mechanistics that pattern the region in the first place. Lineage labelling experiments mainly in birds have helped us to understand basic organisational principles of head, neck and shoulder formation, e.g.[102]. Genetic lineage labelling allows to refine the resolution with which cells can be tracked during development and recent advances in transgenic techniques in model systems other than mouse now render truly comparative data sets in different species possible.

The water-to-land transition about 390 Million years ago represents a major transitional event within the vertebrate group. Hardly any anatomical region was spared in the transformations that occurred in adaptation to the new terrestrial lifestyle; the evolution of the tetrapod middle ear with an insertion of the hyomandibula/ stapes into the wall of the inner ear for the detection of airborne sound is a particularly intriguing example[20,37]. For a long time it was thought that also the tympanon as a structure collecting incoming sound waves at the distal end of the stapes evolved only once within the tetrapod group and was therefore homologous. Nowadays it is generally excepted that a tympanic tetrapod middle ear must have evolved several times independently within the group which raises the interesting question in how far these can be considered homologous and about the shared and divergent genetic mechanistics behind this process[38,39]. Specimen of early tetrapods have been found whose middle ear resemble surprisingly the middle ear in extant frogs like *Xenopus*[154]. The *Xenopus* middle ear can therefore serve as a proxy for such an early tetrapod middle ear and allows to study the genetic patterning of a condition that is otherwise no longer accessible to experimental verification.

With the aim to comparatively study craniofacial patterning, especially the genetic mechanistics behind the formation of the early tetrapod middle ear and to establish homologies between the *Xenopus* and the mammalian middle condition, we took first steps to establish a genetic Cre/LoxP based lineage labelling system in *Xenopus tropicalis* with a new transgenic technique, I-*Sce*I mediated transgenesis. The

establishment of a stable transgenic line for a double fluorescent *Xenopus tropicalis* Cre-reporter as well as the generation and preliminary results for specific Cre-driving constructs are content of this Chapter.

5.2 Table of Contents

5.3 Introduction

5.3.1 Recombinase-based genetic lineage labelling

Higher organisms consist of a multitude of different cell types that originate from a limited number of precursor cells. Tracing the progeny of a precursor provides us with valuable insights into the organisational principles behind the complexity of the organism. The labelling of a cell lineage can be experimentally achieved by different techniques, such as dye injection, transplantation of labelled tissues or by transgenesis-based approaches. Genetic lineage labelling offers the advantage that it does rely less on anatomical landmarks than transplantation techniques, is non-invasive as it does not depend on surgery and is applicable to species with intra-uterine development. The possibility to establish stable and well-characterised transgenic lines further increases the reproducibility of results. The genetic lineage labelling systems that are currently predominantly used in mouse take advantage of site-specific recombinases such as Cre or Flp. The cell-specific and irreversible activation of a genetic reporter with help of Cre or Flp and the inheritance of the persistent reporter activation by all daughter cells thereby allow the tracking of the cell's progeny and establishes a lineage tree.
If lineage labelling experiments help us to understand morphogenetic and developmental processes in one species, comparative lineage labelling between species of relevant phylogenetic positions will provide an additional evolutionary perspective. From a developmental and evolutionary point of view, the vertebrate group is particularly intriguing as the high morphological similarity between embryos of the group contrasts with very diverse adult morphology. Although this phenomenon has already been formulated nearly two hundred years ago (von Baer's Law, 1828)[202], major questions concerning the homology of structures and the genetic networks responsible for the morphological differences, remain unanswered. As the definition of homology on the basis of shared embryonic origin represents the only meaningful way in accordance with developmental and evolutionary processes[5,122], progress in the field will depend on the availability of comparative data sets. So far, limitations in transgenic techniques in species other than mouse have prevented the generation of truly

comparative data but recent advances in transgenesis in teleost and amphibian model systems bring these now within reach. We made use a new technique, I-*Sce*I mediated transgenesis, to establish genetic lineage labelling based on the Cre/ Lox system in *Xenopus* with the final aim to study a particularly intriguing case of tetrapod head evolution, the evolution of the middle ear.

5.3.2 The evolution of the tetrapod middle ear

The fish to tetrapod transition around 390 Million years ago presents an interesting case of the evolution of morphological patterning in adaptation to a new lifestyle. Among the modifications affecting the head/ shoulder region, the evolution of the tympanic middle ear as a way to detect airborne sound is a particularly intriguing phenomenon. In a tympanic ear, aerial sound waves are received by the tympanic membrane (or disc) and transmitted to the liquid-filled inner ear via one or more of middle ear ossicles. The middle ear thereby fulfils the function of a lever and enhances the signal. Aquatic life does not require a middle ear (fish only have an inner ear) as water matches the impedance of the liquid-filled inner ear, but the mechanical enhancement of a middle ear was a prerequisite for the ability to detect airborne sound. A functionally analogous middle ear is present in all living tetrapods (Figure 5.1, note: the tympanon in caecilians was lost secondarily). For a long time, the middle ear of amphibians, reptiles and mammals was considered homologous and thought to be derived from a common middle ear 'proto-type'. Certain anatomical facts let Gaupp to question this homology already in 1912[70], but his view was only accepted many years later with the discovery of early tetrapod fossils lacking the pro-claimed prototype middle ear[111]. Although the concept of several independent evolutions of the tympanic middle ear within the tetrapod group is now generally accepted[38,39], experimental proof remains outstanding. From an evolutionary view point, the frog middle ear is particularly interesting as the recent reconstruction of the middle ear region of early stem-group amphibians (temnospondyls) suggests that the middle ear of extant frogs (*Xenopus*) still strongly

Figure 5.1

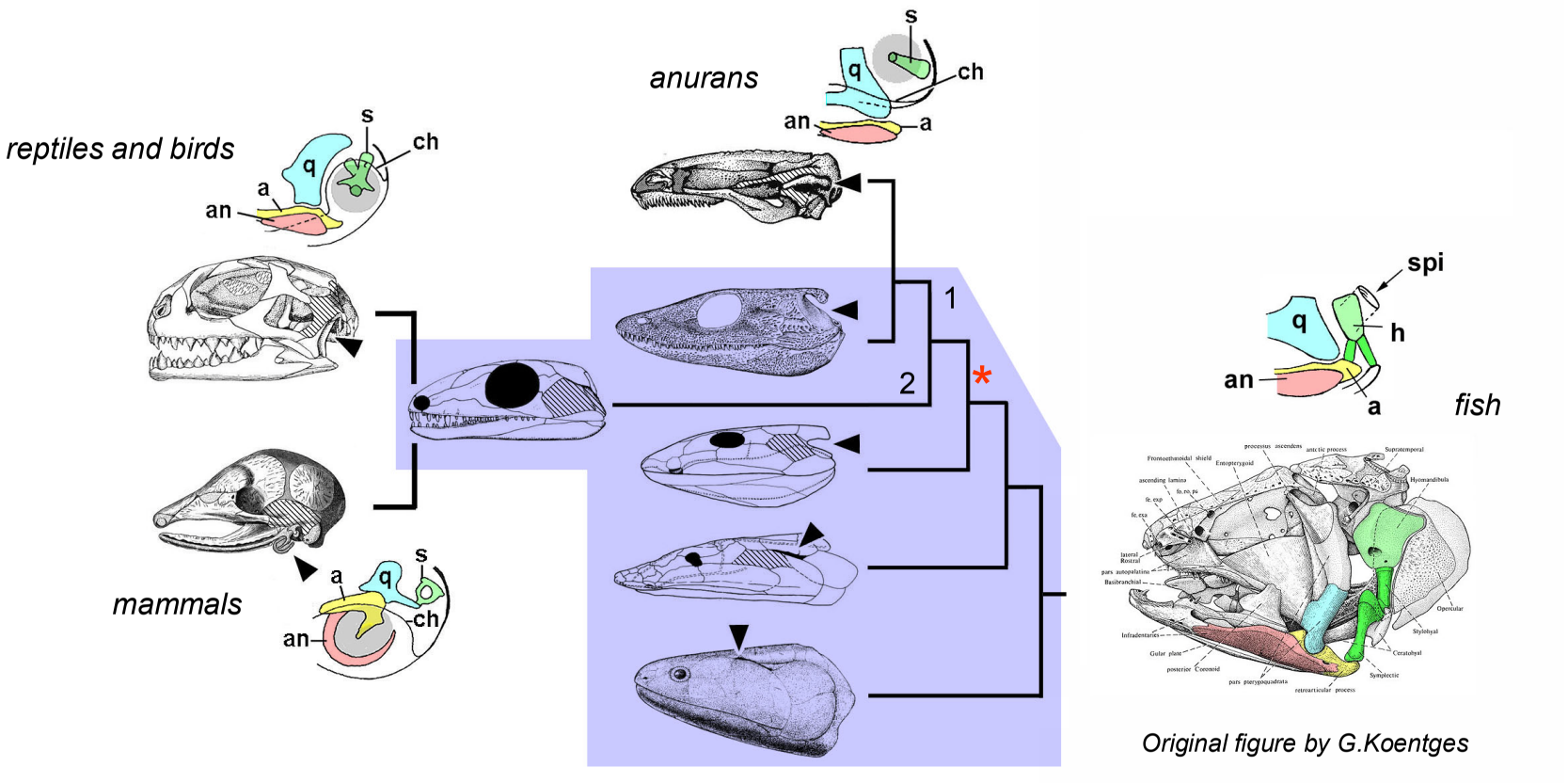

Figure 5.1 The evolution of the tetrapod middle ear

The fish-tetrapod transition is marked with an asterisk.'1' indicates the amphibian and '2' the amniote branch of the tetrapod lineage.

a articular, ***an*** angular, ***ch*** ceratohyal, ***h*** hyomandibula, ***q*** quadrate, ***s*** stapes, ***spi*** spiraculum

extinct species

resembles the ancestral condition[91]. This provides us with an extant model system for an extinct amphibian stem-group and makes an early tetrapod middle ear accessible to experimentation. The amphibian (shown here: *Xenopus*) middle ear consists of a tympanon with a cartilaginous tympanic disc linked by a rod-like stapes (also: columella) to the oval window of the inner ear (Figure 5.2). The middle ears of the two as model systems established *Xenopus* species, *Xenopus laevis* and *Xenopus tropicalis*, look- apart from their difference in size- very much alike (B, C). The amphibian as well as the mammalian stapes are considered to be second branchial arch derivatives and homologous to the fish' hyomandibula (shaded in green in Figure 5.1). The transformation from the hyomandibula into a stapes involved the loss of the distal part of the hyomandibula, a fusion of the proximal part with the (mesodermal) braincase and a re-orientation of the element from sagital to transverse. The fossil record from this transitional period (stem-group tetrapods and crown-tetrapods) provides us with a detailed picture about the sequence of morphological changes leading from the massive structural element of the hyomandibula to the gracile middle ear ossicle of the stapes[20,40]. In mice as a mammalian representative, the boundary between neural crest and mesoderm runs precisely through the stapedial footplate (Figure 5.3), suggesting that the stapes and the oval window evolved simultaneously by a fusion of second arch material with the mesodermal brain capsule under the definition of new skeletogenic boundaries. Genetic lineage labelling for second arch material in *Xenopus* will help us to elucidate whether this situation can be generalised for the tetrapod group or is specific for the mammalian stapes. The analysis of the *Hand*2-Cre mouse provided us with a detailed dataset about skeletal elements originating from the distal part of the first and second branchial arch. Comparative lineage labelling with an equivalent construct in *Xenopus* would allow to directly compare the amphibian with the mammalian condition, potentially also with respect to the origin of the tympanon in both groups.

Figure 5.2- 5.3

A

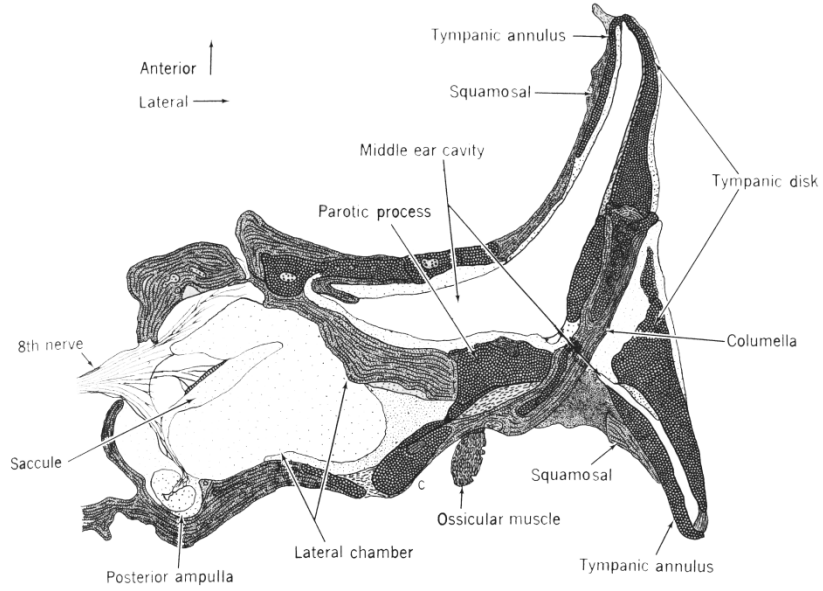

Fig. 5-8. The course and suspension of the columella, and relations to other ear structures in *Xenopus laevis*. Scale 10X. Wever, THE AMPHIBIAN EAR 1985, p 135

B

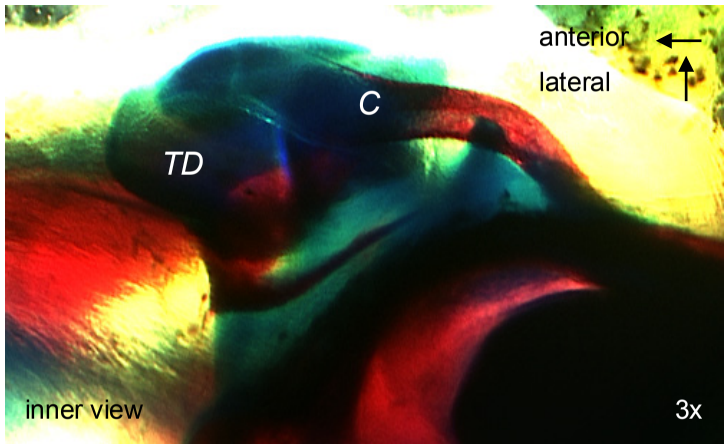

C

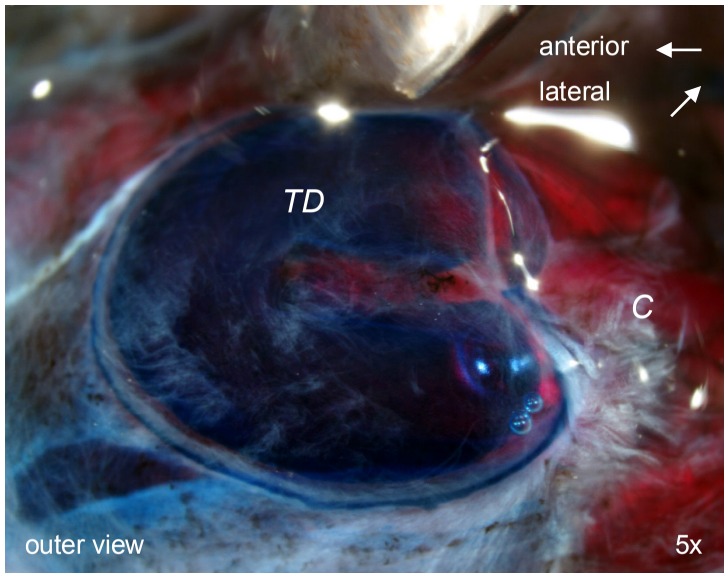

Figure 5.2 *The Xenopus* middle ear

Schematic representation of a *Xenopus laevis* middle ear (**A**) and Alzian-Blue/ Alizarin-Red staining of adult *X.laevis* (**B**) and X.tropicalis (**C**) middle ears.

The amphibian middle ear contains a single ossicle, the columella or stapes. The rod-like columella (*C*) connects with its distal end to a cartilaginous tympanic disk (*TD*).

C columella, ***TD*** tympanic disc

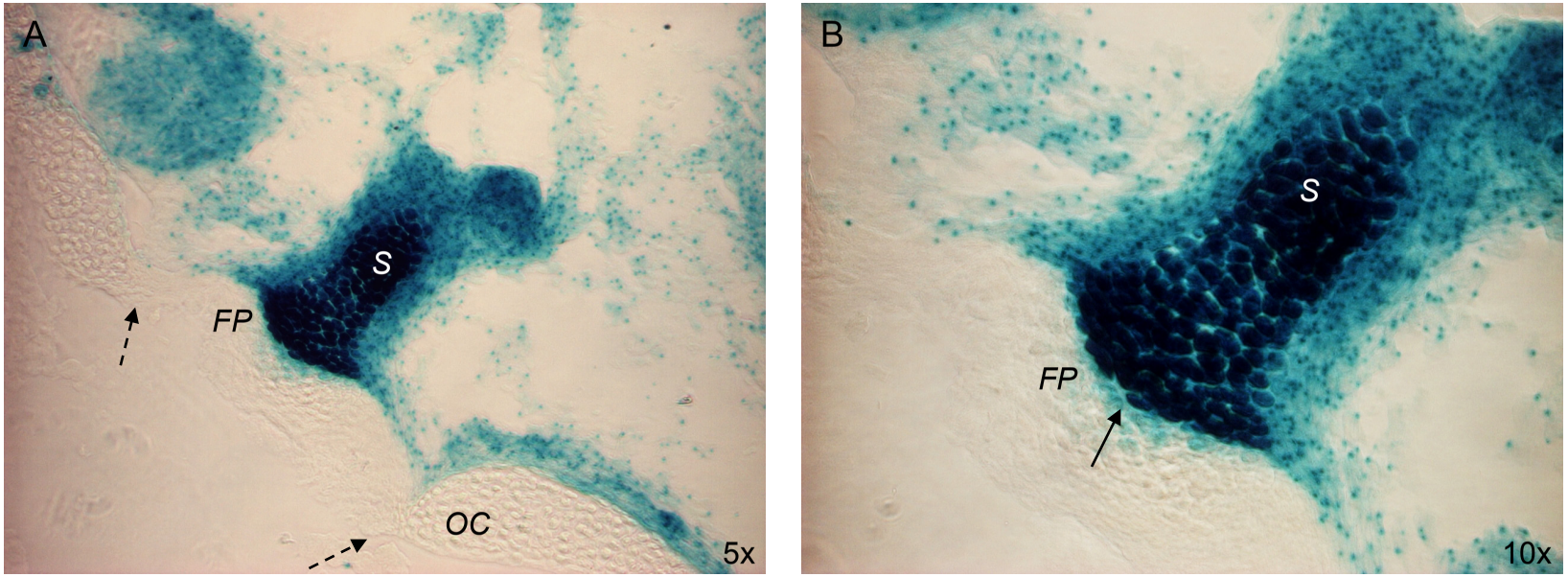

Figure 5.3 The cranial mesoderm/ neural crest boundary runs through the stapedial footplate

X-Gal staining of sagital sections of the otic region of E18.0 Wnt1-Cre mice. Blue labelling indicates neural crest origin.

A The stapes inserts with its footplate *FP* into the oval window (arrows) of the middle ear. Labelling with the Wnt1-Cre transgene shows that the stapes itself but only the outer part of its footplate are neural crest-derived (arrow in **B**). In conclusion, the otic capsulae *OC* and the inner part of the footplate are of mesodermal origin.

FP footplate, ***OC*** otic capsule, ***S*** stapes

5.3.3 Experimental Approach- genetic lineage labelling of neural crest subpopulations in the amphibian head

It has been argued that the only meaningful way to define homology is based on shared embryonic origin (termed 'cellular homology'[5,122]). Lineage labelling allows to follow a distinct cell population and its progeny through development and thereby reveals the embryonic origins of the adult anatomy. Comparative lineage labelling of the same original cell population in different species can then be used to establish cellular homologies between adult elements. Established biological model organisms exist for each of the tetrapod groups (amphibians [e.g. *Xenopus*], amniotes: reptiles including birds [e.g. *Gallus gallus*] and mammals [e.g. *Mus musculus*]) but so far, a detailed embryological map for the skull and the middle ear generated by lineage labelling experiments is only available in birds[45,102,137] (Figure 5.4 B). More recently, the contribution of second branchial arch neural crest to the murine middle ear was determined by genetic lineage labelling in mouse[141] (Figure 5.4 C) but the situation for the amphibian middle ear remains unknown.
Our goal was therefore to generate an embryonic map of the amphibian skull by genetic lineage labelling in *Xenopus tropicalis* that would allow us to compare the amphibian situation with existing avian and mammalian data sets, in particular with the results obtained from the analysis of the *Hand*2-Cre mouse.

As described in detail in the Introduction to this chapter, genetic lineage labelling with the Cre/LoxP method is a transgenic 2-component system with a transgene for a Cre-driver conferring specificity and a transgene for a generic reporter for Cre-activity providing the heritable marker that allows the determining of the cell lineage tree. The method of our choice for *X. tropicalis* transgenesis, I-*Sce*I mediated transgenesis, will be introduced in the next paragraph. The transgenes for a Cre-reporter line and two specific Cre-driving lines and the rationale behind the construct design are described in the following two sections.

Figure 5.4

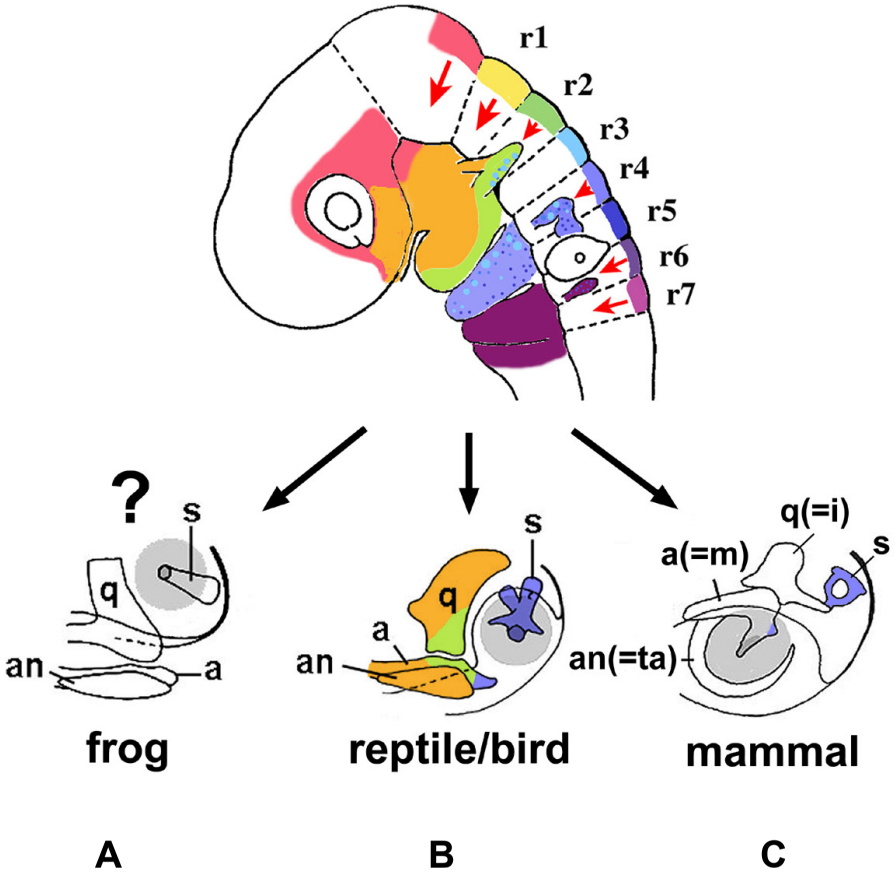

Figure 5.4 The rhombomeric origin of the tetrapod middle ear

The rhombomeric origin of the middle ear is only fully known in birds (**B**). In mammals, the contribution of the second branchial arch to the middle ear has been mapped (**C**). In anurans, the situation is unknown (**A**) .

a articular, ***an*** angular, ***i*** incus, ***m*** malleus, ***q*** quadrate, ***s*** stapes, ***ta*** tympanic anula, **grey**: tympanum

Original figure by G. Koentges

Reference

Kontges, G. & Lumsden, A. Rhombencephalic neural crest segmentation is preserved throughout craniofacial ontogeny. *Development* **122**, 3229-3242 (1996).

5.3.4 I-*Sce*I mediated transgenesis in *Xenopus tropicalis*

We first attempted to genetically lineage label cranial neural crest subpopulations in *Xenopus laevis* by transgenesis with the **R**estriction **E**ndonuclease **M**editated **I**ntegration (REMI) method[8,103] and co-injection of a Cre-reporter and a Cre-driving plasmid (experiments performed by S.Ishibashi/ Amaya group, Cambridge). With the classic REMI method, de-condensed sperm nuclei are incubated with a linearized construct in the presence of a restriction enzyme before being injected into unfertilized eggs[8,103]. Transgenic *X. laevis* embryos from our REMI experiments with simultaneous injection of Cre-reporter and Cre-driver showed a too high degree of mosaicism to allow an interpretation of the results. A further concern was aberrant Cre expression from un-integrated Cre-driving plasmid as genomic integration is required for controlled transgene behaviour[174]. Untimely Cre expression could potentially lead to activation of the Cre-reporter and false-positive results. To overcome both the problem of mosaicism and of un-regulated Cre activity, the decision was made to establish independent stable transgenic *Xenopus* lines for a) a generic Cre-reporter and b) specific Cre-drivers. Both lines would be interbred at later stages to generate double transgenic off-spring for analysis. Its long generation time (normally 1-2 years[59]) does not make *Xenopus laevis* an attractive candidate for the establishment of stable transgenic lines however, so that we chose the closely related *Xenopus tropicalis* that has been recently developed as model organism[81]. Compared to *X. laevis*, *X. tropicalis* offers several advantages: a compact diploid genome (*X. laevis* is tetraploid), smaller-sized adult specimen and most importantly for us, a considerably shorter generation time of 3-5 months[143]. The REMI technique has been already successfully used for transgenesis in *Xenopus tropicalis*[82,142] but injections have been proven technically challenging. In proportion to their overall smaller adult body size, *Xenopus tropicalis* eggs are smaller and more fragile than their *Xenopus laevis* counterparts (0.7–0.8 versus 1.0–1.3 mm, respectively[143]) and are easily damaged by the large injection needle required for REMI transgenesis. For this reason, we opted for an alternative transgenic technique, I-*Sce*I mediated transgenesis, that has recently been reported to allow the generation of fully transgenic founder animals[144]. First established in fish (*Medaka*[184]), I-*Sce*I mediated transgenesis has now been successfully used to generate stable transgenic *Xenopus laevis* and *tropicalis* lines[82,143,144]. The method uses a Meganuclease, originally isolated

from the mitochondriae of the yeast *Saccharomyces cerevisiae*[92,128] to facilitate the integration of a transgene flanked by its recognition sites into the genome. The enzyme recognizes, binds and cleaves a specific 18 base pair consensus sequence (TAGGGATAACAGGGTAAT) that does not naturally occur in the mammalian nor amphibian genome. The exact mechanism by which I-*Sce*I Meganuclease facilitates genomic integration is unknown but might be linked to the fact that the enzyme stays bound to the plasmid after cleavage[150], potentially protecting the linearized fragment from degradation. A major advantage of I-*Sce*I mediated transgenesis results from the fact that the plasmid is- after incubation with I-*Sce*I Meganuclease- directly injected into fertilised *Xenopus* eggs. The higher resistancy of fertilised over un-fertilised eggs and the possibility to use finer injection needles as the injection mix no longer contains fragile sperm result in a considerably higher number of surviving embryos. I-*Sce*I mediated transgenesis has further been reported to lead to fewer transgene insertions with a low copy number[143] which can be advantageous as it reduces the risk of overlapping position variegation effects and potentially facilitates the generation of stable transgenic lines. In our experience, I-*Sce*I mediated transgenesis did not show the expected success and problematic husbandry resulted in *Xenopus tropicalis* generation times of 8 months and more, exceeding the time frame for this PhD project. Nevertheless, we established a stable transgenic *Xenopus tropicalis* line with a double fluorescent Cre-reporter construct and have obtained promising preliminary results for one out of two Cre-driving constructs.

5.3.5 Summary

With the aim of studying the evolution and development of the amphibian middle ear, we planned to establish stable transgenic *Xenopus tropicalis* lines by I-*Sce*I mediated transgenesis that would allow us to perform genetic lineage labelling studies of cranial neural crest subpopulations. As a generic transgenic reporter line for the activity of Cre recombinase comparable to the Rosa26LacZ reporter in mice[176,177] was so far unavailable in *Xenopus tropicalis*, the generation of such a stable transgenic *Xenopus tropicalis* with a double fluorescent Cre-reporter was the first goal of this project and

will be described in section 5.2. In a next step, the generation of specific Cre-driving constructs that would allows us to particularly address the questions of a) the homology of the tympanon within the tetrapod group and b) the proximal fusion of the hyomandibula with the otic capsule and first preliminary results will be described in section 5.3.

5.4 A generic Xenopus tropicalis reporter for Cre-activity for genetic lineage labelling studies

5.4.1 Background

5.4.1.1 A novel generic reporter for Cre-activity in *X. tropicalis*

Over the last ten years, genetic lineage labelling with help of the Cre/LoxP system has become a well-established technique in mice. This was made possible by the availability of a generic and versatile reporter for Cre-activity, the original Rosa26LacZR Cre-reporter, and later versions based on the same principle[176,177]. As described in detail in the Introduction to this chapter, genetic lineage labelling with the Cre/LoxP is a 2-component system with a Cre-driver conferring specificity and a general reporter for Cre-activity providing the heritable marker for the cell lineage. A stable genetically modified Cre-reporter line equivalent to the murine Rosa26 reporters is currently available for *Xenopus laevis* but not for *Xenopus tropicalis* which is much better suited for the generation of stable transgenic lines due to its shorter generation time[81,82,161]. The first goal within our project of genetic lineage labelling of cranial neural crest subpopulations in amphibians was therefore to establish a generic *Xenopus tropicalis* reporter for Cre-activity.

5.4.1.2 Specifications for a *X. tropicalis* Cre-reporter

Since the major goal of this work was to study the embryonic origin of the amphibian head, the activity of the Cre-reporter in the different elements of the head/ shoulder region had to be assured. The ubiquitous activity of the murine Rosa26 Cre-reporter was achieved by targeting of the construct to the Rosa26 locus previously shown to be constitutively and ubiquitously active throughout development[176,214]. A similar gene targeting strategy is not available in *Xenopus*, so that transgenesis was the method of choice for the generation of a Cre-reporter. Because of the transgenic approach, a Cre-reporter construct requires a promoter which thereafter will be essential for reporter activity (leaving aside additional factors like the copy number insertion and position

variegation effects that cannot be controlled by the method). Promoters previously tested in our group showed unreliable expression in mesenchymal derivatives, especially in bone and cartilage, so that particular attention was paid to the choice of the promoter. Viral promoters show many desirable properties (strength, wide-spread activity) but can provoke silencing reactions by the host, particularly during germline passage[36]. The establishment of a stable transgenic Cre-reporter line was our aim, so that preference was given to a promoter of non-viral origin.
In the case of the murine Rosa26 Cre-reporter, it is impossible to assess the activity of the Cre-reporter in the absence of Cre recombinase as only Cre-mediated removal of a Stop cassette leads to the expression of a detectable marker. Absence of signal can therefore not be attributed with certainty to 1. the absence of Cre or 2. the absence of reporter activity or 3. theoretically, the absence of both. Against this background, a change from one to another detectable marker is preferable to an all-or-nothing response and provides an in-built control for reporter activity. In combination with fluorescent markers, it allows the easy screening for positive embryos under a fluorescence dissecting microscope and only potential founders to be raised to adulthood, reducing the number of animals that must be housed and later outbred considerably.
One of the advantages of the *Xenopus* model system is its external embryonic development with small embryos ideal for *in vivo* imaging. Live imaging requires a fluorescent signal that is sufficient for direct detection and the level of fluorescence depends on the combination of promoter strength and the properties of the fluorescent protein, so that we selected fluorescent proteins for their brightness and stability.

Summary of the desirable properties of a *Xenopus tropicalis* Cre-reporter:

- Activity of the Cre-reporter in the head/ shoulder region at relevant stages of development with stable inheritance
- In-built control for reporter activity
- Signal strength sufficient for live imaging to profit from the advantages of the amphibian system with external embryonic development

All components of the Cre-reporter constructs were tested as far as possible to ensure the success of the transgene. The design of a double fluorescent Cre-reporter for

Xenopus transgenesis, the results from the testing of the single components of the Cre-reporter construct and from I-*Sce*I mediated transgenesis in *Xenopus tropicalis* with three different versions of a double fluorescent Cre-reporter, including the final establishment and characterisation of a stable transgenic X. *tropicalis* reporter line for Cre-activity will be described in the next section.

5.4.2 Results Part 1- The design and the generation of a double fluorescent reporter transgene for Cre-activity

5.4.2.1 The design of a double fluorescent Cre-reporter construct for I-*Sce*I mediated transgenesis in *Xenopus tropicalis*

To assess Cre-reporter activity independent of the activity of Cre enzyme, a double fluorescent Cre-reporter was designed for *Xenopus* transgenesis (Figure 5.5):
A ubiquitous promoter is followed by two independent colour cassettes, each encoding a different fluorescent protein (1. RFP, 2. GFP). The first colour cassette contains the coding region of a red fluorescent protein flanked by LoxP sites ('floxed'), the recognition sites for Cre recombinase, and will therefore be removed upon Cre-activity. Default expression of the reporter (A) is defined by the first colour cassette, RFP, represented here by solely red cells. A polyadenylation signal directly downstream of the RFP coding region prevents simultaneous expression from the second cassette, encoding GFP. The activation of Cre in a specific cell (B, arrow, future daughter cells are indicated in grey) leads to excision of the floxed RFP cassette and the subsequent recombination event places the GFP cassette under promoter control. The result is a colour switch from red to green fluorescence, depicted schematically for a single cell in (B). Excision and recombination are practically irreversible, leading to a permanent change on DNA level that is passed on to all daughter cells (green cells in C). This double fluorescent Cre-reporter therefore translate temporally restricted Cre-activity into a permanent colour switch from red to green fluorescence which is then inherited by all progeny, thus defining a cell lineage tree.

The suitability of the promoter of the Cre-reporter construct, the correct change from red to green fluorescence upon the action of Cre and the functionality of the I-*Sce*I recognition sites incorporated in the construct were confirmed in detail and are described in the next paragraphs.

Figure 5.5

5.5

A
B
C
Default
Ubiquitous promoter
LoxP
RFP pA
LoxP
GFP pA
specific Cre-mediated excision and recombination
Lineage- specific
Ubiquitous promoter
LoxP
GFP pA
+
RFP pA
LoxP
Degradation

Figure 5.5 The principle of a double fluorescent reporter for Cre-activity

A schematic representation of the double fluorescent Cre-reporter (DF Cre reporter) with a colour switch from red (**A**) to green (**C**) upon the action of Cre. The appearance of the reporter in cells is illustrated schematically on the right.

A Default expression from the DF Cre-reporter is red fluorescence (Red Fluorescent Protein, RFP), indicated by a red arrow. Read-through into the coding of the downstream protein is prevented by a SV40 polyadenylation signal after the RFP (pA). All cells with the DF Cre-reporter will fluoresce brightly red.

B Upon Cre-activity, the RFP cassette will be removed from the DF Cre-reporter, now placing the coding frame of the second fluorescent protein (Green Fluorescent Protein, GFP) under control of the ubiquitous promoter. Expression from the DF Cre-reporter will consequently change from red to green, this is indicated by the green arrow. Due to RFP stability, fluorescence will change gradually from red over yellow (both RFP and GFP present) to green, indicated for a single cell on the right (arrow). Future progeny is indicated in grey.

C The excision event causes a permanent change on DNA level in the affected cell that will be inherited by all progeny, thus allowing to trace off-spring from the original cell (depicted now as green subpopulation in the comic).

5.4.2.2 A suitable promoter for a double fluorescent *Xenopus* Cre-reporter

5.4.2.2.1 The human Ubiquitin C promoter drives expression in mesenchymal derivatives in *Xenopus laevis*

As detailed in the introduction, our double fluorescent Cre-reporter required a sufficiently strong promoter of preferably non-viral origin with activity in the mesenchymal tissues of the head. The human Ubiquitin C (hUbC) promoter has been shown to drive strong ubiquitous expression in mice[110,163] but had not been used in *Xenopus* before.

We therefore tested the suitability of the hUbC promoter for *Xenopus* transgenesis by the Restriction Enzyme Mediated Integration (REMI) technique in *Xenopus laevis*. For that purpose, the promoter was combined with two different fluorescent proteins, Venus and DsRed2 (Figure 5.6). Transgenic *X. laevis* embryos and tadpoles for p144 (hUbC-Venus) and pSI_hUbC-DsRed2 were easily detected under a fluorescence dissecting microscope due to their bright green respective red fluorescence, proving the functionality of the human UbC promoter in *Xenopus laevis* (Figure 5.6). Green fluorescence was particularly strong in the musculature (Figure 5.6 B1). Even at a late developmental stage, strongly fluorescent muscle fibres are clearly visible through the skin; spider-shaped melanocytes of the typical skin pigmentation of a tadpole can be seen on the green background. Similarly, also red fluorescence is particularly strong in the musculature of the tail (Figure 5.6 D1). To ensure that the hUbC promoter was also active in cranial mesenchymal tissue, the head of the specimen in Figure 5.6 B1 was embedded in OCT (optimal cutting temperature) compound and cryosectioned. Sections of the head region were only counterstained with DAPI and directly analyzed under a Zeiss fluorescence dissecting microscope, the overall expression levels of Venus protein were very high and sufficient for direct imaging (Figure 5.6 B2 and B3). A section through the lower jaw of a transgenic stage 54 *X. laevis* tadpole shows that green fluorescence is readily detectable in bone (arrow) but considerably weaker in cartilage (B2, p144, arrowhead). Also the cell-rich connective tissue of the head fluoresces green (B3, arrow). Under control of the same hUbC promoter, red fluorescence is generally weaker than green fluorescence, but nevertheless clearly present in the musculature, the cartilaginous bars of the branchial basket and the lens of the eye (D).

Figure 5.6

5.6

A

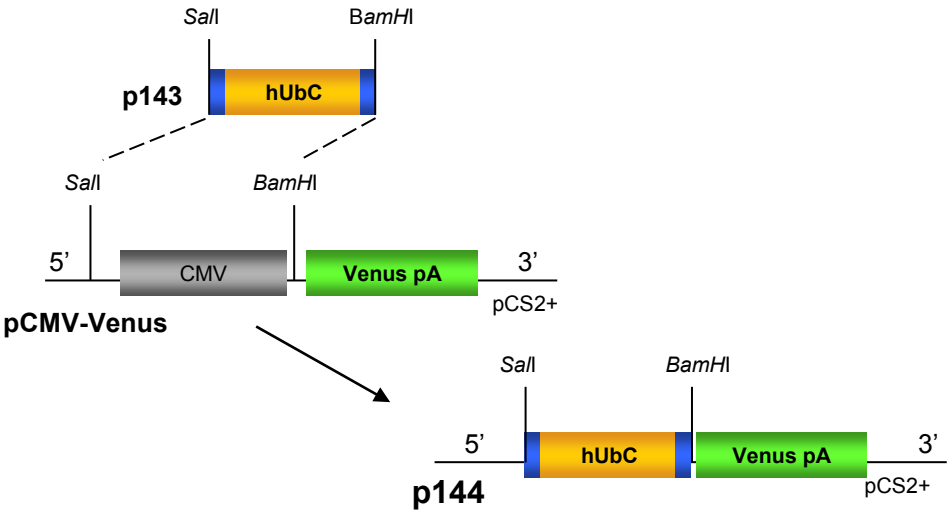

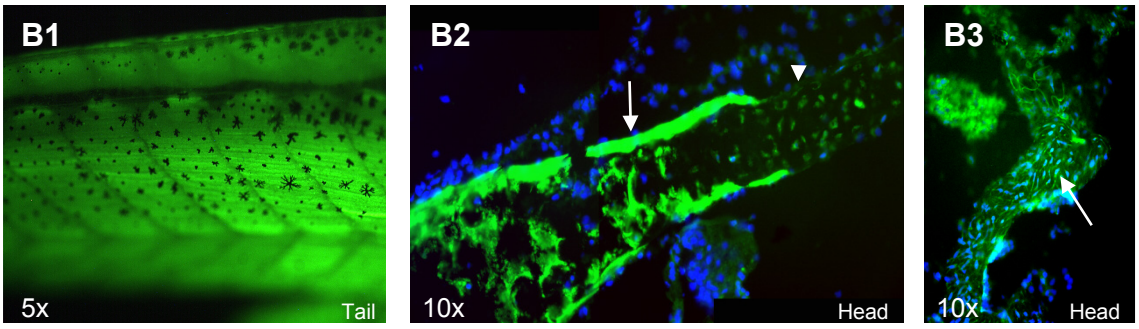

p144

C

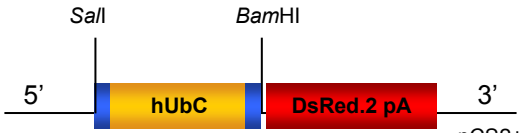

pSI_hUbC-DsRed2

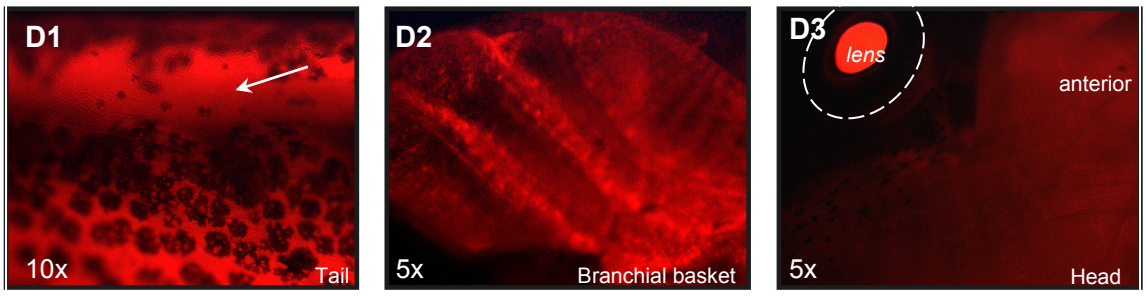

pSI_hUbC-DsRed2

Figure 5.6 The human Ubiquitin C promoter drives ubiquitous expression in *Xenopus laevis*

The human Ubiquitin C promoter (hUbC) was tested by REMI transgenesis in *X.laevis.*

A The generation of plasmid p144 (hUbC-Venus). The CMV promoter of the original plasmid pCMV-Venus (kind gift of R. Moon's lab) was replaced with the human Ubiquitin promoter from p143 (*Sal*I- *Bam*HI fragment).

B1- B3 Analysis of F0 *X.laevis* after injection with p144 (hUbC-Venus).

B1 Strong expression of Venus was seen in the musculature, as shown here for the tail of a living tadpole at stage NF 54.

B2 Direct green fluorescence could be observed on cryosections of the head region (here with a DAPI counterstain, same specimen as in B1): Strong expression was seen in bone (arrow); the expression in cartilage was present but weaker (arrowhead).

B3 Venus is also clearly expressed in the connective tissue of the head region (arrow).

C Construct pSI_hUbC-DsRed2, derived from plasmid p144 by exchange of the Venus coding region against the DsRed2 coding region (the construct was generated by S.Ishibashi/ Amaya laboratory).

D1- D3 Different transgenic tadpoles generated by REMI with pSI-Ubc-DsRed2.

D1 Also with this construct, fluorescence is particularly strong in the musculature; the red fluorescent tail muscles are visible through the skin (arrow, NF>50).

D2 The cartilaginous rods of the branchial basket of a younger tadpole are clearly visible in red fluorescence.

D3 Red fluorescence is also observed in the muscles of the head (the position of the eyecup is indicated by the dashed line, NF> 50).

5.4.2.2.2 Germline transmission of the p144 transgene demonstrates maintained hUbC promoter activity in the F1 generation

The inactivation of transgenes during passage through the germline can jeopardize the establishment of stable transgenic lines. We wished to established whether the hUbC promoter was susceptible to such inactivation despite its non-viral origin. We therefore analyzed outcrosses between transgenic p144 founder (hUbC-Venus) and wildtype *X. laevis* (Figure 5.7): Transgenic p144 off-spring of the F1 generation still showed bright green overall fluorescence (A- C), in particular in the musculature (masticatory muscles in A). Overall levels of fluorescence were sufficient to allow the detection of single muscle fibres, even in the particularly delicate eye muscles (B). Bone still clearly fluoresced green, as shown here for the lower jaw with ossifying dentary bones (C, arrows). Compared to the founder generation, the general fluorescence is lower; this is consistent with a potential loss of transgenic alleles during the outcrossing. Fluorescence on cryosections of tadpoles of the F1 generation was hardly detectable directly (not shown) but immunohistochemistry against GFP (Venus and EYFP are both GFP derivatives and detectable with an anti-GFP antibody) confirmed the widespread expression of Venus (Figure 5.7 D- G). The analysis of a cross-section through the tail of a transgenic p144 *X. laevis* tadpole of the F1 generation demonstrates the maintained activity of the human Ubiquitin C promoter in the central nervous system (neurons of the spinal cord, E), cartilage (part of the vertebral column, F) and muscle (G). Similar to the observation already made in the founder generation, the expression levels in cartilage are lower than in other tissues (B3) and extremely weak in hypertrophic cartilage (F, arrow). These results demonstrate that a transgene containing the human Ubiquitin C promoter can pass the germline in *Xenopus laevis* without a major impairment of its activity.

Based on the results obtained in *Xenopus laevis*, the hUbC promoter was considered a suitable promoter for a Cre-reporter for genetic labelling studies in the head and neck region as

- it shows clear activity in mesenchymal (and also neuronal) derivatives and
- germline passage does apparently not attenuate its activity.

Figure 5.7

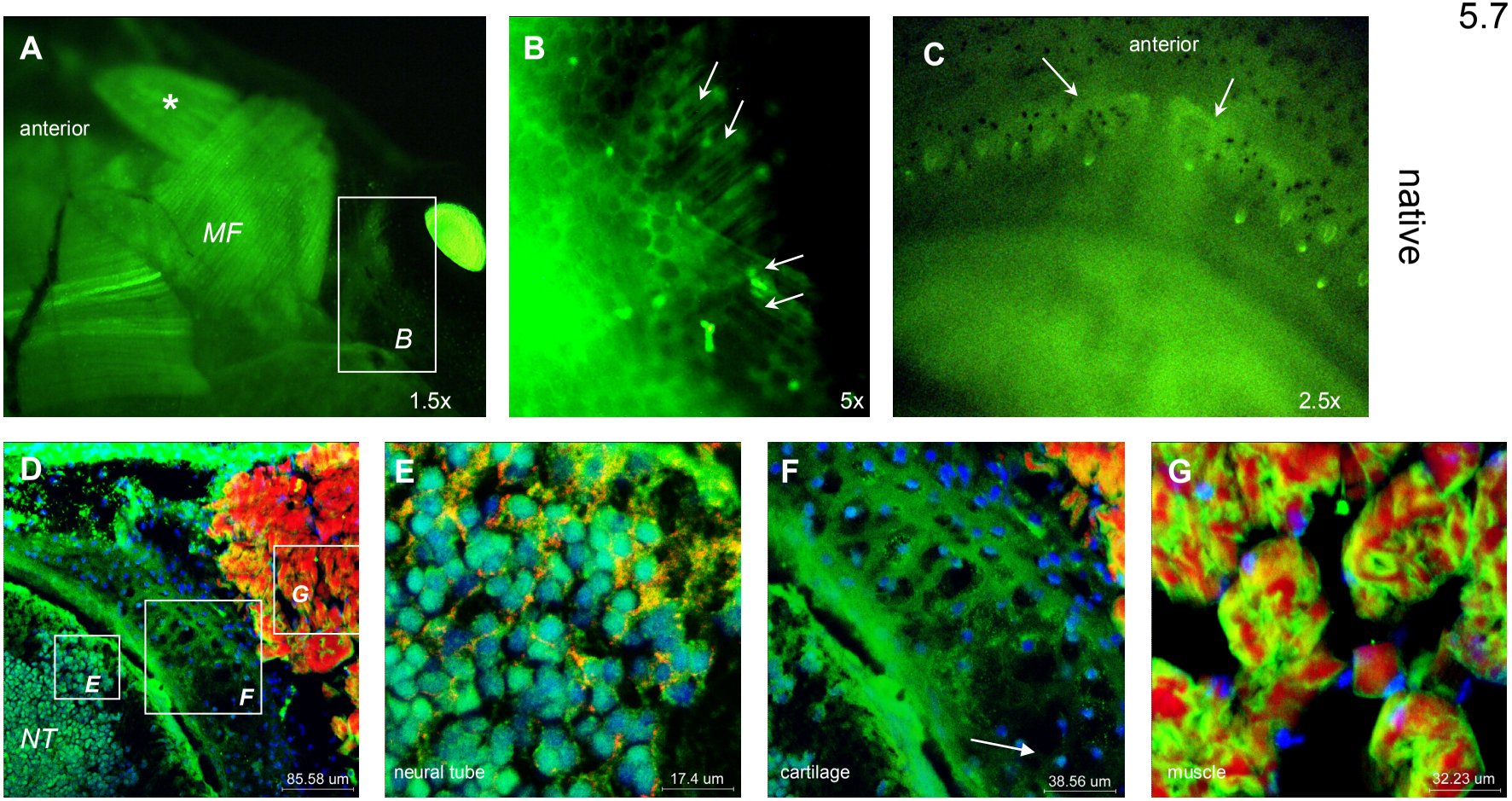

IHC: GFP F-actin DAPI

Figure 5.7 The human Ubiquitin C promoter maintains its activity after passage through the germline

Analysis of transgenic (p144, hUbC-Venus) *X.laevis* of the F1 generation older than stage 50. The transgenic founder had been established by the REMI technique with plasmid p144 and was crossed with wildtype animals for the analysis of the F1 generation. Whole mount views of tadpoles (**A- C**) and confocal images after IHC* for GFP (green) on transverse sections of the tail region, counterstained with Phalloidin633 (F-actin, red) and DAPI (blue) (**D- G**). The anti-GFP (abcam) antibody also recognizes Venus as GFP- derivative.

A- C Whole mount native specimen
A Tadpoles of the F1 generation transgenic for p144 show strong ubiquitous green fluorescence that is directly visible under a fluorescence dissecting microscope; in particular the musculature fluoresces strongle. Here shown are the mouth floor (MF) and the jaw muscles (asterisk).
B Green fluorescence is sufficently strong to allow to distinguish single muscle fibres of the delicate eye muscles, here in a skinned specimen.
C The view of the anterior mouth floor of a different transgenic p144 *X.laevis* F1 tadpole. The positive dentary bones (arrows) are visible through the skin of this specimen.

D- G Immunohistochemistry for Venus/ GFP
D Overview of the section through the tail region of a trangenic p144 *X.laevis* F1 tadpole showing the neural tube (NT), the adjacent vertebra and surrounding muscles. Frames indicate the placement of the details shown in **E**- **G**.
E Neuronal cells in the neural tube stain positive for GFP; this shows activity of the hUbC promoter in the central nervous system.
F Cartilage also stains positive for GFP, with a very weak signal in hypertrophic cartilage (arrow).
G As expected from the whole mount view, muscles (visualized by the Phalloidin staining) stain strongly positive for GFP.

* IHC was performed according to standardized conditions; a detailed description of conditions and antibodies (primary and secondary) can be found in the relevant section under ‘Materials and Methods’ (Chapter 7.5.4).

The design and the generation of double fluorescent Cre-reporter constructs under the control of the human Ubiquitin C promoter for the generation of stable transgenic *Xenopus tropicalis* lines and the generation of such a Cre-reporter line by I-*Sce*I mediated transgenesis are described in the following sections.

5.4.2.3 Double fluorescent Cre-reporter constructs

5.4.2.3.1 Double fluorescent Cre-reporter constructs under control of the hUbC promoter

After the human Ubiquitin C promoter had been identified by REMI transgenesis in *Xenopus laevis* as a suitable promoter for a potential *Xenopus* Cre-reporter, several double fluorescent Cre-reporter constructs were generated on the basis of plasmid p144 (hUbC-Venus, Figure 5.8 and Materials and Methods Chapter 7.2.2.2 for technical details). REMI transgenesis in *Xenopus tropicalis* (plasmid pBR139) proved technically extremely difficult, so the decision was taken to abandon REMI in favour of I-*Sce*I mediated transgenesis, a technique newly established in *Xenopus tropicalis*[144]. Several I-*Sce*I double fluorescent Cre-reporter constructs were therefore created on the basis of plasmid pBR119; we only introduced a single I-*Sce*I recognition site as recommended by our collaborator (S. Ishibashi, Amaya group; plasmids pBR120, pBR135, pBR139).

5.4.2.3.2 Potential enhancement of the activity of the Cre-reporter

In the experiments conducted to test the suitability of the human Ubiquitin C (hUbC) promoter by transgenesis in *X. laevis* it was noted that its activity was inhomogeneous across tissues and that RFP fluoresced considerably less brightly than Venus. These two issues were addressed in the construction of the double fluorescent Cre-reporters by

- the creation of a novel fusion protein between a CMV-immediate early element shown to enhancer promoter function without provoking an anti-viral response from the organism[213] (plasmid pBR120, Figure 5.8 B) and

Figure 5.8

Double fluorescent Cre-reporter constructs

A

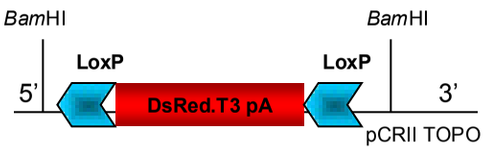

pBR118 LoxP-DsRed.T3 pA-LoxP

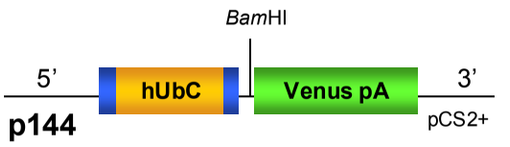

p144

pBR119

hUbC- LoxP-DsRed.T3 pA- LoxP- Venus pA

B

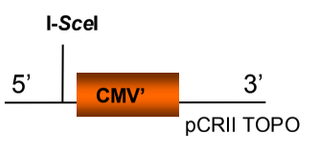

pBR108 I-*Sce*I- CMV IE (CMV')

pBR120

I-*Sce*I- CMV'-hUbC- LoxP-DsRed.T3 pA- LoxP- Venus pA

C

Removal of the CMV' element

pBR135

I-*Sce*I- hUbC- LoxP-DsRed.T3 pA- LoxP- Venus pA

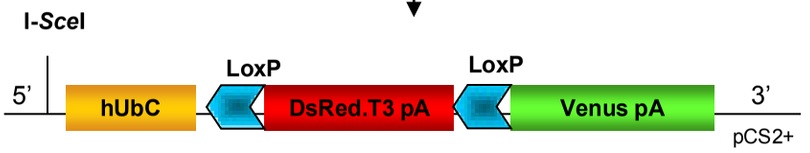

D

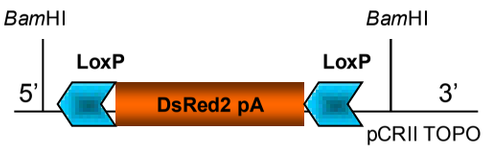

pBR136 LoxP-DsRed2 pA-LoxP

Exchange of the RFP colour cassette

pBR139

I-*Sce*I- hUbC- LoxP-DsRed2 pA- LoxP- Venus pA

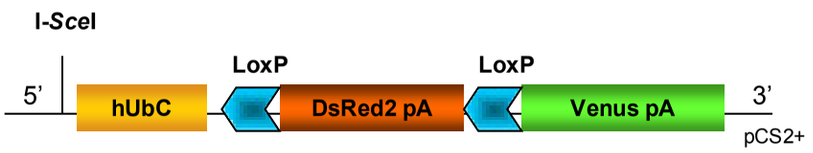

Figure 5.8 Overview of Double Fluorescent Cre-reporter constructs for Xenopus tropicalis transgenesis

A The first Cre-reporter plasmid pBR119 for REMI in *Xenopus tropicalis* was generated by the insertion of a cassette encoding a floxed bright RFP variant, DsRed.T3, followed by an SV40 polyadenylation signal, excised from plasmid pBR118 via *Bam*HI.

B- **D** I-*Sce*I mediated transgenesis made an adaptation of the construct necessary, at the same time different possibilities were explored to potentially enhance the signal strength of the Cre-reporter.

B With the introduction of a 5' I-*Sce*I recognition site into pBR119, a CMV-immediate early element shown to enhance promoter function without inducing an anti-viral response (Yew et al. 2001) was fused to the hUbC promoter to potentially enhance Cre-reporter activity, resulting in construct pBR120.

C Removal of the CMV element from pBR120 by *Pme*I digest and subsequent re-ligation resulted in construct pBR135. Plasmid pBR119 (**A**) and pBR135 are identical except for the 5' I-*Sce*I site.

D As the RFP variant DsRed.T3 had not been tested in Xenopus before, an additional construct with DsRed2 was created by replacing of the coding region of DsRed.T3 by the one of DsRed2, yielding construct pBR139

Intermediate steps and details of the cloning process are described in detail under Materials and Methods (Chapter 7.3.2).

- the usage of a new RFP mutant, DsRed.T3, that shows higher levels of fluorescence, increased stability as well as a shorter maturation time of the fluorescent protein than DsRed2[17] (plasmids pBR119, pBR120, pBR135, Figure 5.8 A, C, D).

In decreasing order, the predicted signal strength from the Cre-reporter was: CMV'-hUbC-fusion promoter in combination with DsRed.T3 (plasmid pBR120), hUbC-DsRed.T3 (pBR135) and hUbC-DsRed2 (pBR139). Although not allowing for absolute quantification, transient transfections in cultured mesenchymal cells confirmed the relative order of Cre-reporter activity (Figure 5.9, C2C12 cells were transfected with identical amounts of DNA and imaged under the same conditions). The fusion of the CMV immediate early element (CMV') to the hUbC promoter resulted in increased expression levels of the fluorescent protein with a higher number of cells above the detection threshold (A' compared to B' and C' and D' compared to E' and F'). As expected, DsRed.T3 is brighter than DsRed2 when driven by the same hUbC promoter (B' and C'). So both the CMV'-hUbC fusion promoter and DsRed.T3 as brighter alternative to DsRed2 are able to increase the signal from the Cre-reporter.

5.4.2.3.3 The double fluorescent Cre-reporters switch colour in response to the activity of Cre

The ability of the double fluorescent Cre-reporters to indicated Cre-activity was tested by transient transfections of the reporter alone or in combination with a Cre-driving plasmid in a mesenchymal cell lineage, C2C12 cells (Figure 5.10 and 5.11). Cre-reporter constructs pBR120, pBR135 (identical to pBR119, except for the 5' I-*Sce*I site) and pBR139 transfected alone demonstrate the default state of the double fluorescent Cre-reporter which is red fluorescence (Figure 5.10). An additional very low emission peak in the green spectrum is explicable by the intermediate green maturation product of red fluorescent proteins[206] (third column, A and B).
When co-transfected with a Cre-driving plasmid (EF1-CREM), the expression from the double fluorescent Cre-reporter construct changes from red to green fluorescence (Figure 5.11). Due to the relative stability of the RFP protein, this colour change occurs gradually. Scanning with very high voltage therefore allows the detection of residual red fluorescence (Figure 5.11 A).

Figure 5.9- 5.11

5.9

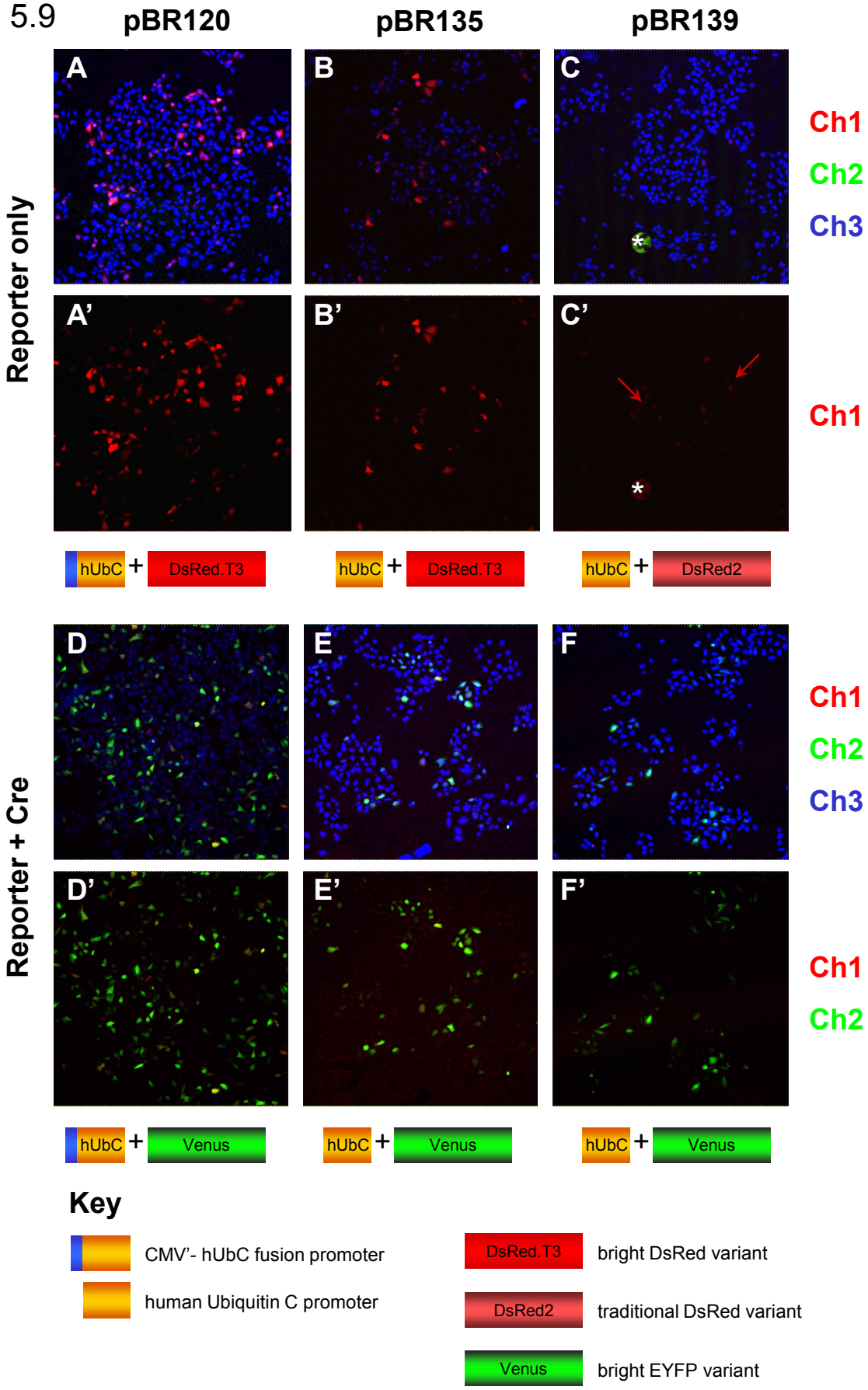
pBR120
pBR135
pBR139
Reporter only
Reporter + Cre
A
B
C
A'
B'
C'
D
E
F
D'
E'
F'
Ch1
Ch2
Ch3
hUbC + DsRed.T3
hUbC + DsRed.T3
hUbC + DsRed2
hUbC + Venus
hUbC + Venus
hUbC + Venus
Key
CMV'- hUbC fusion promoter
human Ubiquitin C promoter
DsRed.T3
bright DsRed variant
DsRed2
traditional DsRed variant
Venus
bright EYFP variant

5.9

Figure 5.9 Estimation of Cre-reporter activity

Transient transfections in C2C12 cells were used to assess Cre-reporter activity and confirm the expected differences (pBR120, pBR135 and pBR139 in order of decreasing activity).

C2C12 cells transfected with the same amount of only a reporter construct pBR120, pBR135 and pBR139 (upper panel, **A**- **C**) or a reporter construct in addition to a Cre-driving plasmid (EF1-CREM, lower panel, **D**- **F**). To allow the comparison of signal strength, confocal images were acquired with identical settings for the red and green channel (Objective HCX PL FLUOTAR 5.0x0.15 COMBI, **PMT 725.7V, PMT 730.9V**).

A- F: overlay of all three channels, **A'-C'**: red channel, **D'-F'**: red plus green channel. The asterisk in **C** indicates an artefact.

The elements responsible for the activity from the Cre-reporter construct are depicted under the corresponding column.

A, D General activity seems strongest from pBR120, the Cre-reporter construct with the bright RFP variant DsRed.T3 under control of the CMV'-hUbC fusion promoter.

B, **C** As expected, under control of the same hUbC promoter DsRed.T3 (pBR135, **B**) appears brighter than DsRed2 (pBR139, **C**).

After Cre-mediated excision and recombination of the RFP encoding colour cassette, the expression levels from pBR120 (**D, D'**) are stronger than from pBR135 (**E, E'**) and pBR139 (**F, F'**), demonstrating the difference in promoter strength between the CMV'-hUbC fusion promoter and the hUbC promoter alone.

Cre-reporter in the default state

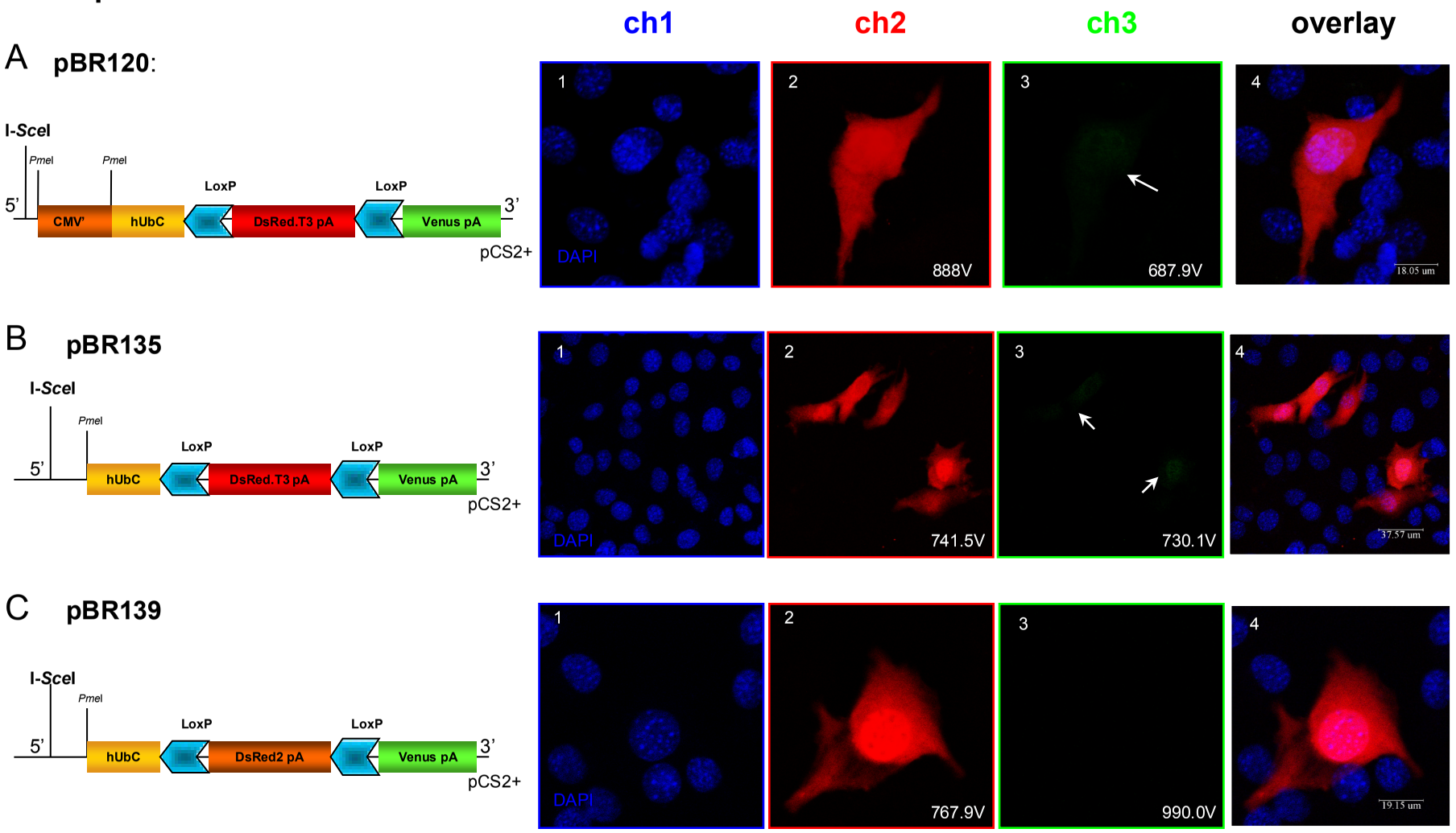

Figure 5.10 The default state of the double fluorescent Cre-reporter

Confocal images of C2C12 cells transfected with Cre-reporter constructs pBR120 (**A**), pBR135 (**B**) or pBR139 (**C**); nuclear counterstain is DAPI (blue). The channels for the detected fluorescence are labelled and colour-coded. The signals for the blue (1), red (2) and green (3) channel are given separately and in overlay (4). To appreciate the relative strength of red to green signal, the Photo Multiplier Tube (PMT) amplification required for the acquisition of the respective image is indicated in the frame (Unit: Volt). Scale bars read 18.05 µm (**A**) , 37.57 µm (**B**) and 19.15 µm (**C**).

The default state for our double fluorescent Cre-reporter in the absence of Cre-activity is red fluorescence. All three Cre-reporter constructs pBR120 (**A**), pBR135 (**B**) or pBR139 (**C**) show the expected red fluorescence (red channel 2). In addition, a week green signal is detected for the Cre-reporter constructs pBR120 and pBR135; these Cre-reporter constructs contain the stronger RFP variant, DsRed.T3 (third column **A** and **B** but not **C**, arrows), most likely due to the green fluorescent intermediate of red fluorescent proteins.

Cre-reporter after Cre-mediated excision and recombination

5.11

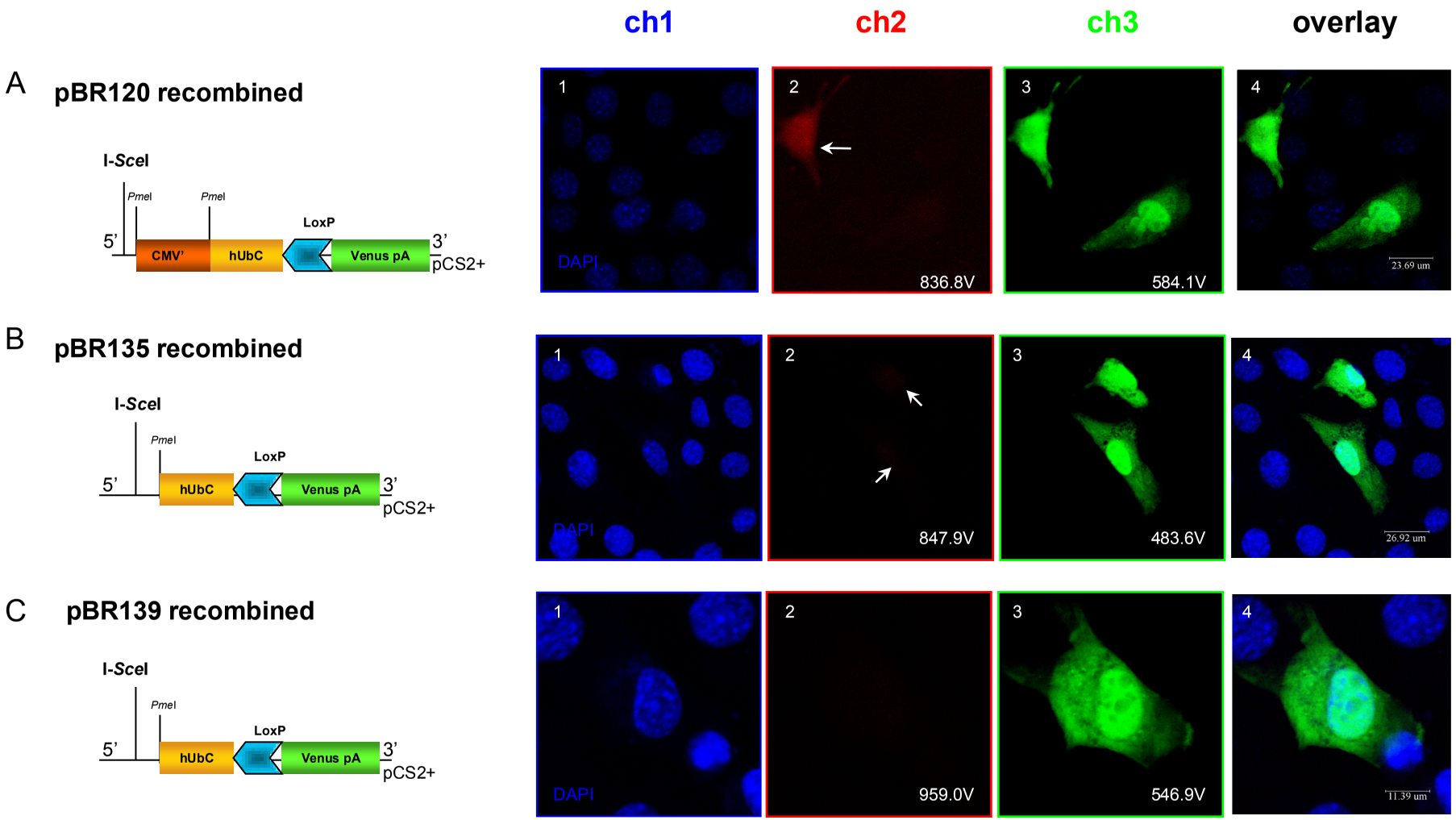

Figure 5.11 Cre-reporter after Cre-mediated recombination

Confocal images of C2C12 cells transfected with EF1-CREM, a Cre-driving construct, in addition to the Cre-reporter constructs pBR120 (**A**), pBR135 (**B**) or pBR139 (**C**); nuclear counterstain is DAPI (blue). The signals for the blue (1), red (2) and green (3) channel are given separately and in overlay (4). To appreciate the relative strength of red to green signal, the Photo Multiplier Tube (PMT) amplification required for the acquisition of the respective image is indicated in the frame (Unit: Volt). Scale bars read 23.69 µm (**A**) , 26.92 µm (**B**) and 11.39 µm (**C**).

After Cre-mediated excision of the RFP cassette and recombination of the construct, the expression from the Cre-reporter changes from red to green fluorescence (third and forth column). Due to relative stability of the RFP protein, the colour switch only occurs gradually; residual red fluorescence can be especially observed for the construct with the stronger CMV'-hUbC fusion promoter, pBR120 (**A** and **B**, second column, arrows).

Cell culture experiments confirm that all three double fluorescent Cre-reporters unambiguously respond to Cre-activity with a colour switch from red to green fluorescence and do not show ‘leaky’ expression that could potentially interfere with the correct interpretation of lineage labelling results.

5.4.2.3.4 I-*Sce*I Meganuclease correctly recognizes the designed I-*Sce*I sites of the double fluorescent Cre-reporter constructs pBR120, pBR135 and pBR139

I-*Sce*I mediated transgenesis relies on the not yet fully understood property of I-*Sce*I Meganuclease to facilitate genomic integration of a transgene[184]. I-*Sce*I Meganuclease-mediated restriction activity is thereby not a predictive factor for successful I-*Sce*I mediated transgenesis[143] but sufficient to prove recognition of the site by the enzyme. Thus, the functionality of the designed I-*Sce*I recognition site (TAGGGATAACAGGGTAAT) of the double fluorescent Cre-reporter constructs pBR120, pBR135 and pBR139 was tested by a restriction digest with I-*Sce*I Meganuclease (Figure 5.12). Cre-reporter plasmids were first linearized with *Xmn*I and subsequently incubated with I-*Sce*I Meganuclease. A plasmid provided by the supplier of the I-*Sce*I enzyme (NEB) served as positive control; as negative control, plasmids were incubated without I-*Sce*I enzyme. Only plasmids incubated with the enzyme showed release of a ~ 1kb fragment, thereby proving a fully functional I-*Sce*I recognition site.

Figure 5.12

I-*Sce*I double fluorescent Cre-reporter plasmids

A **pBR120**

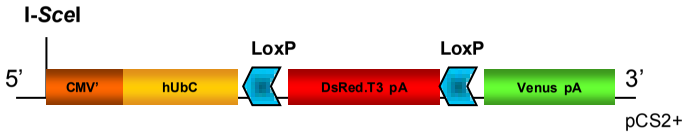

B **pBR135**

C **pBR139**

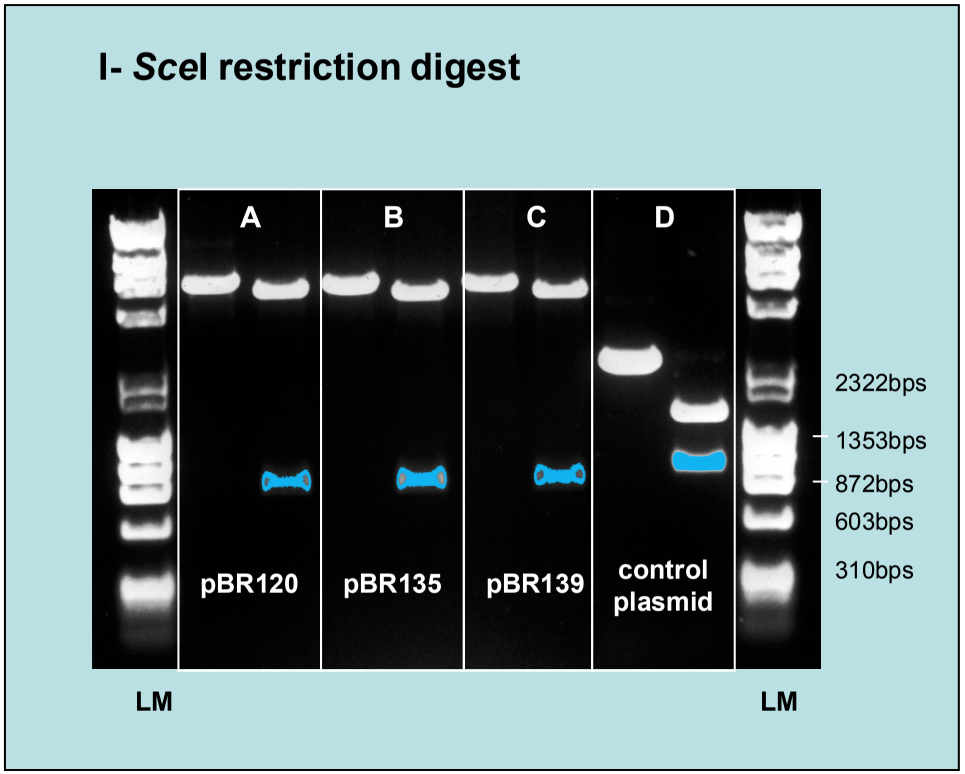

Figure 5.12 Designed I-*Sce*I recognition sites in the Cre-reporter constructs are correctly recognized by I-*Sce*I Meganuclease

The I-*Sce*I recognition site in all three I-*Sce*I Cre-reporter constructs was tested for functionality by a restriction digest with I-*Sce*I Meganuclease. Plasmids pBR120 (**A**), pBR135 (**B**), pBR139 (**C**) were first linearized with the restriction enzyme *Xmn*I over night to later allow the release of an unambigous fragment. Linearized plasmids and a control plasmid from the supplier (NEB) were then digested with I-*Sce*I Meganuclease for 40 min at 37ºC according to the incubation conditions specified for I-*Sce*I mediated transgenesis. As negative control, plasmids were incubated omitting the I-*Sce*I enzyme.

On the left of each lane, the reporter contruct after incubation without I-*Sce*I Meganuclease (negative control). On the right the same reporter construct after incubation in the presence of I-*Sce*I Meganuclease.

All Cre-reporter plasmids (A-C) as well as the supplier's control construct (**D**) show release of a fragment when incubated with I-*Sce*I Meganuclease but not when the enzyme is omitted, providen proof for the full functionality of the I-*Sce*I recognition sites of the Cre-reporter constructs.

LM: Ladder Marker

5.4.2.4 Summary

- The human Ubiquitin C promoter is functional in *Xenopus laevis* and shows wide-spread if not ubiquitous activity. Passage through the germline does not attenuate its activity.
- On the basis of the hUbC promoter, a set of double fluorescent Cre-reporter constructs was generated for I-*Sce*I mediated transgenesis in *Xenopus tropicalis*.
- To potentially enhance Cre-reporter activity, a novel CMV'-hUbC fusion promoter was created and found efficient in cell culture experiments. The exchange of DsRed2 against a new RFP variant, DsRed.T3, increased the detectable level of red fluorescence from the double fluorescent Cre-reporter in cell culture.
- The functionality of the I-*Sce*I recognition site and the correct response of the double fluorescent Cre-reporter constructs to Cre-activity in the form of a switch from red to green fluorescence were confirmed.

I-*Sce*I mediated transgenesis with the double fluorescent Cre-reporter plasmids pBR120, pBR135 and pBR139 and the establishment of a stable transgenic Cre-reporter line in *Xenopus tropicalis* will be described in the next section.

5.4.3 Results Part 2- The establishment of a stable transgenic Cre-reporter line in *Xenopus tropicalis* by I-*Sce*I mediated transgenesis

5.4.3.1 Testing of the Cre-reporter constructs by I-*Sce*I mediated transgenesis

I-*Sce*I mediated transgenesis was performed as described in detail in the Material and Methods section (Chapter 7.4.2.2). Transgenesis with plasmid pBR120, a Cre-reporter construct under the control of the CMV'-hUbC fusion promoter and containing the brighter RFP variant, DsRed.T3, resulted in bright red embryos that developed normally (Figure 5.13, B); this demonstrates that DsRed.T3 is functional and does not impair normal development in *Xenopus tropicalis*. In addition to a relatively uniform red fluorescence at an early stage(B1), we always found bright 'freckles' (arrows B1-3) which Ogino et al.[144] suspect to be caused by un-integrated plasmid. During the development of the embryo, red fluorescence became generally patchy and uneven (B2, 3); the most common phenotype was expression in parts of the tail musculature (B3). The CMV promoter was reported to produce the same type of very strong but patchy expression in *Xenopus* (H.Ogino, personal observation), so we concluded that the patchy expression in our experiments was in all likelihood caused by the CMV' part of the fusion promoter. This conclusion was partially supported by the results from I-*Sce*I mediated transgenesis with Cre-reporter plasmid pBR135 (Figure 5.14). Construct pBR135 differs from the Cre-reporter pBR120 described above in that it only contains the original human Ubiquitin C promoter instead of the CMV'-hUbC fusion promoter (Figure 5.14 A). The red fluorescence in embryos generated with plasmid pBR135 was generally more even than with plasmid pBR120. Areas of brighter expression remained however (B2 and B4), indicating that the CMV'-element was not solely responsible for this phenomenon. Transgenesis with pBR139, a Cre-reporter plasmid that contains the dimmer but established RFP variant, DsRed2 (instead of the DsRed.T3 in pBR120 and pBR135, Figure 5.15), produced embryos with dim but even red fluorescence.

Figure 5.13- 5.15

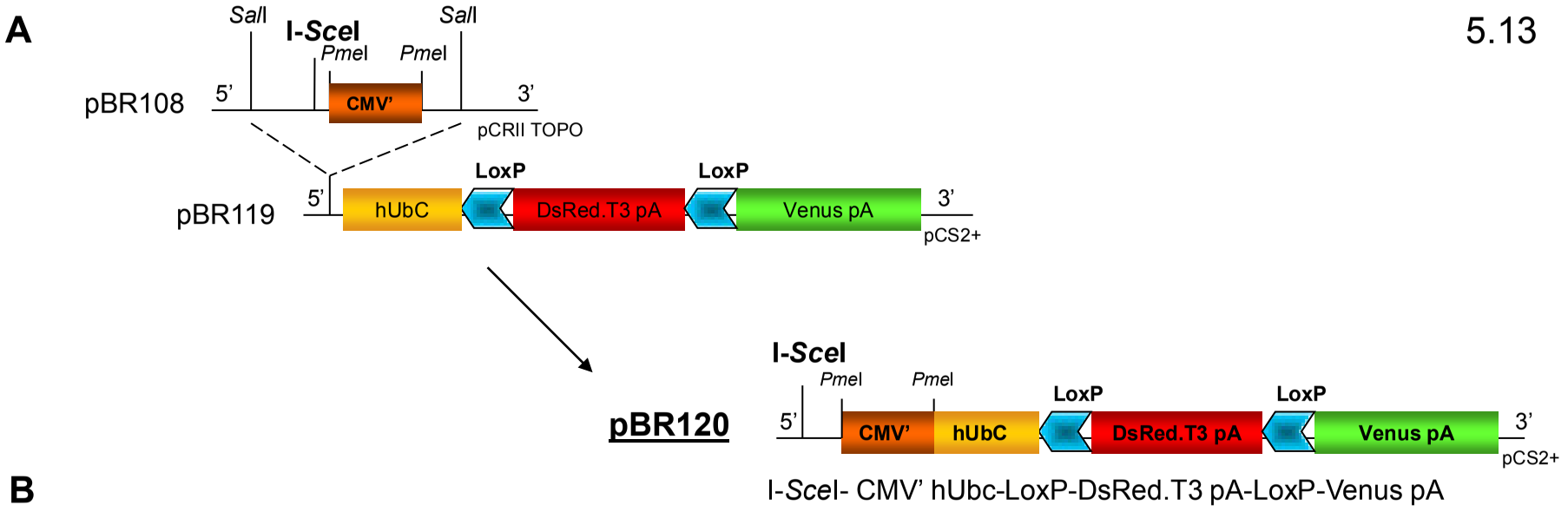
A
SalI
I-SceI
SalI
PmeI
PmeI
pBR108
5'
CMV'
3'
pCRII TOPO
LoxP
LoxP
pBR119
5'
hUbC
DsRed.T3 pA
Venus pA
3'
pCS2+
pBR120
I-SceI
PmeI
PmeI
LoxP
LoxP
5'
CMV'
hUbC
DsRed.T3 pA
Venus pA
3'
pCS2+
I-SceI- CMV' hUbc-LoxP-DsRed.T3 pA-LoxP-Venus pA
B
pBR120
B1
5x
d1
B2
3x
d5
B3
2.5x
d5
B4
2.5x
d5

Figure 5.13 An I-*Sce*I double fluorescent Cre-reporter under control of the CMV'- hUbC fusion promoter (pBR120)

A schematic representation of the generation of the double fluorescent Cre-reporter construct pBR120 (**A**) and its use in I-*Sce*I mediated transgenesis in *X.tropicalis* (**B1**- **4**).

A Generation of construct pBR120: the CMV' part for the CMV'-hUbC fusion promoter with upstream I-*Sce*I site is released from pBR108 by *Sal*I digest and inserted into the unique *Sal*I site of pBR119, creating an I-*Sce*I double fluorescent Cre-reporter under control of a CMV'-hUbC fusion promoter (pBR120).

B1- 4 *X.tropicalis* embryos after I-*Sce*I mediated transgenesis for construct pBR120. Positive embryos show strong red fluorescence, 'freckles' of extremely brightly fluorescing cells (arrowheads) are seen in addition to a more uniform red fluorescence.

B1 A transgenic *X.tropicalis* embryo one day after injection with construct pBR120. Red fluorescence is next to uniform although single strongly expressing cells are present (arrowheads).

B2 A partially transgenic *X.tropicalis* tadpole five days after injection with the same construct. The absence of red fluorescence on one side of the head indicates that the integration of the transgene occurred later than at the 1-cell stage.

B3 The most frequently observed phenotype, here in other transgenic *X.tropicalis* embryos from the same batch as **B2** (five days after injection). Red fluorescence tends to be patchy and is most commonly found in muscles of the tail.

B4 The brightfield view of phenotypically normal tadpoles transgenic embryos shown in **B3** indicates that the transgene itself does apparently not interfere with normal development.

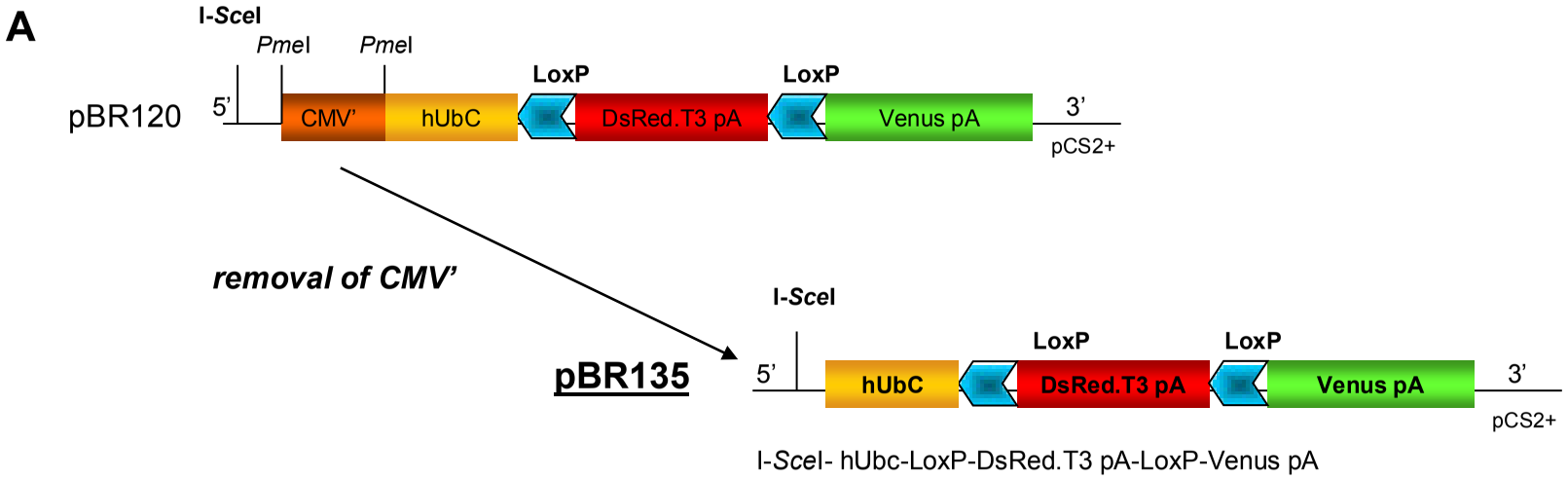
A
I-SceI
PmeI
PmeI
pBR120
5'
CMV'
hUbC
LoxP
DsRed.T3 pA
LoxP
Venus pA
3'
pCS2+
removal of CMV'
pBR135
I-SceI
LoxP
LoxP
5'
hUbC
DsRed.T3 pA
Venus pA
3'
pCS2+
I-SceI- hUbc-LoxP-DsRed.T3 pA-LoxP-Venus pA

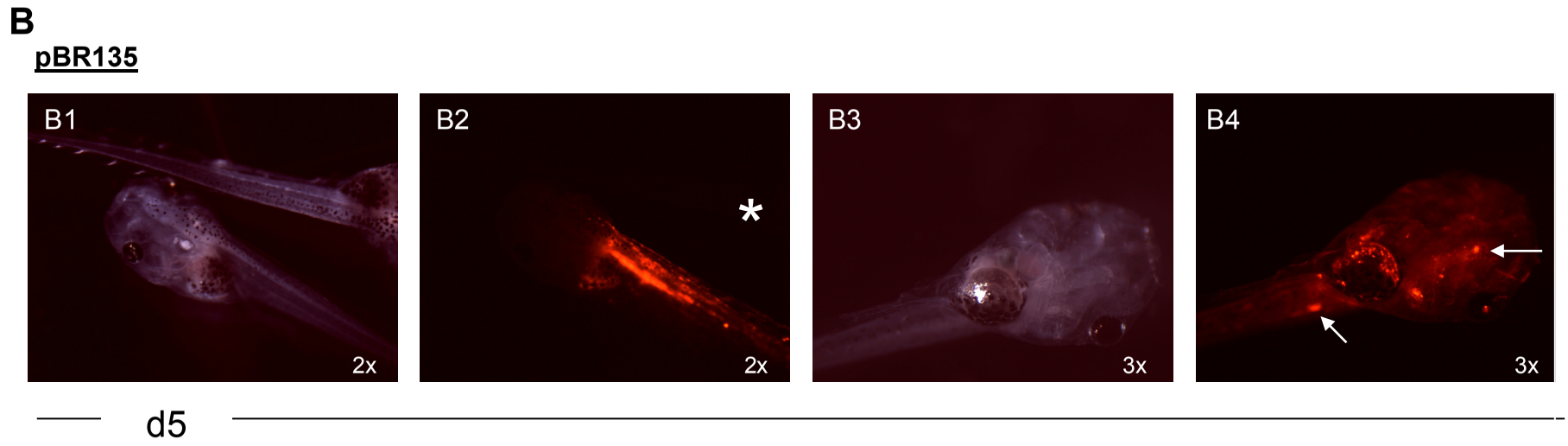
B
pBR135
B1
2x
B2
*
2x
B3
3x
B4
3x
d5

Figure 5.14 The removal of the CMV' element leads to weaker but more homogenous red fluorescence (pBR135)

A schematic representation of the generation of the double fluorescent Cre-reporter construct pBR135 (**A**) and its use in I-*Sce*I mediated transgenesis in *X.tropicalis* (**B1**- **4**).

A Generation of construct pBR135: the CMV' element from construct pBR120 is removed by *Pme*I digest, followed by a re-ligation of the backbone, leaving behind a 5' I-*Sce*I recognition site.

B *X.tropicalis* embryos 5 days after I-*Sce*I mediated transgenesis for pBR135. **B1**, **B3** bright field images of transgenic tadpoles; **B2**, **B4** show the corresponding red fluorescence.

B1, B2 Partially transgenic *X.tropicalis* showing bright red fluorescence in the tail. As a control, an injected but not fluorescent tadpole is shown (asterisk in **B2**).

B3, **B4** Occasionally, tadpoles showed the desired red fluorescence. In comparison with construct pBR120, 'freckles' were reduced but still present (**B4**, arrows).

A **pBR135**

I-*Sce*I- hUbc-LoxP-DsRed.T3 pA-LoxP-Venus pA

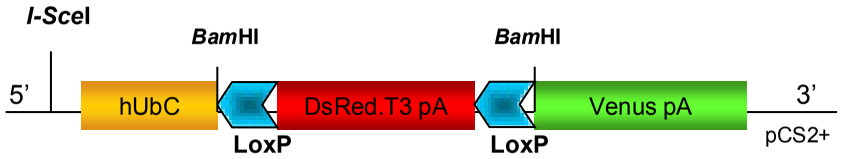

pBR136 LoxP-DsRed2 pA-LoxP

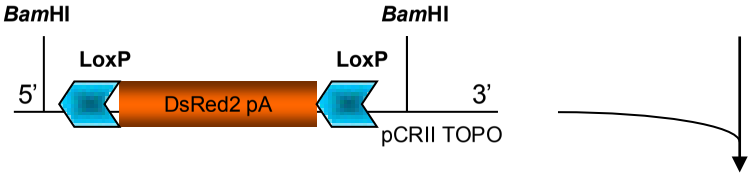

pBR139

I-*Sce*I- hUbC-LoxP-DsRed2 pA-LoxP-Venus pA

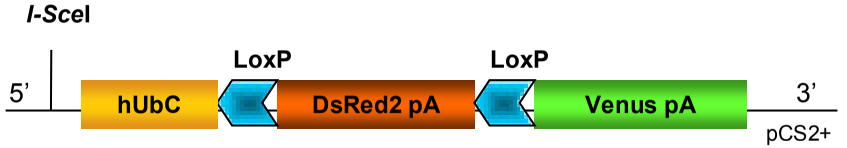

B

pBR139

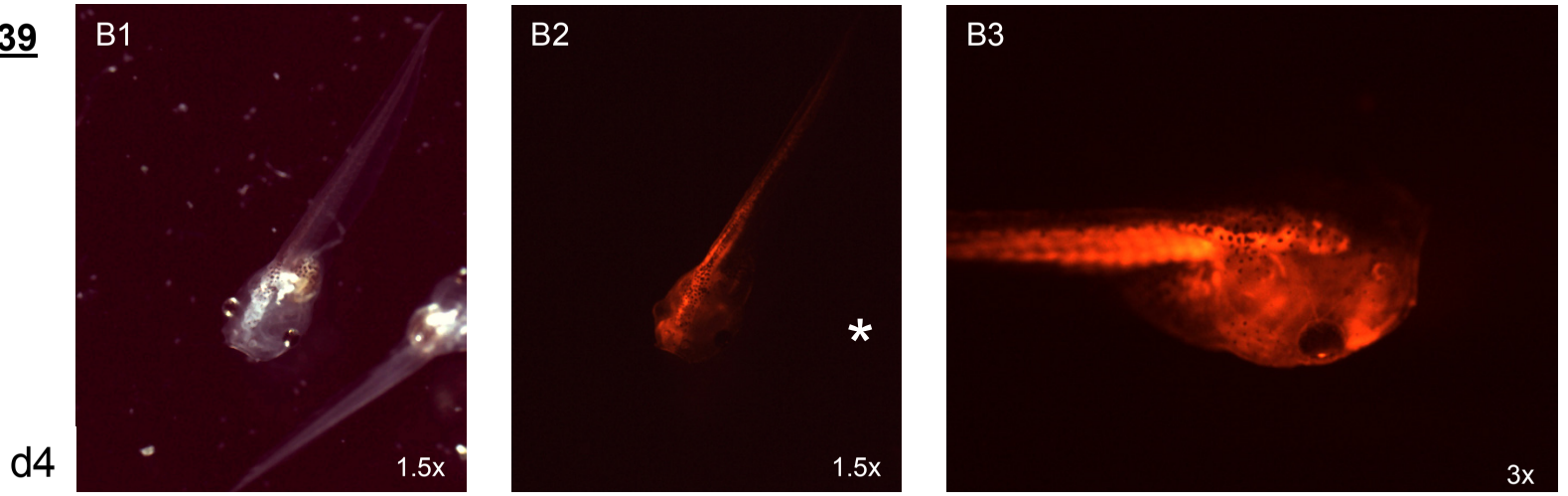

Figure 5.15 DsRed2 expression from the I-*Sce*I double fluorescent Cre-reporter is weak but homogenous (pBR139)

A schematic representation of the generation of the double fluorescent Cre-reporter construct pBR139 (**A**) and its use in I-*Sce*I mediated transgenesis in *X.tropicalis* (**B1**- **3**).

A Generation of construct pBR139: the floxed DsRed.T3 cassette from construct pBR135 is exchanged by *Bam*HI digest against an equivalent cassette containing the in transgenesis widely used DsRed2 from pBR136 (also via *Bam*HI sites).

B *X.tropicalis* embryos after *I-Sce*I mediated transgenesis with construct pBR139 at 4 days after injection. The magnification under which the image was taken is indicated in the right lower corner.

B1, **B2** Bright field and red fluorescence of two tadpoles injected with construct pBR139. One of the tadpoles shows expression in the right body half. The position of the negative tadpole in **B2** is marked by an asterisk.

B3 Higher magnification of the positive embryo shown in B2. The embryo is only half transgenic, the red fluorescence is restricted to the right body half. The overall level of fluorescence is lower than with the previous constructs but appears very even and without extremely bright 'freckles'.

Figure 5.16 shows a comparative overview of the different double fluorescent Cre-reporter constructs that were tested in *Xenopus tropicalis*. As expression from Cre-reporter construct pBR120 was not truly ubiquitous, we decided to focus our efforts on Cre-reporter constructs pBR135 and pBR139. The establishment of a stable transgenic *Xenopus tropicalis* line for one of the constructs, pBR135, is described in the following section.

Figure 5.16

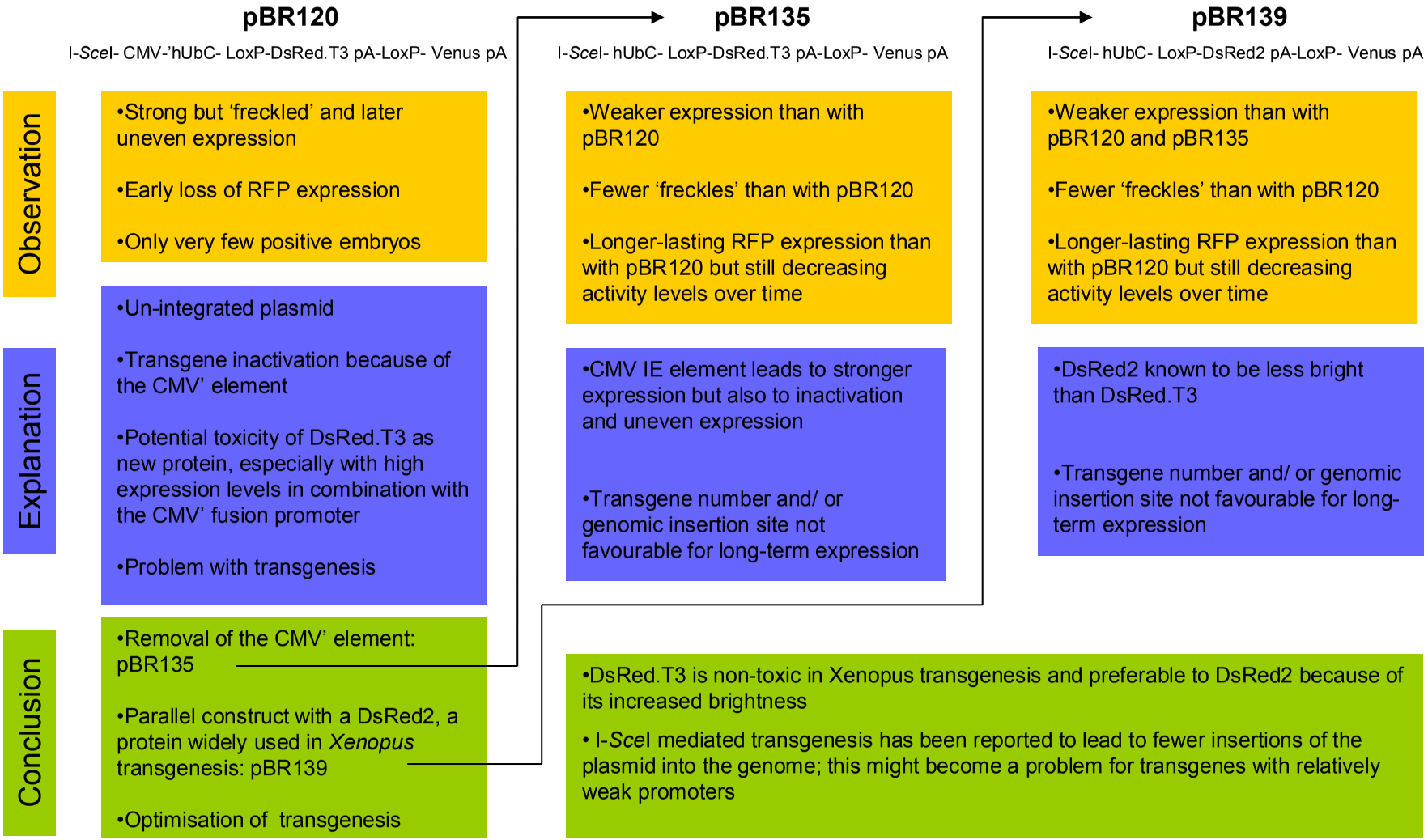

Figure 5.16 I-*Sce*I Cre-reporter constructs in comparison

5.16

5.4.3.2 A stable transgenic *X. tropicalis* Cre-reporter line

A single founder shows germline transmission of the transgene pBR135

After I-*Sce*I mediated transgenesis with constructs pBR135 and pBR139, embryos were screened around stage 20 and positive embryos raised. The screenings were repeated over the following weeks to select for embryos with sustained brightness. Red fluorescence persisted over the course of weeks but eventually decreased and only 13 animals previously identified as fluorescing red could be raised to adulthood, eventually reaching sexual maturity after around eight months. As PCR on DNA from skin swabs had failed and the aim was to establish a stable transgenic Cre-reporter line, germ line transmission of the transgene of these potential founders animals was tested by outcrosses with wild-type *Xenopus tropicalis* . Off- spring of the F1 generation was screened for red fluorescence under a fluorescence dissecting microscope at day 1, 2, 3 and 1 week after fertilisation. One male transgenic animal for construct pBR135 (experiment 9 in Figure 5.17) could be identified as transgenic founder with germline transmission of the transgene. From every outcross, pooled genomic DNA was prepared from at least 200 embryos. PCR using transgene-specific primers confirmed that the male founder No 9 was the only founder with transgenic off-spring (Figure 5.18). The off- spring from founder No 9 showed variable levels of red fluorescence; embryos were classified as ‘bright’, ‘very bright’ or ‘non-fluorescent’ (Figure 5.19) and 67% of all embryos fluoresced brightly (24%) or very brightly (43%). The percentage of malformed embryos was considerably higher in the group of very bright embryos (46%) compared to the bright (23%) or non-fluorescent group (20%). Taking into consideration a higher mortality rate among the malformed embryos, the overall result is consistent with two independent transgene integration events into the genome (theoretically, the Mendelian ratio in the case of two independently inherited alleles would predict 75% positive embryos).

Figure 5.17- 5.19

No	Transgene	Sex	Red fluorescence in F1	Transgene detected by PCR in F1
1	pBR139	F	negative	negative
2	pBR139	F	negative	negative
3	pBR135	M	negative	negative
4	pBR135	M	negative	negative
5	pBR135	M	negative	negative
6	pBR135	M	negative	negative
7	pBR135/ no enzyme	M	negative	negative
8	pBR139	M	negative	negative
9	**pBR135**	**M**	**POSITIVE**	**POSITIVE**
10	pBR139	M	negative	negative
11	pBR135	M	negative	negative
12	pBR135/ no enzyme	M	negative	negative
13	pBR139	F	negative	negative

pBR135

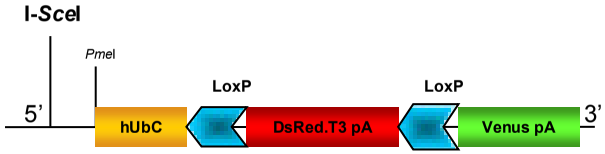

pBR139

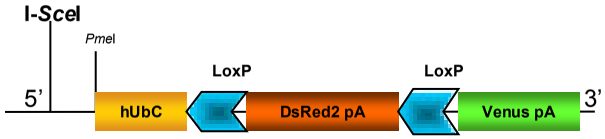

Key

pBR135 I-*Sce*I- hUbC-DsRed.T3 pA-Venus pA

pBR139 I-*Sce*I- hUbC-DsRed2 pA-Venus pA

Figure 5.17 Germline transmission of constructs pBR135 and pBR139

Potentially transgenic *X.tropicalis* founder animals generated by I-*Sce*I mediated transgenesis with the Cre-reporter constructs pBR135 (I-*Sce*I- hUbC-DsRed.T3 pA-Venus pA) and pBR139 (I-*Sce*I- hUbC-DsRed2 pA-Venus pA) were crossed with wildtype animals. The number of the experiment, the transgene and the sex of the founder are indicated. Off-spring of the F1 generation was screened for red fluorescing embryos under a fluorescence dissecting microscope.

In total, 13 potentially transgenic founder animals were analysed. One male injected with construct pBR135 (experiment number 9) produced bright red fluorescent offspring, corresponding to a positive result in the genotyping reaction by PCR (also Figure 5.18). Embryos from all other outcrosses showed no fluorescence, consistent with negative PCR results.

Key: shading reflects the different RFP variants, with DsRed.T3 being brighter than DsRed2

A

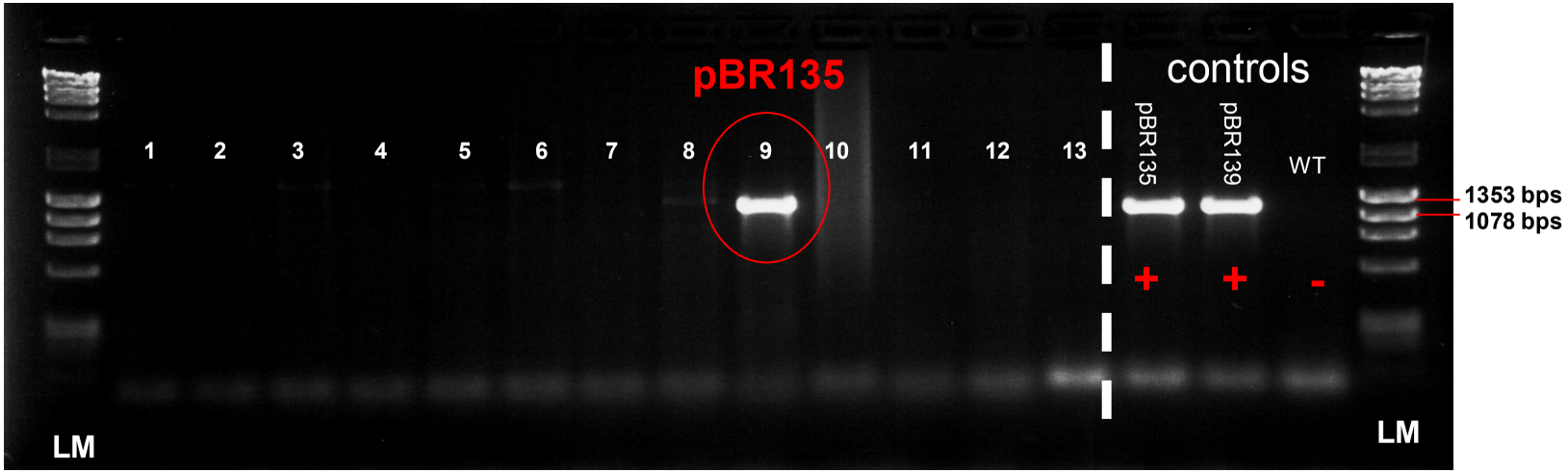

B

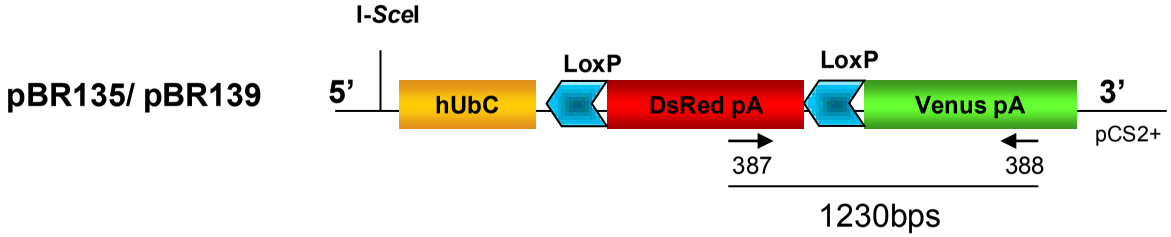

C

PrimBR387 **5'** TTGAATTCTTACTTGTACAGCTCGTCCATG **3'**

PrimBR388 **5'** AGTTCAAGTCCATCTACATGGCCGAAGC **3'**

Figure 5.18 PCR for the transgene in F1 off-spring from potential founder *X.tropicalis*

Result of the PCR reaction to determine the presence of the transgenes pBR135 (I-*Sce*I- hUbC-DsRed.T3 pA-Venus pA) and pBR139 (I-*Sce*I- hUbC-DsRed2 pA-Venus pA) with transgene-specific primers (PrimBR387, 388). Pooled genomic DNA prepared from at least 200 embryos per outcross between a potential transgenic founder and a wildtype *X.tropicalis* was used as template.

A The presence of the transgene could be confirmed by PCR in the off-spring of founder 9 (pBR135, red circle, also see Figure 5.17) but not in off-spring of any other potential founder.

B The amplified fragment of 1230bps encompasses parts of the RFP and GFP coding cassettes and is specific to the double fluorescent Cre-reporter. As DsRed.T3 and DsRed2 only differ in single point mutations, the Primer PrimBR387 aligns with both.

C Primer sequences of PrimBR387 and PrimBR388.

Controls: Positive controls: 0.2 ng pBR135 and 0.2 ng pBR139. Negative control: 500 ng unrelated wildtype *X.tropicalis* genomic DNA.

LM: Ladder marker as described in ‘Materials and Methods’ (Chapter 7.1.3).

pBR135, F1

Screened as	bright	very bright	non-fluorescent
scored	**22/91**	**39/91**	30/91
in %	**24%**	**43%**	33%
out of these were abnormal	5/22	18/39	6/30
in %	23%	**46%**	20%

Fig 5.19 Outcross of the male founder transgenic for pBR135 (founder 9): Screening results in numbers Outcross of the male founder transgenic for pBR135 (founder 9): Screening results in numbers

Embryos were screened at d1 (Nieuwkoop and Faber: early tailbud stages) under a fluorescence dissecting microscope and categorized as bright, very bright or non-fluorescent. 67 % of the embryos ((22+ 39)/91, red boxes) were scored as positive. This result would be consistent with expression from two independent transgene integration sites.

Very bright embryos have a considerably higher proportion of malformed embryos (46%) in comparison to bright (23%) and wild-type embryos (20%).

A time course for pBR135 Cre-reporter activity

In order to establish spatio-temporal Cre-reporter activity in this stable transgenic *Xenopus tropicalis* line, red fluorescence was assessed in the F1 off-spring of transgenic pBR135 founder No 9 between fertilisation and beyond stage 50. Embryos fluoresce uniformly red as early as stage NF20 (Figure 5.20 A shows a stage 23 embryo). Fluorescence then increases and tadpoles are brightest from stage 30- 39 (Figure 5.20 B). After stage 40, the overall level of fluorescence begins to decrease, while staying pronounced in the musculature and the central nervous system (arrows E' and F'). Positive tadpoles can be easily identified till the late 40's stages (D- F, asterisks marking negative siblings for comparison). Past stage 50, tadpoles previously screened as 'very bright' or 'bright' can no longer be unambiguously identified under the fluorescence dissecting microscope (presence of the transgene can be however confirmed by PCR, Figure 5.21 A). On cryosections of the same specimen, residual red fluorescence is found in bone and muscle (red, Figure 5.21 B) and confirmed by immunohistochemistry for RFP (green: anti- RFP, abcam). Under high magnification, very low residual RFP expression is even detectable in cartilage (B').

Interbreeding increases overall brightness allowing confocal imaging with single cell resolution but does not prolong Cre-reporter activity

Since the expression levels from the Cre-reporter decreased with development and a homozygous Cre-reporter line would be beneficial in the future as all off-spring carries the transgene, we interbred transgenic F1 pBR135 animals with the aim to potentially enhance and prolong Cre-reporter expression and to test whether homozygosity for the Cre-reporter was compatible with normal development. Transgenic off-spring of the F2 generation is viable and displays various degrees of red fluorescence, in accordance with the increasing number of possibilities for hetero- and homozygosity for transgenic alleles (Figure 5.22). Despite the fact that interbreeding apparently increases the expression levels of the Cre-reporter, it does not prolong it as F2 pBR135 tadpoles past stage 50 no longer fluoresce red as already observed in the F1 generation (Figure 5.23). Until the early 40's stages, red fluorescence in pBR135 F2 tadpoles was sufficiently strong to allow confocal imaging in single cell resolution of the entire head of the tadpole (Figure 5.24). The time-window in which Cre-reporter activity is directly detectable covers the development of the major structures of the cartilaginous

Figure 5.20- 5.24

5.20

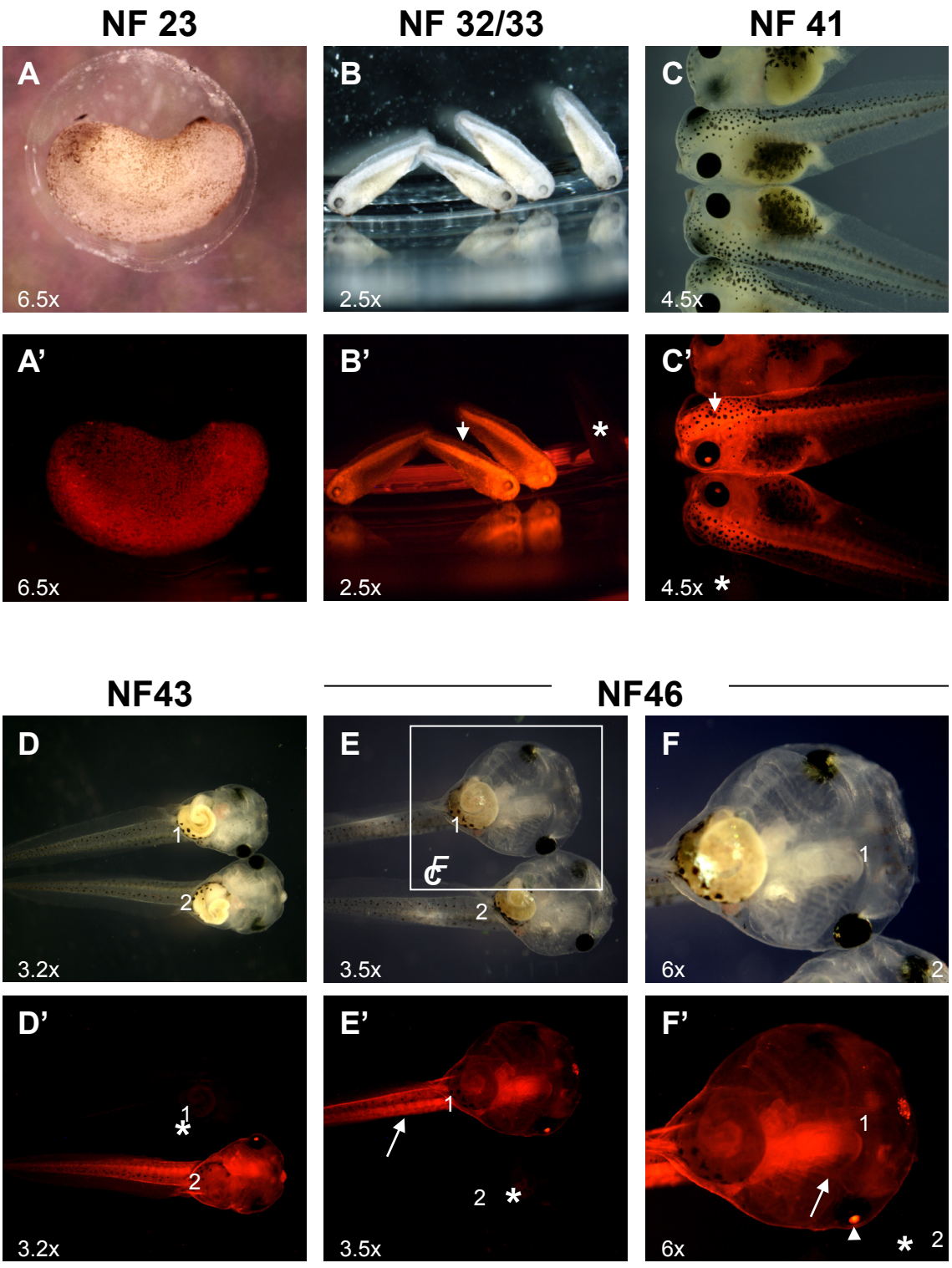

F1 pBR135

5.20

Figure 5.20 Transgenic pBR135 off-spring of the F1 generation shows bright red fluorescence between stage 20 and beyond stage 40

Embryos from a cross between the pBR135 transgenic founder 9 and a wildtype *Xenopus tropicalis* were repeatedly screened under a fluorescence dissecting microscope. Between stage 20 and 46, embryos show bright red fluorescence.

A- F embryos and tadpoles in brightfield, **A'- F'** red fluorescence of the same embryos/ tadpoles. The magnification is indicated in the left corner of the frame.

A Red fluorescence can be detected as early as stage 20, here a stage 23 embryo is shown (**A'**).

B, **C** Transgenic tadpoles develop bright uniform red fluorescence and can clearly be distinguished from non-fluorescent siblings (**B'**, **C'**: asterisks indicate the position of negative embryos). Though the general level of expression is uniform, some tissues like the central nervous system (arrow in **C**') and the musculature (arrow in **B**') show particularly strong expression.

E- **F** Fluorescent and non-fluorescent siblings (asterisks indicate the position of the non-fluorescent sibling) are still easily distinguished in tadpoles past stage 40. However, overall expression levels decrease with development (compare **E'** to **F'**), although red fluorescence in the central nervous system (arrow in **F'**), the musculature of the tail and the lens (arrowhead in **F'**) persists.

Embryos and tadpoles were staged according to Nieuwkoop and Faber.

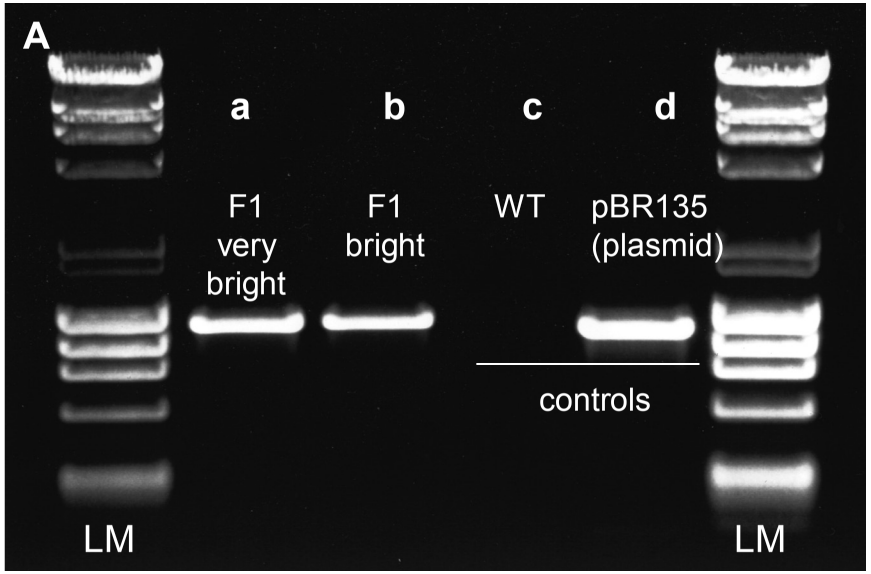

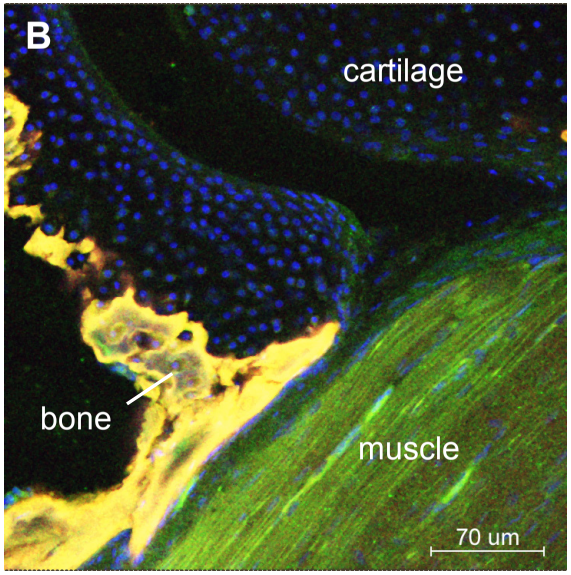

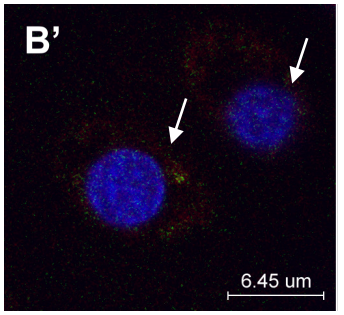

chondrocytes

RFP detected by IHC

RFP (direct fluorescence)

DAPI

Figure 5.21 The pBR135 F1 generation at late developmental stages (past stage 50)

A PCR with transgene-specific primers for the double fluorescent Cre-reporter pBR135 on genomic DNA prepared from off-spring of the F1generation from a cross between a founder and a wild-type animal, tadpoles were older than stage 50. Negative control: unrelated *X. tropicalis* genomic DNA; positive control: pBR135 plasmid.

In late developmental stages (past stage 50), transgenic tadpoles previously screened as 'very bright' and 'bright' no longer show the expected red fluorescence under a fluorescence dissecting microscope. The presence of the pBR135 transgene was however confirmed by PCR (Aa, Ab).

B Immunohistochemistry for RFP on sections of the same 'very bright' specimen as in **Aa**.

IHC* for RFP on a section through the shoulder joint with bone, cartilage and muscle is shown. Green: RFP protein detected by IHC, red: direct red fluorescence from the transgene, blue: DAPI. **B'** shows two cartilage cells (chondrocytes) from **B** in higher magnification.

On sections and sufficient magnification, the red fluorescence from the double fluorescent Cre-reporter is still detectable in bone and muscle (red), confirmed by IHC with anti-RFP antibody (green). Higher magnification (**B**') shows that very low level of RFP and anti-RFP are also present in cartilage cells (chondrocytes, arrows).

* IHC was performed according to standardized conditions; a detailed description of conditions and antibodies (primary and secondary) can be found in the relevant section under 'Materials and Methods' (Chapter 7.5.4).

F2 pBR135

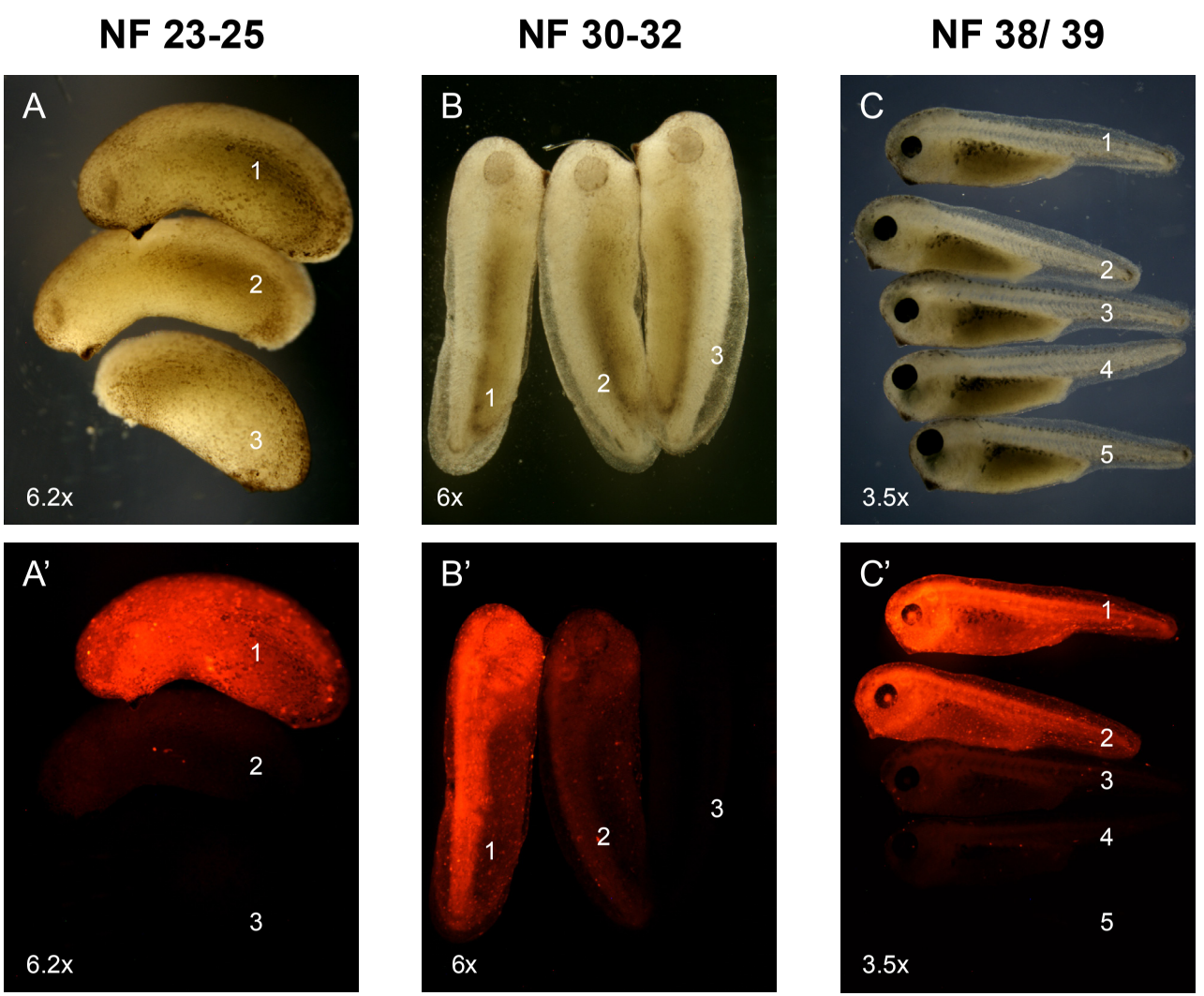
NF 23-25
NF 30-32
NF 38/ 39
A
1
2
3
6.2x
B
1
2
3
6x
C
1
2
3
4
5
3.5x
A'
1
2
3
6.2x
B'
1
2
3
6x
C'
1
2
3
4
5
3.5x

Figure 5.22 The activity of the pBR135 Cre-reporter is maintained in the F2 generation

Off-spring of a cross between two transgenic double fluorescent Cre-reporter *X.tropicalis* (pBR135) of the F1 generation. The animals for the mating had been selected for their particular brightness.

A- **C** brightfield, **A'**- **C'** corresponding red fluorescence of pBR135 F2 tadpoles between stage NF23 and 39. Embryos/ tadpoles are arranged in order of decreasing brightness, '1' indicates the specimen with the strongest fluorescence (**A'**- **C'**).

Embryos and tadpoles of the F1 generation show varying degrees of red fluorescence (**A'**- **C'**), the different level of signal strength are consistent with an increasingly complex genotype.

Even very bright embryos (numbered with (1)) are apparently developing normally (**A**- **C**), indicating that the genomic integration of the transgene did not affect the function of essential genes.

Embryos/ tadpoles were staged according to the classification by Nieuwkoop and Faber.

5.23

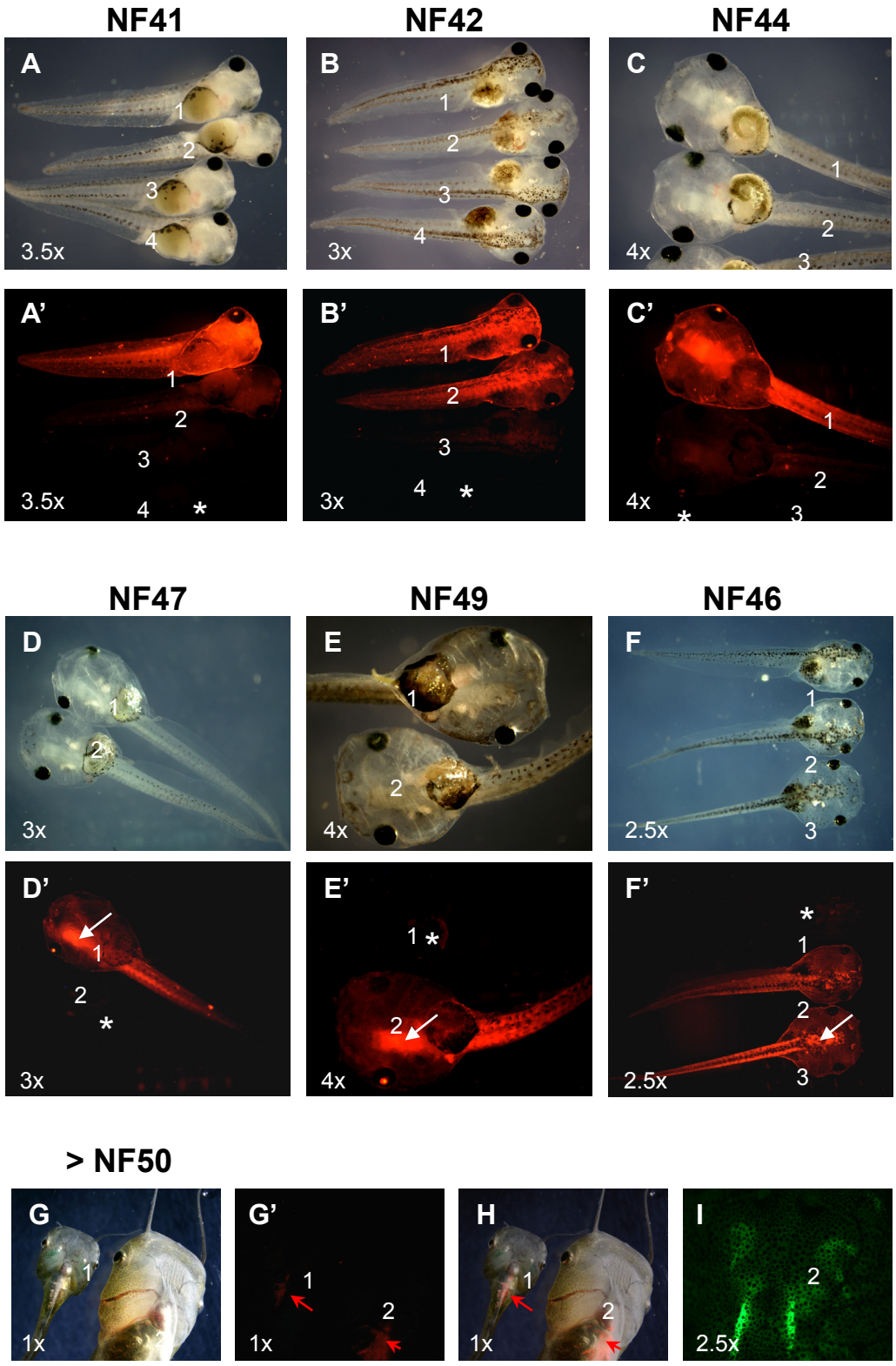

F2 pBR135

Figure 5.23 Interbred off-spring of the F2 generation shows increased levels of red fluorescence but no prolonged activity

Cross between two transgenic *X.tropicalis* (F1 generation, pBR135) that had been previously screened for bright red fluorescence.

A- G brightfield image, **A'- G'** corresponding red fluorescence of tadpoles beyond stage NF40. Embryos/ tadpoles are arranged in order of brightness and negative siblings are marked with an asterisk. The magnification is indicated in the left corner of the frame.

Once identified as positive, tadpoles were raised in the presence of calcein that semi-permanently labels bone and so allowed to trace transgenic animals (**G**- **I**).

Interbred embryos from two transgenic F1 pBR135 Xenopus tropicalis show bright red fluorescence, particularly at early stages (**A**- **C**).
As previously observed for the F1 generation (Figure 5.20), the level of fluorescence in pBR135 F2 tadpoles however also decreases during development (**A'** to **G'**). Also comparable to the F1 generation is the long maintained fluorescence in the central nervous system (**C**', asterisk).

Tadpoles in late stages of development (> NF50) no longer show overall red fluorescence (**G**, **G'**). The only detectable very weak red fluorescence localized to the gut region and must be considered intestinal auto-fluorescence (**H**, arrows). However, calcein staining indicates that the embryos had been screened as brightly red fluorescing at an earlier time-point (**I**).

Embryos and tadpoles were staged according to Nieuwkoop and Faber.

pBR135, F2

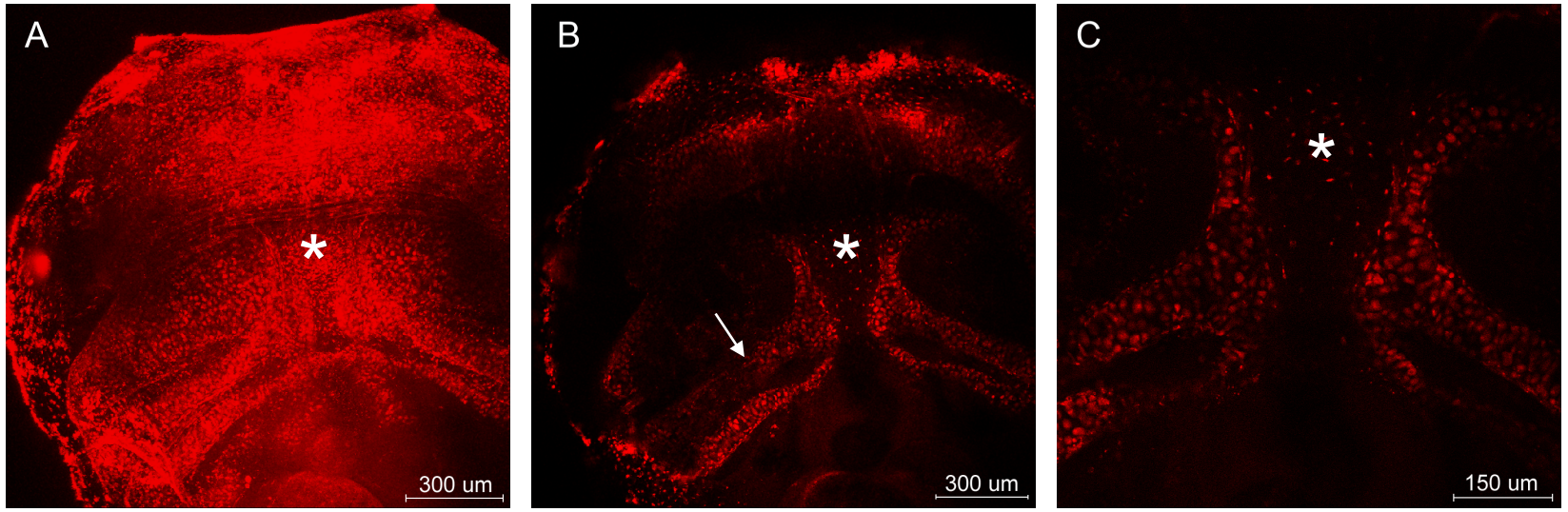

Figure 5.24 Transgenic *X.tropicalis* tadpoles of the F2 generation (pBR135) fluoresce brightly red and allow the detection of single cells by confocal microscopy

A Projection of a confocal z-stack of the lower jaw of a stage 41 F2 pBR135 tadpole in ventral view (143 sections, step-size 2.05 µm). The anatomy of the specimen is clearly visible.

B A thinner optical stack of the same specimen allows to clearly identify single cells, here in the cartilaginous branchial basket (arrow, 66 sections, step-size 0.04 µm)

C A single optical sections in higher magnification of the midline of the same tadpole demonstrates the cellular resolution that can be obtained by confocal microscopy with this Cre-reporter.

asterisk: midline of the specimen

5.24

head skeleton (Figure 5.25), making the pBR135 Cre-reporter a valuable tool for the study of head development.

5.4.3.3 Summary

- The human Ubiquitin C promoter is also functional in *Xenopus tropicalis*, driving wide-spread expression, and is not prone to inactivation during passage through the germline.
- The RFP mutant DsRed.T3 fluoresces brightly in *Xenopus tropicalis* and shows no signs of toxicity, thereby presenting an interesting alternative to the widely used but weaker DsRed2.
- A novel fusion promoter between the CMV immediate early element and the human Ubiquitin C promoter enhances promoter activity in cell culture (C2C12 cells) but leads to uneven expression in *Xenopus tropicalis* transgenesis.
- I-*Sce*I mediated transgenesis potentially allows the generation of a stable transgenic *Xenopus tropicalis* lines, in this case a double fluorescent Cre-reporter line for construct pBR135 (hUbC-DsRed.T3pA-VenuspA).
- Interbreeding of transgenic pBR135 animals of the F1 generation results in viable embryos that develop normally; by this, the expression level from the Cre-reporter can be increased but not prolonged. In F2, the levels of fluorescence around stage 40 allow direct imaging by confocal microscopy in cellular resolution.

A stable generic double fluorescent Cre-reporter line as prerequisite for genetic lineage labelling in *Xenopus tropicalis* was thereby successfully completed. This allows us now to approach the question of the evolution of the tetrapod middle ear with the design of specific Cre-driving constructs, which will be content of the following part of this chapter.

Figure 5.25

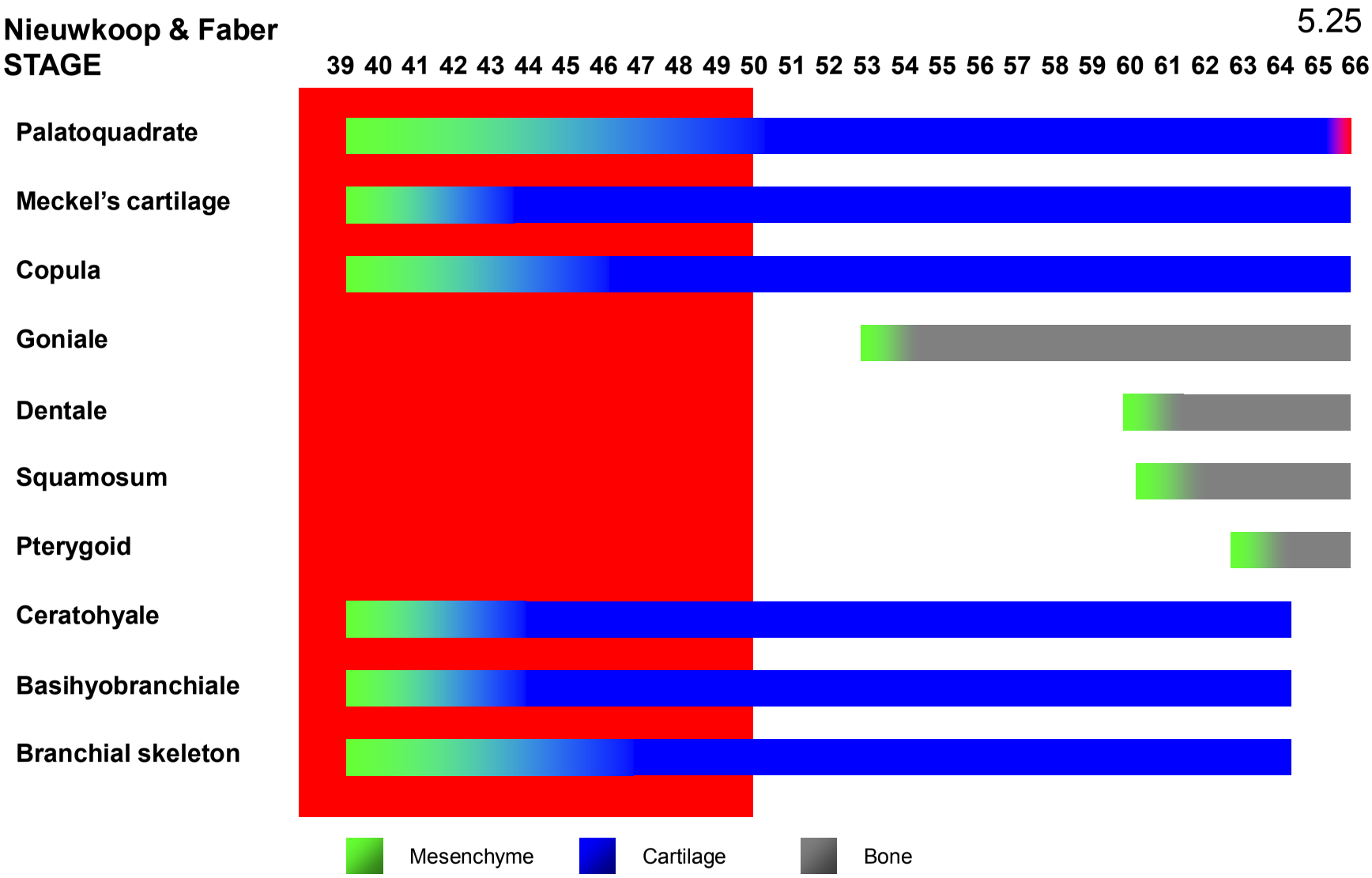
Nieuwkoop & Faber
STAGE
39 40 41 42 43 44 45 46 47 48 49 50 51 52 53 54 55 56 57 58 59 60 61 62 63 64 65 66
Palatoquadrate
Meckel's cartilage
Copula
Goniale
Dentale
Squamosum
Pterygoid
Ceratohyale
Basihyobranchiale
Branchial skeleton
Mesenchyme
Cartilage
Bone

Figure 5.25 Sequence of head and branchial skeleton development in *X.laevis*

First arch elements

Palatoquadrate. Various subparts develop at slightly different time points, overall development from mesenchymal condensations present at NF39 till complete chondrification at NF50.

Meckel's cartilage. Mesenchymal condensation at NF40, pro-cartilaginous at NF41 and cartilaginous at NF43.

Copula or *cartilago labialis inferior*. Mesenchymal condensation at NF40, complete chondrification by NF46.

Goniale (dermal bone). Formation at NF53/54.

Dentale (dermal bone). Formation at NF60.

Squamosum (dermal bone). Formation at NF62.

Pterygoid (dermal bone). Formation at NF63.

Elements of the branchial basket (other branchial arches)

Ceratohyale. Mesenchymal condensation at NF40, pro-cartilaginous at NF41 and cartilaginous at NF43.

Basihyobranchiale. Mesenchymal condensation at NF40, pro-cartilaginous at NF41 and cartilaginous at NF43.

Branchial skeleton. Mesenchymal condensation at NF40 and complete chondrification by NF46.

The entire branchial basket disappears by NF64.

Key: Mesenchyme (green), cartilage (blue) and bone (grey). The red background indicates the window of activity of the pBR135 Cre-reporter. Staging and developmental description according to Nieuwkoop and Faber (Nieuwkoop & Faber. Normal Table of *Xenopus Laevis*. 1994. Garland Publishing)

5.5 Unravelling the origins of the amphibian middle ear

5.5.1 Background

5.5.1.1 Genetic lineage labelling of distinct neural crest subpopulations

Our ultimate goal was to create a rhombomeric fate map of the amphibian anterior skull comparable to the existing results in birds[102] to answer fundamental questions about cranial morphogenesis in amphibians and in particular the origin of the amphibian middle ear. In combination with existing lineage labelling results in other species, this would allow us to gain a better understanding about the ancestral condition of the tympanic tetrapod middle ear and its independent evolution within the different tetrapod groups.

The specificity in the Cre/ Lox system is achieved by the targeted expression of Cre recombinase in a cell population of interest which is achieved by the choice of a suitable genetic enhancer element active in the targeted cell population. The identification of suitable genetic elements which drive specific expression in defined cranial neural crest subpopulations is therefore crucial for this project. The dissection of vertebrate gene regulation and the identification of enhancer elements is still predominantly undertaken in mouse; the sequence conservation of these enhancer elements between species is commonly assumed to reflect functional conservation and significance. We therefore tested reported mouse enhancer elements with relevant activity in neural crest subpopulations for sequence conservation across a wide range of species. Sequence conservation between mouse and *Xenopus* was interpreted as conserved function of the regulatory element and the equivalent *Xenopus* region amplified for our specific Cre-driving constructs. The choice of suitable genetic elements to allow us to address these questions by genetic lineage labelling of cranial neural crest subpopulations, the design and the generation of corresponding constructs and preliminary transgenesis results are presented in the following section.

5.5.1.2 Specifications for a Cre-driving construct

Successful genetic lineage labelling with the Cre/ Lox system is dependent on the specificity of the Cre-driving construct. The specificity of such a Cre-driving construct is defined by the regulatory elements incorporated into the transgene (including species-specificity, enhancer-promoter interactions, the presence or absence of controlling elements and the overall architecture of the regulatory region) and the positive or negative influence of endogenous neighbouring regulatory elements at the transgene insertion site into the genome. Detailed assessment of the activity of Cre is therefore necessary to ensure the correct interpretation of the lineage labelling results. For the later use in I-*Sce*I mediated transgenesis, the specific Cre-driving constructs in this study (plasmids pBR161 and pBR151, Figure 5.29) were designed with a single 5' I-*Sce*I recognition site, as a single I-*Sce*I recognition site was reported to result in higher rates of successful transgenesis than two I-*Sce*I recognition sites that flanked the transgene (personal communication S.Ishibashi, E. Amaya Group).

5.5.2 Results

5.5.2.1 A VenusCrem fusion protein visualises the activity of Cre

In order to simultaneously assess enhancer function and to establish a Cre-driving line at the same time, a fusion protein between Venus, an EYFP mutant[131], and Cre recombinase was generated. After transgenesis, the green fluorescent fusion protein allows an easy screen under a fluorescence dissecting microscope for positive embryos with the correct expression pattern that then can be raised into adulthood, limiting the number of animals that need to be raised and outbred.

A modified version of the Cre recombinase with an intermittent beta-globin intron (designated as 'Crem') was used as the insertion of an artificial intron has been reported to increase transcriptional efficiency in transgenic mice[95,21].

The Venus-Crem fusion protein used for constructs pBR151 and pBR161 was created by a colleague, X. Zhang. When tested by transient transfections in cell culture, this Venus-Cre fusion protein was bright green (Figure 5.26 A) while maintaining enzymatic Cre recombinase activity (B). Due to a nuclear localisation cassette in the coding frame of the Cre recombinase, the fusion protein shows nuclear localisation (A). In combination with the Cre-reporter described in the previous section, red fluorescence will be the reporter default state, green nuclear localisation will indicate the activation of Cre (from the Venus-Crem fusion protein) and green cytoplasmatic fluorescence from the reporter will indicated past and present Cre-activity. The signal from the Venus-Crem fusion protein will therefore not interfere with the signal from the double fluorescent Cre-reporter.

Figure 5.26

A

Fluorescence

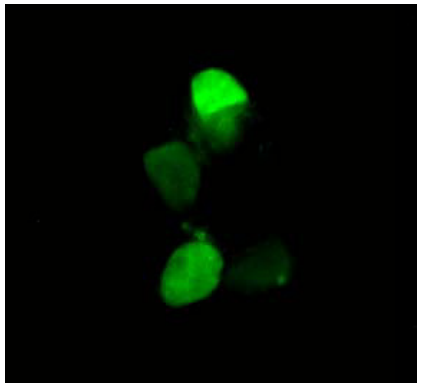

HEK293 cells transfected with

p279 (XT)

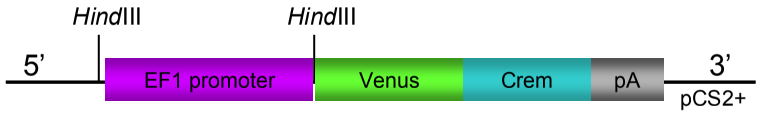

EF1-VenusCrem-pA

B

Recombinase activity

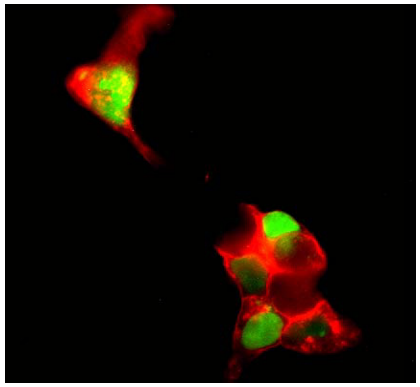

p279 (XT)

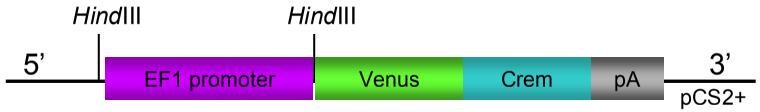

EF1-VenusCrem-pA

+

GAP43DsRed.T4 Cre-reporter (XT)

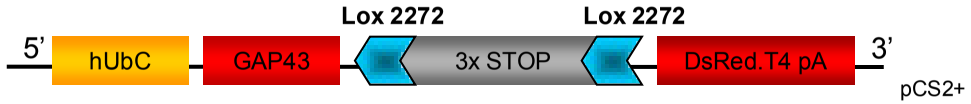

hUbC-GAP43-Lox2272-3xStop-Lox2272-DsRed.T4-rabbit pA

Images courtesy of X. Zhang (XT)

Figure 5.26 Proof of principle: the VenusCrem fusion protein

HEK293 cells were transfected with either a plasmid encoding the VenusCre fusion protein (p279 (pXT_EF1-VenusCrem), Cre with an artifical intron= Crem) alone (**A**) or with p279 (pXT_EF1-VenusCrem) in combination with a Cre-reporter (GAP43DsRed.T4 Cre reporter) (**B**). Experiments and images by X. Zhang.

A The VenusCre fusion protein shows bright green fluorescence. Because of a nuclear localisation signal at the N- terminus of Cre, the VenusCre fusion protein localises to the nucleus.

B The recombinase activity is maintained in the VenusCre fusion protein. In the absence of Cre recombinase, the presence of a STOP cassette prevents the expression of GAP43DsRed.T4 from the GAP43DsRed.T4 Cre-reporter.

Red fluorescence in **B** therefore indicates a past Cre-mediated excision event that removed the intervening STOP cassette and reconstituted the GAP43DsRed.T4 reading frame. Due to the GAP43 signal, DsRed.T4 is membrane-localised.

5.5.2.2 Enhancer elements with specific expression in neural crest subpopulations

The *Hand*2 branchial arch enhancer allows to distinguish between distal and proximal branchial arch origin

Genetic elements driving proximal branchial arch expression have not been identified so far, but the *Hand*2 branchial arch enhancer described in the previous chapters of this thesis labels a distal branchial arch compartment. With help of a Cre transgene containing the *Hand*2 branchial arch enhancer, proximal branchial arch origin can now be defined by the absence of labelling ('non-distal'). Comparative lineage labelling in *Xenopus* with a *Hand*2-Cre construct will generate a dataset directly comparable with the data set of the *Hand*2-Cre mouse.

The branchial arch expression of *Hand*2 is conserved between mammals, amphibians and fish[9]. The *Hand*2 regulatory element directing expression in the distal part of the first and second branchial arch, the previously mentioned branchial arch enhancer, has been identified by mouse transgenesis and is located circa 7.4kb upstream of the transcriptional start site of *Hand*2[29] (Figure 5.27 A). The branchial arch enhancer is conserved on sequence level between mammals, birds, amphibians and fish (Figure 5.27 B). Species-specific function of enhancer and promoter elements despite apparent conservation on sequence level has been reported (unpublished finding by K. Vance in our group, also [198]) so it was decided to use *Xenopus* rather than mouse regulatory elements. To preserve enhancer-promoter specificity and the normal spacing of the elements, the *Xenopus Hand*2 Cre-driver contains the entire *Xenopus* upstream region of *Hand*2 up to and including the conserved branchial arch enhancer element. The amplification of the 4.5kb upstream region proved to be challenging and was finally generated as a set of four separate but overlapping fragments that were re-constituted after extensive sequencing with naturally occurring unique restriction sites (Figures 7.5 and 7.6, Materials and Methods, Chapter 7.2.2.3), resulting in the final plasmid pBR161 (see also Figure 5.29 A).

Figure 5.27

A

***Hand2* branchial arch enhancer**

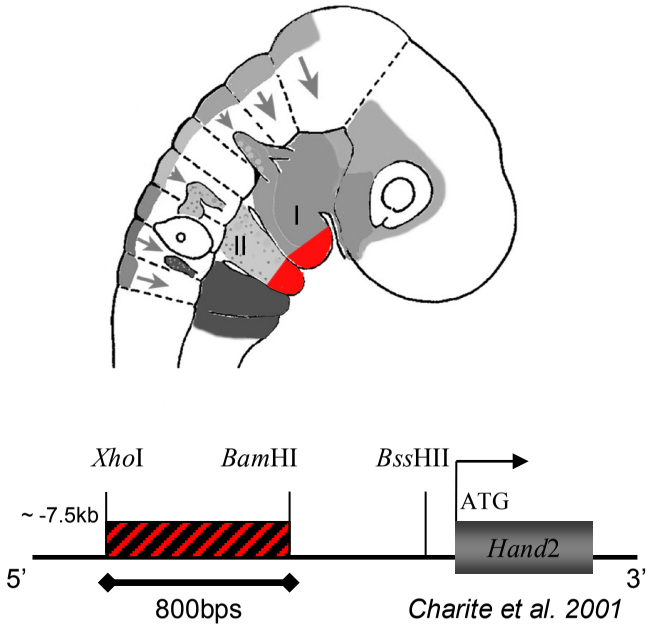

B

Hand2 BA enhancer

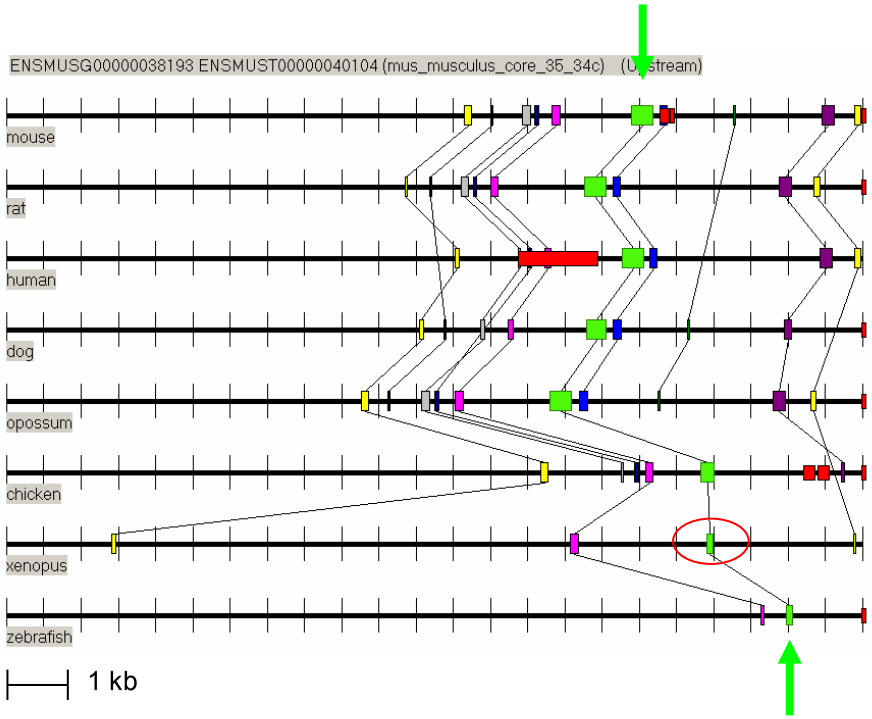

Figure 5.27 A *Hand*2 branchial arch enhancer

A The *Hand*2 branchial arch enhancer labels a distal cell population in the first and second branchial arch (the branchial arches are indicated by roman numbers).

B Multiple sequence alignment performed with RemoGUI Version 1.31 (screenshot). The branchial arch (BA) enhancer is highlighted in green in the multiple alignment and the mouse sequence (first row) corresponds to the *Hand*2 branchial arch enhancer identified by Charite et al. 2001 as depicted in (**A**). The branchial arch enhancer shows evolutionary sequence conservation between mammals, birds, amphibians and teleosts. The *Xenopus* element is encircled.

TSS transcription start site

1 unit represents 1kb sequence

Reference

Charite, J. *et al.* Role of Dlx6 in regulation of an endothelin-1-dependent, dHAND branchial arch enhancer. *Genes Dev.* **15**, 3039-3049 (2001).

A 809 bp *Hox*a2 enhancer for lineage labelling of the second branchial arch

In order to determine the boundary between the second arch-derived amphibian stapes/ columella and the brain case, a genetic element driving expression in the second branchial arch was chosen: *Hox*a2 is expressed in neural crest cells up to the boundary between rhombomere 1 and 2, as well as in the second branchial arch. A non-coding *Bgl*II fragment upstream of *Hox*a2 has been shown to replicate *Hox*a2 expression in rhombomere 3 and 5, as well as in neural crest emigrating from rhombomere 4 and the second branchial arch[117,138]. The 809bps *Hox*a2 second arch enhancer was identified in mouse transgenesis to drive expression in rhombomere 3 and 5 and in the neural crest of the second branchial arch[138]. The enhancer is conserved on sequence level between mammals, birds, amphibians and fish (Figure 5.28). 2kb of the *Xenopus* upstream region including the conserved *Xenopus* second branchial arch enhancer up to the transcriptional start site of *Hox*a2 were therefore amplified by LTPCR and used to finally generate construct pBR151 (Figure 5.29 B).

Figure 5.28- 5.29

A

Hoxa2 r3/r5 (2nd BA) enhancer

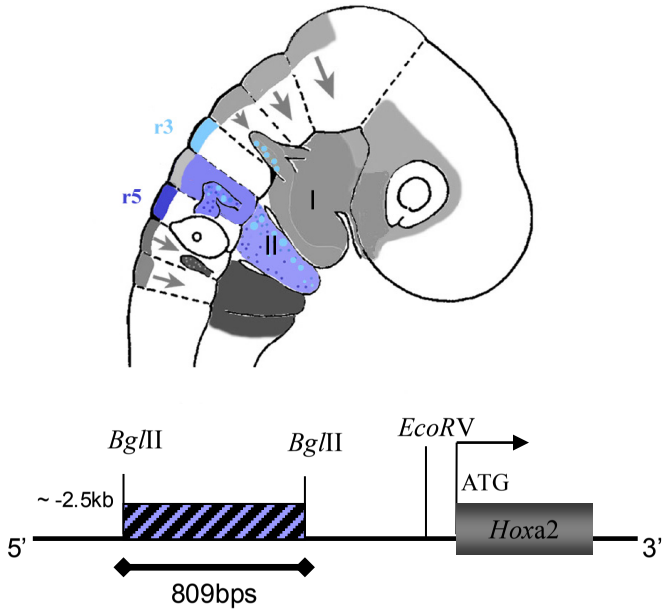

Nonchev et al. 1996, Maconochie et al. 1999

B

Hoxa2 2nd BA enhancer

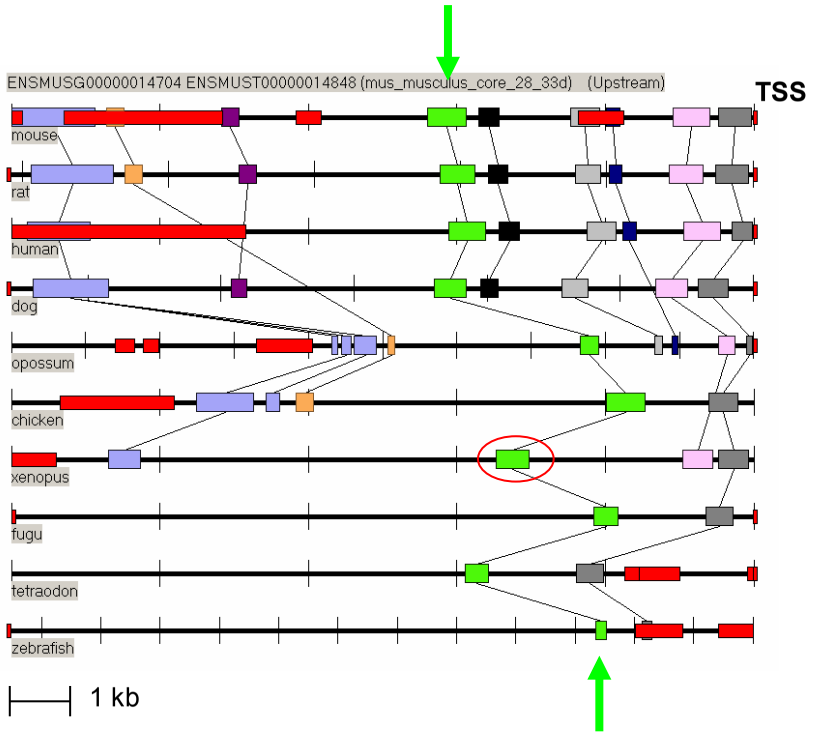

Figure 5.28 The *Hox*a2 second branchial arch enhancer

A The *Hox*a2 2nd branchial arch enhancer identified and tested by Nonchev et al. 1996 and Maconochie et al. 1999 labels rhombomere 3 and 5 and neural crest emigrating from rhombomere 4.

B Multiple sequence alignment performed with RemoGUI Version 1.31 (screenshot). The *Hox*a2 809bps enhancer driving expression in the second branchial arch as identified by Nonchev et al. 1996 is highlighted in green and shows evolutionary sequence conservation between mammals, birds, amphibians and teleosts. The *Xenopus* element is encircled.

TSS transcription start site

1 unit represents 1kb sequence

References

Nonchev, S. et al. Segmental expression of *Hox*a-2 in the hindbrain is directly regulated by *Krox*-20. Development 122, 543-554 (1996).

Maconochie, M. et al. Regulation of *Hox*a2 in cranial neural crest cells involves members of the *AP*-2 family. Development 126, 1483-1494 (1999).

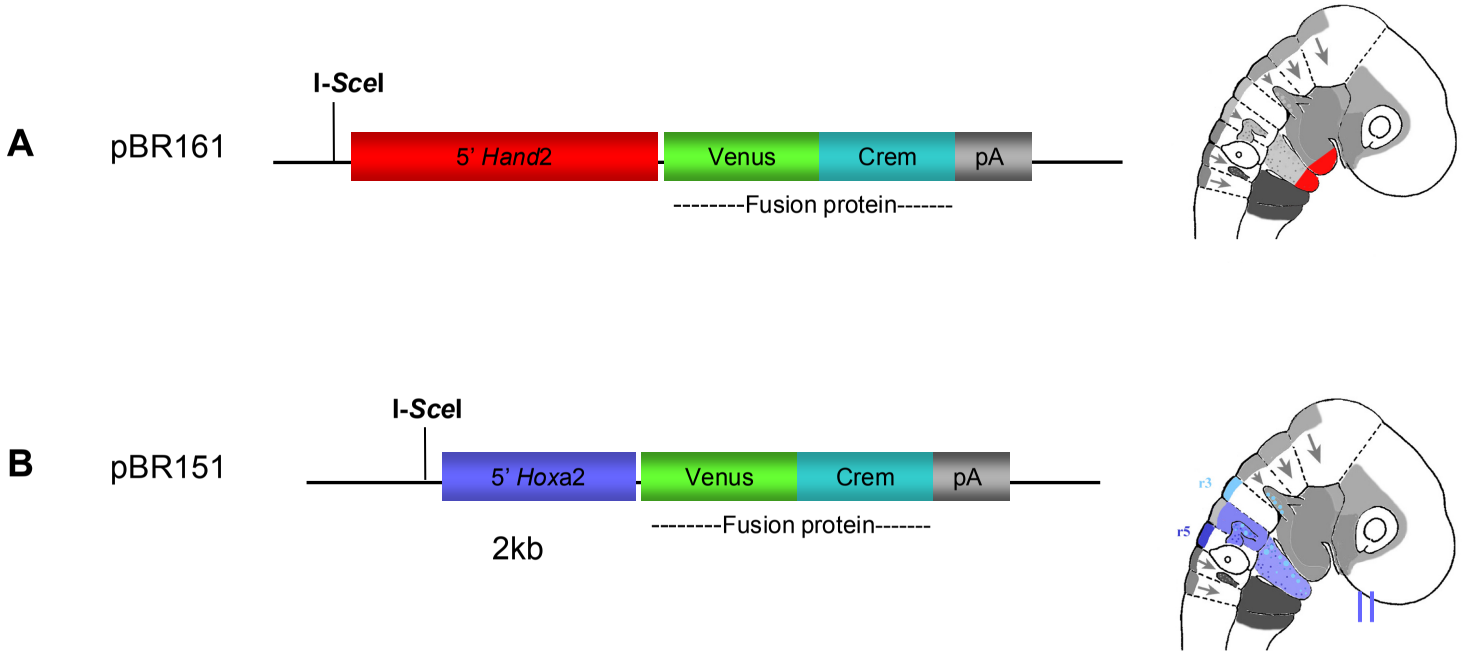

Figure 5.29 Cre-driving constructs under control of *Xenopus* regulatory elements

A Construct pBR161: *Xenopus Hand*2 upstream regulatory region for the labelling of a distal branchial arch compartment.

B Construct pBR151: *Xenopus Hox*a2 upstream regulatory region for the labelling of the second branchial arch.

5.5.2.3 The *Xenopus Hand*2-Venus-Crem construct pBR161 drives distal branchial arch expression in *X. laevis* and in zebrafish

The *Xenopus Hand*2 and *Hox*a2 Cre-driving constructs pBR161 and pBR151 (Figure 5.29) were first tested for activity by the robust REMI technique in *Xenopus laevis*. Both constructs contain the Venus-Crem fusion protein under the control of genomic *X. tropicalis* regions that includes the sequence-conserved *Xenopus* equivalent of enhancer elements previously tested in mouse (Figure 5.26 and 5.27). Transgenic *Xenopus laevis* embryos for pBR161 or pBR151 were therefore expected to show green fluorescence reflecting the activity of the *Hand*2 BA enhancer and the *Hox*a2 809bps enhancer respectively. Unfortunately, no green fluorescence could be observed in *X. laevis* embryos after REMI with construct pBR151 (*Hox*a2-Venus-Crem). However, *X. laevis* embryos injected with construct pBR161 showed green fluorescence reminiscent of *Hand*2 expression (Figure 5.30). At early stages of development, strongly green fluorescent cells were present in the area of the branchial arches; these cells migrated distally (compare B and C), apparently reflecting endogenous *Hand*2 activity as reported by Angelo et al.[9]. Later in development, weak green fluorescence was detectable in the distal part of the branchial arches of transgenic but not control embryos (D, E, arrows). We were not able to replicate this result; further injections by the REMI technique did not generate any further fluorescent *Xenopus* embryos, although transgenesis was successful as the transgenes pBR161 (and also pBR151) were detected by PCR (Figure 5.31). The *Xenopus Hand*2 upstream region was also tested in zebrafish by tol2 transposon-mediated transgenesis. In tol2 transgenesis, a construct with flanking tol2 transposon elements is injected into fertilized eggs together with tol2 transposase mRNA[12] and the enzyme facilitates the integration of the construct into the genome. Construct pBR161 did not contain any transposon elements which made an adaptation of the construct for tol2 transgenesis necessary; the *Xenopus Hand*2 upstream region of pBR161 was therefore inserted into a vector carrying Tol2 elements (Figure 5.32 D). The *Xenopus Hand*2 upstream region was shown to be fully functional in zebrafish (Figure 5.32): Fluorescence was detected in the lower jaw and the distal part of the

Figure 5.30- 5.32

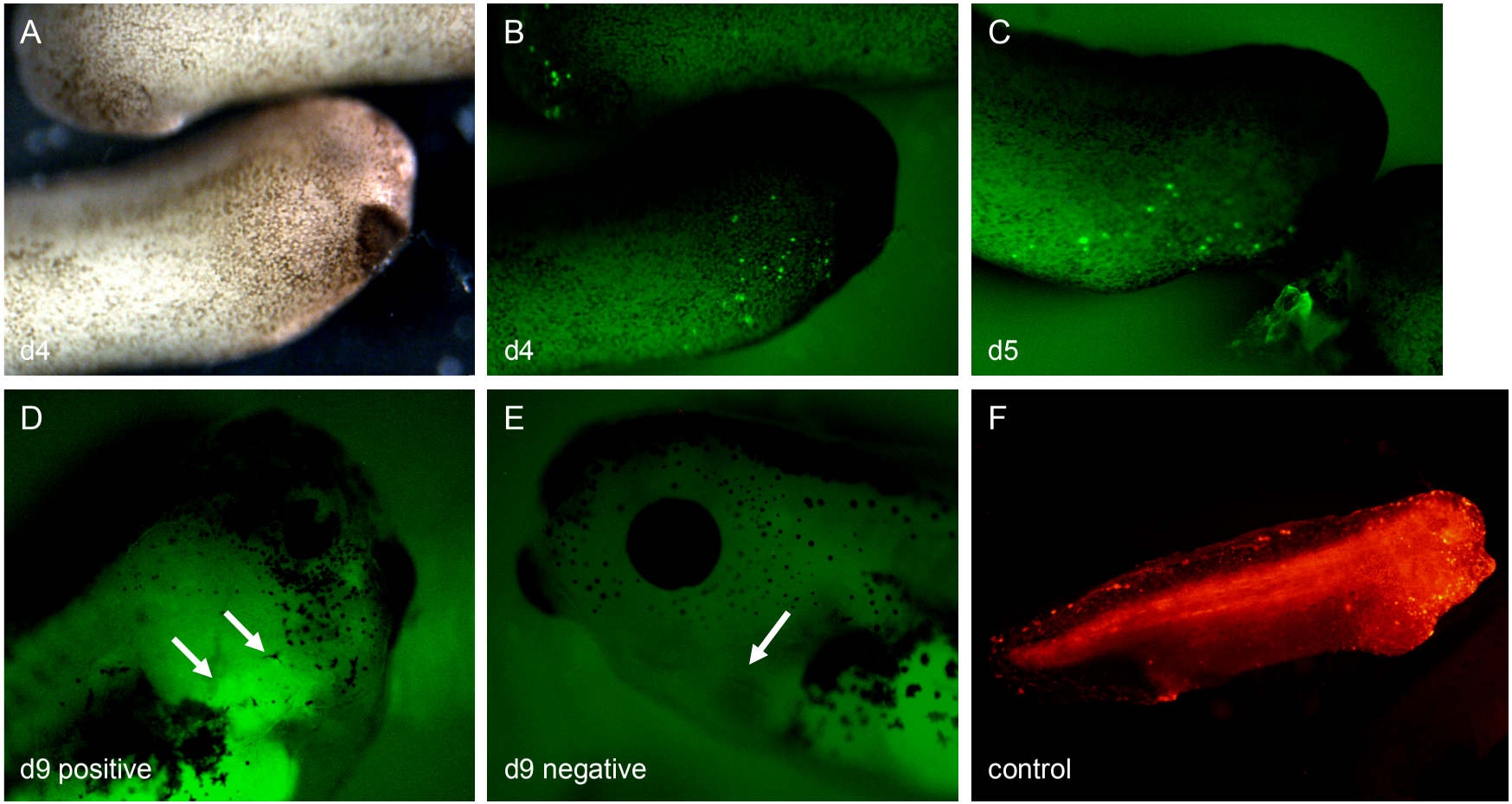
A
d4
B
d4
C
d5
D
d9 positive
E
d9 negative
F
control

Figure 5.30 The *Xenopus Hand*2 upstream region is able to drive specific expression

REMI transgenesis for pBR161 (*Hand*2-VenusCrem) in *Xenopus laevis* resulted in embryos showing expression compatible with endogenous *Hand*2 expression.

A- **D** *Xenopus laevis* tadpoles injected with pBR161 (*X.tropicalis Hand*2-VenusCrem). Brightfield image (**A**) and green fluorescence (**B**- **E**).

After 4 (**B**) respective 5 (**C**) days, bright green speckles were seen in the branchial arch region of some embryos.

D After 9 days, weak green fluorescence was found in the distal part of the branchial arches (arrows) of some specimen.

E For comparison, a tadpole after 9 days with no labelling in the branchial arch region (arrow).

F Control for transgenesis: A *X.laevis* tadpole injected with the control construct pBR162 (I-*Sce*I- hUbC-LoxPDsRed.T3pALoxP-Venus-I-*Sce*I) shows strong ubiquitous red fluorescence demonstrating the success of the REMI transgenesis.

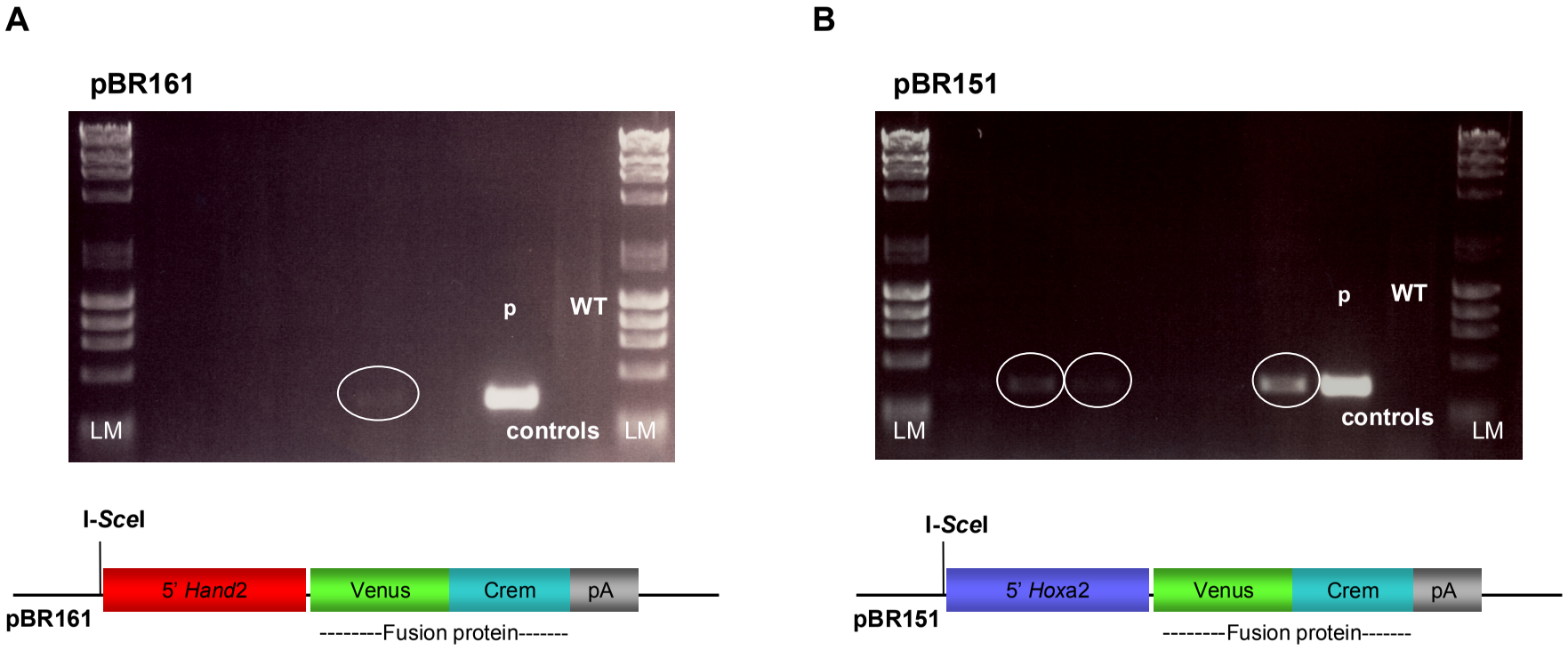
A
pBR161
p
WT
LM
controls
LM
I-SceI
5' Hand2
Venus
Crem
pA
pBR161
--------Fusion protein-------
B
pBR151
p
WT
LM
controls
LM
I-SceI
5' Hoxa2
Venus
Crem
pA
pBR151
--------Fusion protein-------

Figure 5.31 PCR for the transgene after REMI in *X.laevis*

Genomic DNA was prepared by Phenol/ Chloroform extraction of potentially transgenic *X.laevis* tadpoles after transgenesis with the REMI method for the constructs pBR161 (**A**) and pBR151 (**B**). PCRs were performed as standard PCR reactions as described in 'Materials and Methods' as 20 µl reactions with 150 ng gDNA as template.

Primers **TWCre1** (GCTGGTTAGCACCGCAGGTGTAGAG) and **TWCre3** (CGCCATCTTCCAGCAGGCGCACC) amplify a 422bps fragment from the Cre recombinase coding region and have been previously successfully used for genotyping of the *Hand*2-Cre mice (Materials and Methods, genotyping).

In each case, the plasmid originally used for REMI transgenesis is indicated below the gel and was used as positive control in the PCR (plasmid, p). Unrelated wildtype *Xenopus* genomic DNA served as negative control (WT).

Although none of the embryos showed the expected fluorescence when screened under a fluorescence dissecting microscope, the transgene could be detected by PCR in 1/5 cases for pBR161 (Hand2-VenusCrem, **A**) and in 3/6 cases for pBR151 (*Hox*a2-VenusCrem, **B**).

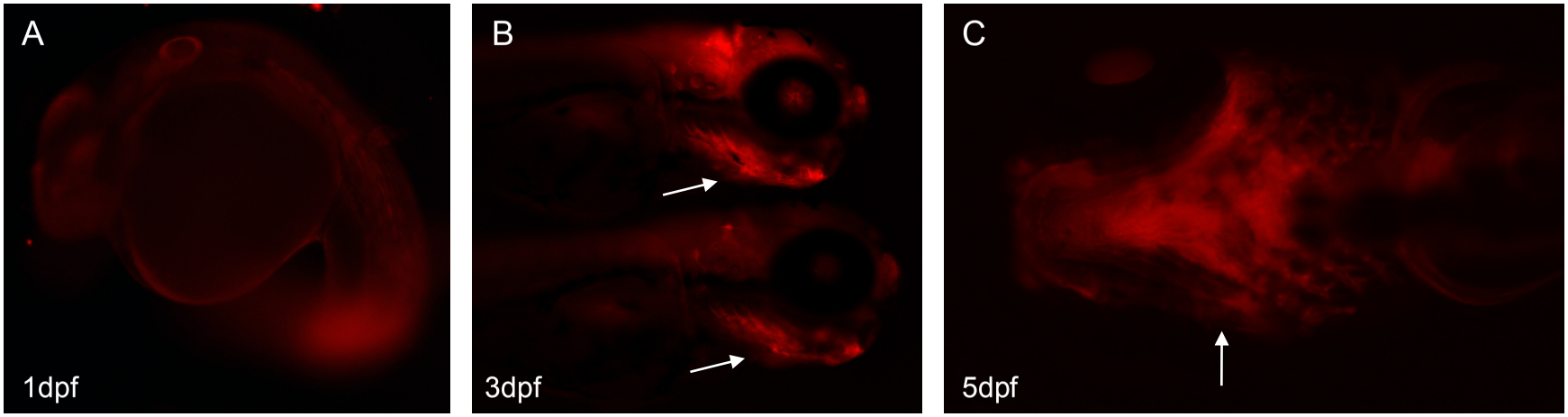

D

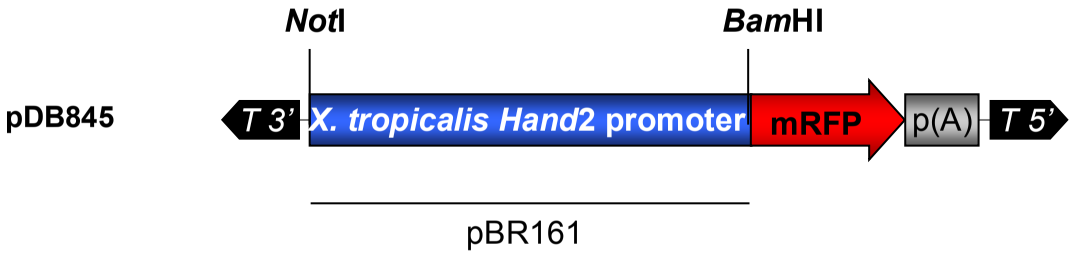

Construct pDB845, injections and images by D. Balciunas

Figure 5.32 The *Xenopus Hand*2 upstream region drives expression in zebrafish

Zebrafish embryo after Tol2 transgenesis with plasmid pDB845 at 1 day (**A**), 3 days (**B**) and 5 days (**C**) post-fertilisation showing red fluorescence in the lower jaw and the distal part of the branchial basket (arrows in **B**, **C**).

The *Xenopus* upstream region is therefore able to replicate an expression pattern consistent with endogenous *Hand*2 expression in zebrafish.

D The adaptation of plasmid pBR161 for Tol2 transgenesis in zebrafish. The *Xenopus Hand*2 upstream region was excised from plasmid pBR161 and inserted into a Tol2 vector to generate pDB845 (last cloning step and transgenesis was performed by D. Balciunas).

C is the same embryo as in Figure 2.2.26

branchial arches (B, C), further in the rays of the fins, reflecting *Hand*2 activity in the limb lateral plate mesoderm (C, also see Chapter 3). An important observation made by D. Balciunas was that signal could only be detected when the *Xenopus Hand*2 upstream region was combined with a standard red fluorescent protein (see Figure 5.32) but not in combination with the Venus-Crem fusion protein. The zebrafish results only became available after the end of the experimental work for this thesis, so that according experiments in *Xenopus* could no longer be performed. All together this suggests that the *Xenopus Hand*2 upstream region is functional in *Xenopus* as well as in zebrafish but that the fluorescence of the Venus-Crem fusion protein in a combination with an endogenous promoter is not strong enough to allow detection. Absence of fluorescence in the case of the other construct, pBR151, might equally rather reflect the insufficient brightness of the Venus-Crem fusion protein rather than lack of enhancer function.

5.5.3 Summary

- The *Xenopus Hand*2 upstream region is functional in *Xenopus* as well as in zebrafish.

- In combination with a strong promoter, the Venus-Crem fusion protein fluoresces green and shows full Cre recombinase activity. Under the control of endogenous promoter sequences, the fluorescence of the fusion protein is too weak to allow detection under a normal fluorescence dissecting microscope.

5.6 Discussion

The establishment of the genetic lineage labelling technique in *Xenopus* proved unfortunately considerably more difficult than anticipated. Despite being highly successful in zebrafish[184], I-*Sce*I mediated transgenesis in *Xenopus tropicalis* did not prove to be the straight-forward and robust technique for the generation of stable transgenic *Xenopus* lines that we had hoped for. In addition, *X. tropicalis* husbandry became a limiting and time-determining factor and affected egg quality, male fertility, embryo survival and the time in which tadpoles reached sexual maturity. Instead of the expected generation time of 3/ 5 months for male/ female *X. tropicalis*, animals bred in our facilities only reached sexual maturity after more than 8 months, significantly delaying the progress of the project (for a time-line, see Figure 5.33). Consequently, the establishment of transgenic *Xenopus tropicalis* lines for genetic lineage labelling became extremely laborious and long-winded, raising in hindsight the question of possible alternative approaches. Transplantation-based techniques analogous to the quail/ chick system used to study the rhombomeric origin of the avian skull are now also available in *Xenopus* and might have represented a faster approach to generate a comparable map of the frog skull. Transplantation experiments in *Xenopus* have been performed as inter-species (e.g. *X. borealis* into *X. laevis*) and intra-species transplantations (labelled donor tissue into unlabelled host or *vice versa*), e.g.[104]. The stable transgenic *X. laevis* line expressing Venus under control of the human Ubiquitin C promoter (Figure 5.6 A and 5.7) that was generated during the work for this thesis would have in effect represented an ideal donor for green fluorescently labelled tissue. As shown in this chapter, the human Ubiquitin C promoter is ubiquitously active in *Xenopus* and drives sufficient levels of fluorescence throughout development. This would not only allow to easily follow transplanted green fluorescing cells over time but also to directly analyse their contribution to adult structures.

Despite the reported difficulties, we nevertheless successfully established the first stable *Xenopus tropicalis* Cre-reporter line reported so far. The double fluorescent Cre-reporter fulfils our specifications in that it indicates Cre-reporter activity independently of Cre-activity, is active in relevant stages of head development and allows confocal live imaging in cellular resolution up to the 40's stages of development, making this an extremely useful generic tool for genetic lineage labelling in *X. tropicalis*. Once the

functionality of the *Xenopus tropicalis* Cre-reporter is confirmed, this reporter will provide a valuable tool for the *Xenopus* community and will be made available through the European Stock Centre for *Xenopus* in Portsmouth.

With a stable Cre-reporter line soon openly available and ever improving transgenic techniques (for example, tol2 transgenesis, another transgenic technique now widely and successfully used in zebrafish[12], shows also promising results in *Xenopus*, e.g.[78]), it will be possible to perform transgenesis for a Cre-driving construct- such as the *Hand*2-VenusCrem construct pBR161- in the transgenic Cre-reporter background. Cre-reporter embryos are easily recognisable due to their ubiquitous red fluorescence and the fact that Cre-reporter animals can be interbred will allow the establishment of a well-characterised homozygous Cre-reporter line with 100% homozygous off-spring in the future. With numerous transgenic embryos available after each round of injections, it will be possible to distinguish between transgene-specific and aberrant results with statistical significance, potentially making the time-consuming establishment of independent Cre-driving lines redundant.

Although we were not able to bring the project to completion due to the unexpected time-line of the experiments, the establishment of the stable double fluorescent Cre-reporter line with construct pBR135 and encouraging preliminary results in *Xenopus* (and zebrafish) with the *Xenopus Hand*2 Cre-driving construct pBR161 represent an important step towards the first truly comparative genetic lineage labelling set of data in species representing the entire gnathostome group and will hopefully allow in the nearer future to experimentally approach the question of the evolution of the tetrapod middle ear.

Figure 5.33

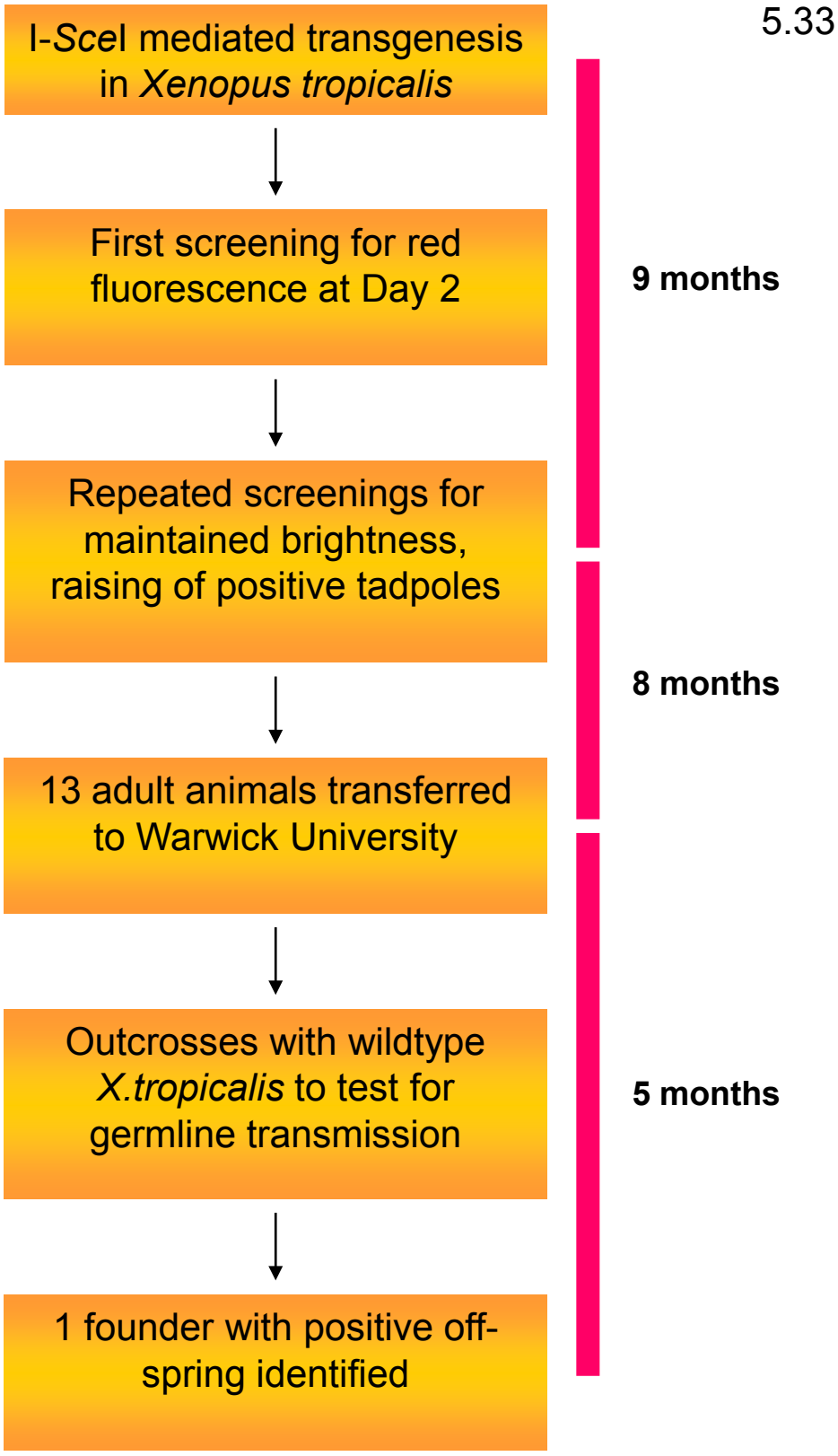

Figure 5.33 Timeframe for the establishment of the stable transgenic pBR135 *X.tropicalis* Cre-reporter line

6 Summarizing conclusion

The work presented in this thesis was driven by the desire to gain a better understanding of the processes directing the development of the highly complex head and neck region in their evolutionary context. Compared to the high complexity of the final structure, the embryonic beginnings are by necessity simple. Understanding how the genetic patterns are laid down in the respective embryonic precursor populations therefore holds the key to the final complexity and will provide us with insights into how the transformation from embryo to adult is mechanistically directed. Genetic lineage labelling with the Cre/ Lox system does not only provide the means to unravel the embryonic origin of adult structures but also to identify shared genetic components between at first sight unrelated structures.

In this study, the *Hand2*-Cre mouse was used for the labelling of sentinel cell populations to study complex morphological processes as the outgrowth of the first branchial arch and the formation of the shoulder blade; the tracing of a defined cell subpopulations within a complex architecture allows to draw conclusions about the overall nature of the process. In the case of the first branchial arch, tracing the fate of the cell population originating from the distal part of the arch reveals that the arch grows according to a compartment-type model and that the distal domain performs an upward and inward rotation during the outgrowth process. The analysis of *dlx* expression domains in relation to the domain defined by the *Hand2* transgene by double and triple fluorescent RNA *in situ* hybridisations suggests that the outgrowth of the branchial arch occurs in a telescopic fashion most likely controlled by the nested expression of *dlx* genes along an ectodermal-endodermal axis.

The same *Hand*2-Cre transgene was then used for the tracing of the lateral plate mesoderm subpopulation associated with the limb to first identify a contribution of the proximal limb structures to the sternum, most likely corresponding to the 'lost' procoracoid of mammals, and second to reveal an interesting general property of the lateral plate mesoderm: although lacking overt segmented behaviour, the initial organisation of the scapula is strict and shows no mixing of cell populations from different embryonic origin. However, once the scapula is established as distinct element, this cellular coherence is apparently released, raising interesting questions about the underlying mechanistics.

Head, neck and shoulder region receive contributions from different embryonic cell populations. Although the boundaries between these different cell populations find no reflection in anatomical boundaries, these are far from random but follow a cryptic rule of ontogenetically preserved connectivity[102] (the 'connectivity rule'). Applied to muscles, the 'connectivity rule' signifies that the attachment and the connective tissue of a given muscle are of cells of the same embryonic origin, while the skeletal element to which the muscle attaches, is not necessarily so. This raises interesting questions how the first contact between the different cell populations is established and how it is then translated into a functional muscle attachment. In the case of the head/ shoulder interface, neural crest-derived muscles of the coracobranchial system attach to a mesodermal shoulder girdle[122]. High resolution imaging in combination with a genetic lineage tracer for neural crest shows that the neural crest provides a 'veneer' of cells on the mesodermal skeleton. This neural crest veneer then serves as muscle anchor point for the equally neural crest-derived coraco-branchial musculature, fulfilling the minimal condition of the 'connectivity rule'. The neural crest-derived muscle attachments in this region are limited to a single cell layer but located directly at the neural crest/ mesoderm interface; neural crest cells sometimes found deeper within the skeletal element at these sites probably reflect a later developmental stage[122].

Development proceeds through a series of increasingly refined patterning events. Although the patterns become more and more elaborated, the underlying gene regulation by which this is achieved does not necessarily so. It has been shown that the same transcriptional network can be re-employed as a morphogenetic tool in the most diverse contexts for entirely unrelated purposes (such as limb outgrowth and the patterning of butterfly wing spots by the transcription factor *distal-less*). This also appears to be the case for the transcription factor *Hand2* and its role in the arrangement of cellular layers, a mechanism that is responsible for the formation of structures as different as the myocardial epithelium[195], the oral ectoderm[208], the dental epithelium and even of dermal bone laminae. The work on the frontal bone presented in this study provides evidence that dermal bone formation does not occur spontaneously within the mesenchyme of the dermis as commonly suggested but is actually a highly organised process relying on the organisation of cellular layer by a control mechanism dependent on the transcription factor *Hand*2.

An evolutionary understanding of head and neck development will depend on the availability of truly comparative lineage labelling data sets in different species of

relevant phylogenetic relationship. In this context, the establishment of a generic reporter for Cre activity in *Xenopus tropicalis* represents an important step towards the accessibility of amphibian data sets, which will be of particular interest with regards to the evolution of the tetrapod middle ear. Considerable advances in both transgenic techniques and general husbandry will still be required before genetic lineage labelling in a model system like *Xenopus tropicalis* or zebrafish will be considered on a par with the mouse system. However, with the establishment of common platforms and resources like Xenbase, Zfin, the European *Xenopus* Resource Centre and the Zebrafish International Resource Centre truly comparative data sets in representatives of the entire gnathostome group will come within reach and help us to address the numerous unanswered questions of head, neck and shoulder development and evolution.

The work presented in this thesis clearly demonstrates the general value of transgenic systems and in particular of genetic lineage labelling as a technique. However, it also becomes clear that transgene behaviour needs to be carefully monitored in order to arrive at valid conclusions about endogenous gene function. As shown in this thesis, the *Hand*2-Cre transgene replicates endogenous *hand*2 expression in the branchial arches rather well at early stages (Figure 2.7 and Figure 6.1 A) but deviates considerably later on (Figure 2.8 and Figure 6.1 A). While the transgene never replicates *hand*2 expression in the lateral plate mesoderm nor the hindlimb, it shows aberrant activity in the forelimb most likely due to missing repressor elements (Figure 6.1 B- D). The difference of transgene behaviour in the limbs suggests that- although *hand*2 endogenously shows the same posterior restricted expression in both buds- *hand*2 expression is independently controlled in forelimb and hindlimb buds. In contrast, later *hand*2 expression domains (between E14 and E16) in dermal bone and in the dental epithelium (Figure 6.1 E and F) are rather well replicated by the *Hand*2-Cre transgene, placing necessary regulatory elements for these patterns within the -7.4kb *Hand*2 upstream region incorporated in the transgenic construct.

To our current understanding, gene expression is controlled by modular genetic elements with defined spatio-temporal activity; the overall gene expression pattern therefore results from the integrative activity of all regulatory elements for a given gene[51]. Regulatory elements can but do not have to be located in the vicinity to the gene they are controlling as long-range enhancers at a considerable distance from the transcription start site have been reported[133]. Against this background it is not surprising

Figure 6.1

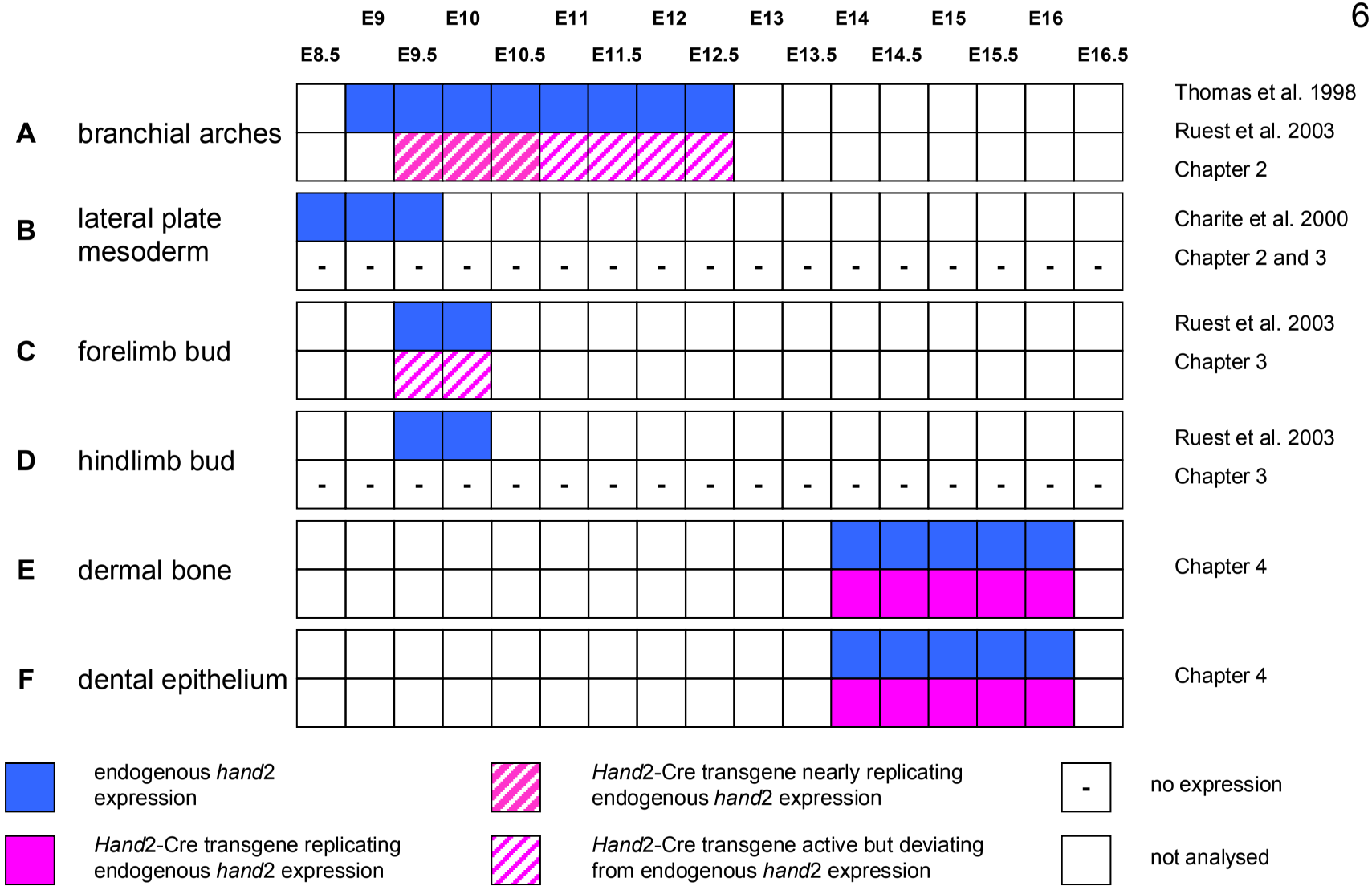
E9
E10
E11
E12
E13
E14
E15
E16
E8.5
E9.5
E10.5
E11.5
E12.5
E13.5
E14.5
E15.5
E16.5
A branchial arches
Thomas et al. 1998
Ruest et al. 2003
Chapter 2
B lateral plate mesoderm
Charite et al. 2000
Chapter 2 and 3
C forelimb bud
Ruest et al. 2003
Chapter 3
D hindlimb bud
Ruest et al. 2003
Chapter 3
E dermal bone
Chapter 4
F dental epithelium
Chapter 4
endogenous hand2 expression
Hand2-Cre transgene nearly replicating endogenous hand2 expression
no expression
Hand2-Cre transgene replicating endogenous hand2 expression
Hand2-Cre transgene active but deviating from endogenous hand2 expression
not analysed

Figure 6.1 Summary of *Hand*2 endogenous expression and *Hand*2-Cre transgene expression

Comparative overview of endogenous *hand*2 expression and the expression driven by the *Hand*2-Cre transgene in the anatomical regions covered by the work of this thesis between embryonic days 8.5 and 16.5: **A** branchial arches, **B** lateral plate mesoderm, **C** forelimb bud, **D** hindlimb bud, **E** dermal bone, **F** dental epithelium. Blue fields indicate endogenous *hand*2 expression, solid magenta fields indicates faithful replication of the endogenous *hand*2 expression pattern by the *Hand*2-Cre transgene, magenta background with white stripes indicates replication with slight deviation, white background with magenta stripes indicate *Hand*2-Cre transgene activity in the correct anatomical region but considerably deviating pattern, white fields marked with a minus ('-') indicate absence of gene or transgene activity and white fields indicate absence of data. If positive results were observed at two time points more than half a day apart, unchanged expression was assumed for the intercalated time points. On the right of the diagram, the data sources on which these reference points are based.

A The *Hand*2-Cre transgene replicates endogenous *hand*2 expression fairly well at early stages (E9.5- E10.5) but later deviates considerably (E11- E12.5).

B The *Hand*2-Cre transgene shows no activity throughout the lateral plate mesoderm although early endogenous *hand*2 expression has been reported here (E8.5- E9.5).

C Analysis at E9.5/ E10 reveals that the *Hand*2-Cre transgene shows activity throughout the forelimb bud in a way that deviates considerably from the endogenous *hand*2 expression pattern.

D The *Hand*2-Cre transgene shows no activity in the hindlimb bud; endogenously, *hand*2 is expressed at the posterior margin.

E Between E14 and E16, *hand*2 is expressed in dermal bone, this expression pattern is replicated by the *Hand*2-Cre transgene.

F *Hand*2 also shows a late expression domain (E14- E16) in the dental epithelium which is replicated by the *Hand*2-Cre transgene.

that the in comparison short stretch (7.4 kb) of *Hand*2 upstream region incorporated in the *Hand*2-Cre transgene is unable to replicate the complete endogenous *Hand*2 expression pattern faithfully, the more so as transgenes can be subject to position variegation effects at their (random) integration sites into the genome.

If the aim is to replicate endogenous gene activity as faithfully as possible, other approaches might therefore be better suited: Bacterial artificial chromosomes (BACs) can carry up to 200 kb of genetic region and have been successfully used for BAC transgenesis[120], not only increasing the likelihood of essential regulatory elements being present in the transgene but also preserving the endogenous architecture of the regulatory region. To protect the transgene from undesired positive and negative influences at the integration site into the genome, transgenes can additionally be flanked by so-called insulator sequences. Insulators have been identified in different species and are known to prevent genetic interaction between elements upstream and downstream of their location, which makes them a valuable molecular tool in transgenesis[15,16,22,68].

Gene-targeting as a further alternative technique makes it possible to insert a marker (such as an enzyme or a fluorescent protein) either at the place or in addition to a gene of interest. In principle, the marker is therefore subjected to exactly the same influences as this particular gene. While technically challenging, this approach can also affect the function of the gene to study, especially when the entire coding region of the gene is replaced, so care has to be taken in how far the resulting condition still reflects the wildtype situation.

With regards to genetic lineage labelling with the Cre/ Lox technique, faithful replication of the entire endogenous activity of a gene might however not be desirable in the first place, as overlapping but unrelated Cre expression domains (in the case of the *Hand*2-Cre transgene: distal branchial arch earlier and bone later, so that not only bone originating from the distal branchial arch is labelled) can interfere with a correct interpretation of the results. As shown in the work of this thesis, even a shorter regulatory region like the *Hand*2 upstream region shows surprisingly complex spatio-temporal activity. In order to be able to reliably trace cells originating from a temporal genetically defined domain with the Cre/ Lox system, it is therefore necessary to ensure that 1. gene and transgene expression are congruent within the time-window of interest and 2. Cre-activity is restricted to this very time-window. While the former can be achieved by the detailed comparison of gene transcript and Cre expression from the transgene by double RNA *in situ* hybridisation (see e.g. Chapter 2), the latter requires an

inducible form of Cre, as for example Cre-ER(T). In Cre-ER (T), the coding frame of Cre recombinase is fused to the estrogen receptor (ER) which renders the expression of the fusion protein Tamoxifen-dependent. The time-window of Cre expression during embryonic development is then controlled by the administration of Tamoxifen to the pregnant female at the appropriate age of gestation, which eliminates confounding effects from premature and/or reactivated transgene activity.
In case of the *Hand*2-Cre transgene, early branchial arch and late bone expression were distinguishable due to difference in levels of ß-Galactosidase in the cells which could point at a problem regarding the analysis of Cre/ Rosa26LacZR crosses by conventional X-Gal staining: While early reporter activation in the *Hand*2-Cre mouse led to ß-Galactosidase levels that were detectable by conventional X-Gal staining, late reporter activation could only be detected by sensitive immunohistochemistry. Conventional X-Gal staining after genetic lineage labelling with the Cre/Lox system in a Rosa26LacZR cross is therefore in all likelihood not suitable to study late developmental processes.

All transgenes and genetic modifications are by nature to some extent artificial; this makes detailed controls and a critical analysis of the obtained data essential before valid conclusions about endogenous gene function can be drawn. In conclusion, it can however be said that transgenes represent despite their limitations highly useful tools that allow us to tackle important developmental questions and will certainly provide us in the future with valuable insights into the mechanistics of the underlying genetic regulation.

7 Materials and methods

7.1 Table of Contents

7.2 *General Molecular Biology*

7.2.1 Plasmid propagation and purification

For propagation, plasmids were grown in chemically competent One Shot® TOP10 *E.coli* (Invitrogen C4040-10/03/06). Transformation was performed according to the manufacturer's protocol: cells were thawed on ice, 0.5- 5 µl ligation mixture added per vial of cells, incubated for 30 min on ice, heat-shocked for 30 sec at 42ºC followed by an incubation on ice for 2 min. After addition of 250 µl room- temperature S.O.C medium, cells were incubated in a 37ºC shaking incubator for 1 hour and plated on pre-warmed selective LB Agar plates. For Blue- White selection, 100 µl X-Gal was spread on the plate and allowed to dry before plating out the transformed cells. Plates were then incubated at 37ºC over night. The following evening, 6 ml LB selective medium were inoculated with a single colony and incubated in a 37ºC shaking incubator over night. Plasmids were routinely purified with Qiagen Miniprep (cat. 27106) or Maxiprep Kits (cat. 12163) according to the manufacturer's protocol without modification.

7.2.2 Visualisation of DNA and RNA fragments

All restriction digests, PCR results and RNA synthesis were routinely checked on standard 1% Agarose (Helena Biosciences) gels in 1X TAE containing 6% Ethidium bromide in 1X TAE buffer at 100-140 Volt. Fragments for purification were separated on 0.8-2% High Quality Agarose (Seakam) 1X TAE, 6% Ethidium bromide gels at 60 Volt.

7.2.3 Ladder Marker

As gel ladder marker for sizing of fragments a mixture of λ *Hind*III DNA and φ174 *Bsu*RI DNA (both Fermentas) with a final concentration of 0.2 mg/ml was used. Ladder maker fragments were sized as indicated below.

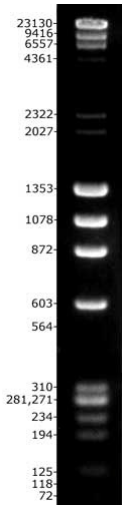

λ *Hind*III/ φ174 *Bsu*RI Ladder Marker

7.2.4 Restriction Digests and Ligation Reactions

Restriction Enzymes were mainly purchased from New England Biolabs. Standard digests for cloning were performed as 30 µl reactions in a 37ºC waterbath or incubator over night. Complete digestion was verified by gel electrophoresis on a standard 1% Agarose gel. Linearized backbone vectors underwent heat-inactivation of the restriction enzyme if possible (20 min at 65ºC or as indicated by the manufacturer) or column purification (Qiagen, QIAquick PCR purification Kit cat. 28106). Linearized plasmids were then de-phosphorylated by Shrimp Alkaline Phosphatase (Roche, Cat. 11758250001) for 3 hours at 37ºC, followed by heat-inactivation of 20 min at 65ºC or by rAPid Alkaline Phosphatase (Roche 04898133001) for 10 min at 37ºC and heat-inactivation of 2 min at 75ºC. Inserts were purified from High Quality Gels (Seakem) with the QIAquick Gel purification Kit (Qiagen 28706) and eluted from the column in RNAse/ DNAse free double-distilled water (Gibco).
Ligations were performed using the NEB Quick Ligation Kit (NEB M2200S or L) according to the manufacturer's protocol, with backbone to insert ratios of 1:0, (1:5), 1:10.

7.2.5 Restriction Digest by I-*Sce*I Meganuclease

I-*Sce*I Meganuclease was purchased from New England Biolabs (NEB). Digests with I-*Sce*I of were performed according to the conditions used for I-*Sce*I mediated transgenesis[144]: 200 ng of plasmid were incubated in 10 µl total volume with 1X I-*Sce*I buffer (supplied with the enzyme) and 0.5 U/ µl I-*Sce*I for 40 min at 37ºC.

7.2.6 Genomic DNA preparation

Genomic DNA for Polymerase chain reactions (PCR) was prepared from fresh tissue by the Phenol/ Chloroform extraction. Fresh tissue was incubated in 0.5 ml Tailing buffer (50mM Tris pH8, 100mM EDTA, 0.5% SDS, 100 mM NaCl) and 0.1 mg/ ml Proteinase K at 55 ºC over night in a shaking water bath, followed by 1:1 Phenol/ Chloroform and 1:1 Chloroform extractions. DNA was precipitated by Isopropanol, the pellet washed with 100% and 70% Ethanol and re-suspended in DNAse/ RNAse-free ddH_2O.

7.2.7 Target DNA amplification by Polymerase chain reaction (PCR)

7.2.7.1 Oligonucleotides

Oligonucleotides as primers for PCR reactions were designed with the Seqbuilder module of the DNAstar package. Primers were between 18 to 100 base pairs long with a balanced purine to pyrimidine content. In order to add new restriction sites or other features (such as LoxP sites or I-*Sce*I sites) to a fragment, so- termed 'recombinant' primers were designed. Recombinant primers consist of a primer part overlapping with the region to amplify and a non-overlapping or 'recombinant' part containing the desired features (such as restriction sites). Primers of this type will be referred to as 'recombinant primers' throughout this thesis. Oligonucleotides were routinely purchased from Operon/ Germany.

7.2.7.2 PCR amplification

All PCR amplifications were carried out on a Mastercycler Gradient (Eppendorf) as 20 µl reactions in thin-walled 0.2 ml stripe PCR tubes (Helena Biosciences). AmpliTaq®DNA Polymerase and buffers were purchased from Applied Biosciences (GeneAmp® PCR Reagent Kit N8010055) and dNTPs were from Roche (Cat.1277049). For the amplification of templates longer than 2kb, the Expand Long Template PCR System from Roche (Cat. 11681834001 or 11681842001) was used.
PCR products were analyzed for correct length on a 1% standard Agarose gel. Fragments of correct size were then purified from a High Quality Agarose gel (Seakam) with the QiaQuick Gel Purification Kit (Qiagen). Purified fragments were routinely sub-cloned into pCRII TOPO (Invitrogen) according to the supplier's protocol and verified for correctness by diagnostic digests and fully sequenced.

1. Standard PCR protocol for templates shorter than 2 kb

PCR reactions for fragments shorter than 2 kb were routinely performed as gradient PCRs with an annealing temperature ranging from 50-70ºC to empirically identify the optimum annealing temperature for a given primer pair.
One master mix was prepared on ice and divided into 12 reactions of 20 µl volume with final concentrations of 25 ng/ µl genomic DNA or 10 pg/ µl plasmid DNA, 500 µM dNTPs, 0.5 µM primer each, 2.5 mM Magnesiumchloride, 1X PCR buffer II and 0.125 U/ µl AmpliTaq®. Amplification from genomic DNA, especially with GC rich templates, sometimes yielded better results with 10 ng/µl gDNA plus 5% DMSO (instead of 25 ng/µl gDNA).

Protocol
Fragments were amplified according to the following protocol:
Initial denaturation: 2 min at 94ºC, followed by 30 cycles of [denaturation (30 seconds at 94ºC) – annealing (30 seconds at 60 +/- 10ºC in a gradient PCR) – extension (1 min per kb at 72ºC)] and a final extension step of 10 min at 72ºC and then kept at 4ºC until analysis.

2. Long Template PCR for templates longer than 2kb

Fragments longer than 2 kb and difficult templates were amplified with the Roche Expand Long Template PCR System in 20 µl reactions by gradient PCRs.
The Expand Long Template kit contains an enzyme blend of Taq DNA polymerase and proof-reading Tgo DNA Polymerase to allow the amplification of long templates with high fidelity (4.8×10^{-6} instead of 1.6×10^{-5} for Taq alone, Roche product description). The kit also provides a choice of three buffers, optimized for fragment length (Buffer 1: <12 kb with 17.5 mM $MgCl_2$; Buffer 2: 12-15 kb with 22.5 mM $MgCl_2$; Buffer 3: 15-20 kb with 22.5 mM $MgCl_2$, DMSO, and detergent).

Reactions were set up as master mixes on ice, with final concentrations of 25 ng/ µl genomic DNA or 10 pg/ µl plasmid DNA, 500 µM dNTPs, 0.5 µM primer each, 1X

Buffer 1-2-3 and 0.1875 U/ µl Taq/Tgo enzyme mix (0.75 µl Enzyme Mix (5 U/ µl) per 20 µl PCR reaction).

Protocol

Fragments were amplified according to the protocol recommended by Roche:
Initial denaturation: 2 min at 94ºC, followed by 10 cycles of [denaturation (10 seconds at 94ºC) – annealing (30 seconds at 60 +/- 10ºC gradient) – extension (1 min per kb at 68ºC)]; followed by 20 cycles of [denaturation (10 seconds at 94ºC) – annealing (30 seconds at 60 +/- 10ºC gradient) – extension (1 min per kb plus 20 additional seconds per cycle at 68ºC)] and a final extension step of 7 min at 72ºC. Reactions were held at 4ºC until analysis.

For subsequent cloning into pCRII TOPO, PCR fragments were gel purified as described above and polyadenylated with standard Taq DNA Polymerase (Applied Biosciences) (750 µM dATP, 1X PCR buffer, 2.5mM $MgCl_2$, 0.25 U/ µl Taq) for 15 min at 72ºC.

7.3 *Specific cloning projects*

7.3.1 Plasmids for RNA probes for RNA *in situ* hybridisation

Plasmids for the generation of RNA probes for RNA *in situ* hybridisations were generated by PCR from mouse genomic DNA, sub-cloned into pCRII TOPO and fully sequenced. The synthesis of the labelled RNA probe will be described in the section 'RNA *in situ* hybridisation' of this chapter.

RNA probe for gene	Plasmid	Primers	detecting
***Hand*1**	**pBR42**	**PrimBR62** **PrimBR63**	**last exon**
***Hand*2**	**pBR43**	**PrimBR65** **PrimBR66**	**last exon**
***Dlx*5**	**pBR44**	**PrimBR69** **PrimBR70**	**last exon**
***Dlx*3**	**pBR45**	**PrimBR67** **PrimBR68**	**last exon**
***Prrx*1**	**pBR47**	**PrimBR73** **PrimBR74**	**last exon excluding the region of similarity with prrx2**
Cre	**p187**	**PrimBR153** **PrimBR154**	**part of the coding frame of Cre recombinase**

7.3.2 Constructs for Xenopus transgenesis

7.3.2.1 The human Ubiquitin C promoter: plasmids p143, p144 and pSI_hUbC-DsRed2

1. Plasmid p143

The human Ubiquitin C promoter was PCR-amplified from human genomic DNA with the recombinant primers PrimBR96 and 97 (Figure 7.1) to add restriction sites for further cloning and the fragment sub-cloned into pCRII TOPO, resulting in plasmid p143. The promoter was sequenced along its entire length with the following primers: T7, PrimBR218seq, PrimBR19seq, TY4 and M13reverse (Figure 7.1 A indicates the positioning of the sequencing primers, primer sequences are listed in the appendix).

2. Plasmid p144

The hUbC promoter was released from p143 by a double restriction digest with *Sal*I and *BamH*I (restriction sites relevant for cloning are indicated in bold in Figure 7.1 C) and used to replace the original CMV promoter flanked by the same sites in pCMV-Venus, resulting in plasmid p144 (hUbC-Venus). The plasmid pCMV-Venus was a kind gift of R. Moon's laboratory and contains the coding sequence for Venus, an Enhanced Yellow Fluorescent Protein (EYFP) variant with additional mutations to increase brightness and stability of the fluorophore [131].

3. Plasmid pSI_hUbC-DsRed2

Replacement of the Venus coding region by the coding region for DsRed2 (Clontech, now discontinued) resulted in pSI_hUbC-DsRed2 (Figure 7.1 C, cloning performed by Shoko Ishibashi, E.Amaya's group).

Figure 7.1

A

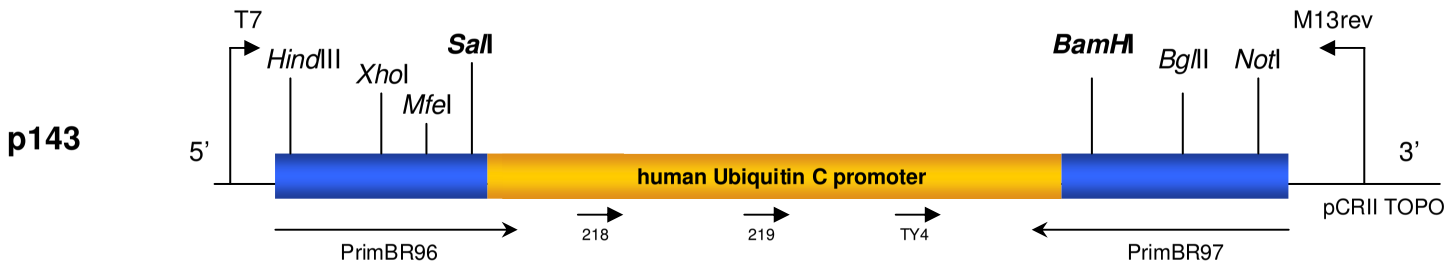

B

PrimBR96

HindIII *XhoI* *MfeI* *SalI*

5'tatccaagcttgtgtcgctcgagacaattgtcgacAGGCTCAGGGAGGT TGAAG **3'**

PrimBR97

NotI *BglII* *BamHI*

5'gcgttgcggccgcatatttgaagatctttcccgcggatccTGTCTAACAAA AAAGCCAAAAACGG **3'**

C

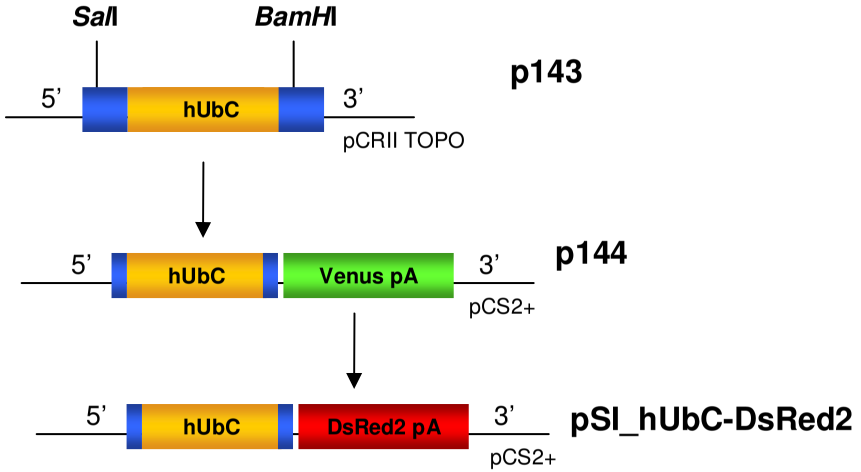

Figure 7.1 The human Ubiquitin C promoter

A The human Ubiquitin C promoter (hUbC) was amplified from human genomic DNA with recombinant primers PrimBR96 and 97 and subcloned into pCRII Topo (p143).

Primers were designed to amplify the sequence shown to drive ubiquitous expression in mice by Lois et al. (Science 2002, yellow box). Recombinant ends (blue boxes) for versatile cloning were added, restriction sites shown in bold indicate the sites that were used in this case. The alignment of recombinant primers and sequencing primers is indicated in.

B Sequence of recombinant primers PrimBR96 and PrimBR97 for fragment amplification by PCR. Restriction sites as annotated; overlap with genomic sequence in upper cases, recombinant part in lower cases.

C Plasmids used in *Xenopus* transgenesis to test the suitability of the hUbC promoter:
Insertion of the hUbC promoter (p143) upstream of Venus resulted in plasmid p144. Replacement of the coding region of Venus of p144 by the one of DsRed2 yielded plasmid pSI_hUbC-DsRed2.

7.3.2.2 Double fluorescent Cre-reporter plasmids pBR119, pBR120, pBR135, pBR139

1. Intermediate constructs pBR118 and pBR136: Red fluorescent proteins flanked by LoxP sites

In order to create a double fluorescent Cre-reporter, a floxed (flanked by LoxP sites) RFP cassette was introduced between the hUbC promoter and Venus of plasmid p144 (Figure 7.2). During the course of this study, a new RFP mutant, DsRed.T3, became available that showed increased brightness and faster maturation[17] than the widely used DsRed2 (Clontech). We therefore decided to test DsRed.T3 and DsRed2 in parallel in our double fluorescent Cre-reporter constructs to potentially enhance expression levels of the reporter. RFP cassettes were first generated as independent plasmids (pBR118 (DsRed.T3) and pBR136 (DsRed2)), fully sequenced and subsequently inserted into the *Bam*HI site of p144, eventually creating plasmids pBR119, pBR120, pBR135 and pBR139. To create floxed RFP cassettes, DsRed.T3 and DsRed2 including their downstream SV40 polyadenylation signals were amplified by recombinant PCR. PCR products were gel purified, sub-cloned into pCRII TOPO to yield plasmids pBR118 and pBR136 respectively and fully sequenced (Figure 7.2 A). Template plasmids for the PCR reactions were kind gifts of B.Glick (DsRed.T3) and S.Ishibashi (DsRed2 containing plasmid, originally Clontech). Flanking inverted LoxP sites were added with the recombinant primer pair PrimBR210 and 211 (Figure 7.2 B). As LoxP sites in forward orientation contain two start codons in different reading frames, the orientation of the LoxP sites in these primers was inverted.

2. Construct pBR119

Insertion of the floxed DsRed.T3 cassette from pBR118 into the *Bam*HI site of plasmid p144 resulted in the first double fluorescent Cre-reporter, pBR119.

Figure 7.2

A

pBR118

LoxP- **DsRed.T3** pA- LoxP

B

pBR136

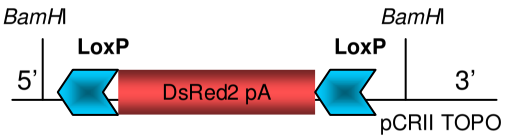

LoxP- **DsRed2** pA- LoxP

C

PrimBR210 *BamHI* **LoxP**

5' aaggatcc**ataacttcgtatagcatacattatacgaagttaat**cgccaccATGGCCTCCTCCGAGGACGT **3'**

PrimBR211 *BamHI* **LoxP**

5' ttggatccagatctgatatcg**attaacttcgtataatgtatgctatacgaagttat**ggtaccTTACGCCTTAAGATACATTGATG **3'**

Figure 7.2 Intermediate plasmids pBR118 and pBR136 with two floxed RFP variants.

Intermediate plasmids: pBR118 (**A**) and pBR136 (**B**).

PCR amplification of DsRed.T3 (for pBR118) and DsRed2 (for pBR136) with the recombinant primer pair PrimBR210 and 211 to add flanking inverted LoxP sites. Fragments were sub-cloned into pCRII TOPO and fully sequenced.

DsRed.T3 was a kind of gift by B.Glick, DsRed2 corresponds to the original Clontech version, kindly supplied by S.Ishibashi.

C Primer sequences for the primer pair PrimBR210 and PrimBR211. LoxP sites are indicated in bold and *BamH*I restriction sites are underlined.

To avoid the creation of artificial transcriptional start sites, LoxP sites were inverted as indicated by the direction of the arrows. Lower cases indicate the recombinant part of the primer, upper cases the overlap with the RFP coding region.

3. Construct pBR120, an I-*Sce*I Cre-reporter construct under control of a novel CMV'-hUbC fusion promoter

The double fluorescent Cre-reporter constructs pBR119 was adapted for I-*Sce*I-mediated transgenesis by addition of a 5' I-*Sce*I recognition site. Following recommendations by our collaborator, only one I-*Sce*I recognition site was introduced into the construct; in their experience, this led to higher success rates in transgenesis than transgenes with two flanking sites (personal communication, S.Ishibashi, Amaya laboratory). Simultaneously to the introduction of the I-*Sce*I recognition site into the construct, a novel fusion promoter was created by fusion of the immediate early element of the CMV promoter (designated as CMV' in this thesis) to the hUbC promoter with the aim to enhance promoter activity. Yew et al [213] had shown that fusion of this CMV' element to a different promoter (in their case, the human Ubiquitin B promoter) led to enhanced promoter activity without the silencing effects typically observed with the full-length CMV promoter (same publication). To be able to introduce the I-*Sce*I recognition site and to create the fusion promoter, the CMV' fragment described by Yew et al [213] was PCR-amplified from a plasmid containing the full-length CMV promoter with the recombinant primer pair PrimBR187 and PrimBR188 (Figure 7.3). The recombinant part of primer PrimBR187 encodes the recognition site for I-*Sce*I Meganuclease, indicated in bold in (B). The PCR product (I-*Sce*I- CMV') was sub-cloned into pCRII TOPO and named plasmid pBR108. Plasmid pBR120, the I-*Sce*I double fluorescent Cre-reporter under control of the CMV'hUbC fusion promoter was created by insertion of the I-*Sce*I-CMV' cassette from pBR108 (via *Sal*I) into the unique *Sal*I site of pBR119 (Figure 5.8).

4. Removal of the CMV' element and exchange of the RFP colour cassette creates two further Cre-reporter constructs, pBR135 and pBR139

After injection with construct pBR120, red fluorescence in transgenic *Xenopus tropicalis* embryos was initially strong but then became patchy and uneven during development. The CMV promoter was reported to produce the same type of very strong but patchy expression in *Xenopus* (H.Ogino, personal observation). As

Figure 7.3

A

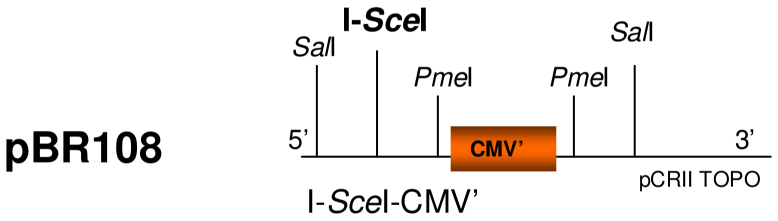

B

PrimBR187 5' agtcgac**tagggataacagggtaat**agtttaaacgcGTTACATAACTTACGGTAAATGG 3'

PrimBR188 5' agtcgacgtttaaacCATGGTAATAGCGATGACTAATACG 3'

Figure 7.3 Predicted enhancement of promoter strength of the hUbC promoter by fusion to an element of the CMV promoter (CMV').

A Yew et al. (Mol.Ther. 2001) showed in their publication that fusion of a part of the CMV promoter to a human promoter could enhance promoter strength without leading to the typically observed silencing of the transgene due to its viral origin.

The equivalent of the fragment used by Yew et al. was amplified by PCR from a plasmid containing the complete CMV promoter sequence and subcloned into pCRII TOPO (pBR108). Recombinant primers were designed to add a 5' I-*Sce*I site and flanking restriction sites.

B The recombinant primers used to add flanking *Pme*I and *Sal* sites for further cloning and a 5' I-*Sce*I site; restriction sites are underlined and the I-*Sce*I site marked in bold.

Lower case indicates the recombinant primer part, upper case shows overlap with the CMV element.

expression from the hUbC promoter alone had never been uneven in *Xenopus laevis*, the CMV' element from the reporter construct pBR120 was the most likely cause for the patchy fluorescence. The CMV' part of the fusion promoter of construct pBR120 was therefore removed by *Pme*I digest and re-ligation, which resulted in a second Cre-reporter construct, pBR135 (hUbC-LoxP-DsRed.T3-LoxP-Venus, Figure 5.8). Constructs pBR120 and pBR135 contain a new RFP variant, DsRed.T3[17] that to our knowledge had not been used in *Xenopus* transgenesis before. To exclude any toxicity effects of the new RFP variant as cause for the uneven fluorescence, the floxed DsRed.T3 cassette of plasmid pBR135 was exchanged against the DsRed2 cassette from plasmid pBR136 (Figure 5.8), creating a third I-*Sce*I Cre-reporter containing the commonly used RFP variant DsRed2, plasmid pBR139 (hUbC-LoxP-DsRed.T3-LoxP-Venus, Figure 5.8)

7.3.2.3 Cre-driving constructs under the control of *Xenopus* regulatory elements, pBR151 and pBR161

1. Plasmid pBR151, a Cre-driving construct under control of 2 kb *Xenopus* Hoxa2 upstream region

The cloning of plasmid pBR151 is shown schematically in Figure 7.4. 2kb of the *X. tropicalis Hox*a2 upstream region were by LTPCR from genomic DNA with the recombinant primer pair PrimBR179 and PrimBR180 (B) to add flanking restriction sites (5' *Asc*I site and 3' *Pme*I site), the amplified fragment gel-purified, sub-cloned into pCRII TOPO and named plasmid pBR109 (1). The *X. tropicalis Hox*a2 region (pBR109 cut with *Asc*I and *Pme*I) then replaced the *Asc*I- *Eco*ICRI fragment of an unrelated plasmid containing a VenusCre fusion protein and the desired 5' I-*Sce*I site (pBR145, (2)), resulting in the final plasmid, plasmid pBR151 (I-*Sce*I- *X. tropicalis Hox*a2- VenusCre).

2. Construct pBR161, a Cre-driving construct under control of the *Xenopus Hand*2 upstream region

All attempts to obtain the *X. tropicalis* 6kb *Hand*2 upstream region containing the sequence-conserved branchial arch enhancer by LTPCR failed. The region was therefore amplified in four separate but overlapping pieces (named A, BC, D and E, Figure 7.5 for a schematic view and the positioning of primers). Endogenous restriction sites (*Swa*I, *Nhe*I and *Bbs*I) were used to subsequently link up the fragments and re- build the 6kb *Xenopus Hand*2 upstream region as detailed below:

3. Amplification of the *Xenopus Hand*2 upstream region

Region A, BC, D and E were amplified from fresh *X. tropicalis* genomic DNA, gel-purified, sub-cloned into pCRII TOPO and extensively sequenced (Figure 7.5). Fragment A, a fragment of 1.8kb length, was amplified by LTPCR with the

Figure 7.4- 7.5

A

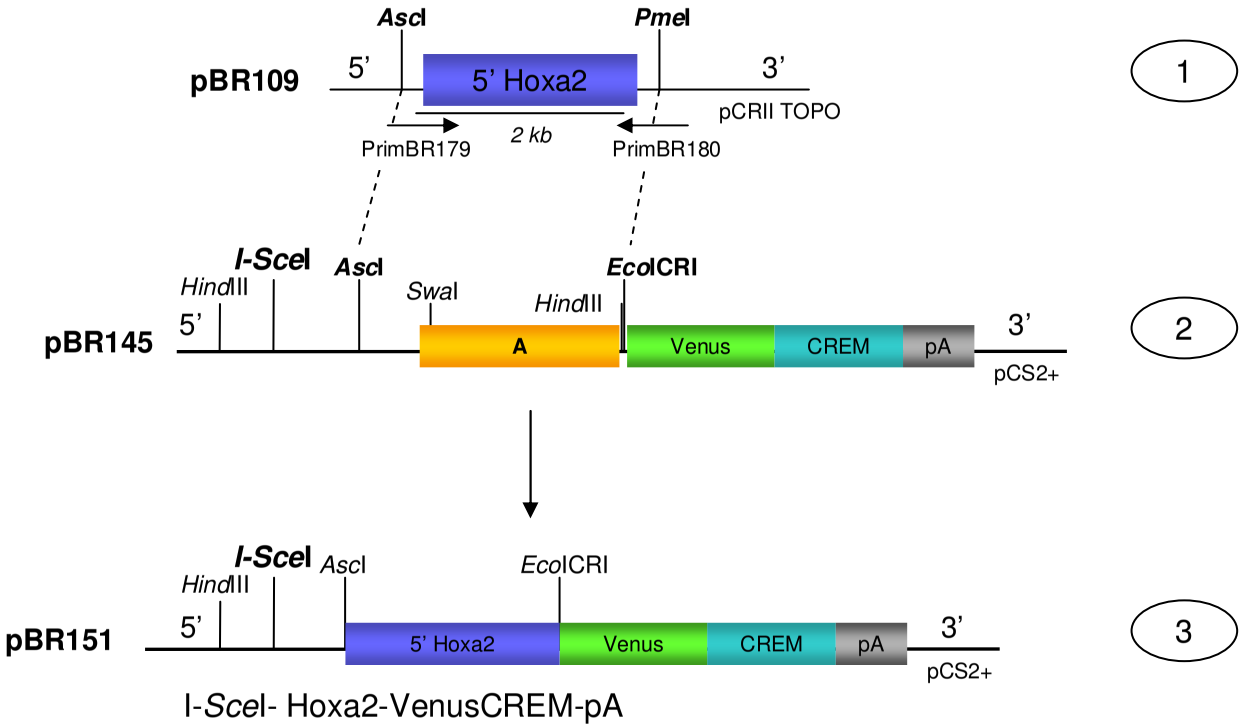

I-*Sce*I- Hoxa2-VenusCREM-pA

B

PrimBR179 5' aaaggtaccatttaaatggcgcgccttaattaaCATATTTTAATTCCCCGTTCTCACCTCTTG 3'

PrimBR180 5' aaaggtaccgtttaaacttaattaaTGGCCCTCTCCTCCAAGCCCTTTAAACAA 3'

Figure 7.4 VenusCre under control of 2kb *Xenopus tropicalis* Hoxa2 upstream region (construct pBR151)

A (1) 2 kb of *Xenopus* Hoxa2 upstream region were amplified by Long template PCR from genomic *X.tropicalis* DNA with the recombinant primer pair PrimBR179 and 180 to add sites for further cloning. The resulting fragment was subcloned into pCRII TOPO and named pBR109.

The Hoxa2 region was released by a double digest with *Asc*I and *Pme*I and cloned between the *Asc*I and *Eco*ICRI site of plasmid pBR145 (2), resulting in the final construct (pBR151), I-*Sce*I- Hoxa2-VenusCREM-pA (3).

B Recombinant primer pair PrimBR179 and PrimBR180. Lower cases indicates the recombinant part of the primer with underlined restriction sites. Upper cases represents overlap with the genomic sequence of the amplified fragment.

A

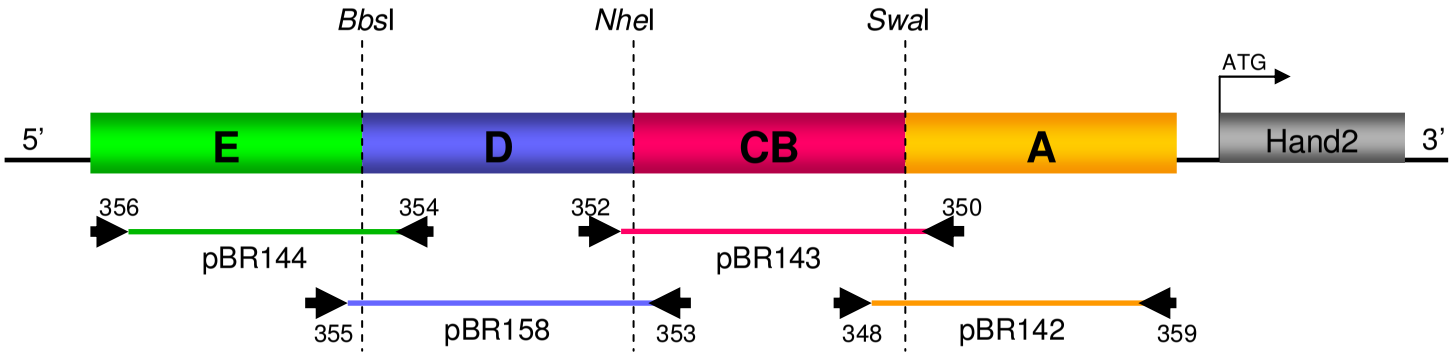

X.tropicalis scaffold 54: 1,282,055-1,285,108 forward strand

B

PrimBR348

*Hind*III **I-SceI** *Asc*I *Not*I

5' aaagctt**tagggataacagggtaat**ggcgcgccctcgaggcggccgcCATGGCATGTATGGGTAATAAAG 3'

PrimBR350

5' GATATTGGCACAACTGTATAGATGG 3'

PrimBR352

5' AGTGTAACCTGGCAACATATGGACTT 3'

PrimBR353

5' GTCCTTTAACATGGCTAATGTACCT 3'

PrimBR354

5' GCACTCTCTGATCTCCCTTCAAGCT 3'

PrimBR355

5' AGTTGTGAGTGGAGCTGCCCCATTA 3'

PrimBR356

5' ACAGCGCTGCGTACCCTTGTGGCGC 3'

PrimBR359

*Hind*III

5' ttaagcttGTCAGCTGGGCTTCCTGGCTAGTCTT 3'

Figure 7.5 The *X.tropicalis* Hand2 upstream region

A The Xenopus tropicalis Hand2 upstream region was amplified in four separate but overlapping fragments (A, BC, D, E) that span endogenous unique restriction sites (*Bbs*I, *Nhe*I, *Swa*I). The sequences of the oligonucleotides used for amplification is given in **B**.

Fragments were subcloned into pCRII TOPO, resulting in the intermediate plasmids pBR142, pBR143, pBR144 and pBR158, and fully sequenced.

The re-constitution of the upstream region to give the final Cre-driving plasmid pBR161 is depicted in Figure 7.4 and described in detail in text.

B All oligonucleotides with the exception of PrimBR348 and PrimBR359 were non-recombinant. PrimBR348 was designed to add 5' *Hind*III-I-*Sce*I-*Asc*I-*Not*I restriction sites for later use in I-SceI-mediated transgenesis and further cloning. PrimBR359 adds a 3' *Hind*III recognition site for subsequent cloning steps as described in Figure 7.4.

recombinant primer pair PrimBR348 and PrimBR359, introducing a 5' I-*Sce*I site for the final construct, and resulted in the intermediate plasmid pBR142. Fragment BC was 1.2kb long and amplified by LTPCR with the primer pair PrimBR352 and PrimBR350, resulting in the intermediate plasmid pBR143. Fragment D (2kb) was very difficult to obtain and finally amplified by LTPCR with the primer pair PrimBR355 and PrimBR353 by LTPCR. As no entirely correct fragment D could be obtained, two complementary partially correct clones were combined to yield the intermediate plasmid pBR158. Fragment E was 1.4kb long and amplified by standard PCR with the primers PrimBR356 and PrimBR354, resulting in the intermediate plasmid pBR144.

4. Generation of the *Hand*2-VenusCrem construct

The generation of the final *X. tropicalis Hand*2-VenusCrem construct pBR161 is schematically depicted in Figure 7.6:
Fragment A with recombinant ends was released by *Hind*III digest from the intermediate plasmid pBR142 (1a) and replaced the EF1 promoter of plasmid p279 (pXT_EF1-VenusCrem) (2a) to result in plasmid pBR145, A-VenusCrem (3a). Fragment CB from the intermediate plasmid pBR143 (4a) was then inserted into plasmid pBR145 as *Swa*I- *Not*I fragment, creating plasmid pBR146, CBA- VenusCrem (5). In parallel, fragment D from the intermediate plasmid pBR158 (1b) was released by double digest with *Bbs*I and *Eco*RV and inserted into plasmid pBR144 (fragment E in TOPO, 2b) linearized with *Bbs*I, resulting in plasmid pBR160 (ED, 3b). Fragment ED from plasmid pBR160 was then inserted as *Nhe*I- *Not*I fragment into the plasmid pBR146, 5' of CBA- VenusCrem (5) to yield the final construct pBR161 EDCBA-VenusCrem= *Xenopus Hand*2-VenusCrem (6).

Figure 7.6

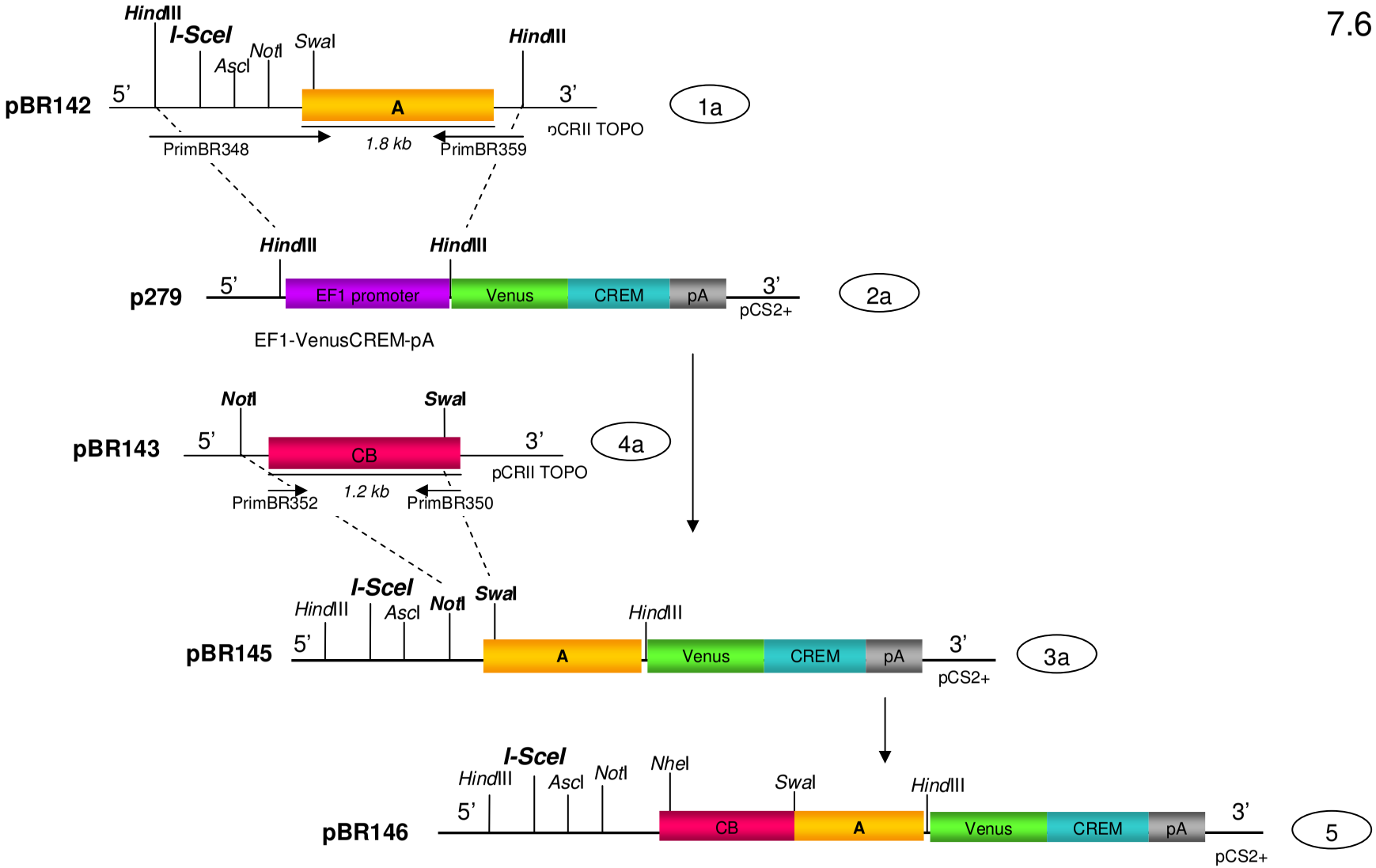
HindIII
I-SceI
AscI
NotI
SwaI
HindIII
pBR142
5'
A
3'
pCRII TOPO
1a
PrimBR348
1.8 kb
PrimBR359
HindIII
HindIII
p279
5'
EF1 promoter
Venus
CREM
pA
3'
pCS2+
2a
EF1-VenusCREM-pA
NotI
SwaI
pBR143
5'
CB
3'
pCRII TOPO
4a
PrimBR352
1.2 kb
PrimBR350
I-SceI
HindIII
AscI
NotI
SwaI
HindIII
pBR145
5'
A
Venus
CREM
pA
3'
pCS2+
3a
I-SceI
HindIII
AscI
NotI
NheI
SwaI
HindIII
pBR146
5'
CB
A
Venus
CREM
pA
3'
pCS2+
5

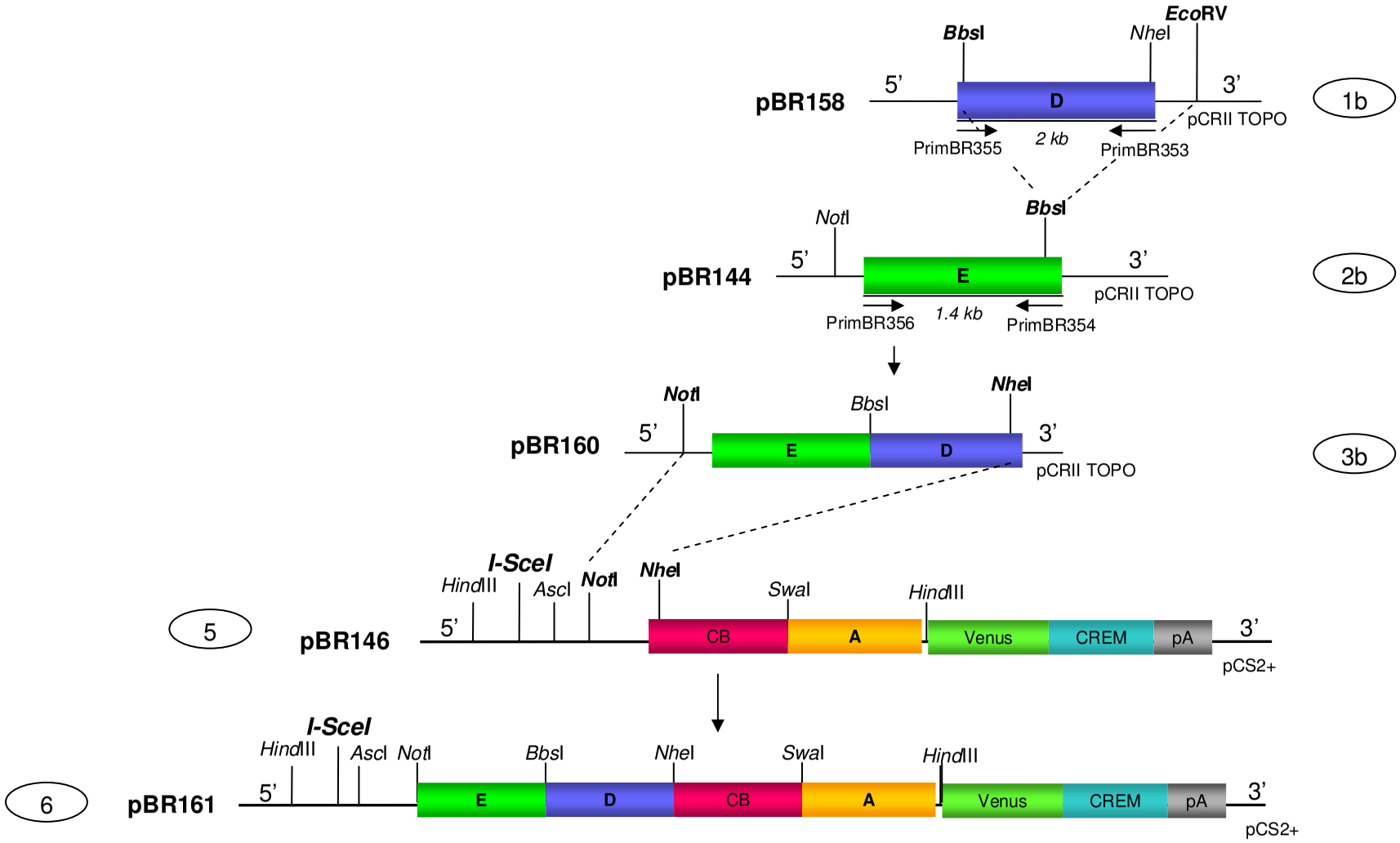

Figure 7.6 A Cre-driving construct under control of the *X.tropicalis* Hand2 upstream region, pBR161
For a detailed description, please see text.

7.4 Cell culture

7.4.1 Transient transfections in C2C12 cells

C2C12 cells were grown on fresh coverslips in 6 well plates in **D**ulbecco's **M**odified **E**agle **M**edium (DMEM) + 10% **F**etal **B**ovine **S**erum (FBS) at 37ºC under 5% CO_2. Transfections were performed at 50-60% cell confluency and plasmid expression was analysed 2 days later.

Reaction set- up

Reagent **A**:

The total amount of 1- 1.5 µg plasmid DNA was incubated with 100 µl Opti-MEM® (Invitrogen) for 30 min at room temperature.

Reagent **B**:

At the end of the incubation period for reagent A, 4.5 µl LIPOFECTAMINE (Invitrogen) was added to 100 µl Opti-MEM® and incubated for 5 min at room temperature, yielding reagent B.

Reagent **B** was added to reagent **A** and mixed carefully.

Transfection

After removal of the growth medium (DMEM +10% FBS) and a wash with pre-warmed PBS, the reagent mix **A+B** was added to 50- 60% confluent C2C12 cells. Cells were incubated at 37ºC for further 2 days before analysis to allow for sufficient protein synthesis.

Preparation for analysis

Coverslips with adherent cells were washed in PBS and stained with DAPI for 10 min. Coverslips were then mounted with Mowiol+ DABCO on glass slides, excess medium removed and coverslips sealed with nail varnish. The mounting medium was allowed to set and transfected cells analysed by confocal microscopy (Leica SP2). A plane in a representative area was scanned in sequential scanning mode to minimize bleed-through.

7.5 *Animal work*

7.5.1 Mouse work

7.5.1.1 Animal supply and husbandry

Transgenic and wildtype mice in a SV129/B6 background were held and bred under Home Office licence according to current legislation in the UK (Animals (Scientific Procedures) Act 1986). Embryos for analysis were collected after timed matings and the plug day was counted as embryonic day E0.
All genetically modified mice lines used for this study are established lines.
Transgenic *Hand*2-Cre mice expressing Cre recombinase under the control of 7kb upstream region of *Hand*2 have previously been described[158] and specimen and mice were kindly supplied by D. Clouthier/ University of Texas, Aurora/ US.
*Wnt*1-Cre mice for the labelling of neural crest cells have also been previously described[50] and were obtained from the Jackson Laboratories/US. Mice heterozygous for the *Hand*2-Cre transgene or the *Wnt*1-Cre transgene were interbred with Rosa26LacZ reporter mice, originally generated and described by Soriano[176], or Rosa26EYFP reporter mice[177]. Rosa26LacZR and Rosa26EYFPR are established reporter lines, mice were obtained from Jackson laboratories/ US and bred to establish reporter mice colonies. Specimen of *Hand*2 branchial arch enhancer knockout mice[211] were kindly provided by H. Yanagisawa/ UT Southwestern/ US. Specimen (torsos) of *Hand*2$^{fl/fl}$, *Wnt*1-Cre$^{+/-}$, Rosa26LacZR$^{+/-}$ mice[79] were also kindly provided by D. Clouthier.

Designation: Transgenic alleles are indicated with a minus (‘-‘), wildtype alleles are indicated with a plus (‘+’).

7.5.1.2 Genotyping

Genotyping to identify transgenic off-spring was performed by PCR with transgene-specific primers on genomic DNA isolated from ear punches or tissue isolated from embryos (for embedded material).

1. *HotSHOT genomic DNA extraction from ear punches for genotyping*

Genomic DNA for genotyping of pups was isolated from single ear punches with the HotSHOT technique[196] according to the following protocol:

1. 75 µl Hotshot alkaline lysis reagent (25mM NaOH, 0.2mM Disodium EDTA; pH12) was added to one mouse ear punch and incubated at 95º for 10- 60min.
To normalize for starting material, only one ear punch per reaction was used.

2. 75 µl Neutralizing reagent (40mM Tris-HCl (Sigma); pH5) was added per sample, giving a solution of neutral pH, and the reaction kept at 4ºC for 1 hr.

3. The final preparation was directly used for PCR (1-5 µl per 20 µl reaction) or stored indefinitely at -20ºC.

2. *PCR protocols for genotyping*

Genotyping for the Rosa26LacZR allele by PCR

Oligonucleotides for genotyping of the Rosa26LacZR allele are used as published[176] and named Sor1,2, and 3:

Sor1 5'-AAAGTCGCTCTGAGTTGTTAT-3'
Sor2 5'-GCGAAGAGTTTGTCCTCAACC-3'
Sor3 5'-GGAGCGGGAGAAATGGATATG-3'

Sor1 and 2 amplify a fragment of ~300bps from the transgene, while Sor1 and 3 amplify a 603 bps fragment from the wild-type allele.

A combination of Sor1,2,3 allows the distinction of wild-type, heterozygous and homozygous animals.

Set-up

PCR reactions were run as 20 µl reactions; per reaction 5 µl gDNA Hotshot preparation was used.
Final concentrations were: 0.5mM dNTP (Roche); 0.5µM Sor1, 0.5µM Sor2, 0.5µM Sor3 (all Operon); 2.5mM $MgCl_2$, 1X PCR buffer, 0.125U/l AmpliTaq® (Kit Roche), filled to 20 µl with DNAse/ RNAse free distilled Water (Utrapure™/Gibco).

Protocol

Initial denaturation	**20 sec at 94ºC**	
30 cycles of	**denaturation-**	**30 sec at 94ºC**
	annealing-	**30 sec at 61ºC**
	extension-	**30 sec at 72ºC**
final extension step	**10 min at 72ºC**	
Hold	**4ºC**	

PCR results were analysed on a 1.8% Agarose/ 6% Ethidium bromide gel.

Genotyping of the Rosa26EYFPR allele by PCR

Oligonucleotides for genotyping of the Rosa26EYFPR allele were:

Sor1 5'-AAAGTCGCTCTGAGTTGTTAT-3'
Sor3 5'-GGAGCGGGAGAAATGGATATG-3'

IMR4982 5'-AAGACCGCGAAGAGTTTGTC-3' (primer suggested by the Jackson Laboratories)

Sor1 and Sor3 amplify a 603bps fragment from the wildtype allele and Sor1 and IMR4982 amplify a 320bps band form the mutant allele.

Set-up

PCR reactions were set up identically to the ones for the Rosa26LacZ allele, with the only difference that the oligonucleotide Sor2 was exchanged against IMR4982.

Protocol

Initial denaturation	**20 sec at 94ºC**	
35 cycles of	**denaturation-**	**30 sec at 94ºC**
	annealing-	**30 sec at 68ºC**
	extension-	**30 sec at 72ºC**
final extension step	**10 min at 72ºC**	
Hold	**4ºC**	

PCR results were analysed on a 1.8% Agarose/ 6% Ethidium bromide gel.

Genotyping for the *Hand*2-Cre transgenic allele by PCR

Oligonucleotides for the genotyping of the *Hand*2-Cre transgene (after a personal communication of D. Clouthier) were:

TWCre1 5'-GCTGGTTAGCACCGCAGGTGTAGAG- 3'
TWCre3 5'-CGCCATCTTCCAGCAGGCGCACC- 3'

TWCre1 and TWCre3 amplify a band of ~ 500bps from the *Hand*2-Cre transgene.

Set-up

PCRs were run as 20 µl reactions; per reaction 2 µl gDNA Hotshot preparation was used. Final concentrations were: 0.5mM dNTP (Roche); 0.5µM TWCre1, 0.5µM TWCre3 (all Operon); 2.5mM $MgCl_2$, 1X PCR buffer, 0.125U/l AmpliTaq® (Kit Roche), filled to 20 µl with DNAse/ RNAse free distilled Water (Utrapure™/Gibco).

Protocol

Initial denaturation	**20sec at 94ºC**	
25 cycles of	**denaturation-**	**30sec at 94ºC**
	annealing-	**30sec at 68ºC**
	extension-	**30sec at 72ºC**
final extension step	**10min at 72ºC**	
Hold	**4ºC**	

PCR results were analysed on a 1.8% Agarose/ 6% Ethidium bromide gel.

Genotyping of the *Wnt*1-Cre transgenic allele by PCR

Oligonucleotides for the genotyping of the *Wnt*1-Cre transgene were (as suggested by the supplier, Jackson laboratories):

IMR0015	5' -CAAATGTTGCTTGTCTGGTG- 3'
IMR0016	5' -GTCAGTCGAGTGCACAGTTT- 3'
IMR1398	5' -CCTCTATCGAACAAGCATGCG – 3’
IMR1399	5' -GCCAATCTATCTGTGACGGC- 3’

Set-up

PCRs were run as 20 µl reactions; per reaction 2 µl gDNA Hotshot preparation was used. Final concentrations were: 0.5mM dNTP (Roche); 0.5µM IMR0015, 0.5µM IMR0016, 0.5µM IMR1398, 0.5µM IMR1399 (all Operon); 2.5mM $MgCl_2$, 1X PCR buffer, 0.125U/l AmpliTaq® (Kit Roche), filled to 20 µl with DNAse/ RNAse free distilled Water (Utrapure™/Gibco).

Protocol

Initial denaturation	**20 sec at 94ºC**	
30 cycles of	**denaturation-**	**30 sec at 94ºC**
	annealing-	**30 sec at 61ºC**
	extension-	**30 sec at 72ºC**
final extension step	**10 min at 72ºC**	

Hold **4ºC**

PCR results were analysed on a 1.8% Agarose/ 6% Ethidium bromide gel.

7.5.2 *Xenopus* work

7.5.2.1 Husbandry

X. laevis and *X. tropicalis* were housed and bred according to current UK Home Office regulations in the animal facility of the National Institute for Medical Research in Mill Hill and in the facility of the Biological Sciences at Warwick University after the move of the Koentges' group to Warwick University in 2005.

7.5.2.2 Transgenesis

7.5.2.2.1 Restriction Enzyme Mediated Integration (REMI) in X. laevis

Transgenesis in *X. laevis* was performed according to the REMI protocol by Kroll et Amaya[103] with omission of the restriction enzyme. Restriction enzyme can be omitted from the protocol if the sperm nuclei are already sufficiently 'damaged', this reduces later developmental defects. First experiments for testing of the human Ubiquitin C promoter in *X. laevis* were performed in collaboration by S.Ishibashi in the laboratory of E. Amaya, then Gurdon Institute. Later REMI injections (pBR151 and pBR161) were performed by E. Jones in her laboratory at Warwick University.

Plasmid preparation before injection

The transgene was released from its vector backbone by restriction digest over night and the fragments separated on a 0.8% High Quality Agarose gel (Seakam). The fragment containing the transgene was gel-purified with the Qiagen QIAquick Gel Extraction Kit (28706) according to the manufacturer's protocol. The eluted fragment was then precipitated with 1/10 volume of 3M Sodium acetate and 2 volumes of Ethanol (100%),

re- dissolved in RNAse/ DNAse free water and adjusted to a concentration of 100 ng/ µl for injection.

Transgenes were released as follows:

plasmid:		**digested with:**
pBR151	***Xenopus Hox*a2 VenusCrem**	***Asc*I, *Drd*I**
pBR161	***Xenopus Hand*2 VenusCrem**	***Xho*I, *Drd*I**
pBR162	**I-*Sce*I- hUbC-LoxP-DsRed.T3 pA-LoxP-Venus pA- I-*Sce*I**	**I-*Sce*I**

Injections

Fertile female *X. laevis* were primed the night before injections according to the following hormone schedule: 100 u FSH 7- 1 day before eggs were needed for injection, 600 u HCG 16 hours before injection, frogs were put in Bart X cooled to 4ºC and allowed to warm up to room temperature.

In preparation for the injection mix, sperm nuclei and egg extract were thawed on ice and the injection mix set up according to the following procedure:

1- 4 µl sperm nuclei and 250 ng linearized plasmid (c= 100 ng/µl) were gently mixed by tapping and incubated at room temperature for 5 min.
2- 18 µl room temperature SDB, 2 µl egg extract (4°C) and 2 µl 0.1M $MgCl_2$ were added, mixed very gently by tapping and incubated at room temperature for 10-15 min.
3- In parallel to the incubation, unfertilized eggs were collected from primed females and de-jellied in fresh 2% Cysteine Solution for 10 min at room temperature.
4- At the end of incubation, 5 µl injection mix were added with cut- off pipette tips to 100 µl SDB (room temperature) to yield the final injection solution. 13.8 µl volume were injected per egg, corresponding to on average 1 sperm nuclei per egg. Injections were preformed under a Zeiss dissecting microscope with a Drummond Nanoject and completed within 45 min.

Screening of embryos

Injected embryos were analysed daily under highest magnification under a Nikon fluorescent dissecting microscope between stage 20 and stage 40 in order not to miss the window of transgene expression.

Genotyping for successful transgenesis: DNA preparation and PCR

DNA preparation

Embryos past stage 40 were collected in single tubes for genomic DNA preparation and euthanized in MS222. The solution was replaced by 500 µl Tailing Buffer + Proteinase K [0.1 µg/µl] and specimen incubated at 55ºC over night. After Phenol-Chloroform extraction, genomic DNA was precipitated and re-eluted in DNAse/RNAse free ddH_2O.

Detection of the transgene (pBR151, pBR161) by PCR

A part of the coding frame for Cre recombinase of the transgenes pBR151 and pBR161 was amplified with oligonucleotides TWCre1 and TWCre3, yielding a band of 422 bps.

TWCre 1 5'- GCTGGTTAGCACCGCAGGTGTAGAG- 3'

TWCre 3 5' –CGCCATCTTCCAGCAGGCGCACC- 3'

Set-up

PCR reactions were run as 20 µl reactions with 200 ng genomic DNA as template. Final concentrations were: 0.5mM dNTP (Roche); 0.5µM TWCre1, 0.5µM TWCre3 (both Operon); 2.5mM $MgCl_2$, 1X PCR buffer, 0.125U/l AmpliTaq® (Kit Roche), filled to 20 µl with DNAse/ RNAse free distilled Water (Utrapure™/Gibco).

Protocol

Initial denaturation	**20 sec at 94ºC**	
25 cycles of	**denaturation-**	**30 sec at 94ºC**
	annealing-	**30 sec at 68ºC**
	extension-	**30 sec at 72ºC**
final extension step	**10 min at 72ºC**	
Hold	**4ºC**	

7.5.2.2.2 I-SceI mediated transgenesis in Xenopus tropicalis

I-*Sce*I mediated Transgenesis in *X. tropicalis* was performed in the laboratory of L. Zimmerman/ NIMR Mill Hill by the author according to the protocol by H. Ogino et al[143,143,144].

Principle

Plasmid DNA containing I-*Sce*I recognition sites is incubated with I-*Sce*I Meganuclease and subsequently microinjected into fertilized *X. tropicalis* eggs. The mechanism by which I-*Sce*I Meganuclease facilitates transgene insertion into the genome is not fully understood, but injections have to be completed within 45 min after fertilisation for successful transgenesis.

Preparation of plasmids for injection

Plasmids containing an I-*Sce*I recognition site were generated as described earlier (7.2)**.** A single I-*Sce*I site was reported to be more efficient than flanking sites (E.Amaya's lab, personal communication), therefore the plasmids for this study were designed with a single I-*Sce*I recognition site. Plasmid DNA was purified with the Qiagen Plasmid Maxi Kit (12163 or 12165), initially followed by Phenol/ Chloroform (Sigma) extraction and Ethanol precipitation. Phenol/ Chloroform extractions were later omitted as injection results after and without extraction did not differ in outcome (also confirmed by H.Ogino). The plasmid concentration was adjusted to 100 ng/µl in RNAse/DNAse free dH_2O (insert).

Preparation of female frogs before injection

Female *X. tropicalis* were primed with 15U HCG (Human Chorionic Gonadotropin) the afternoon before the injection and again with 100U HCG the following morning.
The day of the experiment, male *X. tropicalis* were euthanized in room temperature 0.2% Ethyl 3- Aminobenzoate Methanesulfonate pH7-8 (MS222 Sigma A-5040). Testes were dissected out and transferred into Leibovitz L-15 medium (Sigma L-4386); testes can be kept in Leibovitz medium for 1-2 days at 14ºC.

Once the females started laying eggs, the injection mix up was set up.

Injection Mix

Plasmid (final concentrations: plasmid 40 ng/µl) was mixed with 1X I-*Sce*I Buffer, 0.5 U/µl I-*Sce*I (New England Biolabs R0694)), incubated at 37ºC for 40 min and injected immediately at the end of the incubation period.

***In vitro* fertilisation and preparation for injection**

After the begin of the incubation period of the plasmid, male *X. tropicalis* were euthanized and testes dissected out. Testes were then homogenised in a 1.5ml microcentrifuge tube using a plastic pestle (Sigma, Z359947) in 1X MBS 0.1%BSA. Eggs were gently squeezed out of a female *X. tropicalis* into a Petri dish and fertilized with homogenized testes. Usually, ½- 1 testis was used for 600- 800 eggs. After 2 min, the fertilized eggs were flooded with 0.1X MBS and incubated at room temperature for 10 min.

Jelly coat removal

10 min after fertilisation, the 0.1X MBS was replaced with fresh 0.2% Cysteine (Sigma, C-7352) in 0.1X MBS pH8.0 solution and the embryos swirled until complete removal of their jelly coat (~ 5 min). De-jellied embryos were washed with copious amounts of room temperature 0.1X MBS to remove all Cysteine traces and placed in an injection dish in 0.1X MBS 6% Ficoll 400 (Fisher Scientific, BP525) pH7.5.

Injections

Set- up

All injections were performed with a Narishige IM 300 Microinjector and a Maerzhaeuser Micromanipulator under a Zeiss dissecting microscope.

Needles

Injection needles were made from Borosilicate glass capillaries (1.0 OD/ 0.75 ID Word Precision Instruments, TW100-4) on a Kopf Puller 750 (settings: 17-0-5-0.05-0.1) and broken with a pair of forceps to produce a sharp beveled tip with an outer diameter between 5- 10 µg. Needle shape is essential; fine sharp needles cause less damage to the embryo and lead to higher survival rates.

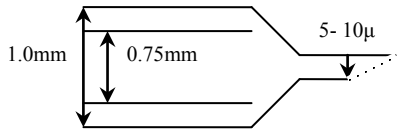

Per embryo, the total amount of 80 ng plasmid DNA was injected in a volume of 2 nl.

Further procedure

Cleaving eggs were sorted after 2 hour incubation at 22ºC and incubated at 22ºC over night in 0.1XMBS. Gastrulating embryos were sorted again the following morning; healthy embryos were cleaned daily and tested for transgene expression under a Zeiss fluorescence dissecting microscope at the appropriate time-point in development. Transgenic embryos were raised at 26ºC according to standard husbandry protocols for *X. tropicalis*. Essential for successful transgenesis is the initial incubation at the lowest possible temperature to slow down development sufficiently for plasmid integration.

7.6 *Staining techniques*

7.6.1 ß-Galactosidase staining

7.6.1.1 Whole mount staining

Freshly harvested embryos were fixed in fresh 4% buffered PFA for 30 min at 4ºC on a nutator, then rinsed twice with PBS, followed by a 5 min and a 25 min wash in Solution A (0.1M Phosphate Buffer pH7.4, 2mM Magnesium chloride $MgCl_2$, 5mM EGTA (all Sigma)). Solution A was replaced with Solution B (0.1M Phosphate Buffer pH7.4, 2mM Magnesium chloride $MgCl_2$, 0.01% Sodium Desoxycholate, 0.02% Nonidet (all Sigma)) and embryos incubated for 10 min at room temperature, followed by a 10 min incubation in pre-warmed Solution B at 37ºC. Solution B was replaced with freshly prepared Staining Solution C (pre-warmed Solution B plus 5mM Ferrocyanide, 5mM Ferricyanide and 1 mg/ ml X-Gal) and embryos stained over night at 37ºC in the dark. The next day, embryos were washed in pre-warmed Solution B for 10 min at 37ºC twice and postfixed in 4% PFA for further storage.
All washes and stainings were performed under gentle agitation to allow even staining.

7.6.1.2 Cryosections

All stainings on sections were performed on cryosections. Cryosections of unfixed tissue were fixed in fresh 4% buffered PFA for 10 min at room temperature, rinsed twice with PBS, followed by two 10 min washes in Solution A (as above) and 20 min in Solution B' (as above without detergents). Slides were then transferred into pre-warmed Solution B' and incubated for 10 min at 37ºC. Solution B' was replaced with Staining Solution C' (as above without detergents) and slides incubated over night at 37ºC in the dark. The next day, slides were washed in pre-warmed Solution B' for 10 min at 37ºC twice and postfixed for 30 min at room temperature with 4% PFA.
Slides were then rinsed with PBS twice and either mounted directly or counterstained for 2 min in Mayer's Hematoxylin (Sigma) followed by 2 min in Blueing Reagent

(Scott's Tap Water Substitute, Sigma) and then mounted in aqueous mounting medium (Mowiol (Calbiochem) or Hydromount (National Diagnostics)).

7.6.2 Calcein staining in *Xenopus tropicalis*

For the staining of bone, *X.tropicalis* tadpoles were allowed to swim freely in frog water with 50 µl/ ml Calcein (Sigma) for up to three days and transferred into fresh frog water half a day before analysis to remove unincorporated Calcein.

7.6.3 RNA *in situ* hybridisation

7.6.3.1 Collection and preparation of material

Mouse embryos

Time-mated pregnant females were culled by neck dislocation and embryos dissected in ice-cold PBS. After removal of all membranes, embryos were rinsed thoroughly in PBS and either directly embedded in OCT for sectioning or fixed over night in 4% buffered PFA at 4ºC on a nutator for whole mount procedures.

Sectioning

Specimen were sectioned on a Cryostat (Bright Instruments) and collected on Superfrost Plus (VWR) slides. Slides were left to dry for 20 min at room temperature and then stored at -80ºC indefinitely.

7.6.3.2 Double and triple fluorescent RNA *in situ* hybridisations on sections

Double and triple fluorescent RNA *in situ* hybridisations on sections were performed according to the protocol established in our group by Dr. X. Zhang (unpublished), based on previous protocols by Scharen-Wiemers, Gerfin-Moser and Josh Sanes.

7.6.3.2.1 Synthesis of RNA probes

RNA probes for *in situ* hybridisation were synthesized from linearized plasmids containing T7, T3 or SP6 phage promoters with the respective RNA Polymerases (Roche) for 2 hours at 37°C.

Plasmid preparation

5 µg plasmid were linearized with an enzyme producing a 5' overhang over night, purified with QIAquick PCR Purification Kit (Qiagen) and eluted in 50 µl DNA/RNA free ddH_2O (Gibco).

RNA synthesis

A 20 µl synthesis reaction was set up with 10 µl elute, 2 µl DIG/ FITC/ DNP labelling mix, 2 µl 10X Transcription Buffer, 2 µl T7/ T3/ SP6 Polymerase (> 20 U/µl, final concentration >2 U/µl) and 0.5 µl RNAseInhibitor (Roche, 40 U/µl, final concentration 1 U/µl) and incubated at 37ºC for 2 hours.

DIG and FITC labelling mixes were purchased ready-made from Roche. The DNP labelling mix was prepared with DNP-11-UTP (Perkin Elmer) and NTPs (Roche, 11277057001) as described by Denkers et al[53].

Successful RNA synthesis was checked on a fresh 1% Agarose gel with 1 µl of the reaction mix. RNA was then precipitated by adding 2.5 µl LiCl and 60 µl Ethanol 100% to the reaction and stored at -20°C over night. RNA was pelleted by centrifugation (20 min at 4°C), washed with 60% Ethanol, air- dried and re-eluted in 50 µl DNA/RNAse free dH_2O (Gibco). Aliquots were stored at -80°C.

7.6.3.2.2 Probes for RNA in situ hybridisation

The following plasmids were used for the generation of RNA probes for the work of this thesis:

probe for gene	plasmid	linearized with	Polymerase
***Barx*1**	**IMAGE8733796**	***Not*I**	**T3**
***Brn*1**	**plasmid kind gift M. Bouchard**	***Sph*I**	**Sp6**
Cre	**p187**	***Xho*I**	**Sp6**
***Dlx*3**	**pBR45**	***Hind*III**	**T7**

***Dlx*4**	**plasmid kind gift of Kawasaki**	***Eco*RI**	**T7**
***Dlx*5**	**pBR44**	***Bam*HI**	**T7**
***Dlx*6**	**pDCDlx6, kind gift of D.Clouthier**	***Spe*I**	**T7**
***Fox*c2**	**IMAGE5308620**	***Age*I**	**T7**
Gsc	**IMAGE3973720**	***Xho*I**	**T3**
***Hand*1**	**pBR42**	***Bam*HI**	**T7**
***Hand*2**	**pBR43**	***Bam*HI**	**T7**
***Msx*1**	**IMAGE4923403**	***Bam*HI**	**T7**
***Pitx*1**	**IMAGE4192818**	***Age*I**	**T7**
***Prrx*1**	**pBR47**	***Bam*HI**	**T7**

7.6.3.2.3 RNA in situ hybridisation

Day 1

Sample preparation

Slides were fixed with 4% PFA in PBS for 10 min at room temperature, followed by 3 washes with PBS for 3 min each. Slides were acetylated in 5.57g Triethanolamine HCl, 536 µl 12.5NaOH, 295 ml dH_2O, 750 µl Acetic Anhydride for 10 min at room temperature, followed by 3 washes with PBS for 5 min each.

Pre-Hybridisation and Hybridisation

Slides were incubated horizontally in a humidified chamber covered with 500 µl Pre-Hybridisation Solution (Hybridisation Solution without probe) for 2 hours at room temperature.

The Pre-Hybridisation Solution was replaced with Hybridisation Solution containing 200- 400 ng/ml DIG- or/ and FITC- or/ and DNP-labeled RNA probe per gene of interest. Probes had been first heated to 80ºC for 4 min and then iced. Slides with Hybridisation solution were coversliped and incubated in a humidified (50% Formamide 5X SSC) hybridisation chamber in a hybridisation oven at 68- 72ºC over night. To avoid cross- contamination, slides with different probes were placed in separate hybridisation chambers.

Day 2

Post-Hybridisation washes

All washes were performed in clean glass jars. Coverslips were briefly removed in 5X SSC pre-heated to hybridisation temperature. Slides were washed twice in pre-heated 0.2X SSC for 30 min at hybridisation temperature, followed by a 5 min 0.2X SSC wash at room temperature.

***Immunological staining**

Slides were placed horizontally and incubated with Solution B1 for 5 min.

B1 was replaced with B2 (Blocking solution, B1 + 10% FCS) and slides incubated at room temperature for at least 1 hour. B2 was replaced with 500 µl B2 plus first antibody

(anti-Fluorescin- POD (Jackson), anti-DIG-POD (Roche), anti-DNP-POD (Perkin Elmer) and slides incubated at 4ºC over night in a humidified chamber.

Day 3

Slides were washed with B1 for 30 min at room temperature for three times.
For tyramide amplification, per slide 3.2 µl Fluorescin/Cy3 /Cy5 conjugated tyramide was diluted in 200 µl 1X Plus Amplification Solution (Perkin Elmer) and the slides incubated at room temperature. Optimal incubation time depended on the probe but usually ranged from 30 min to 2 hours. POD activity was subsequently quenched with 0.01N HCL for 10 min at room temperature.
Slides were washed with B1 for 3 min at room temperature for three times.
For double labelling, the protocol was repeated from the Immunological staining of Day 2 (*) for the second antibody. Usually, probes were developed in the following order: anti-FITC with Fluorescin, anti-Dig with Cy3 and anti-DNP with Cy5.

Counterstain with DAPI

Sections were counterstained with DAPI ($7x\ 10^{-4}$M, 1:1000 in B1) for 5 min at room temperature and then rinsed in dH_2O several times.

Mounting and Storage

Slides were blotted sidewise on paper towels to remove excess water and mounted with 3 drops Mowiol. Once the mounting medium was set, slides were sealed with nail varnish and stored at 4ºC in the dark.

Solutions

PFA

4% Paraformaldehyde in PBS pH7, stored at -20ºC

PBS (Sigma, P4417)

137 mM NaCl **,** 2.7 mM KCl **,** 4.3 mM Na_2HPO_4, 1.47 mM KH_2PO_4, adjusted to a final pH of 7.4

Hybridisation Solution

50% Formamide, 5X SSC, 5X Denhardt's, 250 µg/ ml E.coli (or other) tRNA, 500 µg/ ml herring sperm DNA, stored at -20ºC

SSC 20X stock solution

3.0M NaCl, 0.3M Sodium Citrate

Denhardt's Solution 50X

1% w/v Ficoll 400, 1% Polyvinylpyrrolidone PVP, 1% BSA, stored at -20ºC

B1

0.1M Tris pH7.5, 0.15M NaCl

B2

B1 plus 10% heat inactivated fetal calf serum (FCS)

Mowiol Mounting medium

6g Glycerol (Sigma G-6279), 2.4g Mowiol 4-88 (Calbiochem), 6 ml ddH_2O, 12ml 0.2M Tris Buffer pH8.5

Glycerol, Mowiol and water were slowly mixed on a stirring plate at room temperature for at least three hours. 12 ml 0.2M Tris Buffer pH8.5 were added, the mixture covered with Aluminium foil and stirred at low speed over night on a warm plate. The next morning, the mixture was incubated at 55ºC for 10 min, followed by centrifugation in 50ml Falcon tubes at 5000g and room temperature for 15 min or until the supernatant was clear.

Cleared supernatant was carefully removed and frozen at -20ºC after addition of 2.5% w/v DABCO (1,4-diazobicyclo-[2.2.2]-octane, Sigma) as anti-fade reagent.

7.6.4 Immunohistochemistry

Immunohistochemistry (IHC) was routinely performed on cryosections of material embedded in OCT (Optimal Cutting Temperature) compound according to the standardized protocol below. Newborn specimen and embryos older than E18 were fixed in 4% PFA for 1 hour, rinsed in PBS and equilibrated in an increasing series of Sucrose solution (25% and 40%) before being embedded in OCT compound.

7.6.4.1 Protocol

All IHC stainings were performed following the same protocol: Sections were defrosted and fixed for 10 min at room temperature with fresh PFA (4% in PBS). After 3 rinses with PBS, sections were blocked for at least 1 hour at room temperature in Blocking solution (3 parts Maleic Acid Buffer MAB, 1 part Fetal Bovine Serum FBS, 1 part Roche Western blocking solution, 0.01% Triton and 0.25% H_2O_2 if later POD amplification was used). Sections were then incubated over night at 4ºC with one or more primary antibodies in Blocking solution without H_2O_2. The following day, sections were washed with TBST plus 5% FBS for at least 2 hours with frequent changes and then incubated for 1 hour at room temperature with the secondary antibody in Blocking solution. Slides were washed for another 1- 2 hours with TBST before either tyramide signal amplification (only used for the detection of ß-Galactosidase) or DAPI/ Phalloidin counterstaining. Tyramide signal amplification (Perkin Elmer Kit) was carried out with 5 µl Cy3/5/Fitc conjugated tyramide in 500 µl Ampli-Buffer. After several washes with PBS, sections were counterstained with 1:1000 DAPI and/ or 1:250 Rhodamine-Phalloidin (Chemicon) and mounted with Mowiol.

7.6.4.2 Antibodies

Primary antibodies

Antigen/ species	Dilution	Source/ Reference
Periostin (rabbit)	1:100	Abcam/ ab14041
Col14A1 (mouse)	1:1000	Abnova/ 5F3
Decorin (mouse)	1:1000	Abcam/ ab54728
CRABP1 (mouse)	1:1000	Abcam/ ab2816
Collagen III (mouse)	1:4000	Abcam/ ab6310
Collagen I (rabbit)	1:1000	Abcam/ ab59435
Collagen I (rabbit)	1:100	Abcam/ ab21286
EphA4 (goat)	1:50	R&D/ AF641
RFP (rabbit)	1:2500- 5000	Abcam/ ab62341
*Hand*2 (goat)	15:1000	R&D/ AF3876
Cre (mouse)	1:500- 1000	Abcam/ ab24607
b –Galactosidase (chick)	1:100	Abcam/ ab9361
ZO1 (mouse)	1:40	Hybridoma/ R26.4C
Fibronectin (rabbit)	1:400	Sigma/ F3648
Vinculin (mouse)	1:100	Chemicon/ MAB3574
Laminin (rabbit)	1:100	Sigma/ L9393

Secondary antibodies

Antigen/ species	Dilution	Source/ Reference
a- rabbit 488	1:200	Jackson
a- rabbit Cy5	1:200	Jackson
a- mouse 488	1:200	Jackson
a- chick POD (goat)	1:5000 *	Abcam/ ab6877

* note: same volume of glycerol was added to the antibody upon arrival and the antibody stored at -20ºC, so this would be a dilution of 1:10 000 from the original batch

7.7 *Imaging and image processing*

7.7.1 Confocal microscopy

The confocal images presented in this thesis were acquired on a SP2 Leica and a SP5 Leica laser scanning confocal microscope with objectives ranging from 5x to 100x magnification. Signal in the blue, green, red and infrared channel were acquired with the standard scanning settings provided by the manufacturer. Fluorophores used were DAPI, FITC, Cy3, Cy5 for Fluore*sce*nt RNA *in situ* hybridisations, in addition to Alexa488 and Alexa555 for Immunohistochemistry.
Images were acquired as stacks of optical sections (z- stacks) and collapsed in either average or maximum projection.

7.7.2 Image processing

Images of collapsed z-stacks or single optical planes were processed with the Adobe Photoshop Software. The original grey confocal images were colour-coded and images from different channels superimposed. If necessary, brightness and contrast were adjusted, adjustments were always linear and applied to the entire plane of the image.

7.7.3 Image annotations

For images acquired under a dissecting microscope (fluorescent and brightfield), the magnification is indicated. For images acquired by confocal microscopy, a scale par is provided.

7.8 *Software*

7.8.1 Identification of evolutionary sequence conserved regions with the Regulatory Module Graphical User Interface (ReMoGui)

The ReMoGUI (short for Regulatory Module GUI) is a powerful multiple alignment tool developed by S. Ott in the group of G. Koentges for the identification of potential regulatory modules as short stretches of evolutionary conserved sequence in the proximity of genes that are often missed by other common alignment tools such as BLAST.

To identify potential regulatory modules of a gene of interest, the upstream regions (or gene regions or downstream regions) of the homologous gene from other species are compared by the generation of optimal alignments of sliding windows of 100 bps sequence stretches (step width 5bps) that are scored according to the Needleman-Wunsch algorithm. Scores above 60 were considered significant (the likelihood of a score of 60 is 1:1 Million when aligning non-random 100meres).

7.8.2 Sequence alignment and construct design

Simple sequence alignments were performed with Bioedit or the multiple alignment tool (MegAlign) of the Lasergene® software packet (DNAstar). SeqMan and SeqBuilder of the same packet were used for the design of primers and constructs.

8 Acknowledgments

This work would not have been possible without the support of many and I would like to thank in particular
my supervisor, Georgy Koentges, who introduced me to developmental and evolutionary biology and from whom I learned attention to detail, the importance of quality and to look for the unexpected. My secondary supervisor, Elisabeth Jones, for her enthusiasm and contagious dedication to research and her organisational skills. Thanks for the time you invested in me, for your moral and scientific support- including the testing of my last Cre-driving constructs in *Xenopus laevis*. Thank you for all your helpful comments on my thesis, I have learned a lot. My graduate tutor, Julie Olszweski, for being such a wonderful tutor, for good advice and all your support. A particular thanks for organising my viva! My former graduate tutor, Giti Garthwaite, for telling me a few things I did not want to hear but am still thinking about.

I would also thank our collaborators who were all generous and helpful, namely:
Our first collaborator for work in *Xenopus laevis*, Shoko Ishibashi, in E. Amaya's laboratory, then Gurdon Institute Cambridge, for her skilled injections of my first transgenes. It was a pleasure to work with you, Shoko.
Our collaborators for work in *Xenopus tropicalis*, Lyle Zimmerman, for letting me work in his lab and his infinite knowledge about amphibians. The Zimmerman lab, in particular Michael Reilly, for their technical support and for being such a nice group.
Rob Grainger, for letting me visit his lab to learn about I-*Sce*I mediated transgenesis and all the knowledgeable people in his group whose advice was extremely valuable.
Darius Balciunas, for testing my *Xenopus Hand*2 construct in zebrafish and giving me the permission to use his images in my thesis.
David Clouthier for sending me specimen (*Hand*2-Cre and *Hand*2$^{fl/fl}$;*Wnt*1-Cre;Rosa26LacZ) and mice (*Hand*2-Cre); Hiromi Yanagisawa for sending me specimen (*Hand*2 BAenh$^{-/-}$) and both of them for friendly and helpful communication.
The many people, who was so generous to share their plasmids and reagents with me.

The Koentges' lab for many interesting discussions and the old times in London. In particular Xintao Zhang, for her wonderful triple fluorescent *in situ* protocol, for her version of the VenusCre fusion protein and the images of her control experiments and many stimulating scientific discussions. Keith Vance and Danuta Jeziorska for help with the cell culture experiments. Sascha Ott for the ReMoGui and many helpful discussions about gene regulation. Kate Jordan for continuing to work on my project. Tomoyuki Mitsumori for helping with cloning of some of the early constructs.

Everyone involved in the big collaborative project about bone development and muscle attachment sites- Georgy Koentges, Kate Jordan, David Clouthier and Hiromi Yanagisawa from the biological side, Per Ahlberg, Sophie Sanchez, Kate Trinajstic, Paul Tafforeau and Lovisa Wretman from the palaeontological side-, our discussions in the preparation for the paper helped me to sharpen my argumentation and to arrive at a better understanding of my own data.

My particular thanks goes to Per Ahlberg, for his integrity and generosity, all his intellectual, scientific and moral support and a new perspective which made all the difference.

Many people in technical and scientific support for looking after my transgenic animals, help with imaging, prompt sequencing and many other services. In particular I would like to thank Jacques' team at the Wolfson Institute for Biomedical Research, UCL, and Sam Dixon, Ian Bagley and Paul Jarrett, Syrinda Baghram, Helen Brown and Susan Slade at the University of Warwick.

My family without whom I would not be standing here. My parents who always believed in me. My siblings who always sided with me.

My particular thanks go to Peter Dieter Schoonjans to whom this thesis is dedicated and who shared with me the best and worst moments of the last few years. Thanks for believing in me and never stopping to support and encourage me. Not to mention the IT support and the insistence on taking backups! And Julia and Louisa Schoonjans for having such a lot of patience with their Mum and for being able to lighten up the worst day!

9 Appendix

Head and neck muscles 1	Innervation	Origin			Insertion			Comment
		CT	M	B	CT	M	B	
1st arch	V							
M.temporalis	V	-	-	-	+	-	+	
M.massentericus	V		-		+	-	+	
M.pterygoideus medialis	V	-	-	-	+	-	+	Gradient of positive CT
M.pterygoideus lateralis	V	-	-	-	+	-	+	
• Upper head	V	-	-	-	+	-	+	
• Lower head	V	-	-	-	+	-	+	
M.tensor tympani	V	-	-	-	+	-	+	
M.tensor veli palatini	V	-	-	-	-	-	-	
M.mylohyoideus	V	+	-	+	+	-	(+)	
M.digastricus Venter anterior	V	+	-	+	+	-	(+)	
2nd arch	VII							
Mimic muscles/ platysma	VII	+ or -	-	/	+/-	-	/	depending on location either positive or negative, the boundary can be within the muscle
M.stapedius	VII	-	-	-	-	-	-	
M.stylohyoideus	VII	+	-	+/-	+	-	+/-	styloid process negative with single positive cells but surrounded by positive connective tissue
M.digastricus Venter posterior	VII	+/-	-	+/-	+	-	+	styloid process negative with single positive cells but surrounded by positive connective tissue

Head and neck muscles 2	Innervation	Origin			Insertion			Comment
		CT	M	B	CT	M	B	
Infrahyal Muscles								
M.sternohyoideus		+	-	+	-	-	+[1]/-	1 connective tissue on the muscle outside is positive, in the muscle inside negative
M.sternothyroideus		+	-	+	-	-	+[1]/-	1 connective tissue on the muscle outside is positive, in the muscle inside negative
M.thyrohyoideus		+/-	-	+/-	+/-	-	+/-	1 connective tissue on the muscle outside is positive, in the muscle inside negative
M.omhyoideus		+/-	-	+/-	+/-	-	+[1]/-	1 connective tissue on the muscle outside is positive, in the muscle inside negative
Tongue extrinsic								
M.genioglossus	XII	+	-	+	+	-	+	
M.hyoglossus	XII	+	-	+	+	-	+	
M.chondroglossus		+	-	+	+	-	+	
M.styloglossus	XII	+	-	+/-	+	-	+	styloid process negative with single positive cells but surrounded by positive connective tissue
M.palatoglossus	IX,X, XI	+	-	+	+	-	+	
Others								
M.geniohyoideus	XII	+	-	+	+	-	+	
M.stylopharyngeus	IX	+[2]	-	(+)[1]	+	-	+	1-Styloid composed of labeled and unlabeled cells, surrounding CT labeled with the exeption of the side facing the cranial base 2 CT labeled throughout muscle
M.salpingopharyngeus	IX, X	-	-	-	-	-	-	

Shoulder muscles	Innervation	**Origin**			**Insertion**			**Comment**
		CT	M	B	CT	M	B	
ventral								
M. pectoralis major	Nn pectorales med et **lat** (Plexus brachialis)	+	-	sternum + clavicul a -	+	-	+	
M. pectoralis minor	Nn pectorales **med** et lat (Plexus brachialis)	+	-	ribcage – but CT +	+	-	+	
M. subclavius	N.subclavius (Plexus brachialis)	clavicu la +	-	+	+	-	rib – but CT +	
M. sternocleidomastoideus	XI, Plexus cervicalis	-	-	-	n/a		n/a	labeling varies according to insertion point: no CT labeling close to clavicula, labeling in the CT close to sternuM.
Pars clavicularis		n/a		n/a	-	-	-	
Pars sternalis		n/a		n/a	+*	-	+	
lateral								
M. deltoideus	N. axillaris	+	-	+	+	-	+	
Pars clavicularis		+	-	+	+	-	+	
Pars acromialis		+	-	+	+	-	-/+	
Pars spinalis		+	-	+	+	-	+	
M. supraspinatus	N.suprascap ularis (Plexus brachialis)	+	-	+	+	-	+	
dorsal								

M. infraspinatus	N.suprascapularis (Plexus brachialis)	+	-	+	+	-	arm +	
M. teres minor	N.axillaris	+	-	+	+	-	arm +	
M. teres major	Nn subscapulares	+	-	+	+	-	arm +	
M. latissimus dorsi	N.thoracodorsalis (Plexus brachialis)	+	-	+	+	-	arm +	
dorsal anterior								
M. subscapularis	Nn subscapularis	scapula +	-	+	+	-	+	
M. serratus anterior		-	-	-	-	-	-	
dorsal medial								
M. trapezius	XI	-	-	-	n/a		n/a	
Pars clavicularis		n/a		n/a	+*	-	+	
Pars acromialis		n/a		n/a	+*	-	-/+	
Pars spinalis		n/a		n/a	+*	-	+	
M. levator scapulae	Plexus cervicalis and N.dorsalis scapulae (Plexus brachialis)	-	-	-	-	-	-	
Mm rhomboideii	N.dorsalis scapulae (Plexus branchialis)	-	-	-	-	-	-	
other								

M. omohyoideus	Ansa cervicalis (Plexus cervicalis)	+*but within muscle -	-	+	+*but within muscle -	-	+	
Diaphragma		+	-		n/a			

Glossary and Abbreviations

CT	Connective Tissue
M	Muscle
Mm	Muscles
B	Bone

Facial Nerves

V	Trigeminal Nerve
VII	Facial Nerve
IX	Glossopharyngeal Nerve
X	Vagal Nerve
XI	Accessorial Nerve
XII	Hypoglossal Nerve

Plasmid	Description	Chapter
pBR42	RNA probe for *in situ* Hybridisation for *Hand*1, containing the last exon of the coding region	2
pBR43	RNA probe for *in situ* Hybridisation for *Hand*2, containing the last exon of the coding region	2
pBR44	RNA probe for *in situ* Hybridisation for *Dlx*5, containing the last exon of the coding region	2
pBR45	RNA probe for *in situ* Hybridisation for *Dlx*3, containing the last exon of the coding region	2
pBR47	RNA probe for *in situ* Hybridisation for *Prx*1, containing the last exon of the coding region without homeobox	2
pBR108	intermediate plasmid: *Sal*I-I-*Sce*I-CMV immediated early element for pBR119	5
pBR109	intermediate plasmid for pBR151: 2kb *Hoxa*2 upstream region *(Xenopus*) in pCRII TOPO	5
pBR118	intermediate plasmid for pBR119: floxed DsRed.T3 pA cassette	5
pBR119	hUbC-LoxP-DsRed.T3 pA-LoxP-Venus pA	5
pBR120	I-*Sce*I-CMV'hUbC-LoxP-DsRed.T3 pA-LoxP-Venus pA	5
pBR135	I-*Sce*I-hUbC-LoxP-DsRed.T3-LoxP-Venus	5
pBR136	intermediate plasmid for pBR139: floxed DsRed2 pA cassette	5
pBR139	I-*Sce*I-hUbC-LoxP-DsRed2-LoxP-Venus	5
pBR142	intermediate plasmid: *Xenopus Hand*2 upstream region fragment A in pCRII TOPO	5
pBR143	intermediate plasmid: *Xenopus* Hand2 upstream region fragment BC in pCRII TOPO	5
pBR144	intermediate plasmid: *Xenopus* Hand2 upstream region fragment E in pCRII TOPO	5
pBR145	intermediated plasmid*: Hand*2 fragment A into EF1-VenusCrem after removal of EF1 via *Hind*III	5

pBR146	intermediated plasmid: *Hand*2 fragments CBA- VenusCrem	5
pBR149	intermediate plasmid: *Hand*2 fragments ED in pCRII TOPO	5
pBR151	*Xenopus Hoxa*2- VenusCrem	5
pBR158	intermediate plasmid: *Xenopus Hand*2 upstream region fragment D in pCRII TOPO	5
pBR160	intermediate plasmid: *Xenopus Hand*2 fragment ED in pCRII TOPO	5
pBR161	*Xenopus Hand*2 upstream region fragment EDCBA driving VenusCREM = final construct	5
p144	human UbiquitinC- Venus	5
p187	RNA probe for *in situ* Hybridisation for Cre recombinase, part of the coding region	5
p279	EF1-VenusCREM-pA	5

Primer	No	Sequence	for	purpose	plasmid
PrimBR	62	5' CCTCAGCAGCCCGAAAGCTTCCCTCCT 3'	mouse *Hand*1 last exon	RNA probe	pBR42
PrimBR	63	5' TTATTAAGTCAAGAGCATAGATACTG 3'	mouse *Hand*1 last exon	RNA probe	pBR42
PrimBR	65	5' ATGAGATCTTGAAAAGCACAGTGAGCAG 3'	mouse *Hand*2 last exon	RNA probe	pBR43
PrimBR	66	5' ACACGCAGTGGTTTATTGAATACTTAC 3'	mouse *Hand*2 last exon	RNA probe	pBR43
PrimBR	67	5' GTGAAAATCTGGTTCCAGAACCGCCGCT 3'	mouse *Dlx*3 last exon	RNA probe	pBR45
PrimBR	68	5' ATTAACATTATATATAAAGACTGGTCCAGT 3'	mouse *Dlx*3 last exon	RNA probe	pBR45
PrimBR	69	5' CCATGGTCGAAATAATTTATTTATCCAG 3'	mouse *Dlx*5 last exon	RNA probe	pBR44
PrimBR	70	5' ACAAAAGATCCAAGATCAAGAAGATC 3'	mouse *Dlx*5 last exon	RNA probe	pBR44
PrimBR	73	5' CCATAAGACACCTATCCTGTTCTGT 3'	Cre recombinase (partial)	RNA probe	p187
PrimBR	74	5' ATTGGATGTAGCCTCACAACATC 3'	Cre recombinase (partial)	RNA probe	p187
PrimBR	80	5‘ *ACAGATATCACA*TCGAGAATGAACTGTGCCTTC 3‘	amplification of murine *Hand*2 branchial arch enhancer	PCR	pBR50
PrimBR	82	5‘ *AAGGGCCGGCCATCAGATATCAAA*CGGCAGACTGAG GTCTTCCTGG 3‘	amplification of murine *Hand*2 branchial arch enhancer	PCR	pBR50
PrimBR	112	5‘ *CTTTGTTTAAACGGC*GGTGTGGGTGTCCGCTTCTT 3‘	amplification of murine *Engrailed*2 enhancer	PCR	pBR64
PrimBR	113	5‘ *GCCGTTTAAAC*ACAAACGCTAGTGTAGGCCTGG 3‘	amplification of murine *Engrailed*2 enhancer	PCR	pBR63
PrimBR	114	5‘ *CTTTGTTTAAACGGCGATATC*AAATAGCAGCGAATCTT 3‘	amplification of murine *Hoxa*3	PCR	pBR63

PrimBR	115	5‘ *GCCGTTTAAACCCCGGG*ACGTGTAGGAGGTGAGA 3‘	enhancer amplification of murine *Hoxa*3 enhancer	PCR	pBR63
PrimBR	153	5' ACTATCCAGCAACATTTGGGCCAG 3'	mouse *Prx*1 last exon	RNA probe	pBR47
PrimBR	154	5' CCATCTTCCAGCAGGCGCACCATTG 3'	mouse *Prx*1 last exon	RNA probe	pBR47
PrimBR	179	5' *AAAGGTACCATTTAAATGGCGCGCCTTAATTAA*CATATTTTA ATTCCCCGTTCTCACCTCTTG 3’	amplification of *X.tropicalis Hoxa*2 upstream region	PCR	pBR109
PrimBR	180	5' *AAAGGTACCGTTTAAACTTAATTAA*TGGCCCTCTCCTCCAAGC CCTTTAAACAA 3’	amplification of *X. tropicalis Hoxa*2 upstream region	PCR	pBR109
PrimBR	187	5' AGTCGACTAGGGATAACAGGGTAATAGTTTAAACGCGTTA CATAACTTACGGTAAATGG	I-*Sce*I CMVIE	PCR	pBR108
PrimBR	188	5'AGTCGACGTTTAAACCATGGTAATAGCGATGACTAATACG 3’	I-*Sce*I CMVIE	PCR	pBR108
PrimBR	210	5'*AAGGATCCATAACTTCGTATAGCATACATTATACGAAGTTAATC GCCACC*ATGGCCTCCTCCGAGGACGT 3’	LoxP DsRed	PCR	pBR118
PrimBR	211	5' *TTGGATCCAGATCTGATATCGATTAACTTCGTATAATGTATGCT ATACGAAGTTATGGTACC*TTACGCCTTAAGATACATTGATG 3’	LoxP DsRed	PCR	pBR118
PrimBR	335	5' AGTTGTGAGTGGAGCTGCCCCATTA 3’	sequencing upstream region of *Hand*2 in *X.tropicalis*	sequencing	pBR150
PrimBR	348	5' *AAAGCTTTAGGGATAACAGGGTAATGGCGCGCCCTCGAG GCGGCCGC*CATGGCATGTATGGGTAATAAAGCT 3’	(I-*Sce*I-*Asc*I-*Xho*I-*Not*I-upstream region *Hand*2, part A	PCR	pBR161
PrimBR	349	5' ACAGCGCCATCAATAGGAACTAATA 3’	PCR and sequencing upstream region of *Hand*2 in *X.tropicalis*	sequencing and PCR	pBR150
PrimBR	350	5' GATATTGGCACAACTGTATAGATGG 3’	sequencing upstream region of *Hand*2 in *X.tropicalis*	sequencing	pBR150
PrimBR	350	5' GATATTGGCACAACTGTATAGATGG 3’	upstream region *Hand*2, fragment BC	PCR	pBR161

PrimBR	352	5' AGTGTAACCTGGCAACATATGGACTT 3'	PCR and sequencing upstream region of *Hand2* in *X.tropicalis*	sequencing and PCR	pBR161
PrimBR	353	5' GTCCTTTAACATGGCTAATGTACCT 3'	upstream region, *Hand2* fragment D	PCR	pBR161
PrimBR	354	5' GCACTCTCTGATCTCCCTTCAAGCT 3'	upstream region, Hand2 fragment E	PCR	pBR161
PrimBR	355	5' AGTTGTGAGTGGAGCTGCCCCATTA 3'	upstream region, *Hand2* fragment D	PCR	pBR161
PrimBR	356	5' ACAGCGCTGCGTACCCTTGTGGCGC 3'	upstream region, *Hand2* fragment E	PCR	pBR161
PrimBR	359	5' TTAAGCTTGTCAGCTGGGCTTCCTGGCTAGTCTT 3'	upstream region *Hand2*-*Hind*III, fragment A	PCR	pBR161
PrimBR	387	5' TTGAATTCTTACTTGTACAGCTCGTCCATG 3'	pBR135 and pBR139 partial transgene for genotyping	PCR genotyping	pBR135, pBR139
PrimBR	388	5' AGTTCAAGTCCATCTACATGGCCGAAGC 3'	pBR135 and pBR139 partial transgene for genotyping	PCR genotyping	pBR135, pBR139
PrimBR	155seq	5' CGCGAACATCTTCAGGTTCT 3'	sequencing antisense primer for Crem start	sequencing	pBR150
PrimBR	156seq	5' TCGGCTATACGTAACAGGGT 3'	sequencing upstream region of *Hand2* in *X.tropicalis*	sequencing	pBR150
PrimBR	158seq	5' CAGGTATCTCTGACCAGAGT 3'	sequencing upstream region of *Hand2* in *X.tropicalis*	sequencing	pBR150
PrimBR	159seq	5' ATGGATTTCCGTCTCTGGTG 3'	sequencing upstream region of *Hand2* in X.tropicalis	sequencing	pBR150
PrimBR	19seq	5' GCTGAACTTGTGGCCGTTTA 3'	sequencing antisense primer for VenusGFP start	sequencing	pBR120
PrimBR	218seq	5' GCCACGTCAGACGAAGGGCC 3'	sequencing hUbC promoter	sequencing	p143
PrimBR	219seq	5' CGTGAAGTTTGTCACTGACTC 3'	sequencing hUbC promoter	sequencing	p143

PrimBR	222seq	5' GGATGTTGCCGTCCTCCTTG 3’	internal sequencing primer for VenusGFP	sequencing	pBR120
PrimBR	223seq	5' CCTTGAAGAAGATGGTGCGC 3’	internal sequencing primer for VenusGFP	sequencing	pBR120
PrimBR	336seq	5' AGCCTTCCCTGCTCGCTATT 3’	sequencing upstream region of *Hand*2 in *X.tropicalis*	sequencing	pBR150
PrimBR	337seq	5' GTGATATTTTCTCTACCTCT 3’	sequencing upstream region of *Hand*2 in *X.tropicalis*	sequencing	pBR150
PrimBR	338seq	5' AGTATAGGCTCTTGCACCTT 3’	sequencing upstream region of *Hand*2 in *X.tropicalis*	sequencing	pBR150
PrimBR	339seq	5' GTTTGATAGTAGATAACGAC 3’	sequencing upstream region of *Hand*2 in *X.tropicalis*	sequencing	pBR150
PrimBR	343seq	5' CGTTACTAATACATAAGTAG 3’	sequencing upstream region of *Hand*2 in *X.tropicalis*	sequencing	pBR142 pBR150
PrimBR	344seq	5' TAGAATACTGTACCTGAGCT 3’	sequencing upstream region of *Hand*2 in *X.tropicalis*	sequencing	pBR142 pBR150
PrimBR	348seq	5' CATGGCATGTATGGGTAATAAAGCT 3’	sequencing upstream region of *Hand*2 in *X.tropicalis*	sequencing	pBR150
PrimBR	356seq	5' ACAGCGCTGCGTACCCTTGTGGCGC 3’	sequencing upstream region of *Hand*2 in *X.tropicalis*	sequencing	pBR150
PrimBR	357seq	5' AGATTAAATTCCCCAAGAGAGACCT 3’	sequencing upstream region of *Hand*2 in *X.tropicalis*	sequencing	pBR150
PrimBR	357seq	5' AGATTAAATTCCCCAAGAGAGACCT 3’	sequencing upstream region of *Hand*2 in *X.tropicalis*	sequencing	pBR150
PrimBR	364 seq	5' TGCAGGCGCAGAGTAGACAC 3’	sequencing upstream region of *Hand*2 in *X.tropicalis*	sequencing	pBR150
PrimBR	365seq	5' ATTAGCCTCTGGTATGAAGA 3’	sequencing upstream region of *Hand*2 in *X.tropicalis*	sequencing	pBR150
PrimBR	96_ubc5’	5' TATCCAAGCTTGTGTCGCTCGAGACAATTGTCGAC AGGCTCAGGGAGGTTGAAG 3’	amplification of the human Ubiquitin C promoter	PCR	p143

PrimBR 97_ubc3'	5' GCGTTGCGGCCGCATATTTGAAGATCTTTCCCGCGG ATCCTGTCTAACAAAAAAGCCAAAAACGG 3'	amplification of the human Ubiquitin C promoter	PCR	p143
other				
HC SEQ Primer SEQ 120US	5' CATTTCCCCGAAAAGTGCCA 3'	sequencing 5' in pCS2+ backbone	sequencing	-
PrimSor1	5' AAAGTCGCTCTGAGTTGTTAT 3'	genotyping of ROSA26R allele, Soriano	genotyping	-
PrimSor2	5' GCGAAGAGTTTGTCCTCAACC 3'	genotyping of ROSA26R allele, Soriano	genotyping	-
PrimSor3	5' GGAGCGGGAGAAATGGATATG 3'	genotyping of ROSA26R allele, Soriano	genotyping	-
TWCre1	5' GCTGGTTAGCACCGCAGGTGTAGAG 3'	genotyping primer for *Hand*2-Cre mice	genotyping	-
TWCre3	5' CGCCATCTTCCAGCAGGCGCACC 3'	genotyping primer for *Hand*2-Cre mice	genotyping	-
TY4	5' GCCTAGGGTAGGCTCTCCTG 3'	sequencing hUbC promoter	sequencing	p143

ITALIC primer sequence indicates the recombinant part of the primer

UPPER CASE overlap of the primer with the amplified region

10 Reference List

1. Abe, M. *et al.* Hand2 regulates chondrogenesis in vitro and in vivo. *Bone* (2009).

2. Abe, M. *et al.* Tooth-type specific expression of dHAND/Hand2: possible involvement in murine lower incisor morphogenesis. *Cell Tissue Res.* **310**, 201-212 (2002).

3. Abzhanov, A., Rodda, S. J., McMahon, A. P. & Tabin, C. J. Regulation of skeletogenic differentiation in cranial dermal bone. *Development* **134**, 3133-3144 (2007).

4. Agarwal, P. *et al.* Tbx5 is essential for forelimb bud initiation following patterning of the limb field in the mouse embryo
5. *Development* **130**, 623-633 (2003).

5. Ahlberg, P. E. & Koentges, G. Homologies and cell populations: a response to Sanchez-Villagra and Maier. *Evol. Dev.* **8**, 116-118 (2006).

6. Amar, S., Karcher-Djuricic, V., Meyer, J. M. & Ruch, J. V. The lingual (root analogue) and the labial (crown analogue) mouse incisor dentin promotes ameloblast differentiation. *Arch Anat Microsc. Morphol. Exp.* **75**, 229-239 (1986).

7. Amar, S., Luo, W., Snead, M. L. & Ruch, J. V. Amelogenin gene expression in mouse incisor heterotopic recombinations. *Differentiation* **41**, 56-61 (1989).

8. Amaya, E. & Kroll, K. L. A method for generating transgenic frog embryos. *Methods Mol. Biol.* **97**, 393-414 (1999).

9. Angelo, S. *et al.* Conservation of sequence and expression of Xenopus and zebrafish dHAND during cardiac, branchial arch and lateral mesoderm development. *Mech. Dev.* **95**, 231-237 (2000).

10. Arques, C. G., Doohan, R., Sharpe, J. & Torres, M. Cell tracing reveals a dorsoventral lineage restriction plane in the mouse limb bud mesenchyme
1. *Development* **134**, 3713-3722 (2007).

11. Axelrod, D. Carbocyanine dye orientation in red cell membrane studied by microscopic fluorescence polarization
17. *Biophys. J* **26**, 557-573 (1979).

12. Balciunas, D. *et al.* Harnessing a high cargo-capacity transposon for genetic applications in vertebrates. *PLoS. Genet.* **2**, e169 (2006).

13. Baltzinger, M., Ori, M., Pasqualetti, M., Nardi, I. & Rijli, F. M. Hoxa2 knockdown in Xenopus results in hyoid to mandibular homeosis. *Dev. Dyn.* **234**, 858-867 (2005).

14. Bandyopadhyay, A., Kubilus, J. K., Crochiere, M. L., Linsenmayer, T. F. & Tabin, C. J. Identification of unique molecular subdomains in the perichondrium and periosteum and their role in regulating gene expression in the underlying chondrocytes. *Dev. Biol.* **321**, 162-174 (2008).

15. Bell, A. C. & Felsenfeld, G. Stopped at the border: boundaries and insulators. *Curr. Opin. Genet. Dev.* **9**, 191-198 (1999).

16. Bessa, J. *et al.* Zebrafish enhancer detection (ZED) vector: a new tool to facilitate transgenesis and the functional analysis of cis-regulatory regions in zebrafish
1. *Dev. Dyn.* **238**, 2409-2417 (2009).

17. Bevis, B. J. & Glick, B. S. Rapidly maturing variants of the Discosoma red fluorescent protein (DsRed). *Nat. Biotechnol.* **20**, 83-87 (2002).

18. Bland, Y. S. & Ashhurst, D. E. Fetal and postnatal development of the patella, patellar tendon and suprapatella in the rabbit; changes in the distribution of the fibrillar collagens. *J. Anat* **190 (Pt 3)**, 327-342 (1997).

19. Bolk, L., Goeppert, E., Kallius, E. & Lubosch, W. *Handbuch der vergleichenden Anatomie der Wirbeltiere*. Urban & Schwarzenberg, Berlin und Wien (1938).

20. Brazeau, M. D. & Ahlberg, P. E. Tetrapod-like middle ear architecture in a Devonian fish. *Nature* **439**, 318-321 (2006).

21. Brinster, R. L., Allen, J. M., Behringer, R. R., Gelinas, R. E. & Palmiter, R. D. Introns increase transcriptional efficiency in transgenic mice. *Proc. Natl. Acad. Sci. U. S. A* **85**, 836-840 (1988).

22. Burgess-Beusse, B. *et al.* The insulation of genes from external enhancers and silencing chromatin. *Proc. Natl. Acad. Sci. U. S. A* **99 Suppl 4**, 16433-16437 (2002).

23. Burke, A. C. (Plenum Press, New York,1991).

24. Burke, A. C. & Nowicki, J. L. A new view of patterning domains in the vertebrate mesoderm. *Dev. Cell* **4**, 159-165 (2003).

25. Capdevila, J. & Izpisua Belmonte, J. C. Patterning mechanisms controlling vertebrate limb development. *Annu. Rev. Cell Dev. Biol.* **17**, 87-132 (2001).

26. Carroll, S. B., Grenier, J. K. & Weatherbee, S. D. *From DNA to Diversity*. Blackwell Science, (2001).

27. Cerny, R. *et al.* Developmental origins and evolution of jaws: new interpretation of "maxillary" and "mandibular"
1. *Dev. Biol.* **276**, 225-236 (2004).

28. Cerny, R. *et al.* Combined intrinsic and extrinsic influences pattern cranial neural crest migration and pharyngeal arch morphogenesis in axolotl. *Dev. Biol.* **266**, 252-269 (2004).

29. Charite, J. *et al.* Role of Dlx6 in regulation of an endothelin-1-dependent, dHAND branchial arch enhancer. *Genes Dev.* **15**, 3039-3049 (2001).

30. Charite, J., McFadden, D. G. & Olson, E. N. The bHLH transcription factor dHAND controls Sonic hedgehog expression and establishment of the zone of polarizing activity during limb development. *Development* **127**, 2461-2470 (2000).

31. Chevallier, A. [Role of the somitic mesoderm in the development of the rib cage of bird embryos. I. Origin of the sternal component and conditions for the development of the ribs (author's transl)]. *J. Embryol. Exp. Morphol.* **33**, 291-311 (1975).

32. Chevallier, A. Origine des ceintures scapulaires et pleviennes chez l'embryon d'oiseau. *J. Embryol. Exp. Morphol.* **42**, 275-292 (1977).

33. Chibon, P. L'origine de l'organe adamantin des dents. Etude aumoyen du marquage nucleaire de l'ectoderme stomodeal. *Ann. Embryol. Morphog* **3**, 203-213 (1970).

34. Chibon, P. Analyse expérimentale de la régionalisation et des capacités morphogénétiques de la crête neurale chez l'amphibien urodèle*Pleurodeles waltlii*. *Mém. Soc. Zool. Fr* **36**, pp. 1–107 (1966).

35. Chibon, P. [Nuclear labelling by tritiated thymidine of neural crest derivatives in the amphibian Urodele Pleurodeles waltlii Michah]. *J. Embryol. Exp. Morphol.* **18**, 343-358 (1967).

36. Chou, C. Y., Horng, L. S. & Tsai, H. J. Uniform GFP-expression in transgenic medaka (Oryzias latipes) at the F0 generation. *Transgenic Res.* **10**, 303-315 (2001).

37. Clack, J. A. *Gaining Ground, The Origin and Evolution of Tetrapods*. Indiana University Press, (2002).

38. Clack, J. A. Homologies in the fossil record: the middle ear as a test case. *Acta Biotheor.* **41**, 391-409 (1993).

39. Clack, J. A. Patterns and processes in the early evolution of the tetrapod ear. *J. Neurobiol.* **53**, 251-264 (2002).

40. Clack, J. A. *et al.* A uniquely specialized ear in a very early tetrapod 1. *Nature* **425**, 65-69 (2003).

41. Clarke, J. D. & Tickle, C. Fate maps old and new 48. *Nat. Cell Biol.* **1**, E103-E109 (1999).

42. Coin, R., Haikel, Y. & Ruch, J. V. Effects of apatite, transforming growth factor beta-1, bone morphogenetic protein-2 and interleukin-7 on ameloblast differentiation in vitro. *Eur. J. Oral Sci.* **107**, 487-495 (1999).

43. Colnot, C., Lu, C., Hu, D. & Helms, J. A. Distinguishing the contributions of the perichondrium, cartilage, and vascular endothelium to skeletal development. *Dev. Biol.* **269**, 55-69 (2004).

44. Couly, G., Creuzet, S., Bennaceur, S., Vincent, C. & Le Douarin, N. M. Interactions between Hox-negative cephalic neural crest cells and the foregut endoderm in patterning the facial skeleton in the vertebrate head. *Development* **129**, 1061-1073 (2002).

45. Couly, G. F., Coltey, P. M. & Le Douarin, N. M. The triple origin of skull in higher vertebrates: a study in quail-chick chimeras. *Development* **117**, 409-429 (1993).

46. D'Autreaux, F., Morikawa, Y., Cserjesi, P. & Gershon, M. D. Hand2 is necessary for terminal differentiation of enteric neurons from crest-derived precursors but not for their migration into the gut or for formation of glia. *Development* **134**, 2237-2249 (2007).

47. Dai, Y. S. & Cserjesi, P. The basic helix-loop-helix factor, HAND2, functions as a transcriptional activator by binding to E-boxes as a heterodimer 2. *J Biol. Chem.* **277**, 12604-12612 (2002).

48. Dale, R. M., Sisson, B. E. & Topczewski, J. The emerging role of Wnt/PCP signaling in organ formation 1. *Zebrafish.* **6**, 9-14 (2009).

49. Danielian, P. S. & McMahon, A. P. Engrailed-1 as a target of the Wnt-1 signalling pathway in vertebrate midbrain development. *Nature* **383**, 332-334 (1996).

50. Danielian, P. S., Muccino, D., Rowitch, D. H., Michael, S. K. & McMahon, A. P. Modification of gene activity in mouse embryos in utero by a tamoxifen-inducible form of Cre recombinase. *Curr. Biol.* **8**, 1323-1326 (1998).

51. Davidson, E. H. Genomic Regulatory Systems, Development and Evolution. 2001. academic press. Ref Type: Serial (Book,Monograph)

52. Davy, A., Aubin, J. & Soriano, P. Ephrin-B1 forward and reverse signaling are required during mouse development 6. *Genes Dev.* **18**, 572-583 (2004).

53. Denkers, N., Garcia-Villalba, P., Rodesch, C. K., Nielson, K. R. & Mauch, T. J. FISHing for chick genes: Triple-label whole-mount fluorescence in situ hybridization detects simultaneous and overlapping gene expression in avian embryos. *Dev. Dyn.* **229**, 651-657 (2004).

54. Depew, M. J. *et al.* Dlx5 regulates regional development of the branchial arches and sensory capsules. *Development* **126**, 3831-3846 (1999).

55. Depew, M. J., Lufkin, T. & Rubenstein, J. L. Specification of jaw subdivisions by Dlx genes. *Science* **298**, 381-385 (2002).

56. Depew, M. J., Simpson, C. A., Morasso, M. & Rubenstein, J. L. Reassessing the Dlx code: the genetic regulation of branchial arch skeletal pattern and development. *J. Anat.* **207**, 501-561 (2005).

57. Djiane, A., Yogev, S. & Mlodzik, M. The apical determinants aPKC and dPatj regulate Frizzled-dependent planar cell polarity in the Drosophila eye 7. *Cell* **121**, 621-631 (2005).

58. Duboc, V. & Logan, M. P. Building limb morphology through integration of signalling modules 1. *Curr. Opin. Genet. Dev.* **19**, 497-503 (2009).

59. Duellman, W. E. & Trueb, L. *Biology of Amphibians*. McGraw-Hill, New York (1986).

60. Durland, J. L., Sferlazzo, M., Logan, M. & Burke, A. C. Visualizing the lateral somitic frontier in the Prx1Cre transgenic mouse. *J. Anat* **212**, 590-602 (2008).

61. Evans, D. J. & Noden, D. M. Spatial relations between avian craniofacial neural crest and paraxial mesoderm cells. *Dev. Dyn.* **235**, 1310-1325 (2006).

62. Fanto, M. & McNeill, H. Planar polarity from flies to vertebrates 10. *J. Cell Sci.* **117**, 527-533 (2004).

63. Firulli, B. A. *et al.* Altered Twist1 and Hand2 dimerization is associated with Saethre-Chotzen syndrome and limb abnormalities. *Nat. Genet.* **37**, 373-381 (2005).

64. Franz-Odendaal, T. A., Hall, B. K. & Witten, P. E. Buried alive: how osteoblasts become osteocytes 4. *Dev. Dyn.* **235**, 176-190 (2006).

65. Funato, N. *et al.* Hand2 controls osteoblast differentiation in the branchial arch by inhibiting DNA binding of Runx2. *Development* **136**, 615-625 (2009).

66. Gans, C. & Northcutt, R. G. Neural Crest and the Origin of Vertebrates: A New Head 1. *Science* **220**, 268-273 (1983).

67. Gartner, L. & Hiatt, L. *Color Text Book of Histology*. Saunders (W.B.) Co Ltd, (2001).

68. Gaszner, M. & Felsenfeld, G. Insulators: exploiting transcriptional and epigenetic mechanisms. *Nat. Rev. Genet.* **7**, 703-713 (2006).

69. Gaunt, W. A. The development of enamel and dentine on the molars of the mouse, with an account of the enamel-free areas 2. *Acta Anat (Basel)* **28**, 111-134 (1956).

70. Gaupp, E. "Die Reichertsche Theorie (Hammer-, Amboss- und Kieferfrage)". *Arch. Anat. Suppl. 1912* 1-416 (1912).

71. Gendron-Maguire, M., Mallo, M., Zhang, M. & Gridley, T. Hoxa-2 mutant mice exhibit homeotic transformation of skeletal elements derived from cranial neural crest. *Cell* **75**, 1317-1331 (1993).

72. Gibson, M. C. & Perrimon, N. Apicobasal polarization: epithelial form and function
1. *Curr. Opin. Cell Biol.* **15**, 747-752 (2003).

73. Graham, A., Heyman, I. & Lumsden, A. Even-numbered rhombomeres control the apoptotic elimination of neural crest cells from odd-numbered rhombomeres in the chick hindbrain
1. *Development* **119**, 233-245 (1993).

74. Graham, A., Koentges, G. & Lumsden, A. Neural Crest Apoptosis and the Establishment of Craniofacial Pattern: An Honorable Death. *Mol. Cell Neurosci.* **8**, 76-83 (1996).

75. Grammatopoulos, G. A., Bell, E., Toole, L., Lumsden, A. & Tucker, A. S. Homeotic transformation of branchial arch identity after Hoxa2 overexpression. *Development* **127**, 5355-5365 (2000).

76. Grandel, H. & Schulte-Merker, S. The development of the paired fins in the zebrafish (Danio rerio). *Mech. Dev.* **79**, 99-120 (1998).

77. Hall, B. K. *Bones and cartilage*. (2005).

78. Hamlet, M. R. *et al.* Tol2 transposon-mediated transgenesis in Xenopus tropicalis
3. *Genesis.* **44**, 438-445 (2006).

79. Hendershot, T. J. *et al.* Conditional deletion of Hand2 reveals critical functions in neurogenesis and cell type-specific gene expression for development of neural crest-derived noradrenergic sympathetic ganglion neurons. *Dev. Biol.* **319**, 179-191 (2008).

80. Hendershot, T. J. *et al.* Expression of Hand2 is sufficient for neurogenesis and cell type-specific gene expression in the enteric nervous system. *Dev. Dyn.* **236**, 93-105 (2007).

81. Hirsch, N., Zimmerman, L. B. & Grainger, R. M. Xenopus, the next generation: X. tropicalis genetics and genomics. *Dev. Dyn.* **225**, 422-433 (2002).

82. Hirsch, N. *et al.* Xenopus tropicalis transgenic lines and their use in the study of embryonic induction. *Dev. Dyn.* **225**, 522-535 (2002).

83. Hoerstadius, S. & Sellman, S. Experimentelle Untersuchungen ueber die Determination des Knorpligen Kopfskelettes bei Urodelen. *Nova Acta Soc. Scie. Uppsaliensis, Ser. 4 13* 1-170 (1946).

84. Horiuchi, K. *et al.* Identification and characterization of a novel protein, periostin, with restricted expression to periosteum and periodontal ligament and

increased expression by transforming growth factor beta. *J. Bone Miner. Res.* **14**, 1239-1249 (1999).

85. Hörstadius, S. & Sellman, S. Experimentelle Untersuchungen ueber die Determination des Knorpligen Kopfskelettes bei Urodelen. *Nova Acta Soc. Scie. Uppsaliensis, Ser. 4 13* 1-170 (1946).

86. Huang, L. F., Fukai, N., Selby, P. B., Olsen, B. R. & Mundlos, S. Mouse clavicular development: analysis of wild-type and cleidocranial dysplasia mutant mice
1. *Dev. Dyn.* **210**, 33-40 (1997).

87. Huang, R., Zhi, Q., Patel, K., Wilting, J. & Christ, B. Dual origin and segmental organisation of the avian scapula. *Development* **127**, 3789-3794 (2000).

88. Huang, R. *et al.* Sclerotomal origin of the ribs. *Development* **127**, 527-532 (2000).

89. Hunt, P. *et al.* A distinct Hox code for the branchial region of the vertebrate head. *Nature* **353**, 861-864 (1991).

90. Hunt, P. *et al.* The branchial Hox code and its implications for gene regulation, patterning of the nervous system and head evolution. *Development* **Suppl 2**, 63-77 (1991).

91. J.ROBINSON, P.E.AHLBERG & G.KOENTGES The braincase and middle ear region of Dendrerpeton acadianum (Tetrapoda: Temnospondyli). *Zoological Journal of the Linnean Society* **143**, 577-597 (2005).

92. Jacquier, A. & Dujon, B. An intron-encoded protein is active in a gene conversion process that spreads an intron into a mitochondrial gene. *Cell* **41**, 383-394 (1985).

93. Jiang, X., Iseki, S., Maxson, R. E., Sucov, H. M. & Morriss-Kay, G. M. Tissue origins and interactions in the mammalian skull vault. *Dev. Biol.* **241**, 106-116 (2002).

94. Junqueira & Carneiro *Histologie*. Berlin Heidelberg New York (1991).

95. Kaczmarczyk, S. J. & Green, J. E. A single vector containing modified cre recombinase and LOX recombination sequences for inducible tissue-specific amplification of gene expression. *Nucleic Acids Res.* **29**, E56 (2001).

96. Kardon, G. Muscle and tendon morphogenesis in the avian hind limb
6. *Development* **125**, 4019-4032 (1998).

97. Kardon, G., Harfe, B. D. & Tabin, C. J. A Tcf4-positive mesodermal population provides a prepattern for vertebrate limb muscle patterning
2. *Dev. Cell* **5**, 937-944 (2003).

98. Karner, C., Wharton, K. A. & Carroll, T. J. Apical-basal polarity, Wnt signaling and vertebrate organogenesis
6. *Semin. Cell Dev. Biol.* **17**, 214-222 (2006).

99. Karner, C., Wharton, K. A., Jr. & Carroll, T. J. Planar cell polarity and vertebrate organogenesis
5. *Semin. Cell Dev. Biol.* **17**, 194-203 (2006).

100. Katoh, M. & Katoh, M. Comparative integromics on non-canonical WNT or planar cell polarity signaling molecules: transcriptional mechanism of PTK7 in colorectal cancer and that of SEMA6A in undifferentiated ES cells
2. *Int. J. Mol. Med.* **20**, 405-409 (2007).

101. Klima, M. Early development of the shoulder girdle and sternum in marsupials (Mammalia: Metatheria)
19. *Adv. Anat Embryol. Cell Biol.* **109**, 1-91 (1987).

102. Kontges, G. & Lumsden, A. Rhombencephalic neural crest segmentation is preserved throughout craniofacial ontogeny. *Development* **122**, 3229-3242 (1996).

103. Kroll, K. L. & Amaya, E. Transgenic Xenopus embryos from sperm nuclear transplantations reveal FGF signaling requirements during gastrulation. *Development* **122**, 3173-3183 (1996).

104. Krotoski, D. M., Fraser, S. E. & Bronner-Fraser, M. Mapping of neural crest pathways in Xenopus laevis using inter- and intra-specific cell markers
1. *Dev. Biol.* **127**, 119-132 (1988).

105. Kuo, C. K., Petersen, B. C. & Tuan, R. S. Spatiotemporal protein distribution of TGF-betas, their receptors, and extracellular matrix molecules during embryonic tendon development
1. *Dev. Dyn.* **237**, 1477-1489 (2008).

106. Le Douarin, N. & Kalcheim, C. *The Neural Crest*. Cambridge University Press, (1999).

107. Le Lievre, C. S. Participation of neural crest-derived cells in the genesis of the skull in birds. *J. Embryol. Exp. Morphol.* **47**, 17-37 (1978).

108. Lecuit, T. & Cohen, S. M. Proximal-distal axis formation in the Drosophila leg. *Nature* **388**, 139-145 (1997).

109. Liu, N. *et al.* DNA binding-dependent and -independent functions of the Hand2 transcription factor during mouse embryogenesis
1. *Development* **136**, 933-942 (2009).

110. Lois, C., Hong, E. J., Pease, S., Brown, E. J. & Baltimore, D. Germline transmission and tissue-specific expression of transgenes delivered by lentiviral vectors. *Science* **295**, 868-872 (2002).

111. Lombard, E. Evolution of the tetrapod ear: an analysis and reinterpretation. *Biological Journal of the Linnean Society* **11**, 19-76 (1977).

112. Lumsden, A. & Keynes, R. Segmental patterns of neuronal development in the chick hindbrain
5. *Nature* **337**, 424-428 (1989).

113. Lumsden, A., Sprawson, N. & Graham, A. Segmental origin and migration of neural crest cells in the hindbrain region of the chick embryo. *Development* **113**, 1281-1291 (1991).

114. Luo, Z.-X., Z Kielan-Jaworowska & RL Cifelli In quest for a phylogeny of Mesozoic mammals. *Acta Palaeontol. Pol.* **47**, 1-78 (2002).

115. Luxardi, G., Marchal, L., Thome, V. & Kodjabachian, L. Distinct Xenopus Nodal ligands sequentially induce mesendoderm and control gastrulation movements in parallel to the Wnt/PCP pathway
1. *Development* **137**, 417-426 (2010).

116. Macatee, T. L. *et al.* Ablation of specific expression domains reveals discrete functions of ectoderm- and endoderm-derived FGF8 during cardiovascular and pharyngeal development
1. *Development* **130**, 6361-6374 (2003).

117. Maconochie, M. *et al.* Regulation of Hoxa2 in cranial neural crest cells involves members of the AP-2 family. *Development* **126**, 1483-1494 (1999).

118. Manley, N. R., Barrow, J. R., Zhang, T. & Capecchi, M. R. Hoxb2 and hoxb4 act together to specify ventral body wall formation
1. *Dev. Biol.* **237**, 130-144 (2001).

119. Manzanares, M. & Nieto, M. A. A celebration of the new head and an evaluation of the new mouth
3. *Neuron* **37**, 895-898 (2003).

120. Marshall, V. M., Allison, J., Templeton, T. & Foote, S. J. Generation of BAC transgenic mice
1. *Methods Mol. Biol.* **256**, 159-182 (2004).

121. Massari, M. E. & Murre, C. Helix-loop-helix proteins: regulators of transcription in eucaryotic organisms
1. *Mol. Cell Biol.* **20**, 429-440 (2000).

122. Matsuoka, T. *et al.* Neural crest origins of the neck and shoulder. *Nature* **436**, 347-355 (2005).

123. McFadden, D. G. *et al.* A GATA-dependent right ventricular enhancer controls dHAND transcription in the developing heart. *Development* **127**, 5331-5341 (2000).

124. McFadden, D. G., McAnally, J., Richardson, J. A., Charite, J. & Olson, E. N. Misexpression of dHAND induces ectopic digits in the developing limb bud in the absence of direct DNA binding. *Development* **129**, 3077-3088 (2002).

125. McGonnell, I. M. The evolution of the pectoral girdle. *J. Anat* **199**, 189-194 (2001).

126. McIntyre, D. C. *et al.* Hox patterning of the vertebrate rib cage 1. *Development* **134**, 2981-2989 (2007).

127. Minoux, M., Antonarakis, G. S., Kmita, M., Duboule, D. & Rijli, F. M. Rostral and caudal pharyngeal arches share a common neural crest ground pattern 1. *Development* **136**, 637-645 (2009).

128. Monteilhet, C., Perrin, A., Thierry, A., Colleaux, L. & Dujon, B. Purification and characterization of the in vitro activity of I-Sce I, a novel and highly specific endonuclease encoded by a group I intron. *Nucleic Acids Res.* **18**, 1407-1413 (1990).

129. Morikawa, Y., D'Autreaux, F., Gershon, M. D. & Cserjesi, P. Hand2 determines the noradrenergic phenotype in the mouse sympathetic nervous system. *Dev. Biol.* **307**, 114-126 (2007).

130. Murchison, N. D. *et al.* Regulation of tendon differentiation by scleraxis distinguishes force-transmitting tendons from muscle-anchoring tendons. *Development* **134**, 2697-2708 (2007).

131. Nagai, T. *et al.* A variant of yellow fluorescent protein with fast and efficient maturation for cell-biological applications. *Nat. Biotechnol.* **20**, 87-90 (2002).

132. Nanci, A. *Ten Cate's Oral Histology*. Missouri (2003).

133. Nobrega, M. A., Ovcharenko, I., Afzal, V. & Rubin, E. M. Scanning human gene deserts for long-range enhancers 1. *Science* **302**, 413 (2003).

134. Noden, D. M. An analysis of migratory behavior of avian cephalic neural crest cells. *Dev. Biol.* **42**, 106-130 (1975).

135. Noden, D. M. The control of avian cephalic neural crest cytodifferentiation. I. Skeletal and connective tissues. *Dev. Biol.* **67**, 296-312 (1978).

136. Noden, D. M. The control of avian cephalic neural crest cytodifferentiation. II. Neural tissues. *Dev. Biol.* **67**, 313-329 (1978).

137. Noden, D. M. The role of the neural crest in patterning of avian cranial skeletal, connective, and muscle tissues. *Dev. Biol.* **96**, 144-165 (1983).

138. Nonchev, S. *et al.* Segmental expression of Hoxa-2 in the hindbrain is directly regulated by Krox-20. *Development* **122**, 543-554 (1996).

139. Nowicki, J. L. & Burke, A. C. Hox genes and morphological identity: axial versus lateral patterning in the vertebrate mesoderm. *Development* **127**, 4265-4275 (2000).

140. Nowicki, J. L., Takimoto, R. & Burke, A. C. The lateral somitic frontier: dorso-ventral aspects of anterio-posterior regionalization in avian embryos. *Mech. Dev.* **120**, 227-240 (2003).

141. O'Gorman, S. Second branchial arch lineages of the middle ear of wild-type and Hoxa2 mutant mice. *Dev. Dyn.* **234**, 124-131 (2005).

142. Offield, M. F., Hirsch, N. & Grainger, R. M. The development of Xenopus tropicalis transgenic lines and their use in studying lens developmental timing in living embryos
1. *Development* **127**, 1789-1797 (2000).

143. Ogino, H., McConnell, W. B. & Grainger, R. M. Highly efficient transgenesis in Xenopus tropicalis using I-SceI meganuclease. *Mech. Dev.* **123**, 103-113 (2006).

144. Ogino, H., McConnell, W. B. & Grainger, R. M. High-throughput transgenesis in Xenopus using I-SceI meganuclease. *Nat. Protoc.* **1**, 1703-1710 (2006).

145. Olivera-Martinez, I., Coltey, M., Dhouailly, D. & Pourquie, O. Mediolateral somitic origin of ribs and dermis determined by quail-chick chimeras
1. *Development* **127**, 4611-4617 (2000).

146. Panganiban, G. & Rubenstein, J. L. Developmental functions of the Distal-less/Dlx homeobox genes. *Development* **129**, 4371-4386 (2002).

147. Park, B. K. *et al.* Intergenic enhancers with distinct activities regulate Dlx gene expression in the mesenchyme of the branchial arches. *Dev. Biol.* **268**, 532-545 (2004).

148. Pasqualetti, M., Ori, M., Nardi, I. & Rijli, F. M. Ectopic Hoxa2 induction after neural crest migration results in homeosis of jaw elements in Xenopus. *Development* **127**, 5367-5378 (2000).

149. Pearson, J. C., Lemons, D. & McGinnis, W. Modulating Hox gene functions during animal body patterning
1. *Nat. Rev. Genet.* **6**, 893-904 (2005).

150. Perrin, A., Buckle, M. & Dujon, B. Asymmetrical recognition and activity of the I-SceI endonuclease on its site and on intron-exon junctions. *EMBO J.* **12**, 2939-2947 (1993).

151. Qiu, M. *et al.* Role of the Dlx homeobox genes in proximodistal patterning of the branchial arches: mutations of Dlx-1, Dlx-2, and Dlx-1 and -2 alter morphogenesis of proximal skeletal and soft tissue structures derived from the first and second arches. *Dev. Biol.* **185**, 165-184 (1997).

152. Reichert, K. B. *De embryonum arcubus sic dictis branchialibus*. Berlin 1836. 1836. Berlin.
Ref Type: Thesis/Dissertation

153. Rijli, F. M. *et al.* A homeotic transformation is generated in the rostral branchial region of the head by disruption of Hoxa-2, which acts as a selector gene. *Cell* **75**, 1333-1349 (1993).

154. Robinson, J., Ahlberg, P. E. & Koentges, G. The braincase and middle ear region of Dendrerpeton acadianum (Tetrapoda: Temnospondyli). *Zoological Journal of the Linnean Society* **143**, 577-597 (2005).

155. Robledo, R. F., Rajan, L., Li, X. & Lufkin, T. The Dlx5 and Dlx6 homeobox genes are essential for craniofacial, axial, and appendicular skeletal development. *Genes Dev.* **16**, 1089-1101 (2002).

156. Rodriguez-Guzman, M. *et al.* Tendon-muscle crosstalk controls muscle bellies morphogenesis, which is mediated by cell death and retinoic acid signaling. *Dev. Biol.* **302**, 267-280 (2007).

157. Rosenquist, G. L. & Campbell, G. R. Characteristics of the 19S and 7S response to bacteriophage 0X74 in the fowl
1. *Immunology* **10**, 169-178 (1966).

158. Ruest, L. B. *et al.* dHAND-Cre transgenic mice reveal specific potential functions of dHAND during craniofacial development. *Dev. Biol.* **257**, 263-277 (2003).

159. Ruest, L. B., Xiang, X., Lim, K. C., Levi, G. & Clouthier, D. E. Endothelin-A receptor-dependent and -independent signaling pathways in establishing mandibular identity. *Development* **131**, 4413-4423 (2004).

160. Rychlik, J. L., Gerbasi, V. & Lewis, E. J. The interaction between dHAND and Arix at the dopamine beta-hydroxylase promoter region is independent of direct dHAND binding to DNA
1. *J Biol. Chem.* **278**, 49652-49660 (2003).

161. Ryffel, G. U. *et al.* Tagging muscle cell lineages in development and tail regeneration using Cre recombinase in transgenic Xenopus. *Nucleic Acids Res.* **31**, e44 (2003).

162. Schneider, R. A. & Helms, J. A. The cellular and molecular origins of beak morphology. *Science* **299**, 565-568 (2003).

163. Schorpp, M. *et al.* The human ubiquitin C promoter directs high ubiquitous expression of transgenes in mice
2. *Nucleic Acids Res.* **24**, 1787-1788 (1996).

164. Schweitzer, R. *et al.* Analysis of the tendon cell fate using Scleraxis, a specific marker for tendons and ligaments. *Development* **128**, 3855-3866 (2001).

165. Seckel, L. & Janis, C. Convergences in Scapula Morphology among Small Cursorial Mammals: An Osteological Correlate for Locomotory Specialization. *J. Mammal. Evol* **2**, 261-279 (2008).

166. Sharpe, J. Optical projection tomography as a new tool for studying embryo anatomy
14. *J Anat* **202**, 175-181 (2003).

167. Sharpe, J. Optical projection tomography
12. *Annu. Rev. Biomed. Eng* **6**, 209-228 (2004).

168. Sharpe, J. *et al.* Optical projection tomography as a tool for 3D microscopy and gene expression studies
15. *Science* **296**, 541-545 (2002).

169. Shigetani, Y. *et al.* Heterotopic shift of epithelial-mesenchymal interactions in vertebrate jaw evolution
1. *Science* **296**, 1316-1319 (2002).

170. Shubin, N., Tabin, C. & Carroll, S. Fossils, genes and the evolution of animal limbs
2. *Nature* **388**, 639-648 (1997).

171. Shubin, N., Tabin, C. & Carroll, S. Deep homology and the origins of evolutionary novelty
1. *Nature* **457**, 818-823 (2009).

172. Shulman, J. M., Perrimon, N. & Axelrod, J. D. Frizzled signaling and the developmental control of cell polarity
1. *Trends Genet.* **14**, 452-458 (1998).

173. Simons, M. & Mlodzik, M. Planar cell polarity signaling: from fly development to human disease
1. *Annu. Rev. Genet.* **42**, 517-540 (2008).

174. Sive, H. L., Grainger, R. M. & Harland, R. M. *Early Development of Xenopus laevis, A LABORATORY MANUAL*. Cold Spring Harbor Laboratory Press, Cold Spring Harbor, New York (2000).

175. Smith, S. J., Kotecha, S., Towers, N. & Mohun, T. J. Xenopus Hand2 expression marks anterior vascular progenitors but not the developing heart
1. *Dev. Dyn.* **219**, 575-581 (2000).

176. Soriano, P. Generalized lacZ expression with the ROSA26 Cre reporter strain. *Nat. Genet.* **21**, 70-71 (1999).

177. Srinivas, S. *et al.* Cre reporter strains produced by targeted insertion of EYFP and ECFP into the ROSA26 locus. *BMC. Dev. Biol.* **1**, 4 (2001).

178. Srivastava, D., Cserjesi, P. & Olson, E. N. A subclass of bHLH proteins required for cardiac morphogenesis
1. *Science* **270**, 1995-1999 (1995).

179. Srivastava, D. & Olson, E. N. Knowing in your heart what's right. *Trends Cell Biol.* **7**, 447-453 (1997).

180. Srivastava, D. *et al.* Regulation of cardiac mesodermal and neural crest development by the bHLH transcription factor, dHAND. *Nat. Genet.* **16**, 154-160 (1997).

181. Stock, D. W. *et al.* The evolution of the vertebrate Dlx gene family
2. *Proc. Natl. Acad. Sci. U. S. A* **93**, 10858-10863 (1996).

182. Tao, H. *et al.* Mouse prickle1, the homolog of a PCP gene, is essential for epiblast apical-basal polarity
5. *Proc. Natl. Acad. Sci. U. S. A* **106**, 14426-14431 (2009).

183. te, W. P., Fernandez-Teran, M., Ros, M. A. & Zeller, R. Mutual genetic antagonism involving GLI3 and dHAND prepatterns the vertebrate limb bud mesenchyme prior to SHH signaling. *Genes Dev.* **16**, 421-426 (2002).

184. Thermes, V. *et al.* I-SceI meganuclease mediates highly efficient transgenesis in fish. *Mech. Dev.* **118**, 91-98 (2002).

185. Tickle, C. Genetics and limb development
76. *Dev. Genet.* **19**, 1-8 (1996).

186. Tickle, C. Morphogen gradients in vertebrate limb development
51. *Semin. Cell Dev. Biol.* **10**, 345-351 (1999).

187. Tickle, C. Limb development: an international model for vertebrate pattern formation
46. *Int. J Dev. Biol.* **44**, 101-108 (2000).

188. Tickle, C. Vertebrate limb development and possible clues to diversity in limb form
38. *J Morphol.* **252**, 29-37 (2002).

189. Tickle, C. Patterning systems--from one end of the limb to the other
2. *Dev. Cell* **4**, 449-458 (2003).

190. Towers, M., Mahood, R., Yin, Y. & Tickle, C. Integration of growth and specification in chick wing digit-patterning
1. *Nature* **452**, 882-886 (2008).

191. Towers, M. & Tickle, C. Growing models of vertebrate limb development
5. *Development* **136**, 179-190 (2009).

192. Towers, M. & Tickle, C. Generation of pattern and form in the developing limb
3. *Int. J Dev. Biol.* **53**, 805-812 (2009).

193. Trainor, P. A. & Krumlauf, R. Patterning the cranial neural crest: hindbrain segmentation and Hox gene plasticity. *Nat. Rev. Neurosci.* **1**, 116-124 (2000).

194. Trainor, P. A., riza-McNaughton, L. & Krumlauf, R. Role of the isthmus and FGFs in resolving the paradox of neural crest plasticity and prepatterning. *Science* **295**, 1288-1291 (2002).

195. Trinh, L. A., Yelon, D. & Stainier, D. Y. Hand2 regulates epithelial formation during myocardial differentiation. *Curr. Biol.* **15**, 441-446 (2005).

196. Truett, G. E. *et al.* Preparation of PCR-quality mouse genomic DNA with hot sodium hydroxide and tris (HotSHOT). *Biotechniques* **29**, 52, 54 (2000).

197. Trumpp, A., Depew, M. J., Rubenstein, J. L., Bishop, J. M. & Martin, G. R. Cre-mediated gene inactivation demonstrates that FGF8 is required for cell survival and patterning of the first branchial arch
1. *Genes Dev.* **13**, 3136-3148 (1999).

198. Tumpel, S., Maconochie, M., Wiedemann, L. M. & Krumlauf, R. Conservation and diversity in the cis-regulatory networks that integrate information controlling expression of Hoxa2 in hindbrain and cranial neural crest cells in vertebrates. *Dev. Biol.* **246**, 45-56 (2002).

199. Valasek, P. *et al.* Somitic origin of the medial border of the mammalian scapula and its homology to the avian scapula blade
8. *J Anat* **216**, 482-488 (2010).

200. Vickaryous, M. K. & Hall, B. K. Homology of the reptilian coracoid and a reappraisal of the evolution and development of the amniote pectoral apparatus. *J. Anat* **208**, 263-285 (2006).

201. Vokes, S. A., Ji, H., Wong, W. H. & McMahon, A. P. A genome-scale analysis of the cis-regulatory circuitry underlying sonic hedgehog-mediated patterning of the mammalian limb
6. *Genes Dev.* **22**, 2651-2663 (2008).

202. Von Baer, K. E. *Ueber die Entwicklungsgeschichte der Thiere: Beobachtung und Reflexion*. Bornträger, Königsberg (1828).

203. Wagner, G. Die Bedeutung der Neuralleiste fuer die Kopfgestaltung der Amphibienlarven. *Rev. Suisse Zool.* **56**, 519-620 (1949).

204. Wang, X. P. *et al.* Modulation of activin/bone morphogenetic protein signaling by follistatin is required for the morphogenesis of mouse molar teeth. *Dev. Dyn.* **231**, 98-108 (2004).

205. Wang, X. P. *et al.* Follistatin regulates enamel patterning in mouse incisors by asymmetrically inhibiting BMP signaling and ameloblast differentiation. *Dev. Cell* **7**, 719-730 (2004).

206. Wiehler, J., von, H. J. & Steipe, B. Mutants of Discosoma red fluorescent protein with a GFP-like chromophore. *FEBS Lett.* **487**, 384-389 (2001).

207. Wu, J. & Mlodzik, M. A quest for the mechanism regulating global planar cell polarity of tissues. *Trends Cell Biol.* **19**, 295-305 (2009).

208. Xiong, W. *et al.* Hand2 is required in the epithelium for palatogenesis in mice. *Dev. Biol.* **330**, 131-141 (2009).

209. Xu, H., Firulli, A. B., Zhang, X. & Howard, M. J. HAND2 synergistically enhances transcription of dopamine-beta-hydroxylase in the presence of Phox2a 1. *Dev. Biol.* **262**, 183-193 (2003).

210. Yamagishi, H., Olson, E. N. & Srivastava, D. The basic helix-loop-helix transcription factor, dHAND, is required for vascular development 1. *J Clin. Invest* **105**, 261-270 (2000).

211. Yanagisawa, H., Clouthier, D. E., Richardson, J. A., Charite, J. & Olson, E. N. Targeted deletion of a branchial arch-specific enhancer reveals a role of dHAND in craniofacial development. *Development* **130**, 1069-1078 (2003).

212. Yelon, D. *et al.* The bHLH transcription factor hand2 plays parallel roles in zebrafish heart and pectoral fin development. *Development* **127**, 2573-2582 (2000).

213. Yew, N. S., Przybylska, M., Ziegler, R. J., Liu, D. & Cheng, S. H. High and sustained transgene expression in vivo from plasmid vectors containing a hybrid ubiquitin promoter. *Mol. Ther.* **4**, 75-82 (2001).

214. Zambrowicz, B. P. *et al.* Disruption of overlapping transcripts in the ROSA beta geo 26 gene trap strain leads to widespread expression of beta-galactosidase in mouse embryos and hematopoietic cells. *Proc. Natl. Acad. Sci. U. S. A* **94**, 3789-3794 (1997).

215. Zhang, G. *et al.* Decorin regulates assembly of collagen fibrils and acquisition of biomechanical properties during tendon development 1. *J. Cell Biochem.* **98**, 1436-1449 (2006).